東京市區地帶的沉積軟岩的強度及變形特性

Fumio Tatsuoka
日本東京大學土木工程系

STRENGTH AND DEFORMATION CHARACTERISTICS OF SEDIMENTARY SOFT ROCK IN THE TOKYO METROPOLITAN AREA

Fumio Tatsuoka
Department of Civil Engineering, University of Tokyo, Japan

撮要

本文描述透過數個大型研究和建築工程所得有關東京市區地帶的沉積軟岩的強度及變形特性的資料，其中包括小變形情況下的彈性剛度，在不同應變及壓力下的非線性表現，各向異性的應力應變特性，剪切帶的蠕動及變形特性。高質素岩芯的三軸試驗所得的沉積軟岩彈性剛度與現場剪切波所測數據接近。沉積軟岩的變形和在該岩層上興建的建築物位移可以可靠地利用震波勘測所測量的彈性剛度作出估計，在計算時需要考慮剪切應變及壓力水平對軟岩剛度的影響，而其影響可透過有關的實驗及現場的試驗作出評估。荷載速率效應，可用非線性的模型加以模擬。傳統的取樣方法對岩芯造成不可忽視的擾動。本文最後會討論幾個先進的壓力應變實驗室測驗方法。

STRENGTH AND DEFORMATION CHARACTERISTICS OF SEDIMENTARY SOFT ROCK IN THE TOKYO METROPOLITAN AREA

Fumio Tatsuoka[1]

Abstract : The strength and deformation characteristics of sedimentary soft rock that were evaluated in relation to several large-scale research and construction projects in the Tokyo metropolitan area are described. A large amount of data showing the elastic stiffness at small strains, non-linearity due to strain and pressure level, anisotropy of the stress-strain properties, viscous properties and deformation properties of shear bands is presented. The elastic stiffness of sedimentary soft rock obtained from triaxial tests using high-quality core samples, while measuring stresses and strains accurately, is generally similar to the corresponding value from field shear wave velocity. Deformations of sedimentary soft rock deposits and displacements of structures constructed on and in them at working loads could be reliably predicted based on the elastic stiffness evaluated by field seismic surveys. It was necessary to take into account the dependency of stiffness on shear strain and pressure level, which could be evaluated by relevant laboratory stress-strain tests while referring to results from relevant field loading tests. Loading rate effects due to the material viscous properties, including creep deformation, but not those caused by the migration of pore water pressure, could be simulated by a non-linear three-component model. Core samples retrieved by conventional rotary core tube sampling method could be noticeably disturbed. Several advanced laboratory stress-strain testing methods developed in the course of this long-term study are described.

INTRODUCTION

Since the 70's, a number of large important civil engineering structures, including foundations for long suspension bridges, high-rise buildings, large and deep excavations for underground energy storage tanks, railway and highway tunnels, rockfill dams and etc, have been constructed on and in sedimentary soft rock deposits in Japan (e.g., Tatsuoka and Shibuya 1991; Tatsuoka and Kohata 1995; Tatsuoka et al. 1995a; Tatsuoka 1999a, 2001; Koseki et al. 2001). In such projects the prediction of ground deformation and structural displacements is one of the major design steps. In the mid 80's, when the author started assisting several major construction projects in or on sedimentary soft rock deposits, it was normal that the observed full-scale field deformations of sedimentary soft rock deposits largely deviated from those predicted in advance. The situation at that time is summarized below:

1) When based on stiffness values obtained from conventional laboratory stress-strain tests, such as unconfined compression tests and oedometer tests, full-scale field ground deformations and structural displacements were often largely over-estimated. Thus, practicing civil engineers naturally tended to not rely on laboratory stress-strain tests, although the reasons for the cited disagreement usually could not be identified. This is a somewhat different situation from the one in the UK, where sample disturbance was considered to be responsible for the over-estimation of full-scale field ground deformation when based on laboratory stress-strain tests (mostly triaxial compression tests) using samples retrieved from the field (e.g., Jardine et al. 1991;

[1] Professor, Department of Civil Engineering, University of Tokyo, Japan

Hight and Higgins 1995; Jardine 1995). It was found later that the main cause for the cited over-estimation was that non-linear stress-strain behaviour at small strains which were relevant to the full-scale field cases and effects of recent stress history were not properly taken into account in these predictions (e.g., Burland 1989; Jardine et al. 1991; Hight and Higgins 1995; Jardine 1995).

2) Engineers tended to rely on results obtained from plate loading tests (PLTs) and pressure-meter tests (PMTs or bore hole lateral loading tests BHLTs) that were analysed based on the conventional isotropic linear theory and assuming homogeneous ground conditions. When predicting the settlement of a footing for a bridge or a heavy structure, PLTs were preferred because the loading conditions in PLTs are similar to those in the full-scale field case. However, it is not possible to perform PLTs at elevations below the present seabed where typical footing base is to be placed at offshore sites. For example, in the Akashi Strait Bridge project, a great number of conventional pre-bored PMTs were performed in a number of boreholes at the offshore sites. An empirical method was proposed to convert measured PMT stiffness $(E)_{PMT}$ (evaluated based on isotropic linear theory) to equivalent PLT stiffness $(E)_{PLT}$ that would be used in the prediction of the instantaneous settlement of footings to be constructed on a sedimentary soft rock deposit (Kobe group of the Pliocene epoch) for the Akashi Strait Bridge (e.g., Takeuchi et al. 1981). In this correction method, the ratio $(E)_{PLT}/(E)_{PMT}$ increases with a decrease in $(E)_{PMT}$. In the design, non-linearity of stress-strain behaviour due to strain and pressure level as well as effect of loading history on the stress-strain behaviour was not taken into account in an explicit way when evaluating the stress-strain properties of sedimentary soft rock. The correction method described above is representative of such a situation.

3) A link among the stiffness values obtained from laboratory stress-strain tests, field loading tests (PLTs and PMTs), field seismic surveys and full-scale field measurements was missing. Typically, a large difference was often observed between dynamically measured elastic stiffness (such as those from field seismic survey) and statically measured 'elastic' stiffness (such as E_{50} values from conventional laboratory stress-strain tests and reloading stiffness values from PLTs). It was explicitly or implicitly considered that the reason for the above is that a given mass of sedimentary soft rock has two different types of elastic stiffness, the dynamic and static elastic stiffness values. In the case when discontinuities (such as joints, cracks and faults) are densely distributed within a given mass of sedimentary soft rock, the elastic Young's modulus of the mass evaluated by seismic survey could be much larger than the value back-calculated from the full-scale field observations even when non-linearity of stress-strain behaviour is taken into account, but it would be smaller than the elastic Young's modulus accurately evaluated at very small strains by laboratory stress-strain tests using core samples not containing such discontinuities. As shown below, however, the effects of discontinuities on the average stress-strain properties of a mass of sedimentary soft rock are usually not significant, unlike cases involving hard rock masses. Rather, the so-called 'elastic' stiffness from conventional laboratory stress-strain tests could be much smaller than the value from field seismic survey and full-scale field behaviour. This was usually due to technical problems in the conventional laboratory stress-strain tests and/or effects of sample disturbance. The current SOA of this issue is summarised in Tatsuoka et al. (2001b).

In the late 80's, the authors and their colleagues started a comprehensive series of studies on the following topics with respect to the stress-strain-time properties of sedimentary soft rock utilising predominantly laboratory stress-strain tests:

1) Development of relevant laboratory stress-strain testing methods (i.e., triaxial and plane strain compression tests and true triaxial tests) to accurately evaluate the stress-strain behaviour.
2) Stress-strain behaviour at small strains, including the elastic behaviour:
   a) A comparison between elastic stiffness values from laboratory stress-strain tests and field shear wave velocities.
   b) Relevant definitions of elastic deformation properties and its constitutive modelling.
3) Non-linearity due to strain and pressure level of pre-peak stress-strain behaviour.
   a) Evaluation of non-linearity and its constitutive modelling.

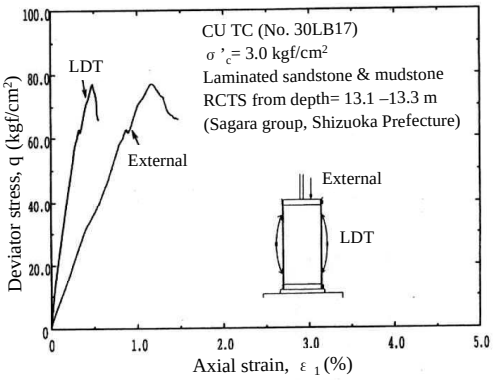

a)

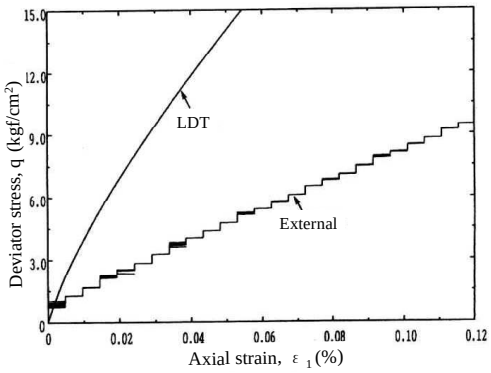

b)

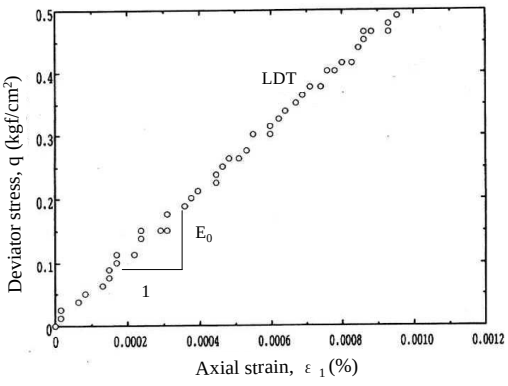

c)

Figure 2.1. Deviator stress-axial strain relations from a CU TC test on a sedimentary soft rock of sand-mudstone from Sagara group (Pliocene epoch), Shizuoka Prefecture (Tatsuoka and Shibuya 1991).

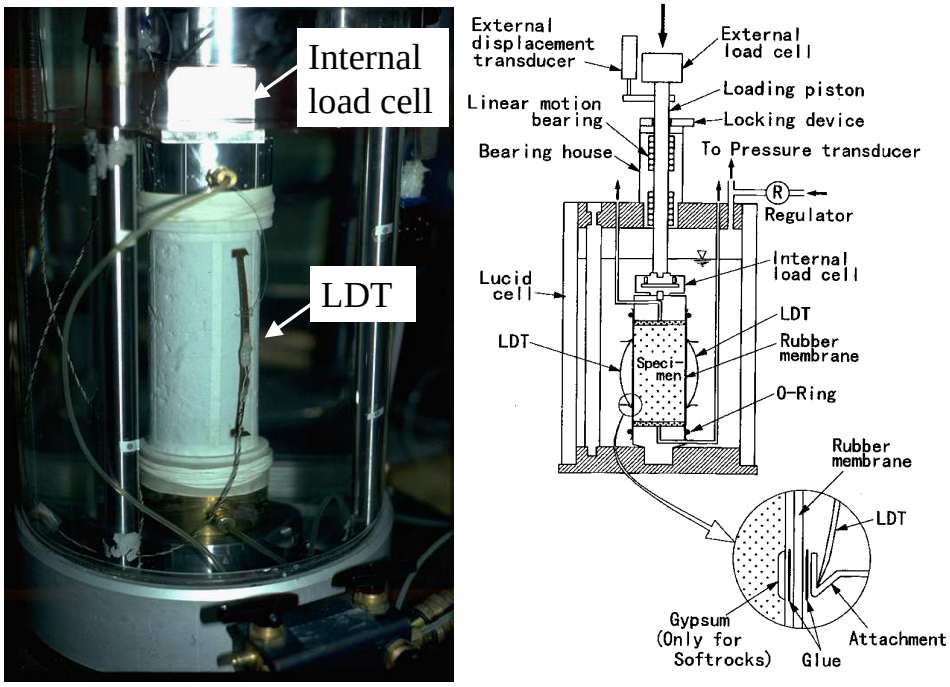

a) b)

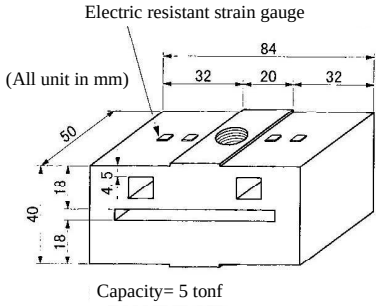

Figure 2.2. a) & b) Triaxial compression test system with local axial strain measurements by using a pair of LDTs (the specimen is sedimentary soft rock); and b) details of internal load cell (Tatsuoka et al. 1999a, b).

b) Analysis of full-scale field ground deformation and structural displacements and results from filed loading tests based on the elastic deformation properties from field shear wave velocities measured and the non-linearity of stress-strain behaviour from laboratory stress-strain tests on core samples retrieved from the site.

4) Inherent and stress system-induced anisotropy of the strength and deformation properties.

5) Shear banding characteristics related to failure analysis.

6) Sample disturbance:
   a) Different degrees of sample disturbance among different sampling methods (i.e., rotary core tube sampling and block sampling and direct coring at the exposed ground surface).
   b) Effects of sample disturbance on the elastic stiffness, non-linearity in the pre-peak stress-strain behaviour and peak strength.

7) Loading rate effects due to the material viscous properties and its constitutive

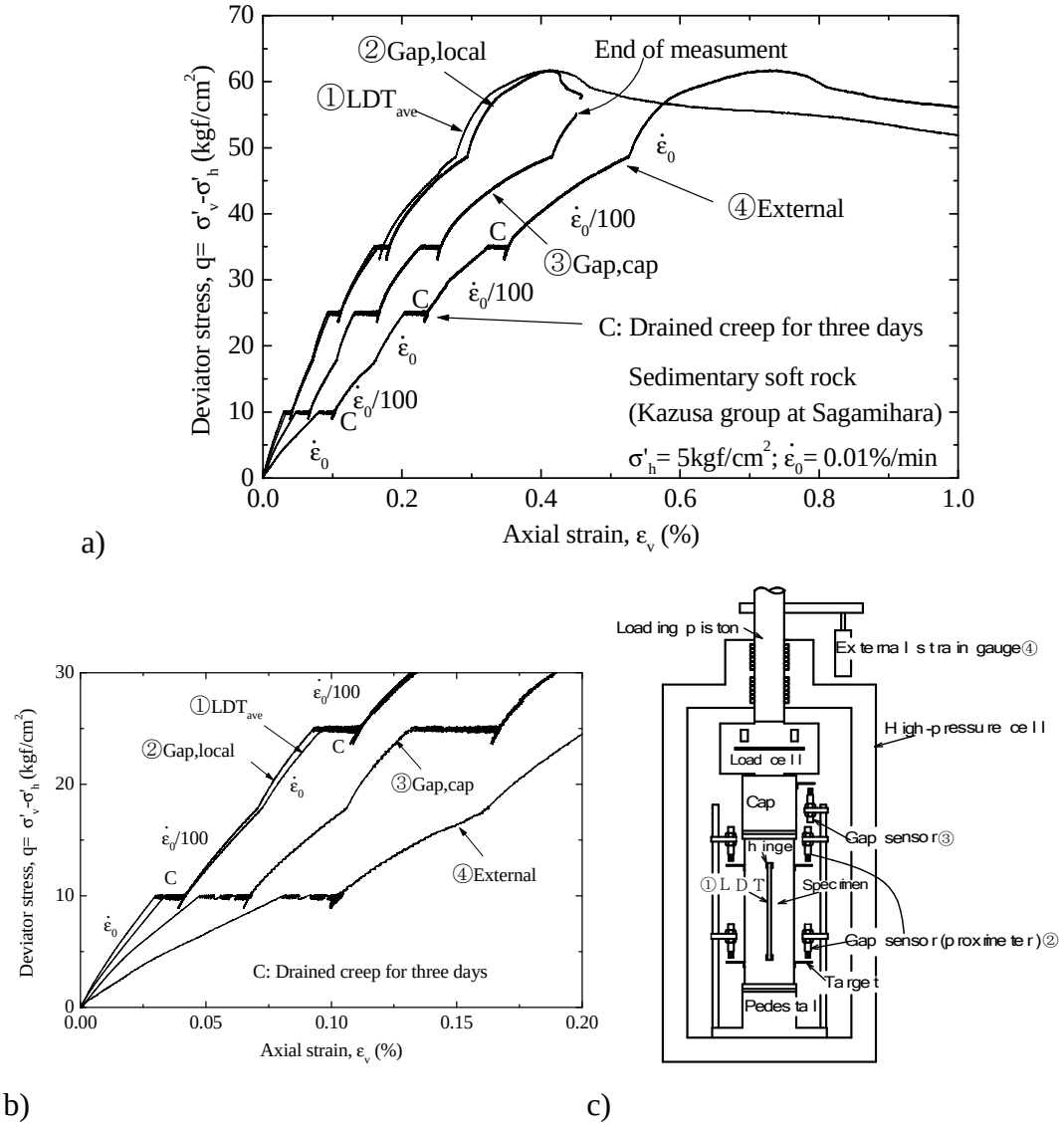

Figure 2.3. Comparison of axial strains measured by four methods in a CD TC test including creep loading stages and step changes in the strain rate, sedimentary soft rock of silt-sandstone, Kazusa group of Pleistocene epoch at Sagamihara; a) overall stress-strain relationship; b) stress-strain relationship at small strains; and c) four methods of axial strain measurement (Hayano et al. 2001).

modelling.

The following is a summary of the results from these research programs, including the latest unpublished test results.

RECENT ADVANCES IN LABORATORY STRESS-STRAIN TESTING METHODS

Accurate and Sensitive Evaluation of Strains by Local Measurements

Vertical LDTs for axial strains: In the late 80's, the authors and their colleagues performed a large number of triaxial tests on core samples retrieved from full-scale test fills of cement-mixed sand placed underwater and found the importance of local strain measurements

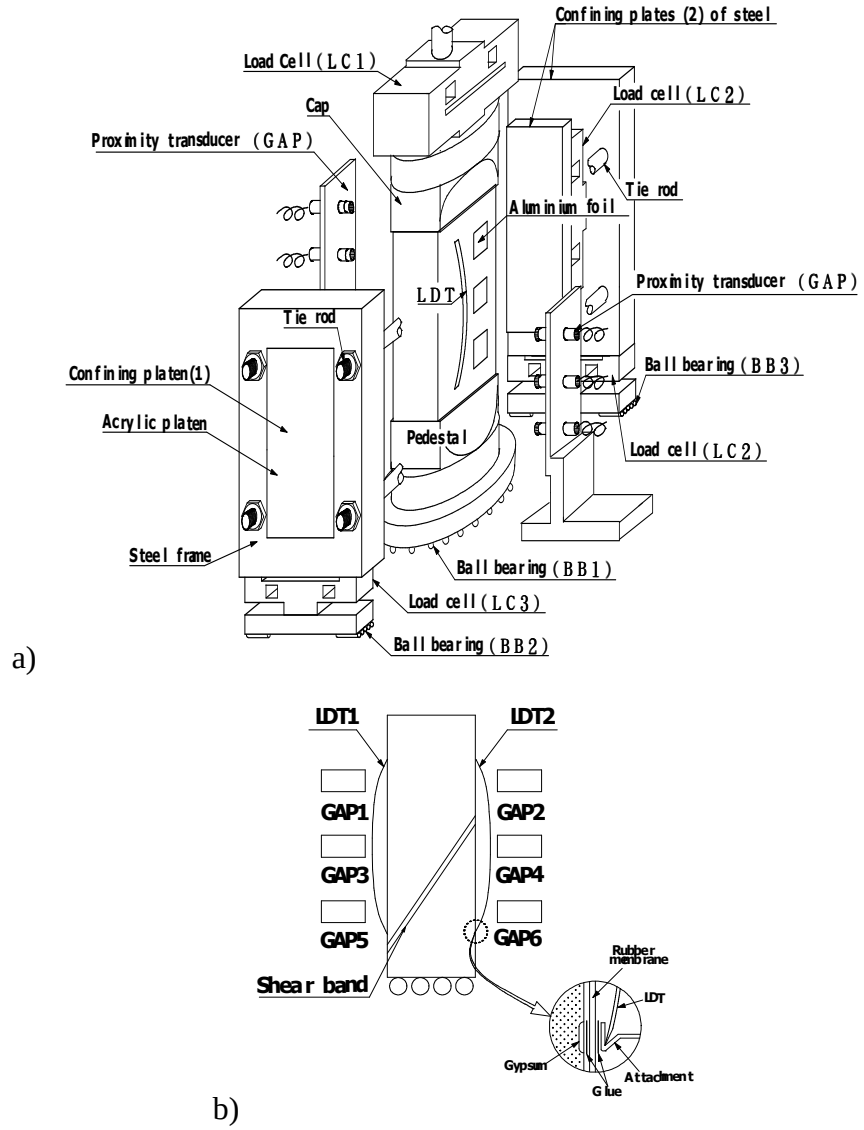

Figure 2.4. a) Plane strain compression testing system to observe the deformation of shear bands for sedimentary soft rock; and b) local measurement system for axial and lateral deformations (Hayano et al. 1999b).

for the accurate and reliable evaluation of pre-peak stress-strain properties of stiff geomaterial (Tatsuoka and Shibuya 1991; Tatsuoka et al. 1997b). We obtained the same conclusion with sedimentary soft rock from results of a series of unconfined and triaxial compression tests on core samples from a site where a high embankment for an airport was to be constructed over an existing railway tunnel that had been constructed in a sedimentary soft rock deposit of the Pliocene epoch (Sagara group) in Shizuoka prefecture (Tatsuoka and Shibuya 1991; Tatsuoka et al. 1993). The age of the deposit is greater than five million years and it consists mainly of mudstone with sandstone layers. **Fig. 2.1** shows a result from a CD TC test on a core sample of sand-mudstone (with a diameter of 5 cm and a height of 10 cm) performed at an axial strain rate of 0.01 %/min, which is typical of the many tests performed related to this project. **Fig. 2.2** shows the triaxial testing system used for the tests. In this series of tests, a local axial strain gauge, called the local deformation transducer (LDT), was used for the first time in TC tests on sedimentary soft rock samples, after a number of TC tests on cement-mixed sand had been performed using a pair of LDT. The LDT, developed by Goto

et al. (1991), is a type of clip gauge and consists of a phosphor bronze strip that is placed the ends of specimen diameter on the lateral surface of specimen. A set of electric-resistant strain gauges consisting of a full bridge is attached to both sides of the central part of the strip to detect the axial deformation of specimen very accurately. The LTD has become one of the most popular local axial strain measuring methods in Japan for relatively stiff geomaterials.

In the project for which the TC test described in Fig. 2.1 was performed, it was necessary to evaluate whether the weight of the embankment would damage the concrete lining of the railway tunnel, which had been constructed in a deposit of sedimentary soft rock. At that time it was the standard engineering practice to use the stiffness E_{PMT} from conventional pre-bored PMTs in the numerical analysis to predict the ground deformation in

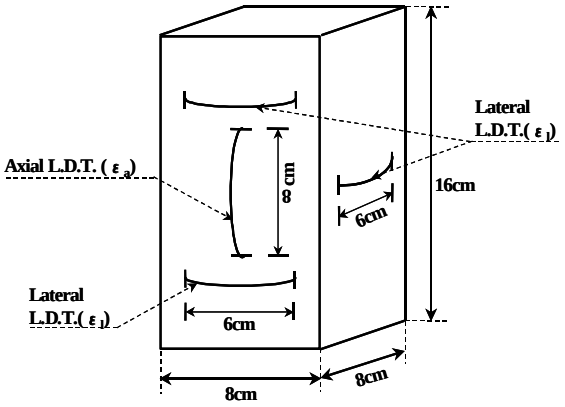

Figure 2.5. Rectangular prismatic specimen with vertical and lateral LDTs for triaxial compression tests of sedimentary soft rock (Hayano et al. 1997).

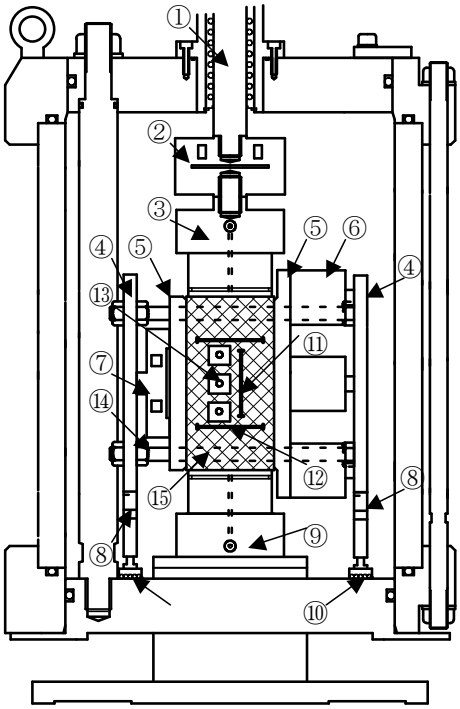

① Loading rod (ϕ 30mm)
② Load cell (LC1)
③ Cap
④ End plate
⑤ Confining plate
⑥ Oil cylinder
⑦ Load cell (LC2)
⑧ Load cell (LC3)
⑨ Pedestal
⑩ Slide bearing
⑪ Vertical LDT (ε_z)
⑫ Horizontal LDT (ε_y)
⑬ Gap sensor and target (ε_x)
⑭ Tie rod
⑮ Specimen

Figure 2.6. True triaxial testing system with vertical and lateral LDTs for sedimentary soft rock (Hayano et al. 1999a; Hayano 2001).

such a case. In that project, the tangent Young's modulus evaluated at a half of the peak strength, $(E_{tan})_{50}$, was evaluated from the relationship between the deviator stress and the externally measured axial strain from unconfined compression tests (Tatsuoka et al. 1993). These $(E_{tan})_{50}$ values were generally similar to the E_{PMT} values from primary loading curves obtained by conventional PMTs performed at the site. On the other hand, a series of CU and CD TC tests were performed using a pair of LDTs at the Geotechnical Engineering Laboratory, the University of Tokyo (Tatsuoka and Shibuya 1991; Tatsuoka et al. 1993). The initial Young's modulus (E_0) at strains less than about 0.001 % evaluated from the relationship between the deviator stress and the locally measured axial strains obtained from TC tests (as shown in Fig. 2.1c) was essentially the same as the elastic stiffness from field shear wave velocities. The values of the secant modulus E_{sec} at the strain level that was expected in the field were also evaluated, which were only slightly lower than the E_0 values while much higher (by a factor of about 4) than the $(E_{tan})_{50}$ values. Numerical analysis using the E_{PMT} or $(E_{tan})_{50}$ values predicted that the concrete lining of the tunnel would be damaged. It was predicted, however, that the tunnel would not be damaged if the analysis was based on the E_{sec} values evaluated from field shear wave velocities taking into account the non-linearity of stress-strain behaviour from the results from TC tests locally measuring axial strains as shown in Fig. 2.1.

From the beginning of 2002, a partial excavation of the surface soil layer and sedimentary soft rock deposit overlying the tunnel for the construction of a protection structure to reduce the load by the weight of embankment applied to the tunnel started. The protection structure is under construction at the time of writing this paper (the beginning of August 2002). The deformations of the tunnel and surrounding sedimentary soft rock deposit that have been so far observed have shown that the stiffness evaluated based on the elastic deformation properties from field shear wave velocity is consistent with the field behaviour while the values of E_{PMT} and $(E_{tan})_{50}$ are utterly too small. The details of this case will be reported in the near future.

It is now well known that such a large discrepancy between externally and locally measured axial strains, as seen in Fig. 2.1, is due to the significant effects of bedding error at the top and bottom ends of the specimen. When axial strains are measured with an external axial gauge placed outside the triaxial cell, errors due to the deformation of the apparatus (i.e., system compliance) are also included in measured axial strains. The bedding error could be due to;

a) a lack of parallelism between the specimen ends and the contact surfaces of the cap and pedestal;
b) undulation of specimen ends; and
c) extra-compression of disturbed thin layers formed during specimen preparation (and drainage filter paper when used as in the case of the test described in Fig. 2.1).

Even when an excellent contact between the specimen ends and the cap and pedestal is ensured by capping the specimen ends by using gypsum, the effects of item c) above would not become negligible, as observed from the result from a CD TC test presented in **Fig. 2.3**. In this test, the core sample obtained at the Sagamihara test site (as described in detail later in this paper) was used. In this test, axial strains were measured by using: (1) a pair of LDTs; (2) two pairs of proximity transducers (or gap sensors), both set at the ends of specimen diameter along the lateral surface of the specimen; (3) a proximity transducer measuring the

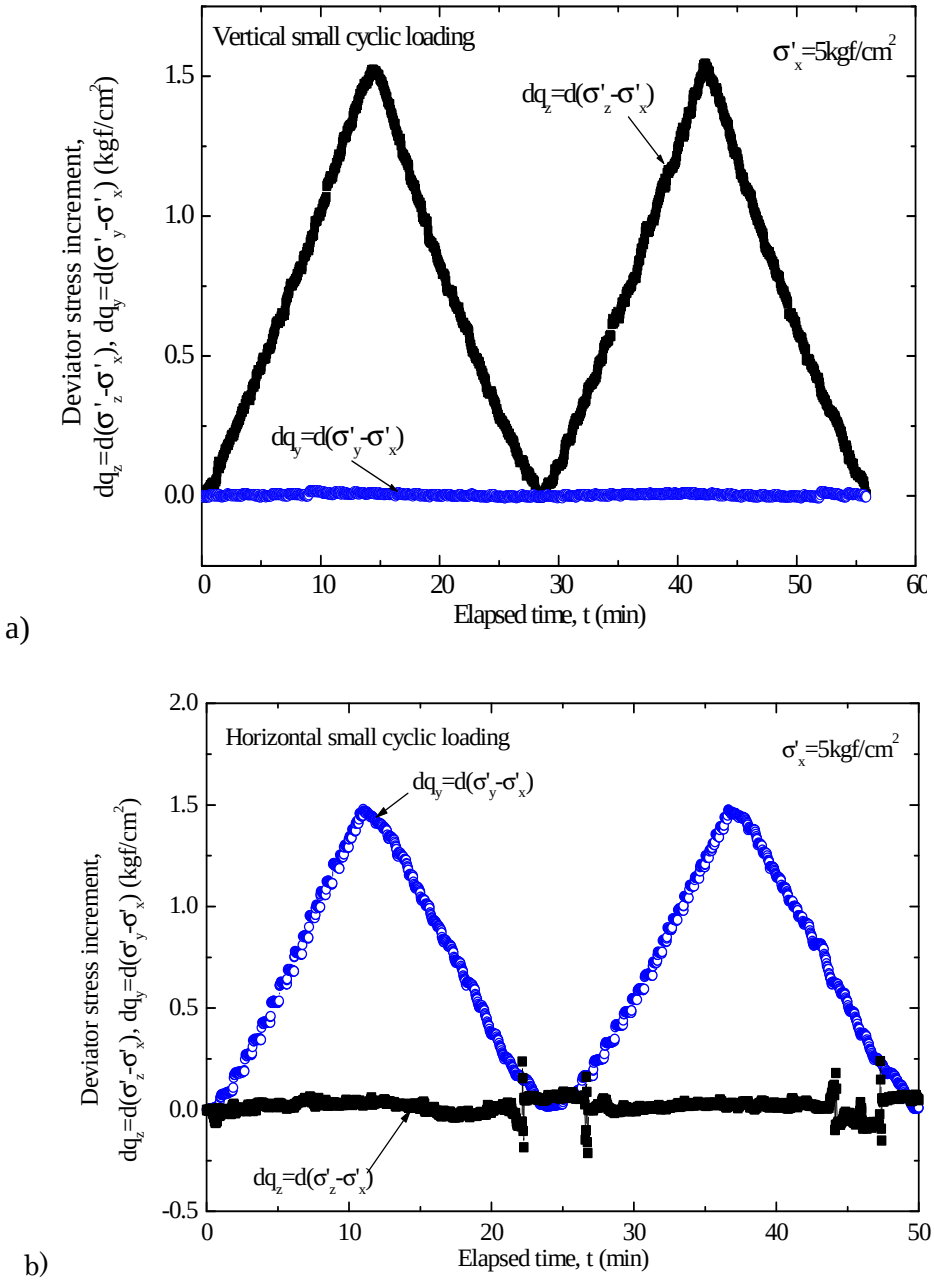

Figure 2.7. Time histories of vertical and horizontal stresses in cyclic loading tests on sedimentary soft rock (Kazusa group at Sagamihara); a) cyclic loading of vertical stress at constant horizontal and lateral stresses; and b) cyclic loading of horizontal stress at constant vertical and lateral stresses (Hayano et al. 1999a).

axial displacement of the specimen cap; and (4) an external axial gauge placed outside the triaxial cell measuring the axial displacement of the loading piston. It may be seen that the axial strains measured by using "(3) a proximity transducer (denoted as (3)Gap,cap)" exhibits large bedding error during not only monotonic loading but also creep loading stages. The difference in the axial strains measured with "(3) a proximity transducer" and "(4) an external axial gauge (denoted as (4) External)" is due to the system compliance.

After the above described project, the authors were involved in a number of projects

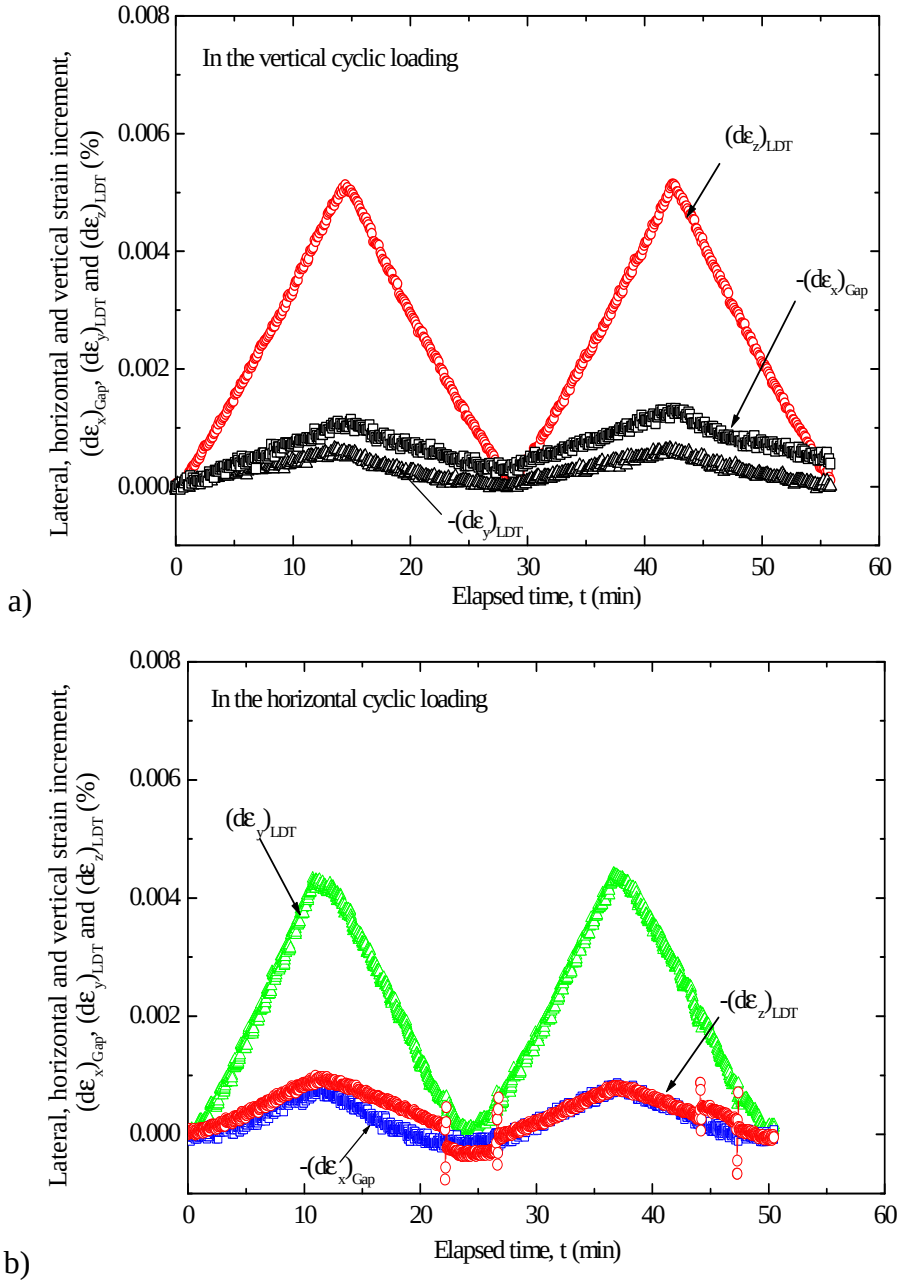

Figure 2.8. Time histories of vertical and horizontal strains in cyclic loading tests on sedimentary soft rock (Kazusa group at Sagamihara); a) cyclic loading of vertical stress at constant horizontal and lateral stresses; and b) cyclic loading of horizontal stress at constant vertical and lateral stresses, corresponding to Fig. 2.7 (Hayano et al. 1999a).

for bridge foundations, high-rise building, deep vertical shafts, subway tunnels and etc. constructed on or in sedimentary soft rock deposits, as summarized by Tatsuoka and Shibuya (1991), Tatsuoka et al. (1995a), Tatsuoka and Kohata (1995) and Tatsuoka et al. (1999a).

Before starting an experimental study into the viscous properties of sedimentary soft rock in the early 90', the authors considered that the effects of bedding error would not be significant on strain increments that develop during a creep loading test, in which the axial stress is kept constant. This assumes that the bedding error is a function of effective axial stress. Most of the creep tests on sedimentary soft rock that could be found in the literature

used an external axial gauge to evaluate axial strain increments developed during creep loading. It was found from a series of TC tests, however, that the effects of bedding error during monotonic loading could become larger with a decrease in the axial strain rate and the effects could be significant during creep loading tests (Matsumoto et al. 1999; Tatsuoka et al. 1999b: Hayano et al. 2001). Fig. 2.3 shows results typical of test results indicating the above. It may be seen that the difference between the axial strains measured with "(3) a proximity transducer" and "(3)&(4) two types local axial strain gauges" increases also at the creep loading stages.

Vertical LDTs are also useful to evaluate the deformation of shear bands that develop in sedimentary soft rock in triaxial compression tests and plane strain compression tests (Tatsuoka and Kim 1995; Hayano et al. 1999b). **Fig. 2.4** shows a plane strain compression test system developed for this purpose. Several ball bearing systems are used to enhance the free development of shear bands. Test results from PSC tests using this system are reported later in this paper.

Load cell: For reliable evaluation of the stress-strain behaviour of sedimentary soft rock, not only at small strains but also spanning the whole pre-peak regime, it is necessary to use a load cell having not only a high resolution but also a large capacity, in addition to a relevant local axial strain gauge. To this end, an internal load cell as shown in Fig. 2.2 was developed and has been used at the authors' laboratory. More details of this load cell are described in Tatsuoka (1988).

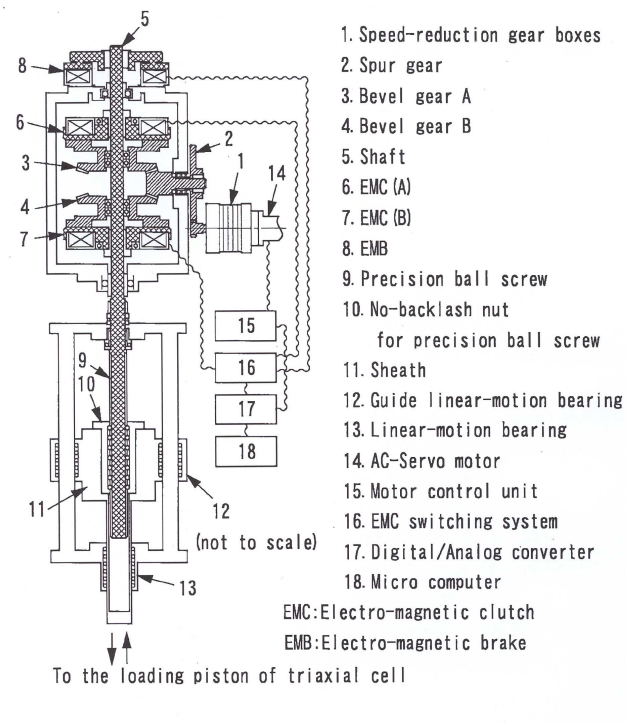

Figure 2.9. Precision gear-type axial loading apparatus (Tatsuoka et al. 1994: Santucci de Magistris et al. 1999).

Horizontal LDTs for lateral strains: It is very difficult to evaluate reliable lateral

strains of a cylindrical specimen of geomaterial by measuring changes in the specimen diameter when the effective lateral stress changes. This is due to effects of bedding error at the lateral surface of the specimen that could be very large with sedimentary soft rock. Errors in the lateral strains could also be very large when they are obtained from locally or externally measured axial strains combined with volumetric strains obtained from the amount of water sucked into or expelled from a saturated specimen. To evaluate lateral strains of specimens of granular material (i.e., sand and gravel) in triaxial compression tests when the effective lateral stress changes, Hoque et al. (1996) used eight LDTs placed horizontal on the flat lateral surfaces of a rectangular prismatic specimen (23 cm x 23 cm in cross-section x 57 cm in height).

This method becomes more difficult when applied to smaller specimens of sedimentary soft rock. Hayano et al. (1997) used lateral LDTs having a length of 60 mm to evaluate lateral strains of sedimentary soft rock specimens with dimensions of $80 \times 80 \times 160$ mm in triaxial compression tests (**Fig. 2.5**). This method is now the standard testing method in the Geotechnical Engineering Laboratory of the University of Tokyo to accurately and sensitively evaluate the lateral strains of specimens composed of sand, gravel and stiff cement-mixed soil and sedimentary soft rock in triaxial compression tests in which the effective lateral stress changes (Jiang et a. 1997; Tatsuoka et al. 1999b; Anh Dan et al. 2001; Kongsukprasert et al. 2001; Nawir et al. 2001).

Fig. 2.6 shows the true triaxial testing system using a rectangular prismatic specimen with dimensions of 60 mm (in the direction of cell pressure σ'_3) x 80 mm x 160 mm (Hayano et al. 1999a). Axial strains in the vertical direction (z direction) are locally measured by using a pair of vertical LDTs. In addition, normal strains in one lateral direction (denoted as the horizontal direction and y direction), which are free from bedding errors that would occur at the side surface of the specimen when the effective confining pressure changes, are measured locally by using two pairs of laterally placed LDTs (in total four). Normal strains in the other lateral direction (x direction) are measured by using a set of proximity transducers (in total six), which would include effects of bedding error when the effective lateral stress σ'_x changes. **Fig. 2.7a** shows the time histories of axial and horizontal stresses from a typical cyclic loading test of the vertical stress σ_z with two constant stresses σ_y and σ_x. **Fig. 2.7b** shows the time histories of σ_y and σ_z from a typical cyclic loading test of the horizontal stress σ_y with two constant stresses σ_z and σ_x. These cyclic loading tests were performed to evaluate the elastic deformation properties of sedimentary soft rock from Sagamihara. **Figs. 2.8a** and **b** show the corresponding time histories of normal strains in the three normal directions. Hayano et al. (1999a) reported the inherent and stress system-induced anisotropy in the quasi-elastic deformation characteristics in terms of Young's modulus and Poisson's ratio of sedimentary soft rock. This issue is discussed later in this report.

Versatile Loading Method

Loading method to evaluate material viscous properties of test specimen: Hayano et al. (1997; 2001) showed that loading rate effects arising from the material viscous properties on the stress-strain behaviour of sedimentary soft rock could be significant. Because of the very complicated nature of the viscous properties of sedimentary soft rock (and other types of geomaterials), it is necessary to evaluate the loading rate effects not only by performing monotonic loading tests at different constant strain rates and creep loading tests but also by applying more general loading histories of strain rate, including the following

(Tatsuoka et al. 2000, 2001a):

1) restart of ML at different constant strain rates following a creep loading stage;
2) gradual and sudden changes in the strain rate during otherwise ML at a constant strain rate;
3) strain relaxation tests;
4) application of unload/reload cycles with a small strain amplitude during otherwise ML loading and creep loading to evaluate the effects of stress state and loading history on the elastic deformation characteristics; and
5) application of these loading schemes 1-5) described above during otherwise global unloading and reloading.

With respect to item 4) above, it is necessary to evaluate an irreversible strain increment for a given stress increment at a given stress state to study the viscous properties of a given material. To this end, it is essential to evaluate accurately the elastic deformation characteristics at any given stress state and for any given loading history.

Fig. 2.3 shows results from a CD TC test on sedimentary soft rock (mudstone), including many of the loading schemes described above, performed to evaluate loading rate effects due to the material viscous properties. A precision gear-type axial loading apparatus was used in this test, which can control an axial strain much less than 0.001 % for a specimen height of 10 cm with practically no backlash during load reversal (**Fig. 2.9**; Tatsuoka et al.

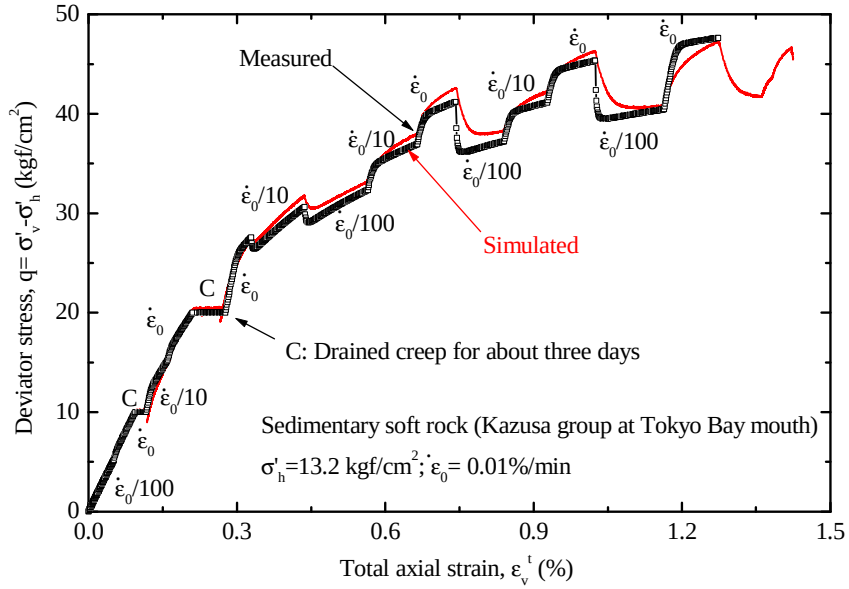

a)

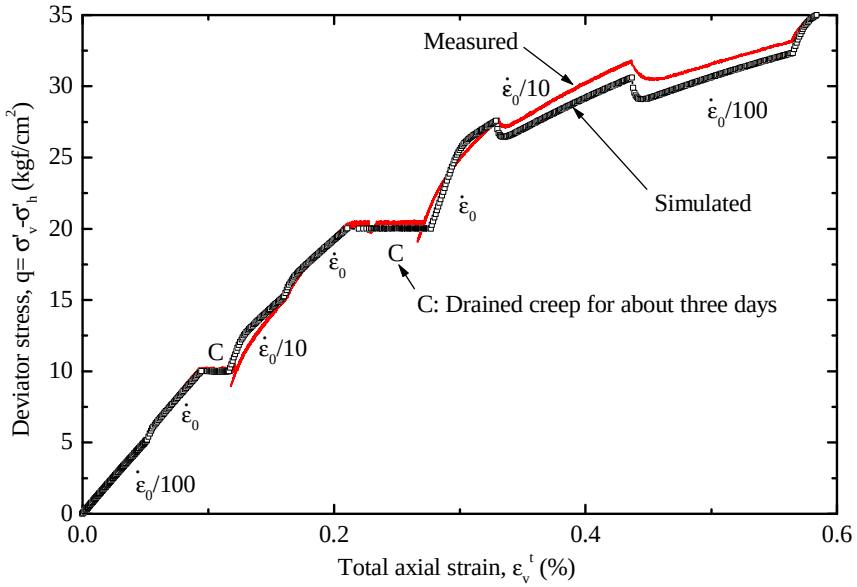

b)

Figure 2.10. Loading rate effects in a CD TC test on sedimentary soft rock of Kazusa group from Tokyo Bay mouth (Hayano et al. 2001).

1994; Santucci de Magistris et al. 1999). **Fig. 2.10** shows a similar result from a drained TC test on a core sample of sedimentary soft rock core sample of the Kazusa group from the mouth of the Tokyo Bay. The sample was isotropically reconsolidated to the field effective vertical stress. The results of the model simulation presented in this figure are explained later in this paper.

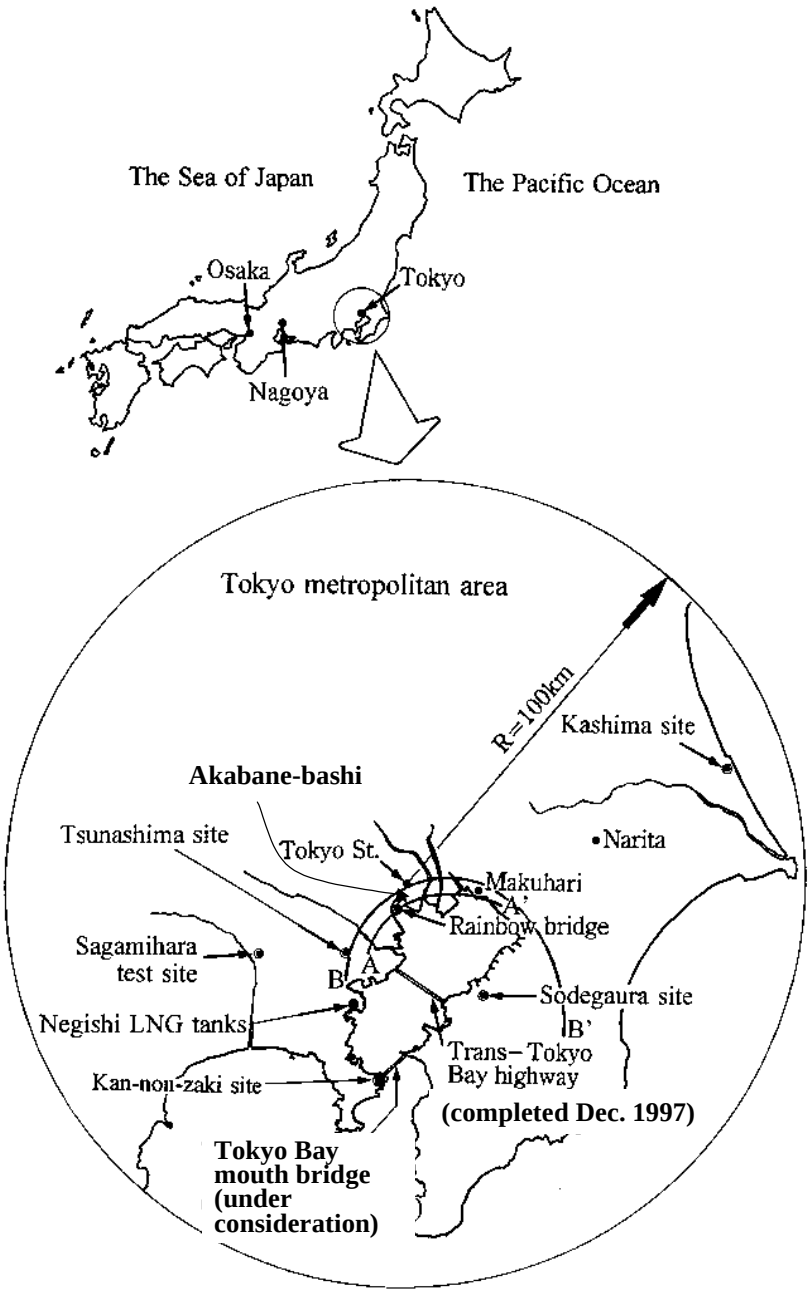

Figure.3.1. Locations of the sites where the stress-strain behaviour of sedimentary soft rocks were investigated (modified after Tatsuoka et al. 1995a).

SITE DESCRIPTIONS AND GENERAL TRENDS OF STRENGTH AND STIFFNESS

General

The following two projects in the Tokyo metropolitan area (**Fig. 3.1**) were selected to

discuss on the primary characteristic features of the stress-strain-time properties of sedimentary soft rock:

1) a full-scale field experiment at Sagamihara; and
2) geotechnical investigations for a suspension bridge at the mouth of the Tokyo Bay,

The discussions are based on results from laboratory stress-strain tests and field loading tests, full-scale field behaviours and their simulations. Engineering issues and related stress-strain properties of sedimentary soft rock at other sites, reported by Tatsuoka and Kohata (1995) and Tatsuoka et al (1995a), are also referred to where necessary.

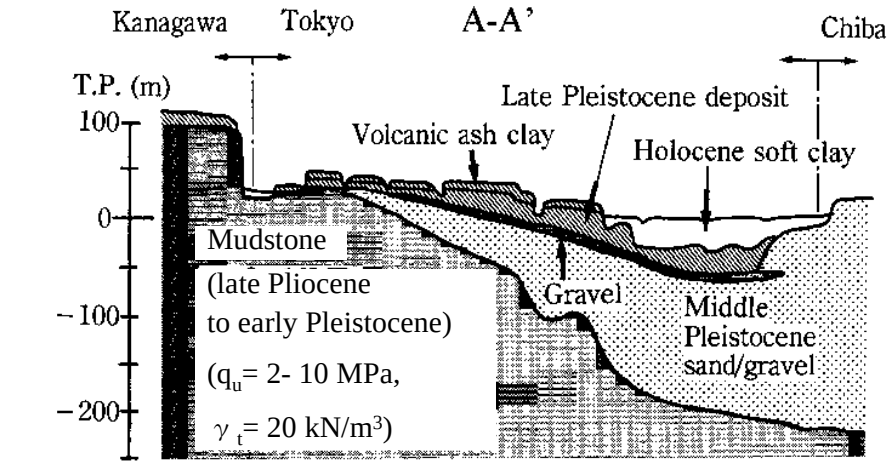

a)

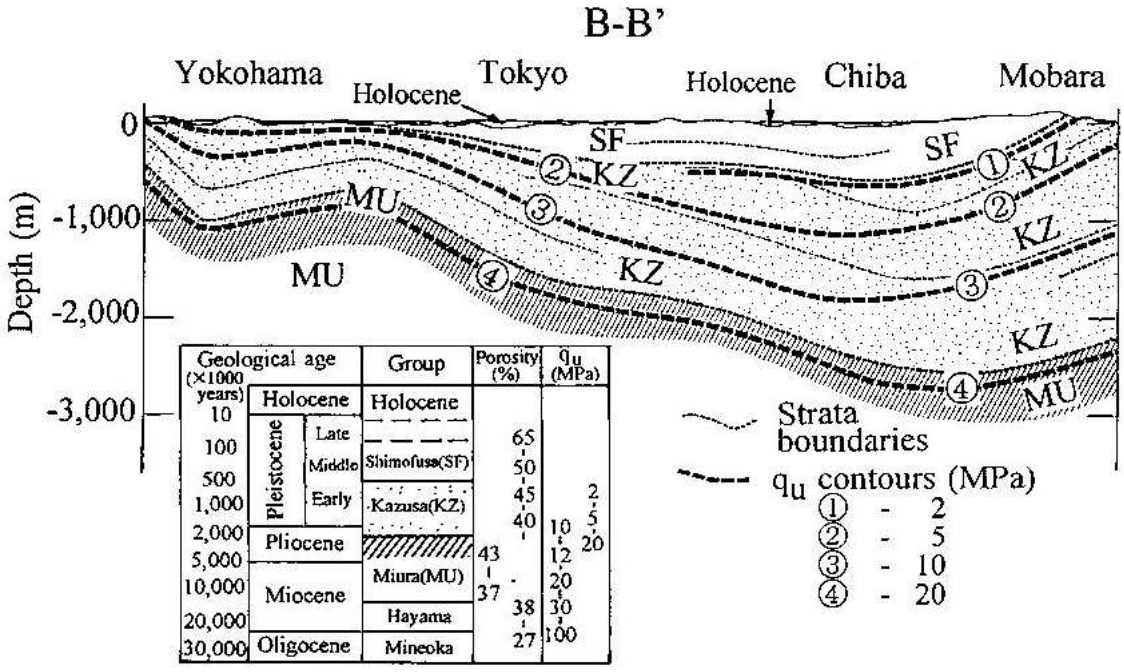

b)

Fig. 3.2 Geological cross-sections along lines A-A' (Tatsuoka et al., 1995a) and B-B' (Hoshino 1993) in Fig. 3.1.

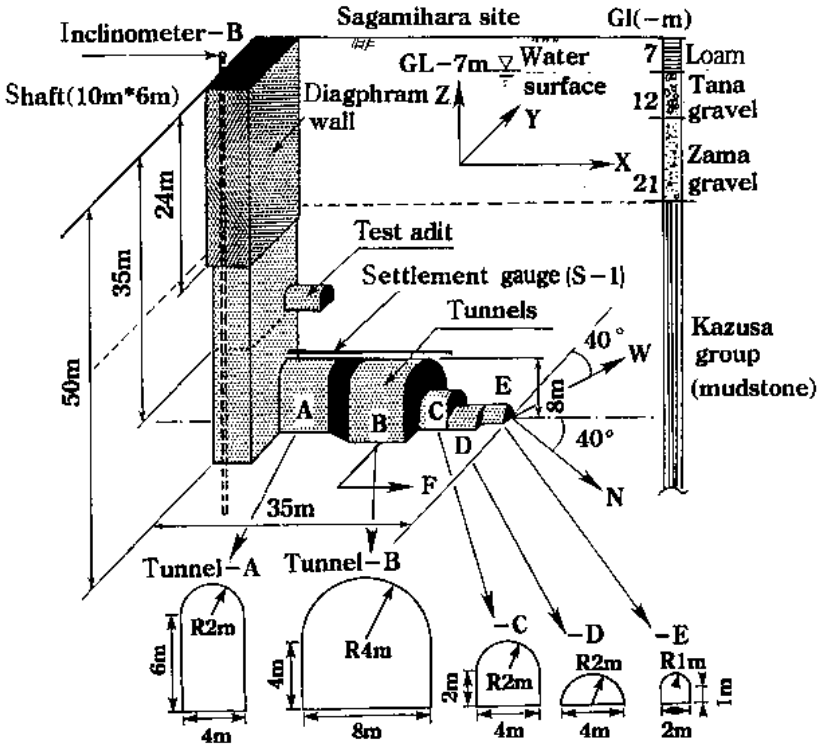

Figure 3.3a. General configurations of full-scale field experimental excavation (first stage of experiment) and ground conditions at Sagamihara test site (Ochi et al. 1993, 1994; Tatsuoka and Kohata 1995; Tatsuoka et al. 1997a).

In the Tokyo metropolitan area (Fig. 3.1), as seen from **Fig. 3.2**, Holocene and Pleistocene uncemented soil deposits are underlain by a thick sedimentary soft rock deposit of the Kazusa group. The Kazusa group is about one to two million years old of the late Pliocene to the early Pleistocene epochs. The Kazusa group deposit is underlain by an older sedimentary soft rock deposit of the Miura group of the late Miocene epoch to the Pliocene epoch of the Tertiary period. The top of the Kazusa group deposit becomes deeper towards the center of a depressing basin in the north of the Tokyo Bay area. The original soil types of these sedimentary soft rock deposits are clay (mud), silt and sand, which change from one site to another and from one depth to another. Mudstone is generally well cemented, while fine sandstone is less uncemented. In the deposits of the Kazusa group, sometimes nearly uncemented coarse sand layers can be found between well-cemented mudstone layers (e.g., Tatsuoka et al. 1997a). A reason (or reasons) for high cementation of mudstone compared with its relatively young geological age (about one to two million years with the Kazusa group) is (are) not well understood. Except for those exposed in the air, the soft rock deposits of the Kazusa and Miura groups have not been noticeably weathered, while some zones have been slightly disturbed by tectonic forces.

In the past, these sedimentary soft rock deposits were considered as a very good foundation having sufficiently high strength and stiffness to support ordinary non-massive civil engineering structures including RC buildings, bridge foundations and so on. In these cases, their detailed mechanical properties were not critically evaluated. For the last two decades, however, a number of large-scale important structures were constructed on or in and large-scale deep ground excavations were performed in the sedimentary soft rock deposits of the Kazusa group. Therefore, many detailed geotechnical investigations for research and design were performed.

Sagamihara Test Site

General: As shown in **Fig. 3.3a**, a 50 m-deep experimental shaft and a series of short tunnels at the bottom of the shaft were excavated from 1989 until 1992 in a sedimentary soft mudstone deposit of the Kazusa group without using stiff supports as has been used in other construction projects under similar conditions (Ochi et al. 1993, 1994; Tatsuoka et al. 1995b, 1997a). The excavation for the extension of the shaft to deeper levels and the construction of an underground dome (**Fig. 3.3b**) started in January 1995 and ended in March 1996 (Matsumoto et al. 1999, 2000). The observation of the ground behaviour continued for the following several years.

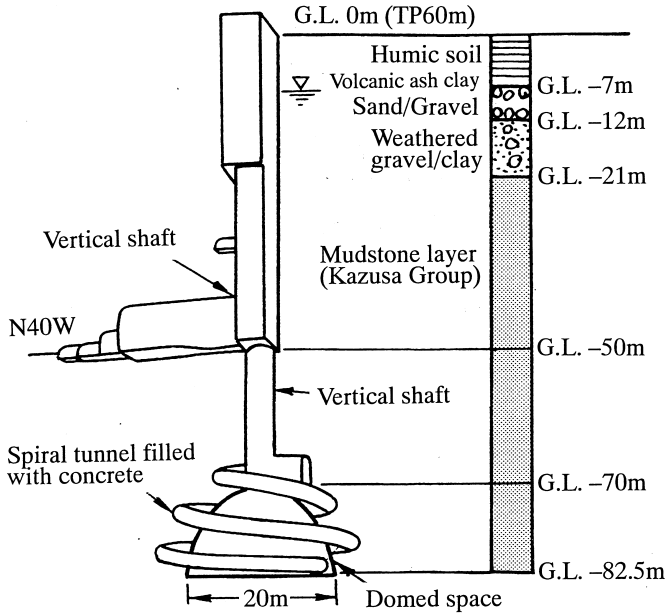

Figure 3.3b. Final experiment configurations at Sagamihara test site (Matsumoto et al. 1999, 2000).

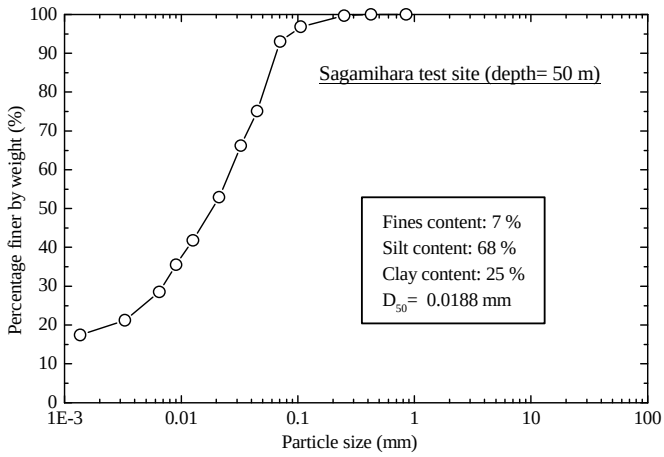

Figure 3.4. Grain size distribution of sedimentary soft rock (mudstone), Sagamihara test site (Kim et al. 1994; Hayano 2001).

The deformation and strength characteristics of the sedimentary mudstone of the Kazusa group at the Sagamihara test site were investigated in great detail (Kim et al. 1994, Tatsuoka and Kohata 1995: Tatsuoka et al. 1995b, 1997a). **Fig. 3.4** shows the grading curve

Table 3.1. Some physical quantities of sedimentary soft rock (Sagamihara test site, for depths down to 50 m; Kim et al. 1994).

Specific gravity G_s	2.73	Natural water content, w_n	20.6~29.6 %
Total density ρ_t	1.88~2.06 g/cm^3	Void ratio e	0.64~0.86

Figure 3.5. A RCTS sample with a shear plane after a TC test, Sagamihara test site.

obtained from samples retrieved from a depth of around 50 m, which is typical of the mudstone at the site. This grading curve and other similar ones presented in this paper were obtained by first breaking each oven-dried sample with a hand-held hammer followed by crushing and grinding the broken pieces in a mould until all the material passed through a sieve with an opening of 0.42 mm. **Table 3.1** shows the material properties of the samples retrieved from depths down to about 50 m that were used for triaxial compression tests performed by Kim et al. (1994). **Fig. 3.5** shows one of the core specimens used in the TC tests, which exhibited a clear shear plane along which a fossil of leaf happened to have been embedded.

Compressive strength: **Fig. 3.6** shows the distribution with depth of the compressive strength of core samples; i.e., q_u from unconfined compression tests (U tests) and q_{max} from CU and CD triaxial compression (TC) tests. In the TC tests, the specimens were isotropically consolidated to the respective in-situ effective overburden pressure $(\sigma'_v)_0$. The axial strain rate (in terms of externally measured one) was 0.01 %/min. The core samples were retrieved by the following three methods:

1) Block sampling (BS): Large blocks of mudstone were carved out from the excavated ground surface inside the tunnels (Fig. 3.3a), from which core samples for laboratory stress-strain tests were cored using a rigidly fixed diamond core barrel in the laboratory.

2) Direct coring (DC): Samples for laboratory stress-strain tests were cored using a rigidly fixed diamond core barrel inside the shaft and tunnels.

3) Rotary core tube sampling (RCTS): Core samples were retrieved by using a double-tube rotary core sampler from the bottom of respective borehole drilled from the ground surface. All the core samples used for the U tests (except the one presented in Figs. 3.7 and 3.8) were obtained by this method.

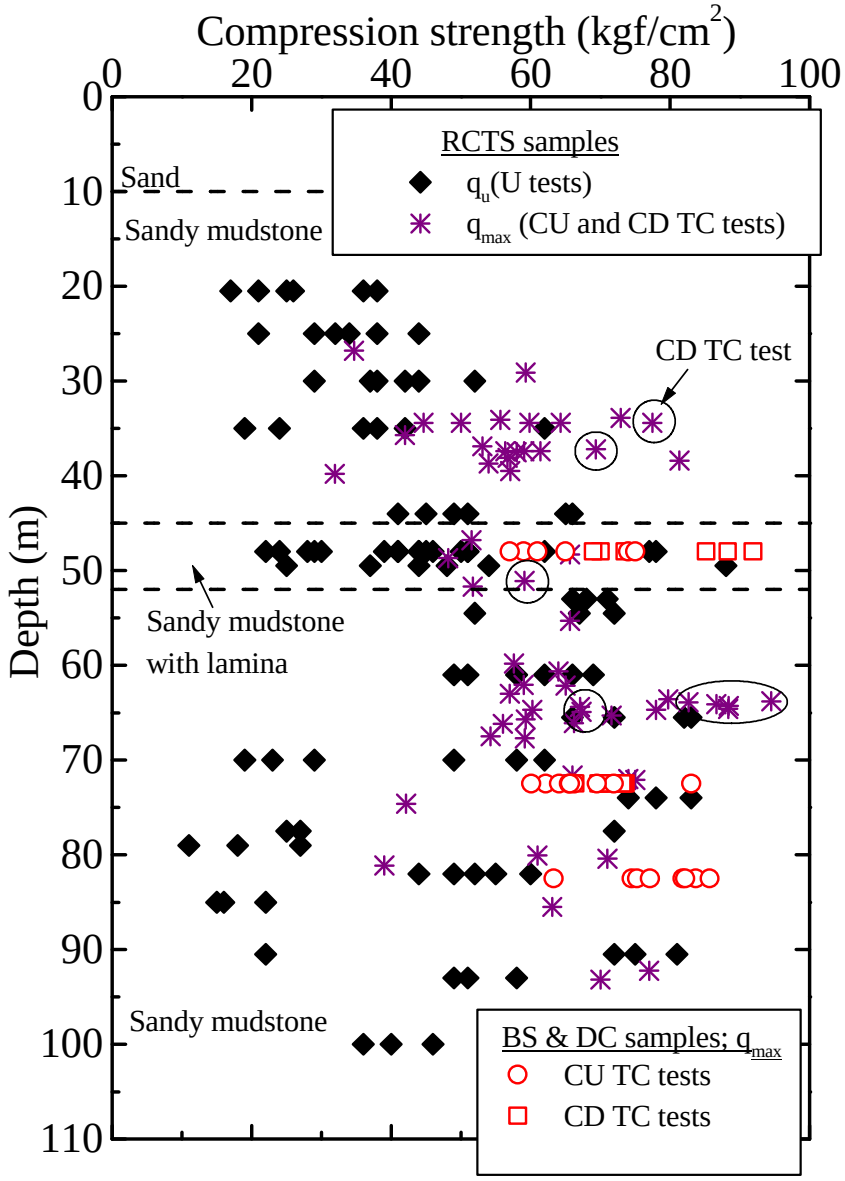

Figure 3.6. Distribution of compressive strengths from unconfined and triaxial compression tests, Sagamihara test site (Wang 1996; Hayano et al. 2000).

It may be observed from Fig. 3.6 that the unconfined compression strength exhibits a much larger scatter and a much smaller average value than the triaxial compression strength. It could be inferred from this result that; a) the deposit is somehow heterogeneous; and b) the compressive strength of this mudstone largely depends on the confining pressure. However, this inference is biased by effects of sample disturbance, which could be particularly large on

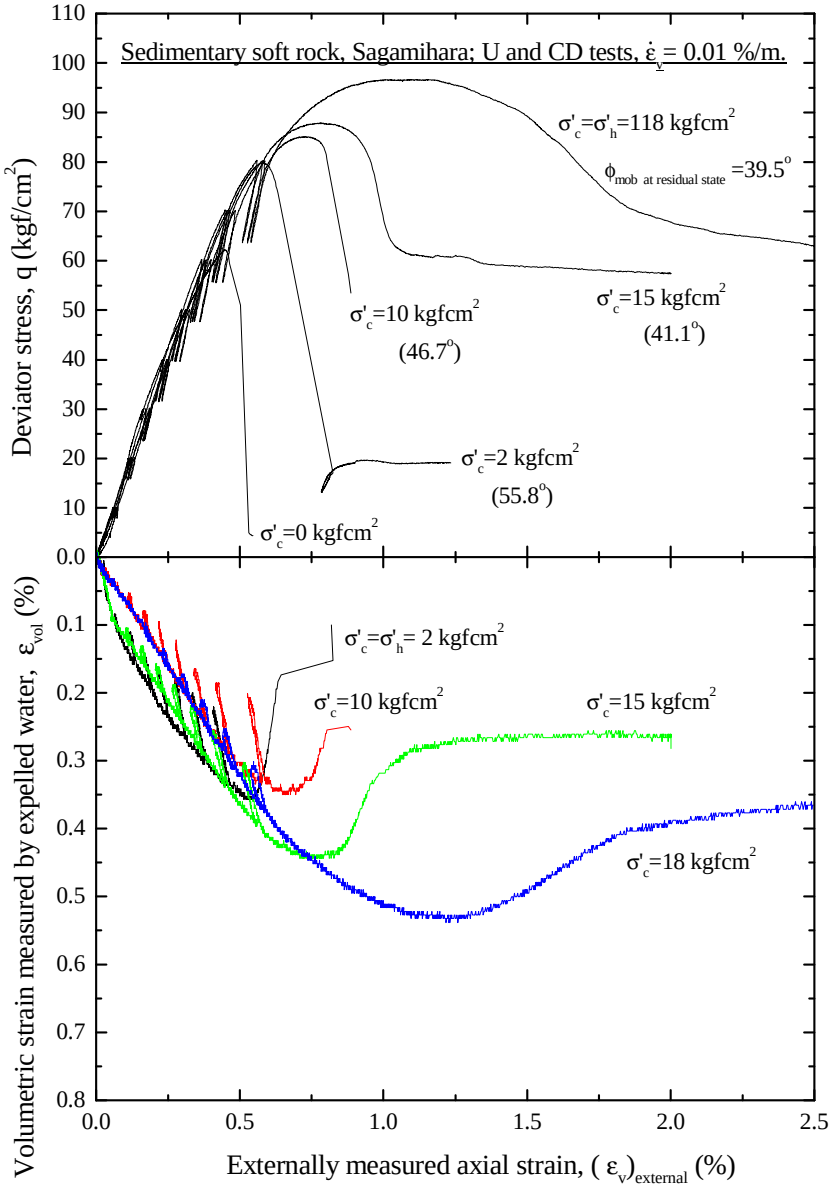

Figure 3.7 Results from U test and a series of CD TC tests at different consolidation pressures using core samples from single block retrieved in the tunnel at a depth of 50 m, Sagamihara site (Wang 1996; Hayano et al. 1999b).

the unconfined compression strength from U tests using RCTS samples, as discussed below.

Fig. 3.7 shows the stress-strain behaviour from a U test and a series of CD TC tests at different consolidation pressures using core samples obtained from a single large block retrieved by BS at a depth of 50 m in the tunnel. The volumetric strain was not measured in the U test. **Fig. 3.8a** summarises the peak strength from these compression tests. The following trends of behaviour may be seen from these figures:

1) For a set of core samples from a single large block, the peak strength increases moderately with an increase in the consolidation pressure. The difference between the q_u strengths from U tests (using RCTS samples) and

the q_{max} values from TC tests presented in Fig. 3.6 is much larger than the one that could be deduced from the results presented in Figs. 3.7 and 3.8a. This fact indicates that the q_u strengths of RCTS core samples are generally smaller than those of core samples obtained by BS. This is due to the effects of sample disturbance in RCT sampling (Tatsuoka et al. 1995a).

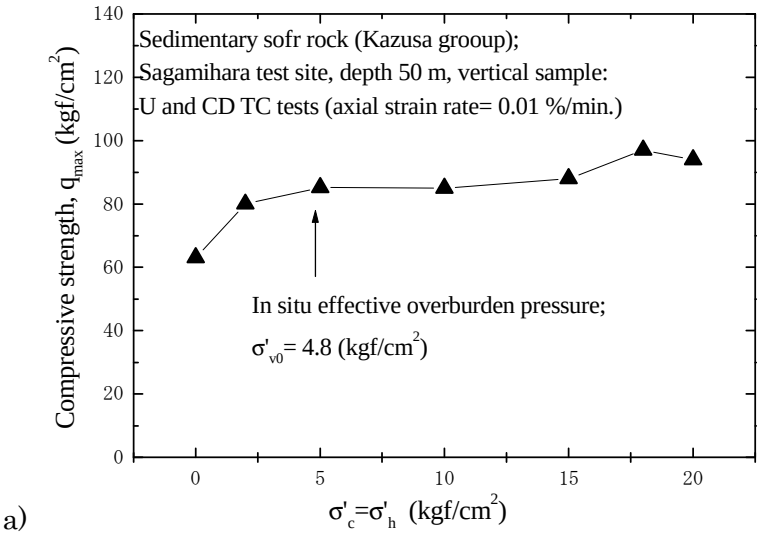

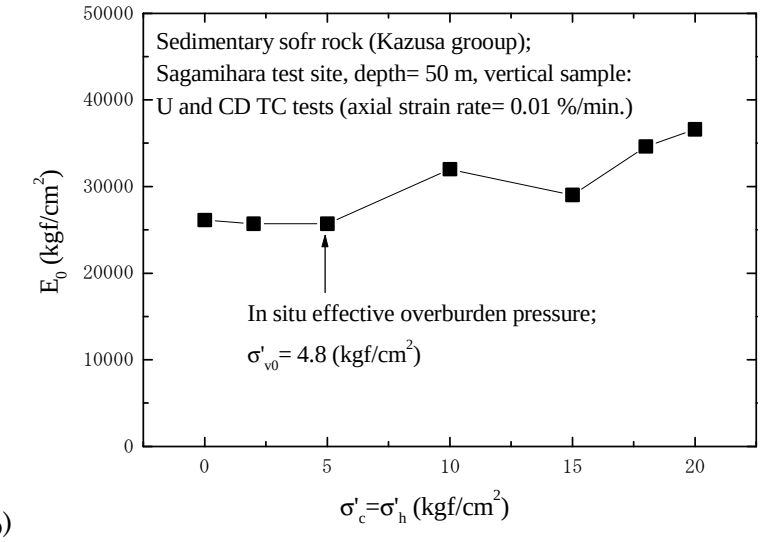

Figure 3.8. Dependency on the isotopic pressure of; a) peak strengths; and b) initial Young's modulus (based on locally measured strains less than about 0.001 %) from the compression tests presented in Fig. 3.7 (Wang 1996).

2) Generally the q_{max} strength from a CD TC test is larger than the one from a CU TC test under otherwise the same testing conditions.

3) The CU and CDTC strengths, q_{max}, of RCTS core samples are also generally smaller than those of BS and DC core samples. This is also due to the effects of sample disturbance in RCT sampling. However, this difference in the compressive strength between RCTS samples and BS & DC samples is generally much smaller with the TC tests than the one with the U tests. It seems that reconsolidation to the respective in-situ pressure reduced the

effects of sample disturbance on the TC strength of RCTS samples.

4) When based on the compressive strength, q_{max}, from CU TC tests, the compressive strength under field stress conditions gradually increases with depth. This trend of behaviour is not evident with the q_u values at depths larger than about 50 m. This fact would suggest that the effects of sample disturbance with RCTS become larger with increasing depth.

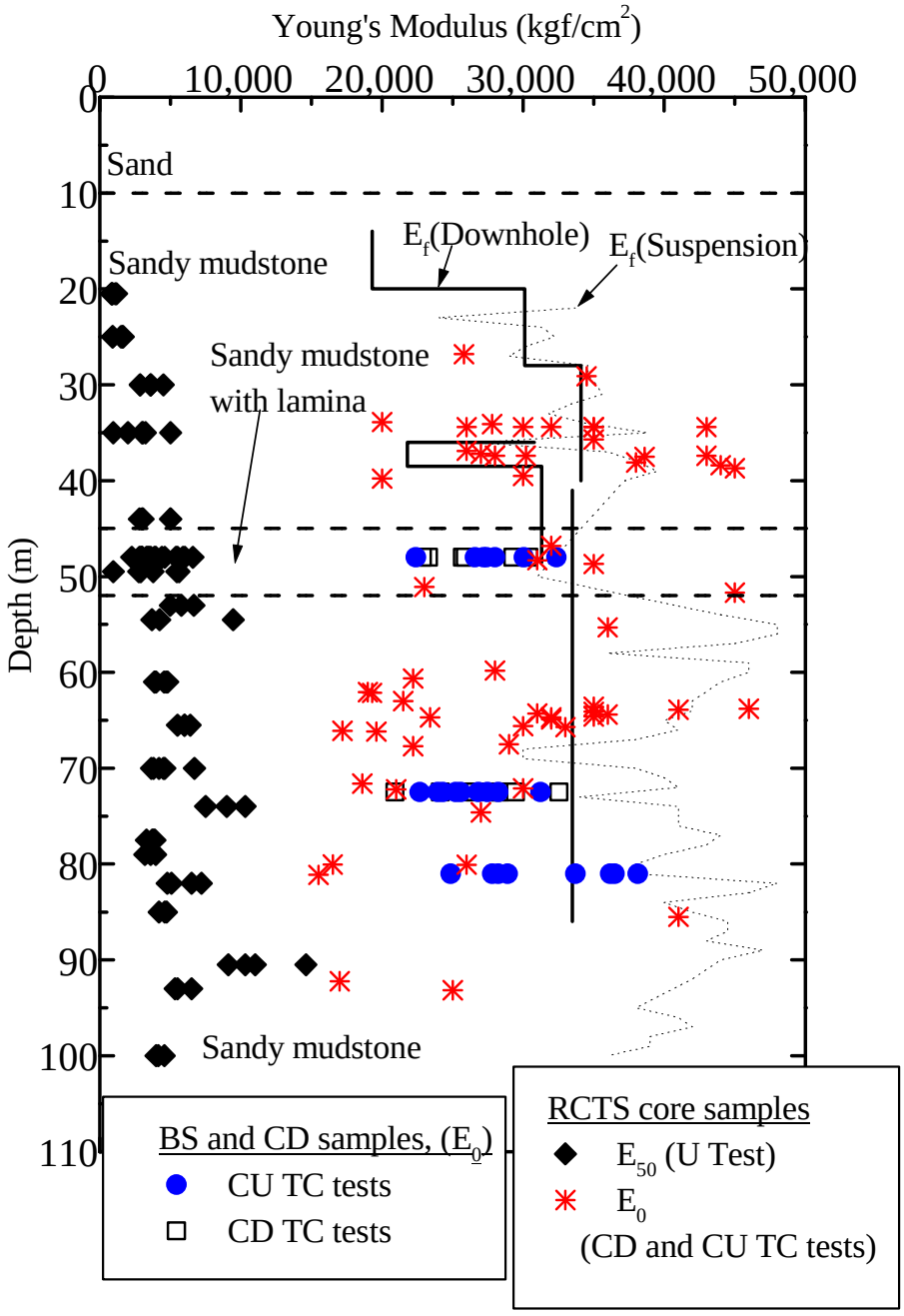

Figure 3.9. Distribution of Young's modulus from unconfined compression tests and triaxial compression tests and field seismic surveys (Wang 1996; Hayano et al. 2000).

These results indicate that the combined effects of confining pressure and sample disturbance on the unconfined compressive strength, q_u, of core samples retrieved by RCTS could be significant. Thus, the compressive strength of sedimentary soft rock under

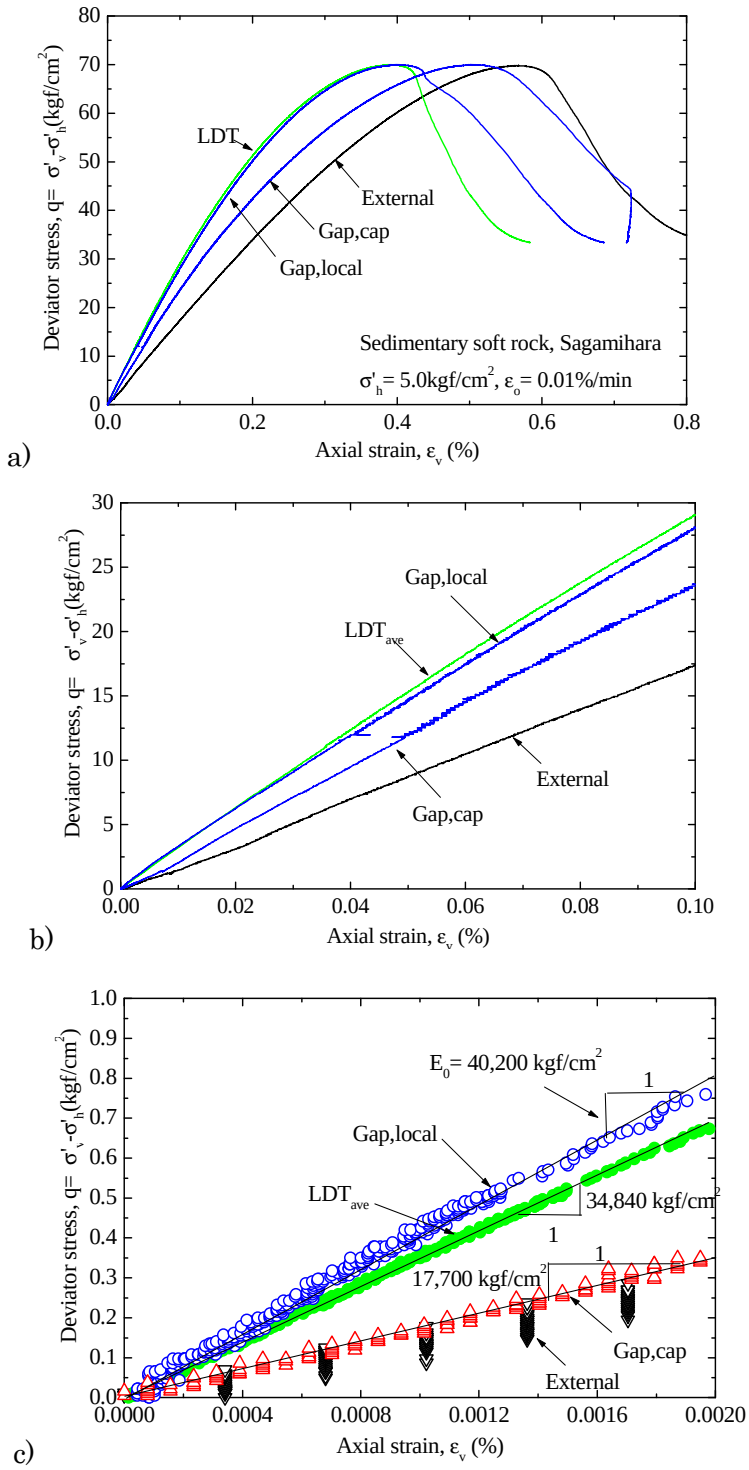

Figure 3.10. Deviator stress-axial strain relations from a CD TC test, sedimentary soft rock, BS sample, Sagamihara test site, depth= 50 m (see Fig. 2.3c for four methods of axial strain measurement; Hayano 2001).

confined conditions in the field could be seriously underestimated when evaluated based on these q_u values. Similar examples were obtained at Kashima and Sodegawara sites (shown in Fig. 3.1) by Kawasaki et al. (1993) (Fig. 2.29 of Tatsuoka and Kohata 1995) and at the site of Akashi Strait Bridge (see Fig. 2.26 of Tatsuoka and Kohata 1995). It is likely that, during the operation of rotary core tube sampling, a core sample retrieved in the inner sampling tube

could be largely damaged when the rocking motion of the sampler becomes too large and/or excessive compressive or tensile axial force is applied to the sampling tube.

Small strain stiffness: **Fig. 3.9** shows the distribution with depth of the following different Young's modulus values:

1) Undrained elastic Young's modulus E_f from down-hole seismic surveys performed in bore holes. The values of E_f were obtained as: $E_f = 2(1+\nu_u)\cdot G_f$, where ν_u is the undrained elastic Poisson's ratio, which is assumed to be equal to 0.43 in this case; and G_f is the elastic shear modulus equal to $\rho\cdot[(V_s)_{VH}]^2$, where ρ is the total density and $(V_s)_{VH}$ is the velocity of the shear wave propagating in the vertical direction with horizontal particle movements. Vertical and horizontal line segments in Fig. 3.9 indicate the E_f values obtained by this method.
2) Undrained elastic Young's modulus E_f from the suspension method (local up-hole seismic survey) performed in the same bore holes in which the down hole seismic surveys were performed. A dotted line indicates the E_f values obtained by this method.
3) Initial Young's modulus E_0 defined at axial strains less than about 0.001 % from CD and CU TC tests measuring locally axial strains with a pair of LDTs. **Fig. 3.10** shows results from a typical CC TC test using a BS sample. The results of BS and DC core samples are distinguished between CU and CD TC tests in this figure, while those of 4) E50 values from unconfined compression tests (measuring axial strains externally) using RCTS core samples are not.

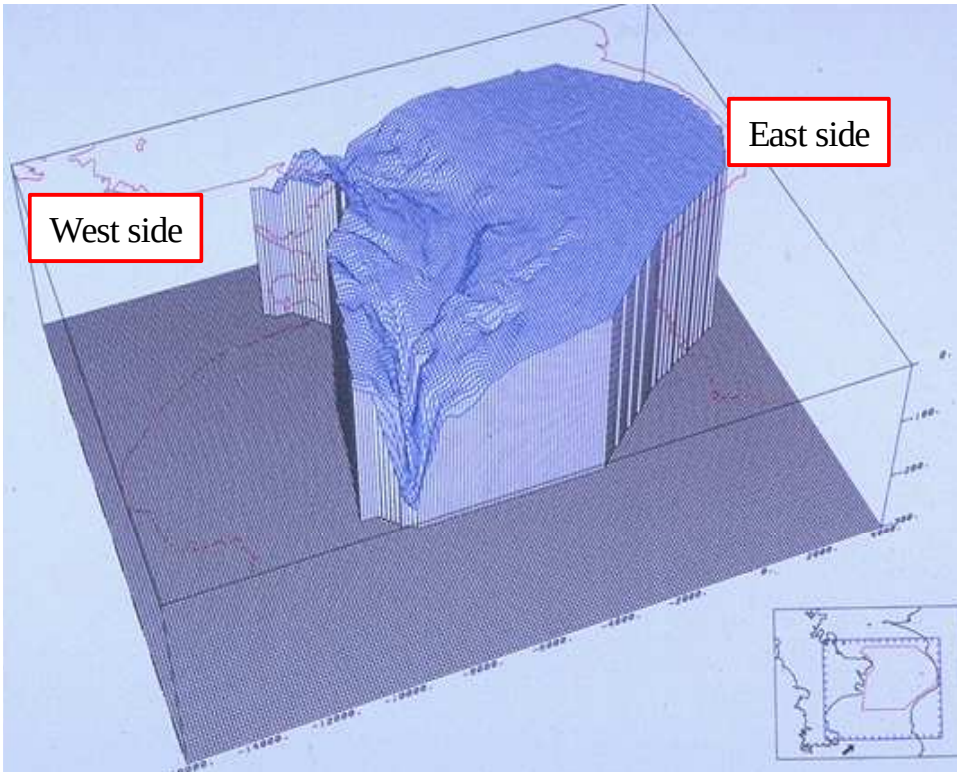

Figure 3.11. Seabed at the mouth of Tokyo Bay (by the courtesy of Ministry of Land, Infrastructure and Transport).

4) E50 values from unconfined compression tests (measuring axial strains externally) using RCTS core samples.

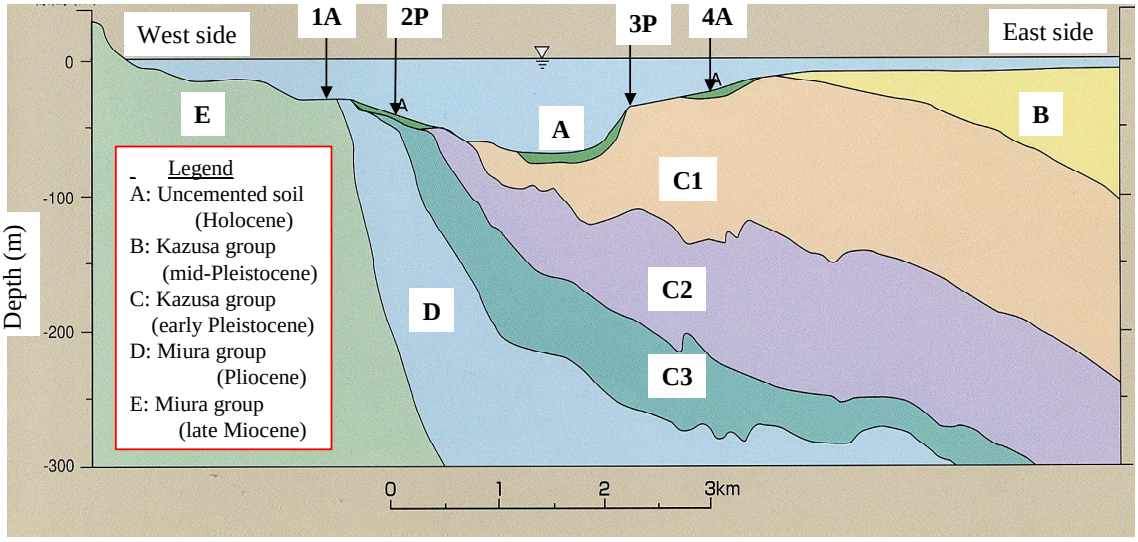

Figure 3.12. Geological profile and planned locations of the foundations for a bridge, the mouth of Tokyo Bay (by the courtesy of Ministry of Land, Infrastructure and Transport).

The following trends of behaviour may be seen from Fig. 3.9:

1) The E_{50} values from the unconfined compression tests are utterly not representative of thesmall strain stiffness of sedimentary soft rock under field stress conditions. This significant discrepancy of the E_{50} values from the E_0 and E_f values are due to the following factors:

i) *Confining pressure*: **Fig. 3.8b** shows the effects of consolidation pressure on the E_0 values from U and CDTC tests measuring locally axial strains with a pair of LDTs on core samples obtained for one large block retrieved in the tunnel. It may be seen that the effect of this factor is small with these least disturbed core samples. However, it is not the case with noticeable disturbed RCTS samples.

ii) *Sample disturbance:* The effect of this factor on the stiffness evaluated by unconfined compression tests using RCTS samples could be large. It may be seen from Fig. 3.9, however, that, with the sedimentary soft rock at the Sagamihara test site, the effect of this factor is not significant on the stiffness evaluated by TC tests on samples reconsolidated to the field pressure level.

iii) *Bedding error:* The effect of this factor becomes larger at lower confining pressure (Kim et al. 1994). Therefore, the effect is larger in U tests than in TC tests under otherwise the same conditions.

iv) *Strain level:* The locally measured strain level at which E_{50} is defined at a strain that is much larger than the elastic limit strain, which is about 0.2 % in the data presented in Fig. 3.7. The axial stress becomes much larger than the initial value by that strain level. As the pressure level-dependency becomes larger, the E_{50} value could be still similar to the initial value E_0 under otherwise the same conditions if the effects of strain

level and pressure level are balanced with each other. With the sedimentary soft rock of mudstone type at the Sagamihara test site, the pressure level-dependency of E_0 is not significant, as seen from Fig. 3.8b. It appears, therefore, that the effect of this factor the E_{50} value is not masked by the effect of pressure level.

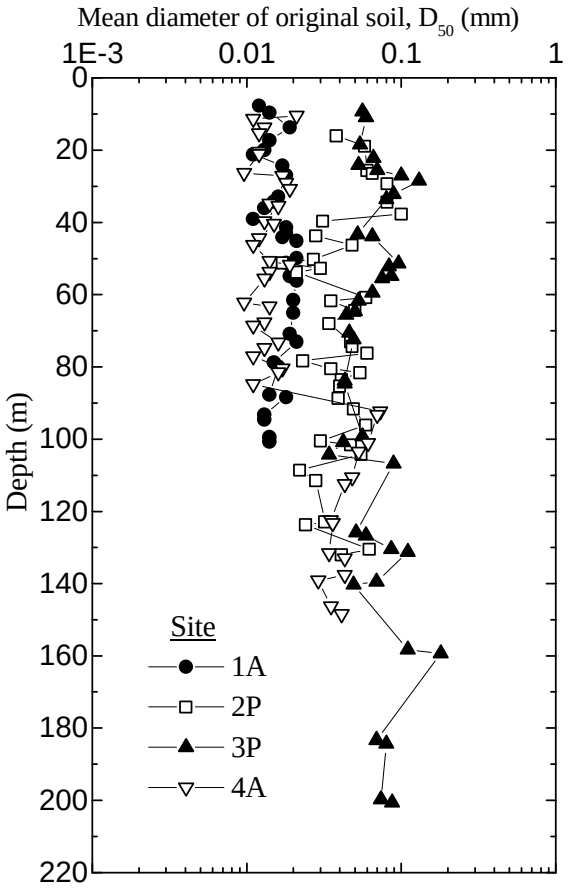

Figure 3.13. Comparison of mean diameter of mother soils among sites 1A, 2P, 3P and 4A, Tokyo Bay mouth (Kodaka et al. 2000; Hayano 2001).

With the sedimentary soft rock at the Sagamihara test site, it seems that combined effects of these factors could be significant. The unconfined compression test has been the most popular laboratory stress-strain testing method in Japan to evaluate the strength and deformation characteristics of sedimentary soft rock. One of the main reasons for the above would be that the effects of these factors i) – iv) become evident only by referring to such data as presented in this paper, which is usually very difficult. Another reason would be a relatively low cost for testing. It has been shown by Tatsuoka and Kohata (1995) and Tatsuoka et al. (1995b, 1999a), however, that the use of such E_{50} values from U tests measuring axial strain externally on RCTS samples could result into a significant over-estimate of full-scale field ground deformation and structural displacements related to sedimentary soft rock.

2) The scatter in the E_0 values obtained from TC tests is generally larger with RCTS samples than with BS and DC samples. Moreover, at depths greater than about 70 m, the average of E_0 values of RCTS samples is noticeably

Table 3.2(a). Physical properties of sedimentary soft rock (Tokyo Bay mouth, site 1A).

Depth (m)	Soft rock type	Water content (%)	Total density ρ_t(g/cm^3)	Content (%)	
				Coarser than 0.074 mm	Finer than 0.074 mm
～19.0	Sandy mudstone	35	1.84	15	85
19.0～35.0	Sandstone, mudstone & sandy mudstone	36	1.85	20	80
35.0～49.0	Sandy mudstone	36	1.83	7	93
49.0～76.0	Sandy mudstone	34	1.87	13	87
76.0～85.0	Sandy mudstone	35	1.85	7	93
85.0～	Sandy mudstone	40	1.78	7	93

Table 3.2(b). Physical properties of sedimentary soft rock (Tokyo Bay mouth, site 2A)

Depth (m)	Soft rock type	Water content (%)	Total density ρ_t(g/cm^3)	Content (%)	
				Coarser than 0.074 mm	Finer than 0.074 mm
11.5～22.3	Muddy fine-sandstone	23	2.01	36	64
22.3～41.2	Tuff-sandy mudstone	26	1.99	49	51
41.2～56.4	Sandy mud	29	1.96	27	73
56.4～72.4	Tuff-sandy mudstone	30	1.93	38	62
72.4～	Tuff-sandy mudstone	26	1.99	36	64

smaller than the value of BS and DC samples. It is likely that these two observed trends of behaviour are due to larger effects of sample disturbance with RCTS samples. This issue is discussed in more details later in this paper.

3) The E_f values from the two methods of field seismic survey are essentially the same at depths shallower than about 50 m. On the other hand, at depths greater than about 50 m, the E_f values from the down hole method are generally smaller than those from the suspension method. The underlying reason(s) is (are) not known to the present authors.

4) The E_0 values from CU and CD TC tests performed under otherwise similar conditions are not significantly different from each other. The main reason appears to be that the strain rate is not slow enough to ensure fully drained conditions at small strains immediately after the start of CD TC loading. This issue is discussed in detail later in this paper.

5) The E_0 values from CU and CD TC tests using BS and DC samples are generally in good agreement with the corresponding E_f value, particularly with the value from the down-hole method. However, the E_0 value becomes relatively smaller than the corresponding E_f value at greater depths. This result suggests that BS and DC samples retrieved from large depths are not totally free from the effects of sample disturbance caused by a relatively large pressure relief. Other possible reasons for this discrepancy are;

a) inherent anisotropy in the elastic deformation properties at this site;

Table 3.2(c). Physical properties of sedimentary soft rock (Tokyo Bay mouth, site 3P).

Depth (m)	Soft rock type	Water content (%)	Total density ρ_t(g/cm^3)	Content (%)	
				Coarser than 0.074 mm	Finer than 0.074 mm
～12.5	Muddy fine-sandstone	25	2.00	40	60
12.5～42.0	Muddy sand & Sandy mudstone	26	1.96	51	49
42.0～65.3	Muddy fine-sandstone	25	1.99	50	50
65.3～78.0	Muddy fine-sandstone	25	2.01	27	73
78.0～102.0	Sandy mudstone	25	2.00	32	68
102.0～110.0	Muddy sandstone	31	1.89	40	60
110.0～125.0	Gravel-containing coarse sandstone	27	2.00	38	62
125.0～157.0	Muddy fine-sandstone	24	2.03	49	51
157.0～178.0	Tuff-coarse-sandstone	25	1.99	63	37
178.0～211.1	Muddy fine-sandstone	27	1.97	54	46
211.1～220.0	Muddy fine-sandstone & Tuff-coarse-sandstone	27	1.95	59	41
220.0～	Tuff-gravel-containing coarse-sandstone	23	1.92	79	21

Table 3.2(d). Physical properties of sedimentary soft rock (Tokyo Bay mouth, site 4A).

Depth (m)	Soft rock type	Water content (%)	Total density ρ_t(g/cm^3)	Content (%)	
				Coarser than 0.074 mm	Finer than 0.074 mm
5.9～87.5	Sandy mudstone	33	1.88	11	89
87.5～109.0	Muddy fine-sandstone	28	1.97	46	54
109.0～126.6	Muddy fine-sandstone	25	2.00	26	74
126.6～142.8	Muddy fine-sandstone	25	1.98	25	75
142.8～	Muddy fine-sandstone & sandy mudstone	24	2.02	25	75

b) effects of different strain rate between the TC tests and the seismic surveys.

It is shown later in this paper that the effects of these factors would not be significant with the sedimentary soft rock at this site. A direct comparison between the E_0 and E_f values for a number of sites, including the Sagamihara test site, is shown later in this paper.

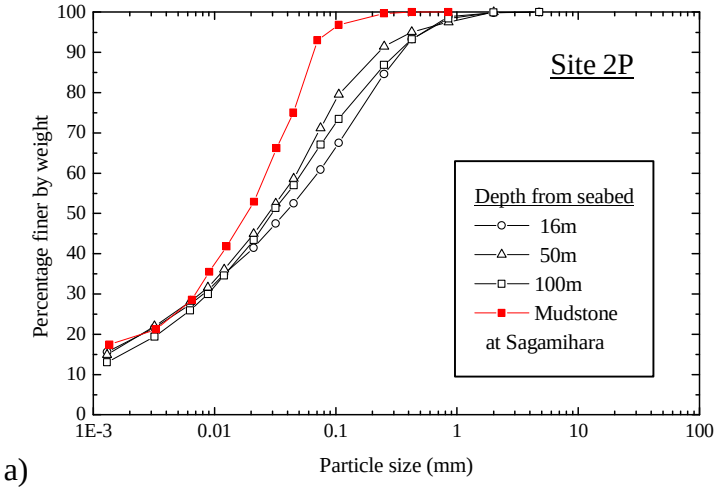

a)

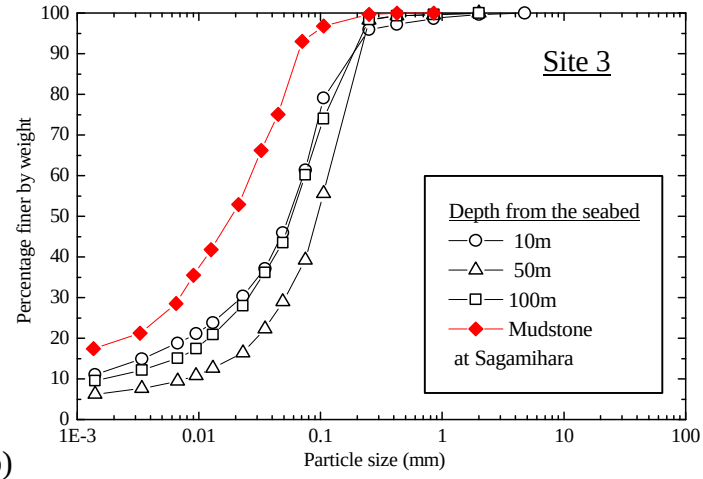

b)

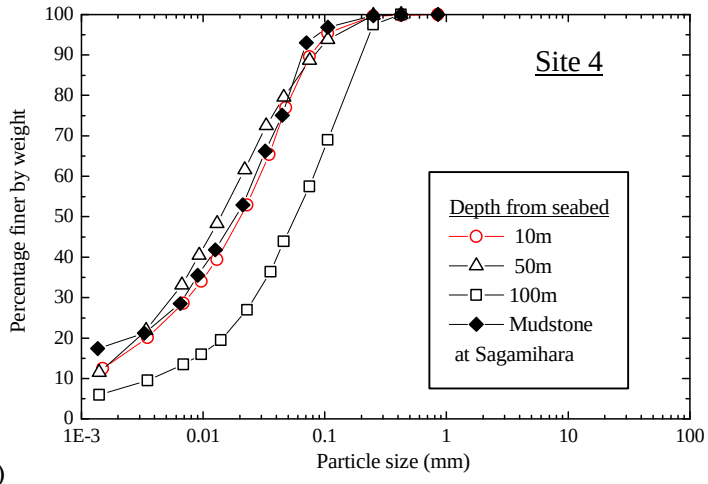

c)

Figure 3.14. Grain size distributions of mother soil at Tokyo Bay mouth (sites, 2P, 3P and 4A), compared with the one at Sagamihara test site (Kodaka et al. 2000; Hayano 2001).

Tokyo Bay Mouth Bridge Project

General: A long suspension bridge is being planned to be constructed at the mouth of the Tokyo Bay to complete a loop of highway encircling the Tokyo Bay (Fig. 3.1). **Fig. 3.11** shows the seabed at the mouth of the Tokyo Bay, while **Fig. 3.12** shows the geological

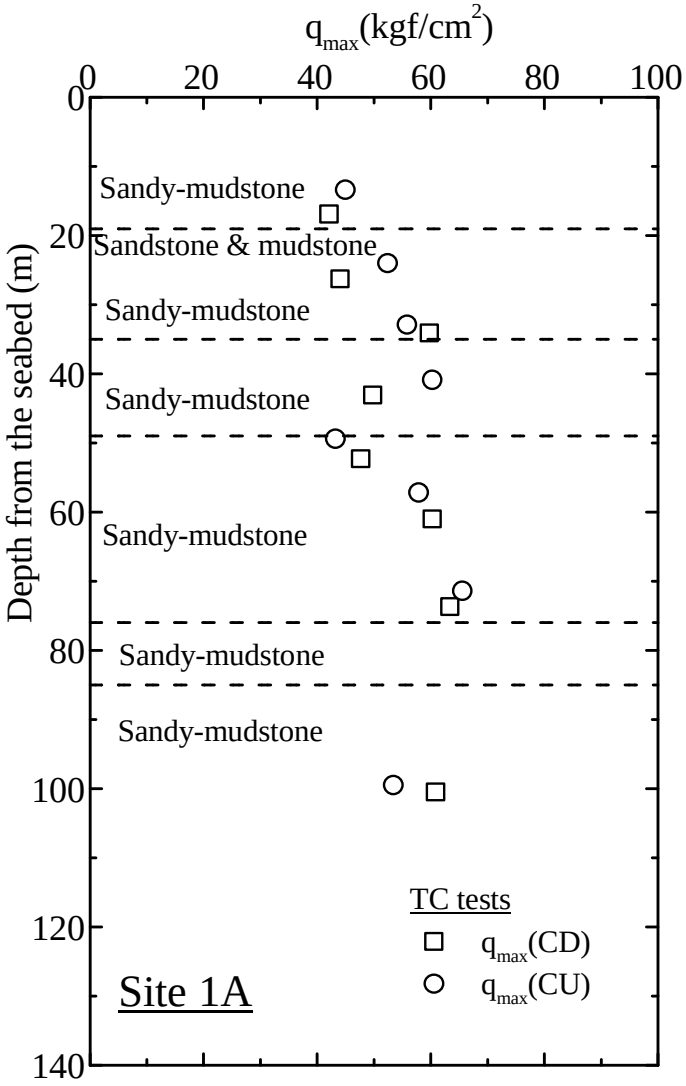

Figure 3.15a. Distribution with depth of compressive strength from TC tests, sedimentary soft rock, Tokyo Bay mouth, site 1A (U tests were not performed at this site) (Kodaka et al. 2000; Hayano 2001).

profile along the planned route of the bridge indicating the locations of the two anchorages, 1A and 4A, and the two piers, 2P and 3P. The side and central spans of the bridge are planned to be 720 m-long and 2,250 m-long. This large central span, which is larger than the 2,000 m of the Akashi Strait Bridge, is necessary to span over a relatively wide depression at the center of the channel at the mouth of the Tokyo Bay (see Fig. 3.11). The supporting ground of the bridge is basically sedimentary soft rock deposits with the bedding direction inclined as shown in Fig. 3.12. On the eastern side, younger deposits of the Kazusa group (the early Pleistocene epoch) dominate, while on the western side, older deposits of the Miura group (the late Miocene and Pliocene epochs) dominate.

From the early 90's, a detailed and advanced geotechnical investigation started. Based on experiences gained from the geotechnical investigations and their evaluation by comparing the predictions based on their results with the observed behaviours of the foundations for the Akashi Strait Bridge and Rainbow Bridge, it was decided to perform advanced SOA geotechnical investigations. The investigations aimed at accurate

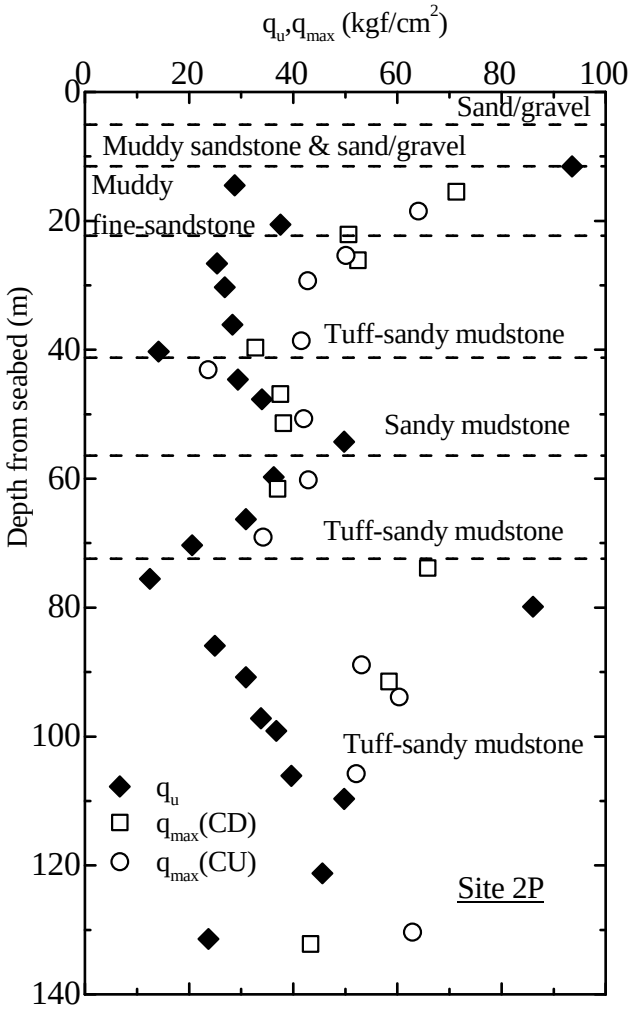

Figure 3.15b. Distribution with depth of compressive strength from U and TC tests, sedimentary soft rock Tokyo Bay mouth, site 2P (Kodaka et al. 2000; Hayano 2001).

characterization of the stress-strain-time properties of the concerned sedimentary soft rock, particularly those at relatively small strains that would be actually operated in the ground. Differently from the previous similar cases, including the Akashi Strait Bridge, the following SOA technologies were utilized in a systematic way in these investigations, performed at the design stage:

1) A large number of field in-bore-hole seismic surveys were performed not only to identify the geological conditions, but also to evaluate the elastic deformation properties for the use in numerical analysis to predict the ground deformations and the displacements of the footings under static as well as dynamic loading conditions.
2) A large number of PMTs were performed with a control of strain level involved so that the results could be interpreted taking into account the non-linearity of stress-strain behaviour.
3) A great number of core samples were retrieved by means of the SOA technology of RCTS.
4) A great number of triaxial tests were performed on RCTS samples. In

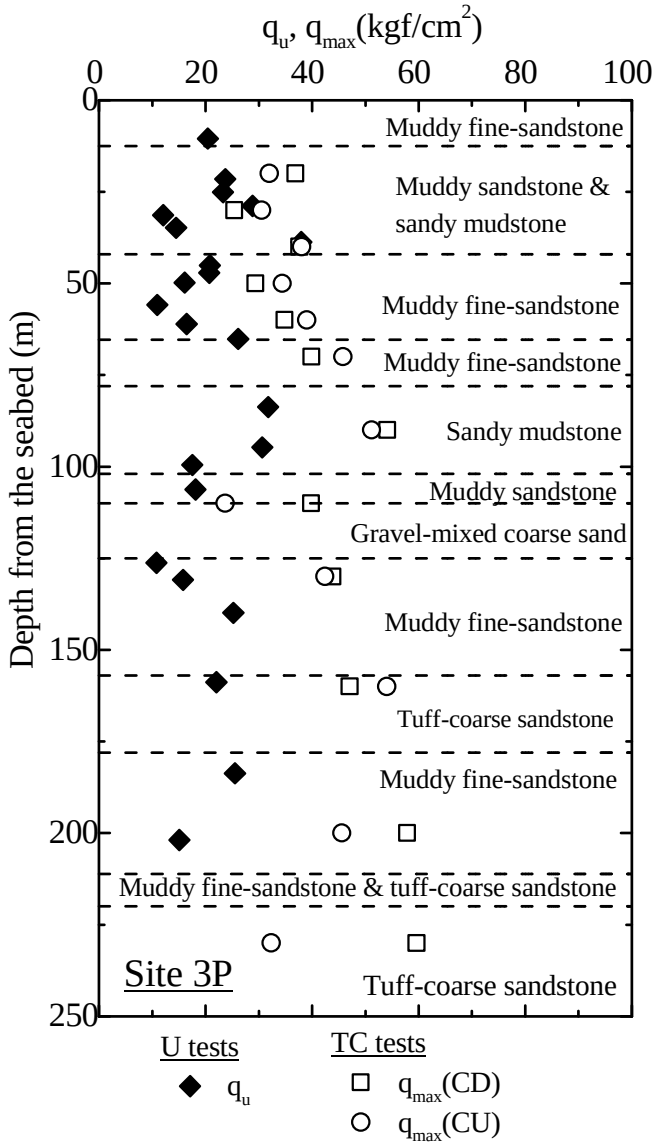

Figure 3.15c. Distribution with depth of compressive strength from U and TC tests, sedimentary soft rock Tokyo Bay mouth, site, site 3P (Kodaka et al. 2000; Hayano 2001).

these tests, axial strains were locally measured by using LDTs and various loading histories were applied to evaluate not only the whole pre-peak stress-strain behaviour and peak strength but also the stress state-dependency of elastic deformation properties and viscous properties.

Another reason for such detailed and advanced geotechnical investigations as above is that it is necessary to evaluate as accurate as possible the strength and deformation characteristics of the sedimentary soft rock deposits supporting the foundations so that the following two contradicting requirements could be satisfied:

a) It is requested to make the construction cost as low as possible. To this end, with respect to the foundation design, it is necessary to make the footing

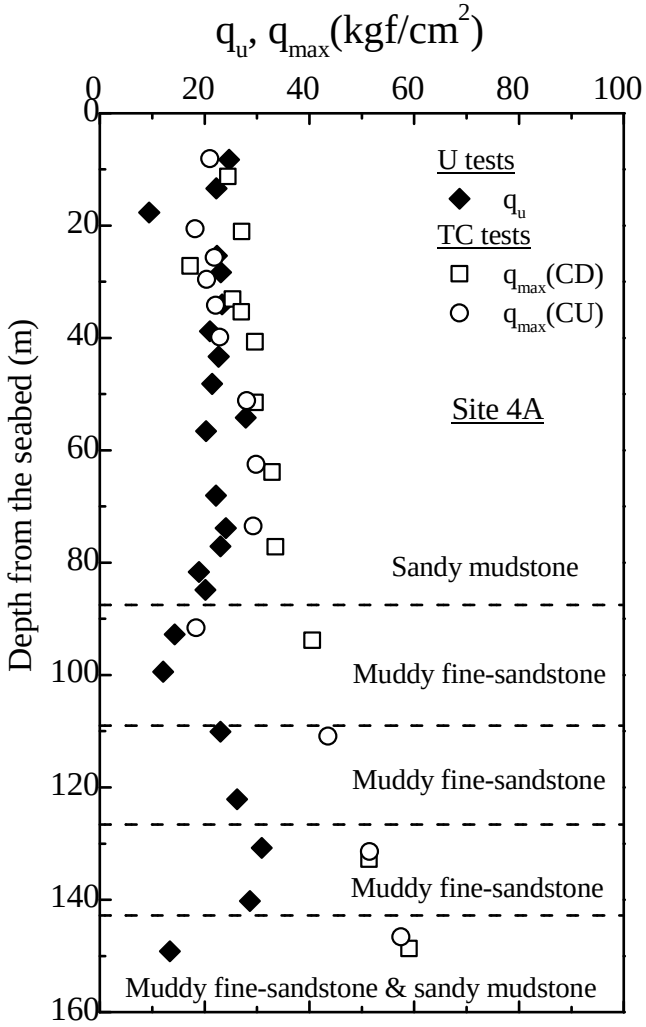

Figure 3.15d. Distribution with depth of compressive strength from U and TC tests, sedimentary soft rock Tokyo Bay mouth, site 4A (Kodaka et al. 2000; Hayano 2001).

dimensions as small as possible and to make the elevations of the footing base as shallow as possible.

b) The design seismic load for civil engineering structures has increased significantly after a great number of civil engineering structures were seriously damaged during the 1995 Kobe Earthquake (the Hyogo-ken-nambu Earthquake). Moreover, the planned location of the bridge is inside one of the highest seismic activity zones in Japan, close to the epicenter of the 1923 Great Kanto Earthquake.

A number of difficulties were encountered during these geotechnical investigations because of offshore investigations at a relatively deep sea. Part of the results obtained from these investigation performed so far is reported below.

Soft rock type: The geological age becomes younger on the eastern part of the site. The grain size of the mother soil type at shallow parts of the sedimentary soft rock deposits are not uniform. As seen from **Fig. 3.13** and **Table 3.2**, the grain size is relatively coarser at sites 2P and 3P than at sites 1A and 4A. This trend can also be seen from the grain size distributions of the crushed and ground sedimentary soft rock samples retrieved from several depths at sites

2P, 3P and 4P (**Fig. 3.14**). This characteristic trend of grain size distribution reflects in different ratios between the compressive strengths from unconfined compression tests and those from CU and CD TC tests at different sites, as shown below.

Compressive strength: **Figs. 3.15a** through **3.15d** show the distribution with depth of compression strength from U tests (except for site 1A) and CU and CD TC tests, all using RCTS core samples. In the TC tests, the specimens were reconsolidated isotropically to the respective field effective vertical stress. The axial strain rate was 0.01 %/min. It is seen that the difference in the q_{max} value between the CU and CD tests is not as obvious as at the Sagamihara test site. It may also be observed that the difference between the q_u and q_{max} values is generally larger in the layers where sandstone is dominant, typically at site 3P. At the early stage of investigation performed in the 70's, only unconfined compression tests were

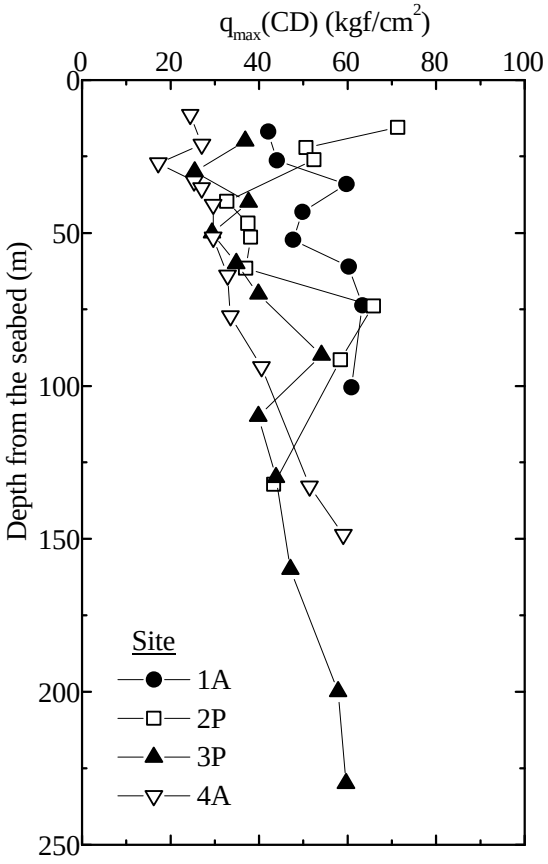

Figure 3.16. Comparison of q_{max} from CD TC tests at the four sites, Tokyo Bay mouth (Kodaka et al. 2000; Hayano 2001).

performed on RCTS core samples as laboratory stress-strain tests. It can be readily seen again from the results presented in Fig. 3.15 that the unconfined compression strength is not at all representative of the compressive strength under field stress conditions, especially with the sandstone of sedimentary soft rock.

Fig. 3.16 compares the q_{max} values from CD TC tests on RCTS samples retrieved from the four sites. It may be seen that the strength at sites 1A and 2P (on the western side), where the deposits are older, is generally larger than that at sites 3P and 4A (on the eastern side).

Fig. 3.17 shows the dependency of the shear strength $\tau_{max} = q_{max}/2$ on the effective minor principal stress at failure, σ'_{3f}, at site 3P, where the stability of the foundation was deemed to be lowest among the four sites. They were obtained from CU and CD TC tests using RCTS samples. The effective failure envelope has a rather large friction component, reflecting the fact that sandstone is dominant at this site. The failure envelope appears to be relatively unique for different depths and for drained and undrained conditions, which means that this failure envelope can be used conveniently in the failure analysis of the ground at site 3P based on the effective stress.

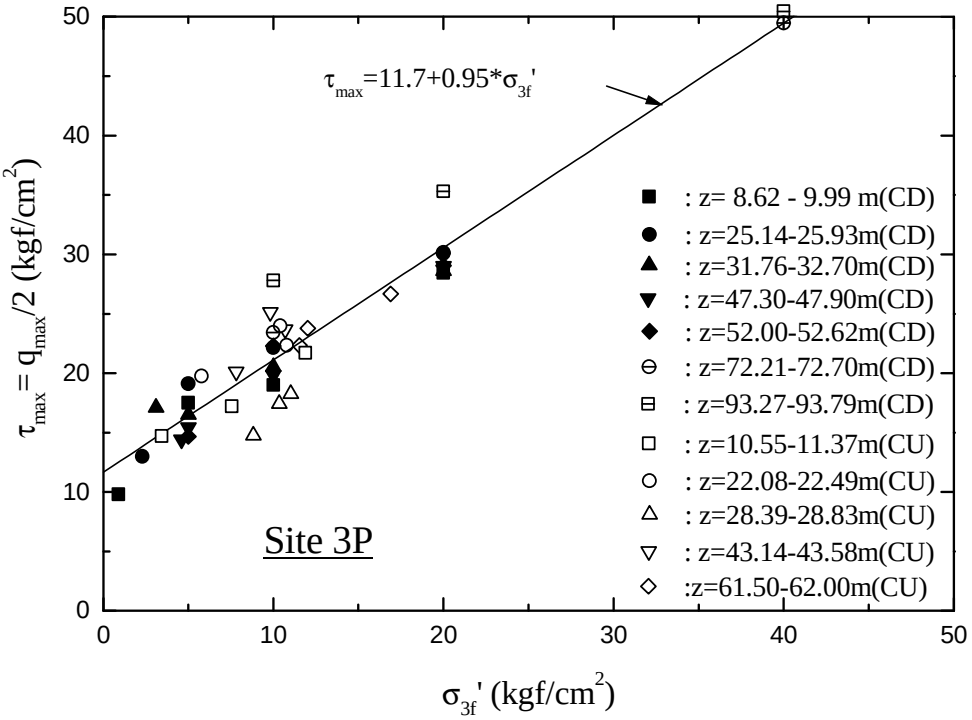

Figure 3.17. Failure envelope in effective stress from CU and CD TC tests for sedimentary soft rock, site 3P, Tokyo Bay mouth (Wang 1996).

Small strain stiffness: **Figs. 3.18a** through **3.18d** show the distribution with depth of the following different Young's modulus values:

1) Undrained elastic Young's modulus, $E_f = 2(1+\nu_u)\cdot G_f = 2(1+\nu_u)\cdot\rho\cdot\left[(V_s)_{VH}\right]^2$, obtained from the suspension method (local up-hole seismic survey) performed in the offshore bore holes from which core samples were retrieved by RCTS: The average E_f value in each sub-layer is indicated by a segment of vertical line.
2) Initial Young's modulus, E_0 (= $(E_v)_0$), defined at axial strains less than about 0.001 % from CD and CU TC tests locally measuring axial strains with a pair of LDTs using RCTS samples: **Fig. 3.19** shows results obtained from a CD TC test on a sedimentary soft rock retrieved from site 4A, which is typical of the above. These E_0 values are denoted as E_0*(CU)* and E_0*(CD)* in Fig. 3.18.
3) E_{50} values from unconfined compression tests (measuring axial strains externally) using RCTS samples (except for site 1A).
4) E_{PMT} values from pre-bored pressure-meter tests evaluated based on the

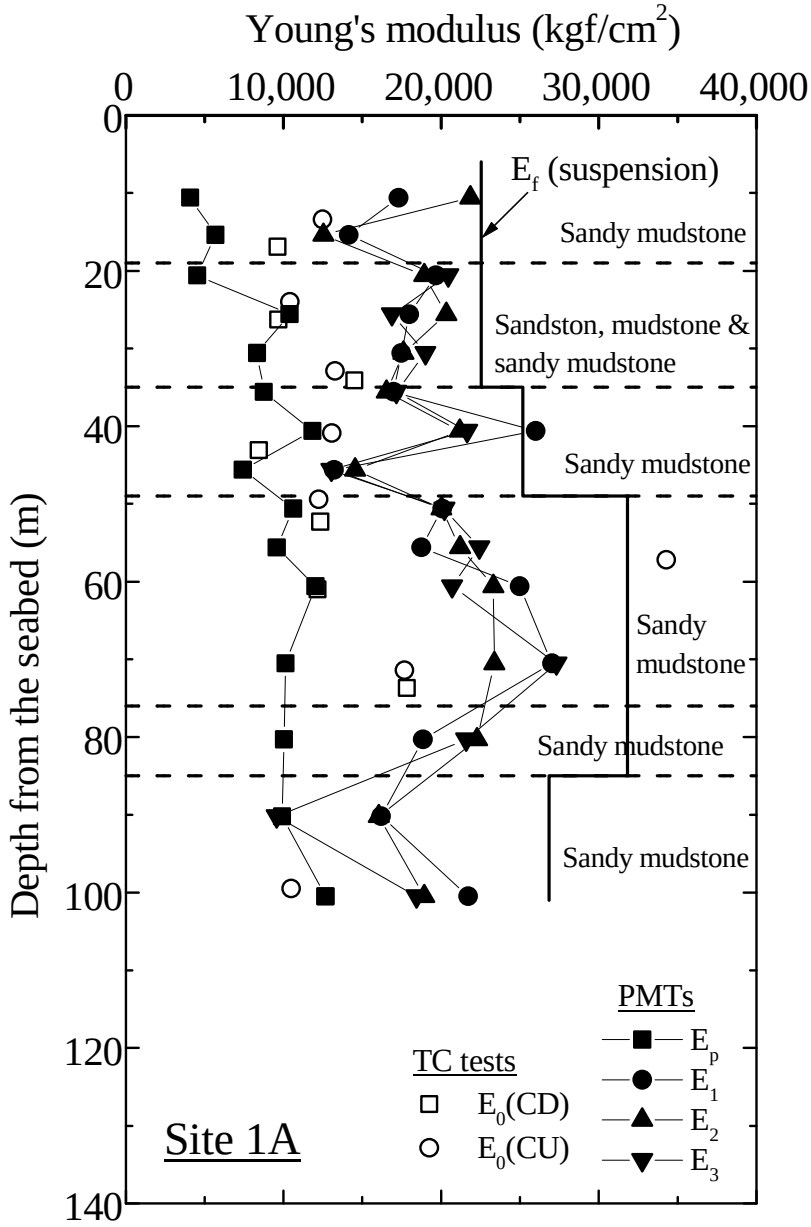

Figure 3.18a. Distribution with depth of Young's modulus from TC tests and PMTs and field seismic survey, Tokyo Bay mouth, site 1A (Kodaka et al. 2000; Hayano 2001).

isotropic linear theory using a Poisson's ratio equal to 0.3. As schematically illustrated in **Fig. 3.20**, the E_{PMT} values were obtained from the average slope of the primary loading curve above the lift-off pressure (i.e., after the balloon became in contact with the bore hole wall) and the reload curves of small amplitude unload/reload cycles applied during otherwise monotonic loading. These E_{PMT} values are denoted as E_p, E_1, E_2 and E_3 in Fig. 3.18.

The following trends of behaviour may be seen from Figs. 3.18a through 3.18d:

1) The E_{50} values from the unconfined compression tests are utterly not representative of the small strain stiffness of sedimentary soft rock under

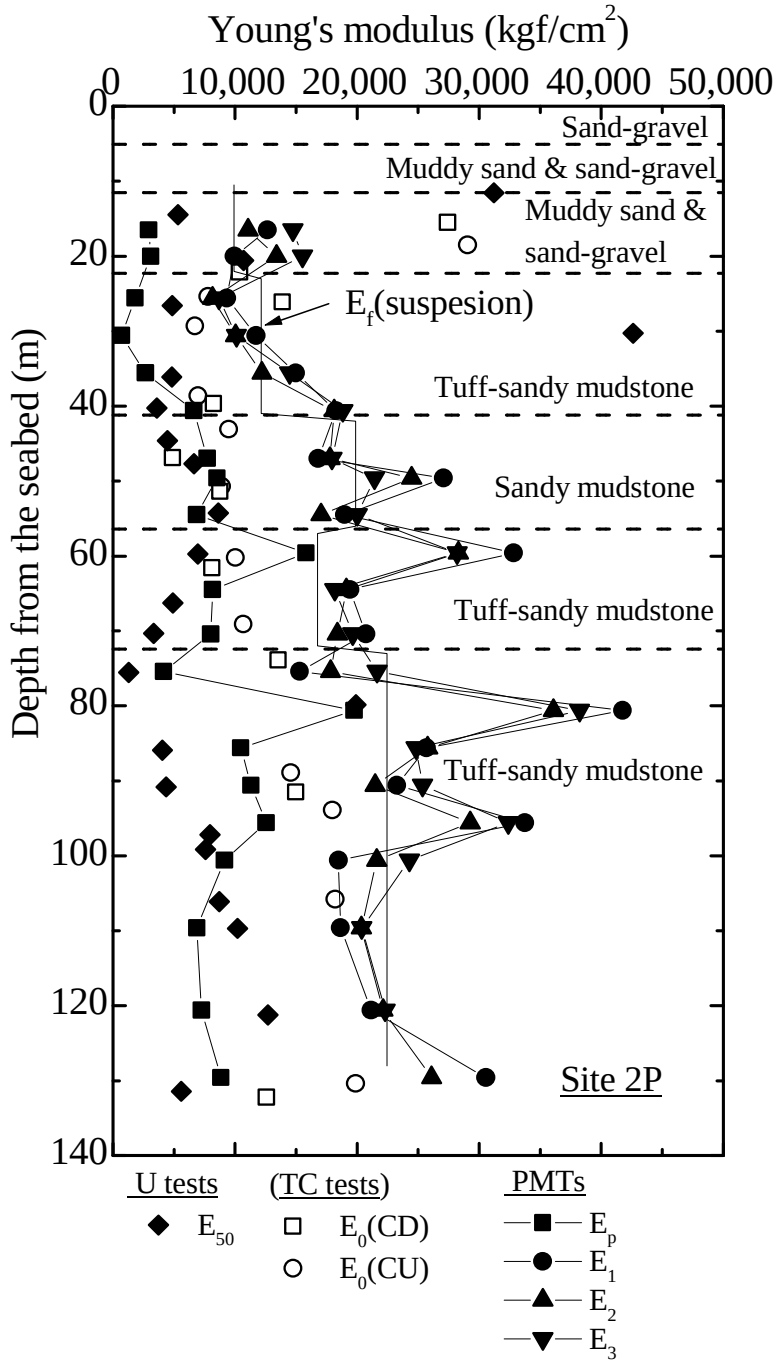

Figure 3.18b. Distribution with depth of Young's modulus from TC tests and PMTs and field seismic survey, Tokyo Bay mouth, site 2P (Kodaka et al. 2000; Hayano 2001).

field stress conditions.

2) The E_0 values from CD and CU TC tests (using RCTS samples) at a respective similar depth are not particularly different from each other. These E_0 values are generally slightly smaller than the E_f value. This result suggests that most of the RCTS samples were somewhat disturbed, which is inevitable because the RCTS was performed at offshore sites where the sea was relatively deep.

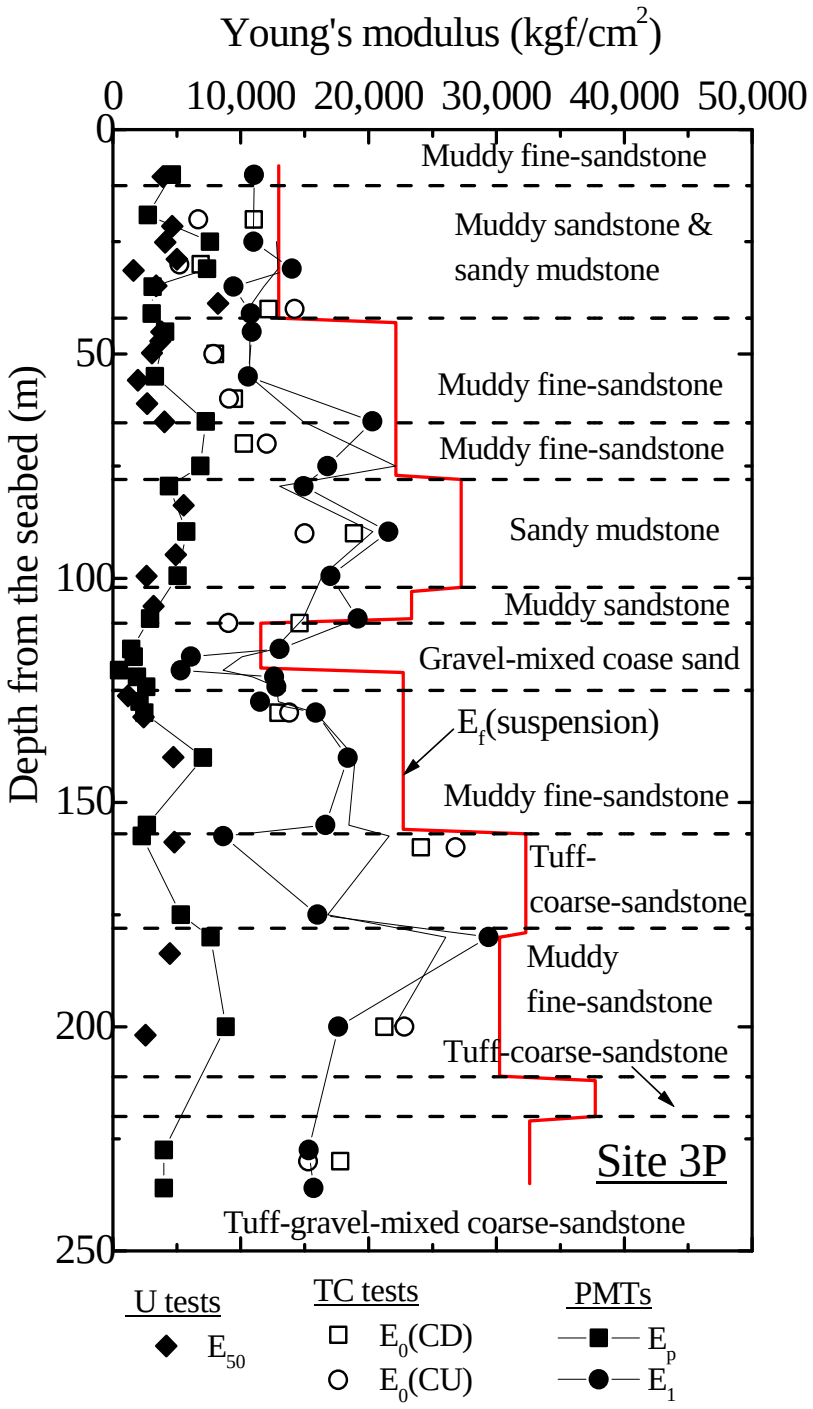

Figure 3.18c. Distribution with depth of Young's modulus from TC tests and PMTs and field seismic survey, Tokyo Bay mouth, site 3P (Kodaka et al. 2000; Hayano 2001).

The above two trends of behaviour are similar to those observe at the Sagamihara test site.

3) The E_{PMT} values from the average slope of primary loading curve (denoted as E_p) are generally similar to the E_{50} values from the U tests. This result also explains why the full-scale field ground deformation and structural displacements are often over-estimated by conventional analysis using such E_{PMT} values (Tatsuoka and Shibuya 1991; Tatsuoka and Kohata 1995;

Tatsuoka et al. 1995a & 1999a). In comparison, the values of E_1, E_2 and E_3 are noticeably larger than the E_p value at the same depth and some data show values that even exceed the E_f values. It is likely that these trends of behaviour described above are due not only to decreased strain amplitudes and decreased effects of disturbance at the bore hole wall during unload/reload cycles from which the values of E_1, E_2 and E_3 were evaluated, but also to increased pressure levels at which these stiffness values were evaluated. In fact, the effects of pressure level are noticeable on the small strain stiffness evaluated by triaxial tests applying unload/reload cycles with a small strain amplitude at various isotropic stress states using RCTS samples from these sites (**Figs. 3.21a** though **d**). This result shows that effects of both strain and pressure level (and those of loading history, inherent anisotropy, heterogeneity and etc.) should be taken into account when interpreting data from field loading tests, such as PLTs and PMTs.

The data obtained from a series of geotechnical investigations performed for the design of the suspension bridge at the mouth of the Tokyo Bay are well consistent with those obtained from a number of previous projects described in the precedent sections. Yet, well-controlled laboratory stress-strain tests evaluating the effects of influencing factors are necessary to have a general framework of the stress-strain-time properties of sedimentary soft rock, which are described in the following sections.

RECENT FINDINGS OF STRESS-STRAIN-TIME PROPERTIES

General

In this section some recent findings regarding the stress-strain-time properties of sedimentary soft rock obtained from a comprehensive series of laboratory stress-strain tests on sedimentary soft rock are summarized. The tests were performed to interpret and better understand the relationship between laboratory and field tests and between test results and full-scale field observations, as described above.

Small strain stiffness

Engineering implications of elastic deformation characteristics: Compared with uncemented relatively soft soil, the stress-strain behaviour of sedimentary soft rock is generally more linear. In the test described in Fig. 3.19, for example, a small amplitude unload/reload cycle was applied many times during otherwise monotonic loading to evaluate the elasticity and its stress state-dependency at different stress states. It may be seen from Fig. 3.19b that the stress-strain behaviour is rather linear and recoverable until the axial strain becomes 0.01 %. Moreover, the tangent stiffness at an axial strain of 0.1% is still about a half of the initial stiffness (Fig. 3.19d). When the linearity of stress-strain behaviour is relatively high, as described above, the stiffness at small strains (say less than 0.001 %), which represents essentially the elastic deformation properties, could be linked to stiffness values that are back-calculated from full-scale field observations in construction projects on or in sedimentary soft rock deposits. Tatsuoka and Kohata (1995), Tatsuoka et al. (1995a, 1997a, 1999a) and Izumi et al. (1997), among others, reported that when the non-linearity due to strain and pressure level (or more generally stress state) and the effects of loading history, among other factors, are properly taken into account, the stress-strain properties to use in the numerical analysis for the evaluation of full-scale field ground deformation and structural displacements could be deduced rather confidently based on the elastic deformation stiffness

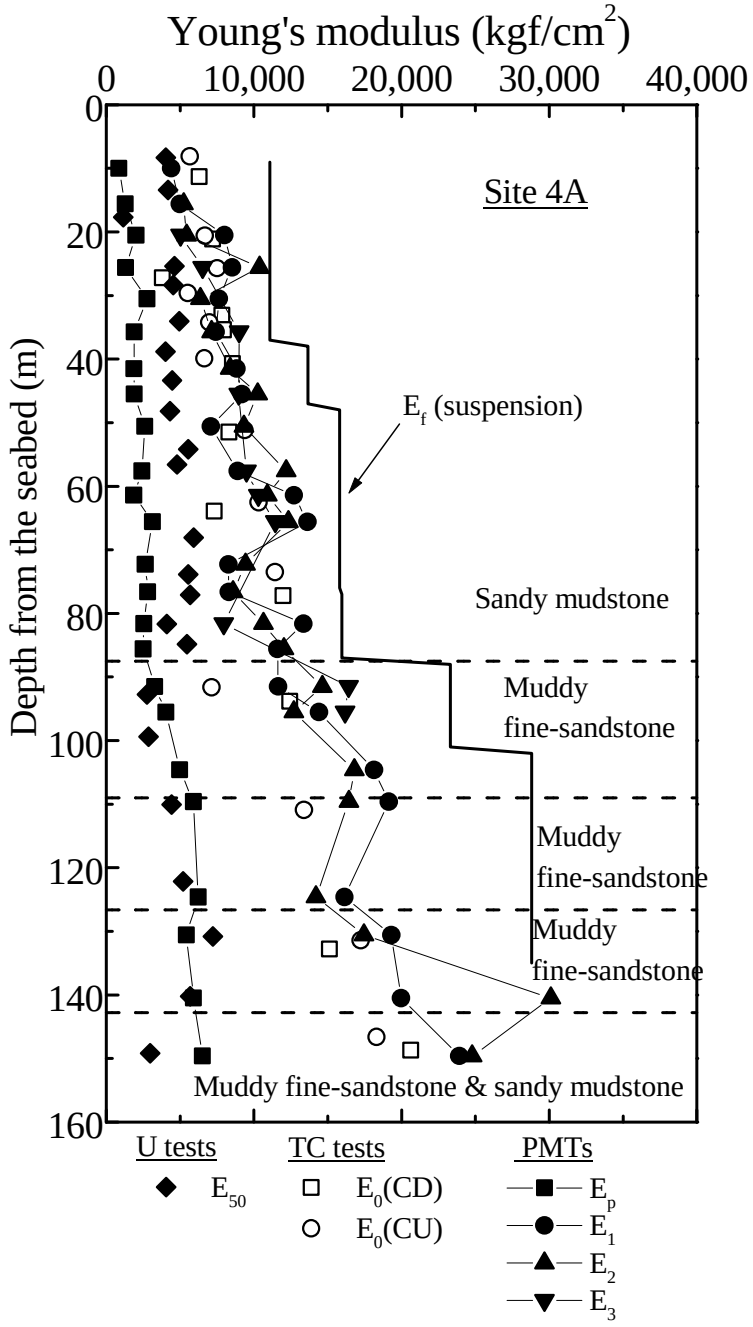

Figure 3.18d. Distribution with depth of Young's modulus from TC tests and PMTs and field seismic survey, Tokyo Bay mouth, site 4A (Kodaka et al. 2000; Hayano 2001).

evaluated from field shear wave velocities, as shown below.

Fig. 4.1 summarizes the relationships between the ratio of the secant Young's modulus E_{sec} to the average undrained Young's modulus E_f from field shear wave velocities for depths (equal to 3.2 GPa) and the major principal strain ε_1 (in the logarithmic scale) obtained from an extensive series of investigations performed at the Sagamihara test site to evaluate the stress-strain properties of sedimentary soft rock. Here, the values of secant Young's modulus E_{sec} were evaluated by the following different methods for the deposit of sedimentary soft rock for depths down to about 50 m performed at the first stage of

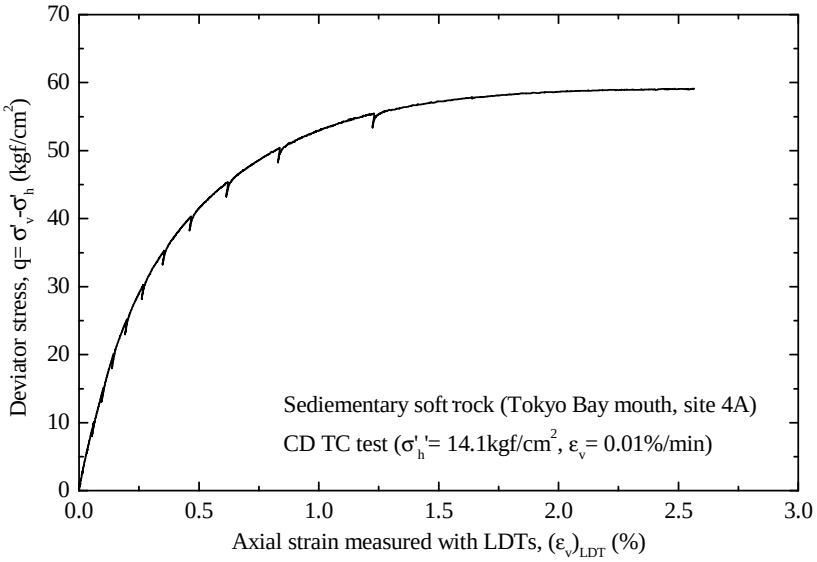

a)

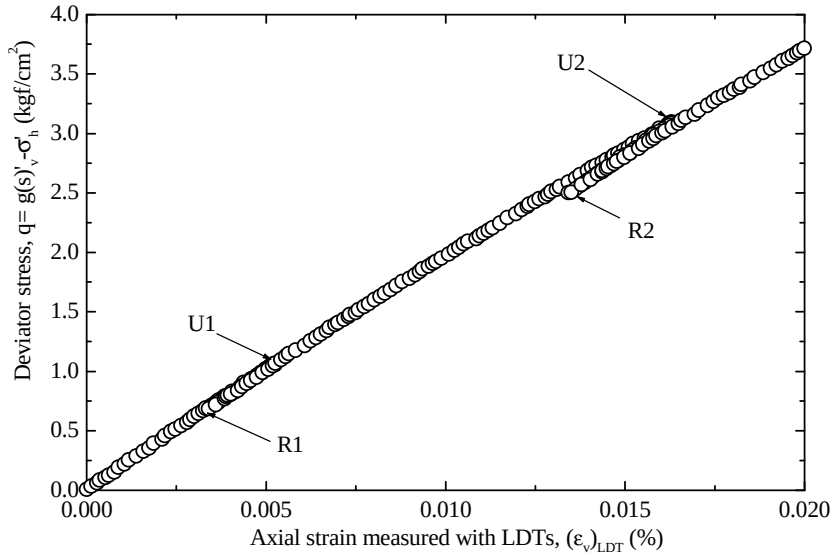

b)

Figure 3.19a&b. Deviator stress and axial strain relation from a CD TC test, sedimentary soft rock, Tokyo Bay mouth, site 4A (Hayano 2001).

experiment described in Fig. 3.3a:

1) *CU and CD TC tests locally measuring axial strains on core samples from the site:* It is assumed for this plot that the initial and maximum value of E_{sec} from the CU TC tests, denoted as $E_{v0(CU)}$, is the same as the average value of E_f (equal to 3.2 GPa), which is deemed to have been obtained under undrained conditions. It is also assumed that the value of E_0 from the CD TC test is smaller by a factor of $(1+\nu_d^e)/(1+\nu_u^e)$ than the value from the CU TC test performed under otherwise the same condition. Here, ν_d^e is the drained elastic Poisson's ratio, which is assumed to be equal to 0.2 and ν_u^e is the undrained elastic Poisson's ratio, which is assumed to be equal to 0.43 for the sedimentary soft rock at the site. Then, the value of $(1+\nu_d^e)/(1+\nu_u^e)$

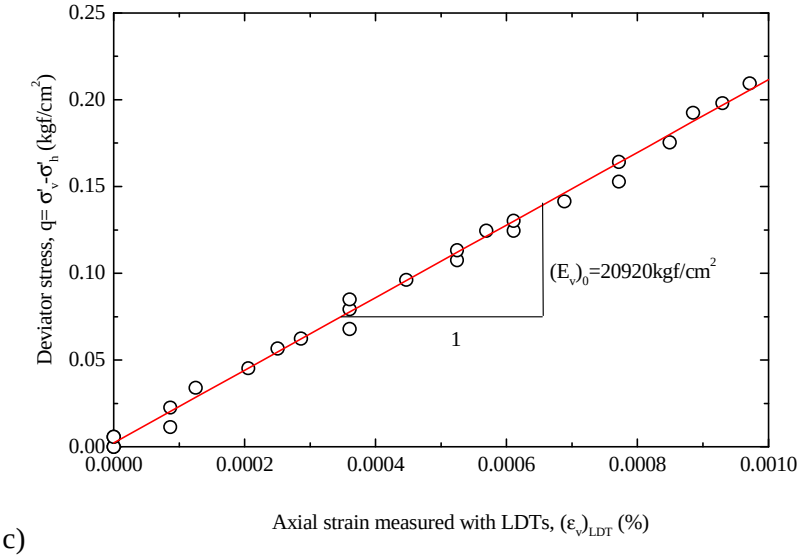

c)

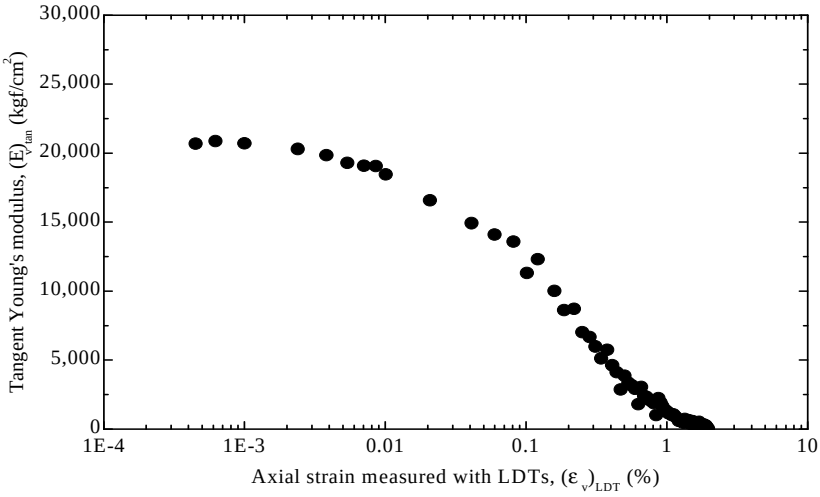

d)

Figure 3.19c&d. c) Deviator stress and axial strain relation at very small strains; and b) tangent Young's modulus and axial strain relation from a CD TC test, sedimentary soft rock, Tokyo Bay mouth, site 4A (Hayano 2001).

becomes equal to 0.84. The continuous relationships denoted as BS(CU) and BS(CD) were obtained from CU and CD TC tests using BS or DC core samples, which were least disturbed among those used in this study. The relationships denoted as Patterns I, II and III mean the results from TC tests using RCTS samples, which were generally more disturbed in the increasing order of I, II and III. Based on the TC test results performed by Kim et al. (1994), it is assumed that the average value of E_0 is the same between the BS and DC samples and the RCTS samples.

2) *Plate loading tests using a rigid plate with a diameter of 30 cm or 60 cm:* Plate loading tests (PLTs) were performed in the test adit at a depth of 35 m and the tunnel at a depth of 50 m. $E_{PLT}(D)$ denotes the values of Young's modulus obtained based on the isotropic linear theory from the relationships between the plate load and the plate settlement during primary loading. In this case, the values of Young's modulus from unloading/reloading curves were only slightly larger (by about 20 %) than the values from the primary loading curves. The ε_1 value in this plot is equal to the plate settlement

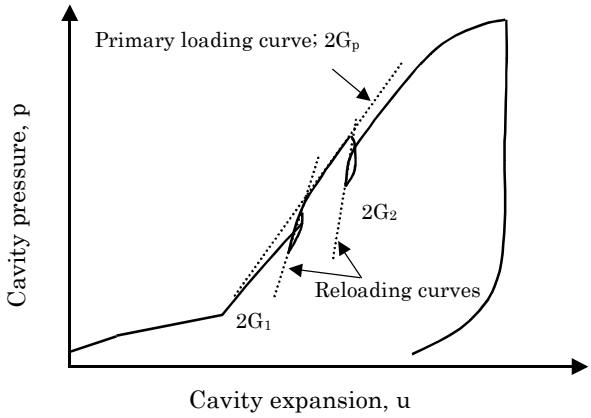

Figure 3.20. Schematic diagram showing the definitions of shear modulus in PMTs.

divided by the plate diameter. $E_{PLT}(S)$ denotes the values of Young's modulus obtained based on isotropic linear theory from measured vertical normal strains in the ground along the central axis of plate. When compared with $E_{PLT}(D)$, these values of $E_{PLT}(S)$ are deemed to be more accurate being free from the effects of bedding error at the ground surface, including extra compression of a thin disturbed zone formed during trimming the ground surface. On the other hand, $E_{PLT}(S)$ scatters much more than $E_{PLT}(D)$, perhaps because $E_{PLT}(S)$ reflects much more sensitively the non-uniformity of the ground.

3) *Pressure-meter tests (or bore hole lateral loading tests; BHLTs):* Two types of pre-bored pressure-meter tests (PMTs) and one type of self-bored PMT were performed. $E_{BHLT}(M)$ denotes the values of Young's modulus obtained from pre-bored PMTs in which only monotonic primary loading was performed and both cavity expansion and cavity wall pressure were measured by using pick-ups located above the ground surface. On the other hand, $E_{BHLT}(C)$ denotes the values of Young's modulus from the self-bored PMTs in which small unload/reload cycles were applied during otherwise monotonic loading (as schematically illustrated in Fig. 3.20), while both cavity expansion and cavity wall pressure were measured by using pick-ups installed inside the balloon. In both cases, isotropic linear theory was used to evaluate the shear modulus, from which the Young's modulus was obtained by using an undrained Poisson's ratio. The ground strain ε_1 shown in Fig. 4.1 is the value at the borehole wall. It may be seen that the value of ε_1 is much larger with $E_{BHLT}(M)$, and therefore, the values of $E_{BHLT}(M)$ are much lower than the values of $E_{BHLT}(C)$.

4) *Back analysis of the full-scale field behaviour during excavation of the shaft, test adit and tunnels and their behaviour during earthquakes:* The respective E_{sec} value was obtained from the maximum strain in the ground (plotted as the ground strain ε_1 in Fig. 4.1) and the corresponding stress back-calculated by the FEM in the respective case.

The following trends of behaviour may be seen from Fig. 4.1:

1) The relationship labeled BS(CU) (from CU TC tests using highest quality core samples obtained by BS or DC) is consistent with the results from the

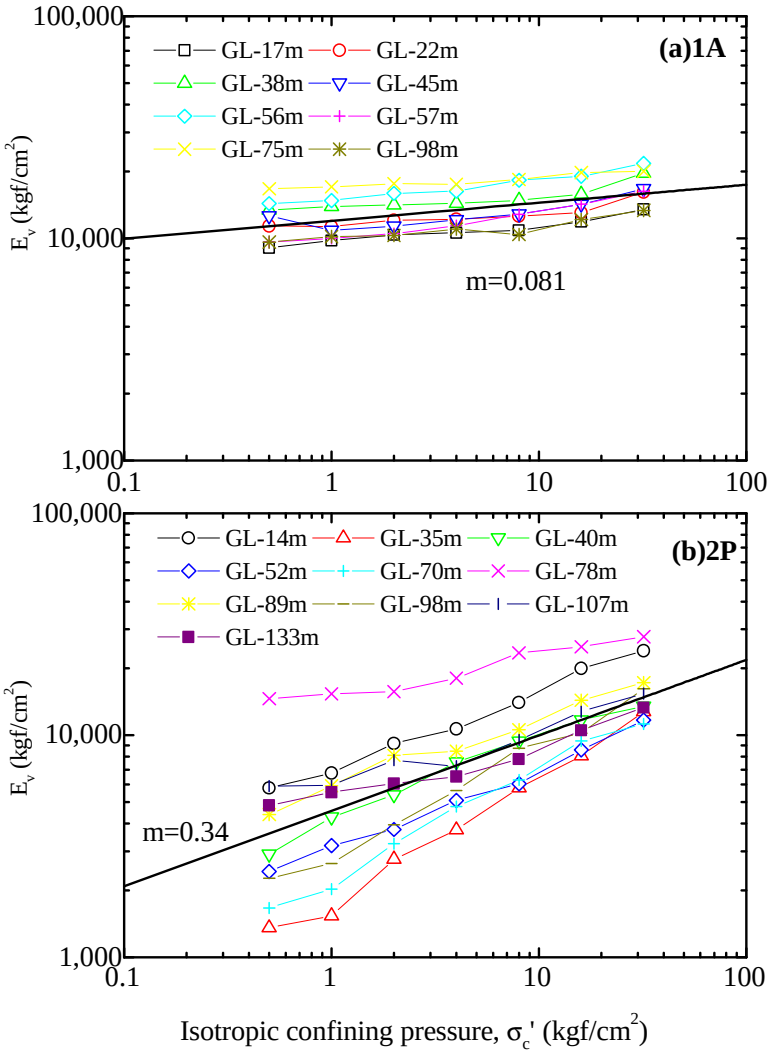

Figures 3.21a&b. Dependency of E_0 on the isotropic confining pressure from TC tests, Tokyo Bay mouth, sites 1A & 2P (Kodaka et al. 2000; Hayano 2001).

field loading tests and the full-scale field observations at relatively small strains, while the one labeled BS(CD) is consistent with the results from the field data at relatively large strains. This is perhaps because the drained condition becomes more prevalent with an increase in the strain level. This good agreement can also be attributed to the fact that the effects of pressure level on the stress-strain behaviour are insignificant in this case (see Fig. 3.8).

2) Among the relationships denoted by Patterns I, II and III (from TC tests using RCTS samples), those denoted as Patterns I(CU) and I(CD) are most consistent with the results from PLTs and PMTs and the full-scale field observations. It may also be seen that the relationships labeled Patterns II and III, in particular Pattern III, are not representative of the field behaviour.

3) Despite the use of a very light support system in this experimental excavation, the largest ε_1 is relatively small, about 0.2 %, at the walls of the shaft and the tunnel.

4) It is significant that the E_{sec} values from the field loading tests and full-scale field behaviour can be linked to the average E_f value by referring to the

strain-non-linearity of stiffness evaluated by the TC tests on core samples that are not seriously disturbed (i.e., BS core samples and RCTS samples exhibiting Pattern I relation). This good agreement can also be attributed to the fact that the effects of pressure level on the stiffness are insignificant in this case.

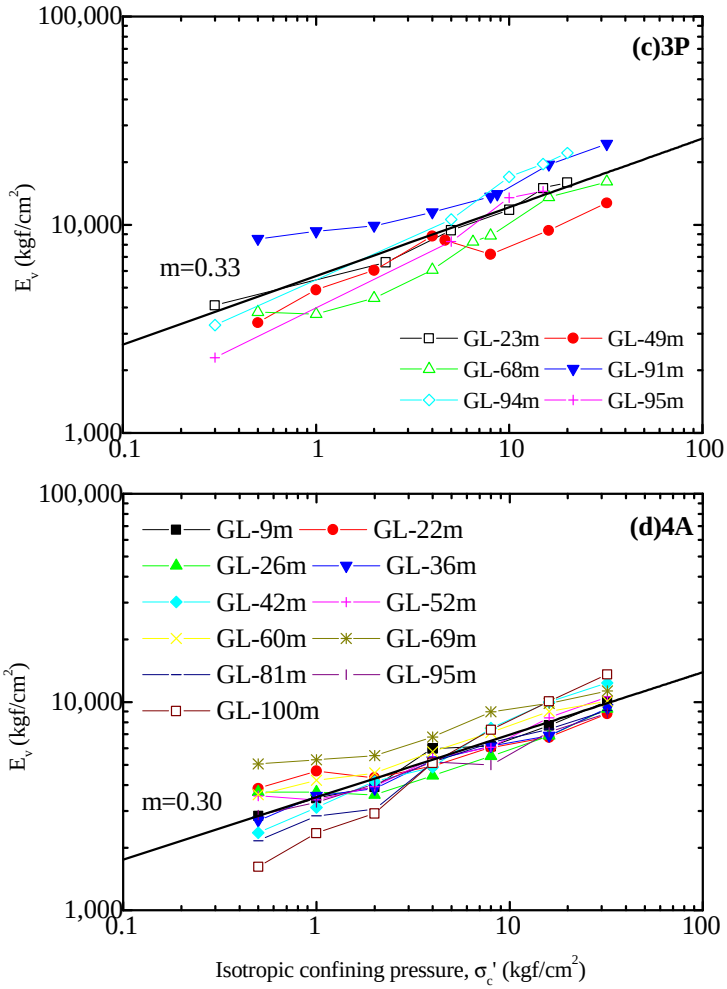

Figures 3.21c&d. Dependency on the isotropic confining pressure of E_0 from TC tests, Tokyo Bay mouth, sites 3P and 4A (Kodaka et al. 2000; Hayano 2001).

A similar comparison with the sedimentary soft rock of the Kazusa group has been obtained from the full-scale field observations obtained during the construction of the foundations for an 800 m-long suspension bridge (Rainbow Bridge) and related field and laboratory tests (Izumi et al. 1997). Part of the results is presented in **Fig. 4.2**. The effects of pressure level on the stress-strain behaviour are also insignificant in this case. Therefore, a comparison of stiffness considering only the strain-non-linearity is relevant. This result also shows the importance of the elastic properties for the prediction of the deformation of relatively stiff geomaterial, such as sedimentary soft rock, and related structural displacements at working loads.

Fig. 4.3 summarises the relationships between the ratio of E_{sec} to E_f and the major

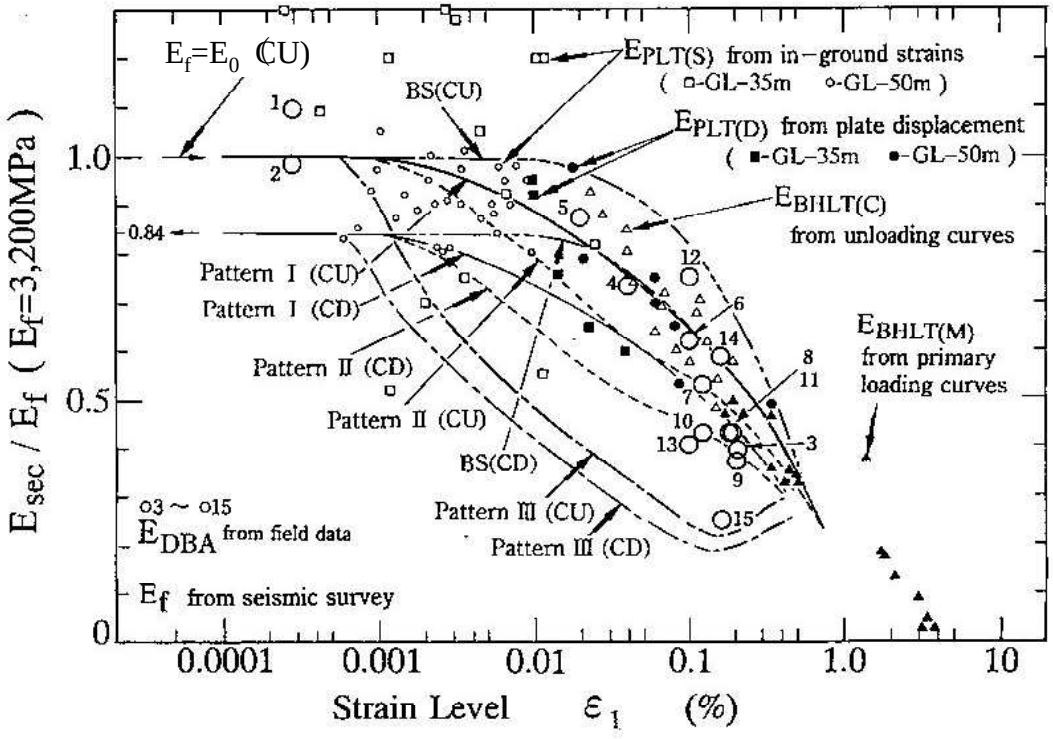

Figure 4.1. Comparison of Young's modulus from laboratory and field tests and full-scale field behaviour, sedimentary soft rock (Kazusa group), Sagamihara test site (Tatsuoka et al. 1997a).

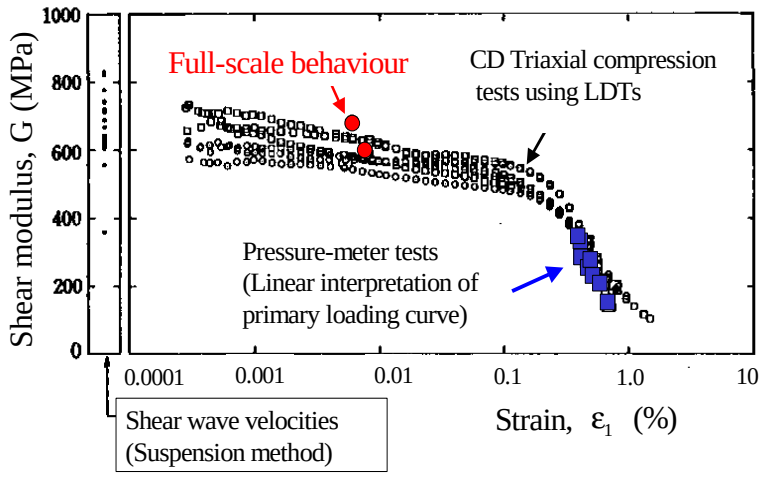

Figure 4.2. Comparison of Young's modulus from laboratory and field tests and full-scale field behaviour when constructing anchorage 4A, sedimentary soft rock (Kazusa group), depth= 54- 74 m, Rainbow bridge site (Izumi et al. 1997; Tatsuoka et al. 1997a).

principal strain ε_1 (in the logarithmic scale) obtained from the full-scale behaviour of the ground supporting piers 2P and 3P for the Akashi Strait Bridge. Pier 2P was constructed on an uncemented gravel layer (Akashi group of the early Pleistocene epoch), while pier 3P was constructed on a sedimentary soft rock deposit (Kobe group of the Pliocene epoch with a geological age of about four million years). The vertical strains in the ground below the respective footing were evaluated from vertical displacements of ground measured at many

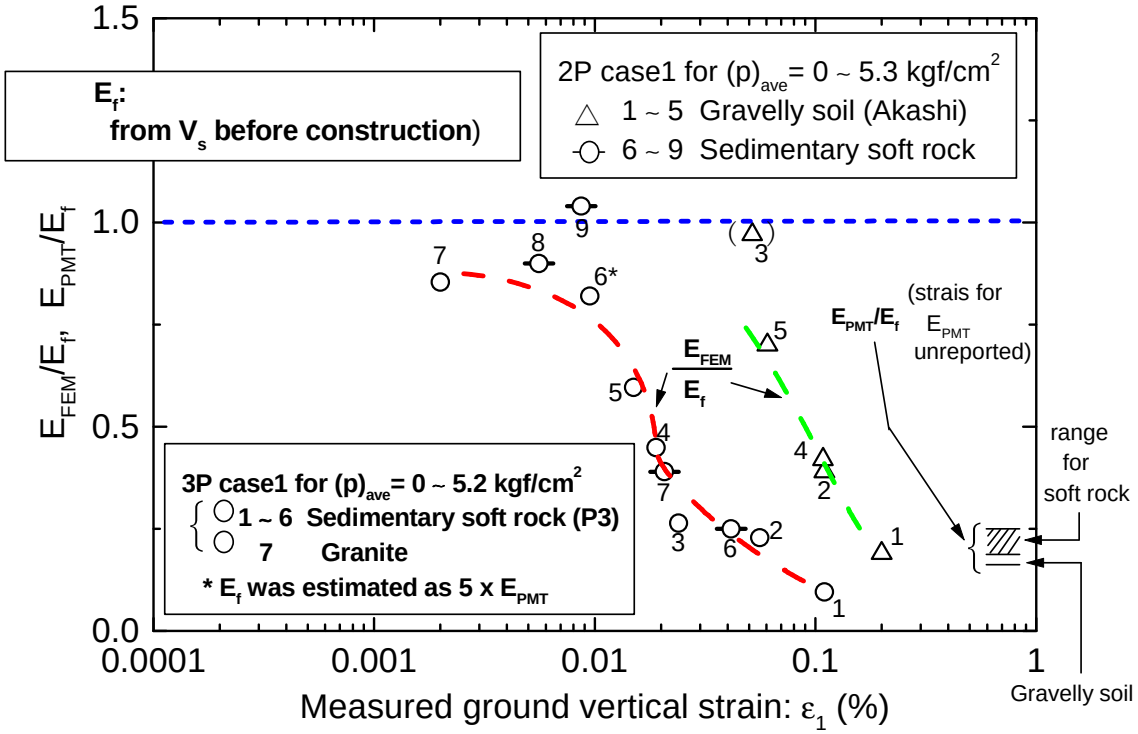

Figure 4.3. Comparison of Young's modulus from field tests and field full-scale behaviour, sedimentary soft rock (Kobe group) and gravel (Akashi group), sites 2P and 3P, Akashi Strait Bridge (Yoshida et al. 1993; Tatsuoka and Kohata 1995).

depths along the central axis of the footing. The numerals that are indicated beside each data point denote the numbers of the sub-layers counted from the top layer. The E_{sec} values from the full-scale field behaviour were obtained by linear 3-D FEM analyses. The analysis used the in-ground strains observed until an intermediate construction stage when the average pressure at the bottom of the footing became about a half of the final value at the completion of the pier construction (about 12 kgf/cm^2) (Yoshida et al. 1993). The respective back-calculated E_{sec} value is denoted as E_{FEM}, which has been divided by the respective E_f value of each sub-layer measured by the down-hole PS logging performed before construction. E_{PMT} denotes the Young's modulus from primary loading curves in pre-bored PMTs evaluated based on the isotropic linear theory. Since the strain levels in the PMTs performed at the sites were not reported, they were estimated to be about 0.7 % by referring to the similar test results.

The following trends of behaviour may be noted from Fig. 4.3:

1) The largest ground strain was about 0.2 %, which is similar to the full-scale field behaviour exhibited at the Sagamihara test site.
2) The sedimentary soft rock and uncemented gravel deposits showed two clearly separate relationships.
3) These two relationships exhibit a marked non-linearity, while the ratio E_{FEM}/E_f approaches 1.0 as the ground strain decreases towards 0.001 % or less. It should be noted, however, that the trend of non-linearity of these two curves have been made larger by effects of a pressure decrease on the stiffness of the sedimentary soft rock (sandstone) and the gravel. That is, the stiffness values at shallower sub-layers should have decreased noticeably

by a decrease in the pressure during the excavation of ground prior to the construction of the piers, which was to a depth of 14 m for pier 2P and 19 m for pier 3P.

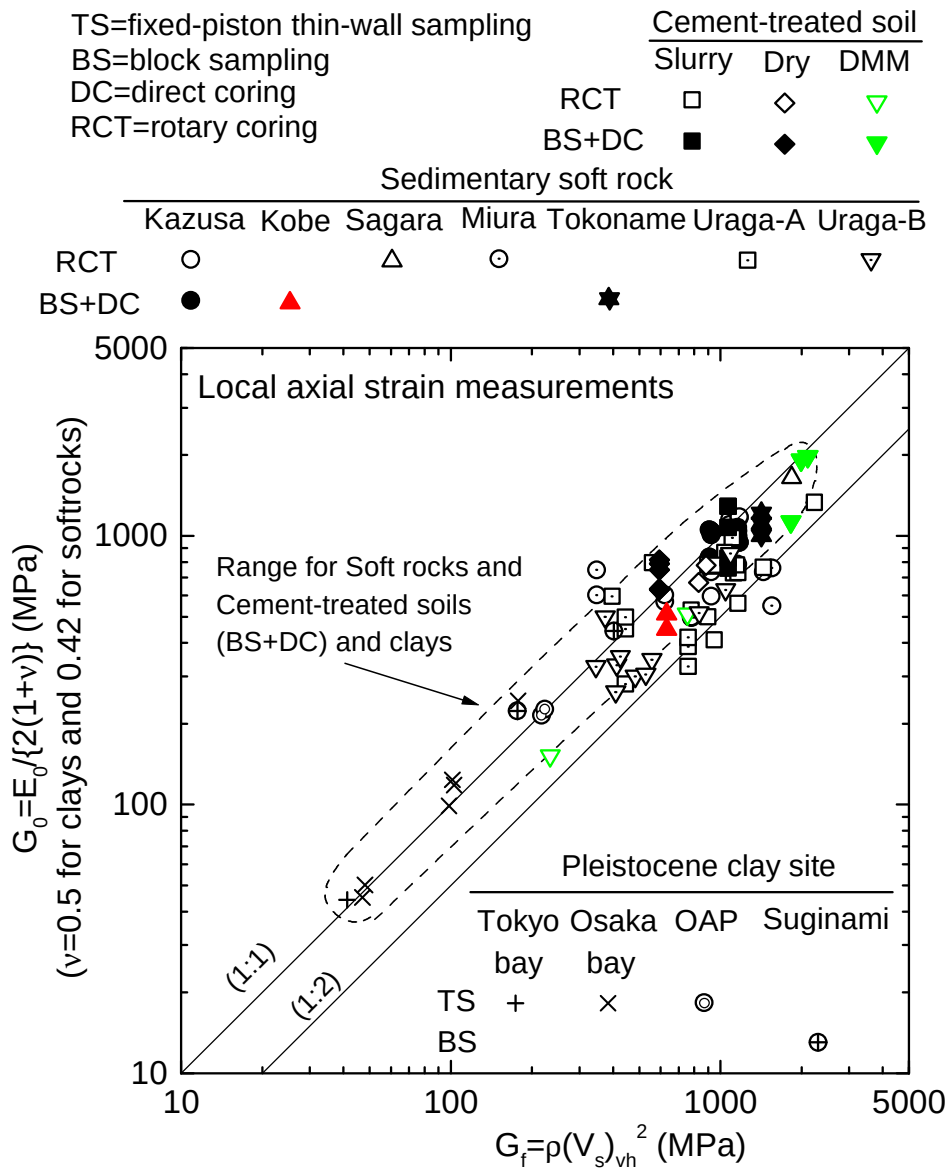

Figure 4.4a. Comparison between G_0 from TC tests and G_f from field shear wave velocity for Pleistocene clays, sedimentary soft rocks and cement-mixed soils (Tatsuoka et al. 1999a).

4) It appears that the values of E_{PMT}/E_f become higher than the E_{FEM}/E_f values at the same strain level. This would be due mainly to the fact that the E_{PMT} values were measured at pressure levels that were much higher than the values in the ground before construction while the E_{FEM}/E_f values became smaller by a decrease in the pressure level associated with ground excavation.

It has been shown that the FEM analysis can simulate the full-scale behaviour of the piers 2P and 3P when based on the Young's modulus E_f from field shear wave velocity and the non-linearity by strain and pressure level evaluated by triaxial tests (Siddiquee et al. 1994, 1995; Tatsuoka and Kohata 1995; Tatsuoka et al. 1999a). The triaxial tests were performed

on core samples of sedimentary soft rock (Kobe group) and 30 cm-diameter 'undisturbed' samples of the gravel (Akashi group) (Tatsuoka et al. 1991).

Comparison of elastic stiffness between laboratory and field measurements: To confidently use the elastic deformation characteristics of sedimentary soft rock evaluated by either laboratory stress-strain tests or field seismic surveys as a basis for the prediction of full-scale field ground deformation and structural displacements, it is essential and necessary to ensure that the elastic stiffness from laboratory stress-strain tests, such as triaxial tests using high-quality undisturbed samples (as shown in Figs. 3.10 and 3.19), and the corresponding value from field shear wave velocity are consistent with each other. **Fig. 4.4a** shows a comparison of the elastic shear modulus G_0 from TC tests and the elastic shear modulus G_f from field shear wave velocity obtained in relation to a number of research and construction projects in Japan for a decade preceding 1997. The geomaterial types for these data are Pleistocene stiff clay, sedimentary soft rock, soft clay improved by in-situ cement-mixing (denoted as DMM; the deep mixing method) and cement-mixed sand used to construct large-scale offshore fills (denoted as Slurry and Dry). The latter two types of cement-mixed soil technologies were developed and used in the Trans-Tokyo Bay highway projects (Tatsuoka et al. 1997b). The G_0 values were obtained from Young's modulus E_0 evaluated by TC tests or small amplitude cyclic loading triaxial tests assuming that the elastic undrained Poisson' ratio $(\nu_{vh})_0$ is equal to 0.42 and 0.5 for, respectively, sedimentary soft rock and clay.

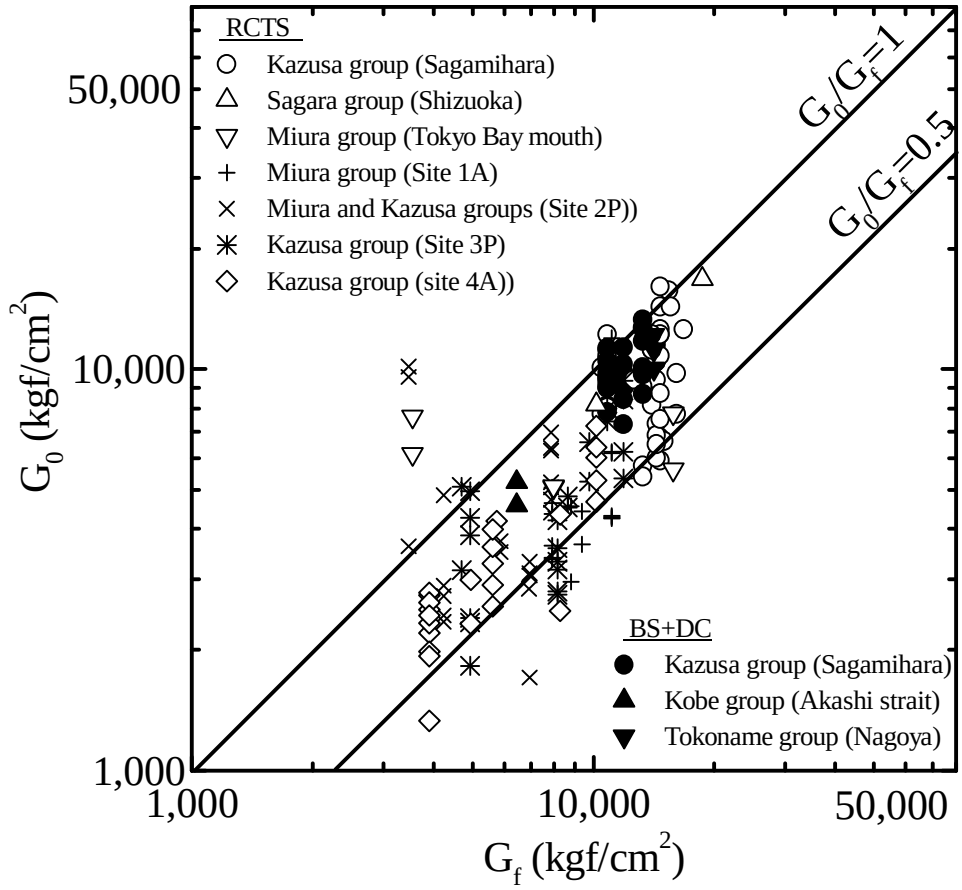

Figure 4.4b. Comparison between G_0 from TC tests and G_f from field shear wave velocity for sedimentary soft rocks (Kodaka et al. 2000).

Fig. 4.4b (Kodaka et al. 2000) shows a similar summary for sedimentary soft rock. Also **Fig.**

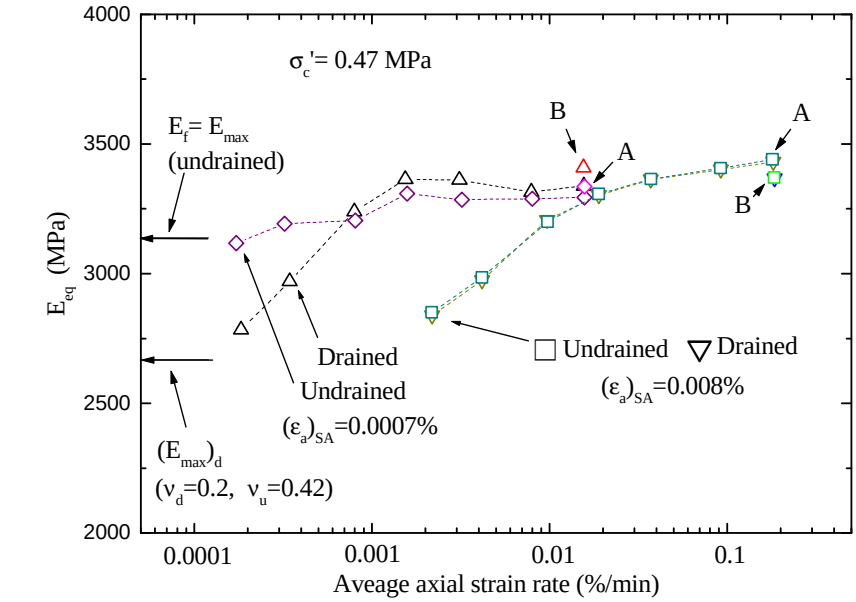

a)

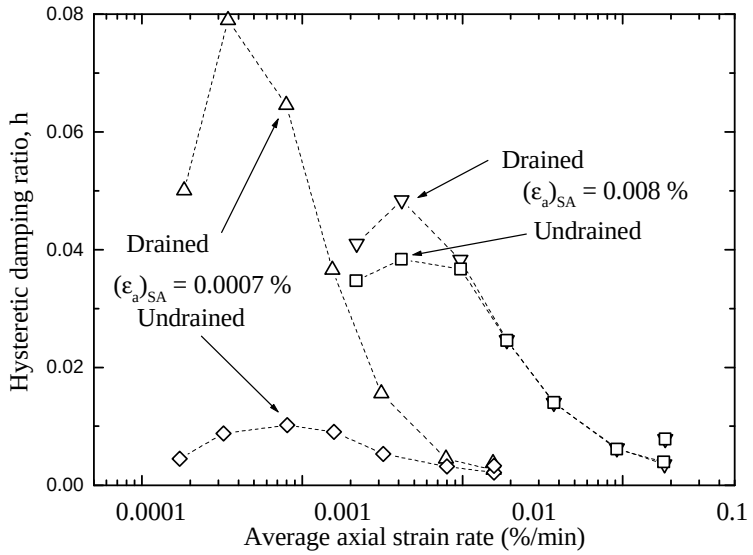

b)

Figure 4.5. a) Peak-to-peak secant Young's modulus E_{eq} and b) damping ratio h, plotted against average axial strain rate from CD and CU cyclic triaxial tests using a single specimen of sedimentary soft rock from Sagamihara test site (Tatsuoka and Kohata 1995; Kohata et al. 1997).

4.4b (Kodaka et al. 2000) shows a similar summary for sedimentary soft rock. Also included in this figure is the data that was obtained after the summary presented in Fig. 4.4a was made from the geotechnical investigations performed for the design of the suspension bridge being planned for construction at the mouth of the Tokyo Bay.

The following trends of behaviour may be seen from Figs. 4.4a and 4.4b:

1) The values of G_0 and G_f are generally in a reasonably good agreement with each other not only for sedimentary soft rock, but also for Pleistocene clay and cement-mixed soil.
2) With sedimentary soft rock, the agreement is generally better with the G_0

values obtained by triaxial tests using undisturbed samples retrieved by block sampling (BS) or direct coring (DC). It is also the case with cement-mixed soil (Fig. 4.4a). That is, for the same value of G_f, the value of G_0 of RCTS samples is generally smaller than the value of BS and DC samples.

3) The scatter is noticeably larger with the G_0 values of RCTS samples than with those of BS and DC samples. Despite the scatter due to effects of anisotropy and/or heterogeneity in the sedimentary soft rock deposits, it is very likely that RCTS samples were more-or-less disturbed and the degree of sample disturbance was not consistent at different depths and different sites and during different sampling operations (Tatsuoka et al. 1995b).

It could be concluded based on the results presented in Figs. 4.4a and 4.4b that;

a) for a given mass of sedimentary soft rock under a given stress condition, there exists only one kind of elastic modulus, which can be evaluated by either relevant static stress-strain tests or shear wave velocity measurements (field measurements in practical cases); and

b) the elastic deformation properties could be the essential basis to obtain the stiffness values to use in the prediction of full-scale field ground deformation and structural displacements.

Detailed evaluation of elastic deformation characteristics: To get a deeper insight into the link between statically and dynamically evaluated stiffness values at small strains, it is necessary to better know about the deformation reversibility and the effects of strain rate on the stress-strain behaviour at small strains, say less than about 0.001 %.

Fig. 4.5 shows the values of peak-to-peak secant Young's modulus, E_{eq}, and damping ratio, h, plotted against the average axial strain rate between respective peak stress states in each cycle. These data were obtained from drained and undrained cyclic triaxial tests using a single specimen (5 cm in diameter and 10 cm in height) of sedimentary soft rock from the Sagamihara test site (Kohata et al. 1995; Tatsuoka and Kohata 1995). The sample was isotropically reconsolidated to the field effective vertical stress (4.8 kgf/cm^2). The axial strain amplitude applied was first 0.0007 % and then 0.008 %. In each set of cyclic loading tests with the same strain amplitude, ten cycles of sinusoidal stresses under first undrained and then drained conditions were applied from the highest strain rate (data point ***A***) toward smaller strain rates. The data points denoted as ***B*** were obtained at the end of a series of cyclic loading with the same strain amplitude at different strain rates. It may be seen that the effects of cyclic loading history on the measured Young's modulus and damping ratio were insignificant (in particular when the axial strain amplitude was 0.0007 %).

The following trends of behaviour could be seen from Fig. 4.5:

1) At axial strain rates exceeding about 0.0008 %/min, in both cases where the axial strain amplitude was 0.0007 % and 0.008 %, the E_{eq} value from drained cyclic loading tests (in which the drainage valves were kept open) is essentially the same as the value from undrained cyclic loading tests (in which the drainage valves were kept closed) performed under otherwise the same conditions. This test result shows that the fully or nearly fully drained conditions can be ensured only when cyclic loading tests are performed at sufficiently low strain rates with this mudstone of sedimentary soft rock.

2) The drained Young's modulus that would be observed in 'drained' cyclic loading tests with an axial strain amplitude of 0.0007 % at sufficiently low

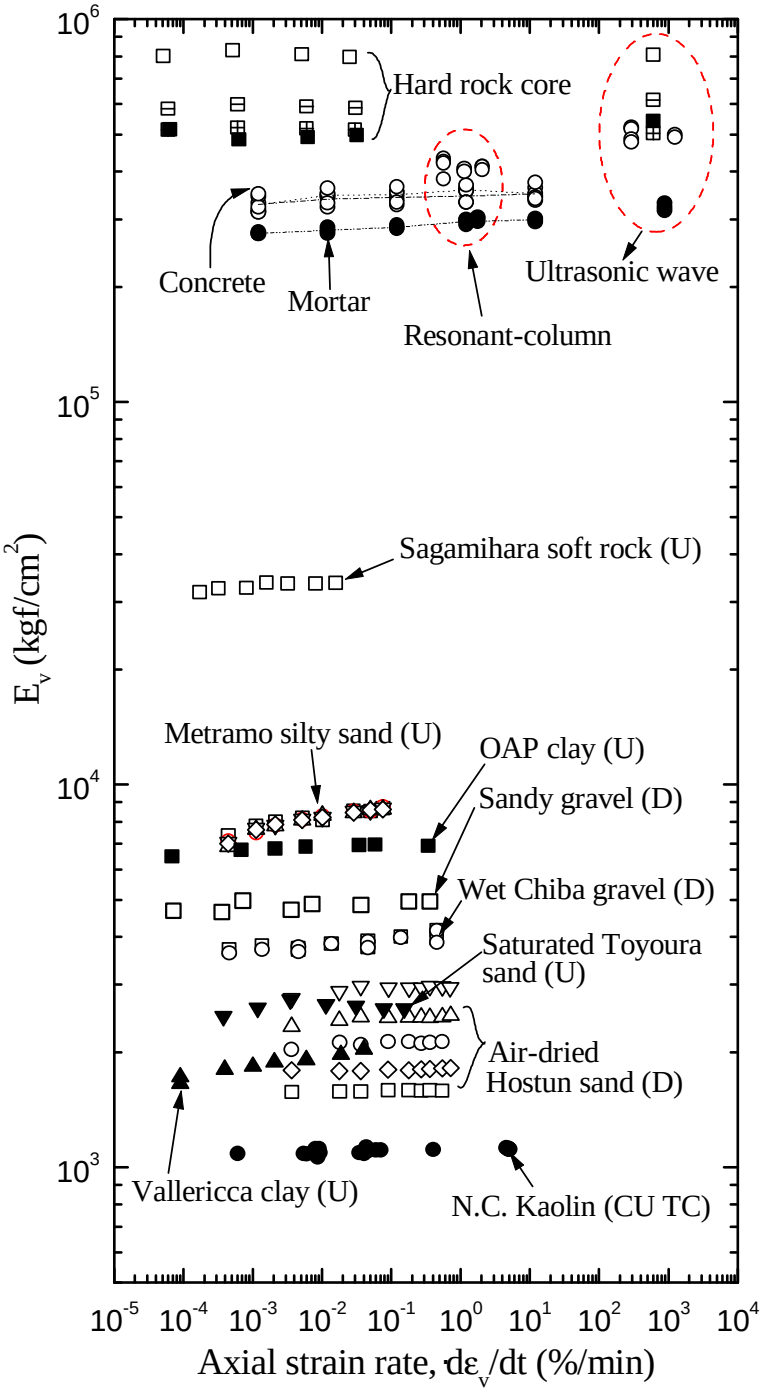

Figure 4.6. Summary of the dependency of quasi-elastic Young's modulus E_v on strain rate (Tatsuoka et al. 1999a, b), obtained from:

1) *Cyclic triaxial tests (U; undrained and D; drained) :* Sagamihara soft mudstone, OAP clay and gravel, air-pluviated Toyoura sand (e= 0.658 and $\sigma'_v = \sigma'_h$ = 1.0 kgf/cm^2); air-pluviated Hostun sand (e= 0.72 and σ'_v = 0.8～2.5 kgf/cm^2 and σ'_h = 0.8 kgf/cm^2); compacted Metramo silty granite sand (σ'_h = 4.0 kgf/cm^2; Santucci de Magistris et al. 1999); Vallericca clay (ditto).
2) *CU TC tests:* NC kaolin (p_c' = 3.0 kgf/cm^2, K_c= 0.6～1.0).
3) *Unconfined cyclic tests and ultrasonic tests:* hard rocks, concrete and mortar (Sato et al. 1997a, b).

strain rates is noticeably smaller than the undrained Young's modulus for the same strain rate. This would be due to the fact that the shear modulus is essentially the same under undrained and drained conditions, while the Poisson's ratio is noticeably different under undrained and drained conditions.

3) The damping ratios, *h*, under undrained conditions are not totally negligible even at an axial strain amplitude of 0.0007 %. The truly elastic behaviour during cyclic loading should exhibit zero damping ratios, which may be approached at strain amplitudes lower than 0.0007 %. Therefore, the deformation modulus evaluated at strains (or strain amplitudes) of around 0.001 % should be called "the quasi-elastic modulus" (Tatsuoka et al. 1999a).

4) A high rate of increase in the damping ratio with a decrease in the strain rate evaluated for an axial strain amplitude of 0.0007 % under 'drained' conditions is due to the complicated interaction between the fabric of sedimentary soft rock and migrating pore water.

Di Benedetto and Tatsuoka (1997) showed that the dependency of E_{eq} and h on the strain rate under undrained conditions seen in Figs. 4.5a and 4.5b (and similar behaviours under undrained and fully drained conditions exhibited by different types of geomaterials) could be simulated by a linear three-component model. The model consists of a linear elastic component connected in series to a pair of another linear elastic component and a Newtonian dashpot connected in parallel. It is shown later in this paper that a non-linear three-component model, which is an extension of the linear one, are able to simulate the whole loading rate effects on the stress-strain behaviour of geomaterials, including creep behaviour, different pre-peak stress-strain behaviours and peak strengths during monotonic loading at different constant strain rates and effects of change in the strain rate on the stress-strain behaviour.

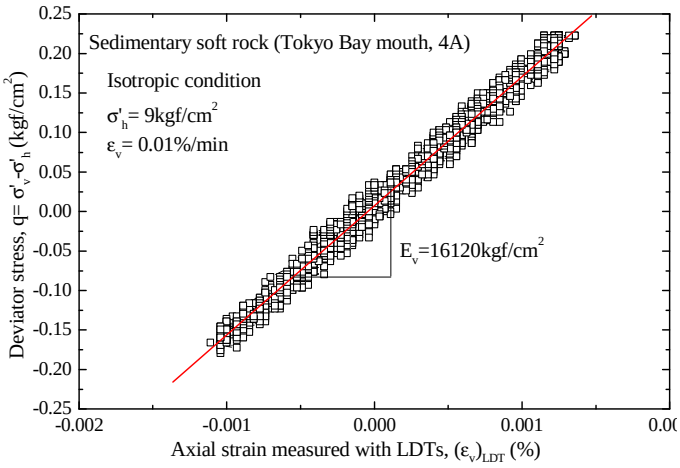

Figure 4.7. Eleven unload/reload cycles applied at isotropic stress state, sedimentary soft rock, Tokyo Bay mouth, site 4A (Hayano et al. 1999b; Hayano 2001).

Fig. 4.6 summarizes the effects of strain rate on the quasi-elastic Young's modulus E_v (i.e., the values of E_0 defined for an axial strain of 0.001 % from ML tests and E_{eq} values for an axial strain amplitude of about 0.001 % from cyclic loading tests) for different types of geomaterial (Tatsuoka et al. 1999a, b). The following trends of behaviour may be seen from

Fig. 4.6:

1) The E_v value is generally more dependent on the strain rate with less stiffer materials.
2) The dependency of E_v on the strain rate becomes smaller with the increase in the strain rate, becoming negligible at strain rates larger than a certain value (see also Fig. 4.5).

A number of experimental results have shown that for fine-grained geomaterials, such as sand and clay, the E_v value evaluated by static (monotonic and cyclic loading) stress-strain tests performed at a strain rate that is not extremely low is comparable with the value from shear wave velocity measured by, for example, the bender element method under

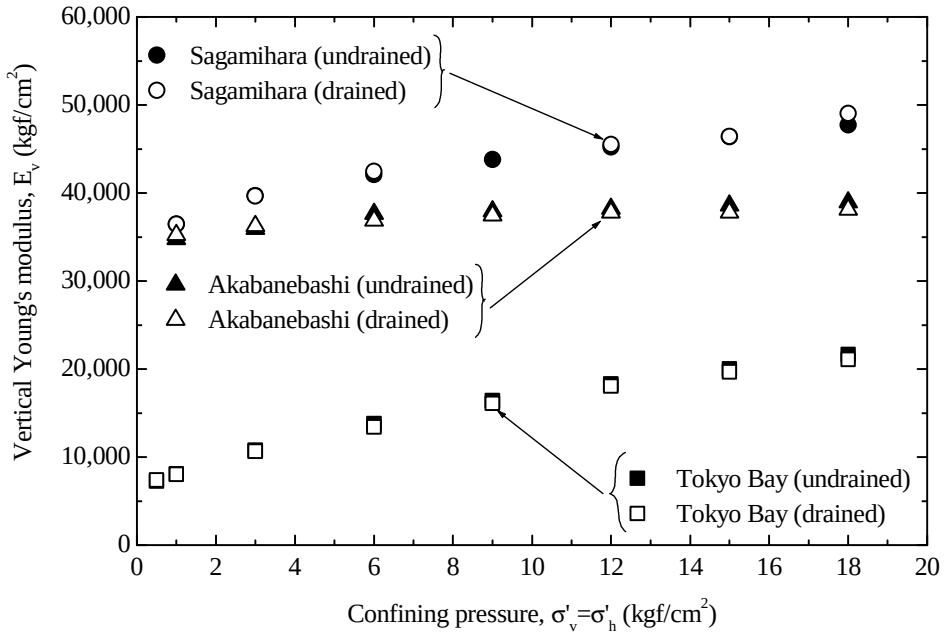

a)

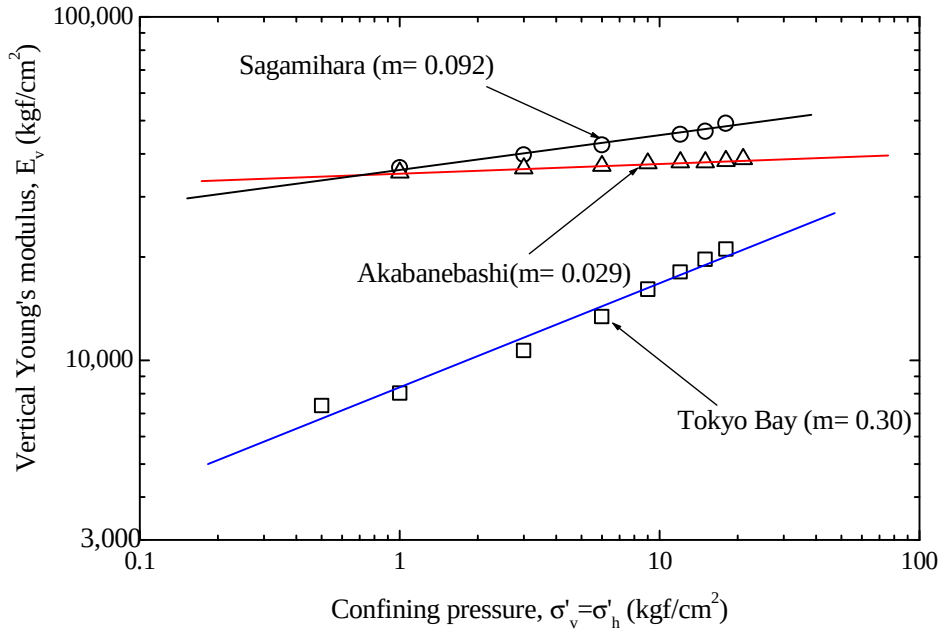

b)

Figure 4.8. Dependency of quasi-elastic Young's modulus on isotropic confining pressure for sedimentary soft rock at three sites; a) arithmetic plot; and b) log-log plot (Hayano 2001).

otherwise the same test conditions (e.g., Tatsuoka 1994; Tatsuoka et al. 1994, 1995c, 1999a&b). The trend of behaviour 2) described above is consistent with this fact. That is, the elastic (or quasi-elastic) deformation characteristics of geomaterials, including sedimentary soft rock that does not include discontinuities significantly, can be evaluated by relevant static stress-strain tests (Shibuya et al. 1992; Tatsuoka 1994; Tatsuoka et al. 1994, 1995c, 1999a&b).

Dependency of elastic modulus on the isotropic confining pressure: The elastic (or quasi-elastic) deformation properties of sedimentary soft rock (in particular less cemented ones, such as sandstone) could noticeably depend on the instantaneous stress state. **Fig. 4.7** shows typical stress-strain behaviour during eleven unload/reload cycles of deviator stress with an axial strain amplitude (single) of about 0.001 % applied to an isotropically reconsolidated sample obtained from site 4A at the mouth of the Tokyo Bay. The

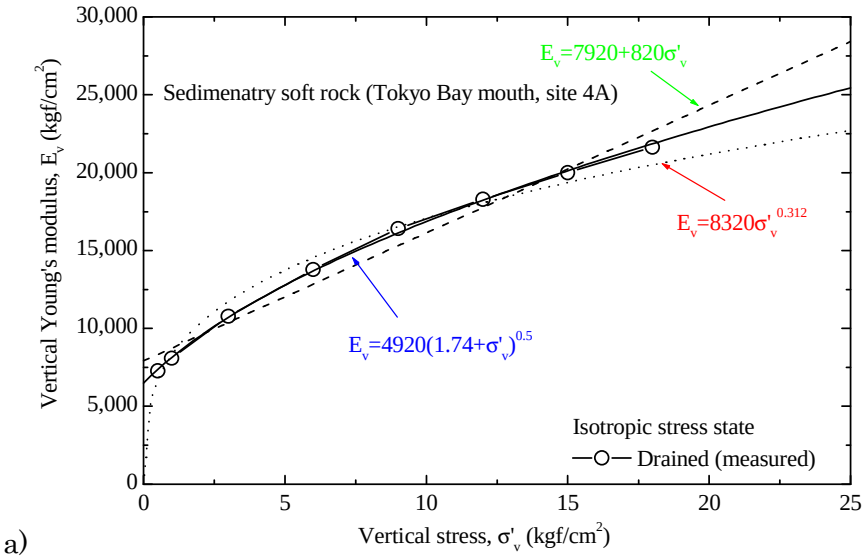

a)

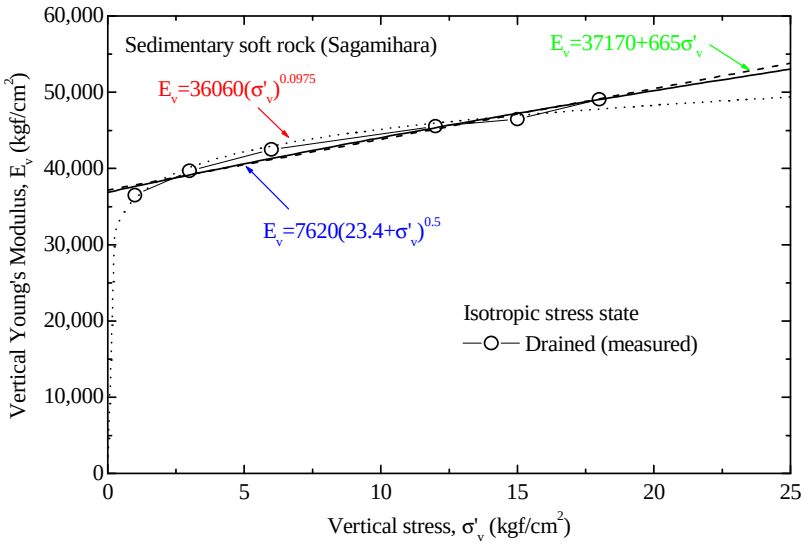

b)

Figure 4.9 a&b. Dependency of vertical quasi-elastic Young's modulus on the vertical stress; comparison of different functions: a) Tokyo Bay mouth, site 4A; and b) Sagamihara test site (Hayano 2001).

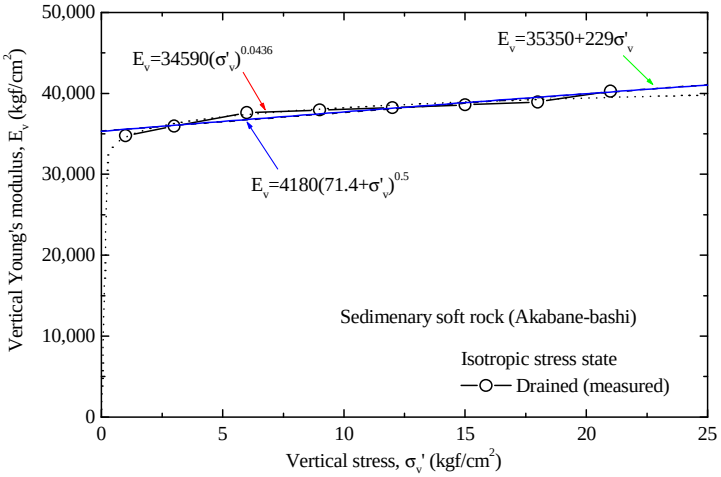

Figure 4.9c. Dependency of vertical quasi-elastic Young's modulus on the vertical stress; comparison of different functions; Akabane-bashi (Hayano 2001).

quasi-elastic Young's modulus in the vertical direction, E_v, was defined as shown in this figure. **Fig. 4.8a** shows the relationships between the quasi-elastic Young's modulus, E_v, obtained from undrained and drained conditions and the effective confining pressure, evaluated at various isotropic stress states using core samples of sedimentary soft rock retrieved from three sites (Sagamihara, 4A at Tokyo Bay mouth and Akabane-bashi), including those presented in Fig. 4.7. The axial strain rate in these tests was 0.01 %/min. The core samples from the three sites are all from sedimentary soft rock deposits of the Kazusa group, obtained by BS (Sagamihara and Akabane-bashi) and RCTS (Tokyo Bay mouth). The in-situ effective overburden pressure $(\sigma'_v)_0$ is about 5.0 kgf/cm^2 (Sagamihara), about 13.5 kgf/cm^2 (Tokyo Bay mouth) and about 1.0 kgf/cm^2 (Akabane-bashi). It may be seen from Fig. 4.8a that a pair of E_v values evaluated under undrained and nominally drained conditions are essentially the same, perhaps for the same reason described in relation to the data presented in Fig. 4.5. It may also be seen that the E_v value is noticeably pressure-dependent and the relationship is significantly non-linear.

Fig. 4.8b shows the same relationships plotted on a full-logarithmic scale. The data presented in this figure could be fitted with linear relationships:

$$E_v = (E_v)_0 \cdot \left(\sigma'_c / \sigma'_0\right)^m \tag{4.1}$$

where $(E_v)_0$ is the value of E_v when σ'_c is equal to σ'_0; and m is the exponent. Note that Eq. 4.1 cannot represent properly the measured relationships as the confining pressure σ'_c approaches zero. The following equation is therefore better than Eq. 4.1 to represent the E_v-σ'_c relation for a wider range of σ'_c starting from $\sigma'_c = 0$:

$$E_v = (E_v)_0 \cdot \left[\left(C + \sigma'_c / \sigma'_0\right)/(1+C)\right]^{0.5} = B \cdot \left(C \cdot \sigma'_0 + \sigma'_c\right)^{0.5} \tag{4.2}$$

where C and B are constants (B= $(E_v)_0 / \left[\sigma'_0 \cdot (1+C)\right]^{0.5}$). An exponent equal to 0.5 is used considering that the cohesive property of sedimentary soft rock is reflected in the coefficient C, while the pressure-dependency becomes the same as the average value for uncemented geomaterials, which is about 0.5, when the coefficient C is introduced.

Figs. 4.9a, **b** and **c** compare Eqs. 4.1 and 4.2 and another linear relation with the

respective measured relation. It may be seen that Eq. 4.1 can represent very well the respective measured relationship except when σ'_c is very close to zero. When it is necessary to fit the data for a range of σ'_c starting from zero to a certain value, Eq. 4.2 would be more relevant. Despite the limitations expressed above, the exponent *m* of Eq. 4.1 is used below to represent the pressure level-dependency of E_v, because the m values have been obtained for many other available sets of data. It may also be seen from Fig. 4.9 that a linear relation is not relevant.

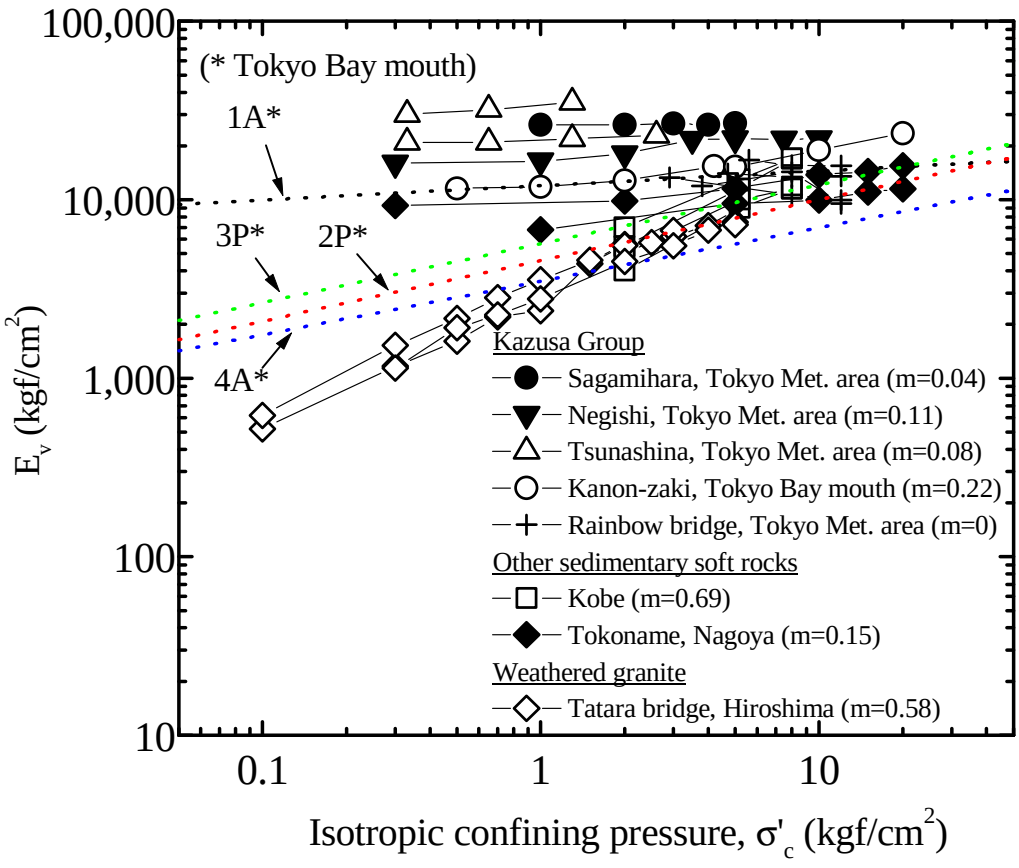

Figure 4.10. Pressure-dependency of vertical quasi-elastic Young's modulus of various types of sedimentary soft rock (Kodaka et al. 2000; Hayano 2001).

Fig. 3.21 shows the E_v - $log_{10}(\sigma'_c)$ relationships in the full-logarithmic scale, similar to those presented in Fig. 4.8b, obtained for the sedimentary soft rock deposits at the mouth of the Tokyo Bay. A close examination of the data presented in this figure shows that the exponent *m* is generally larger for larger particle diameters of the mother soil and for smaller geological ages. **Fig. 4.10** summarizes such relationships for different types of uncemented and cemented geomaterials, reported by Kohata et al. (1997), together with the average relations presented in Fig. 3.21.

The values of the exponent *m* for different types of geomaterial obtained as described above are plotted against the respective mean diameter D_{50} in **Fig. 4.11**. The values of D_{50} of sedimentary soft rock were obtained by crushing and grinding the respective oven-dried core sample until all the material passed a sieve with an opening of 0.42 mm. The geological ages for the sedimentary soft rocks referred to in this figure are as follows;

a) *Kazusa group at Sagamihara site;* The Kazusa group has a geological age

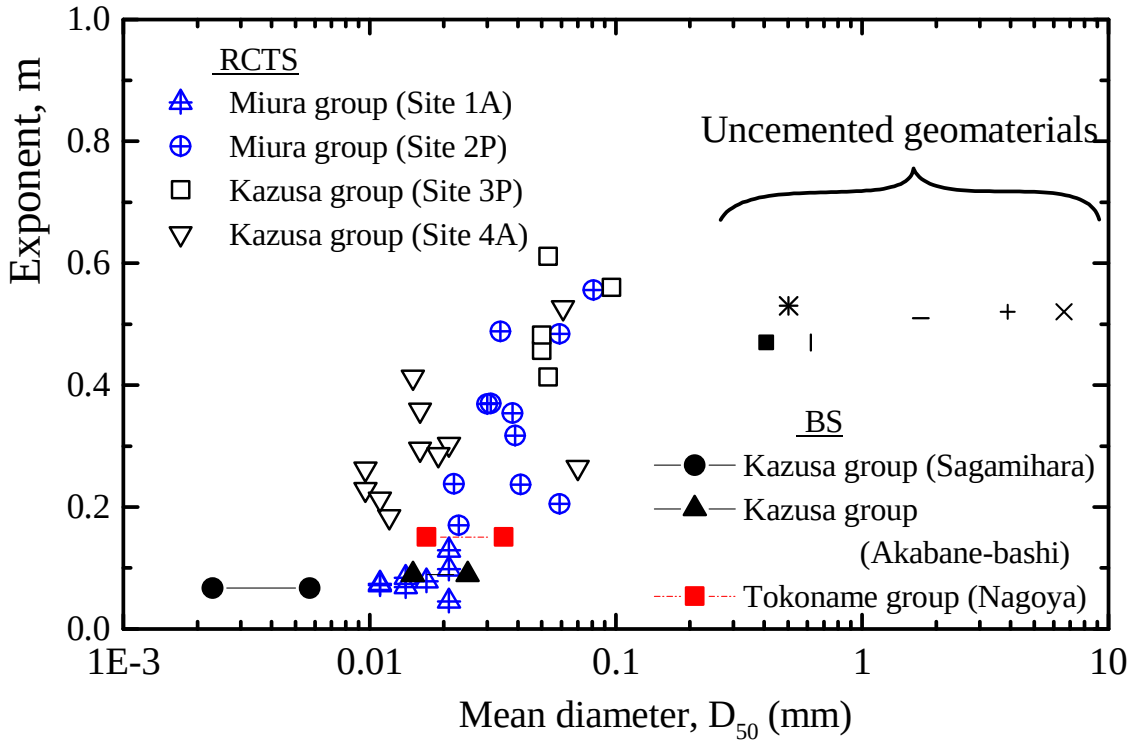

Figure 4.11. Relationship between the exponent *m* and the mean diameter D_{50} and the geological age (Hayano et al. 2000; Hayano, 2001).

from about one to five million years (the Pliocene to early Pleistocene epochs). The geological age at a depth of 50 m at the Sagamihara test site, from which the core samples that were used to obtain the data presented in Fig. 4.11 were retrieved, is estimated to be about 1.7 million years.

b) *Kazusa group at Akabane-bashi;* The core samples for the data presented in this figure were obtained by BS from a Kazusa group deposit at a construction site of a subway in the mid Tokyo (Miyazaki et al. 1999). The geological age of the deposit is estimated to be about two million years.

c) *Tokoname group in the Chita Peninsula (close to Nagoya City):* The geological age of the Tokoname group is about two to six million years of the late Miocene to Pliocene epochs. The core samples for the data presented in this figure were retrieved from the upper part of the deposit of this group.

d) *Tokyo Bay mouth;* The geological origin of the deposits changes from the Miura group (the Miocene epoch) on the western side to the Kazusa group (the Pliocene to early Pleistocene epochs) on the eastern side.

The following trends of behaviour may be seen from Fig. 4.11:

1) For the similar geological age, the exponent *m* for the sedimentary soft rock tends to become larger with an increase in D_{50}, approaching the average value for unbound granular materials reconstituted in the laboratory, which is about 0.5. This fact suggests that the development of cementation at inter-particle contacts is faster with soil having a smaller D_{50}.

2) For the same D_{50} value, the exponent *m* tends to become smaller with an increase in the geological age, approaching zero.

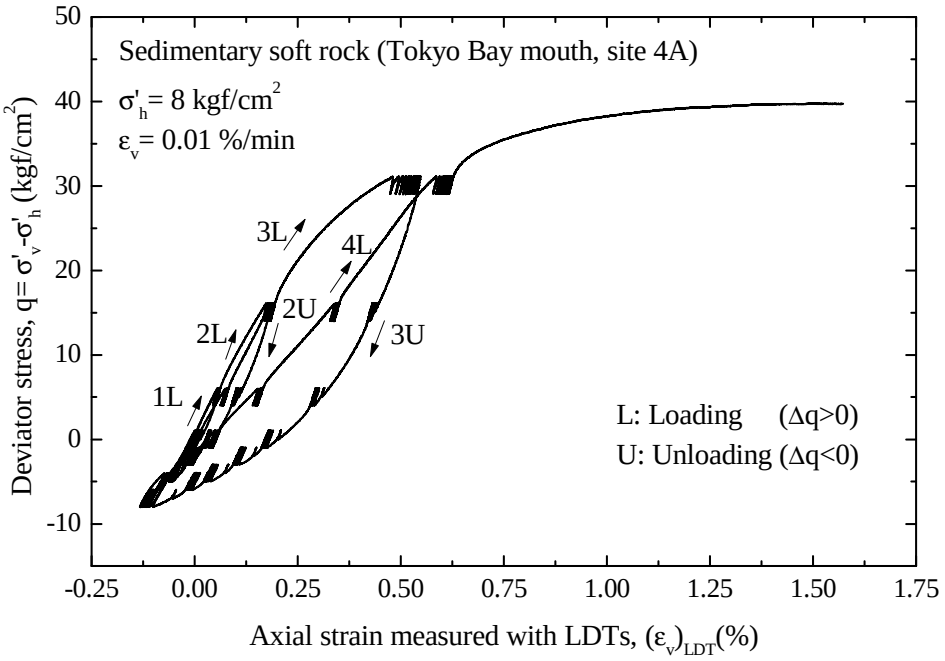

Figure 4.12. Overall stress-stress relation from a CD cyclic triaxial test measuring quasi-elastic properties, sedimentary soft rock, Tokyo Bay mouth, site 4A; Hayano et al. 1999b; Hayano 2001).

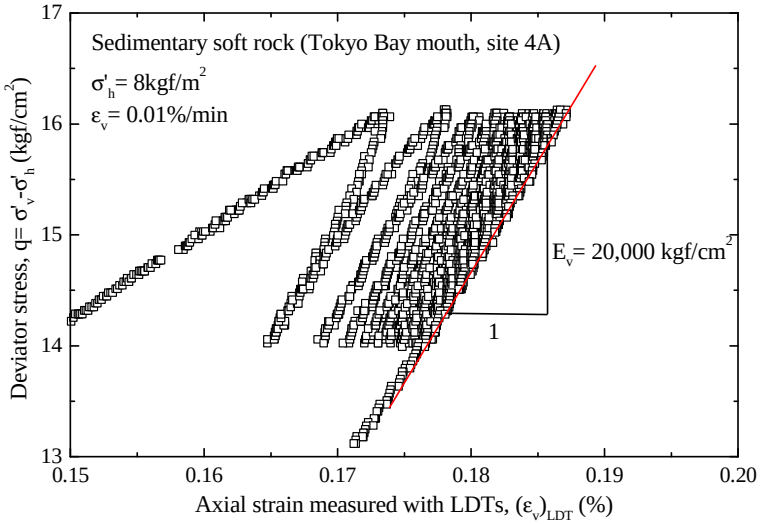

Figure 4.13. Stress-stress relations during small amplitude unload/reload cycles to measure quasi-elastic properties, sedimentary soft rock, Tokyo Bay mouth, site 4A; Hayano et al. 1999b; Hayano 2001).

3) Under otherwise the same conditions, the exponent *m* from TC tests using RCTS samples are generally higher than the values from TC tests using BS samples. Some RCTS samples of sedimentary soft rock of the Kazusa and Miura groups retrieved from the mouth of the Tokyo Bay that have D_{50} values of around 0.05 mm to 0.1 mm exhibit exponents *m* that are noticeably higher than 0.5. One of the reasons for this would be the effect of sample disturbance. Although this factor should be taken into account when estimating the exponent *m* under field stress conditions, the details of the effect of sample disturbance on the exponent *m* are not known.

Dependency of elastic Young's modulus on general stress states: With unbound (or uncemented) granular materials, the Young's modulus, E_x, defined for a major principal strain increment, $d\varepsilon_x = d\varepsilon_1$, taking place in the *x* direction is a rather unique function of the normal stress, σ'_x, acting in the *x* direction (Hardin 1978; Roesler 1979; Jamiolkowski et al. 1991; Tatsuoka et al. 1999a&b). Therefore, the ratio of the values of vertical and horizontal quasi-elastic Young's modulus E_v / E_h increases in a non-linear fashion with an increase in the stress ratio σ'_v / σ'_h, showing the stress system-induced anisotropy (Tatsuoka et al. 1999a-d).

Fig. 4.12 shows the overall stress-strain relationship from a special triaxial test in which a set of eleven 'drained' unload/reload cycles with a small strain amplitude were applied many times during otherwise drained monotonic loading and unloading in triaxial compression and extension. The test was performed at a constant effective confining pressure equal to the in-situ effective vertical stress (8 kgf/cm^2). The axial strain rate was

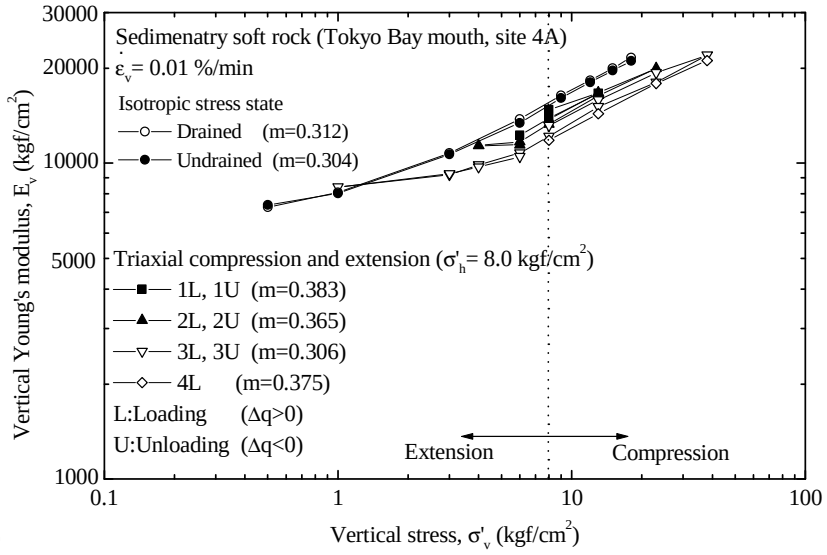

a)

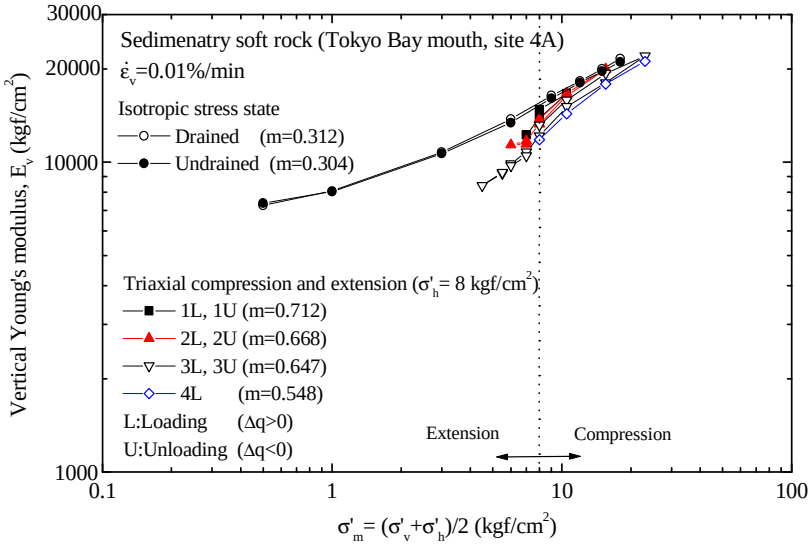

b)

Figure 4.14a&b. Dependency of vertical quasi-elastic Young's modulus on; a) vertical stress; and b) average stress, sedimentary soft rock, Tokyo Bay mouth, site 4A (Hayano et al. 1999b; Hayano 2001).

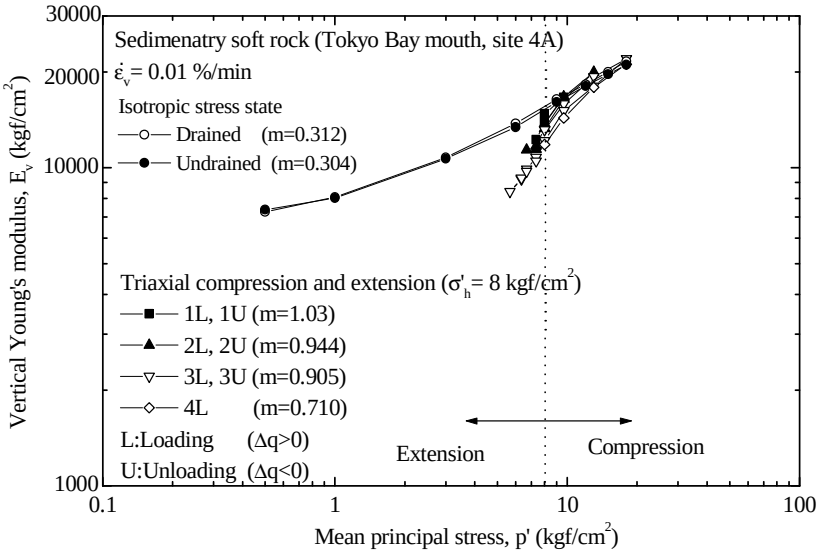

Figure 4.14c. Dependency of vertical quasi-elastic Young's modulus on mean principal stress, sedimentary soft rock, Tokyo Bay mouth, site 4A (Hayano et al. 1999b; Hayano 2001).

kept always equal to 0.01 %/min. An RCTS sample retrieved from site 4A at the mouth of the Tokyo Bay was used in this test. **Fig. 4.13** shows unload/reload stress-strain relations obtained at an anisotropic stress state in this test. The hysteresis loops at the initial stage of cyclic loading are not closed due to the development of residual strain caused by the viscous properties. The quasi-elastic Young's modulus E_v was defined for the last cycle where the viscous deformation had become negligible.

Fig. 4.14a shows the relationships between the E_v values under drained and undrained conditions and the vertical stress σ'_v evaluated at various isotropic stress states as well as those between the E_v values under drained conditions and σ'_v evaluated at various anisotropic stress states during otherwise globally cyclic triaxial loading (shown in Fig. 4.12). The following trends of behaviour may be seen from this figure:

1) The values of quasi-elastic Young's modulus, E_v, evaluated under undrained and nominally drained conditions at various isotropic stress states are generally similar. This indicates again that the drained conditions in these nominally drained tests could be essentially undrained.
2) The E_v values evaluated at various isotropic and anisotropic stress states are a rather unique function of σ'_v (as represented by Eqs. 4.1 and 4.2). On the other hand, the E_v values are not a unique function of the mean stress $\sigma'_m = (\sigma'_v + \sigma'_h)/2$ (**Fig. 4.14b**) nor the mean principal stress $p' = (\sigma'_v + 2\sigma'_h)/3$ (**Fig. 4.14c**). This conclusion could not be obtained confidently when the values of E_v were measured only under triaxial compression stress conditions.
3) In Fig. 4.14a, the E_v value becomes gradually smaller during global reloading, unloading and reloading when compared with those at the same σ'_v value at the isotropic stress states. This trend becomes stronger as the maximum and minimum shear stresses become larger during global cyclic loading. This phenomenon is due to effects of damage to cementation.

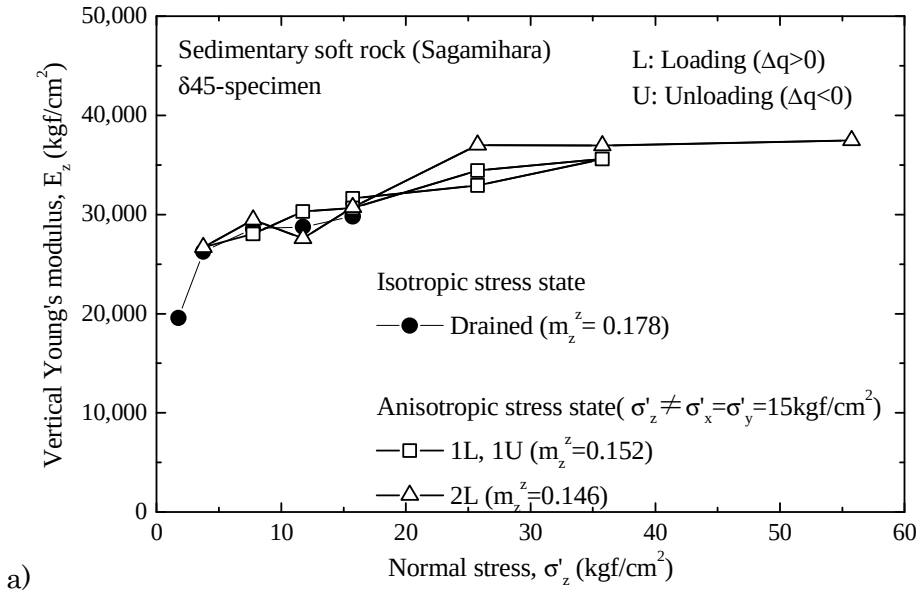

a)

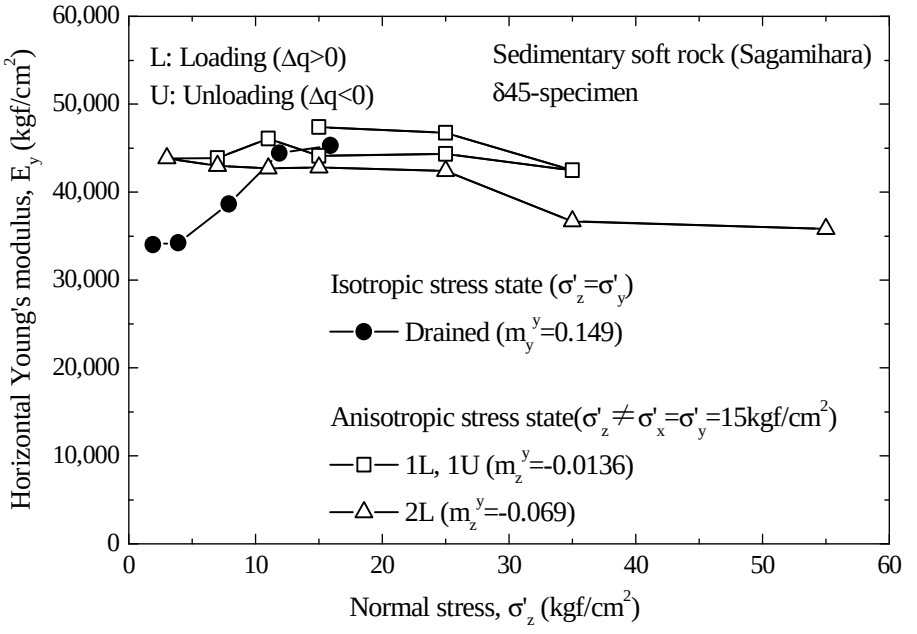

b)

Figure 4.15. Dependency of horizontal quasi-elastic Young's modus on the vertical stress at isotropic and anisotropic stress states, sedimentary soft rock, Sagamihara test site (δ = 45 degree sample) (Hayano et al. 1999a; Hayano 2001).

Figs. 4.15a and **4.15b** show the relationships between the E_z value and the normal stress σ'_z in the vertical direction and between the E_y value and σ'_z obtained from a true triaxial test using a rectangular prismatic specimen described in Fig. 2.6. The vertical direction of the sample during this true triaxial test is inclined at an angle of 45 degrees from the vertical direction in the field. In this test the values of E_z and E_y were evaluated at various isotropic stress state where $\sigma'_z = \sigma'_y$ and also during otherwise global cyclic loading of the axial stress σ'_z with a large amplitude at a constant σ'_y = 15 kgf/cm^2 (Hayano et al. 1999a). The following trends of behaviour may be seen from these figures:

1) The vertical elastic modulus, E_z, is a rather unique function of the vertical normal stress σ'_z irrespective of the stress ratio σ'_z/σ'_y, which is in

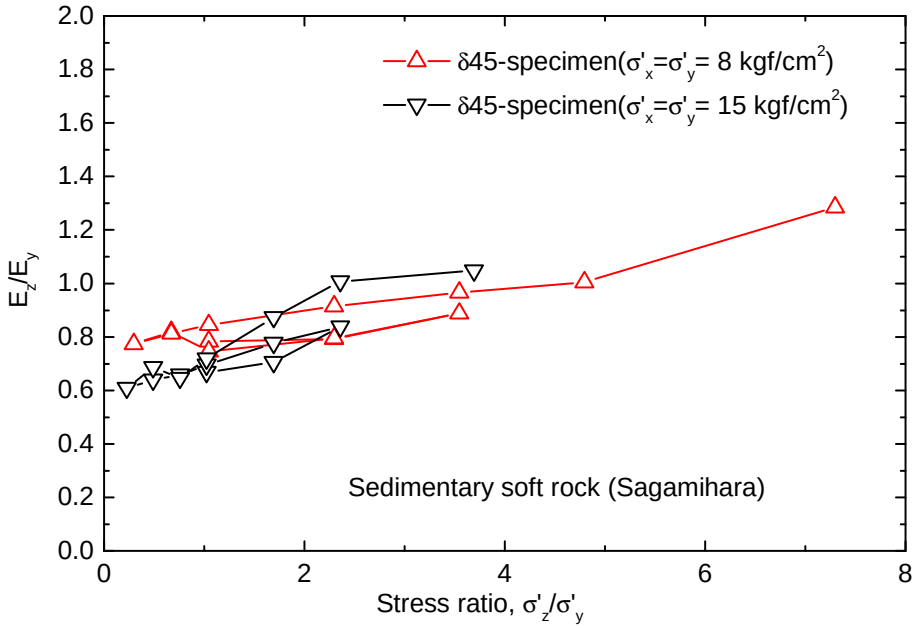

Figure 4.16. Dependency of the ratio of vertical to horizontal quasi-elastic Young's modulus on the stress ratio at various isotropic and anisotropic stress states, sedimentary soft rock, Sagamihara test site (δ = 45 degree sample) (Hayano et al. 1999a; Hayano 2001).

accordance with the results presented in Fig. 4.14. m_z^z means the exponent in Eq. 4.1 when the Young's modulus is E_z (as represented by the super-script *z*) and the normal stress is σ_z (as represented by the sub-script *z*); that is, m_z^z shows the effects of σ_z on E_z.

2) The horizontal elastic Young's modulus E_y increases noticeably with an increase in $\sigma'_z = \sigma'_y$ at the isotropic stress states. The exponent m_y^y shows the effects of σ_y on E_y. However, E_y is not sensitive to the change in the value of σ'_z when the horizontal normal stress σ'_y is kept constant. The exponent m_z^y shows the effects of σ_z on E_y. During global cyclic loading of σ'_z at a constant σ'_y, the values of E_y decreases gradually with an increase in the maximum value of σ'_z (i.e., as the previous maximum stress ratio σ'_z/σ'_y increases), which is likely due to the effects of damage.

Fig. 4.16 shows the relationships between the ratio of E_z/E_y and the stress ratio σ'_z/σ'_y obtained from the test described in Fig. 4.15 and another similar test. It may be seen that the ratio E_z/E_y noticeably increases with an increase in the stress ratio σ'_z/σ'_y, which is basically the same trend of behaviour as uncemented soils. A similar result of sedimentary soft rock was obtained by Kohata et al. (1995).

The test results presented above show that the elastic deformation properties of sedimentary soft rock, in particular those having the elastic deformation characteristics that are noticeably dependent on pressure level, could become more anisotropic at more anisotropic stress states in the similar way as uncemented granular materials.

Non-linearity due to Strain

As described above, the dependency of stiffness on pressure level of sedimentary

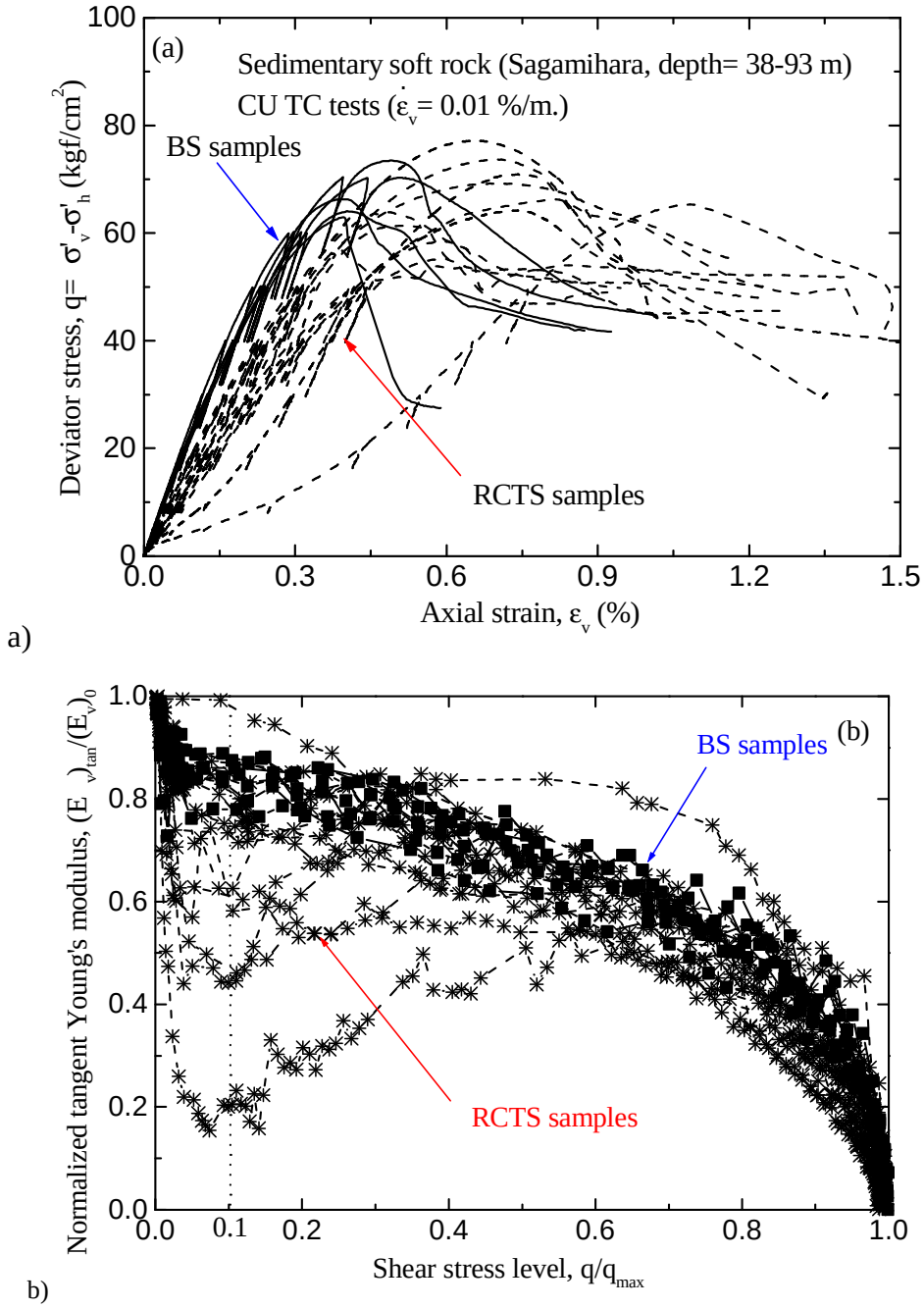

Figure 4.17. a) Deviator stress and axial strain relations; and b) normalized tangent Young's modulus and shear stress level relations of BS and RCTS samples, sedimentary soft rock, Sagamihara site (Wang 1996).

mudstone of the Kazusa group at the Sagamihara test site is relatively small. Thus, the non-linearity of stress-strain relation observed in CD or CU TC tests of BS samples (as shown in **Fig. 4.17a**) is due mostly to the non-linearity due to strain (or shear load level q/q_{max}).

The non-linearity of stress-strain relation could be sensibly represented by the relationship between $(E_v)_{tan}/(E_v)_o$ and q/q_{max} (Shibuya et al. 1991; Tatsuoka and Shibuya 1992), as those from CD TC tests shown in **Fig. 4.17b**, where $(E_v)_{tan}$ is the tangent Young's modulus and $(E_v)_o$ is the initial and maximum value of $(E_v)_{tan}$ (i.e., the elastic Young's modulus at the isotropic stress state, E_0). When the stiffness is noticeably dependent on pressure level, the non-linearity observed in a CD TC test is due to combined effects of strain

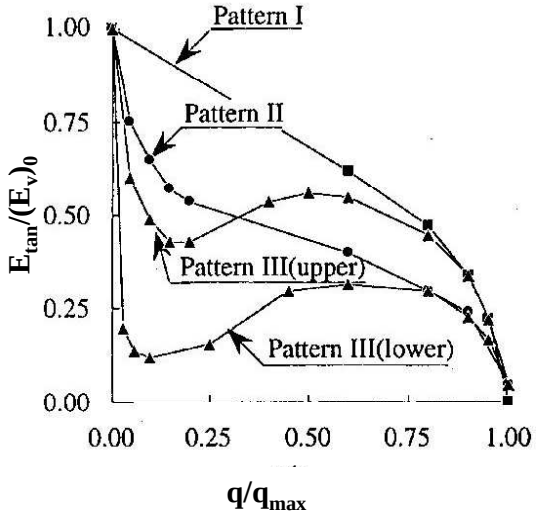

Figure 4.18. Four patterns of normalized tangent Young's modulus and shear stress level relations of RCTS samples, sedimentary soft rock, Sagamihara site (Tsubouchi et al. 1994; Tatsuoka et al. 1997a).

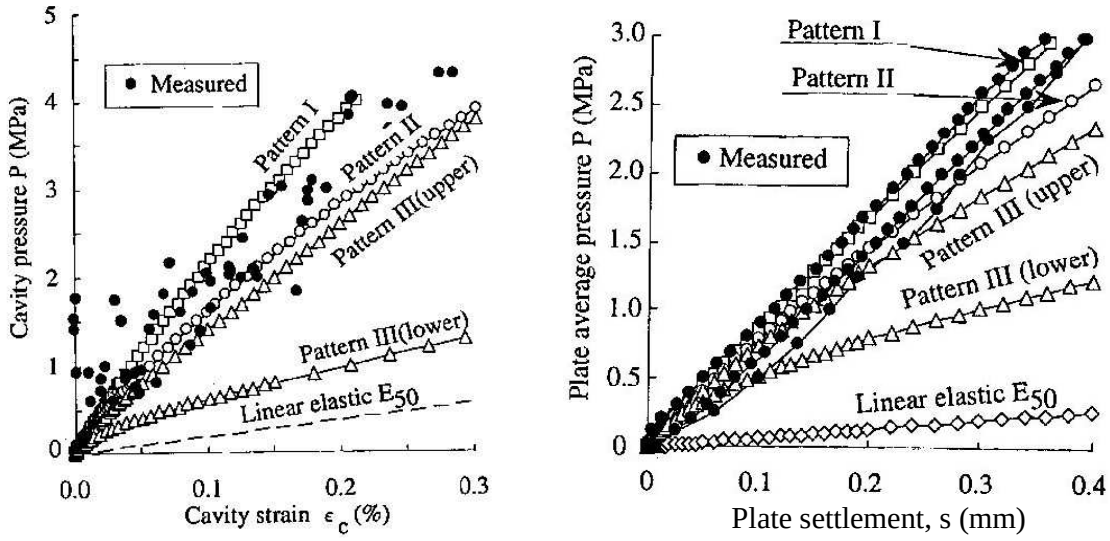

a) b)

Figure 4.19. Comparison between results from a) PMTs; and b) PLTs; and their FEM analysis based on different patterns of stress-strain relations of RCTS samples, Sagamihara site (Tsubouchi et al. 1994; Tatsuoka et al. 1997a).

(or q/q_{max}) and pressure level, as discussed in detail by Kohata et al. (1997). To obtain the value of pressure level-dependent $(E_v)_{tan}$ at an given stress state, Tatsuoka et al. (1999a) proposed an approximate method using the pressure level-independent $(E_v)_{tan}/(E_v)_o$ and q/q_{max} relationship while taking into account the effects of pressure level on the values of $(E_v)_o$ and q_{max}. It is to be noted that the stiffness of sedimentary soft rock becomes more pressure-dependent by sample disturbance. Therefore, an increased degree of non-linearity with the RCTS samples seen in Fig. 4.17 is associated with an increased pressure-dependency of stiffness.

It may also be seen from Figs. 4.17a and b that the non-linearity of stress-strain relationship is largely different between the BS and RCTS samples. In addition, the trend of

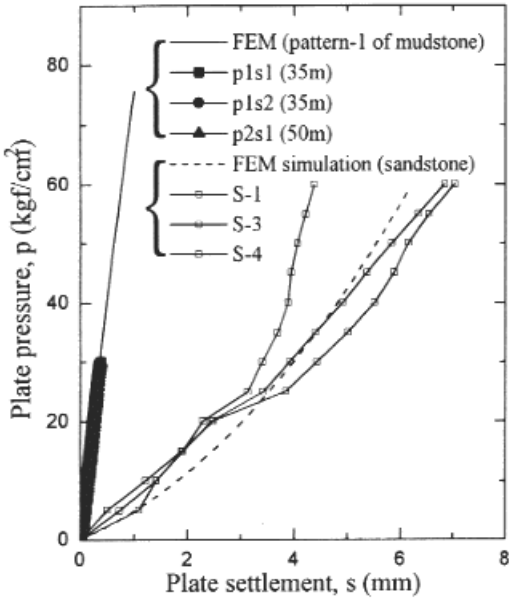

Figure 4.20. Comparison between results at larger strains from PLTs and their FEM analysis based on the field elastic shear wave velocity and non-linearity from laboratory stress-strain tests (based on Pattern I stress-strain relation of RCTS samples for Sagamihara site) (Tsubouchi et al. 1994; Tatsuoka et al. 1997a).

non-linearity is very similar among the BS samples (retrieved from a depth of about 50 m), while the variation in the non-linearity is tremendous among the RCTS samples. This is due to the effect of sample disturbances, which could be significantly different among different RCTS samples.

Tatsuoka et al. (1994) and Tatsuoka et al. (1997a) categorized the relationships between $(E_v)_{tan}/(E_v)_o$ and q/q_{max}, of the RCTS samples presented in Fig.4.17b into three different patterns, I, II, III(upper) and III(lower), as shown in **Fig. 4.18**. The curves denoted as Patterns I and II represent the respective average relationship, while the curves denoted as III (upper) and III (lower) show the upper and lower bounds. These relationships in the form of $E_{sec}/E_f (= E_{sec}/E_0) - \varepsilon_1$ relations are also presented in Fig. 4.1. Tsubouchi et al. (1994) and Tatsuoka et al. (1997a) also showed that the numerical analysis using the stress-strain relation Patterns I is most consistent with the results from PMTs (**Fig. 4.19a**) and those from PLTs (**Figs. 4.19b** and **4.20**). Fig. 4.20 also compares results from similar analysis of PLTs performed on a sandstone deposit of the Kobe group at the bottom of the excavation to a depth of 61 m where anchorage 1A for the Akashi Strait Bridge was constructed (Siddiquee et

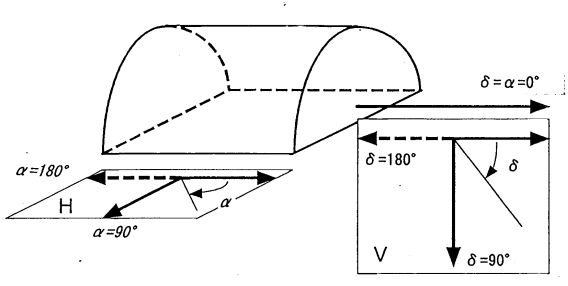

Figure 4.21a. Directions of DC sampling in the tunnel (at a depth of 50 m); Sagamihara site (Tatsuoka et al. 1997a).

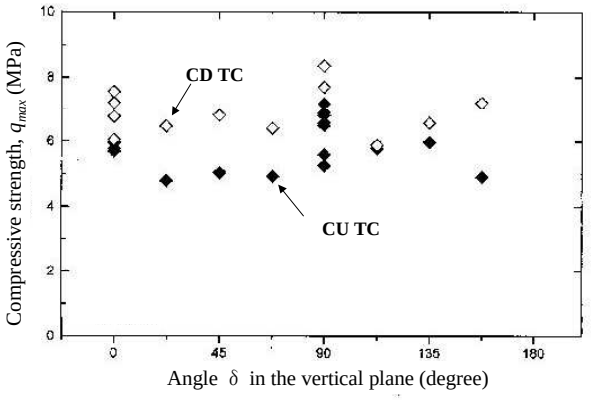

b)

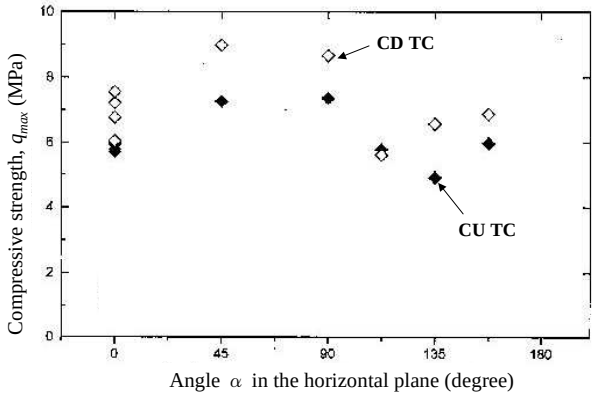

c)

Figure 4.21b&c. Compressive strength in different directions in the field from TC tests, Sagamihara site (Tatsuoka et al. 1997a).

al. 1994, 1995). In this analysis, the field stress-strain behaviour was estimated based on the field shear wave velocity and non-linearity due to strain and pressure level from laboratory stress-strain tests (i.e., TC tests). The effects of pressure level on the stiffness, which are usually much more important with sandstone than mudstone for a similar geological age, were taken into account by the approximate method described above.

Other Important Issues

Inherent anisotropy: **Fig. 4. 21** shows the compressive strength, q_{max}, and the initial and maximum Young's modulus, E_0, obtained from CU and CD TC tests performed on DC core samples retrieved from different directions in the tunnel at a depth of 50 m at the Sagamihara test site (Fig. 3.3a) (Tatsuoka et al. 1997a). It may be seen that the degree of inherent anisotropy in the deformation and strength characteristics is not significant, although it is not negligible. To obtain more general conclusions regarding this issue, a more systematic investigation at many other different places is necessary.

Strain localisation: Sedimentary soft rock exhibits shear banding when failing under pressure higher than a certain level. Hayano et al. (1999b) investigated this issue by performing plane strain compression (PSC) tests on BS core samples (12 cm high, 4 cm wide in the σ_3 direction and 6 cm long) of mudstone retrieved from a depth of about 50 m at the Sagamihara test site. The PSC apparatus is depicted in Fig. 2.4a. The deformation of shear bands was obtained by locally measuring both axial and lateral deformation as shown in Fig. 2.4b. They also performed TC tests on RCTS samples from the mouth of the Tokyo Bay to evaluate the deformation characteristics of shear bands by a method similar to the one

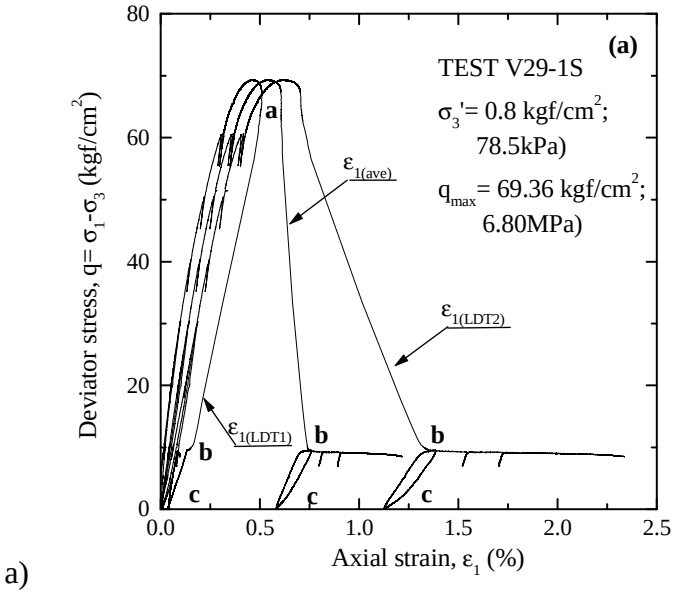

a)

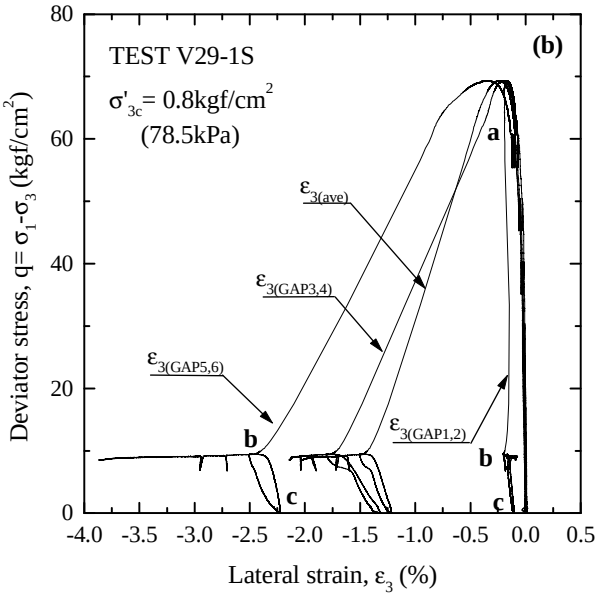

b)

Figure 4.22. Relationship between deviator stress and a) local axial strains and their average; and b) local lateral strains and their average from a PSC test, sedimentary soft rock, Sagamihara site, depth= 50 m (Hayano et al. 1999b).

illustrated in Fig. 2.4b

Figs. 4.22a shows the relationships between the deviator stress and the locally measured axial strains measured on the two opposite lateral planes, where σ'_3 was acting, and their average obtained from a PSC test at a confining pressure of 0.8 kgf/cm^2. **Figs. 4.22b** shows the relationships between the deviator stress and the lateral strains measured locally at three levels across a specimen width and their average from the PSC test. It may be seen from these figures that local strains $\varepsilon_{1(LDT1)}$ and $\varepsilon_{3(GAP1,2)}$, representing the deformation of the zones not including a shear band, exhibit an elastic rebound in the post-peak regime. **Fig. 4.23** shows the relationships between the shear stress acting along the shear band and the shear deformation of the shear band obtained from a series of PSC and TC tests. It may be seen that the shear stress drops from the peak value to the residual value

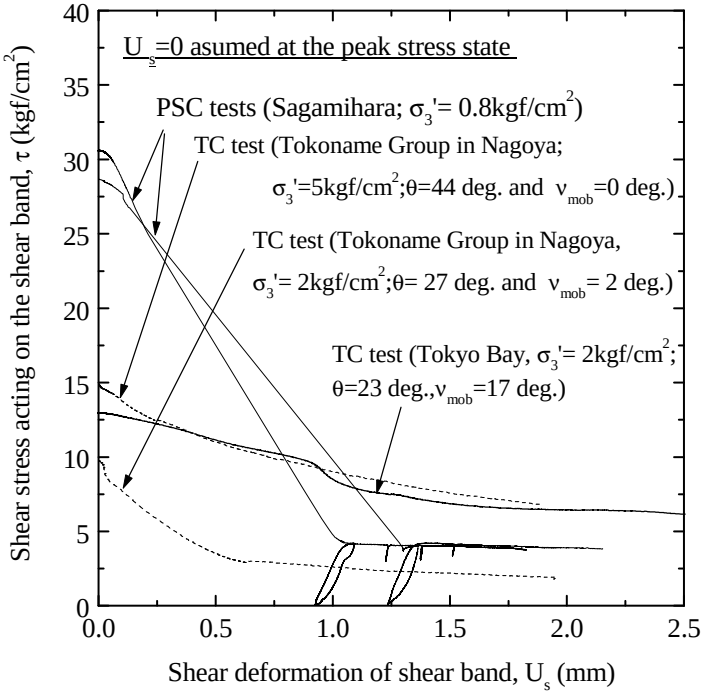

Figure 4.23. Relationships between shear stress and shear deformation of shear band from TC and PSC tests on several types of sedimentary soft rock (Hayano et al. 1999b).

after only a shear deformation increment in the order of 1 mm. Further study is necessary regarding the effects of soft rock type and confining pressure on this behaviour.

Viscous properties: The loading rate effects due to material viscous properties on the stress-strain behaviour of geomaterials, including sedimentary soft rock, could be significant, in particular as approaching the shear failure state (e.g., Tatsuoka et al. 2000, 2001). The stress-strain behaviour presented in Fig. 2.10 was obtained from a CD TC test in which the strain rate was changed stepwise several times and a couple of creep loading stages were included during otherwise monotonic loading. This behaviour was simulated by a non-linear three-component model illustrated in **Fig. 4.24** (Hayano et al. 2001). As the non-linear three-component model is described in details by Di Benedetto et al. (2002) and Tatsuoka et al. (2002), only the basic framework is presented below.

According to this model, a given strain increment is decomposed into elastic and inelastic (or irreversible) components as:

$$d\varepsilon = d\varepsilon^{e} + d\varepsilon^{ir} \tag{4.3}$$

The elastic strain increment is obtained by the hypo-elastic model（e.g., Hoque and Tatsuoka 1998; Tatsuoka et al., 1999a&c）as:

$$\&\& = \&/ E^{e}(\sigma) \tag{4.4}$$

where $E^e(\sigma)$ represents the elastic modulus (or more generally the elastic deformation stiffness matrix), which is a function of instantaneous stress σ as well as other soil parameters including instantaneous void ratio, stress history and etc. A given stress is decomposed into the inviscid (non-viscous) and viscous components as:

$$\sigma = \sigma^f + \sigma^v \tag{4.5}$$

where σ^f is the inviscid stress, which is a non-linear function of ε^{ir} (and stress history parameter in the case of cyclic loading). The loading rate-independent $\sigma^f \sim \varepsilon^{ir}$ relation, as represented as $\sigma^f(\varepsilon^{ir})$, is called the reference stress-strain relation. σ^v is the viscous stress representing the viscous properties. When σ^v is a unique function of the instantaneous irreversible strain ε^{ir} and its rate $\dot{\varepsilon}^{ir} = \partial\varepsilon^{ir}/\partial t$ (and others) irrespective of loading history in the case of monotonic loading, where $\dot{\varepsilon}^{ir}$ is always positive, this type of viscous property is called the isotach type (Suklje 1969). Generally, this type of viscous property could be represented as:

$$\sigma^v_{iso} = H''(\varepsilon^{ir}, \dot{\varepsilon}^{ir}, p, d, ...) \tag{4.6}$$

where σ^v_{iso} represents the viscous stress of the isotach type; and *H"* denotes a function of instantaneous values of ε^{ir} and $\dot{\varepsilon}^{ir}$ as well as other parameters, among which *p* and *d* represent the effects of instantaneous pressure level and specimen void ratio. As σ^f is a function of ε^{ir}, *p* and *d*, Eq. 4.6 could be simplified into:

$$\sigma^v_{iso} = H'(\sigma^f, \dot{\varepsilon}^{ir}) \tag{4.7}$$

where *H'* denotes a function of instantaneous values of σ^f and $\dot{\varepsilon}^{ir}$. The experimental results showed that the following specific form is relevant to geomaterials (Tatsuoka et al. 1999b, 2002):

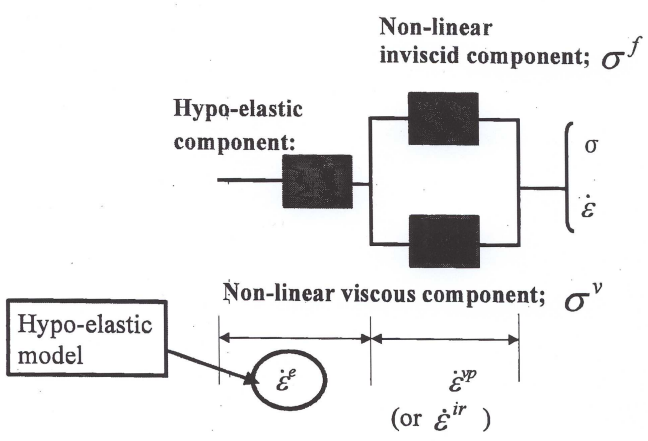

Figure 4.24. Framework of the non-linear three-component model (Di Benedettto et al. 2002; Tatsuoka et al. 2002).

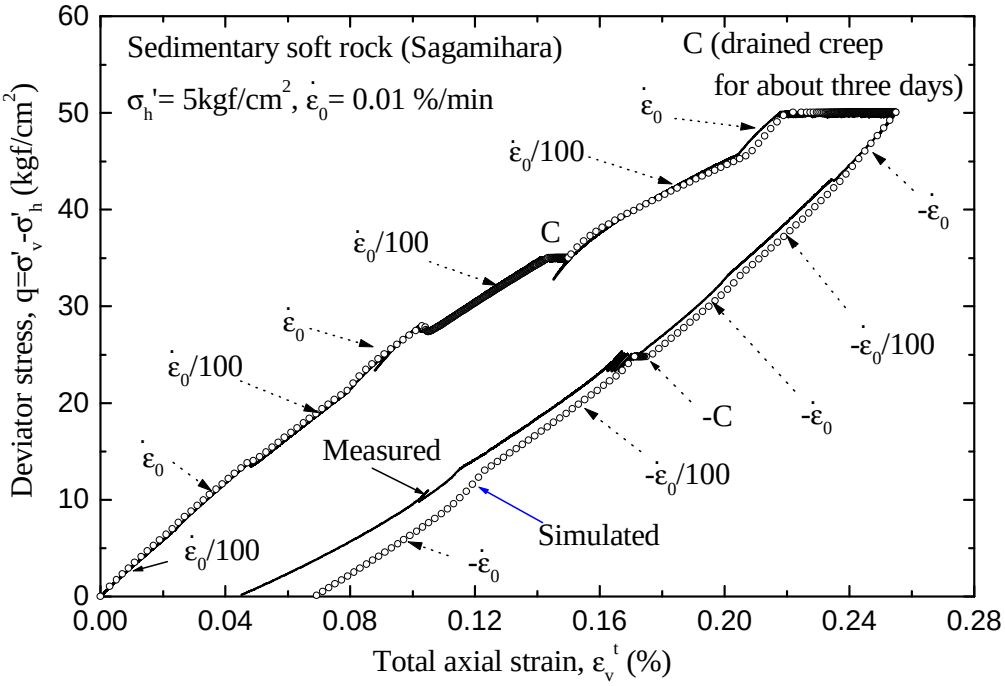

Figure 4.25. Simulation of deviator stress and axial strain relation from a CD TC test, sedimentary soft rock, Sagamihara site, depth= 50 m (Hayano 2001).

$$\sigma^{v}_{iso} = H_v(\sigma^f)\cdot g_v(\dot{\varepsilon}^{ir}). \tag{4.8}$$

where $H_v(\sigma^f)$ means a function of σ^f; and $g_v(\dot{\varepsilon}^{ir})$ is a non-linear function of $\dot{\varepsilon}^{ir}$, called the viscosity function. The simplest form of Eq. 4.8 is:

$$\sigma^{v}_{iso} = \sigma^f \cdot g_v(\dot{\varepsilon}^{ir}) \tag{4.9}$$

When Ea. 4.9 is relevant, from Eqs. 4.5 and 4.9, we have:

$$\sigma = \sigma^f\left(\varepsilon^{ir}\right) + \sigma^v\left(\dot{\varepsilon}^{ir}\right) = \sigma^f\left(\varepsilon^{ir}\right)\cdot\{1+g_v(\dot{\varepsilon}^{ir})\} \tag{4.10}$$

The previous study (Tatsuoka et al. 1999d: Di Benedetto et al. 2002: Tatsuoka et al. 2002) showed that the following non-linear function of $\dot{\varepsilon}^{ir}$ is relevant for $g_v(\dot{\varepsilon}^{ir})$:

$$g_v(\dot{\varepsilon}^{ir}) = \alpha\cdot[1-\exp\{1-(\frac{\dot{\varepsilon}^{ir}}{\dot{\varepsilon}^{ir}_f}+1)^m\}] \quad (\geq 0) \tag{4.11}$$

where α, $\dot{\varepsilon}^{ir}_f$ and m are the positive constants. According to Eq. 4.11, $g_v(\dot{\varepsilon}^{ir}) = 0$ when $\dot{\varepsilon}^{ir} = 0$, then we have a elasto-plastic response with $\sigma = \sigma^f\left(\varepsilon^{ir}\right)$. Therefore, this model could be perfectly continuous with any conventional elasto-plastic model. In addition, we have $g_v(\dot{\varepsilon}^{ir}) = \alpha$ when $\dot{\varepsilon}^{ir} = \infty$, which means another elasto-"plastic" response with $\sigma = (1+\alpha)\cdot\sigma^f\left(\varepsilon^{ir}\right)$. The model as formulated above has been called the new isotach model, since the model is based on the original proposal of Suklje (1964) while modifying some basic concepts (Tatsuoka et al. 1999d; 2000; 2001a). For the simulation of the test result presented in Fig. 2.10, the deviator stress $q = \sigma'_v - \sigma'_h$ is selected for the stress parameter σ. It may be seen from Fig. 2.10 that all the details of loading rate effects due to the material viscous properties are well simulated by the three-component model using the same

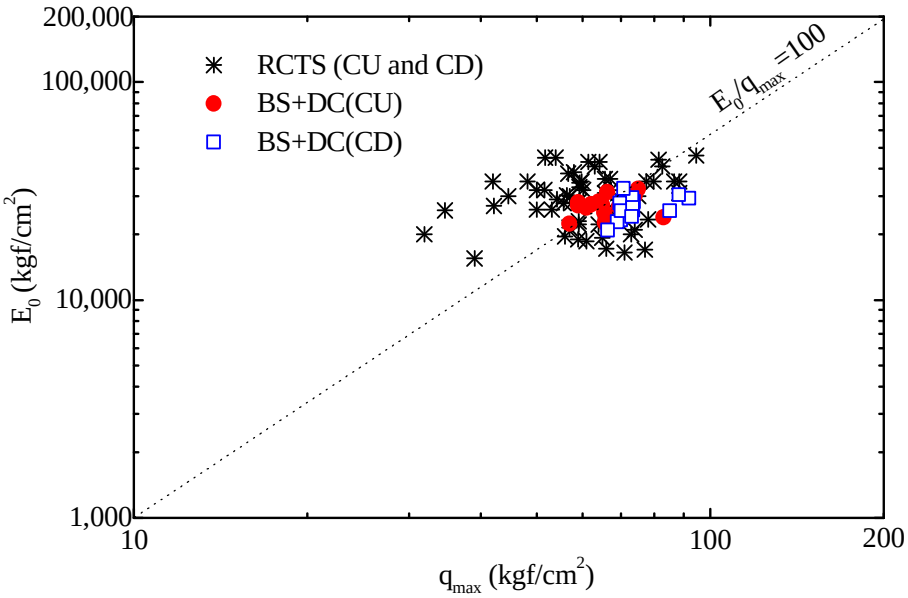

Figure 4.26. Comparison between initial Young's modulus and compressive strength from TC tests, sedimentary soft rock, Sagamihara site (Hayano et al. 2000; Hayano 2001).

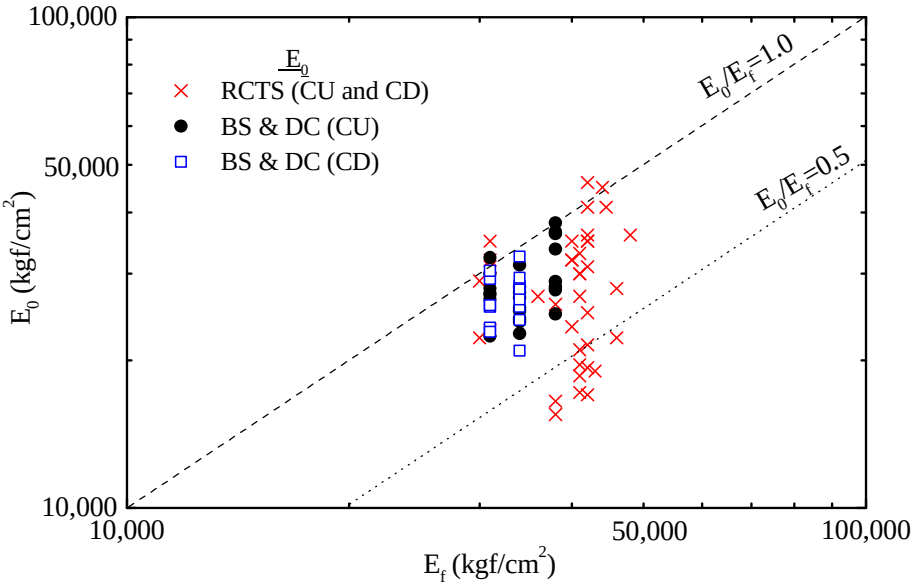

Figure 4.27. Comparison between initial Young's modulus from TC tests on RCTS and BS&DC samples and elastic Young's modulus from field shear wave velocity, sedimentary soft rock, Sagamihara site (Hayano et al. 2000; Hayano 2001).

parameters for the whole of the test result.

Fig. 4.25 shows part of the result from another CD TC test with several stepwise changes in the strain rate and creep loading stages during otherwise global loading and unloading and its simulation by the non-linear three-component model. In this test, the axial strain increment at the creep loading stage during otherwise global unloading is negative (i.e., the creep recovery phenomenon). It may also be seen that the non-linear three-component model is able to simulate the loading rate effects due to the viscous properties (i.e., effects of step change in the strain rate and creep deformation) of sedimentary soft rock during not only

global loading but also global unloading. More detailed discussions on this model simulation of the stress-strain-time behaviour of sedimentary soft rock are given in Hayano et al. (2001).

Note that the non-linear three-component model is a direct extension of the conventional elasto-plastic modelling by introducing the viscous stress component. That is, the conventional elasto-plastic model is equivalent to the three-component model lacking the viscous stress component.

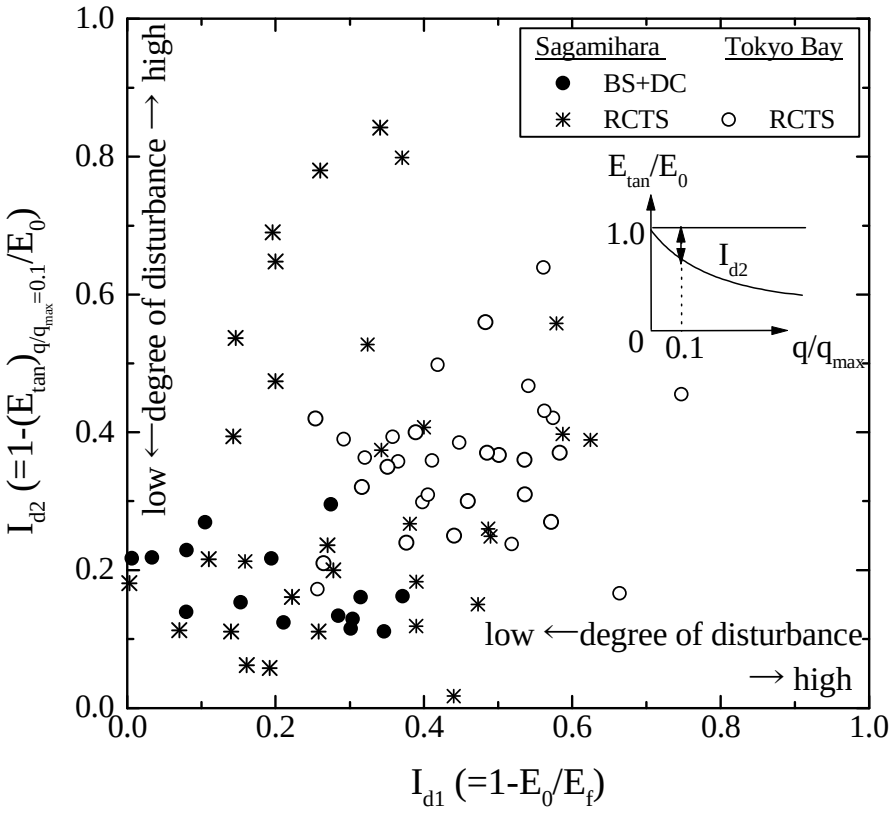

Figure 4.28. Correlation between two indexes for sample disturbance for sedimentary soft rock (Hayano et al. 2000; Hayano 2001).

Sample Disturbance

It may be seen from Fig. 4.17 that the effects of sample disturbance on the non-linearity due to strain and pressure level of pre-peak stress-strain relationship could be significant. Tatsuoka et al. (1995b) showed that the effects of sample disturbance with RCTS samples of sedimentary soft rock are generally larger in the order of the non-linearity of pre-peak stress-strain relationship, the peak strength and the initial Young's modulus. This point is also discussed below referring to a large amount of data including those obtained after the previous paper (Tatsuoka et al. 1995b).

Fig. 4.26 compares the relationships between the initial Young's modulus E_0 ($=(E_v)_0$) and the compressive strength q_{max} for the BS & DC samples and the RCTS samples retrieved from the Sagamihara test site. **Fig. 4.27** shows the relationship between the initial Young's modulus E_0 and the elastic Young's modulus from field shear wave velocity,

corresponding to those presented in Fig. 4.26. It may be seen from Fig. 4.26 that with the RCTS samples, the scatter of initial Young's modulus E_0 is much smaller than that of compressive strength q_{max}. Yet, as seen from Fig. 4.27, the scatter of initial Young's modulus E_0 is much larger with the RCTS samples than with the BS & DC samples. In addition, the E_0 value is generally smaller than the field value E_f to a large extent with the RCTS samples than with the BS and DC samples. It is also to be noted that even the E_0 values of the BS and DC samples are generally smaller than the field value E_f.

Based on the facts described above, the following two indexes were proposed to represent the degree of sample disturbance with sedimentary soft rocks (Hayano et al. 2000; Hayano 2001):

1) Index $I_{d1} = 1 - E_0 / E_f$
2) $I_{d2} = 1 - (E_v)_{tan.q/q_{max}=0.1} / E_0$, where $(E_v)_{tan.q/q_{max}=0.1}$ is the tangent Young's modulus $(E_v)_{tan}$ when the shear stress level q/q_{max} is equal to 0.1.

The index I_{d2} was proposed considering that the value of $(E_v)_{tan}$ tends to become the minimum when q/q_{max} becomes around 0.1 (see Fig. 4.17b). Core samples having $I_{d1} = I_{d2} = 0.0$ are considered to have not been disturbed at all, while those having higher values of I_{d1} and I_{d2} are considered to be highly disturbed. **Fig. 4.28** shows the relationship between these two indexes for the data of the core samples of sedimentary soft rock retrieved from the Sagamihara test site and the mouth of the Tokyo Bay.

The following trends of behaviour may be seen from this figure:

1) The values of I_{d1} and I_{d2} are generally higher with the RCTS samples than with the BS and DC samples.
2) The correlation between I_{d1} and I_{d2} is not high. In particular, the value I_{d2} is relatively large opposed to relatively small values of I_{d1} for a number of data. This fact means that the comparison between the laboratory value E_0 $(=(E_v)_0)$ and the field value E_f may not be sufficient to evaluate the effects of sample disturbance on the whole stress-strain properties of a given core sample of sedimentary soft rock, but another index, such as I_{d2}, is necessary for a more confident evaluation of the effects of sample disturbance.

CONCLUSIONS

The following conclusions can be derived from the results from laboratory and field tests and full-scale observations with respect to the strength and deformation characteristics of sedimentary soft rock:

1. Relevant laboratory stress-strain tests can play essential roles in characterizing the non-linear stress-strain-time properties of sedimentary soft rock as it has been the case in a number of research and construction projects in the Tokyo metropolitan area and others in Japan.
2. The elastic (or quasi-elastic) deformation characteristics could be evaluated by triaxial tests using high-quality samples while measuring stresses and strains accurately. In particular, axial strains could be evaluated accurately and sensibly by using a local gauge, such as LDTs. The elastic stiffness defined at strains less than about 0.001 % from such triaxial tests as described above is consistent with the field value from shear wave

velocities measured by field seismic surveys in a number of research and construction projects.

3. The elastic deformation characteristics are a function of instantaneous stress, which could be formulated by a hypo-elastic model, in a similar manner with the one for uncemented granular materials.
4. The deformation of a sedimentary soft rock deposit and displacements of structures constructed on and in it at working loads could be reliably predicted or simulated based on the elastic stiffness evaluated by field seismic survey, while taking into account the dependency of stiffness on strain and pressure level evaluated by relevant laboratory stress-strain tests using high-quality core samples.
5. The degree of inherent anisotropy in the strength and deformation characteristics of sedimentary soft rock (mudstone) at the Sagamihara test site was not significant.
6. In the post-peak regime in PSC and TC tests, the shear stress drops from the peak value to the residual value after only a shear deformation increment in the order of 1 mm.
7. Loading rate effects due to the material viscous properties, including creep deformation and changes in the stress associated with step and gradual changes in the strain rate, not due to the migration of pore water, could be reasonably simulated by a non-linear three-component model, called the new isotach model.
8. Core samples retrieved by the conventional rotary core tube sampling method could be noticeably disturbed. Two indexes are proposed to represent the sample disturbance of sedimentary soft rock.

ACKNOWLEDGEMENTS

The authors are grateful to Dr. Yamamuro, J.A., the University of Delaware, for his kind review of the manuscript.

REFERENCES

Anh Dan,L.Q., Koseki,J. and Tatsuoka,F. 2001. Viscous deformation in triaxial compression of a dense well-graded gravel and its model simulation, *Advanced Laboratory Stress-Strain Testing of Geomaterials* (Tatsuoka et al. eds), Balkema, pp.187-194.

Burland,J.B. 1989. Small is beautiful -the stiffness of soils at small strains, *Canadian Geotechnical Journal*, Vol.26, pp.499-516.

Di Benedetto,H. and Tatsuoka,F. 1997. Small strain behaviour of geomaterials: Modelling of strain rate effects, *Soils and Foundations*, Vol.37, No.2, pp.127-138.

Di Benedetto,H., Tatsuoka,F. and Ishihara,M. 2002. Time-dependent deformation characteristics of sand and their constitutive modelling, *Soils and Foundations*, 42-2, pp.1-22.

Goto.S, Tatsuoka,F., Shibuya,S., Kim,Y.-S., and Sato,T. 1991. A simple gauge for local small strain measurements in the laboratory, *Soils and Foundations*, Vol.31, No.1, pp.169-180.

Hardin,B.O. 1978. The nature of stress-strain behavior for soils, *Proc. Geotech. Div. Specialty Conf. on Earthquake Eng. and Soil Dynamics, ASCE, Pasadena*, Vol.1, pp.3-90.

Hayano,K., Sato,T. and Tatsuoka,F. 1997. Deformation characteristics of a sedimentary softrock from triaxial compression tests rectangular prism specimens", *Géotechnique*,

Vol.47, No.3, pp.439-449.
Hayano,K., Tatsuoka,F. and Yoshiizumi,N. 1998. Modeling pre-failure stress-strain properties of sedimentary softrocks based on very small strain stiffness, *Nondestructive and Automated Testing for Soil and Rock Properties, ASTM STP 1350* (Marr & Fairhurst eds.), pp.259-275.
Hayano,K., Tatsuoka,F., Koseki,J. and Sato,T. 1999a. Small strain deformation characteristics of sedimentary soft mudstone from true triaxial tests, *Proc. Second Int. Conf. on Pre-Failure Deformation Characteristics of Geomaterials, IS Torino '99* (Jamiolkowski et al., eds.), Balkema, Vol.1, pp.191-198.
Hayano,K., Maeshiro,T., Tatsuoka,F., Sato,T., Wang,L. and Kodaka,T. 1999b. Shear banding in a sedimentary soft mudstone subjected to plane strain compression, *Geotechnical Testing Journal, ASTM*, Vol.22, No.1, pp.67-79.
Hayano,K., Matsumoto,M., Tatsuoka,F. and Koseki,J. 2001. Evaluation of time-dependent deformation property of sedimentary soft rock and its constitutive modeling, *Soils and Foundations*, Vol.41, No.2, pp. 21-38.
Hayano,K., Tatsuoka,F. and Koseki,J. 2000. The effect of sample disturbance on the deformation characteristics of sedimentary soft rocks and its evaluation", *Proc. of JGS Symposium on Rotary Sampling Techniques and Evaluation of Properties on Soft Rocks and Hard Soils,* pp.105-08 (in Japanese).
Hayano,K. 2001. Pre-failure deformation characteristics of sedimentary soft rock, *PhD thesis, University of Tokyo* (in Japanese).
Hight,D.W. and Higgins,K.G. 1995. An approach to the prediction of ground movements in engineering practice: Background and application, *Proc. of Int. Symposium Pre-Failure Deformation of Geomaterials* (Shibuya et al., eds.), Balkema, Vol.2, pp.909-945.
Hoque,E., Tatsuoka,F. and Sato,T. 1996. Measuring anisotropic elastic properties of sand using a large triaxial specimen, *Geotechnical Testing Journal*, ASTM, Vol.19, No.4, pp.411-420.
Hoque,E., and Tatsuoka,F. 1998. Anisotropy in the elastic deformation of materials, Soils and Foundations, *Soils and Foundations*, Vol.38, No.1, pp.163-179.
Hoshino,K. 1993. Geological evolution from the soil to the rock: mechanical lithification and change of mechanical properties, *Geotechnical Engineering of Hard Soils- Soft Rocks* (Anagnostopoulos et al. eds.), Balkema, Vol.1, pp.131-138.
Izumi,K., Ogihara,M. and Kameya,H. 1997. Displacements of bridge foundations on sedimentary softrock; a case study on small strain stiffness, *Gèotechnique*, Vol.47, No.3, pp.619-632.
Jamiolkowski,M., Leroueil,S., and Lo Presti,D.C.F. (1991): Design parameters from theory to practice, Theme Lecture, *Proc. Geo-Coast '91, Yokohama,* Vol.2, pp.877-917.
Jardine,R.J., St.John,H.D., Hight,D.W. and Potts,D.M. 1991. Some practical applications of a non-linear ground model, *Proc. 10th European Conference on SMFE*, Firenze, Vol.1, pp.223-228.
Jardine,R.J. 1995. One perspective of the pre-failure deformation characteristics of some geomaterials, *Proc. of Int. Symposium Pre-Failure Deformation of Geomaterials* (Shibuya et al., eds.), Balkema, Vol.2, pp.855-885.
Jiang,G.L., Tatsuoka,F., Flora,A. and Koseki,J. 1997. Inherent and stress state-induced anisotropy in very small strain stiffness of a sandy gravel, *Géotechnique,* Vol.47, No.3, pp.509-521.
Kawasaki,S., Nishi,K. and Fujikawa,Y. 1983. Mechanical properties of deep soft rock ground in the suburbs, *Geotechnical Engineering of Hard Soils- Soft Rocks* (Anagnostopoulos et al. eds.), Balkema, Vol.1, pp.593-600.

Kim,Y.-S., Tatsuoka,F. and Ochi,K. 1994. Deformation characteristics at small strains of sedimentary soft rocks by triaxial compression tests", *Géotechnique*, Vol.44, No.3, pp.461-478.

Kodaka,T., Koseki,J., Hayano,K., Hojo,Y. and Itabashi,T. 2000. Study on the deformation and strength characteristics of soft rock at the Tokyo Bay mouth from field stress-strain tests and laborartory tests, *Proc. of JGS Symposium on Rotary Sampling Techniques and Evaluation of Properties on Soft Rocks and Hard Soils*, pp.161-166 (in Japanese).

Kohata,Y., Wang,L., Tatsuoka,F., Ochi,K. and Tsubouchi,T. 1995. Inherent and induced anisotropy of sedimentary softrock", *Proc. of the 10th Asian Regional Conf. on S.M.F.E., Beijing*, Vol.1, pp.33-36.

Kohata,Y., Tatsuoka,F., Mukabi,J.N. and Suzuki,M. 1995. Effects of strain rate and drainage on deformation characteristics at small stain of geomaterials, *Earthquake Geotechnical Engineering (*Ishihara eds.), Balkema, pp.151-156.

Kohata,Y., Tatsuoka,F., Wang,L., Jiang,G.L., Hoque,E. and Kodaka,T. 1997. Modelling the non-linear deformation properties of stiff geomaterials, *Géotechnique*, Vol.47, No.3, pp.563-580.

Kongsukprasert,L., Kuwano,R and Tatsuoka,F. (2001): Effects of ageing with shear stress on the stress-strain behavior of cement-mixed sand, *Advanced Laboratory Stress-Strain Testing of Geomaterials* (Tatsuoka et al. eds.), Balkema, pp.251-258.

Koseki,J., Tatsuoka,F., Yoshimine,M., Hatanaka,M., Uchida,K., Yasufuku,N. and Furuta,I. 2001. Report on applications of laboratory stress-strain test results of geomaterials to geotechnical practice in Japan, *Advanced Laboratory Stress-Strain Testing of Geomaterials* (Tatsuoka et al. eds.), Balkema, pp.111-184.

Matsumoto,M., Hayano,K., Sato,T. and Tatsuoka,F. 1999. Time effects on stress-strain properties at small strains of sedimentary soft mudstone, *Proc. Second Int. Conf. on Pre-Failure Deformation Characteristics of Geomaterials, IS Torino '99* (Jamiolkowski et al., eds.), Balkema, Vol.1, pp.313-321.

Matsumoto,M., Hayano,K., Tatsuoka,F. and Koseki,J. 2000. Long-term Deformation of Sedimentary Soft Rock Associated with Underground Excavation, *Tsuchi-to-Kiso*, Vol. 48, No. 2, pp. 13-16 (in Japanese).

Miyazaki,K., Hayano,K., Tatsuoka,F. and Koseki,J. 1999. Deformation of sedimentary soft rock in deep excavation, *Proc. Second Int. Conf. on Pre-Failure Deformation Characteristics of Geomaterials, IS Torino '99* (Jamiolkowski et al., eds.), Balkema, Vol.1, pp.809-817.

Nawir,H., Kuwnao,R. and Tatsuoka,F. (2001): Effects of stress path on the flow rule of sand in triaxial compression, *Advanced Laboratory Stress-Strain Testing of Geomaterials* (Tatsuoka et al., eds), Balkema, pp.287-294.

Ochi,K, Tsubouchi,T. and Tatsuoka,F. 1993. Stiffness of sedimentary soft rock from in situ and laboratory tests and from field behaviour, *Proc. of Inter. Conf. on Geotechnical Engineering of Hard Soils - Soft Rocks* (Anagnostopoulos et al. eds.), Vol.1, Balkema, pp.707-714.

Ochi,K., Tsubouchi,T. and Tatsuoka,F. 1994. Deformation characteristics of sedimentary soft rock evaluated by full-scale excavation", *Proc. of Int. Symposium Pre-Failure Deformation of Geomaterials* (Shibuya et al., eds.), Balkema, Vol.1, pp.601-607.

Roesler,S.K. (1979): Anisotropic shear modulus due to stress anisotropy, *Jour. of GE Div., ASCE*, Vol.105-GT7, pp.871-880.

Santucci de Magistris,F., Koseki,J., Amaya,M., Hamaya,S., Sato,T. and Tatsuoka,F. 1999. A triaxial testing system to evaluate stress-strain behaviour of soils for wide range of strain and strain rate, *Geotechnical Testing Journal, ASTM*, Vol.22, No.1, pp.44-60.

Sato,M., Ueda.M, Hasebe,N. and Kondo,H. 1997a. Comparison among wave velocities from seismic observation waves and field tests for hard rock mass, *Journal of Japanese Society for Civil Engieers,* Vol.III-38, pp.75-87 (in Japanese).

Sato,M., Ueda.M, Hasebe,N. and Umehara,H. 1997b. Dynamic elastic modulus of dam concrete earthquake motion, *Journal of Japanese Society for Civil Engieers,* Vol.V-35, pp.43-55(in Japanese).

Shibuya,S., Tatsuoka,F., Abe,F., Kim,Y.-S., Park,C-S. and Mukabi,J.N. 1991. A new look at stress-strain relations of soils and soft rocks, *Proc. of the 9th Asian Regional Conf. on SMFE,* Bangkok, Vol.1, pp.63-66.

Shibuya,S., Tatsuoka,F., Teachavorasinskun,S., Kong,X.J., Abe,F., Kim,Y.S. and Park,C.-S. 1992. Elastic Deformation Properties of Geomaterials", *Soils and Foundations,* Vol.32, No.3, pp.26-46.

Siddiquee,M.S.A., Tatsuoka,F., Hoque,E., Tsubouchi,T., Yoshida,O., Yamamoto,S. and Tanaka,T. 1994. FEM simulation of footing settlement for stiff geomaterials, *Proc. of Int. Symposium Pre-Failure Deformation of Geomaterials* (Shibuya et al., eds.), Balkema, Vol.1, pp.531-537.

Siddiquee,M.S.A., Tatsuoka,F., Kohata,Y., Yoshida,O. and Yamamoto,Y. and Tanaka,T. 1995. Settlement of a Pier Foundation for Akashi- Kaikyo Bridge and its numerical analysis, *Proc. Int. Workshop on Rock Foundation of Large-Scale Structures,* Tokyo, Balkema, pp.413-420.

Suklje, L. 1969. Rheological aspects of soil mechanics. *Wiley-Interscience,* London.

Takeuchi,T., Tanaka,S., Tanaka,T. and Nishida,K. 1981. Analysis of various actors influencing deformation, *Proc. Int. Symposium on Weak Rocks,* Tokyo, Vol.1, pp375-380.

Tatsuoka,F. 1988. Some recent developments in triaxial testing system for cohesionless soils, *Advanced Triaxial Testing of Soil and Rock, ASTM STP No.977,* pp.7-67.

Tatsuoka,F., Yamada,K., Yasuda,M., Yamada,S. and Manabe,S. 1991.Cyclic undrained behaviour of an undisturbed gravel for aseismic design of a bridge foundation, *Proc. of the Second Int. Conf. on Recent Advances in Geotechnical Earthquake Engineering and Soil Dynamics,* St Louis (Prakash eds.), Vol.1, pp.141-148.

Tatsuoka,F. and Shibuya,S. 1991. Deformation characteristics of soils and rocks from field and laboratory tests, Keynote Lecture for Session No.1, *Proc. of the 9th Asian Regional Conf. on SMFE,* Bangkok, Vol.2, pp.101-170.

Tatsuoka,F., Kohata,Y., Mizumoto,K. Kim,Y.-S., Ochi,K. and Shi,D. 1993. Measuring small strain stiffness of soft rocks, *Geotechnical Engineering of Hard Soils- Soft Rocks* (Anagnostopoulos et al. eds.), Balkema, Vol.1, pp.809-816.

Tatsuoka,F., Sato,T., Park,C.-S., Kim,Y.-S., Mukabi,J.N. and Kohata,Y. 1994. Measurements of elastic properties of geomaterials in laboratory compression tests, *Geotechnical Testing Journal, ASTM,* Vol.17, No.1, pp.80-94.

Tatsuoka,F. 1994. Measurement of static deformation moduli in dynamic tests, Panel Discussion on Deformation of soils and displacements of structures, *Proc. of the 10th European Conf. on S.M.F.E., Florence,* Vol.4, pp.1219-1226.

Tatsuoka,F and Kim,Y.-S. 1995. Deformation of shear zone in sedimentary soft rock observed in triaxial compression, *Localisation and Bifurcation Theory for Soils and Rocks* (Chambon et al., eds.), Balkema, pp.181-187.

Tatsuoka,F. and Kohata,Y. 1995. Stiffness of hard soils and soft rocks in engineering applications. Keynote Lecture, *Proc. of Int. Symposium Pre-Failure Deformation of Geomaterials* (Shibuya et al., eds.), Balkema, Vol.2, pp.947-1063.

Tatsuoka,F., Kohata,Y., Ochi,K. and Tsubouchi,T. 1995a. Stiffness of soft rocks in Tokyo metropolitan area - from laboratory tests to full-scale behaviour, Keynote Lecture,

Proc. Int. Workshop on Rock Foundation of Large-Scale Structures, Tokyo, Balkema, pp.3-17.

Tatsuoka,F., Kohata,Y., Tsubouchi,T., Murata,K., Ochi,K. and Wang,L. 1995b. Sample disturbance in rotary core tube sampling of softrock", *Conf. on Advances in Site Investigation Practice, Institution of Civil Engineers,* London, pp.281-292.

Tatsuoka,F., Lo Presti,D.C.F. and Kohata,Y. 1995c. Deformation characteristics of soils and soft rocks under monotonic and cyclic loads and their relationships, SOA Report, *Proc. of the Third Int. Conf. on Recent Advances in Geotechnical Earthquake Engineering and Soil Dynamics, St Luois* (Prakash eds.), Vol.2, pp.851-879.

Tatsuoka,F., Ochi,K., Tsubouchi,T., Kohata,Y. and Wang,L. 1997a. Sagamihara experimental underground excavations in sedimentary softrock, *Geotechnical Engineering, Proc. Instn Civ. Engrs,* 125, Oct., pp.206-223.

Tatsuoka,F., Uchida,K., Imai,K., Ouchi.T. and Kohata,Y. 1997b. Properties of cement-treated soils in Trans-Tokyo Bay Highway project, *Ground Improvement,* Thomas Telford, Vol.1, No.1, pp.37-58.

Tatsuoka,F., Jardine,R.J., Lo Presti,D., Di Benedetto,H. and Kodaka,T. 1999a. Characterising the Pre-Failure Deformation Properties of Geomaterials, Theme Lecture for the Plenary Session No.1, *Proc. of XIV IC on SMFE, Hamburg,* September 1997, Vol.4, pp.2129-2164.

Tatsuoka,F., Modoni,G., Jiang,G.L., Anh Dan,L.Q., Flora,A., Matsushita,M., and Koseki,J. 1999b. Stress-Strain Behaviour at Small Strains of Unbound Granular Materials and its Laboratory Tests, Keynote Lecture, *Proc. of Workshop on Modelling and Advanced testing for Unbound Granular Materials, January 21 and 22, 1999, Lisboa* (Correia eds.), Balkema, pp.17-61.

Tatsuoka,F., Correia,A.G., Ishihara,M. and Uchimura,T. 1999c. Non-linear Resilient Behaviour of Unbound Granular Materials Predicted by the Cross-Anisotropic Hypo-Quasi-Elasticity Model, *Proc. of Workshop on Modelling and Advanced testing for Unbound Granular Materials, January 21 and 22, 1999, Lisboa* (Correia eds.), Balkema, pp.197-204.

Tatsuoka,F., Santucci de Magistris,F. and Momoya,M. and Maruyama,N. 1999d. Isotach behaviour of geomaterials and its modelling, *Proc. Second Int. Conf. on Pre-Failure Deformation Characteristics of Geomaterials, IS Torino '99* (Jamiolkowski et al., eds.), Balkema, Vol.1, pp.491-499.

Tatsuoka,F., Santucci de Magistris,F., Hayano,K., Momoya,Y. and Koseki,J. 2000. Some new aspects of time effects on the stress-strain behaviour of stiff geomaterials", Keynote Lecture, *The Geotechnics of Hard Soils – Soft Rocks, Proc. of Second Int. Conf. on Hard Soils and Soft Rocks, Napoli,* 1998 (Evamgelista and Picarelli eds.), Balkema, Vol.2, pp1285-1371.

Tatsuoka,F., Uchimura,T., Hayano,K., Di Benedetto,H., Koseki,J. and Siddiquee,M.S.A. 2001a. Time-dependent deformation characteristics of stiff geomaterials in engineering practice, the Theme Lecture, *Proc. of the Second International Conference on Pre-failure Deformation Characteristics of Geomaterials, Torino, 1999, Balkema* (Jamiolkowski et al., eds.), Vol. 2, pp.1161-1262.

Tatsuoka,F., Shibuya,S. and Kuwano,R. 2001b. Recent advances in stress-strain testing of geomaterials in the laboratory, *Advanced Laboratory Stress-Strain Testing of Geomaterials* (Tatsuoka et al. eds.), Balkema, pp.1-12.

Tatsuoka,F. 2001. Impacts on Geotechnical Engineering of Several Recent Findings from Laboratory Stress-Strain Tests on Geomaterials, 2000 Burmister Lecture at Columbia University, Geotechnics for Roads, Rail Tracksand Earth Structures (Correia & Brandle eds.), Balkema, pp. 69-140.

Tatsuoka,F., Ishihara,M., Di Benedetto,H. and Kuwano,R. 2002. Time-dependent shear deformation characteristics of geomaterials and their simulation, *Soils and Foundations*, 42-2, pp.103-129.

Tsubouchi,T., Ochi,K. and Tatsuoka,F. 1994. Non-linear FEM analyses of pressure-meter tests in a sedimentary soft rock, *Proc. of Int. Symposium Pre-Failure Deformation of Geomaterials* (Shibuya et al., eds.), Balkema, Vol.1, pp.539-544.

Wang,,L. 1996. Study into the field deformation characteristics of sedimentary soft rock by means of triaxial tests, *PhD. Thesis, University of Tokyo* (in Japanese).

Yoshida,O., Yamagishi,K. and Nasu,S. 1993. Ground deformation supporting Akashi Strait Bridge Tower Foundations: observation and back-analysis, *Proc. of Domestic Symposium on Utilization of Deep Underground Space, Japanese Geotechnical Society,* pp.149-156 (in Japanese).

開挖工程之回顧

陳嘉正
奧雅納工程顧問

OBSERVATIONS FROM EXCAVATIONS – A REFLECTION

Andrew K C Chan
Ove Arup & Partners Hong Kong Limited

撮要

本文介紹了兩組分別在香港及亞洲其他軟土地區進行的不同深度之基坑開挖工程實例，討論了在工程進行時所觀察到的牆身位移和影響其因素以及預測未來開挖工程所需之設計參數等。

由於結果來自現場觀察，故較適用於與上述例子類似之開挖工程。尤爲重要的是，從累積的觀察結果中增加對設計方案之信心，從而啓發創新及具經濟效益之設計。

最後引出兩例，一例在香港的填海區，另一例則在曼谷之軟土區，作爲本文總結。

OBSERVATIONS FROM EXCAVATIONS – A REFLECTION

Andrew K C Chan [1]

Abstract: Observed wall movements from two sets of case histories for a range of deep excavations are presented. The first from excavations in Hong Kong and the second from excavations on soft clay sites around Asia. These cases are discussed and general observations made regarding factors affecting the observed movements and design parameters relevant to the prediction of behaviour in future excavations. Observations alone are only sufficient for future design if these designs are within the range of experience represented by past cases. More importantly observations are needed to gain confidence in design procedures so that these procedures can then be used to extrapolate to innovative and more economical designs. The paper ends by showing two examples where this has been done, one in a recent reclamation in Hong Kong and the other a soft clay site in Bangkok.

INTRODUCTION

The geotechnical engineering design process can never rely on calculations alone. Observations from previous similar projects in similar ground conditions enable these design processes to be refined and unnecessary conservatisms to be removed. In this way confidence in the design process can be developed leading to confidence in extrapolating the design experience into more 'adventurous' and economic construction.

This paper presents a series of case histories that are associated with deep excavations. The main emphasis observation presented here is the observed maximum lateral movement of the retaining wall element during the excavation process. A series of observations contrasts two types of ground profiles common in Southeast Asia. The first is a residual soil profile such as found in Hong Kong where the soils have been weathered from the parent rock. As such the stress history and the state of stress in the ground is difficult to quantify. In this case a common design approach has been used and the selection of suitable soil parameters, especially the soil stiffness empirically correlated with SPT 'N' values, is investigated by back analysis of field measurements. The second is an alluvial or marine clay profile common in the coastal areas of many Southeast Asian cities including Singapore, Bangkok, Taipei, Shanghai and parts of Hong Kong. For these profiles, the deposition and stress history can be assessed with some degree of accuracy and reasonable assessments made of the predicted behaviour under changes in stresses due to engineering construction. Key factors that influence the observed movements including the effectiveness of various construction methods are discussed. The final part of the paper shows examples of where the design process has been used to extrapolate previous experience to enable innovative and more economical construction methods to be employed.

It must be stated that this paper is not intended as an exhaustive or even extensive review of relevant projects. The author has deliberately selected projects that the author's company has been associated with over the last 20 years or so, and these have been selected to illustrate the main principles of the use of case histories for the design of retaining walls for deep excavations.

---

[1] Chairman, Ove Arup & Partners Hong Kong Limited

DEEP EXCAVATIONS IN HONG KONG

The case histories of deep excavations in Hong Kong cover a wide variety of ground conditions. Most involve a thickness of fill that overlies residual soil, usually completely decomposed granite. In a couple of cases there is a layer of marine or alluvial deposits over the residual soil. The fill varies significantly from a thin superficial layer of disturbed ground to 20m thick layer of engineered fill placed as part of a reclamation process. The case histories are presented in order of their construction and are as follows.

Chater Station, Central

The paper by Davies and Henkel (1980) describes this project, now referred to as 'Central Station', in some detail. Many geotechnical difficulties were encountered during the construction. Significant settlement was observed to adjacent structures primarily due to the effects of dewatering but was also due to the installation of the diaphragm walls panels and the subsequent excavation. As this paper is concentrating on the effects of excavation only the lateral wall movements associated with the excavation are presented.

Figure 1 shows a summary of the ground conditions that comprise 8m of fill over 8m of marine deposits over completely decomposed granite (CDG). The excavation at this site was 26m deep and a 1.2m thick diaphragm wall was used to support the excavation. The station was excavated using the top-down method with the permanent station floor slabs supporting the retaining walls as the excavation progressed downwards. The observed wall movement is also shown in the figure. Unfortunately the movements were only recorded after the upper slab of the station, the roof, was constructed.

The wall has been re-analyzed using the *Oasys* program FREW (Pappin et al 1986) to determine the soil stiffness values that give rise to best agreement to those observed. This computer program represents the wall as line of linear elastic bending beam finite elements and attaches the wall to a block of soil on either side of the wall (see Figure 2). The stiffness of the soil block is assessed using a method based on two dimensional finite element analyses. The soil stresses are limited to remain within the active and passive force limits and internal arching within the soil mass is allowed. Groundwater pressures are also modeled in the analysis.

In common with standard practice in Hong Kong the soil Young's Modulus E value has been expressed as a function of the SPT N value (blows per 300mm). As shown in Figure 1 good agreement with observed measurements for the remaining stages of the excavation are observed when an E value of 1.5N(MPa) is used for the Fill and Marine deposits, E=2N(MPa) for the CDG, and E=4N(MPa) for CDG/HDG.

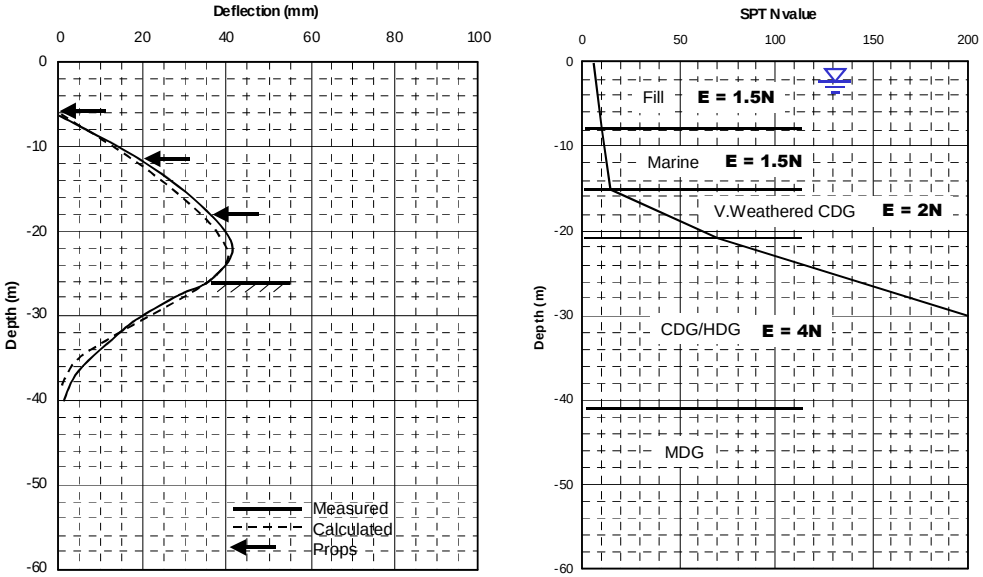

Figure 1 – Chater Station

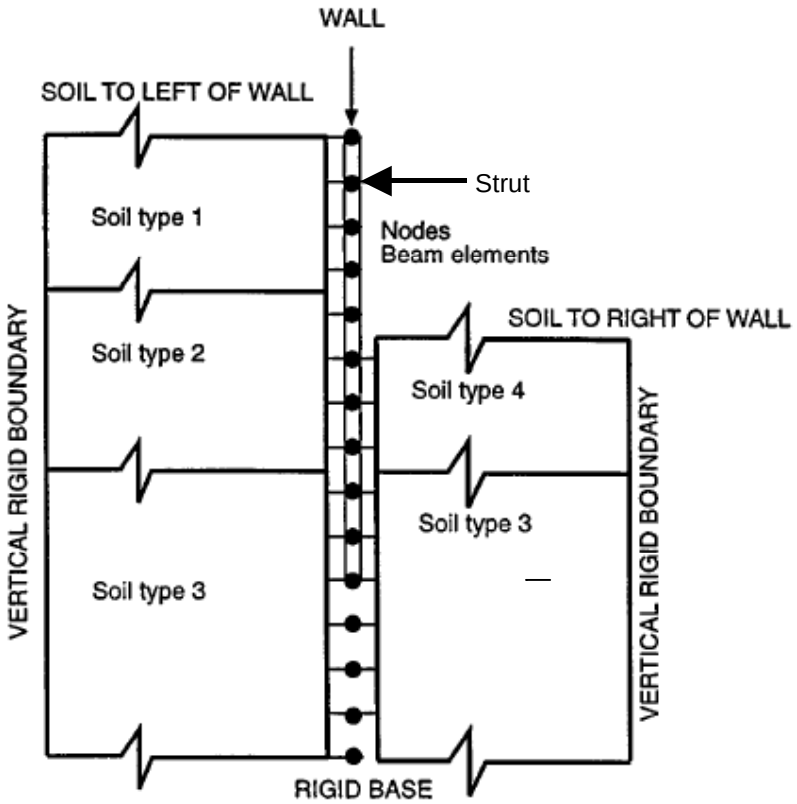

Figure 2 – Wall and Soil Model Used in *Oasys* FREW

The Hongkong & Shanghai Bank Headquarters, Central

Two sections have been analyzed for the Hongkong & Shanghai Bank Headquarters Building in Central. Both are north-south sections, one being across Queen's Road Central, and the other across Des Voeux Road. Humpheson et al (1986) gives details of the soil conditions, construction method and observed movements. The ground conditions for Queen's Road and Des Voeux Road are shown in Figures 3 and 4. It can be seen that the CDG under Queen's Road has noticeably higher N values than that at the same level under Des Voeux Road. Both sections have about 7m of fill and/or alluvium over the CDG. A 1m thick diaphragm wall was used and the basement was excavated using the top down method with the permanent basement floor slabs supporting the retaining walls as the excavation progressed downwards. The depth of excavation varied between 16 and 18m as shown on the figures.

The maximum observed lateral movement of the retaining wall varied from 30mm on the Queen's Road section to 42mm on the Des Voeux Road section. The back analysis shows the best agreement is achieved with E equal to 1.5N(MPa) for the fill and alluvium and E equal to 2N(MPa) for the CDG. This is observed for both sections.

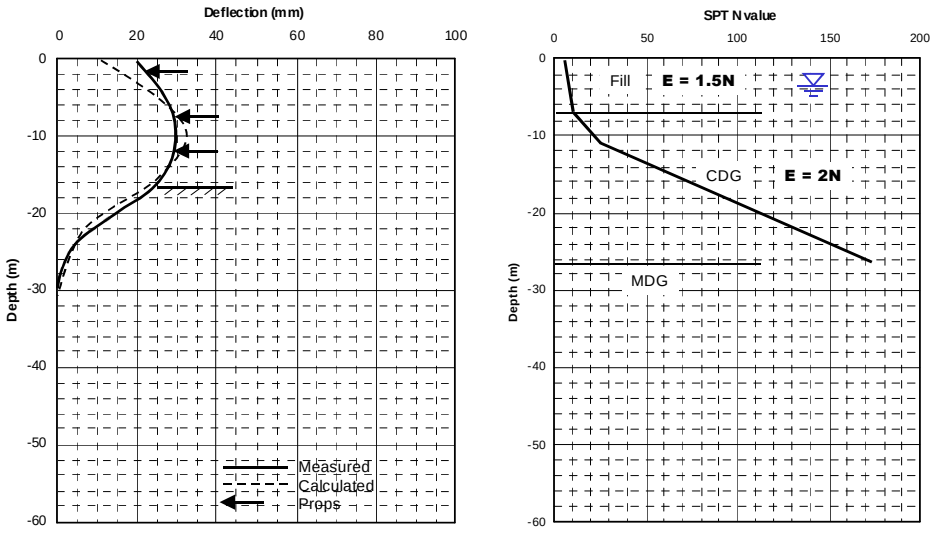

Figure 3 – Hongkong Bank Headquarters (Queen's Road)

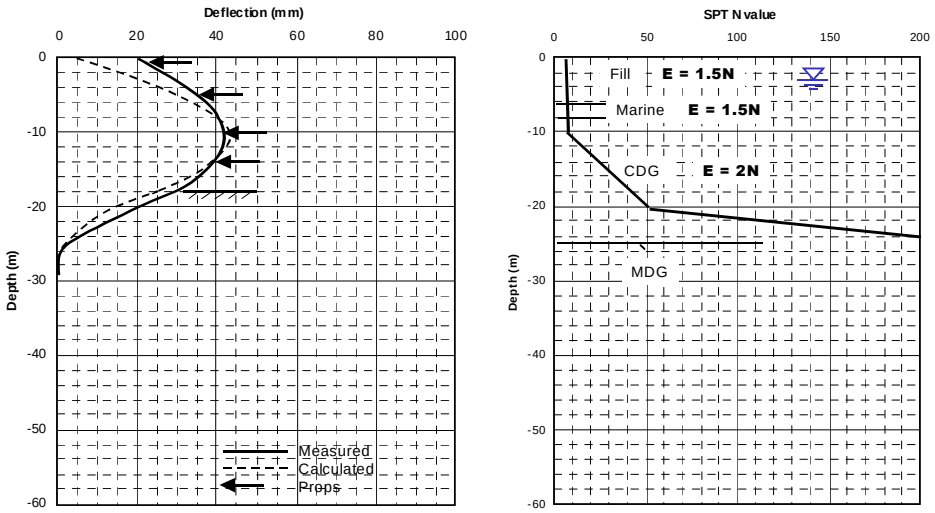

Figure 4 – Hongkong Bank Headquarters (Des Voeux Road)

Evergreen Hotel, Wan Chai

This project is described in detail in Walsh and Fung (1989). Figure 5 shows the ground conditions at this site. The depth of excavation was 11.5m and a 24m long sheet pile wall was used as the retaining system. An array of temporary props at about 2m vertical spacing were used to support the wall. It can be seen that the horizontal movement of the sheet pile wall during excavation amounted to about 25mm.

Again this excavation has been reanalyzed using *Oasys* FREW to determine the soil stiffness values that give rise to best agreement to those observed. For this case, the best agreement is achieved when an E value of 1.5N(MPa) is used for the fill and alluvial sand and an E value of 3N(MPa) for the completely decomposed granite (CDG). The computed displacement using these values is shown in Figure 5. It should be noted however that prior to the excavation, the pile foundations for the project were installed. The piles comprised driven H piles and the presence of these piles may have enhanced the soil stiffness somewhat.

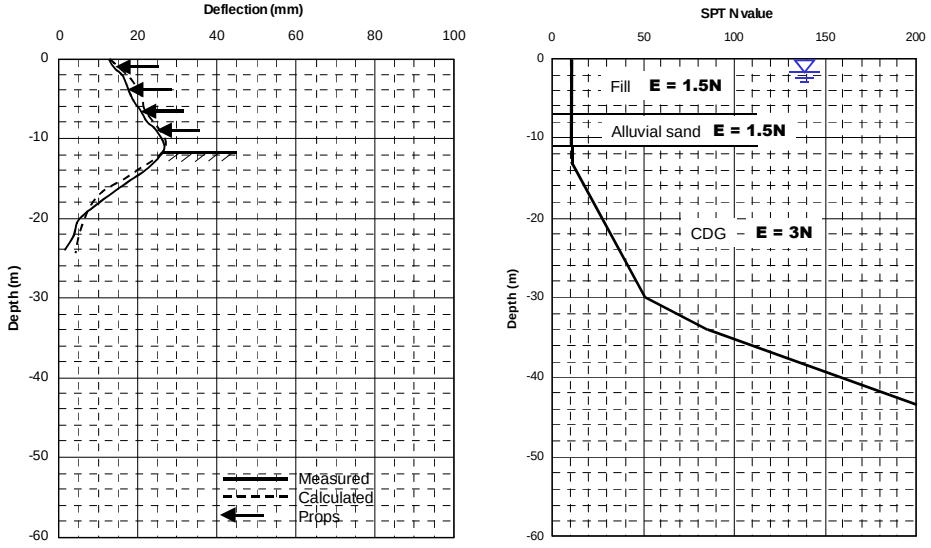

Figure 5 – Evergreen Hotel

Dragon Centre, Sham Shui Po

Full details of the ground conditions, construction method and observed movements due to construction have been published previously, Lui and Yau (1995). The ground conditions are summarized in Figure 6 and comprise 4m of fill over 6m of marine deposits over an extensive thickness of CDG. In this case a 1.2m thick diaphragm wall was used and again the top down method of excavation was used to support the wall as the 26m deep excavation progressed. It should be noted that within 100m distance from the site, the structures are either supported on footings or driven piles and are without basement. Hence the site can be regarded to comprise of a 'virgin' soil profile which had not been subjected to previous dewatering effects.

In common with standard practice in Hong Kong, a pumping test was carried out before any excavation was started to demonstrate that the wall was adequate to allow draw-down of water within the excavation without leading to excessive draw-down in the ground surrounding the excavation. Interestingly, this pumping test caused a significant amount of

movement and this is also shown in the figure. When the pumping test was completed and the water allowed to rise again within the excavation, the wall displacement reduced to about half of that observed during the pumping test.

The lateral movement of the diaphragm wall at the completion of the excavation, at a typical section, is shown in Figure 6. Back analysis of the movement using *Oasys* FREW, reported by Lui and Yau, (1995), shows that good agreement is observed with an E equal to N(MPa) in the fill and alluvium and E increasing from 1.5N to 2N(MPa) in the underlying CDG. The calculated movement is shown in Figure 6. It is of interest to note that these E/N values are similar to those inferred from earlier pumping test for the construction of the MTR Wan Chai Station by Davies (1987). The movement of the wall during the pumping test is better modeled if the K_0 value in the CDG is set close to the active pressure coefficient K_a.

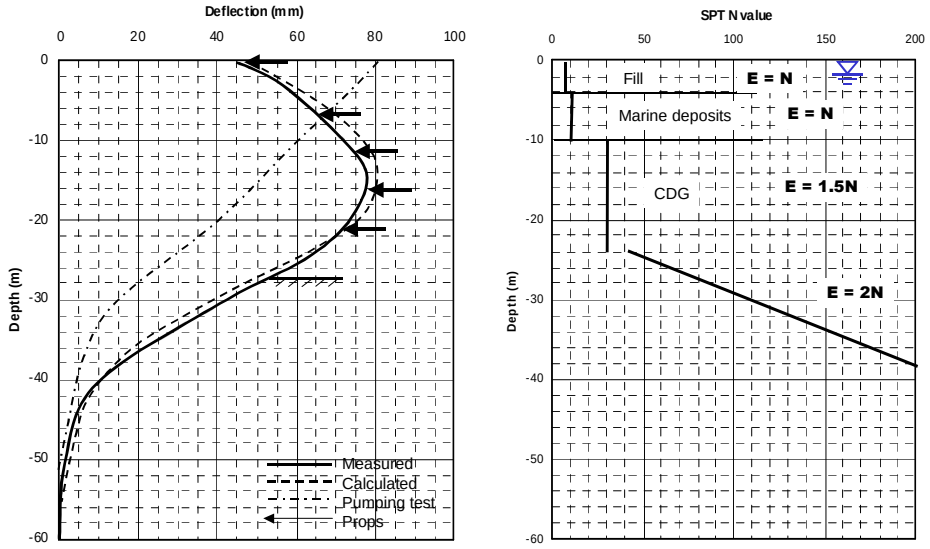

Figure 6 – Dragon Center

Festival Walk, Kowloon Tong

The geotechnical aspects of this shopping center and office complex project are described in some detail in Lee at al (2001). A section through the deepest excavation at Festival Walk is shown in Figure 7. This 33m deep excavation is located below Tat Chee Avenue at the northern end of the development. The ground comprises a thin layer of fill over CDG as shown in the figure. A 1.2m thick diaphragm wall was used to retain the soil and the construction method was initially an anchored wall for the top two levels of struts and the top down method commencing at the third level of props. This method was necessary because the ground level on the opposite side of the site is about 15m lower than that at Tat Chee Avenue.

The observed displacement of the wall is also shown in Figure 7. It can be seen that the top of the wall has moved out by about 50mm. This was partly due to the anchors behaving in a flexible manner and partly due to the building itself leaning away from Tat Chee Avenue when the anchors were de-stressed. Back analysis of the movement using *Oasys* FREW shows that reasonable agreement is observed with an E equal to 2N(MPa) in the CDG. It must be emphasized however that in this calculation the overall wall movement is very sensitive to the assumption of anchor stiffness.

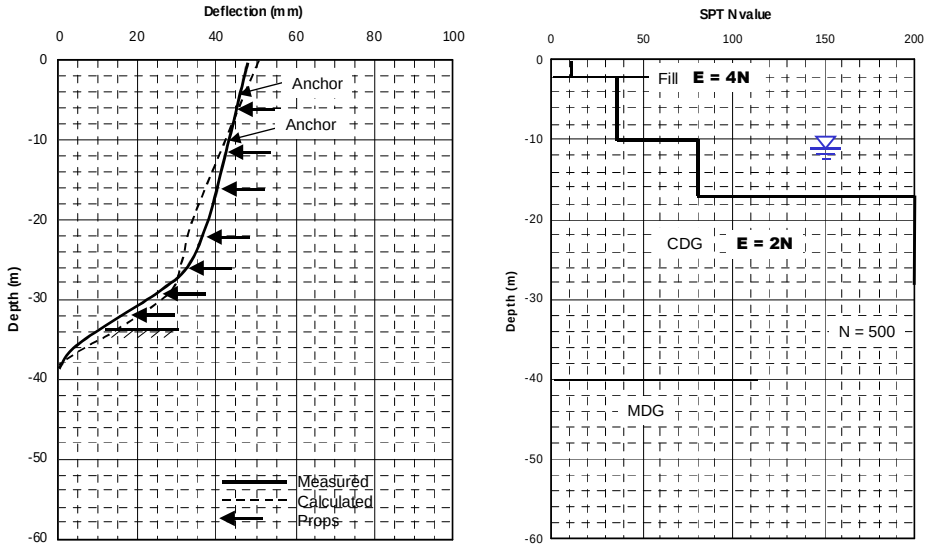

Figure 7 – Festival Walk

Hong Kong Station, Northern Development, Central

Young (2003) gives details of the geotechnical aspects of this project. The section selected for this paper is a section through the drum ramp at the western end of the Northern Development and is shown in Figure 8. The ground conditions comprise 22m of recently completed sand fill over 8m of alluvium over more than 30m of CDG. A 1.5m thick diaphragm wall was used and the top down method of excavation was used for this 23m deep excavation. The observed lateral displacement of the wall that occurred during excavation is shown in Figure 8. Again back analysis has been carried out and, as shown in Figure 8, reasonable agreement is observed between the observed and calculated lateral displacements if a value of E equal to 4N(MPa) is used for all materials. It should be emphasized that the upper layers of fill had been compacted after placement and pile foundations had been installed on the passive side before the excavation.

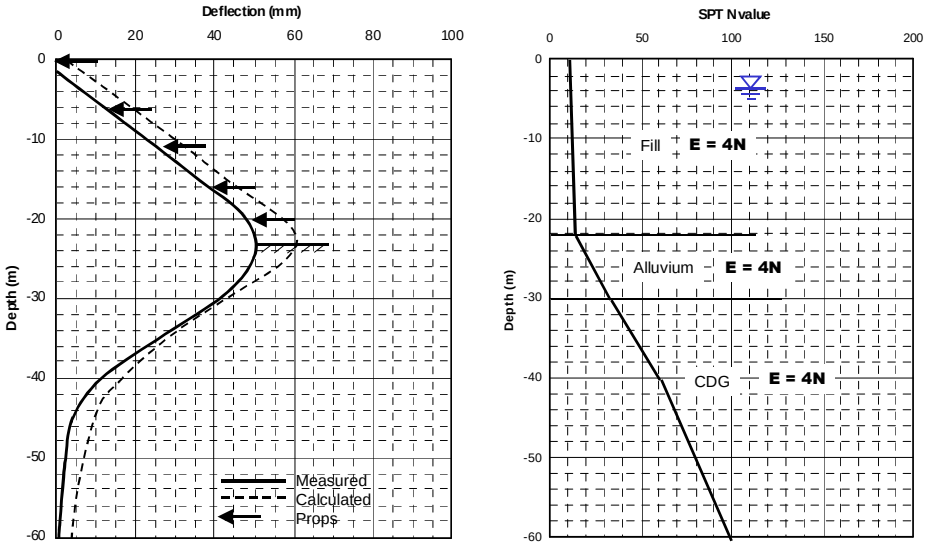

Figure 8 – Hong Kong Station Northern Development

Discussion

Comparison can be made with previously published observations from deep excavations. Long (2001) gives an extensive database of lateral movements associated with deep excavations. Figure 9 shows his summary for excavations in soil where the thickness of soft soil is less than 60% of the depth of the excavation. The vertical axis is the maximum lateral wall displacement divided by the depth of excavation (δmax/H) and the horizontal axis is the Clough et al (1989) system stiffness parameter, which is equal to the wall EI value divided by the unit weight of water and the strut spacing to the fourth power. Also shown is the Clough and O'Rourke (1990) relationship for excavations where the factor of safety on base heave is at least three.

The data from the case histories described above are plotted in Figure 9. The observed movement from the recent Chater House project, reported in Sze and Young (2003) to this seminar has also been added. It can be seen that the data generally gives a δmax/H value of about 0.2%. The deep Festival Walk excavation gave a lower value of 0.15% and the Dragon Centre job gave a higher value of about 0.3% of the depth of excavation. Considering all these excavations were well controlled with stiff walls and good propping systems, the implication is that it will be very difficult to reduce the lateral displacement to smaller values.

It is also noted that in the Hong Kong case histories presented above a relationship was derived between the soil Young's Modulus and the SPT N value (blows per 300mm). It is recognised that, given the variability of a weathered granite profile, there are uncertainties in arriving at an average SPT N profile from scattered test results and in the description of the materials. There is some evidence that the E/N ratio increases at higher values of SPT (Davies 1987), for CDG/HDG. Alternatively, the observations could reflect the higher stiffness now observed in a variety of soil profiles at small strains. Generally it is seen that if an E/N value of 1.5(MPa) is used for fill, alluvium and marine deposits and an E/N value of 2(MPa) is used for CDG, then a reasonable and conservative estimation of lateral displacement will be calculated.

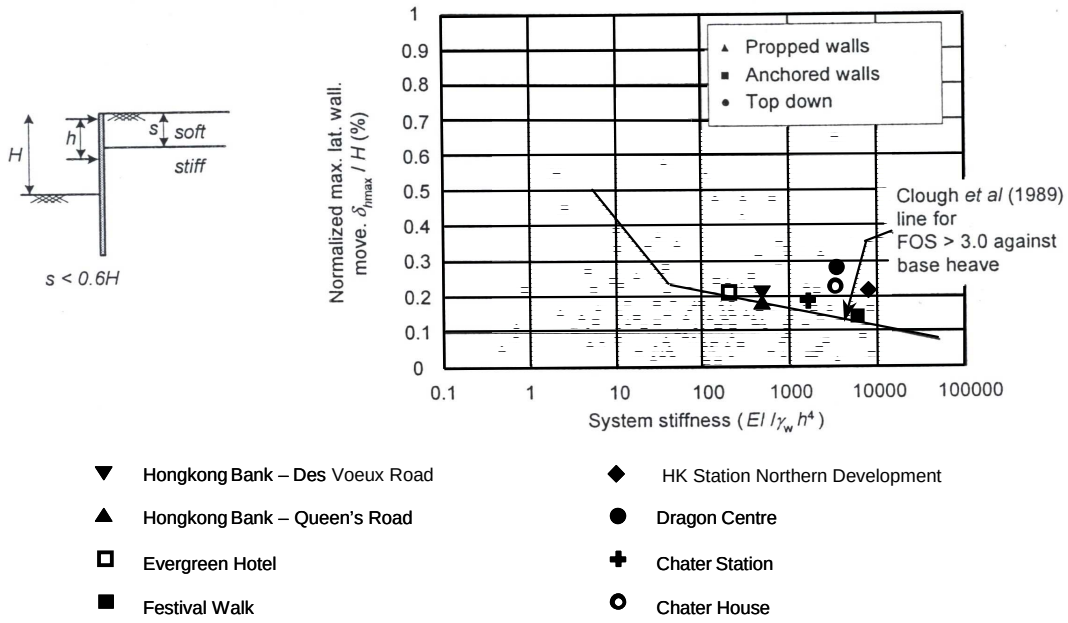

Figure 9 – Comparison with Long (2001)

DEEP EXCAVATIONS IN SOFT CLAY IN ASIA

Sites comprising a significant thickness of soft silty clay are common in the coastal cities of Southeast Asia. Many of these alluvial or marine deposits have similar characteristics. The case histories are from Singapore, Taipei and Shanghai and are again presented in order of construction. The thickness of the soft clay layer is the greatest in Shanghai.

Newton Station, Singapore

This project has previously been published by Nicholson (1987) and Gaba (1990). The ground conditions are illustrated in Figure 10. The overall depth of excavation was 14.5m and a 0.8m thick diaphragm wall was used to support the retained soil. The method of excavation was a top-down construction with permanent concrete floor slabs that also acted as props to the wall, being cast as the excavation progressed. The excavation was initiated at the eastern end of the station and a typical observed lateral movement of the retaining wall is shown in Figure 10. The maximum wall movement is about 0.7% of the excavation depth.

Near the western end of the station, the marine clay became significantly thicker as shown in Figure 11. An added complication was the presence of neighboring buildings becoming quite close to the station. The observed movements at the eastern end, while being somewhat less than those predicted would not be tolerable at the western end and the presence of deeper clay would have meant that unacceptably large building displacements would be likely to occur. A jet grout raft, installed prior to commencing the excavation, was therefore adopted in that area. Figure 11 shows the depth of the jet grout raft and the movement that resulted from the excavation at that area. It can be seen that the jet grout raft was very effective in reducing the movement. The wall movement in this case is about 0.2% of the excavation depth.

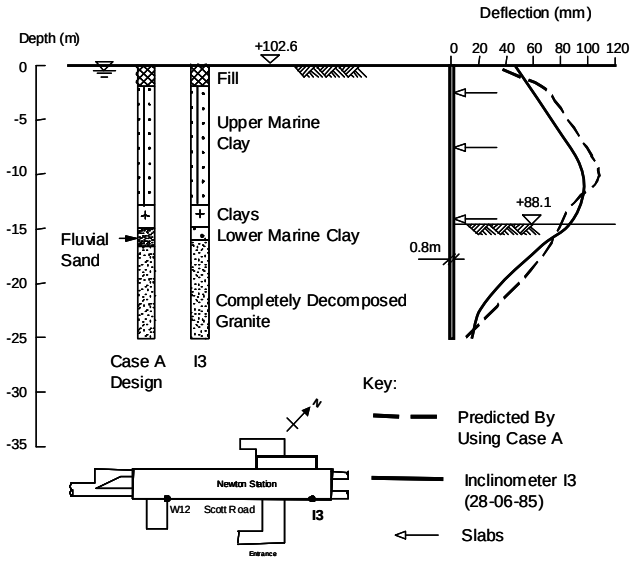

Figure 10 – Predicted and Measured Wall Deflection without Jet Grout (Newton Station)

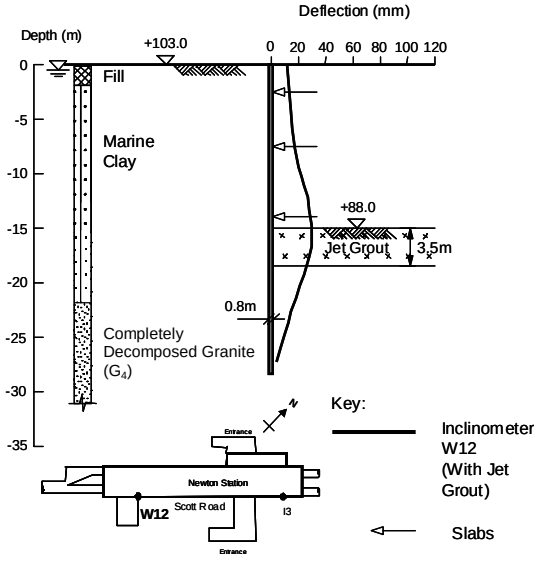

Figure 11 - Measured Wall Deflection with Jet Grout (Newton Station)

Station BL14 of Nankang Line, Taipei

Several stations (BL13 to 16) of the Nankang Line were designed between 1989 and 1991 and constructed in the early to mid-90's. These involved deep excavations in a thick bed of silty clay and other alluvial materials. The project area lies in the so-called K1 Zone of the Keelung deposits and the geotechnical characteristics of the clay layers known as the Sungshan Formations are described by Woo and Moh (1990).

Figure 12 shows a section of station BL14 and the foundations of adjacent buildings. The construction required an excavation of 17.7m, supported by 1.2m thick diaphragm walls and essentially by top-down method. Stringent limits on permissible movements were imposed (e.g. 25mm) by the Client. At the start of the design process, three local case histories on projects in the same area were back-analyzed using *Oasys* FREW to calibrate parameters to be used. Early analysis, and indeed from empirical rule, e.g. Clough et al (1989), indicates maximum wall deflection in the order of 80 to 90 mm and this when translated into building settlements would be unacceptable. Having considered various methods to reduce ground movements, and from the experience of Newton Station in Singapore, it was decided to introduce a 3m thick jet-grout raft at below the excavation level.

Figure 13 shows the simplified soil engineering profile and the computed lateral wall deflection profiles with and without the jet-grout raft. The actual "undrained" deflection profile measured by a typical inclinometer is also shown. The jet-grout raft was effective in reducing the lateral wall deflection to about 22mm and contributed significantly to the protection of the sensitive buildings. The value of $\delta max/H$ measured is about 0.12%, being well below the normal range measured from other projects in Taipei with no jet grouting. Further data from this and other stations indicated rational analysis by FREW gave close approximation of measured wall deflection profiles.

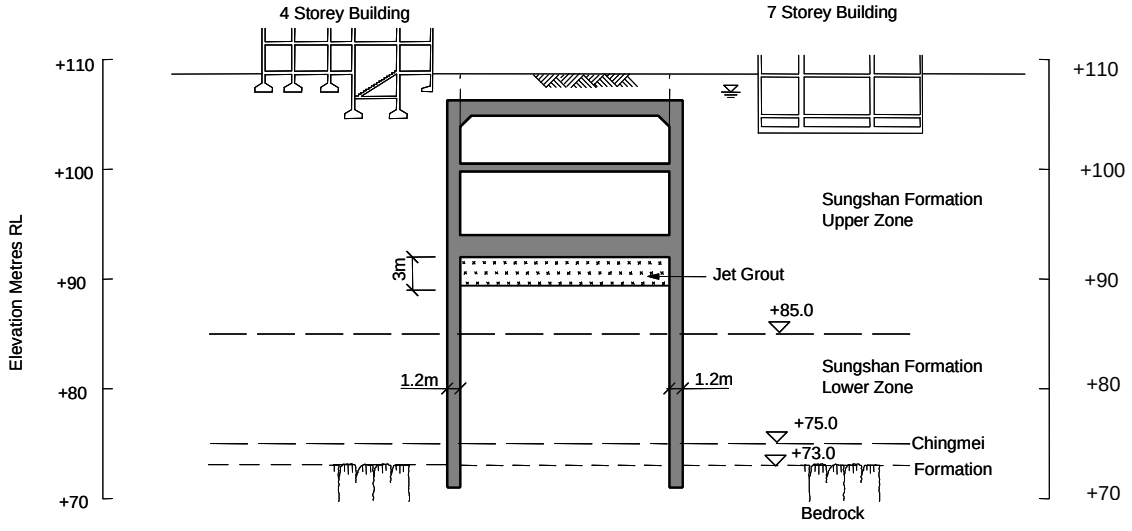

Figure 12 – Section of Station BL14

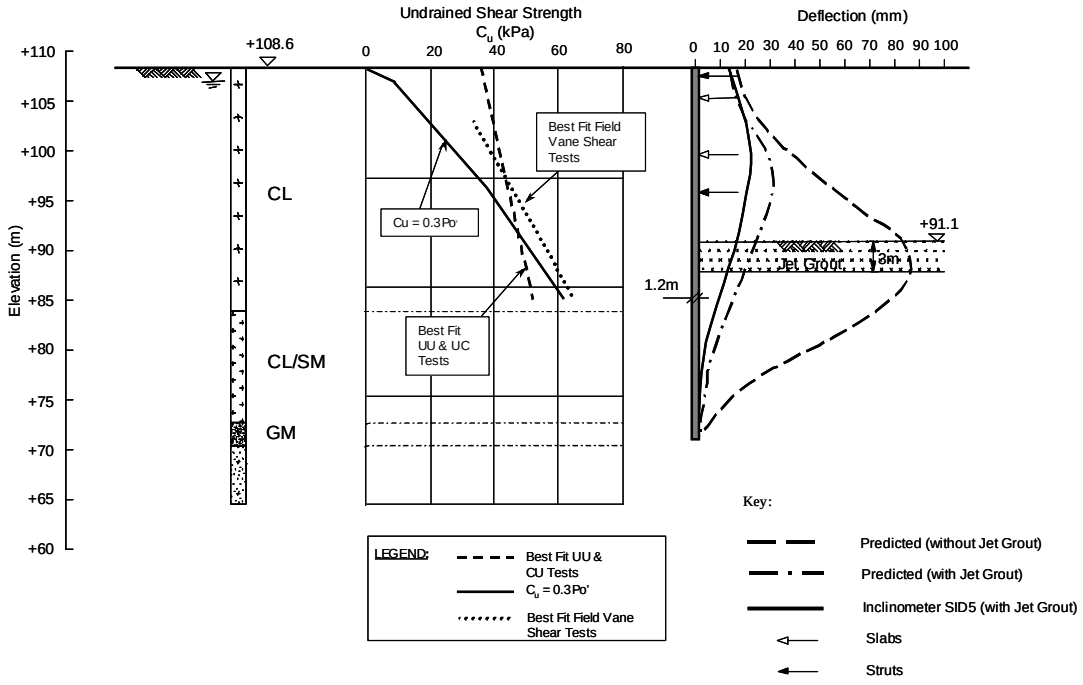

Figure 13 - Predicted and Measured Wall Deflection (Station BL14, Taipei)

New World Centre, Shanghai

A very large number of building projects were being constructed in the mid to late 1990's in Shanghai. The 250m tall New World Centre, located at the heart of the Lu Wan District, is a typical example. General ground conditions have been described by Chan et al (1996), and this project involved excavation of a 3-level basement. The site is along the busy Huai Hai Road Central, and the Shanghai MRT Line 1 Huang Pi Station and the running tunnels are at a distance of about 10m from the site boundary (see Figure 14).

Early work on the Shanghai Metro (Liu, 1993) and building basement excavations (e.g. Mak and Liu, 1996) in the soft Shanghai clays indicate that large ground movements can occur particularly where workmanship was less than ideal. In the case of the New World Centre basement, it was decided to carry out the excavation in two phases (Figure 14). Phase I, further away from the station and tunnels to avoid potentially excessive movements affecting the metro facilities, has an excavation depth of 17.7m, was constructed first to allow the tower erection to proceed. To reduce ground movements, it was further decided to introduce a buried 'waling' of 6m thickness using deep mixed cement columns as shown in the figure.

Figure 15 shows results of FREW analyses and measured wall deflection profiles. The maximum measured deflection was about 40mm. When Phase I was complete, Phase II excavation (for building podium area), two meters shallower at 15.7m, started with a jet-grouted layer (buried 'prop') below excavation level covering a large part of the site. This stronger measure was taken to further ensure effects on the metro works are minimized.

Figure 15 shows the jet grouting was effective in limiting the maximum deflection to about 20mm and the project was successfully completed without causing any undesirable problem. The value of δmax/H with ground treatment measured at various parts of the site is very low at about 0.12% to 0.23%.

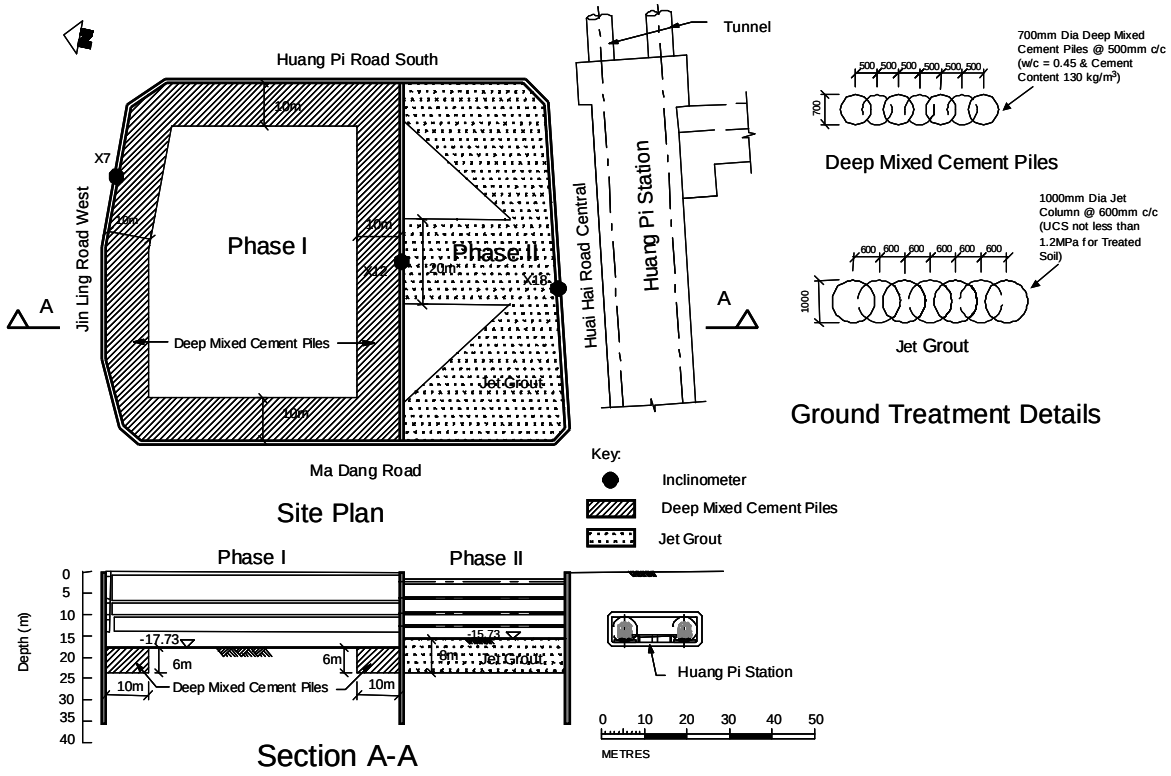

Figure 14 – Shanghai New World Centre

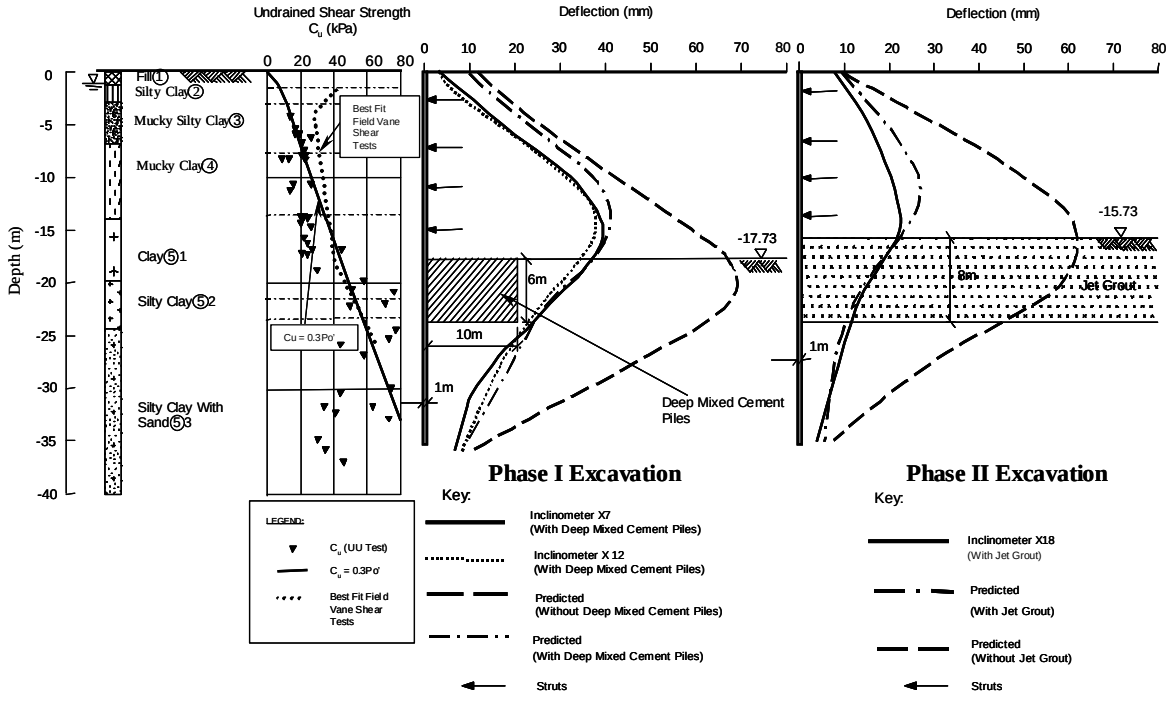

Figure 15 – Predicted and Measured Wall Deflection

Discussion

Excavations carried out in soft silty clay deposits can cause relatively large wall movements. Experience from different sites in Asian cities shows similarity and consistency in observed behaviour. Empirical rules such as Clough and O'Rourke (1990) give reasonable first estimate of maximum wall movement. Analyses using FREW with a set of soil parameters from standard measurements (e.g. strength) and from empirical correlations (e.g. stiffness, earth pressure coefficients) can give good enough predictions of the maximum movement and profile. Clearly, more high quality monitoring data specific to each location will enhance the confidence in our ability to predict, perhaps with more sophisticated numerical analysis and soil stress-strain models.

It should be noted that movements in soft clay profiles are particularly affected by actual details of the excavation method and workmanship, and may be time-dependent. To be of real value, case histories need to record as much relevant details as possible.

Stringent requirements are often set by building control or mass transit authorities for protection of properties adjacent to deep excavations, some being absolutely necessary. In clay profiles, these movement limits are difficult if not impossible to satisfy and ground treatment, such as jet grouting before excavation, becomes necessary. From the cases presented, it is shown that such strengthening or 'buried props' can be effective in achieving a $\delta max/H$ of about 0.2% or below.

EXTRAPOLATION TO ENABLE INNOVATIVE DESIGN

In this section two examples are presented where established design methods, calibrated against previous experience, have been used to produce innovative and economical solutions in problems involving deep excavations. The first is in a recent reclamation in Hong Kong, followed by one in Bangkok.

Tseung Kwan O Station, Hong Kong

This project, previously published by Ho et al (2001), involved the use of precast concrete props in deep trenches such that they were in position just below the final excavation level. The ground profile comprised about 12m thickness of recent reclamation fill over 10m of soft marine clay over 20m of fine and coarse alluvium over a varying thickness of completely decomposed volcanic residual soil. Originally the 1.2m thick diaphragm wall was designed by Arup to use a jet grout raft just below the deepest excavation. The jet grout raft was required to limit the bending moments in the wall to manageable levels rather than to restrict lateral deformations.

The Contractor, Leighton-China State JV, proposed an alternative scheme comprising underwater excavation. The wall was constructed and the excavation commenced. At this stage it became apparent that the marine clay, which originally had not reached full primary consolidation under the action of the recent fill, was steadily gaining strength as it approaches normal consolidation. The contractor wished to explore the possibility of eliminating the underwater excavation scheme and approached Arup to develop a more conventional alternative scheme. The use of precast concrete props lowered into 7m deep trenches, placed just below the final excavation level and secured to the wall with tremie concrete was jointly developed between Arup and the contractor. Figure 16 shows a schematic construction sequence for this work. Again this sequence of temporary propping was required to limit the bending stresses within the already completed diaphragm wall.

The scheme progressed using the precast beams. The marine clay continued to gain strength and the observed movements of the wall showed that the predicted displacements were too large. A back analysis procedure using FREW was therefore adopted and revised soil stiffness parameters developed to match the observed displacement. These revised parameters, described in details in Pan et al (2001), and illustrated in Figure 17, were then used in an application of the Observational Method to eliminate the buried prop in the latter part of the excavation. All of this work was carried out under the Buildings Department approval procedure.

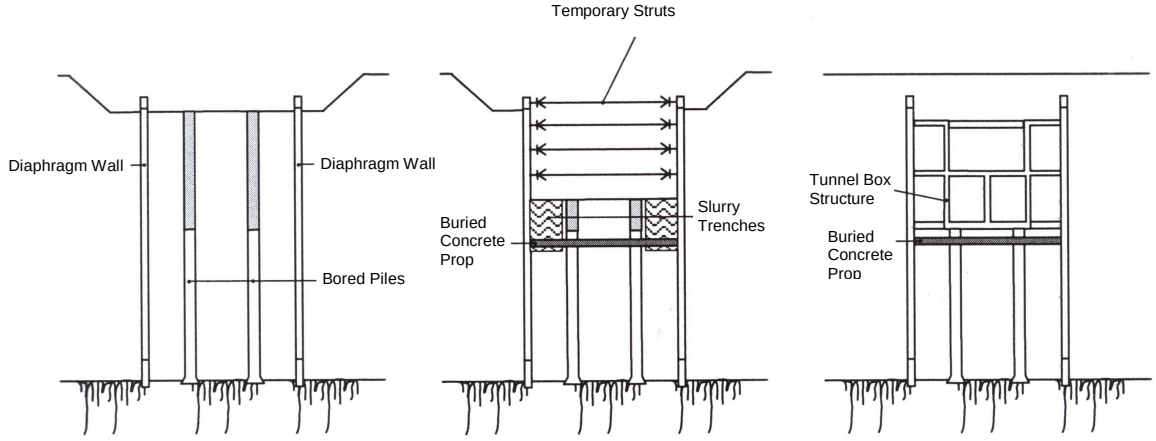

Figure 16 - Excavation sequence at Tseung Kwan O Station

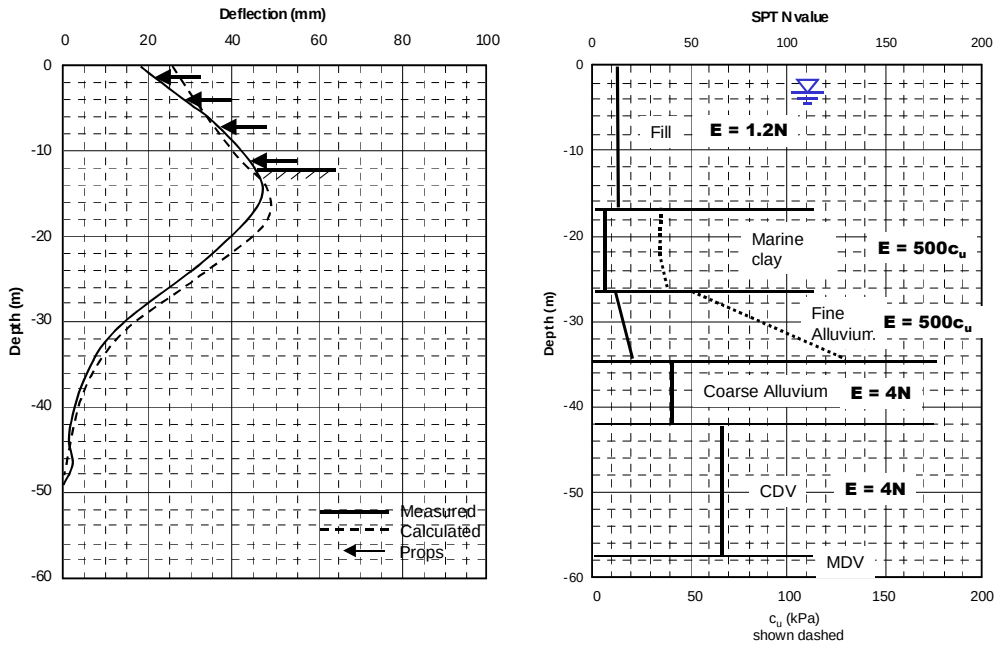

Figure 17 - Tseung Kwan O Station

MRTA Northern Section, Bangkok

An innovative scheme was adopted in this project to optimize the construction process of this major metro construction project in Bangkok, see Davies et al (2001). Tunnel Boring Machines were driven through three station boxes prior to the completion of the excavation within these boxes. Figure 18 shows the work arrangement at this stage. To facilitate unimpeded construction progress, tunnel "eyes", reinforced with glass fibre reinforcement polymer, were designed at the end walls of the station box. The construction clearance between the main diaphragm walls and the tunnel and between the internal stanchions and the tunnel was about 1m. After the tunnels were completed the station excavation was progressed using the top down method and eventually the tunnels within the station box demolished. Based on experience of using FREW, a detailed finite element numerical analysis was carried out to evaluate the interaction between the tunnel, the walls and the station stanchions and the effects of excavation within the station box on these elements. Figure 19 shows the analysis of the tunnelling stage of the excavation. The site investigations carried out for the design included self boring pressure meter testing to determine the small strain stiffness of the soil profile and give appropriate values for the station design. The field and laboratory test results, in combination with the numerical analysis allowed the design to be expeditiously undertaken and the tunnelling to proceed with confidence. This is the first time concurrent tunnelling and station construction has been undertaken on this scale.

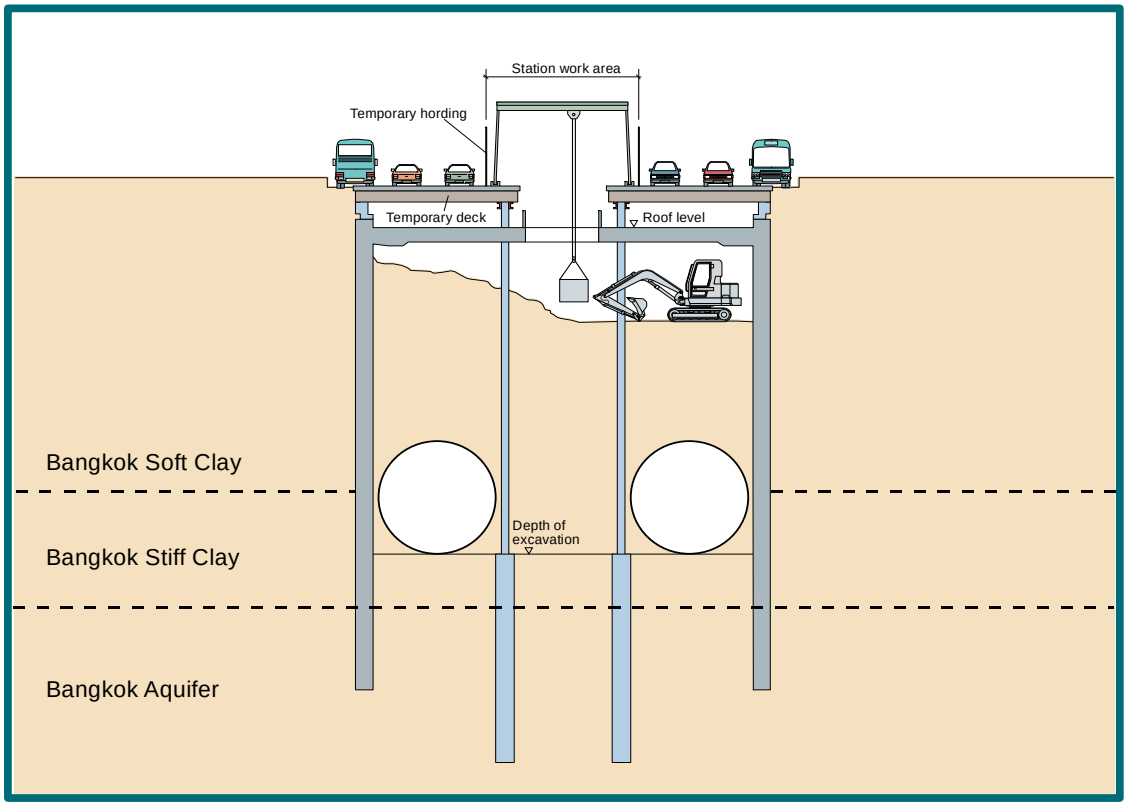

Figure 18 – Construction Arrangement of Bangkok MRTA

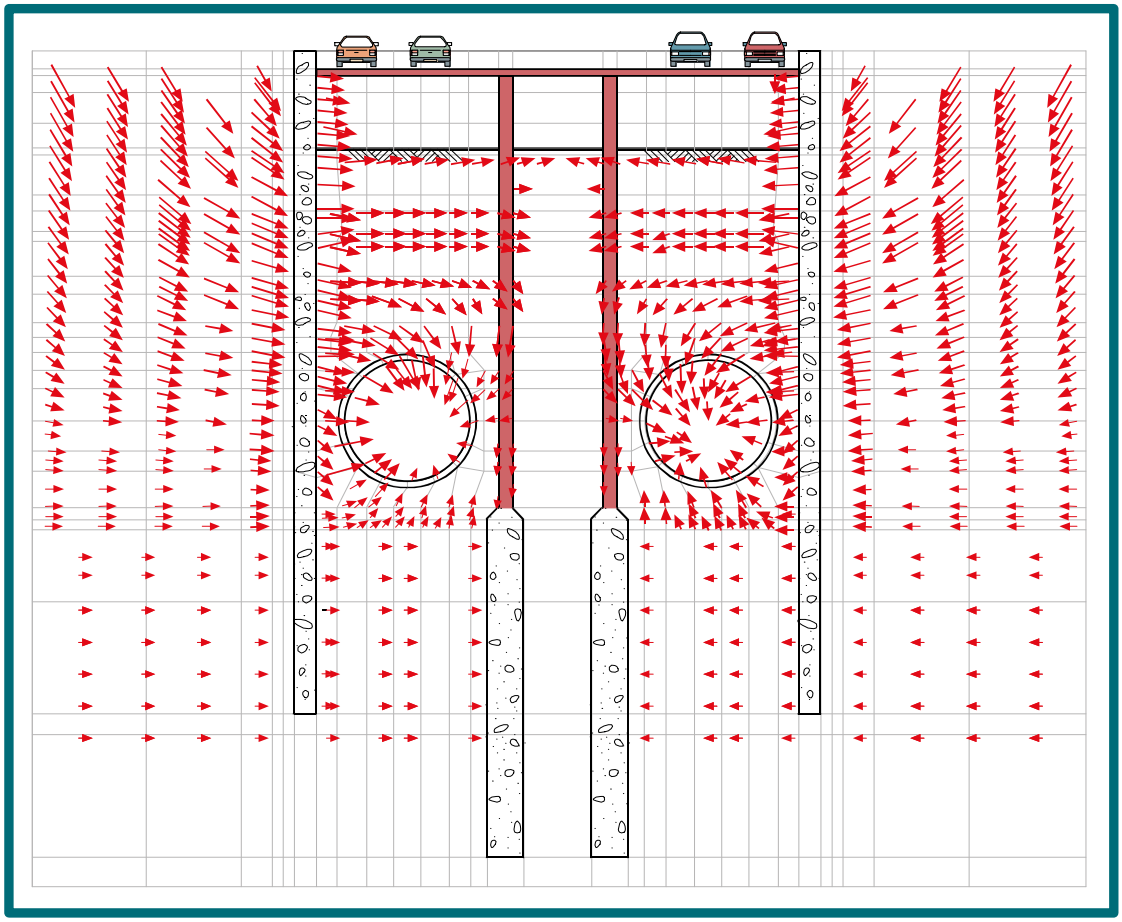

Figure 19 – Numerical Analysis Result at Tunnelling Stage

CONCLUSIONS

The above case histories of showing observed maximum lateral movements of retaining walls due to deep excavations forms a valuable resource of previous experience in these problems. They show that a combination of good quality field data and rational analysis can give the engineer confidence in the design predictions.

They also lead to the following observations:

1. Well-controlled deep excavations in urban Hong Kong are likely to cause maximum lateral displacements of the retaining walls that will be between 0.15% to 0.3% of the final excavation depth.

2. Back analysis of excavation lateral movements in Hong Kong shows that for movement prediction purposes, reasonable and conservative estimates of displacement are likely to be achieved by using an Young's Modulus (E) for soil of 1.5N(MPa) for fill and alluvium and a value of E = 2N(MPa) for completely decomposed granite. Higher E/N values are relevant for CDG/HDG with high 'N' values.

3. Experience from soft clay sites is widely applicable and can be used with reasonable confidence for sites around the region.

4. Observations in themselves are only sufficient for a robust design if the current design situation fits within the range of previous experience. To enable extrapolation to larger and/or more economical design, it is necessary to use back analysis to validate and give confidence in the employed design methods. This process enables these design methods to be used to extrapolate to innovative and economical designs with some confidence.

REFERENCES

Chan A.K.C., Lui, J.Y.H., Yau, K.F. and Yin, K.K. (1996) "Aspects of Geotechnical Practice in China with particular reference to foundations in Shanghai" *Proc. of the 16th HKIE Geotechnical Division Annual Seminar.*

Clough, R.W. and O'Rourke, T. D. (1990). "Construction induced movements of insitu walls". *Proc. ASCE Conf. on Design and Performance of Earth Retaining Structures, Geotech. Spec. Publ. No. 25, pp. 439-470.*

Clough, R.W., Smith, E.M. and Sweeney, B.P. (1989) "Movement control of excavation support systems by iterative design", *Proc. ASCE Foundation Engineering: Current Principles and Practices., Vol. 2, ASCE, New York, pp 869-884.*

Davies, J.A. (1987) "Groundwater control in the design and excavation of a deep excavation". *Proc. of the 9th European Conference on Soil Mechanics & Foundations Engineering, Dublin, pp139-144.*

Davies, J., Thompson, P. and Young, S.T. (2001) "A comparison between tender, detailed design and the field performance of diaphragm walls in Bangkok". *Proc. of the 14th Southeast Asian Geotechnical Conference.*

Davies, R.V. and Henkel, D.J. (1980). "Geotechnical Problems Associated with Construction of Chater Station". *Proc. of the Conference on Mass Transportation in Asia, Hong Kong.*

Gaba, A.R. (1990). "Jet Grouting at Newton Station, Singapore". *Proc. 10th Southeast Asian Geotechnical Conf. Vol. 2, pp77-79.*

Ho J., Hope S., Pappin J.W. and Blair C (2001). "Buried Concrete Prop for Tseung Kwan O Station and Tunnels". *Proc. of the 20th HKIE Geotechnical Division Annual Seminar.*

Humpheson, C., Fitzpatrick, A.J.& Anderson J.M.D. (1986). "The basements and substructure for the new headquarters of the Hongkong and Shanghai Banking Corporation, Hong Kong". *Proc. Institution of Civil Engineers, Vol. 80, London, pp851-883.*

Lee, D.M., Pappin, J.W. and Buckler, J.G. (2001). "Control of ground movement in the construction of Festival Walk". *Proc 14th Southeast Asian Geotechnical Conference.*

Liu, J.H. (1993) "The Prediction of Ground Movements around Slurry Wall Supported Deep Excavations". *Proc. Sino-American Technology Engineering Conference, Infrastructure Construction Session, Beijing, pp84-85.*

Long, M. (2001). "Database for Retaining Wall and Ground Movements due to Deep Excavations". *ASCE Journal of Geotechnical and GeoEnvironmental Engineering, pp. 203-224.*

Lui, J.Y.H. and Yau, P.K.F. (1995). "The Performance of the Deep Basement for Dragon Centre". *Proc. of the 15th HKIE Geotechnical Seminar on Instrumentation in Geotechnical Engineering.*

Mak, L.M. and Liu, J.H. (1996) “Geotechnical problems associated with substructures construction above Metro Tunnels” *Proc. of the 16th HKIE Geotechnical Division Annual Seminar*.

Nicholson, D.P. (1987) “ The Design and Performance of the retaining Wall at Newton Station”. *Proc. of the Singapore MRTC Conference, Singapore, pp147-154.*

Pan J.K.L., Pappin J.W., Cowan S. & Lam L. W. Y. (2001) “An Application of the Observational Method at Tseung Kwan O Station and Tunnels”. *Proc. of the 20th HKIE Geotechnical Division Annual Seminar*.

Pappin, J.W., Simpson, B., Felton, P.J. and Raison, C. (1986). “Numerical analysis of flexible retaining walls” Symposium *on computer applications in geotechnical engineering, The Midland Geotechnical Society, April*.

Sze, W.C.J. and Young, S.T. (2003). “Design and Construction of a Deep Basement through an existing Basement at Central”, *Proc. of the 22nd HKIE Geotechnical Division Annual Seminar.*

Walsh, N.M. and Fung, K. (1989) “The Use of Inclinometers to Improve the Modeling of Retaining Walls”. *Proc of the 9th HKIE Geotechnical Division Annual Seminar*.

Woo, S.M. and Moh, Z.C. (1990) "Geotechnical Characteristics of Soils in the Taipei Basin", *Proc. of the 10th Southeast Asian Geotechnical Conference, Taipei, Volume II.*

Young, S.T. (2003). “Slurry Wall Design for Hong Kong Station”. *Proc. of Conference “Earth Retention Systems 2003” jointly organised by ASCE Metropolitan Section Geotechnical Group, The Deep Foundation Institute and ADSC: The International Association of Foundation Drilling, May 2003, New York City.*

ACKNOWLEDGEMENT

The measurements for the cases in Taipei and Shanghai are taken from internal files of Arup Hong Kong. Assistance from many colleagues in Arup Geotechnics, particularly Dr Jack Pappin and Ir Mark Choi, is gratefully acknowledged.

挖坑導致岩土工程意外的個案

歐陽仁生　　江純敏
香港特別行政區政府土木工程署土力工程處

CASE HISTORIES IN TRENCH EXCAVATION FAILURES

Y S Au Yeung and Jessie S M Kwong
Geotechnical Engineering Office, Civil Engineering Department
Government of the Hong Kong Special Administrative Region

撮要

挖坑工程主要是爲社區敷設或維修公共設施及溝渠。根據土木工程署土力工程處的研究結果，由一九八六年至二零零零年期間，共有最少十五宗因挖坑導致的塌坑及山泥傾瀉事件，一共造成十人死亡和四人受傷。該研究亦發現在一九六六年發生一宗十分嚴重的擋土牆崩塌意外，造成六人死亡及十六人受傷，而牆腳的挖坑工程是導致該宗慘劇的主因。隨後在二零零零至二零零三年二月期間，再發現多四宗與挖坑有關的岩土工程意外，造成多四人受傷。從研究這二十宗已知與挖坑有關的岩土工程意外得知，導致坑道崩塌的主因，是由於承建商未有建造有足夠支支撐力的臨時橫撐。至於導致與挖坑有關的山泥傾瀉意外，其主因之一是由於排水設施不足以至地面水進入坑道，最終造成山泥傾瀉。本文載有這二十宗因挖坑導致意外的詳情以及可能引致意外原因的分析。

CASE HISTORIES IN TRENCH EXCAVATION FAILURES

Y S Au Yeung[1] and Jessie S M Kwong[2]

Abstract: Trench excavations are carried out principally to allow installation or repair of public utilities, drains and sewers to serve populated areas. A study carried out by GEO (2001) found that between 1986 and 2000, there were at least ten deaths and four injuries caused by fifteen trench excavation failures or trench-induced slope failures. The study also discovered a very serious single incident in 1966, in which a retaining wall collapsed killing six people and injuring sixteen others and trench excavation at the toe of the wall was the main cause of the tragedy. Further information obtained between 2000 and February 2003 showed another four geotechnical failures related to trench excavations, adding another four injuries. The observations on these twenty known trench-related geotechnical failures revealed that the common causes of trench collapses could be attributed to inadequate shoring. In the case of trench-related slope failures, one of the main contributory factors was found to be inadequate drainage provisions to prevent water ingress into open trenches. This Paper will present the factual details of the twenty failure cases and diagnoses into the possible causes of the failures.

INTRODUCTION

A search of existing files and information has discovered at least twenty trench excavation failures causing casualties or serious trench-related landslides in Hong Kong. These twenty trench-related failures resulting in the total casualties of sixteen deaths and twenty-four injuries will be reviewed in this Paper.

SOURCES OF INFORMATION

This study includes a review of the readily available information on past trench failures. The sources of information came from various Government Departments, utility undertakers and newspaper agents. Special attention is paid to those trench failures affecting slopes and retaining walls (collectively termed slopes in this Paper) and causing public safety concerns. Detailed studies to diagnose the probable causes of four of the trench-induced landslides were undertaken by GEO's Landslide Investigation Consultants.

[1] Chief Geotechnical Engineer, Geotechnical Engineering Office, Civil Engineering Department, Government of the Hong Kong Special Administrative Region
[2] Senior Geotechnical Engineer, Geotechnical Engineering Office, Civil Engineering Department, Government of the Hong Kong Special Administrative Region

CASE STUDIES OF TRENCH EXCAVATION FAILURES

Trench excavations are normally carried out to allow installation or repair of public utilities. Many regard the works being minor in nature and thus tend to ignore the necessary safety measures. However, it should be noted that the shallowest excavated depth of the failed trenches reported in this Paper was 1.3 m. In fact, the excavated depths were less than 2 m in seven out of the twenty failure cases and seven cases with depths ranging between 2 m and 3 m when failed. These statistics highlight the potential danger even in shallow excavations, and precautionary measures should not be neglected. The twenty trench-induced failure cases are reviewed, and their modes and probable causes of failures are also discussed. The trench-induced geotechnical failures are categorized into five modes, viz. collapse of trench, collapse of slope below trench, collapse of slope above trench, collapse due to vibrations and collapse due to poor backfilling/reinstatement work.

(A) Collapse of Trenches

The primary causes of trench collapses reviewed in this Paper were due to inadequate or absence of shoring, improper working procedure or excessive surcharge imposed on trench sides. Such problems may have been caused by unsatisfactory contract specification of the shoring requirements, or by non-compliance with specified shoring details, or both.

According to the information collected, eleven out of the twenty failure cases involved trench collapsing and caving-in, in which eight workers were killed and seven injured.

(A1) 30.6.1986 – Kellet Bay near Shek Pai Wan Road, 2.5 m deep trench, one fatality
(A2) 22.2.1987 – Nga Tsin Long Road, 1.3 m deep trench, one fatality
(A3) 11.1.1990 – Along the Fanling bound carriageway of Sha Tau Kok Road, 2.4 m deep trench, one fatality
(A4) 6.1992 – Near Lam Kam Road roundabout towards Shek Kong direction, trench depth unknown, closure of main road
(A5) 26.2.1993 – Castle Peak Road near Pok Oi Hospital, 4 m deep trench, one fatality, one injury
(A6) 4.7.1993 – Ping Ha Road, Yuen Long

Workers were laying pipes inside a 3 m deep unsupported trench when a cave-in occurred. One of the workers was killed and another one was injured by the collapsed soil. The collapse was likely to have been caused by the absence of shoring support and the external loading induced by a heavy vehicle parked at the trench side.

(A7) 24.12.1994 – Junction of Ferry Street & Man Wui Street, 1.7 m deep trench, one fatality

(A8) 15.4.1996 – Wang Lee Street, Yuen Long

An excavated trench caved in and a worker was killed by collapsed soils. The open trench was about 2.2 m deep. The probable cause of the failure was reported to be insufficient shoring.

(A9) 5.11.1999 – Sam Mun Tsai Road, Tai Po

Workers were preparing for the installation of support when the trench side collapsed. The unsupported trench was 2.8 m deep. The failure caused one death and one injury.

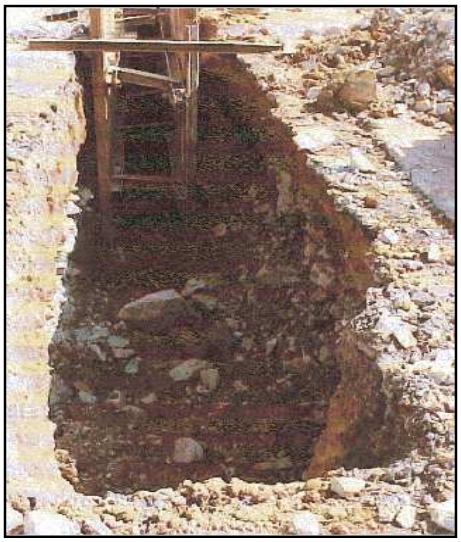

(A10) 5.4.2001 – La Salle Road, Kowloon Tong, 3 m deep trench, two injuries

(A11) 19.2.2003 – Lai Chi Kok Road, Cheung Sha Wan

Two workers were injured, one seriously and one critically, by the collapsed trench. They were working inside the unsupported 1.5 m deep trench at the time of the failure.

(B) Collapse of slopes below trenches

Infiltration of rainwater into slopes is one of the main causes of landsides in Hong Kong. Open trenches, being more susceptible to infiltration, could lead to failure of adjacent slopes below if drainage is not adequately provided.

The following cases were landslide cases likely to have been induced by trench excavations at the slope crest. Although no fatality was reported in these cases, there were near misses. In fact, one person was injured in one case and the economic consequences (such as, closure of major roads) were significant.

(B1) <u>24.8.1999 – Kennedy Road near 6 Hau Fung Lane</u>

The trench was located at the crest of a slope and excavation work was in progress. The open trench was left uncovered during a heavy rainstorm. It was likely that because of inadequate drainage provision on site, water was allowed to enter the trench and infiltrated into the slope below. A landslide occurred as a result of rise in groundwater level.

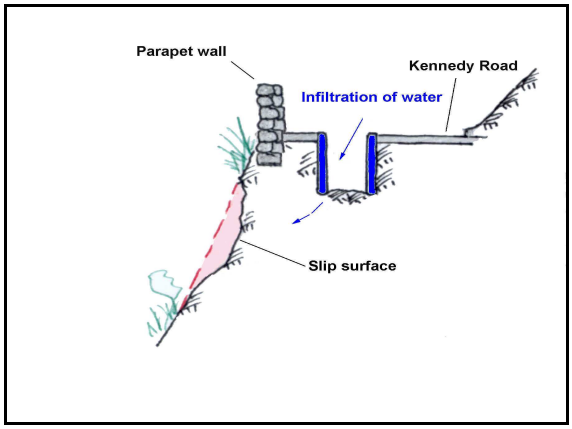

(B2) <u>2000 – Kennedy Road</u>

A trench of 3 m deep was being excavated at the crest of a fill slope to facilitate laying of cables. Sheet piling was installed to support the trench sides. The open trench was left uncovered during a heavy rainstorm. Surface water was likely to have entered and accumulated inside the trench, and subsequently infiltrated into the fill slope below. The fill slope collapsed injuring one passer-by and causing damages to building and closure of two major roads.

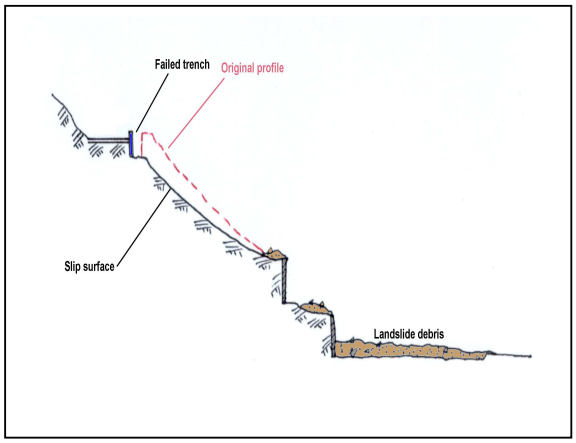

(C) Collapse of slopes above trenches

When a trench is excavated near the toe of a slope, special attention should be given in order not to undermine the stability of the slope due to the loss of toe support.

Trenching works at the toe of the slopes without proper supports led to the collapse of the following two slopes. The failures of which resulted in the deaths of two workers and six passers-by, plus the injuries of sixteen others.

(C1) <u>8.6.1966 – Adjacent to La Salle Primary School, Boundary Street</u>

A trench was excavated to facilitate the laying of cable in the pavement in front of a section of a masonry wall. The 2 m high, 15 m section of the 76 m long masonry wall forming the boundary of La Salle Primary School collapsed outwards onto Boundary Street during heavy rainfall. The wall collapsed on a bus queue full of school children at 12:30pm, killing six and injuring 16 others.

Professor Lumb in his investigation report concluded that "the collapse of the wall at La Salle Primary School was due to a combination of (a) water pressure behind the wall, (b) poor quality of the mortar in the wall, and (c) the excavation at the foot of the wall". He went on to say that "Failure might not have occurred if there had been no trench excavated, but the prime cause of the collapse was water pressure…".

(C2) <u>6.5.1993 – Tung Chung Road</u>

A pipe was being laid when a worker inside the trench was struck by a rock falling from an adjacent upslope. The trench was 1.5 m deep and support was not installed throughout. It was likely that the slope was disturbed and its stability undermined by the excavation of the trench, resulting in the rock fall and one fatality.

(D) Collapse due to vibrations

The stability of slopes with loose boulders or rocks on surface, or sub-vertical masonry or brick facing may be vulnerable to vibration induced by heavy machinery operating in close proximity. Two cases of vibration-induced failures were found.

(D1) 16.1.1991 – Between the pavement of Lung Cheung Road and ventilation building of Diamond Hill MTR Station

A worker was hit and killed by pieces of fallen sand brick skin wall while breaking up a concrete slab at the bottom of a 1.7 m deep trench using a pneumatic breaker. The sand brick skin wall was attached to the external wall of a building adjacent to the trench. The integrity of the wall was affected by vibration induced by concrete breaking.

(D2) July 2000 – Slope No. 11SW-D/C547, Middle Gap Road

Two landslides occurred at the slope shortly after workers started to excavate a shallow trench using a pneumatic hammer to break up the existing carriageway during road kerb construction near the slope toe.

The detailed study of the landslides carried by GEO concluded that "…The close correlation of timing between the works and the occurrence of the landslides, together with the location of the active works in close proximity to the landslides site, suggest the possibility that vibrations caused by the hammering action could have been a contributory factor to the failures." The landslides resulted in the temporary closure of the southbound lane of Middle Gap Road.

(E) Collapse due to poor backfilling/reinstatement work

Loosely compacted trenches will permit lateral flow of water along the trench through the backfilled material. They will also lead to excessive settlement of roads which will damage the road structure and will cause damage to the underlying utilities. Infiltration through cracked pavement into the loose soil can lead to the failure of the adjacent downslopes. Three landslides related to poorly compacted trenches were reported.

(E1) 9.1.1996 – Opposite Tsang Tai Uk, Lion Rock Tunnel Road

When the backfilling work of a trench excavated at the toe of a fill slope was found not up to standard, the backfill material had to be dug up and re-compacted. After a lapse of four months, it was noted that continuous cracks had developed on the fill slope.

An investigation report indicated that there were a number of factors that contributed to the development of the cracks. The inadequate compaction of the backfill material during the trench work had triggered some movement of the slope above, and the removal of toe support during the second trench works had worsen the slope condition. The incident resulted in the recompaction of the entire fill slope.

(E2) 24.8.1999 – Pokfulam Road, opposite the Chinese Christian Cemetery

A landslide occurred at a cut slope above Pokfulam Road. Trench excavation works had been going on along a 3 m wide berm above the landslide site. The GEO

investigation report concludes "It is probable that inadequate drainage provisions associated with the construction works along the berm immediately above the failure led to a change in site condition sufficient to affect the stability of the slope at time of rainfall. There was evidence to indicate that concentrated surface water runoff from the hillside above the berm had flowed across the recently completed conduit and onto the unprotected portion of slope above the landslide. This occurred due to a lack of appropriate drainage and protection measures along the newly constructed conduit in the vicinity of the failure. Furthermore, standing water of 100 mm to 200 mm deep found in the unlined trench of 2 m deep would have led to a concentrated source of infiltration into the slope. These conditions are considered to have generated elevated water pressures in the materials in the vicinity of the landslide leading to the failure of the slope."

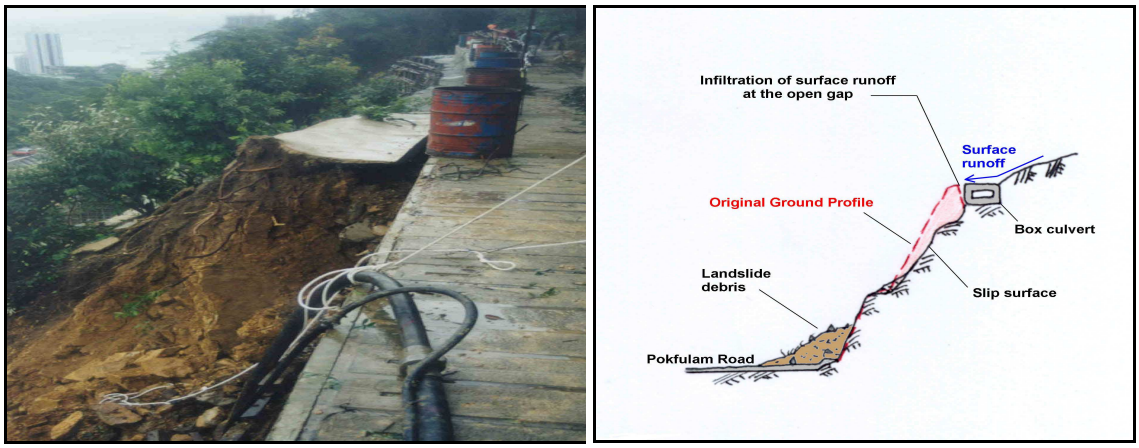

(E3) 2.9.2001 - Kwun Ping Road, North of Tsz Wan Shan

An investigation carried out by GEO reported that "A deep backfilled trench runs along the crest of a fill slope beneath Kwun Ping Road. The backfill material within the trench was found to be loose at depths with 0.9 m of the ground surface. Extensive cracks and ground settlement of the pavement of Kwun Ping Road had developed on the surface of the road probably as a result of the settlement of the loose backfill to the trench."

A section of the road verge collapsed with the landslide undermining a narrow portion of the road pavement. The report concluded "the failure was probably triggered by the saturation of the backfill to the trench immediately behind the main scarp and the build-up of transient groundwater pressure within the relatively thin layer of loose fill".

Summary of the Main Causes of Failures and Recommendations

It is clear from the information on past failure cases that the stability of the trench and adjacent slopes can be affected if trench excavations are not properly carried out. The main factors contributing to the failure of trenches and slopes are : inadequate shoring, inadequate drainage provision leading to ingress of runoff from the surface and infiltration, and loss of toe support. Compaction of backfill upon completion of excavations is also important as trenches loosely backfilled with soil will permit almost as much infiltration from the surface as an open

trench. These common causes of failures could be due to inadequate contract specifications of the works or non-compliance with specifications or both. In view of the problems and deficiencies, a Guide to Trench Excavations (HyD & CED, 2003) has been prepared and published to enhance safety of trench excavations, particularly on the aspects of shoring support and drainage measures. The Guide is intended to promote a safe and healthy working environment for all personnel in construction sites and the third parties which may be affected by trench-induced slope failures. The Guide includes the following major recommendations, among others, :

a) No worker should be permitted to work in an unsupported trench with depth greater than 1.2 m.
b) Excavation of trenches located on or above man-made or natural slopes should be avoided during the wet season if possible. If excavation during the wet season cannot be avoided, adequate drainage provisions must be provided to ensure that the stability of the adjacent slopes will not be adversely affected by any water ingress from the trench.
c) Trench excavation must be closely supervised to ensure compliance with the statutory requirements and contract specifications.
d) Upon completion of the trench work, the trench must be backfilled with suitable material compacted to the required density (e.g. 95% of the maximum dry density).

CONCLUSIONS

The review of the past failures of trench excavations known to GEO has discovered at least twenty trench excavation failures or trench-induced landslides, which resulted in the total casualties of sixteen deaths and twenty-four injuries. Therefore, the risk associated with shallow excavations is not low. A Guide to Trench Excavations (HyD & CED, 2003) has therefore been prepared and published to enhance safety standards of trench excavations in Hong Kong. This Guide is available for download at Highways Department Website <http://www.hyd.gov.hk> and Hong Kong Slope Safety Website <http://hkss.ced.gov.hk>.

REFERENCES

GEO (2001). *A Study on Past Failures of Trench Excavations*. Special Project Report SPR 2/2001, Geotechnical Engineering Office, Civil Engineering Department, the Government of the HKSAR, 68p.

HyD & CED (2003). *Guide to Trench Excavations (Shoring Support and Drainage Measures).* Highways Department and Civil Engineering Department, the Government of the HKSAR, 42p.

ACKNOWLEDGEMENTS

This paper is published with the permission of the Director of Civil Engineering, Government of the Hong Kong Special Administrative Region.

在新填海區的筏式基礎

朱沛坤　　邱國輝
邁進土木結構工程顧問有限公司

RAFT FOUNDATION ON NEWLY RECLAIMED LAND

Reuben P. K. Chu & Paul K. F. Yau
Meinhardt (C&S) Limited

撮要

在填海區，一般典型土層包括填土，填土下便是較軟弱沖積土或淤泥粘土層。由於填土附加荷載關係，長期粘土壓密沉降會隨時間出現，因此大部份建築結構物都採用樁基礎支撐。但是樁基礎經濟取向性，是取決於負摩擦力大小、堅固土層深度、結構荷載和型式等。同時，樁基結構由於沉降相對較少，因而樁基建築結構與外圍非樁基建築物設施相對產生較大差異沉降。另一選擇方案，淺型筏式基礎配合一些地基改良方法，以達到控制地基沉降要求來承托建築結構是較爲有效方案。

本文簡述其中一個應用於香港新填海區的筏式基礎成功例子，介紹有關詳細土力工程設計考慮。

RAFT FOUNDATION ON NEWLY RECLAIMED LAND

Reuben P.K. Chu[1] and Paul K. F. Yau[2]

Abstract: In reclamation areas, the typical sub-soil profile is a layer of fills underlain by soft clay layers such as marine and alluvium deposits overlying decomposed rock. Owing to the soft cohesive and silty nature of the deposits, large ongoing consolidation settlement would occur over a fair long period of time after completion of reclamation. As a result, most of the building structures are supported by piled foundation. However, the economy of the piled foundation is much governed by factors such as negative skin friction on the piles, the depth of firm stratum, the type of structures and the intensity of loadings. Meanwhile, the piled foundation supporting structures would have created an interface problem between the pile-supported structure and the on-grade supported services laid on the newly reclaimed land. An alternative of shallow raft foundation with appropriate ground treatment would be a more effective option when the raft foundation settlements are controlled within the acceptable limits of building structures.

This paper presents one of the case histories in which shallow raft foundation has been adopted for the development on a newly reclaimed land in Hong Kong. The detailed geotechnical design considerations for the practical applications of raft-type foundation on the reclaimed land are illustrated.

INTRODUCTION

In November 1995, Hong Kong Aircraft Engineering Company (HAECO) commissioned Meinhardt Consulting Engineers to design and take up the project management of the construction of the Aircraft Base Maintenance Facilities at the western end of the reclaimed Airport platform at Chek Lap Kok. The facility consists of a three bay Aircraft Hanger, adjoining four-storey workshop and office buildings, and external pavement. The two key challenges were to create a column clear space 220mx70m capable of accommodating 3 no. 747-700 Boeing and 2 no. A230 Airbus aircraft and the cost-effective foundation design for the whole complex. The programme required the application of fast track philosophy to both the design and construction. The master plan prepared by Meinhardt was signed off in February 1996. The construction began in October 1996 and completed in July 1998. The foundation solution supporting the structure is of a shallow raft footing to cater for the nature of the ground, the structure types, the intensity of the loadings, and acceptance criteria of the foundation settlement. This paper presents the raft foundation adopted on a newly reclaimed land in Hong Kong. The detailed design considerations including ground investigation, performance review of reclamation work, foundation option with ground improvement techniques, foundation settlement analysis, and comprehensive structure settlement monitoring and review are briefly described.

1 Director, Meinhardt (C&S) Limited
2 Technical Director, Meinhardt (C&S) Limited

SITE LOCATION AND GROUND INVESTIGATION

The site is located at the western end of the reclaimed Airport platform at Chek Lap Kok, about 50m from the vertical seawall (Figure 1). It has a total of about 260mx180m in plan area. As revealed from the construction records of the reclaimed platform, the western most part of the site was reclaimed with Type A/B rock fill with a surface capping of Type C sand fill, while the remainder of the site has been reclaimed with Type C sand fill. The site is of a general flat platform. A site investigation was carried out at the site to identify the ground conditions, and to establish the sub-soils properties and geotechnical design parameters for the foundation design. The investigation consisted of the following:

- 15 vertical boreholes with regular sampling and standard penetration tests
- 22 piezo-cone penetration tests
- 6 seismic cone penetration tests
- 3 spectral analysis of surface waves tests
- Pore water pressures and hydraulic conductivity measurements
- Laboratory testing of the undisturbed mazier samples, and bulk samples of sand fill

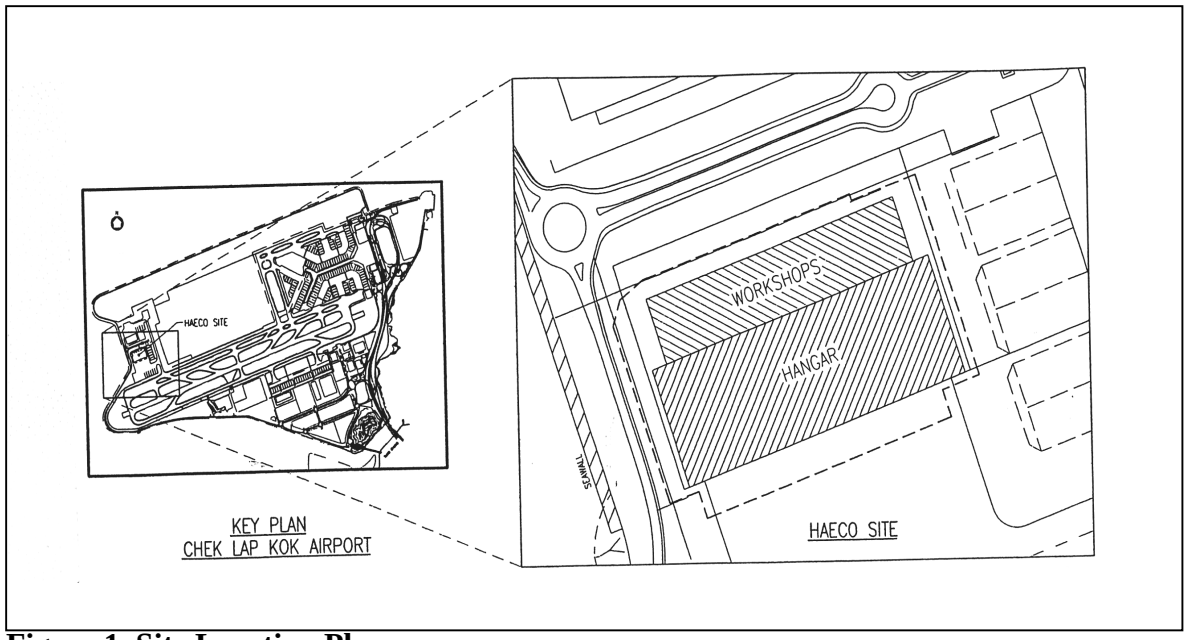

Figure 1. Site Location Plan

GEOLOGICAL CONDITIONS

The typical stratigraphy of the site revealed from the site investigation, is summarized as follows:

Table 1: Summary of typical geological profiles

Ground Levels	Soil Profiles
+6 mPD	Ground profile formation Level
-18 mPD to +6 mPD	Fill (Type C or Type A/B)
-47 mPD to –18mPD	Alluvium, consisting of sands, silts and clays
-53 mPD to –47mPD	Completely decomposed granite
Below –53 mPD	Bedrock of decomposed granite

The investigation indicated that the upper 24m of the ground mainly consisted of fill placed during the platform reclamation. The area of Type C sand fill and Type A/B rock fill is consistent with the construction records. The sandfills met the reclamation performance specifications and that the rock fill mainly conformed to Type B rock fill which contained more fines than the Type A rock fill. The specification for Type B was a grading from 0.002mm up to 300mm. Type A rock fill was a well-graded material with a maximum boulder size of 2m. The nature of the alluvial materials was clearly identifiable in the boreholes, and cone penetration tests. The formation of alluvium varied over the site, which consisted of inter-layered sands, silts and silty clay. Up to 18m of silty clay of alluvium was encountered in some locations. The granite bedrock was located at about 55m to 60m below the ground. The groundwater level at the site was generally close to the sea level ranged from +1.5mPD to +2.5mPD. The typical geological conditions across the site are illustrated in Figure 2.

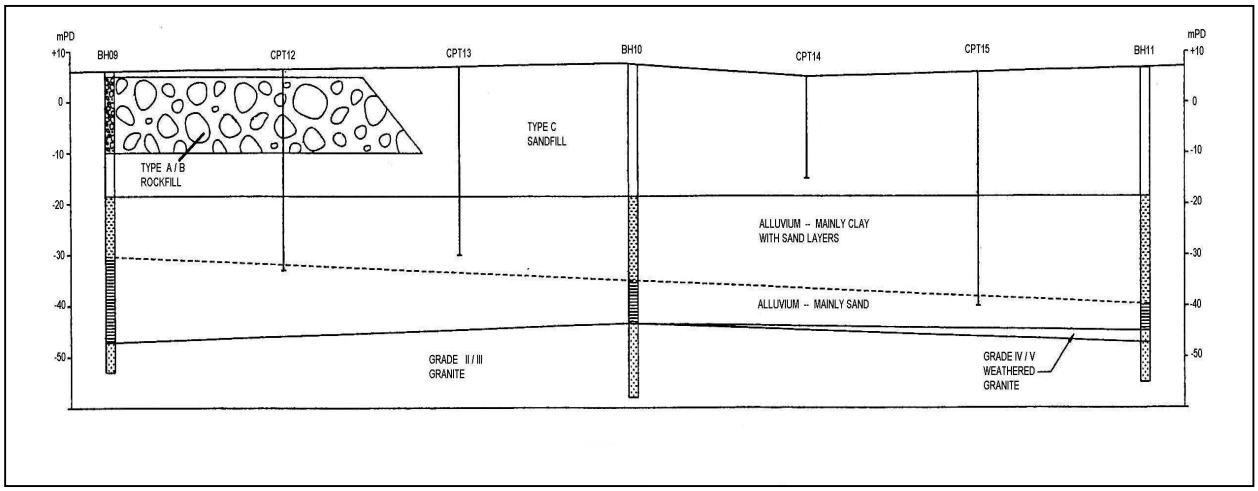

Figure 2. Typical geological cross section across the site

PERFORMANCE REVIEW OF PLATFORM RECLAMATION

Of particular significance is the long-term residual settlement of the newly reclamation of the airport platform. The review of the site performance on the residual settlement and liquefaction potential of placed sand fills is considered.

Long term settlement of airport platform

The design of platform reclamation is a dredged reclamation to remove all soft marine deposits prior to the placing of fill. Because of the relatively recent reclamation of the Chek Lap Kok airport platform at the time of the design of the project, significant settlements due to the consolidation of alluvial soils and/or creep settlement of the reclamation fills are still anticipated. The pore pressures measurements had been obtained from the nearby instruments and the instruments installed in the ground investigation works. The excess pore water pressure at the depth in the alluvium showed that the excess pore water pressure was of less than a meter. The measurements were apparently constant, suggesting that the primary consolidation of the alluvial clays was essentially complete. The secondary compression would be the dominant mode of the long-term settlement in the alluvium.

The long-term settlement of the airport platform has been reviewed by the extrapolation of the settlement monitoring information from the nearby extensometers and by calculations from the laboratory testing results for the alluvial soils. Based on the above review, the suggested

long term platform settlement for a design life of 50 years would range from 100 to 250mm with an average value of 150mm. The differential settlement of the secondary compression due to the varying thickness of the alluvium and fill would be much less and not a controlling factor for the development. The available settlement monitoring information during and after the reclamation is useful for the back-analysis of the sub-soils settlement behaviour for the design of the shallow raft foundation on the reclaimed land.

Liquefaction potential of sand fill

Liquefaction during dynamic loadings such as seismic case is an important consideration for saturated clean sand fill. However, the sand fill at the site has been densified by vibroflotation such that the minimum tip resistance of cone penetration test was 8Mpa. The site investigation also indicated that the sand fill met the specification requirements with the average tip resistance of approximately 12Mpa. An analysis of the liquefaction potential of these sand fill indicates that the densified sand at the site lies well below the lower limits of observed liquefaction of the sand for the appropriate seismic loadings at Chek Lap Kok.

FOUNDATION OPTIONS

All foundation options considered have to satisfy the economy, technical and programme aspects. The two main foundation systems considered as feasible options are pile foundations and shallow foundation with appropriate ground treatment.

Piled foundation

Piled foundations such as driven steel piles and bored piles were considered but they were discounted from the value engineering workshops due to the following results:

- Low bearing capacity of the piles to cater for negative skin friction due to ongoing settlement of the thick alluvial clay extending almost down to rockhead and long piles are therefore required
- Driven steel piles not suitable due to high negative skin friction and no sufficiently firm bearing stratum exists above rockhead
- Much higher construction capital cost for larger diameter bored piles bearing on rock
- Long construction programme and higher risk for delay
- Greater differential settlement between piled building and adjacent aircraft pavements and underground utilities

Shallow raft foundation

For the shallow raft foundation option considered, the most suitable system in terms of constructibility, flexibility for underground services, acceptance of differential settlement, less construction programme and cost are fully evaluated. The greatest concerns of the shallow footing foundation option are of differential settlement, total settlement and allowable bearing capacity of the ground. In the design considerations, the controlling criteria of shallow footing foundation on sand/rock fill much depends on settlement performance instead of the allowable bearing capacity. The factors affecting the shallow foundation settlement performance on the subject site are:

- Whole airport reclamation platform residual settlement
- Additional loadings as a result of shallow footing loadings from the workshop and hanger structures
- The different properties of sand fill and rock fill
- The different loadings applied from the heavier workshop building and the hanger pylon

In terms of reclamation settlement, nothing could be done to eliminate the settlement however

the performance review confirmed that the primary consolidation settlement was complete. The long-term residual settlement would be much less and have no adverse effects to the facilities. The remaining three factors were considered in the shallow footing options. It was concluded that and they could be further minimized if an effective ground treatment was carried out.

Ground treatment by dynamic compaction

The type A/B rock fill was placed by the end dumping method and no compactive effort was applied. Due to the nature of the ground to be treated, dynamic compaction was selected as the most practical method to improve the stiffness of the Type A/B rock fill while the Type C sand fill covering most of the site had been densified by vibro-flotation, which was further confirmed by the ground investigation results and further treatment was not required. The dynamic compaction was therefore intended to allow the treatment of the rockfill to achieve the similar performance to the vibro-compacted Type C sand fill. The acceptance criteria was based on comparing the results of shear wave velocity measured by spectral analysis of surface waves, Menard pressuremeter and loading tests for both Type A/B rock fill and Type C sand fill before and after the ground treatment. The foundation design should also take into account that the settlement performance of the rock fill and sand fill, and the interface between sand fill and rock fill could be different from the geotechnical engineering design point of view.

SHALLOW RAFT/PAD FOOTING FOUNDATION DESIGN CONSIDERATIONS

The final form of banded plate-raft foundation system which consisted of a 600mm thick base slab with 1.2m deep overall upstand beam is adopted for the workshop building foundation while the spread footing foundation is adopted for the hanger pylon foundation as shown in Figure 3. The design of the shallow footing foundation on sand/rock fill depend much on the settlement performance rather than the bearing capacity. The allowable bearing capacities have been assessed based on the geometry of the footings, founding depth, and appropriate soil strength parameters. The calculated allowable bearing capacities against shallow shear failure, and deep seated failure resulting from the alluvial clay had adequate factor of safety of at least 3.

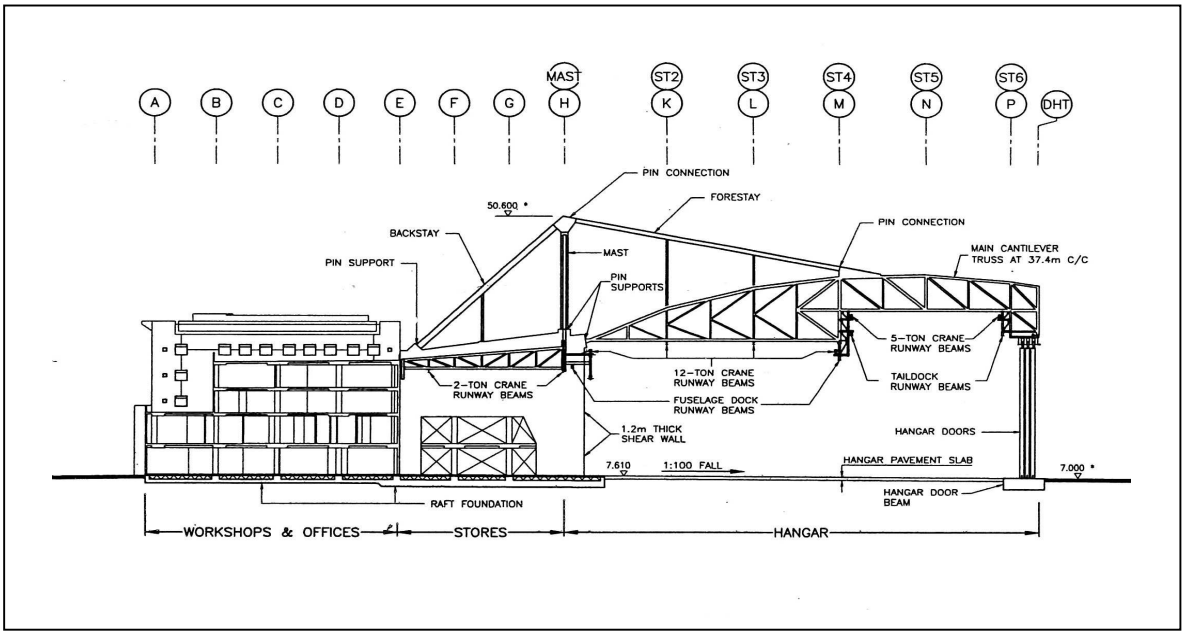

Figure 3. Shallow raft / pad footing foundation arrangement

Foundation settlement assessment

The foundation settlement of the site would occur as a result of:

- Whole reclamation platform settlement which is mainly the secondary compression of the alluvial soils and creep settlement of fills
- Elastic settlement and consolidation settlement of the reclamation fills and the underlying alluvial clays due to the applied raft and footing loadings

Estimation of the settlements was carried out based on a review of reclamation settlement, ground investigation results and the loading of the foundation. The settlement at the critical locations of the foundation was analyzed which included immediate settlement, consolidation settlement and secondary compression. The total settlement due to the workshop building raft of a plan area 40mx200m of about 150kPa and the hanger pylon's pad footing of about 300kPa were calculated. This settlement was in addition to the reclamation platform settlement. The estimated total settlements in a design life of 50 years are ranged from 300mm to 450mm.

The main concern on the settlement effects to the foundation and structures is of the differential settlement rather than total settlement. The differential settlement will depend on the variations in individual loading distribution, variability of the sand or rock fill and differences in the thickness of the alluvial clays and the stiffness of the foundation structures. The final raft foundation design maintained the foundation settlement below a maximum angular distortion of 1:300 between any two-column positions. The workshop building and cantilever foundations would also settle more than the hanger pavement due to the applied foundation loads. These different movements were also accommodated by the articulated transitional slab structures.

Soil-structure interactions

For the foundation design purposes, the raft foundation has been analysed as a slab supported a series of elastic soil springs to simulate the settlement effects to the structures. Using the finite element program "SAFE", a different combination of soil stiffness and loading were modelled for a 3-D raft foundation structure analysis. Of particular concern, the following settlement cases for the different soil stiffness have been assessed:

- Settlement of foundations as a result of the applied structure loading
- Settlement of foundations as a result of platform reclamation
- Settlement across the sand / rock fill transition

In the raft analysis, the soil sub-grade modulus had been allowed to vary from 0.6MN/m^3 to 20MN/m^3 to cater for the predicted settlement effects. The combinations were examined for the more onerous results to be used for design purposes.

Foundation settlement monitoring

The settlement markers at the critical locations of the building workshop and hanger structures are set up for the settlement monitoring and performance review. Since construction began on site in October 1996, settlement monitoring has been continuously taken. The typical measured total settlement and differential settlement against time are produced in Figure 4 and 5. The predicted time-settlement curves for the raft foundation on the reclaimed land are also given in Figure 4. It could be seen that the measured total settlements up to Mid 2002 ranged from 200mm to 400mm and differential settlement between nearby settlement monitoring points ranged from 20mm and 40mm. The calculated maximum angular distortion between nearby settlement monitoring points was about 1:700. The measured settlement and differential settlement are compared within the computed range. The structures have performed as predicted. Clearly, the past settlement records show that the settlement rate has been diminished at 1 to 2 years after the end of construction. The recorded differential settlements come to a more stable level at around 1 year after the end of construction. Generally speaking, the

settlement effects would be reduced to about 50% to 80% of total settlement, 1 to 2 year after the end of building construction.

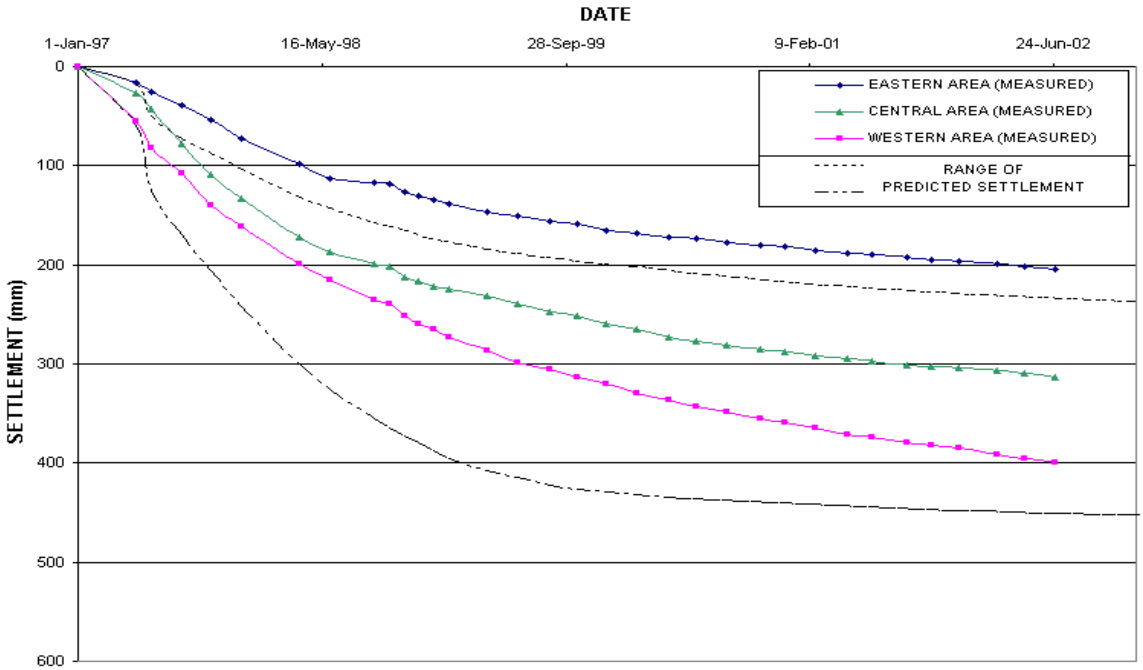

Figure 4. Predicted and Measured total settlement

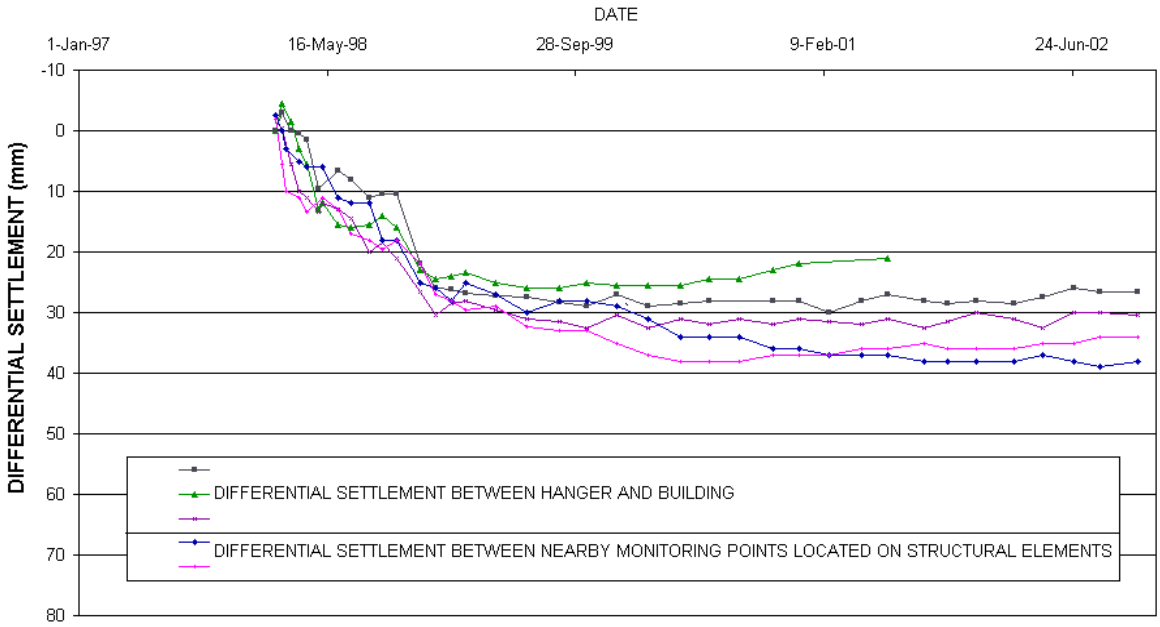

Figure 5. Measured differential settlement

CONCLUSION

The project demonstrated the importance of understanding the geotechnical and structural design of using a shallow footing foundation with appropriate ground treatment rather than the piled foundation to support the facilities on a newly reclaimed land. It also provides the

valuable knowledge and experience in terms of foundation and geotechnical engineering design and construction. In addition, the fast track programme requires an optimization of engineer decision-making and project management to produce a fully integrated design.

REFERENCES

Fang H.Y. (1990). Foundation Engineering Handbook, 2nd Edition.

American Concrete Institute (1988). "Suggested analysis and design procedures for combined footings and mats" Report by ACI Committee 336, J. Am. Concr. Inst., May-June.

Geotechnical Control Office (1991). " Review of earthquake data for Hong Kong region" GCO publication No. 1/91, Hong Kong.

竹篙灣填海工程第一期
如何有效減少沙質填海物料的蠕變

麥克 (前任職)偉信顧問集團有限公司
(現任職)GCG(ASIA)LTD
繆義仁　　偉信顧問集團有限公司

PENNY'S BAY RECLAMATION – STAGE 1
EFFECTIVE REDUCTION OF CREEP IN SAND FILL

Michael S Hendy
Formerly Scott Wilson Ltd, now GCG (Asia) Ltd
Ian C Muir
Scott Wilson Ltd

撮要

竹篙灣的二百公頃填海工程已於二零零零年五月八日展開。最近，首項工程"竹篙灣填海工程第一期"剛剛完成，而基建工程亦正快速地進行中。填海工程中，所使用的填土主要成份爲海相砂，其來源不僅在香港水域之內，亦包括香港水域以外的地方。而工程中，所採用的土地加固技術包括海相沉積軟土之挖掘、部份砂質填土之振動壓實及加載（預壓）。

在設計考慮中，填土的蠕變固結沉降被認定爲長期殘餘沉降的主要成份。故該工程在竹篙灣安裝了全面的土力工程監測儀器裝置，此裝置能夠提供高質素的參考數據於土力工程師，用于測量出殘餘沉降值。本文指出，振動壓實結合相對地適度的加載可以可觀地減少砂質填土蠕變所引起的長期沉降。

PENNY'S BAY RECLAMATION – STAGE 1
EFFECTIVE REDUCTION OF CREEP IN SAND FILL

Michael S Hendy[1] and Ian C Muir[2]

Abstract: Construction of the 200 ha reclamation at Penny's Bay commenced on 8 May 2000. The first Contract – Penny's Bay Reclamation, Stage 1 – has recently been completed and the follow on Works for Infrastructure is progressing rapidly. The fill used in the reclamation has comprised predominantly marine sand, which has been sourced from various locations within and outside of Hong Kong waters. Ground treatment has included dredging of the soft marine deposits, partial vibrocompaction of the sand fill and surcharging.

At the time of the design, creep in the fill was identified as a major component of the long-term residual settlement. The comprehensive programme of geotechnical instrumentation installed at Penny's Bay has provided some good quality data for quantifying residual settlement. This paper demonstrates that vibrocompaction combined with relatively moderate surcharging has significantly reduced the long-term settlement due to creep in the sand fill.

INTRODUCTION

Penny's Bay Reclamation – Stage 1 (Contract CV/99/12) is the site formation Contract for Hong Kong Disneyland under the direction of the Civil Engineering Department.

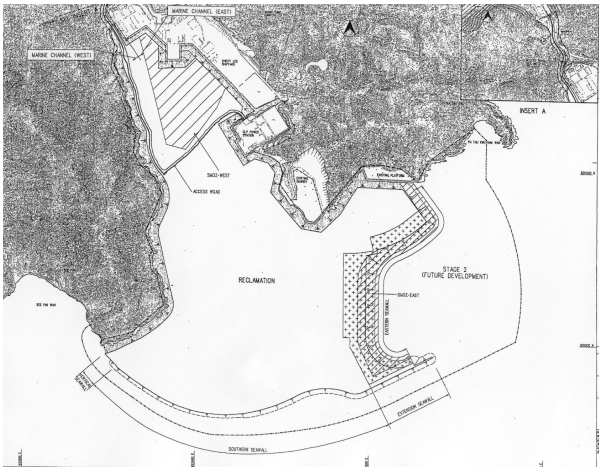

Figure 1 – Site Plan

The chosen site at Penny's Bay offers the benefits of an area of sheltered water at the north east end of Lantau and with appropriate infrastructure is strategically placed for future access by road, rail and sea. The site had been previously designated for the construction of a Container Terminal back-up area and had been investigated during the early 1990's under the LAPH study. Figure 1 is a key plan of the site.

Early studies by the British Geological Society had identified the presence of thick sediments (marine deposits) to a maximum depth of about 30m and this meant that parts of the site would be dredged in order to meet the tight development programme. A summary of the ground conditions at the site was presented in a paper to the South East Asian

[1] Formerly with Scott Wilson Ltd, now GCG (Asia) Ltd
[2] Scott Wilson Ltd

Geotechnical Conference in 2002 (Hendy & Brown (2002)). The paper summarised the site deposits as comprising up to 30m of Hang Hau Formation overlying Chek Lap Kok up to 20m thick with underlying bedrock of predominantly granite and rhyolite. The Hang Hau Formation thins towards the coast and the inner bay where it reduced to a depth of about 15m. The Hang Hau Formation is typical of the area with soft to firm grey silty clay with shell fragments and occasional shell beds. The underlying alluvium comprises typically firm to stiff, locally soft grey-brown to orange clay interbedded with silty sand. Estuarine deposits are encountered locally including some organics.

One of the key requirements for the proposed theme park was that post-construction settlement was kept small to accommodate simple foundations for the proposed low-rise buildings and theme park attractions. In less sensitive areas where soft deposits were retained, ground treatment included vertical drains and surcharging. Vibrocompaction with nominal surcharging was adopted to densify the thick layer of imported sand fill forming the reclamation.

Vibrocompaction has been used regularly in Hong Kong over the last decade to densify granular deposits (eg Berner (1998), Carter (1996)). However, with the exception of rule-of-thumb equations, there has generally been little data available to quantify long-term settlement behaviour after ground treatment through back-analysis of the creep settlement coefficient, $C\alpha$. The Penny's Bay site has included clusters of geotechnical instrumentation for examining settlement behaviour during construction. The site has therefore provided a unique opportunity to investigate the range of post-treatment $C\alpha$ for a vibrocompacted sand fill.

RECLAMATION PROGRESS

Reclamation commenced on 8 May 2000 with dredging in areas of the inner bay for early construction of the main site access road. Grab dredgers were deployed in this area due to the shallow depth to the seabed. The central portion of the inner bay was designated for a future water recreation centre and soft deposits were retained in this area. Following the initial grab dredging operations, a fleet of trailer suction hopper dredgers (TSHD's) were mobilised to site. The TSHD's significantly increased the rate of dredging and filling and enabled the deeper dredging and filling to be carried out systematically. Towards the end of the dredging/filling programme, the size of the dredgers once again decreased. The variation of dredger capacity and type varied throughout the Contract as summarised on Table 1 and Figure 2, which also give an indication of the capacity of each dredger and filling production rates.

DREDGE	CAPACITY
Rotterdam	21,000m^3
Amsterdam	17,000m^3
Nile River	17,000m^3
Pearl River	17,000m^3
Lange Wapper	13,700m^3
JFJ de Nul	11,750m^3

Table 1 Dredger Capacities

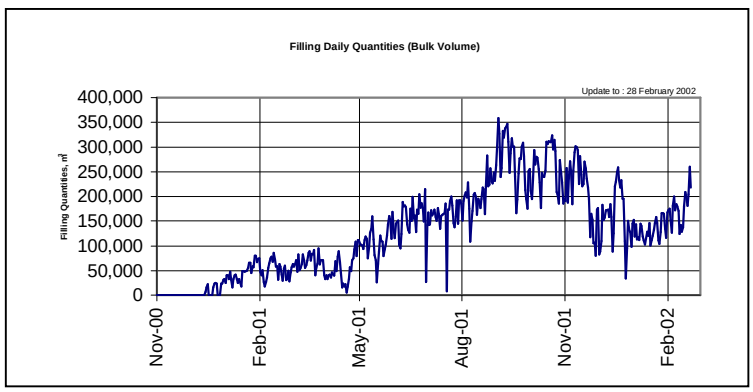

Figure 2 Daily Filling Volumes

GROUND TREATMENT

As previously mentioned, ground treatment in dredged areas comprised vibrocompaction and nominal surcharging. Figure 3 shows the vibrocompaction in progress. The design intent was generally to densify the top 15m of the sand fill to provide a 'stiff' upper layer in the sand fill profile. In more sensitive areas of the site or where greater loadings were anticipated, vibrocompaction was specified to full depth.

Figure 3 Vibrocompaction in Progress

Densification of the top 15m of sand fill provided two benefits:

Firstly, it reduced residual settlement within the treated zone by reducing the void space. Secondly it provided a stiff but flexible raft, which would assist with bridging soft or weaker areas at depth (local soft spots) and would thus assist with reducing differential settlement at the surface. Limiting the extent of full depth vibrocompaction also reduced the cost of the ground treatment.

The design formation level varied across the site to allow for future drainage requirements and also to allow for settlement. The follow-on infrastructure contracts would require additional filling and re-profiling to suit the final layout – information not available during the reclamation design. Nonetheless, it was recognised that to minimise re-compaction of the imported sand fill during follow-on Contracts, compaction to formation level was required during the reclamation. This was achieved by specifying vibrocompaction to Formation level, which had the additional benefit of reducing the risk of settlement due to soft spots near the surface. In order to ensure there would be sufficient confinement of the vibrating equipment near the surface, a nominal 2m high surcharge was specified as part of the design.

The Specification for the vibrocompaction was based on well-known correlations between relative density and CPPT. A 50m grid of CPPTs specified after completion of vibrocompaction was used as a basis for acceptance of the ground treatment. The Specified CPT profile in the Contract is presented as Figure 4**.**

Several compaction trials were carried out prior to undertaking the production vibrocompaction. The trials assisted with development of an efficient grid spacing and helped determine the most appropriate type of equipment for vibrocompaction.

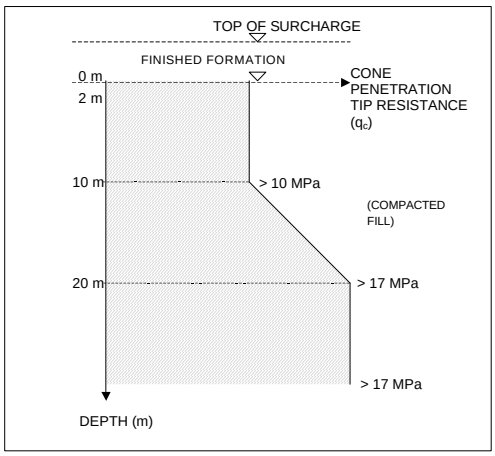

Figure 4 Specified CPPT Profile

A spacing of 2.3m was determined for the vibrocompaction points from the trial. The achievable insitu relative density depends on the sand quality as well as the available equipment for vibrocompaction. During the design stage, East Lamma Channel was known to be an available source for some of the 65 million m^3 of sand required for the project, whilst the remainder of the sand had to be sourced from outside of Hong Kong waters. The quality of the sand at East Lamma was known to be generally good for vibrocompaction but natural variation in the sand quality was inevitable and the source of sand from outside of Hong Kong waters was unknown prior to tender. To ensure that clean sand was used on site, a tight grading envelope with a reduced limit on fines content was specified.

One of the biggest single factors affecting the density of the as-placed sand is the method of placement. At the time of design, the placement method was unknown although it was likely that the sand would be placed hydraulically given the volume of fill and programme for the Works. The Specification was therefore chosen to accommodate all placement methods. In fact, the Contractor adopted a hydraulic method. Hydraulically placed clean sand is frequently very dense above the water table due to the rapid drainage and force of placement, depending on the sand quality. As-placed relative densities of up to 90% or more can be achieved without vibrocompaction above the water table. Below the water table the relative density is less affected by the placement method and a relative density in the range 40% to 50% is more likely. The Specification was designed to provide a relative density of greater than 85%.

The objective of the vibrocompaction was, in part, to provide a consistent degree of compaction across the site. As expected, the as-placed relative density was found to be high near to the surface prior to vibrocompaction, and generally dropped suddenly at the water table (sea-level) to well below the Specification. It was therefore necessary to vibrate through the dense surface layer to ensure a satisfactory degree of compaction had been achieved in the lower layers and throughout the vibrocompacted profile. The effect of vibrocompaction can be seen from a typical CPPT tip resistance profile in the sand before and after vibrocompaction presented as Figure 5.

The method of placement had a second effect where fines could accumulate in low points. The effect of such segregation could only be controlled by carefully layering the fill during placing and by avoiding extensive settling ponds. High fines, where it had accumulated, would generally reduce the effectiveness of the vibrocompaction. A detailed methodology for acceptance of the vibrocompaction was therefore established at an early stage of the site trials to agree acceptance criteria and to minimise disruption during the production work.

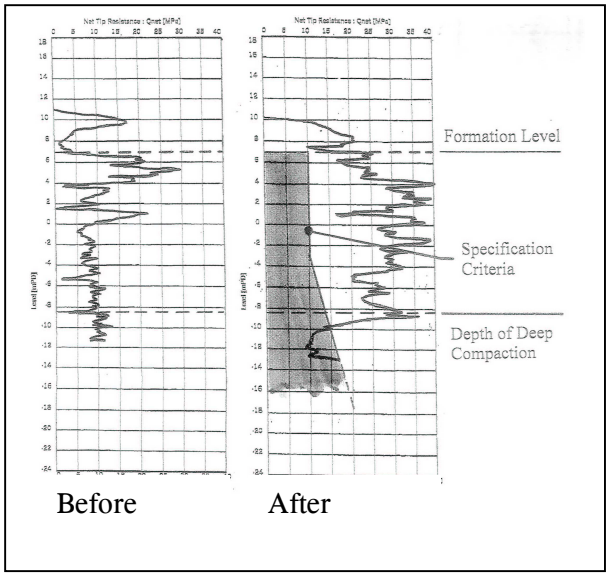

Figure 5 CPPT Profiles before and after vibrocompaction

SETTLEMENT BEHAVIOUR

Instrumentation monitoring data indicating the settlement behaviour of the reclamation during surcharging was used to estimate residual settlements and thereby the long-term settlement performance of the reclamation. Instrumentation included deep settlement plates (placed on the seabed prior to filling and shallow settlement markers placed near formation level. Vibrating wire piezometers were installed where settlement of the underlying alluvial deposits were a concern or where vertical drains were installed in retained soft deposits.

Figure 6 presents a set of time v settlement plots for a sample location, E16N26, situated in the central portion of the reclamation and within an area subjected to full-depth vibrocompaction. The upper plot comprises settlement data from the shallow settlement marker, and the lower plot data from the deep settlement marker. The data covers approximately 3 months and illustrates the sudden settlement at the time of vibrocompaction. In this case, the vibrocompaction resulted in immediate settlement of approximately 400mm, or 1.5% of the layer thickness.

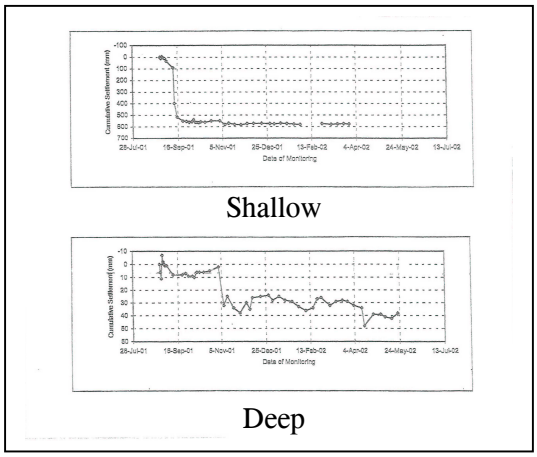

Figure 6 Settlement v Time at E16N26

The back-analysis of the creep settlement coefficient, $C\alpha$, for the full thickness of settling deposits was possible from review of the shallow settlement marker data alone. To identify the creep settlement behaviour in the sand fill, the settlement recorded at the deep settlement marker could be subtracted from the settlement recorded at the shallow settlement marker. Obviously, the zones of full depth vibrocompaction offered the best opportunity to identify $C\alpha$ values for the treated sand, and these areas have formed the basis of the work presented here.

Data from approximately 50 settlement markers at various locations across the site subjected to treatment over the full depth of the sand fill have been reviewed and $C\alpha$ values back-analysed. The results of this work are displayed graphically in Figure 7, with $C\alpha$ plotted against fill layer thickness. The plot indicates no apparent relationship between the two variables.

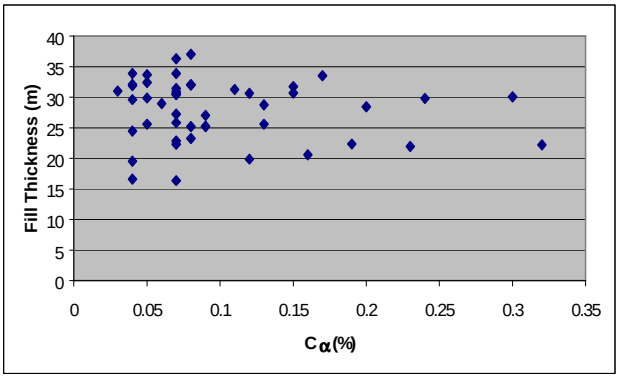

Figure 7 $C\alpha$ versus depth

Values of $C\alpha$ ranged from around 0.05% to in excess of 0.30% and it can be seen that a cluster of results occurs at about 0.10%. Statistical analysis of the data, in fact, indicated a mean $C\alpha$ value of 0.10%, and a standard deviation in the results of 0.07%. The upper 95% confidence limit coincides with a $C\alpha$ value of about 0.20%. These values compares well with other ranges determined previously for sand fill (e.g. Hendy et al (2001) and Muir et al (2001)).

The results of the data review indicate the following:

(i) Creep settlement continues to occur in sand fill following vibrocompaction

(ii) The rate of creep settlement with time for the treated zone should mostly lie within a range of 0.2*%/mm/log cycle* or less, indicating the upper bound of this range would provide a suitable value for use in design.

CONCLUSION

A major reclamation has been constructed at Penny's Bay in a short period of time with good quality sand (low percentage of fines) sourced both from within Hong Kong and outside of Hong Kong waters. The sand fill has been placed hydraulically with modern dredgers and vibrocompacted to various depths around the site. An assessment of the settlement monitoring data indicates that significant densification of the sand occurs due to vibrocompaction and this is dramatically illustrated by the sudden increase in settlement during the vibrocompaction process. Following the vibrocompaction, the rate of settlement in the sand is significantly reduced. From the data examined for this paper, a C_α value of 0.2% is indicated as a suitable design value for a good quality sand fill treated using vibrocompaction.

REFERENCES

Berner P. (1998) Ground Improvement at Chek Lap Kok: Review of vibrocompaction at Hong Kong's new airport; Tansactions, HKIE; 5(1) 1-5.

Carter M. (1996) A Settlement Prediction Method Developed for Macau International Airport; Tansactions; HKIE; 3(1) 35-40.

Hendy M.S. & Brown C.J. (2001), *Hong Kong Disneyland Penny's Bay Reclamation – Stage 1 Site Characterisation*. Proc. 14th South East Asian Geotechnical Conference, Hong Kong., December 2001.

Muir I.C., Hendy M.S., & Ching P.T (2001), *Creep Settlement in Reclamation Sand Fill, Analytical Review and Early Predictions*; Proc. Deformations and Movements, HKIE Geo Seminar; Hong Kong.

Hendy M.S., Ching P.T & Muir I.C (2001), *Creep Settlement in Reclamation Sand Fill, A Case Study*. Proc. Geotechnical Deformations and Movements, HKIE Annual Geotechnical Seminar; Hong Kong.

ACKNOWLEDGEMENTS

The authors would like to thank the Director of Civil Engineering, Hong Kong SAR Government for granting permission to publish this paper. Acknowledgement is also given to Ham-Hong Kong Construction JV and their sub-Contractors who undertook the reclamation contract and collected the data used in this paper.

市區地盤地下連續牆的設計與施工

何智凌
新利地基工程有限公司
李啓信　　林早妮
李啓信工程顧問有限公司

DESIGN AND CONSTRUCTION OF DIAPHRAGM WALL IN A DIFFICULT URBAN SITE

Nick C. L. Ho
Sunley Engineering & Construction Co. Ltd.
K.S. Li and J. Lam
Victor Li & Associates Ltd.

撮要

本文描述了一幢佔有三層地庫的商業樓宇，它座落於觀塘一個市區重建的地盤，鄰近有其他大廈及地下鐵路站。此樓宇的地庫是用地下連續牆建造。在建造過程中，有很多障礙物需要清除，包括現有地庫、樁帽和混凝土樁。雖然有部分障礙物已清除，但仍然有部分大直徑的混凝土樁不能清除，所以在設計地下連續牆時需要作出特別考慮。本文描述了一些設計和施工方法，以便解決此牆在建築上的困難，並介紹在香港新採用的地下連續牆接頭。

DESIGN AND CONSTRUCTION OF DIAPHRAGM WALL IN A DIFFICULT URBAN SITE

Nick C.L. Ho[1], K.S. Li[2] and J. Lam[3]

Abstract: A commercial building with a 3-level basement, flanked by existing buildings and located in close proximity to the Mass Transit Railway station was constructed at an urban redevelopment site at Kwun Tong. The basement was constructed using diaphragm walls. It was necessary to overcome many obstructions, including existing basement, pile caps, unreinforced concrete piles and reinforced concrete bored piles. Some of the obstructions were removed during construction, but the large diameter bored piles had to be left in place. Treatment works were necessary to accommodate the existing bored piles. The paper describes the techniques used to tackle the problems and some new joint details used for construction of diaphragm wall.

INTRODUCTION

A commercial building with a 3-level basement, flanked by existing buildings and located in close proximity to the Mass Transit Railway station was constructed at an urban redevelopment site at Kwun Tong. Figure 1 shows the location of the site which was divided into two main areas, namely Areas 1 and 2. The basement, covering both areas, was constructed using diaphragm walls in a top-down method. The foundation contractor was responsible for the design and construction of the diaphragm wall. The layout of the diaphragm wall panels is also shown in Figure 1.

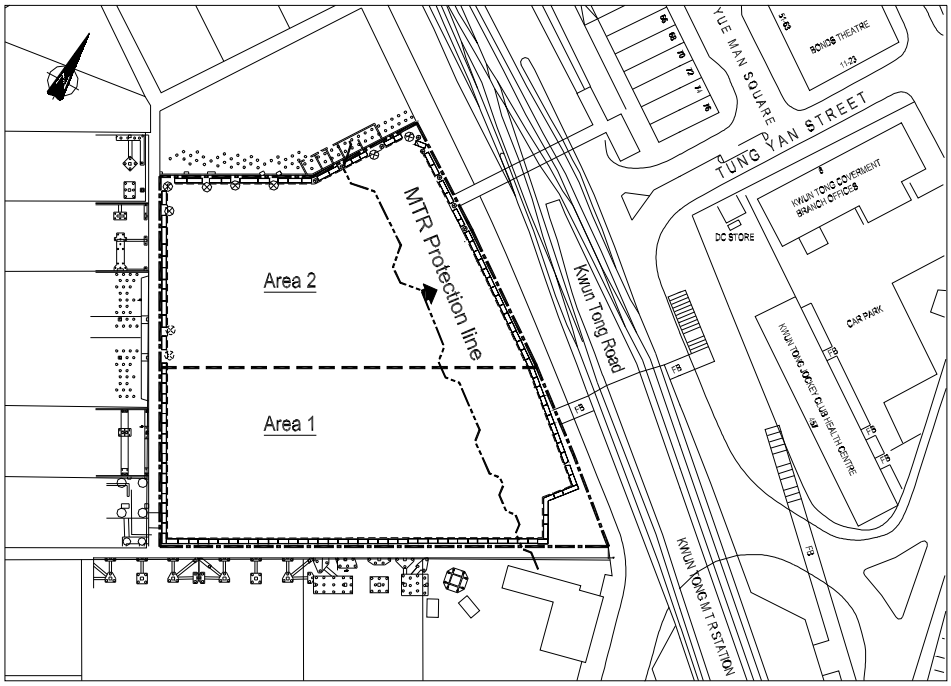

Figure 1 Site location and diaphragm wall layout plan

[1] Senior Contracts Manager, Sunley Engineering & Construction Co. Ltd.
[2] Director, Victor Li & Associates Ltd.
[3] Engineer, Victor Li & Associates Ltd.

The project location was an old redevelopment site. Area 1 was previously occupied by a pre-existing building with a basement of 5m in height, which covered the whole of Area 1. The building had been demolished prior to the re-development, but the basement remained in place. To minimize the construction difficulty, the outer faces of the diaphragm walls were set back from the site boundaries by 500mm to 800mm to avoid the old basement wall.

A redevelopment project was previously planned for Area 2. Bored piling works within the site had been completed and sheetpiles were installed along most of the site boundaries of Area 2. However, the redevelopment project was shelved at the stage, leaving abandoned bored piles and sheetpiles along the alignment of the proposed diaphragm wall.

GROUND CONDITIONS

The site is characterized by a stratigraphic sequence of Fill, Marine Deposit, Alluvium and weathered granite of different weathering grades. Figure 2 (a) shows a typical soil profile of the site along the northwestern site boundary where the diaphragm wall was more significantly affected by existing bored piles. A simplified section of the basement for the new commercial development is shown in Figure 2(b).

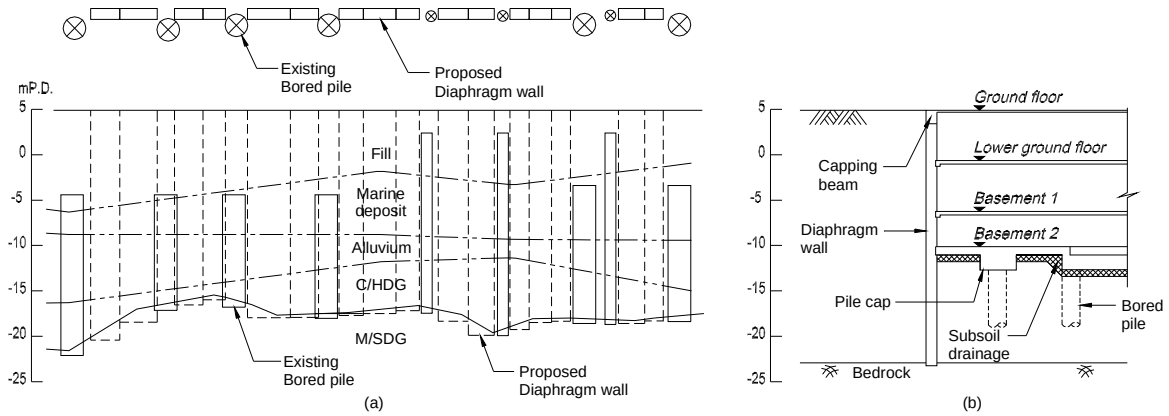

Figure 2 Typical soil profile and details of basement

DESIGN OF DIAPHRAGM WALL

General

The diaphragm wall was a 1.2m thick wall which ran along the perimeter of entire site, except at locations affected by existing bored piles and sheetpiles. The design of diaphragm wall in Hong Kong is generally more conservative than that in many other countries, such as Taiwan, in terms of wall thickness and reinforcement content. The reasons being that:

a. Stringent settlement limits are usually imposed for deep excavation in Hong Kong. Therefore, a stiffer wall with a higher wall thickness is often necessary to control ground settlement.

b. Diaphragm walls are usually constructed in urban sites where the groundwater tables are generally high. As a result, the majority of lateral pressure acting on the diaphragm wall is water pressure rather than earth pressure. In most cases, a conservative

groundwater level and hydrostatic distribution of water pressure are adopted for the design of diaphragm wall to cover the extreme conditions. In Hong Kong, structural design of diaphragm wall is commonly based on the British code BS8110 or the Code of Practice for The Structural Use of Concrete published by the Buildings Department. In these codes, the load factors or partial factors used for structural design is 1.4 or higher, which are considered too conservative when used to calculate the design bending moment and shear force induced by conservative design water pressures for reinforced concrete design.

Design of Treatment Works

As shown in Figure 1, there were many existing bored piles (1.2m or 2.5m in diameter) along alignment of the diaphragm wall in Area 2. Percussive excavation was not allowed within the MTRC protection zone (i.e. Figure 1). This had rendered the most commonly used methods for overcoming obstruction, namely, chiselling, down-the-hole hammer or preboring using the so-called Odex method inapplicable. Even if percussive excavation were permitted, the reinforcement bars in the existing bored piles would make the excavation difficult, slow and costly. While consideration was given to remove the existing bored piles by jacking, it was also ruled out due to technical difficulties and, more importantly, the risk of excessive ground disturbance. A decision was therefore made to leave the existing bored piles in place or to partially remove them later during bulk excavation. Treatment works were necessary to seal off the gap between an existing bored pile and its adjacent diaphragm wall panels. Figure 3 shows the design of some typical treatment works carried out for the project. The salient features of the design scheme of treatment works are described below.

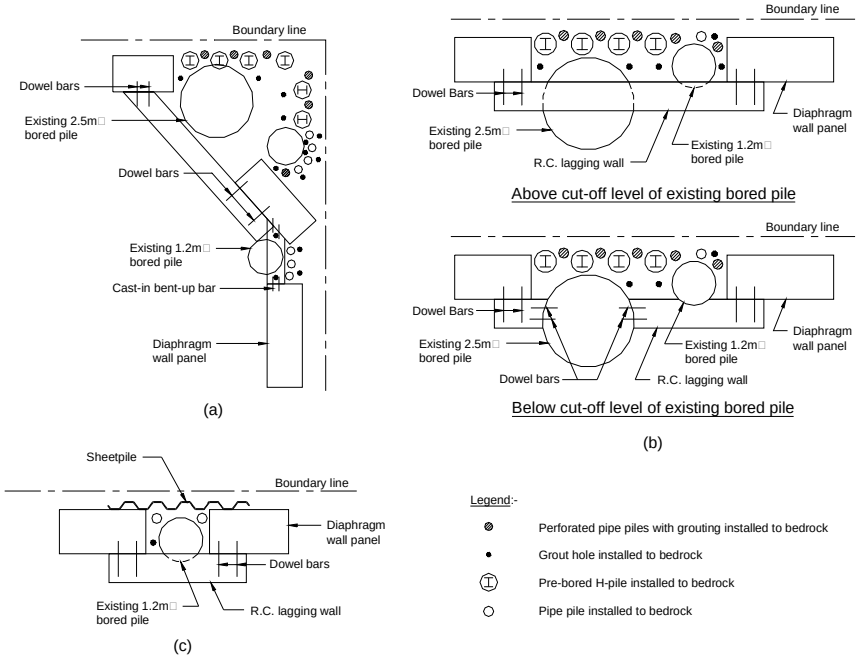

Figure 3 Typical treatment works

a. Diaphragm wall panels were constructed as close to existing bored piles as practicable to minimize the extent of treatment works. The gap widths between existing bored piles and diaphragm wall panels were to a certain extent controlled by the size of the trench cutters or hydraulic grabs used for excavation. The maximum gap width was

about 0.8m. The minimum size of a diaphragm wall panel was also controlled by the excavation equipment. Some of the existing bored piles were so close to each other that it was not possible to install a wall panel between two adjacent bored piles. Therefore, treatment works had to be carried out for a larger extent. At some location, the orientation of the diaphragm wall panel had to be shifted from its main alignment in order to insert a diaphragm wall panel into the gap between two existing bored piles close to each other, as indicated in Figure 3(a).

b. The cut-off levels of the existing bored piles were several metres below ground surface. Therefore, the soils above and behind an existing bored pile had to be supported during bulk excavation for basement construction, which was effected by the installation of temporary pipe piles, prebored H-piles or sheetpiles. The choice of retaining elements was governed by site conditions.

- For the existing bored piles with a cut-off level near the ground surface, sheetpiles were used because of a lower risk of encountering obstructions. Even if obstructions were encountered, they might be removed by local excavation using a backhoe.

- For existing bored piles with a low cut-off level or where it was not possible to insert a diaphragm wall panel in the gap between existing bored piles, pipe piles or prebored H-piles were adopted to support the soil during bulk excavation. When the lateral extent of treatment works was significant and if space permitted, prebored H-piles were used as they could provide stronger and safer structural elements to retain the soil during bulk excavation. Otherwise, 273mm diameter 6mm thick pipe piles were used.

- The provision of sheetpiles, pipe piles or prebored H-piles could not induce a watertight condition during excavation. Therefore, grouting was carried out to provide a grout curtain down to the bedrock as part of the treatment works. Some pipe piles were perforated to allow soils outside these pipe piles to be grouted when grouting was carried out inside the pipe piles.

Sheetpiles, prebored H-piles or pipe piles were only used as temporary structural elements to support the soil during bulk excavation. For permanent installation, lagging walls would be constructed between adjacent diaphragm wall panels and/or existing bored piles, based on the same concept as soldier piles. The lagging walls were designed to resist the water and earth pressures. The loadings from the lagging walls were in turn transferred to the diaphragm walls and/or bored piles. For this reason, the diaphragm wall panels to which the lagging walls were connected were heavily reinforced to resist the additional shear force and bending moment.

To facilitate construction, the lagging walls were designed as two-way beams as illustrated in Figure 4. During excavation, the lagging wall was designed as a simply supported beam spanning across two diaphragm wall panels as indicated in Figure 4(a). The tension forces at the end supports were resisted by dowel bars embedded in the diaphragm wall panels. The dowel bars were secured to the diaphragm wall panel by use of high strength bonding agent. If the lagging wall was designed as a simply supported beam in the horizontal direction, its performance would very much rely on the long-term integrity of the dowel bars. As a safeguard, the lagging wall was also designed as a continuous vertical beam propped by

the basement slabs as indicated in Figure 4(b). When the entire basement structure was complete, the anchor bars would become redundant. The construction of the lagging walls was carried out in phase with the excavation works, with the aid of couplers to connect the vertical reinforcement bars during construction.

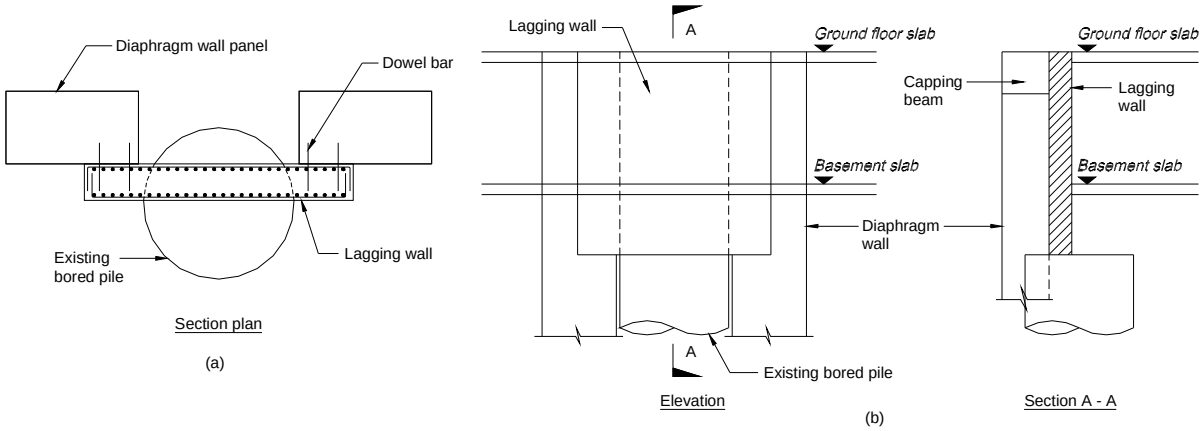

Figure 4 Design of lagging wall

CONSTRUCTION OF DIAPHRAGM WALL AND TREATMENT WORKS

Some general aspects of construction of diaphragm wall and treatment works for the project have been described earlier by Ho & Chan (2001). Only some new features for diaphragm wall construction and techniques used to overcome the construction difficulties for this project will be described in this section.

General

The equipment used for trench excavation included 2.8m and 3.2m wide hydraulic grabs and a 2.8m wide trench cutter. All these equipment had a thickness of 1.2m. Hydraulic grabs were mainly used for constructing primary panels with steel end plates as will be described later.

Bentonite was used to stabilize the trench during excavation. The verticality of slurry trench was continuously monitored by a built-in inclinometer in the hydraulic grab and trench cutter. The vertical alignment of the grab could be slightly adjusted to maintain verticality of the slurry trench by hydraulically controlled head movement of the grabs. The same can be achieved for trench cutters by adjusting movement of the shear plates.

Removal of Obstructions at Area 1

At Area 1, the existing basement, some pile caps and concrete piles could obstruct the construction of diaphragm wall. To facilitate diaphragm wall construction, part of the basement slab and pile caps had been removed during demolition of the building with the help of shoring works shown in Figure 5. Initially, the void space left after partial removal of the basement slab and pile caps was filled with mass concrete according to the original design. The backfilled mass concrete, though weaker than reinforced concrete, was still difficult to be removed by a hydraulic grab. If a hydraulic grab was to be used, closely spaced holes had to be formed in the mass concrete before the materials could be broken up and removed by grabs. Subsequently, no-fines concrete, which could be broken up and removed by hydraulic grabs,

was used for backfilling of the partially demolished basement slabs and pile caps at the advice of the foundation contractor.

Apart from the basement slab and pile caps, there were still 28 concrete piles lying along the diaphragm wall alignment. These concrete piles were unreinforced, except that dowel bars were present near the pile head. Some of these piles were located partially below the basement screen wall and it made their removal by chiselling or reverse circulation drilling not feasible. In addition, the vibration and the possible associated ground settlement caused by chiselling might adversely affect surrounding utilities, buildings and MTRC facilities.

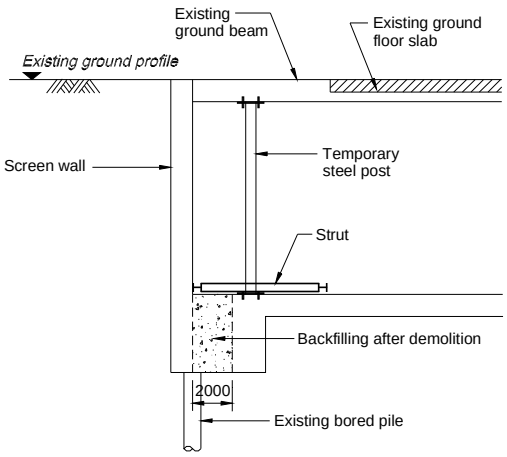

Figure 5 Method for removing obstructions at existing basement

The top portions of the concrete piles with dowel bars were first removed by a hydraulic grab. A trench cutter was then used to remove the unreinforced concrete of the pile. During this process, bentonite slurry was used to maintain stability of the excavation. After removal of the whole concrete pile, the trench would be backfilled by lean concrete. The diaphragm wall panel at the location of the concrete pile would be constructed immediately after removal of the existing concrete piles.

Type of Panel Joints

Steel End Plate Joint System

Steel end plate joints (SEP joints) were adopted in this project for the first time in Hong Kong. For this project, they were used for panels excavated using a hydraulic grab. Details of the SEP joints are shown in Figure 6. The design of the SEP joints was modified from the overlapping joint, which is widely used in Japan and Taiwan (Tasi *et al*, 1991) and has also been used in Egypt (El-Razek, 2000). The SEP joint was formed by a 6mm thick steel end plate fabricated with steel angles which acted as guide rails for cleaning of the joint. The steel angles could also lengthen the drainage path of water along the joint and therefore improve the water tightness of the SEP joint.

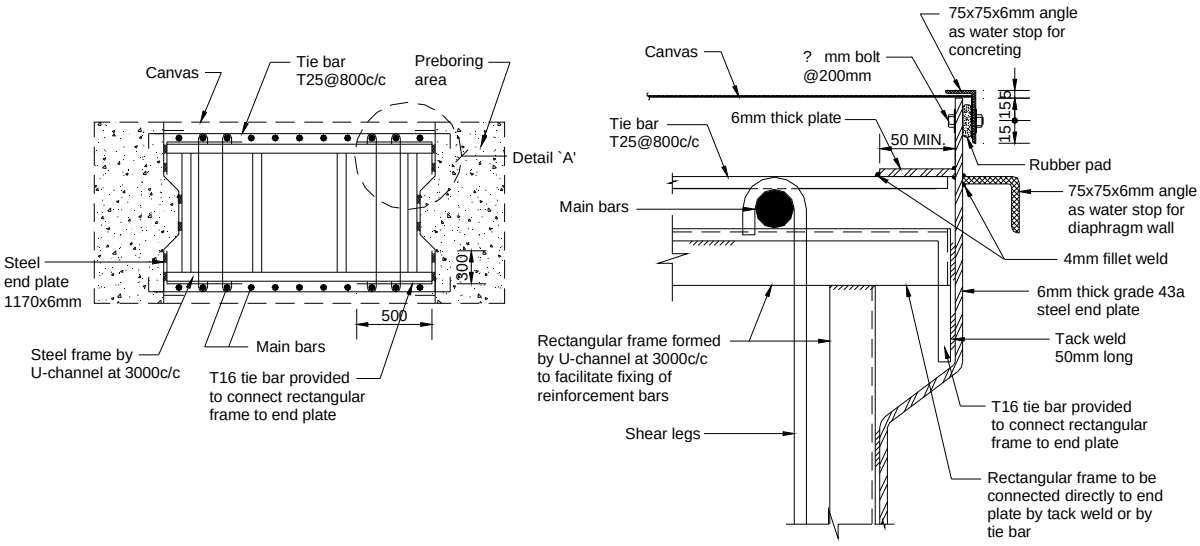

Figure 6 Details of steel end plate joints

The sequences of construction of panels with SEP joints are illustrated in Figure 7 and described as follows:

a. A slurry trench for the primary panel was excavated to the required founding level of the diaphragm wall panel.

b. Before placement of reinforcement cages, a koden test was carried out to check for presence of excessive overbreak. If necessary, plywood with polystyrene sheets would be fixed to the reinforcement cage at the location of overbreak to prevent excessive loss of concrete.

c. The reinforcement cage was placed inside the trench and the steel end plate was set back from the ends of the slurry trench, usually by a distance of about 0.5m, to prevent it from being damaged during excavation of the secondary panel. The areas outside the steel end plates are called the preboring areas which will not be concreted during construction of a primary panel.

d. Concreting of primary panel was carried out, during which the steel end plates and the canvas attached to them would prevent tremie concrete from flowing into the preboring areas. To avoid instability of the steel end plates due to differential pressure head during concreting, the preboring areas were backfilled with aggregates in phase with concreting. If leakage of concrete was detected, more aggregates would be filled in the preboring areas to keep the top level of the aggregates above that of the concrete to prevent further leakage.

e. After completion of two successive primary panels, a slurry trench was formed between the primary panels for construction of the secondary panel. The aggregates previously placed in the preboring areas of the primary panels would be removed during excavation of the secondary panel.

f. The construction of the secondary panel would then proceed in a similar way as the primary panel. Before concreting of the secondary panel, the steel end plates would be

cleaned by a tailor-made steel brush that could fit into the area embraced by the steel angles outside the steel end plate to facilitate cleansing. No steel end plates need to be provided for the reinforcement cage of the secondary panel. The concrete of the secondary panel would be cast against the steel end plates of the primary panels.

The steel end plates were welded to steel frames, each with a 3m spacing. The steel frames were used to hold the end plates in place during fabrication, to facilitate fixing of reinforcing bars and to strengthen the reinforcement cage so as to prevent distortion of the assembly during lifting of the reinforcement cage. Canvas was used at both faces of panel to minimize leakage of concrete to the preboring areas.

SEP joint not only enhances the structural performance but also the water-tightness of the diaphragm wall as the steel end plates are left in place in the primary and successive panels. It also minimizes the possible damage of joint and/or other problems which may arise when extracting a temporary end plate of the traditional CWS joint.

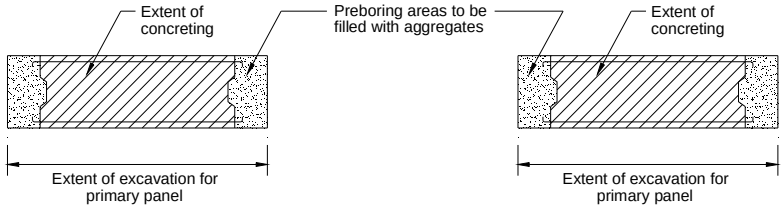

(a) Construction of primary panels

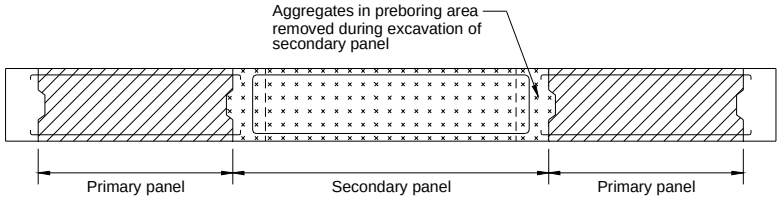

(b) Construction of secondary panels

Figure 7 Construction sequence for SEP joints

Overcut Joint

Overcut joints were formed when constructing diaphragm wall panels using the trench cutter. The construction sequences of overcut joints are illustrated in Figure 8 and described below:

a. Two successive primary panels were constructed. While steel end plates were not needed for the overcut joint, the reinforcement cage was set back from the ends of the slurry trench by 0.4m.

b. After completion of two successive primary panels, a slurry trench was formed between the primary panels by trench cutting. The trench cutting would over cut the concrete of the primary panels by 0.15m when forming the slurry trench.

c. Trench cutting would also be carried out to clean the overcut concrete surface of the primary panel before concreting of the secondary panel.

(a) Construction of primary panels

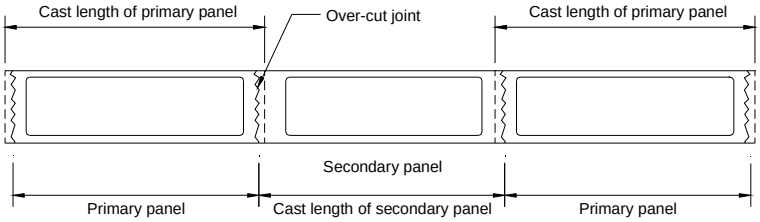

(b) Construction of secondary panel

Figure 8 Construction sequence for overcut joint

Other construction details of diaphragm wall panels with overcut joints are similar to those of diaphragm wall panels with SEP joints.

Precautionary Measures

A prime concern for the design of treatment works was the collapse of grouted soils between prebored H-piles and pipe piles during bulk excavation. When bulk excavation reached a deep level, the grouted soils had to resist a significant water pressure from outside the site. To minimize the risk of soil collapse, the following precautionary measures were taken: -

a. The lagging walls were constructed in vertical depths of 2m at maximum for each step. To minimize the extent of exposed soil and the soil exposure time, the lagging walls would be constructed as soon as the extent of local excavation was sufficient to allow sufficient working space to construct the lagging wall.

b. If water leakage in the grouted soils was detected, sand bags would immediately be placed at the point of leakage. A concrete pad would then be constructed to support the soils at the point of leakage to prevent the leakage point from developing into a bigger soil cavity. A discharge pipe would be installed in the concrete pad to relieve the water pressure.

c. Re-grouting would then be carried out at the pre-existing vertical grout holes or newly installed grout holes near the leakage point. Horizontal grout holes would be installed through the concrete pad into the soils to stop the water leakage.

The above precautionary measures were proven to be effective as significant leakage of water had occurred only at two different levels of the same area of treatment works for the entire basement construction. Figure 9 shows the additional works carried out to control the leakage. When leakage first occurred at a depth of about 5m below ground, a concrete pad was constructed at the point of leakage and horizontal grout holes were installed to stop the water seepage. Additional grout holes were then installed outside the pipe pile wall as precautionary measures before further excavation. The second leakage occurred at a depth of

7m below ground when the lagging wall was almost ready for concreting. Sand bags were used to temporarily control the seepage before casting the concrete for the lagging wall.

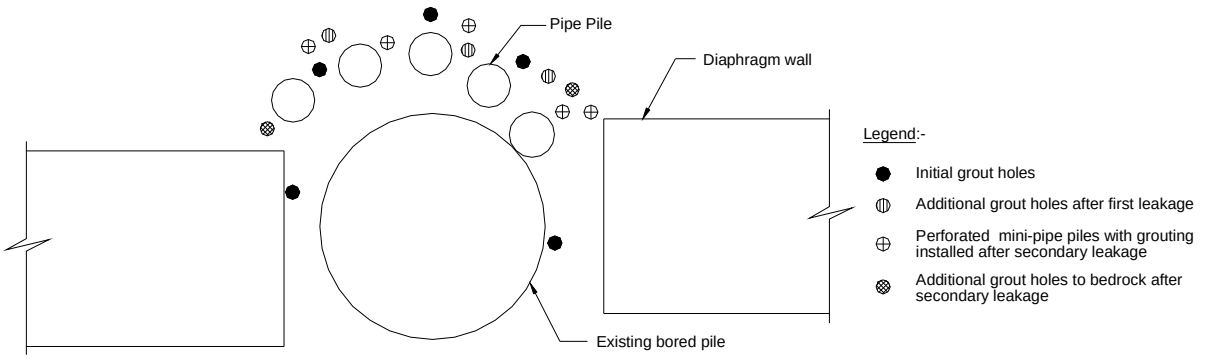

Figure 9 Additional works to control water leakage

After the second leakage, there was a concern that the grouting of soils might not be effective at this treatment works area due to poor soil conditions. 75mm diameter perforated mini-pipe piles were therefore installed behind the larger diameter pipe piles already constructed at the area. Given that the mini-pipe piles could act as physical barriers to water flow, they were considered more effective measures for stopping seepage flow than conventional grouting which relies on grouted soil as a means of seepage control. Grouting was carried out inside the perforated mini-pipe piles. While the grout mixtures would permeate through the perforations to grout the soils around the mini-pipe piles, additional conventional grout holes were also sunk to strengthen the soils and enhance water tightness. No further leakage of water occurred at this treatment works area during further excavation after the above additional precautionary works were completed.

CONCLUSIONS

The design and construction of diaphragm wall in a difficult urban site are presented. Techniques for overcoming obstructions caused by existing basement, pile caps and concrete piles are described. In areas where large diameter reinforced bored piles could not be removed, the treatment works were designed to allow these bored piles to be left in place or be partially removed during bulk excavation. Precautionary measures were implemented to prevent and tackle the problem of leakage during excavation. Steel end plate and overcut joints were successfully adopted for the project and found to be effective in controlling the leakage of water.

REFERENCES

Ho, N.C.L and Chan, T.F. (2001). "Diaphragm wall construction in a difficult redevelopment site at Kwun Tong", *Proc. Design and Construction of Diaphragm Wall*, Centre for Research & Professional Development, 103-116.

El-Razek, M.E.A. (2000). "New method for construction of diaphragm walls", *Journal of Construction Engineering and Management*, ASCE, pp.233-241.

Tasi, K.W., Ou, C.D and Lee, K.H. (1991). "Watertight and earthquake resistant joints for diaphragm walls", *Proc. Geotechnical Engineering Congress*, ASCE, 1991.

鑽孔灌注樁的施工工序對其樁側摩擦力的影響

林早妮　　李啓信
李啓信工程顧問有限公司

INFLUENCE OF CONSTRUCTION METHOD ON SHAFT FRICTION OF BORED PILE – A CASE STUDY

J. Lam and K.S. Li
Victor Li & Associates Ltd.

撮要

香港的樁基設計人員大多忽略了施工工序是會影響大型排土樁〈如鑽孔灌注樁，矩形樁〉的樁側摩擦力。用不同的方法在同類岩土性質的地盤建造兩支類似的樁基，其樁側摩擦力也可能有很大的差別。

本文敘述了一個研究個案，對一條裝有永久性環狀套筒，**1.5** 米直徑的灌注樁作荷載測試。測試顯示環狀套筒會令灌注樁樁側的摩擦力大爲減低。

INFLUENCE OF CONSTRUCTION METHOD ON SHAFT FRICTION OF BORED PILE – A CASE STUDY

J. Lam[1] and K.S. Li[2]

Abstract: There is a general lack of appreciation by foundation designers that the development of shaft friction along a replacement pile, e.g. bored piles, barrette, is very much influenced by the construction procedures. Two sites with similar soil profiles can produce vastly different shaft friction along the piles. The paper presents a case study involving a full-scale test of a 1.5m diameter bored pile constructed using a permanent liner. The test pile demonstrated that the use of a permanent liner would result in very low shaft friction along bored piles.

INTRODUCTION

Bored piles are commonly used in Hong Kong to resist heavy building loads. In an earlier study by Lo & Li (1999), it was pointed out that the development of shaft friction along bored piles would be significantly influenced by the installation procedures. Permanent liners are sometimes used in the construction of bored piles. From a theoretical standpoint, the provision of a permanent liner will reduce the shaft friction of bored piles. In this paper, we will describe the mechanism which leads to the low shaft friction along bored piles with permanent liner and present a case study which confirms the significant reduction of shaft friction by the use of a permanent liner.

CONSTRUCTION OF BORED PILES WITH PERMANENT LINERS

Bored piles are commonly constructed with the help of a temporary steel casing to prevent cave-in of soils during excavation. The temporary casing can be sunk by a vibrator, an oscillator or a rotator. Very often, it may not be necessary or sometimes not feasible to sink the temporary casing to the full depth of very deep drilled shafts. The sinking of a single temporary casing to a great depth will require a high-capacity equipment to overcome the significant frictional force that may develop along the temporary casing. It is also difficult to remove the casing when significant frictional resistance has already developed during casing insertion.

An alternative means to sink a long temporary casing is to adopt the technique of telescoping casing. In this technique, a large diameter outer temporary casing is sunk to a certain depth into the ground, followed by a second temporary casing with a smaller diameter placed inside the outer casing. The process can be repeated until the required level is reached. As the inner casing is shielded by the outer casing, the soil friction that can develop along the inner temporary casing will be reduced and the temporary casing can then be sunk to a greater depth using less heavy-duty equipment. The technique of telescoping casing involving three temporary casings has been used in Hong Kong for constructing long bored piles or bored piles which

[1] Engineer, Victor Li & Associates Ltd
[2] Director, Victor Li & Associates Ltd.

penetrate through multiple cavities in marble areas. The major limitation of the technique is the requirement of a higher capacity crane to lift the inner temporary casing during installation or extraction. There is therefore a practical limit for the maximum length of inner temporary casing that can be installed using a given crane.

When full-depth casing cannot be sunk, some foundation contracts may require the provision of a permanent liner inside the temporary casing before concreting. The installation of permanent liner can help eliminate certain pile defects, such as fresh concrete mixing with the soils collapsed from the otherwise unsupported shaft during concreting or necking of concrete during extraction of temporary casing.

A permanent liner is usually a corrugated circular tube made from steel sheets. To avoid the placement of the permanent liner being blocked or the liner being lifted by the temporary casing during its extraction, the size of the permanent liner must be smaller than that of the temporary casing. As the temporary casing is extracted, a gap will thus be formed temporarily between the soil and the permanent liner. The gap will be larger if telescoping casing is used for pile excavation. If the excavated shaft is stable after removal of the temporary casing, a permanent gap will be left outside the permanent liner. Otherwise, lateral movement or cave-in of soils will occur to fill up the gap.

THEORETICAL CONSIDERATIONS

As discussed by Lo *et al* (2001), there are two possible mechanisms, namely fill-in mechanism and close-in mechanism, by which the gap between the permanent liner and the excavated shaft would disappear after casing extraction as illustrated in Figure 1. In the fill-in mechanism, the excavated shaft formed in the stronger material is temporarily stable after extraction of the temporary casing. Soils will collapse from the unstable excavated shaft above and fill up the gap. In the close-in mechanism, the excavated shaft cannot maintain its stability, with soil moving towards the permanent liner as the temporary casing is being extracted.

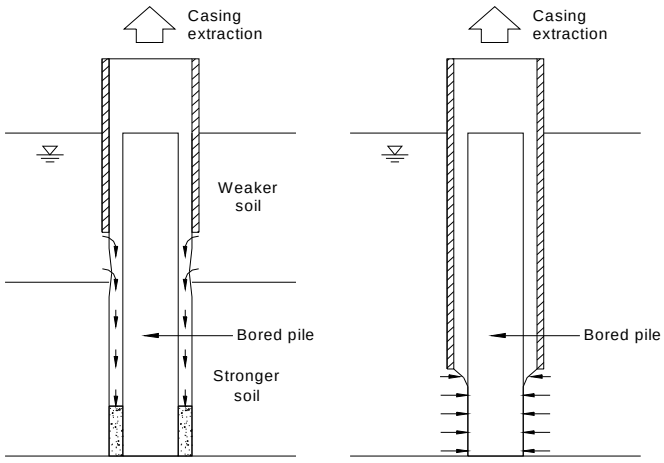

(a) Fill-in mechanism (b) Close-in mechanism

Figure 1 Collapse mechanism

From a theoretical standpoint, the shaft friction that can develop along a bored pile with permanent liner is small for both mechanisms. This can be explained by using the following equation, which governs the shaft friction along a bored pile:-

$$\tau = \sigma_h \tan \delta \tag{1}$$

where σ_h is the effective horizontal stress acting on the pile-soil interface and δ is the interface friction angle.

For the fill-in mechanism, the re-worked soil that collapses into the annular void is likely to be loose while a stable excavated shaft in the stronger soil implies a low value of σ_h. The friction angle δ and the horizontal stress σ_h around the pile and hence the shaft friction at the pile-soil interface are expected to be low. For the close-in mechanism, lateral movement of soil towards the permanent liner will trigger the arching effect to develop in the surrounding soils. The arching effect of a circular excavated shaft was studied by Terzaghi (1943) from which the following equation for the confining stress required to maintain stability of an excavated shaft can be derived:-

$$\sigma_{ro} = \frac{1}{(\mathrm{N}_\phi + 1)(N_\phi - 1)} \cdot \left\{ \frac{2 \cdot \left((N_\phi - 1)\, \gamma \, \mathrm{z} + 2\, \mathrm{c} \sqrt{N_\phi} \right)}{\left(\frac{r_e}{r_o} \right)^{(N_\phi - 1)}} - 2\, \mathrm{c} \sqrt{N_\phi} \right\} \tag{2}$$

where c = cohesion of soil; ϕ = angle of shearing resistance of soil; γ = unit weight of soil;
σ_{ro} = horizontal stress at wall of the excavated shaft at depth z below ground surface;
r_o = radius of excavated shaft;
r_e = outer radius of the zone of plastic equilibrium at depth z;
$N_\phi = \tan^2 (45° + \phi/2)$

The definitions of the notations used in Eq.2 are explained in Figure 2. Some parametric studies have been carried out to estimate the magnitude of σ_{ro} required to maintain stability of the excavated shaft based on the above equation using the shear strength parameters of soil given in Figure 3. The lateral stress σ_{ro} required to maintain stability of the excavated shaft is low. When close-in of the excavated shaft occurs, further movement of the soils around the bored pile will stop when the lateral pressure developed at the pile-soil interface is equal to σ_{ro}. This implies that the horizontal stress σ_h acting on the bored pile will also be small. According to Eq.1, the shaft friction will also be low.

The above deduction based on simple theoretical considerations have been verified by Lo *et al* (2001) using more sophisticated numerical analysis performed by the program FLAC. Figure 4 shows the results of predicted lateral stress around a bored pile presented by Lo *et al* (2001). It can be observed that the lateral stress is low for both collapse mechanisms, a conclusion which is in line with that drawn from the simple equation of Eq.2.

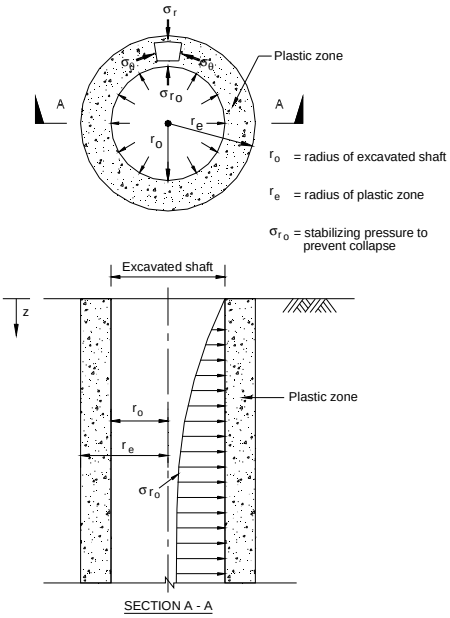

Figure 2 Arching effect of a circular excavated shaft

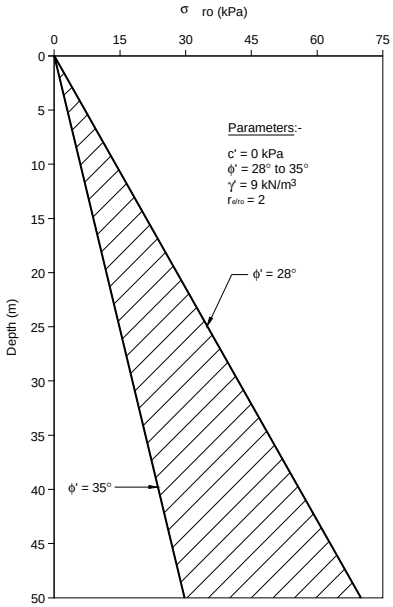

Figure 3 Lateral stress required to maintain stability of excavated shaft

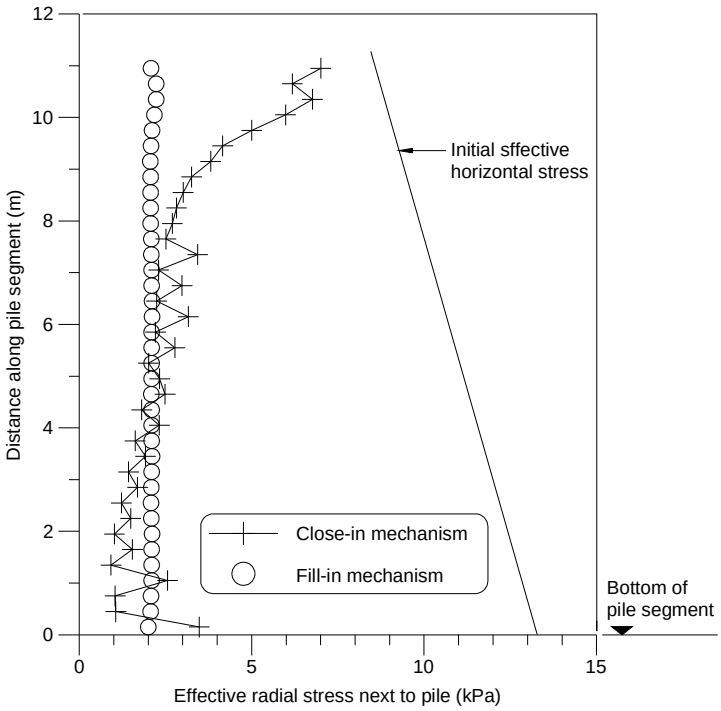

Figure 4 Lateral stress predicted by FLAC

CASE STUDY

A development project was proposed in a reclamation site at Tseung Kwan O. The site is characterized by a stratigraphic sequence of fill, marine deposit, alluvium, and decomposed tuff of different weathering grades. Figure 5 shows a typical soil profile of the site. The proposed development comprised several tower blocks supported by bored piles. The bored piles were all constructed with permanent liners along the full length of the piles. The bored piles for the tower blocks were either 2.25 or 2.55m in diameter with a bell-out ranging from 3.50 to 4.50m.

Abnormal behaviour involving significant drop in piezometric pressure below the marine deposit as indicated in Figure 5 emerged in late 1999 when construction of the tower blocks was in progress. This had resulted in unexpected subsurface ground settlements within the alluvium and completely decomposed tuff (CDT) layers as shown in Figure 6. Such settlements were believed to have been caused by dewatering in bedrock during the construction of a deep tunnel near the site (TDD, 2000). According to Figure 6, the CDT layer gradually rebounded to a level above the datum, at which the initial settlement measurement was taken after the deep tunnel had been lined to minimize water seepage.

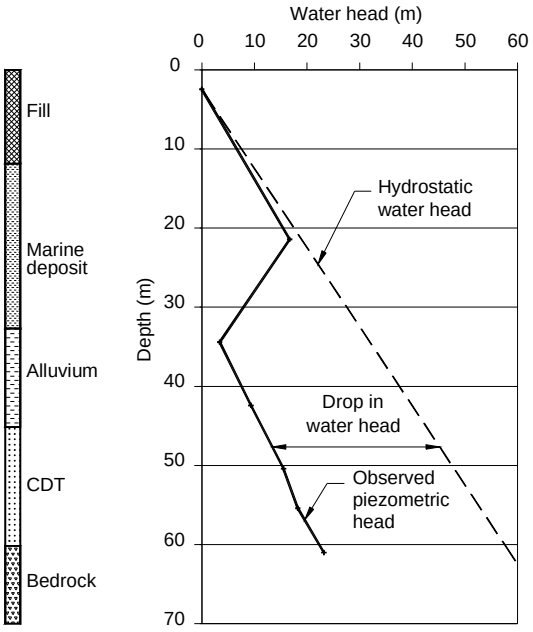

Figure 5 Soil profile and drop in piezometric pressure at the reclamation site

In the original foundation design, allowance had only been made for negative skin friction (NSF) that might develop along the length of bored piles within the fill and marine deposit soil layers. The design NSF calculated using the conventional textbook analysis was high with values of between about 8200 and 12200 kN. However, the occurrence of subsurface settlement below the marine deposit down to the bedrock would also trigger the development of NSF along the full length of the bored piles. There was a concern that the capacity of the completed bored piles might not be adequate to resist the additional NSF.

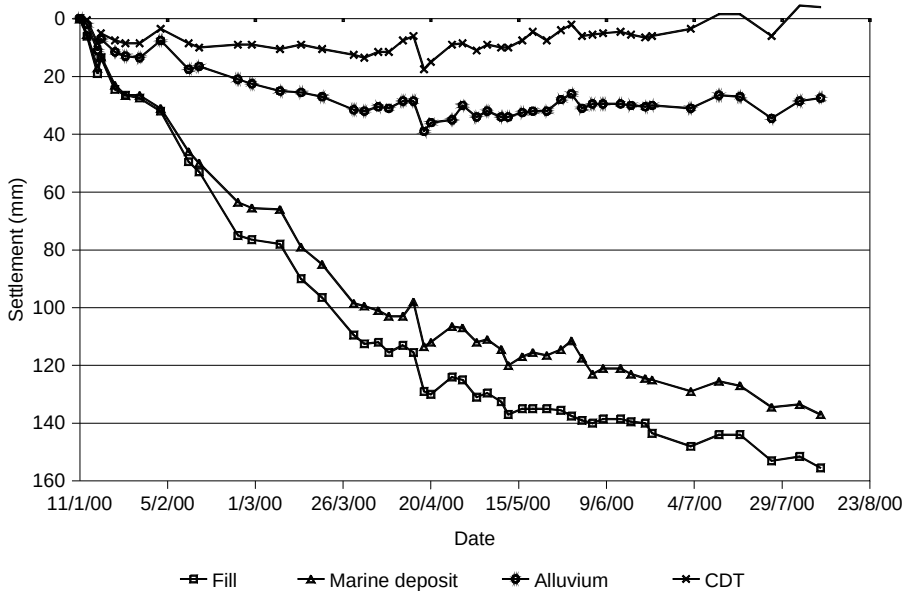

Figure 6 Subsurface ground settlement occurred at the reclamation site

Based on the theoretical considerations discussed in the preceding section, it was considered that shaft friction along bored piles with permanent liners would be much lower than that calculated using the conventional procedures in the original design. Simple calculations based on Eq.1 and Eq.2 also indicated the design NSF allowed for in the original design would be sufficient to resist the actual NSF that might develop along the full length of the bored piles.

An instrumented test bored pile was constructed at the site to affirm the theoretical prediction of low shaft friction. The test bored pile had a diameter of 1.5m, constructed to a depth of 55m below ground. The bored pile was constructed using a 2m diameter temporary steel casing with the provision of a permanent liner down to 1m above the toe level. Figure 7 shows details of the test bored pile. To eliminate the base resistance during the loading test, a sand box was provided at the base of the bored pile. The sand box was welded to the bottom segment of the reinforcement cage. Two reservation tubes were provided for the full length of the test bored pile and welded onto the top steel cover of the sand box. The sand inside the sand box would be flushed out by pressurized water prior to commencement of pile loading test.

The total shaft resistance along the full length of the test bored pile can be considerable when calculated using the conventional method. In GEO Publication No.1/96 (GEO, 1996), shaft friction coefficient β of between 0.15 and 0.6 has been quoted as typical values for soils ranging from loose sand to dense sand. For a 55m long test bored pile, the estimated total shaft resistance can amount to over 20000 kN if the upper bound value of β is used for calculation. To cater for this extreme condition, the test bored pile was designed for a maximum test load of 30000 kN. As there was no working space available at the site for setting up a massive kentledge for pile loading test, a decision was therefore made to use an anchor system as shown in Figure 8 for the reaction system. A total of 6 anchors were installed in the bedrock. The anchors were installed prior to construction of the test bored pile to minimize the effect on development of shaft friction of the test bored pile. The anchors were fixed to the 6 corners of a hexagonal-shaped reaction

frame, keeping a distance of 7.5m from the centre of the test bored pile. During the pile loading test, the hydraulic jacks, which were placed between the reaction frame and the test pile, would be pressurized to thrust the test bored pile downwards by jacking against the reaction frame held in position by the anchors.

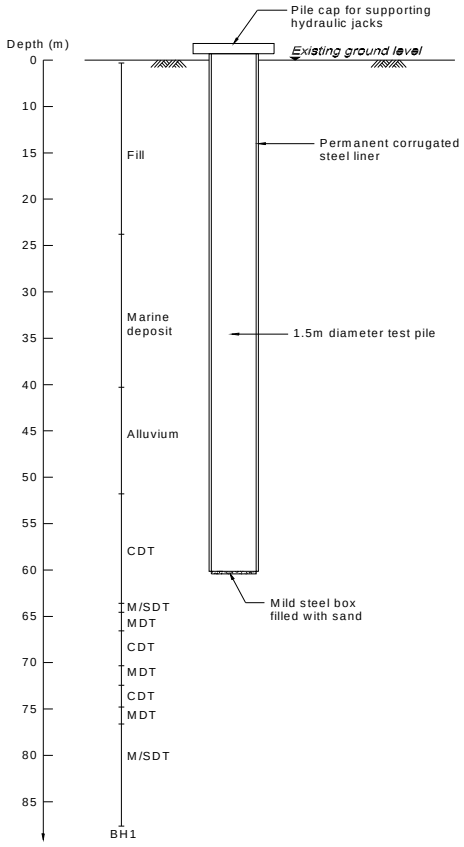

Figure 7 Details of the test bored pile

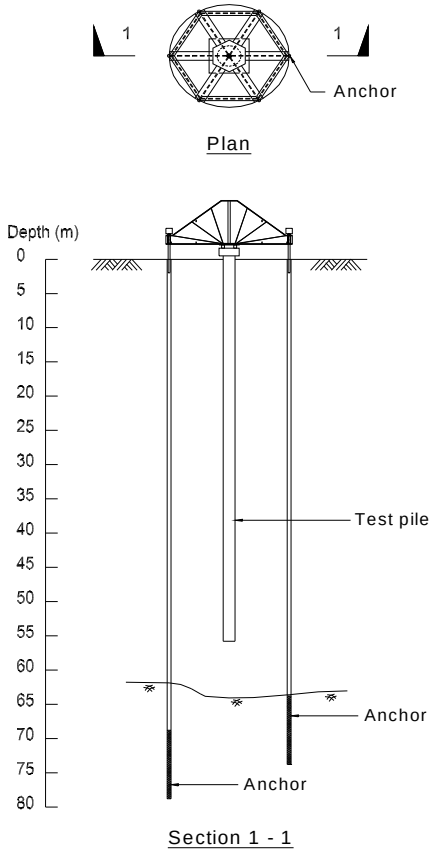

Figure 8 Reaction system for test bored pile

The test bored pile was constructed using the same procedures as those adopted for constructing the completed bored piles of the tower blocks. A temporary steel casing was progressively sunk to the toe level of the test bored pile by an oscillator, while keeping the base of the temporary casing below the excavation level inside the casing at all times. Once excavation for the pile shaft had been completed, a permanent liner, the prefabricated steel box filled with sand and the reinforcement cage were lowered into the temporary casing in sequence.

The excavated shaft was cleaned by air-lifting prior to concreting. During concreting, the temporary casing was extracted progressively by the oscillator while maintaining the top of the tremie concrete at a certain depth above the base of the temporary casing at all times. After concreting, the depths of the two reservation tubes were measured to ensure that they had not been blocked during concreting. The duration of construction of the test bored pile was 17 days, from commencement of excavation to concreting of the pile. After the concrete of the test bored pile had hardened, two openings were formed in the top cover of the sand box by coring through

the reservation tubes. This would facilitate the flushing of sand out of the sand box prior to the commencement of pile loading test. After the sand box had been emptied, the test bored pile would then be loaded by its self-weight. The loading test was carried out one month after completion of construction of the test bored pile to permit the hardened concrete to cool down to a low and steady temperature.

TEST RESULTS

The top level of the soil in the annular gap around the test bored pile had been constantly monitored in four directions after extraction of the temporary casing. The monitoring results are shown in Figure 9. It can be observed that the excavated shaft was stable up to a depth of over 40m even when left unsupported within a short period after full extraction of temporary casing. Progressive closing up of the gap occurred, most likely by the fill-in mechanism. The unsupported excavated shaft formed in the fill and marine deposit layers remained stable up to a depth of approximately 23m one month after its construction. The fact that the deep unsupported excavation shaft had remained stable for such a long period of time has clearly demonstrated that arching effect could be very significant in maintaining stability of an excavated shaft, thus rendering a reduction in lateral stress acting on the bored pile.

Figure 10 shows the load-settlement curve of the test bored pile. The test pile was loaded to failure when a very small applied load of 2600kN was reached. The self-weight of the bored pile and the steel reaction frame was found to be sufficient to load the test bored pile to failure. In hindsight, the costly anchor system was not necessary. With an unsupported depth of 23m of the excavated shaft, the test bored pile was only in contact with the surrounding soils for the bottom 32m of the pile. Dividing the failure load by the contact area yielded an average ultimate shaft friction of 17kPa for the test bored pile. The low shaft friction was in line with the theoretical prediction discussed earlier.

The NSF acting on the completed bored piles for the development project at Tseung Kwan O was re-assessed based on the results of the test bored pile. A reduction factor of 0.17 was obtained by comparing the observed total resistance of the test pile at failure with the pile resistance calculated using the conventional approach. The reduction factor was then applied to the NSF along the bored piles calculated using the conventional approach. The re-assessed NSF along the whole bored pile was mostly between 4000kN and 10,000kN. It was found that the conservative design NSF estimated using the conventional procedures for the soil layers of fill and marine deposit in the original foundation design was even larger than the re-assessed total NSF for the entire length of the completed bored piles. Therefore, the original design was adequate despite the unexpected subsurface ground settlement. Overloading of the bored piles was not a concern for the project and the development project could proceed as planned without compromising the structural safety of the buildings.

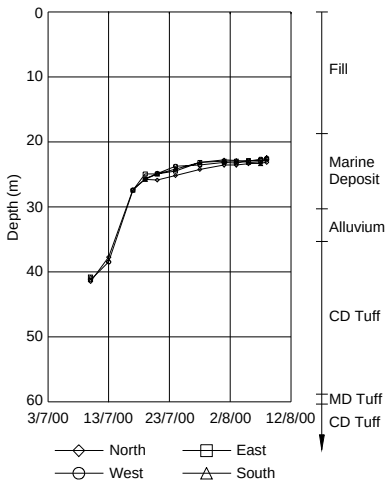

Figure 9 Monitoring results of top of the level of the soil in the annular gap around the test bored pile

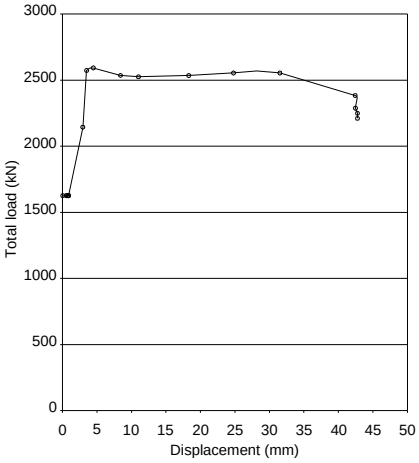

Figure 10 Load-settlement curve test bored pile

DISCUSSION AND CONCLUSION

The provision of a permanent liner will significantly reduce the shaft friction of a bored pile, as clearly demonstrated by the pile loading test results of the test bored pile. The same conclusion is drawn by the case studies of bored piles constructed using permanent liners reported by Kwok (1987). The conventional approach to estimating shaft friction will grossly overestimate the shaft friction along bored piles with permanent liners.

If bored piles are designed to be friction bored piles, permanent liners should not be used. On the contrary, the provision of a permanent liner is a very effective means for reducing the NSF of bored piles constructed in a new reclamation site underlain by soft soils.

REFERENCES

Kwok, D. W. (1987). *Construction of Large Diameter Bored Piles Founded on Soil*, MSc. Thesis, The University of Hong Kong.

Geotechnical Engineering Office (GEO) (1996). *Pile Design and Construction*, GEO Publication No. 1/96.

Lo, S-C.R. and Li, K.S. (1999). "Challenges in the design and construction of large diameter bored piles founded on decomposed granite", *Proc. Construction Challenges into the Next Century*, Hong Kong Institution of Engineers, 84-91.

Lo,S-C.R., Gnanendran, C.T. and Li, K.S. (2001). "The application of numerical analysis to geotechnical engineering", *Proc. 14th Southeast Asian Geotechnical Conference*, Vol.1, 383-388.

Terzaghi, K. (1943). *Theoretical Soil Mechanics*, John Wiley & Sons.

Territory Development Department (TDD) (2000). *Final Report on Investigation of Unusual Settlement in Tseung Kwan O Town Centre*, consultancy report prepared by Maunsell Consultants Asia Ltd. in association with Maunsell Geotechnical Services Ltd.

安達臣道石礦場採用的傳統及機械式岩石挖掘方法

林奕創　　沈鵬搏　　盧耀宗
茂盛土力工程顧問有限公司

CONVENTIONAL AND MECHANICAL ROCK EXCAVATION METHODS EXERCISED AT THE ANDERSON ROAD QUARRIES

Y. C. Lam, Barry Sum and Joseph Lo
Maunsell Geotechnical Services Ltd., Hong Kong

撮要

本港在進行隧道挖掘工程時普遍採用傳統的鑽孔及爆破方法。不過，由於機械式岩石挖掘科技正不斷改進，現時很多基建工程漸多採用隧道鑽探機器**(TBM)**。向上提升鑽孔技術是其中一種透過利用隧道鑽探機器的機械式岩石挖掘方法。安達臣道石礦場於一九九八年建造了兩條橫向的隧道及三個垂直豎井的隧道，目的是加快運送開礦而來的泥石。本文件會介紹該工程在設計上，特別是使用隧道鑽探機器進行工程的考慮。由於採用隧道鑽探機器，本文件改良岩石構造評級方法**(RSR)**，並建議一設計圖表，可直接於 **Q-SYSTEM** 中作調整。本文件並會簡單討論隧道及豎井的建造工程。

CONVENTIONAL AND MECHANICAL ROCK EXCAVATION METHODS EXERCISED AT THE ANDERSON ROAD QUARRIES

Y.C. Lam[1], Barry Sum[2] and Joseph Lo[3]

ABSTRACT

In Hong Kong, conventional drilling and blasting has been commonly adopted in tunnel excavation projects. However, as the technology of mechanical rock excavation is being improved, Tunnel Boring Machine (TBM) is increasingly accepted in many current infrastructure projects. Raise boring technique is one of the mechanical rock excavation methods with the use of TBM. To facilitate the mucking process at the Anderson Road Quarries, two tunnels with three vertical shafts were constructed in 1998. Design considerations for this project, especially on TBM construction are presented in this paper. By modifying the Rock Structure Rating (RSR) approach, a design chart is proposed for direct adjustment on Q-system due to TBM operation. In addition, a brief discussion on the both tunnel and shaft construction is also included.

INTRODUCTION

The Anderson Road Quarries (ARQ) are composed of two quarries, namely the Tai Sheung Tok Quarry at the northern area and the Anderson Road Area 3 Quarry at the southern side. At the Tai Sheung Tok Quarry, Tunnel A was excavated with a typical span of 5.5m, length of about 100m and up gradient of 1.6%. Two vertical shafts, which have diameters of 2.75m and heights of about 75m, are connected with the enlarged end of Tunnel A. A geological section of Tunnel A is shown in Figure 1. At the Anderson Road Area 3 Quarry, Tunnel B with a typical span of 4.6m extends 80m from the portal with an up gradient of 1.5%. It connects with another vertical shaft of 70m high at the end. A geological section for Tunnel B is shown in Figure 2. Crushed rocks from surface excavation are to be dumped through the shafts and transported out from the tunnels by means of feeder systems.

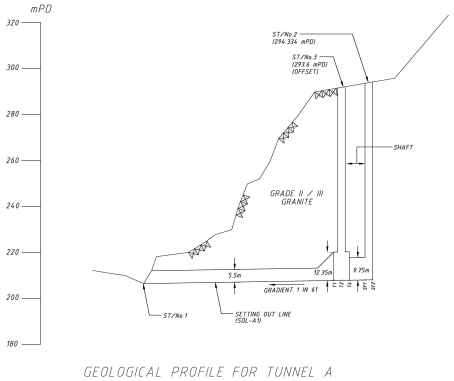

Figure 1: Geological Section of Tunnel A

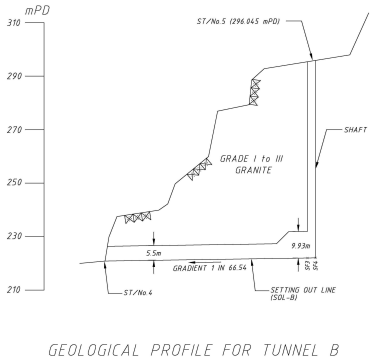

Figure 2: Geological Section of Tunnel B

[1]Geotechnical Engineer, Maunsell Geotechnical Services Ltd.
[2] Geotechnical Engineer, Maunsell Geotechnical Services Ltd.
[3] Executive Director, Maunsell Geotechnical Services Ltd.

DESIGN CONSIDERATIONS

Empirical Design Approach

Drill & Blast Tunnels

Drill and blast tunneling method was adopted for construction of Tunnel A and Tunnel B. Based on the Rock Tunneling Quality Index (Q-system) developed by Barton, Lien, and Lunde (1974) of Norwegian Geotechnical Institute, rock mass characteristics and tunnel support were determined. According to the Q-systems, Rock Mass Quality (Q) is estimated by six parameters, namely the RQD - rock quality designation (Deere et al 1967), Jn - joint set number, Jr - joint roughness number, Ja - joint alteration number, Jw - joint water reduction factor, and SRF - stress reduction factor. The formula is given as below:

(a) (b) (c)

$$Q = (RQD/Jn) \times (Jr/Ja) \times (Jw/SRF) \quad (1)$$

Factor (a) represents the structural quality of the rock mass and indicates the size of the rock blocks implicitly. In other words, a higher value of factor (a) gives a larger size of the rock blocks. Factor (b) represents the shear strength, roughness and frictional characteristics of the joint walls or infilling. Higher value means a stronger interlocking strength. Factor (c) can be reckoned as a total stress parameter. In addition to the above parameters, ESR - excavation support ratio, which reduces the effective span according to the construction practice.

In the ARQ project, ESR of 1.6 (as a permanent mining tunnel) was adopted because the tunnel was built with heavy machinery and a design life of 14 years (Figures 3 & 4). The average RQD was above 90%; Jn was 6 (i.e. two joint sets plus random); Jr and Ja were both in unity (i.e. rough, planar and unaltered joint walls); Jw was also in unity with minor water inflow; under medium stress condition, SRF of 1 was adopted. Hence, the typical Q value for the main tunnels A & B was estimated to be 15 and the tunnels were supported by spot bolts normally. Although the quality of the granitic rock was considered to be good in this quarry, the lowest Q value logged was 0.1 due to other factors such as locally high water inflow and adverse joint characteristics.

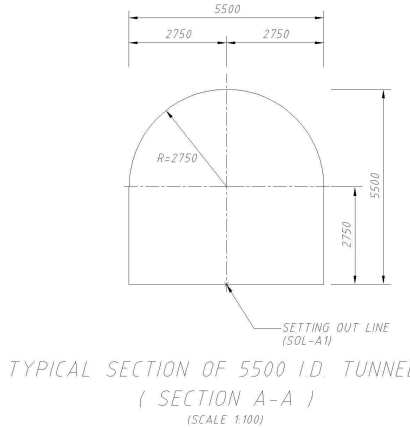

Figure 3: Cross Section of Tunnel A

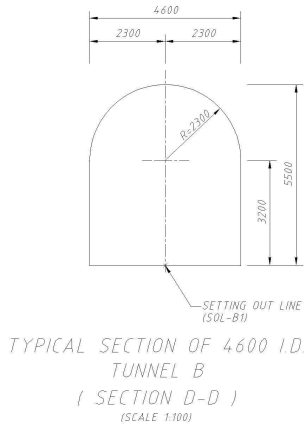

Figure 4: Cross Section of Tunnel B

For the enlarged tunnel section, tunnel height instead of span was used for the design. Referring to Figure 5 with enlarged tunnel height of 12.5m, different tunnel supports such as pattern bolting and shotcreting with various thickness were applied in accordance with the ground reference condition.

However, an adjustment should also be made for the tunnel wall support (Qw) by applying the formula below:

$$Qw = (2 \times \log Q + 3) \times Q \qquad (2)$$

The formula is valid with Q value in between 0.1 and 10. For Q value below 0.1, Qw = Q; for Q value over 10, Qw = 5 x Q.

The above design procedures were only for the main and enlarged tunnels. However, some parameters such as Jn and ESR should be factored for designing tunnel support at portals and intersections. At the portal areas, additional tunnel support by means of steel rib installation was adopted for safety purpose.

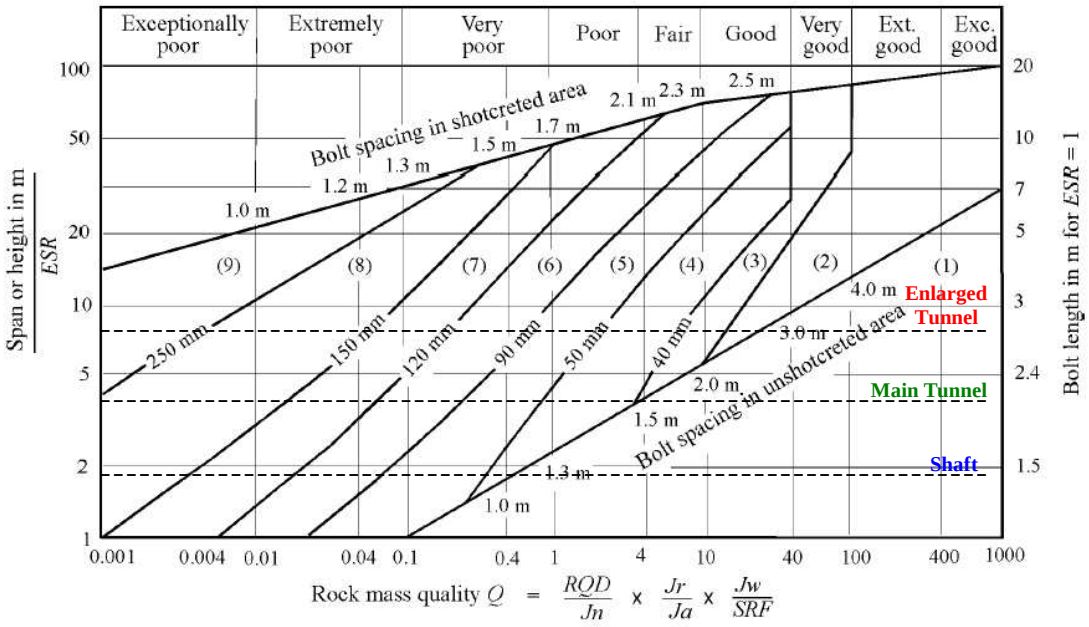

REINFORCEMENT CATEGORIES

1) Unsupported
2) Spot bolting
3) Systematic bolting
4) Systematic bolting with 40-100 mm unreinforced shotcrete
5) Fibre reinforced shotcrete, 50 - 90 mm, and bolting
6) Fibre reinforced shotcrete, 90 - 120 mm, and bolting
7) Fibre reinforced shotcrete, 120 - 150 mm, and bolting
8) Fibre reinforced shotcrete, > 150 mm, with reinforced ribs of shotcrete and bolting
9) Cast concrete lining

Figure 5: Estimated Support Categories based on the Tunnelling Quality Index Q (after Grimstad and Barton 1993)

Vertical Shaft by Raise Borer (TBM)

Mechanical Tunnel Boring Machine (TBM) method was used in the vertical shafts construction for this project. A raise borer from Robbins (Plate 1) was used to carry out the work. A pilot hole was initially drilled down from the peak platform. As the pilot hole intersected with the horizontal tunnel, the raise borer head was installed. The vertical shaft was then bored from bottom up. The process is known as raise boring.

Plate 1: Robbins Raise Borer

By using TBM method, rock structure around the machine driven tunnel should have a better condition because less disturbance to the incipient rock joints and tighter rock structures are expected. Nevertheless, the adopted rock classification method (Q-system) had no adjustment made for the enhanced rock quality at the time when tunnels and shafts of this project were designed.

With respect to the enhanced rock quality, an adjustment factor was introduced by George Wickham (1972) by means of the Rock Structure Rating (RSR) system (Figure 6). The RSR system was initially developed for the U.S. Bureau of Mines to describe the "quality" of rock structure that in turn determines the need for ground support. The index is on a scale of 20 to 100 (normal range is 25 – 70) and is calculated by considering three parameters. Parameter A combines the rock type, strength and geologic structure. Parameter B relates the joint pattern with direction of drive. Parameter C determines the overall rock quality by summing the parameters A & B, and taking into account the joint and groundwater conditions. Contrary to the Q-system, the RSR method provides ground support requirements prior to excavation.

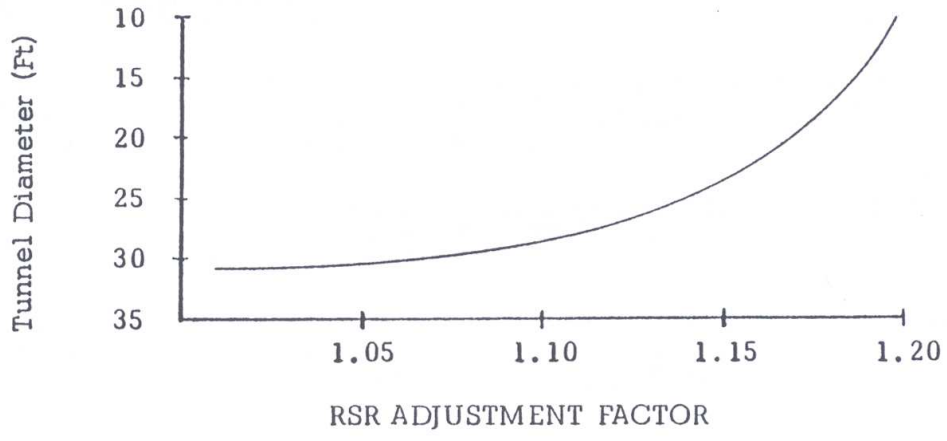

Figure 6: RSR Adjustment for TBM Operation
(George E. Wickham, 1972)

In order to adjust tunnel support requirements determined by the Q-system, a transitional approach involving the Rock Structure Rating (RSR) was adopted. Therefore, instead of using the RSR method, a correlation was made to convert the RSR value to Q value. With this conversion, the entire tunnel support system would still be developed as usual by the Q-system. By using the correlations suggested by Bieniawski, 1976 and Rutledge, 1978, a direct relationship is proposed between RSR and the Q value:

$$Q = e^{(0.144\ RSR - 6.68)} \qquad (3)$$

With the use of a boring machine, the RSR value would be adjusted upward to reflect a better condition of the penetrated rock structure. However, RSR value should not be adjusted if tunnel diameter is over 9m or 30ft. The adjustment curve is developed empirically as below:

$$F_{RSR} = Ax^4 + Bx^3 + Cx^2 + Dx + E \qquad (4)$$

where F_{RSR} = TBM Adjustment Factor (RSR method)
x = Tunnel Diameter (m)
A = -0.000273 ; B = 0.00555 ; C = -0.0418 ; D = 0.127 ; E = 1.067

Remarks : The formula is applicable to TBM tunnel with diameter within the range of 2.5m to 9m

1) Example of this project with vertical shaft of 2.75m (Indirect Correlation)

Shaft Diameter,	$x = 2.75m$	
Adjustment Factor (RSR),	$F_{RSR} = 1.199$	applying (4)
Typical Q value,	$Q_{original} = 7$	
Unadjusted RSR,	$RSR_{original} \approx 60$	applying (3)
Hence,	$RSR_{TBM} = 60 * 1.199 \approx 72$	
	$Q_{TBM} = e^{(0.144 * 72 - 6.68)} \approx 40$	applying (3)

After the adjustment of Q to Q_{TBM}, the value was boosted up by almost 6 times from 7 to 40. Since the shaft diameter was relatively small, only spot bolting was required even applying the Q adjustment. However, effect of the TBM adjustment can be demonstrated in Example 2 where shear zone was encountered locally at the shaft.

Based on the formulae (3) and (4), an adjustment chart is developed solely for the Q-system (Figure 7). The adjustment factor using this chart is termed as F_Q. An example will be shown below with the application of this adjustment chart.

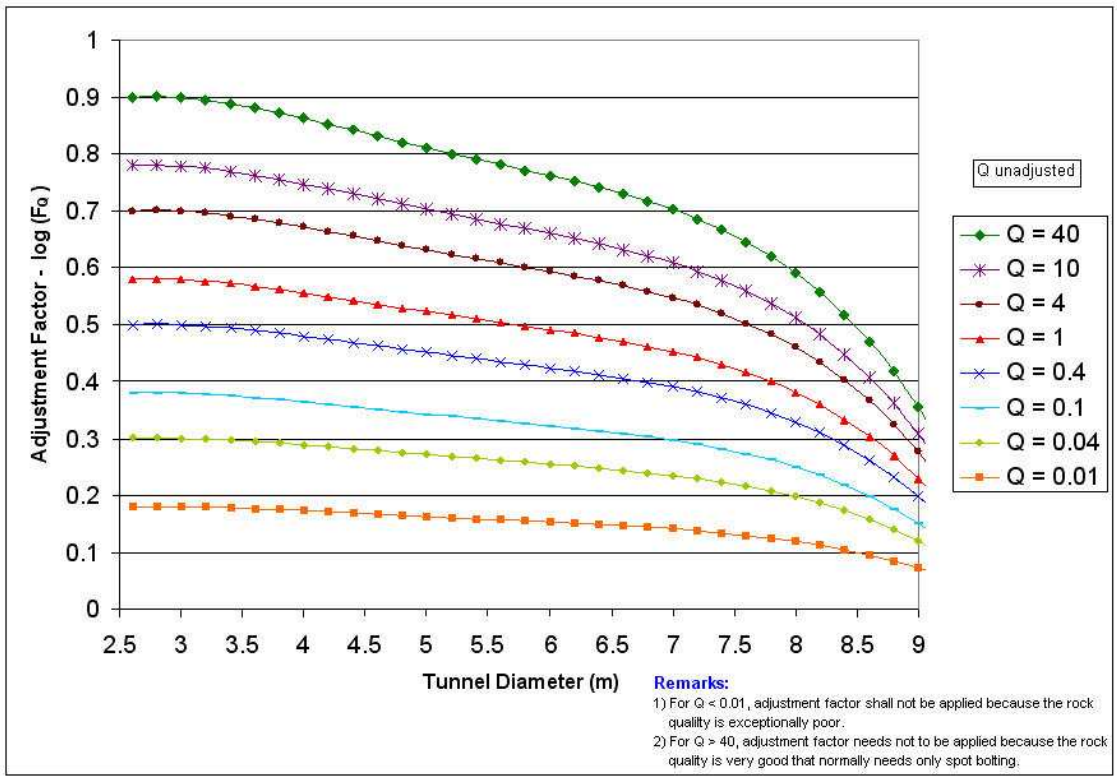

Figure 7: Adjustment Chart for Q value under TBM Operation

When the shear zone was encountered at about 260mPD of vertical shaft at Tunnel A, TBM adjustment was made for Q in addition to another adjustment proposed by Loset, 1990. The Loset formula was applied to determine a more realistic Q value.

$$\text{Log } Qm = \frac{b \log Qz + \log Qr}{4b + 1} \qquad (5)$$

where Qm = mean Q value for zone and side rock
Qz = Q value of weakness zone
Qr = Q value of adjacent rock
b = breadth of weakness zone (in metre)

2) <u>Example of this project with shear zone thickness of 3m at Shaft A</u>

Q of adjacent rock, Qr = 7
Q of weakness zone, Qz = 0.014
Breadth of weakness zone, b = 3m

a) Indirect TBM adjustment by RSR method,

Mean Q value, Qm = 0.017 applying (5)
Unadjusted RSR, RSRm ≈ 18 applying (3)

Adjustment Factor (RSR), $F_{RSR} = 1.199$
Hence, $RSR_{TBM} = 18 * 1.199 \approx 22$
$Qm_{(TBM)} \approx 0.03$ applying (3)

b) Direct TBM adjustment by Figure 7,

Mean Q value, $Qm = 0.017$
Adjustment Factor (Q), $\log (F_Q) = 0.22$, or $F_Q \approx 1.66$ applying Figure 7
Hence, $Qm_{(TBM)} \approx 0.03$

With ESR=1.6, Support Category 6 is required (Figure 5).

Hence, 120mm mesh/fibre reinforced shotcrete was recommended instead of 150mm thick if Q value was unadjusted.

As TBM technology grows rapidly, a review on TBM tunnelling was carried out recently by Barton in year 2000. A new Q_{TBM} method was built onto the six Q-system parameters. The newly introduced parameters for TBM include the ratio of rock mass strength SIGMA, cutter force F, cutter life index CLI, the quartz content of the rock q, and the estimated stress level at the tunnel face σ_ϕ. The modified formula is given as below:

$$Q_{TBM} = Qo \times \frac{SIGMA}{F^{10}/20^{9}} \times \frac{20}{CLI} \times \frac{q}{20} \times \frac{\sigma_\phi}{5} \qquad (6)$$

where Qo = oriented Q value (based on RQD in the tunneling direction)

Back to Example 2, Qm is re-calculated by using formula 6. Normalized values for SIGMA, F, CLI, and q suggested by Barton are adopted here. The $Qm_{(TBM)}$ is calculated as 0.025, which is lower than the previously calculated value of 0.03. This discrepancy may be due to the cutter force value and other machine-specific parameters.

Numerical Design Approach

Although the tunnel support designs were basically determined by the empirical approach, numerical design approach was also applied to verify the adequacy of the support system. Analytical models were developed by UNWEDGE and Phase^2.

UNWEDGE was used to determine the potential wedge block and design the bolting system accordingly. It provided a 3 dimensional view of how the potential wedges affecting the stability of the tunnel. Major joint sets mapped at Tunnel A during the construction were categorized into 3 groups, namely (78,240), (85,335), and (30,320). With the tunnel trend of 21.5^o, potential wedges were generated by the program. According to the empirical design, spot bolts of 3m long had been adopted. Results output by UNWEDGE verified that the provision of the 3m spot bolts is adequate for stabilizing the potential wedge formed (Figures 8 & 9).

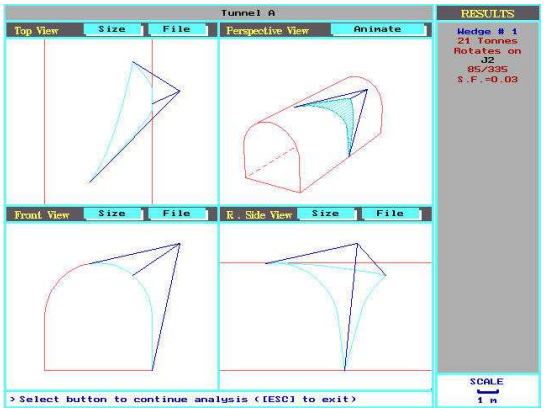

Figure 8: Potential Wedge of 21 tonnes

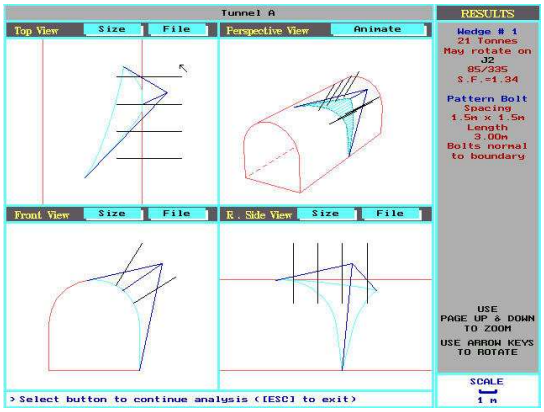

Figure 9: Provision of Spot Bolts

Phase[2] is an analytical computer program using finite element approach to model the behavior of deep excavation. For this project, it was used to predict the ground behavior at the intersections between the vertical shafts and the enlarged tunnel sections. Since the empirical approach by the Q-system had taken into account the intersection factor, numerical analysis was carried out as a supplement to the Q-system to confirm the support requirements. With the provision of steel ribs, pattern bolts, and fibre reinforced shotcrete, the maximum deformation was estimated as 20mm (Figure 10) and stress distribution is shown on Figure 11.

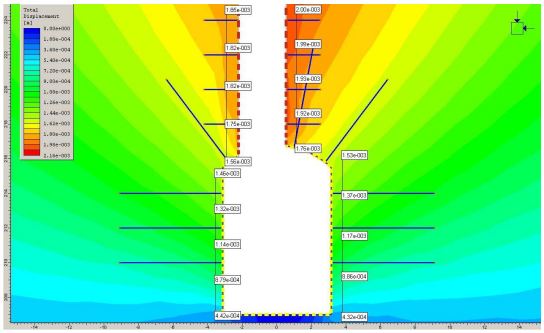

Figure 10: Estimated Deformation at Tunnel A

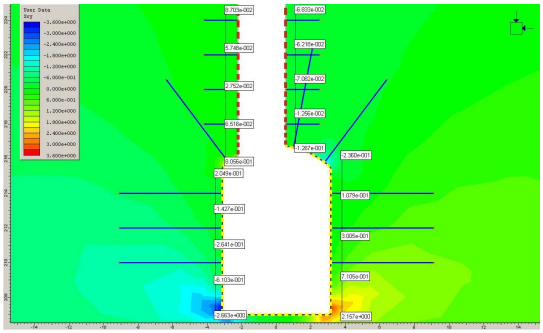

Figure 11: Stress Distribution at Tunnel A

PERFORMANCE OF TWO EXCAVATION METHODS

Drill & Blast Tunnelling

For the normal section of Tunnel A, the span and height of this section are 5.5m. In order to minimize disturbance to the public, a maximum of two blasting cycles per day could be achieved. Depending on the rock quality, the average advance rate was 2m per day. For the enlarged section of Tunnel A with various spans from 5.5m to 6.8m and heights from 5.5m to 12.5m, the advance rate was less than 1m per day. Including the support installation, Tunnel A with the extension was completed within 6 months.

For the normal section of Tunnel B, the span and height are 4.6m and 5.5m respectively. As the rock encountered was mainly fresh to slightly decomposed, the advance rate was about 2m to 2.5m per day, which was faster than at Tunnel A because of the smaller tunnel size and better rock (i.e. less support required). The rate for the enlarged section was about the same as it was at the enlarged section of Tunnel A, which was about 1m per day. Tunnel B with its shaft was completed within 5 months including both tunnel excavation and support installation.

When the tunnels were excavated, support was not installed immediately. An unsupported length was estimated according to the ground reference condition (Figure 12). In other words, the rock mass was allowed to deform sufficiently so that the load-bearing capability of the rock mass could be fully mobilised. This process is known as the arching effect (Proctor & White, 1968). As the rock mass pressure was redistributed to tunnel walls, acting loads on the support system were reduced to below the supporting strength. Hence, the residual load and the weight of loosened rock mass became the only acting loads on the tunnel support system.

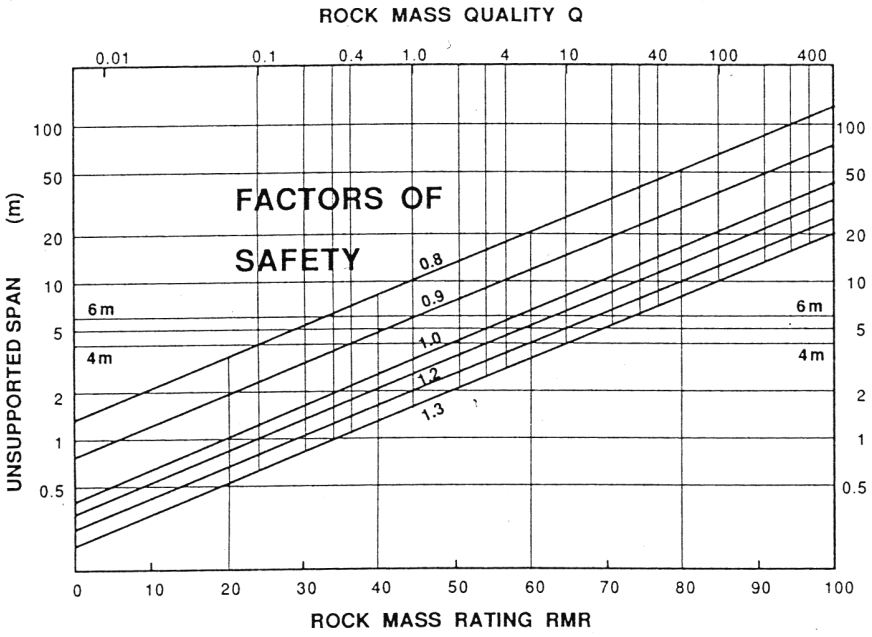

Figure 12: Estimated FOS for unsupported excavation as a function of span, Q, & RMR (Houghton and Stacey, 1980)

TBM Tunnelling – Raise Boring

A separate raise boring team was recruited from Australia under RaiseBore Australia Pty Ltd. Once the setting out of the locations of two shafts were carried out, concrete platforms were constructed at the crest of Tunnel A and then at Tunnel B. The machinery mobilisation was completed in about 3 days. Consequently, pilot hole for Shaft A at ST/No. 2 was commenced after Tunnel A was excavated and supported. The hole was driven down at a rate of 0.8m to 1.2m per hour depending on the rock quality. The entire process was done within a week. The pilot hole drilling bit was then replaced

by a reaming cutter head at the end of Tunnel A (i.e. bottom of the Shaft A). Back-reaming was then carried out at an average rate of 0.5m per hour (i.e. equivalent to 4m per day). For each 2m of reaming, spoils of about 20 tons were mucked out by trucks. Each cycle took about 5 - 6 hours and the Shaft A was drilled through in about 3 weeks. Similar procedures were carried out at Shaft B (ST/No. 3) and Shaft C (ST/No. 5). The entire raise boring process was done within three months (i.e. equivalent advance rate of 80m per month).

With the enhanced rock quality due to the machine drilling, no support was actually required except at the stratum where shear zone was encountered, a 120mm thick of shotcrete was applied. Additional supports were installed at the intersections between the shafts and tunnels.

CONCLUSIONS

The combined use of a quantitative classification Q-system and a flexible NMT reinforcement techniques was ideally suited to this project as tunnels were driven in a wide range of jointed but competent rocks. However, this empirical method has been updating with more ongoing case records. It is important for designers or practitioners to update their knowledge on using this system so that tunnels can be more effectively designed. In addition, some add-on tools as mentioned in this paper should be applied to the raw quality numbers of rock mass logged.

With the use of tunnel boring machine, the Q value would be adjusted upward to reflect a better condition of the penetrated rock structure. The correlation chart in this paper provides engineers a more direct way to design machine driven tunnels with the widely adopted Q-system. However, the authors strongly suggest that more case study records should be reviewed and the chart should be updated accordingly in future.

Under the review by Barton in year 2000, hybrid solution combining TBM and drill-and-blast was suggested; for instance, while waiting for TBM delivery, one or both portals can be driven by drill-and-blast method. A similar hybrid concept adopted in ARQ project reveals that Barton's recommendation is feasible and should be recommended to the tunneling industry.

REFERENCES

Barton, N. (2000). "Rock Mass Classification for choosing between TBM and Drill-and-Blast or a Hybrid Solution." Tunnels and Underground Structures, Zhao, Shirlaw & Krishnan (eds), Balkema, Rotterdam, pp. 35-50.

Barton, N., and Grimstad, E. (1994). "The Q-System following Twenty Years of Application in NMT Support Selection." Felsbau 12 (1994) Nr. 6, pp. 428-436.

Barton, N., and Grimstad, E. (1993). "Updating of the Q-System for NMT." Proceedings of the International Symposium on Sprayed Concrete – Modern Use of Wet Mix Sprayed Concrete for Underground Support, Fagemes, 1993, (Eds Kompen, Opsahl and Berg. Norwegian Concrete Association, Oslo).

Barton, N., Lien, R., and Lunde, J. (1977). "Estimation of Support Requirements for Underground Excavations." Proceedings of 16th Symposium on Design Methods in Rock Mechanics, Minnesota, 1975. Published by ASCE, N.Y. 1977, pp. 163-177. Discussion pp. 234-241.

Bell, F. G. (1992). "Engineering in Rock Masses." Butterworth Heinemann.

Bieniawski, Z. T. (1989). "Engineering Rock Mass Classifications." John Wiley & Sons.

GEO Geoguide 4 (1992), "Guide to Cavern Engineering", Geotechnical Engineering Office, Civil Engineering Department, Hong Kong SAR Government.

Hoek, E. and Brown, E. T. (1980). "Underground Excavations in Rock". Institution of Mining and Metallurgy, London.

Milne, D., Hadjigeorgiou J., and Pakalnis R. (1998). "Rock Mass Characterization for Underground Hard Rock Mines."

Proctor, R. V., and White, T. L. (1968). "Rock Tunnelling with Steel Supports." Commercial Shearing and Stamping Co., Youngstown, Ohio, 1946. (reprinted 1956, revised 1968).

Rutledge, J. C., and Preston, R. L. (1978). "New Zealand Experience with Engineering Classifications of Rock for the Prediction of Tunnel Support." Tunnelling under Difficult Conditions. Proceedings of the International Tunnel Symposium, Tokyo, 1978, pp. 23-29.

Skinner, E. H. (1988). "A Ground Support Prediction Concept: The Rock Structure Rating (RSR) Model." Rock Classification Systems for Engineering Purposes, ASTM STP 984, Louis Kirkaldie, Ed., American Society for Testing and Materials, Philadelphia, 1988, pp. 35-51.

Wickham, G. E., Tiedemann H. R., and Skinner, E. H. (1972). "Support Determinations based on Geologic Predictions." Proceedings of the First North American Rapid Excavation and Tunnelling Conference, Vol. 1, pp 43-64.

面震法在新田東排水渠計劃的應用

劉永佳　　林建忠
香港特別行政區政府土木工程署土力工程處

APPLICATION OF VIBROFLOTATION TECHNIQUE IN THE SAN TIN EASTERN DRAINAGE CHANNEL PROJECT

Kenneth W.K. Lau and K.C. Lam
Geotechnical Engineering Office, Civil Engineering Department
Government of the Hong Kong Special Administrative Region

撮要

渠務署現正在新界西北區，深圳河附近的低地興建一條 **2.2** 公里長的排水渠；並在落馬洲非常鬆軟的土地上，建造一所抽水站。由土木工程署進行的設計評估顯示，石柱是承托抽水站最理想的方案。現時，超過 **1,500** 支石柱正在建造中。本文詳述了該工地的土力特性、獨特的設計要求、設計方案的評估、設計論據和獨特的設計元素、與設計施工程序。而且，本文亦有介紹初步的載重測試結果和石柱承托成效監測計劃。

APPLICATION OF VIBROFLOTATION TECHNIQUE IN THE SAN TIN EASTERN DRAINAGE CHANNEL PROJECT

Kenneth W.K. Lau[1] and K.C. Lam[1]

Abstract: The Drainage Services Department is constructing a 2.2 km long drainage channel to drain floodwater from the low lying areas around the northwestern New Territories to the Shenzhen River. A pumping station for the drainage channel will be constructed on very soft ground near the Lok Ma Chau area. Option assessment undertaken by the Civil Engineering Department during the conceptual design stage indicated stone columns to be the desirable design option for this project; and currently, over 1,500 stone columns are under construction. This paper summarizes the challenging soil conditions and design requirements that prompted the stone column solution, elucidates the philosophy and critical elements of the stone column design, and highlights the design considerations for construction. The field testing program with preliminary load test results and the scheme of performance monitoring for the stone column supported structures are also introduced.

INTRODUCTION

Located in the northwestern New Territories, the low lying areas around San Tin are often subject to flooding. To alleviate the flooding risk and to drain the floodwater more effectively, a 2.2 km long drainage channel is being constructed between Castle Peak Road and the Shenzhen River, Figure 1. Running in parallel and adjacent to the Lok Ma Chau border road, the major proposed works include:

- 2 embankments with height between 4 and 5 m and side slope gradient of 1:2;
- a pumping station with its base slab level at -3 mPD and the final ground level at 6.7 mPD near the Lok Ma Chau border crossing bridge, with a typical cross-section shown in Figure 3; and
- two vehicular bridges across the channel, one near Castle Peak Road and the other near the Shenzhen River.

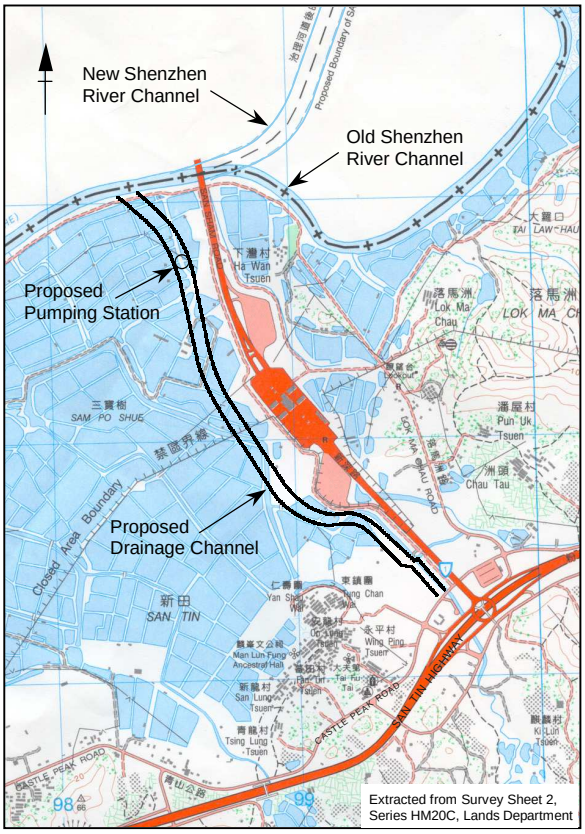

Figure 1 – Site Location Plan

[1] Geotechnical Engineering Office, Civil Engineering Department, Government of the Hong Kong Special Administrative Region.

The Geotechnical Engineering Office of the Civil Engineering Department (CED) was commissioned by the Drainage Services Department (DSD) to carry out a robust and cost-effective geotechnical design for the pumping station and its associated structures, which are underlain by very soft pond deposits and marine clay with thickness up to 12 m and undrained shear strength as low as 10 kPa.

The total contract sum for the civil engineering works is around 319 million Hong Kong Dollars. Construction of the project commenced in October 2002 and is expected to be completed by June 2006.

GROUND CHARACTERIZATION AND GEOTECHNICAL DESIGN PARAMETERS

The proposed pumping station is located at about 200 m from the Shenzhen River, and the ground is characterized by fishponds with average ground levels of the pond beds and the bunds at about 1.0 and 3.0 mPD, respectively. With the groundwater levels varying between 0 and 1.0 mPD, a water level at 2.0 mPD has been adopted for design under the short-term conditions. The long-term design water level is about 4.4 mPD, corresponding to the 1 in 200 year flood level.

The site is typically underlain by the Hang Hau Formation, which comprises about 2 m of grayish brown to dark gray pond deposits (PD), 10 m of dark fossiliferous gray marine clay (MC), 5 m of marine sand (MS) or alluvial sand (AS). The bedrocks are normally encountered at depth less than 25 m, consisting mainly of metasandstone or metasiltstone with localized calcareous zones, undivided phyllite, schist and graphite schist. The borehole record indicates that some shell fragments and organic materials were occasionally found, but no peat was encountered.

The PD and MC are very soft to soft, normally to slightly consolidated silty clays with 50 – 100% fine contents of which 15 – 50% are clay size particles. They have intermediate to very high plasticity (plasticity index and liquid limit in the ranges of 10 – 40% and 25 – 75%, respectively), suggesting their clay minerals are predominantly illite with some kaolinite, Lau (2002a). The mean void ratio and moisture content of the PD and MC are 1.27 (0.60 – 1.82) and 46.6% (23.8 – 66.1%). The PD and MC are normally active with an average activity of 0.76.

Table 1 – Geotechnical Design Parameters for the Pumping Station (After Lau 2002a)

Soil or Rock	Unit Weights		Shear Strength Parameters			Consolidation Parameters					
	γ_b (kN/m^3)	γ_d (kN/m^3)	c' (kPa)	ϕ' (^{o})	S_u (kPa)	p_c (kPa)	m_v (m^2/MN)	C_v (m^2/yr)	1st CR (Note 3)	Re-CR (Note 3),	2nd CR (Note 3)
Fill	20	17	5	33	---	---	---	---	---	---	---
PD	16	11	3	30	Note (1)	Note (2)	1	0.8	0.22	0.030	0.003
MC	17	12	2	32	Note (1)	Note (2)	1	1	0.25	0.025	0.003
MS	19	16	0	37	---	---	---	---	---	---	---
AS	20	18	0	38	---	---	---	---	---	---	---
CDR	19	16	3	35	---	---	---	---	---	---	---

Notes (1) $S_u = 10$ kPa for $h \le 4m$; $S_u = 1.25h + 5$ kPa for $h > 4m$

(2) $p_c = 35$ kPa for $h \le 4m$; $p_c = 10h - 5$ kPa for $h > 4m$

(3) CR = Compression Ratio

Typical undrained shear strength is very low at about 10 kPa in the uppermost 4 m, beyond which it increases to about 20 kPa at 12 m depth. The sensitivity is relatively low at 2 – 3, which is typical of the PD/MC in the region (Lau and Cowland 2000). A summary of the geotechnical design parameters determined from a comprehensive program of soil exploration is given in Table 1. Due to the particle size distribution, the insensitive and inactive nature of the relatively peat free PD/MC, the application of vibro-replacement technique is considered technically feasible for this project (Greenwood 1970).

DESIGN OPTION ASSESSMENT

A typical cross-section of the pumping station, which has a maximum design pressure of 164 kPa, is shown in Figure 3. The raised platform for the pumping station, at 6.7 mPD, is supported mostly by 1:2 gradient perimeter embankments and a small 3.7 m high retaining wall in the southwestern corner of the site. Cost-effectiveness and robustness are the primary design requirements of the Drainage Services Department.

Due to the very soft nature of the PD/MC, full dredging by open excavation is not considered environmentally friendly since it will involve disposal of an unnecessarily large amount of soft mud into our precious mud disposal sites. Deep excavation of more than 15 m by sheet piling in very soft ground with high groundwater table, on the other hand, will entail a relatively high risk of bottom heaving and a strenuous task of dewatering.

With relatively shallow bedrock, H-steel piles would have been very robust and cost effective, and can be easily installed. However, the site is located in the vicinity of the Mai Po Nature Reserve, which is the home to numerous bird species, including a quarter of the world's endangered and much celebrated Black-faced Spoonbills. The reserve has been formally designated as a recognized Ramsar Site – an international convention in Wetlands signed in Ramsar, Iran, in 1971. Noise control is in force and pile driving will require special permission from the relevant authorities.

Bored piles, in either large or small diameters, will be more expensive to construct for the pumping station and its associated structures; and yet ground treatment will still be required for the raised platform. Therefore, the design option assessment was extended to various ground treatment methods.

Table 2 – Comparison of Various Ground Treatment Techniques

Methods / Attributes	Stone Columns	Deep Cement Mixing (DCM)	Vacuum Surcharging	Electro-osmotic Consolidation
Cost	Lower	Higher	Lower	Higher
Stability Improvement	Good	Very good	Limited to top layers	Good
Settlement Reduction	Good	Very good	Moderately good	Good
Construction Noise	Quiet operation	Quiet operation	Very quiet operation	Very quiet operation
Water Pollution	Precaution may be needed	Precaution needed	Clean operation	Clean operation
Type of Contracts	Engineer Design	Design and Build	Design and Build	Design and Build
Local Contractors	Available	Available (marine only)	Not readily available	Not readily available
Construction	Easy and rapid	Easy and rapid, if available	Vacuum leaking	Supply of high amperage
Quality Control	Stringent	Very stringent	Very stringent	Very stringent
Sustainability	Good to very good	Moderately good	Very good	Very good
Field Tests and Monitoring	Required	Required	Required	Required

Stone columns have been successfully used to treat soft clays with undrained shear strength as low as 7 kPa, provided that the soft clays are not highly sensitive and do not contain peat with more than 1 m thickness (Greenwood 1970). Based on noise control, cost-effectiveness, robustness, stability and serviceability, sustainability and various construction aspects as summarized in Table 2, it is apparent that the stone column is the most desirable design option.

BASIS OF STONE COLUMN DESIGN

Unit Cell Concept

To facilitate the determination of the strength parameters of the composite ground for stability and settlement analyses, the tributary circular area surrounding a stone column can be conveniently idealized as a unit cell representative of the composite ground as depicted in Figure 2. The equivalent diameter of the unit cell, D_e, and the area replacement ratio, a_s, (the ratio of the area of the stone to the area of surrounding soil) can be expediently expressed in terms of the spacing and the patterns of the stone columns.

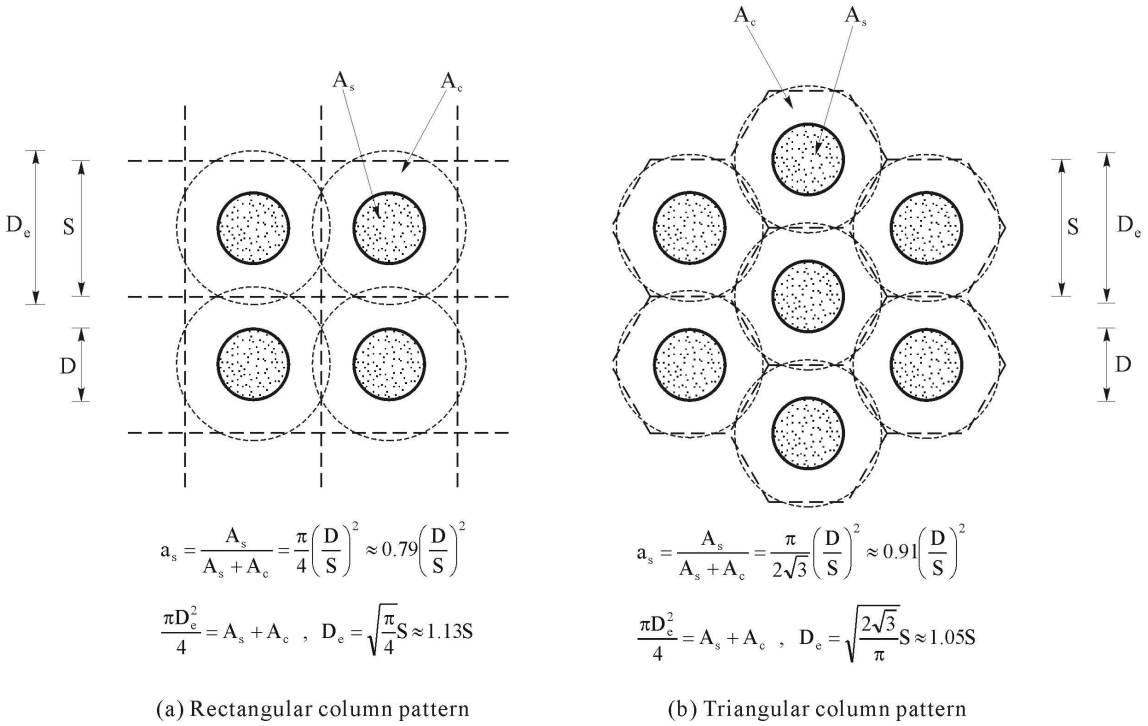

Figure 2 – Unit Cell Representation of the Stone Column Treated Composite Ground

Stress Concentration

When the composite ground is loaded, arching of stress will occur, resulting in an increase in stress on the stone columns and a decrease in stress on the surrounding clays. The stress concentration factor, *n*, which is defined as the ratio of the stress on stone column to the stress on the clay, apparently depends on the area replacement ratio, the stress level in the unit cell, and the relative stiffness of the stones, the clay and the foundation. Based on documented results of model laboratory tests and full-scale field measurements, Bergado et al (1996) and Ye et al (1994) recommended the *n* values to be ranged between 2 and 4 for most applications. Recent field measurement by Watts et al (2000) also indicated the *n* values in the range of 2 – 4 for soft clays with undrained shear strength as low as 7 kPa. An *n* value of 3, therefore, was adopted in the design analysis.

Factors of Safety

The recommended global safety factor for raft foundations is 3 for dead load and not more than 2 for a combination of dead load and extreme live load according to Terzaghi et al (1996). Hence, the adoption of a global safety factor of 3 for a combination of dead load and live load for the stone column supported raft foundations is considered a conservative expedient. The external stability of the retaining wall was checked by partial safety factors in accordance with *Geoguide 1* (GEO 1994). For long-term overall stability of the embankment and the retaining wall, a global safety factor of 1.4 was used in compliance with *Geotechnical Manual for Slopes* (GCO 1984). As immediate stability will improve with time due to the dissipation of the excess pore water pressure, a safety factor of 1.1 was adopted against short-term undrained failures.

Ultimate Bearing Capacity

The most probable failure mode of an isolated single stone column is bulging failure, occurring at a depth of about *1.5D* from the top of the stone column (Bergado et al 1996). The ultimate bearing capacity of single columns is based on the assumption that the lateral bulging of the stones are resisted by the ultimate passive resistance of the surrounding clay. The method developed by Hughes and Withers (1974), based on the approximation of the bulging failure of stone column by cylindrical cavity expansion in a pressuremeter, was adopted in the design analysis. This method accounts for the effect of overburden pressure, yet it does not require design parameters to be determined from specific model tests.

Other modes of failure – bearing capacity of single columns at the founding depth, bearing capacity of stone column groups, and stability against lateral squeezing – were also analyzed in terms of classical soil mechanics with strength parameters of the composite ground represented by the unit cell concept, Figure 2. These modes of failure, however, are not critical according to the results of detailed design analyses (Lau 2002b).

Settlement Reduction

Upon loading, stress concentration on the stone columns will cause a decrease in stress acting on the clay; thus resulting in a reduction of the overall foundation settlement. The settlement reduction can be simply determined by considering simple force equilibrium and strain compatibility of a unit cell of the composite ground, Figure 2. This simplistic idealization of the unit cell concept, however, tends to give a lower bound estimate of the settlement reduction when compared to field performance according to Bergado et al (1996). Priebe's method (Priebe 1978) was adopted since it gives reasonably conservative settlement prediction for fully penetrating stone columns by including the effect of the strength and area replacement ratio of the stones.

Accelerated Rate of Consolidation

The total degree of consolidation at a given time *t*, $U_T(t)$ in the composite ground is determined according to Carrillo (1942) by assuming that the dissipation of the excess pore water pressure takes place in the horizontal and vertical directions simultaneously, i.e.,

$$U_T(t) = 1 - (1 - U_v)(1 - U_r) \qquad (1)$$

where U_v is the average degree of consolidation in the vertical direction and is determined by Terzaghi's classical 1-D consolidation theory. U_r is the average degree of consolidation in the radial/horizontal direction and is given by Barron's method of sand drain analysis (Baron 1948) with a smearing ratio of 2 (Hansbo 1979).

Increase in Undrained Shear Strength

The increase in undrained shear strength, S_u, of the slightly to normally consolidated PD/MC is based on the following empirical relationship proposed by Mesri (1975):

$$S_u = 0.22\left(\sigma'_p \text{ or } \sigma'_{ov}\right) \qquad \textit{whichever is the larger} \qquad (2)$$

where σ'_p = *preconsolidation pressure*

σ'_{ov} = *effective overburden pressure*

This empirical correlation was also found to be reliably conservative for the Shenzhen River mud (Lau and Cowland 2000), which is located in the vicinity of the pumping station.

ELEMENTS OF THE STONE COLUMN DESIGN

5 stone column works zones – Zones A, B, C, D and E as summarized in Table 3 – were designed to cater for the different design requirements of the pump hall, the flow diversion chamber, the outlet chambers, the boundary retaining wall and the fill platform. Comprehensive design details are given in Lau (2002b), and the critical design elements instrumental to the robustness and cost-effectiveness of the stone columns are highlighted in the following sections.

Table 3 – Summary of the 5 Stone Column Treatment Zones

Treatment Zones / Design Details	Pump Hall (Zone A)	Flow Diversion Chamber (Zone B)	Outlet Chamber Nos. 1 & 2 (Zone C)	Boundary Retaining Wall (Zone D)	Fill Platform/ Embankment (Zone E)
Stone Column Pattern	Square	Square	Square	Triangular	Triangular
Stone Column Spacing, S (m)	2.0	2.0	1.8	2.0	2.5
Stone Column Diameter, D (m)	1.2	1.0	0.8	1.0	0.8
Diameter of Unit Cell, D_e (m)	2.3	2.3	2.0	2.1	2.6
Typical Unit Cell Area, A (m^2)	4.0	4.0	3.2	3.5	5.4
Area Replacement Ratio, a_s (%)	28.3	19.6	15.5	22.7	9.3
Diameter to Spacing Ratio, D/S	0.60	0.50	0.44	0.50	0.32

Area Replacement Ratio of Stone Columns

The area replacement ratios, a_s, for the 5 treatment zones should commensurate with the magnitude of the design pressures, i.e., a_s should be larger for the load bearing structures (15.5 – 28.3%) and smaller for the fill platform/embankment area (9.3%). The purpose of the stone columns in the fill platform is primarily for speeding up the consolidation process and enhancing the short-term stability of the fill embankment during construction.

Grid Pattern of Stone Columns

Since an equilateral triangular pattern will give the densest packing, stone columns for the retaining wall and the fill platform were configured in this manner. On the other hand, stone columns arranged in square or rectangular pattern will be more compatible for foundations that are mostly rectangular in area. Hence, approximately square patterned stone columns were configured for the load bearing foundations with their edges resting on one entire row of stone columns instead of the soft clay.

Depth of Treatment

Since floating stone columns will result in a one-way drainage, the degree of dissipation of porewater pressure and consolidation will be considerably longer. In addition, primary and secondary consolidation of the clay below the column tips will lead to an increase in foundation settlement. Hence, all the stone columns were designed to be penetrating the PD/MC completely with a minimum of 1 m embeddment into the layer of alluvial sand or marine sand, Figure 3.

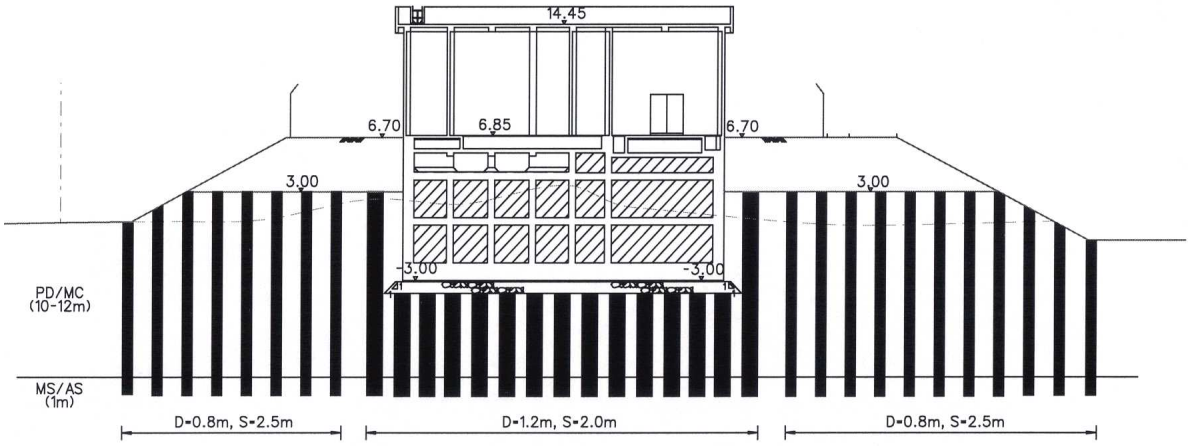

Figure 3 – Typical Cross-section of Stone Column Treatments

Diameter and Spacing

The diameter, *D*, and spacing, *S*, play an important role in the cost-effectiveness and robustness of stone columns. The optimal *D/S* ratios for the 5 stone column treatment zones as shown in Table 3 are the results of due considerations given to the homogeneity of the composite ground, minimization of ground disturbance and economics. A more homogeneous composite ground can be accomplished by more closely spaced, smaller stone columns; but they are generally more expensive to install due to larger number of mobilization runs of the vibroflots. On the other hand, larger stone columns at wider spacing will be more economical to construct for a given area replacement ratio although they will normally result in a less homogenous composite ground.

Types and Grading of Stones

The stones should be easily compacted in a dense packing with minimal machine energy, and they should not react or degrade with the in-situ ground. As such, clean, hard, inert and natural crushed rocks with a grading of a nominal single-sized material within the range of 20 – 75 mm and less than 5% fines were specified.

Surcharge on the Composite Ground

To further reduce foundation settlement, a 4.5 m surcharge will be applied to the composite ground treated with stone columns, resulting in a surcharge load greater than the net foundation pressure of the pump house. At 7.5 mPD level, the surcharge will be maintained for a minimum period of three months or until 90% realization of consolidation settlement. With the consolidation settlement corresponding to the surcharge predicted at about 0.78 m and the final formation level of the elevated platform at 6.7 mPD, only minimal backfilling will be required subsequently.

(a) Accelerated Degree of Consolidation

Since the proposed stone columns will have diameters ranging from 0.8 m to 1.2 m, the action of radial drainage will be much more effective than that of conventional sand drains or prefabricated band drains. As shown in Figure 4, about 90% of consolidation can be achieved for the load bearing composite ground after 1 month of surcharge. Thus, a surcharge period of three months is considered to be a conservative expedient.

(b) Increase in Undrained Shear Strength

Due to stress concentration around the stone columns, the actual overburden pressure acting on the clay will be less than the average surcharge pressure, resulting in the lower bound profile of strength gain as shown in Figure 5. This lower bound of strength gain was conservatively adopted in the stability analysis. Specifically designed stress concentration relief caps, in the form of square pyramid of matching dimensions, will be placed on designated load bearing stone columns to nullify the effect of stress concentration. The scenario that the stress concentration relief caps just offset the stress concentration effect is illustrated by the upper bound profile of strength gain in Figure 5. The stress concentration relief caps are expected to further enhance the robustness of the design by reducing the overall and differential settlement of the stone column supported foundations.

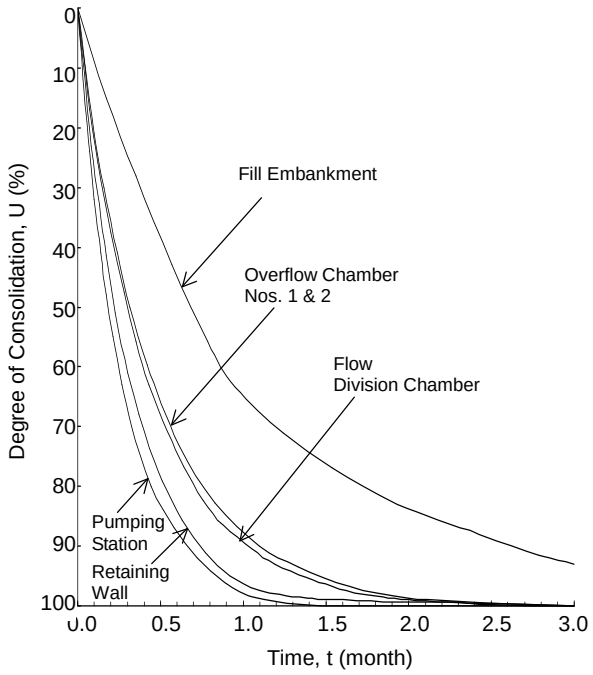

Figure 4 – Predicted Degree of Consolidation

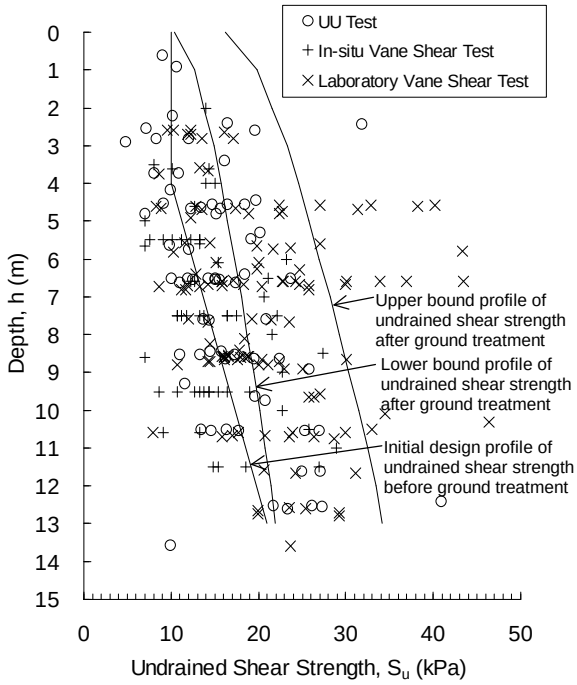

Figure 5 – Undrained Shear Strength Profiles

CONSTRUCTION

Prior to the installation of the stone columns, a layer of sand blanket/drainage materials is placed up to the 3 mPD level to facilitate installation, improve short-term stability and enhance serviceability. The sand blanket serves as a working platform for the required machinery to install the stone columns and to facilitate drainage. It helps forcing the occurrence of bulging failure of single stone columns to greater depths, thus enhancing the bearing capacity. It also facilitates initial setting out, planning of sedimentation ponds for the silt-laden flushing water before disposal, and the setting up of a site office.

Over 1,500 stone columns are being constructed by a wet top-feeding process, in which the vibroflot penetrates into the ground by the combined effects of its own weight and the vibrating action of its eccentrically mounted motor. Water jetting out at the bottom and along the sides of the vibroflot will facilitate penetration, flushing out loose particles from the hole, and maintaining the stability of the hole, Figure 6. At the required depth, the vibroflot is withdrawn slightly and the pressure of the jetting water is reduced to maintain the stability of the hole. A charge of stone is fed into the hole by a front-end loader on the working platform, and the vibroflot is then re-penetrated into the hole to compact the stones into the required diameter. This process is repeated, with the vibroflot remaining inside the hole for stability, until the stone column is formed to the ground surface.

Figure 6 – Installation of Stone Columns by Wet Top-Feeding Process

After installation of the working stone columns and prior to the placement of the 4.5 m surcharge, the square pyramid stress concentration relief caps will be placed on designated load bearing stone columns. Instrumented field tests will be carried out and completed by the end of the surcharge period. All functioning instruments including pressure cells, settlement sensors and piezometers used in the field tests will be re-used in monitoring the long-term performance of the stone column supported structures.

FIELD TESTS

A comprehensive field test program has been planned to evaluate the adequacy of construction process, ultimate bearing capacity, load and settlement characteristics, and gain in undrained shear strength of the in-situ ground (Lau 2002b). The field tests being carried out on site include proof load tests, cell load tests, zone load tests and vane shear tests.

Proof Load Tests

A proof load test is essentially a quality control test since the test load is applied quickly onto a working stone column by jacking against heavy construction plant such as a crane or a tractor mounted rig. A total of 7 proof load tests with test loads 1.5 – 2.5 times the equivalent working loads are being carried out to determine the immediate load settlement relationship. Preliminary proof load test results given in Figure 7 indicate that the test column was properly installed with satisfactory immediate load settlement characteristics.

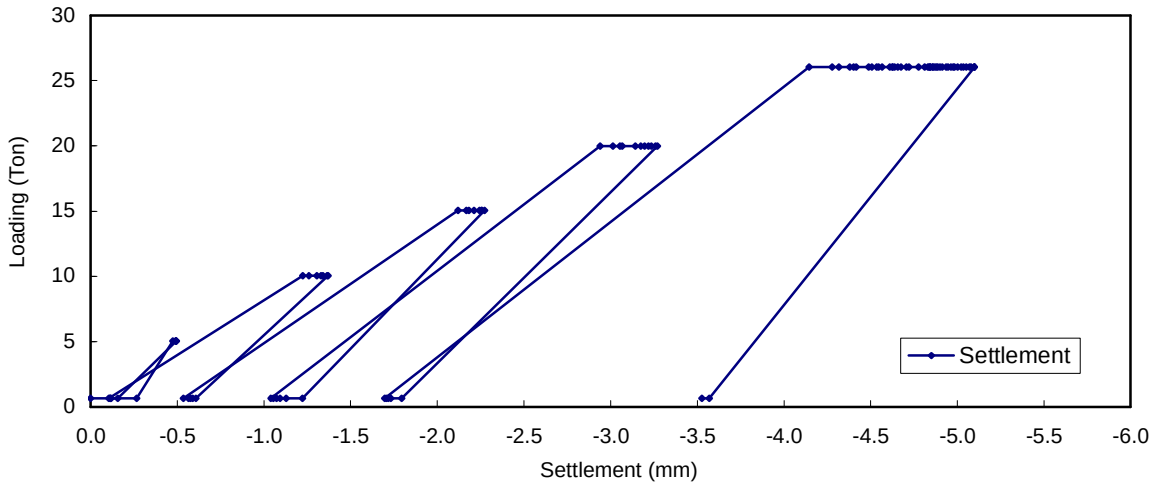

Figure 7 – Load Settlement Characteristics of a Typical Proof Load Test

Cell Load Tests

Three cell load tests as illustrated in Figure 8 will be carried out to determine the load settlement relationship and stress concentration of three single working stone columns. Each loading area will correspond to the unit cell area, which is the area tributary to a single stone column as defined in Figure 2. The test load will be equivalent to the ultimate bearing capacity of a single stone column with at least 5 load increments.

Zone Load Test

A practical zone load test covering 9 stone columns will also be carried out for the pump hall. The 6 m x 6 m square zone will be loaded at the 3 mPD level by kentledge. Flat jack pressure cells will be placed on the top of stone columns and on the surrounding clay to gage the stress concentration effect with time. The test will be maintained until at least 90% of consolidation settlement has been recorded, and preferably be extended to cover part of the secondary settlement behavior. With a surcharge period of three months and the predicted degrees of consolidation given in Figure 4, it is anticipated that the zone load test will yield valuable data on the consolidation settlement behavior of the composite ground.

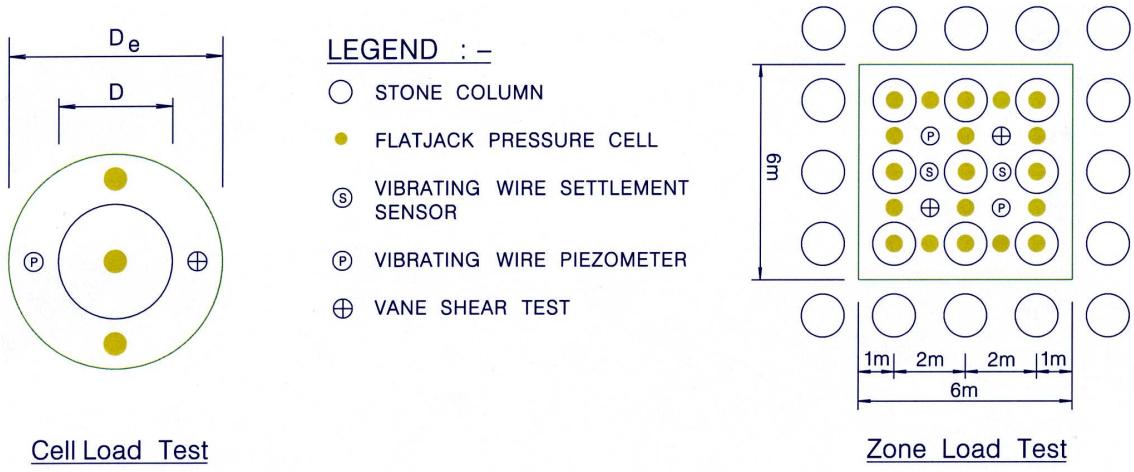

Figure 8 – Typical Layout of the Cell Load Tests and the Zone Load Test

In-situ Vane Shear Tests

The load carrying capacity of stone columns is directly dependent on the gain in shear strength of the clay due to the surcharging load. Therefore, in-situ vane shear tests will be carried out for each load test and at the foundation level of the pumping station to confirm the gain in shear strength.

INSTRUMENTATION AND MONITORING

Instrumentation has a crucial role in the design of stone columns in this project. The purpose is essentially to confirm the design assumptions, to control the rate of construction, or to modify the design if necessary, such that the stability of the pumping station and its associated structures can be ensured during and after construction. Hence, a comprehensive network of geotechnical instruments has been specified (Lau 2002b). The instruments include monitoring points, settlement plates, earth pressure cells, magnetic extensometers, vertical and horizontal inclinometers, settlement sensors and settlement profilers, vibrating wire piezometers and double standpipe piezometers.

It is envisaged that monitoring will reveal the satisfactory performance of the raft foundations, retaining wall and embankments supported by stone columns, since the design of the stone columns was based on well established design methodology with reasonably conservative design assumptions. The monitoring results will also yield valuable information on the long-term behavior of stone column treated composite ground; and such data may facilitate more cost-effective stone column design in future.

CONCLUSIONS

A rare combination of challenging soil conditions (low shear strength and high compressibility) and special design requirements (cost-effectiveness, robustness and noise restriction) for this project have prompted a unique opportunity to employ vibroflotation technique in Hong Kong. It has been shown that application of the stone columns was executed to its fullest technical and economic advantages for the lightly loaded pumping station with relatively deep founding level.

The stone column design, which was based on simple and well-established design principle with reasonably conservative assumptions, has been elucidated. Methodology to assess the acceleration of consolidation, increase in shear strength, improvement of stability and reduction of settlement, has been demonstrated. The application of surcharge at a level commensurate with the final formation level and the use of specially designed stress concentration relief caps will further enhance the robustness of the design. Other critical design elements – diameter, spacing, pattern and area replacement ratio – that could influence the performance of the pumping station have been presented in details.

Design considerations for construction to facilitate installation of stone columns and to improve short-term stability have been highlighted. The comprehensive field testing program with preliminary results of proof load tests and the scheme of an extensive network of geotechnical monitoring are also introduced. It is envisaged that the results of the field tests and monitoring will confirm the design assumptions, substantiate the performance of the stone column supported structures, and yield valuable information on the long-term behavior of the stone column treated composite ground.

REFERENCES

Barron, R.A. (1948). "Consolidation of fine-grained soils by drain wells," *Trans. ASCE, 113*, pp. 718 – 754.

Bergado, D.T., Anderson, L.R., Miura, N. & Balasubramaniam A.S. (1996). *Soft Ground Improvement in Lowland and other Environments*, ASCE Press, New York, 427p.

Carrillo, N. (1942). "Simple two and three-dimensional cases in theory of consolidation of Soils, *J. of Math. & Physics*, Vol. 21, No. 1, pp. 1-5.

Greenwood, D. A. (1970). "Mechanical Improvement of Soils Below Ground Surface", *Proc. of Conf. on Ground Eng., ICE*, pp. 11 – 22, London, 1970.

Geotechnical Control Office (1984). *Geotechnical Manual for Slopes*, 2nd Edition, 295p.

Geotechnical Engineering Office (1993). *Geoguide 1: Guide to Retaining Wall Design*, 2nd Edn., 268p.

Hansbo, S. (1979). "Consolidation of clay by band-shaped pre-fabricated drains," *Ground Engineering*, 12, No. 5, pp. 16 – 25.

Hughes, J.M.O. & Withers N.J. (1974). "Reinforcing soft cohesive sold with stone columns", *Ground Engineering*, Vol. 7 No.3, May 1974, pp.42 – 49.

Lau, K.W.K. (2002a). *Flood Protection Works for East San Tin*, Advisory Report ADR 12/2002, Geotechnical Engineering Office.

Lau, K.W.K. (2002b). *Geotechnical Design of Stone Columns for the San Tin Eastern Drainage Channel*, Advisory Report ADR 13/2002, Geotechnical Engineering Office.

Lau, K.W.K and Cowland, J.W. (2000). "Geosynthetically Enhanced Embankments for the Shenzhen River", Proc. of Geo-Denver 2000, ASCE Geotechnical Special Publication No. 103, pp. 140 – 161.

Mesri, G. (1975). "New design procedure for stability of soft clays", Discussion, *J. Geotech. Eng*., ASCE, Vol. 101, No. 4, pp. 1090 – 1093.

Priebe, H. J. (1978). *Abschatzung des Scherwiderstandes eines durch Stopverdichtung verbesserten Baugrundes.* Die Bautechnik, (55), 8, 282-284.

Terzaghi, K, Peck, R.B. and Gholamreza, M. (1996). *Soil Mechanics in Engineering Practice*, John Wiley & Sons, 3rd Edition, 549p.

Watts, K.S., Johnson, D., Wood, L.A. & Saadi, A. (2000). "An instrumented trial of vibro ground treatment supporting strip foundation in a variable fill", *Geotechnique*, Vol. 50, No. 6, pp. 699 – 708.

Ye, S.L., Han, J., & Ye, G.B. (1994). *Foundation Treatment and Underpinning Technology*, (In Chinese), 2nd Edition, China Construction Industry Press, 662p.

ACKNOWLEDGEMENTS

This paper is published with the permission of the Head of Geotechnical Engineering Office, the Director of Civil Engineering and the Director of Drainage Services of the Government of the Hong Kong Special Administrative Region. Acknowledgements are extended to Mr. T.F. Chong, formerly of the CED and currently of the DSD, for his involvement in the design stage of the project, Ir K.W. Mak and Miss P.N.Y. Lau of the CED, who are now providing geotechnical input in the construction stage. Helpful comments from Ir W.M. Wong and Ir C.L. Leung of the DSD and technical support provided by Mr. H.K. Yiu of the CED are also gratefully acknowledged.

打樁公式新建議的初步的研究

李啓信
李啓信工程顧問有限公司
陳少德
香港特別行政區政府香港房屋委員會
林早妮
李啓信工程顧問有限公司

AN ALTERNATIVE PILE DRIVING FORMULA – A PRELIMARY STUDY

K. S. Li
Victor Li & Associates Ltd.
S. T. Chan
Hong Kong Housing Authority
Government of the Hong Kong Special Administrative Region
J. Lam
Victor Li & Associates Ltd.

撮要

本文討論了兩條香港常用的打樁公式，即是希利公式和香港建造商協會建議的打樁公式。根據打樁數據顯示，希利工式用是有不足之處。

本文建議應用另一條可行的公式，它可以解決現常用打樁公式的不足之處。根據一個地基工程的試樁資料，這建議公式相當準確。本文亦建議放鬆對現時訂定打入樁的最終貫入度表的規限。

AN ALTERNATIVE PILE DRIVING FORMULA – A PRELIMINARY STUDY

K. S. Li[1], S. T. Chan[2] and J. Lam[3]

Abstract: This paper reviews two pile driving formulae commonly used in Hong Kong, namely, the Hiley formula and the formula proposed by the Hong Kong Construction Association (HKCA). Data which illustrate the limitations of the Hiley formula are presented. An alternative pile formula which removes some of the limitations of the Hiley formula and HKCA formula is proposed. The accuracy of the proposed alternative pile driving formula is ascertained by pile loading test results from a foundation project. Recommendations are made for relaxing the applicable range of allowable maximum final set values in preparing the final set tables for pile driving.

INTRODUCTION

Driven piles are usually designed to achieve a certain ultimate capacity. Pile driving formulae have been and are still widely used to determine the allowable maximum final set value for a given hammer weight, drop height and design ultimate pile capacity. Although more sophisticated and arguably more reliable methods based on Pile Driving Analyzer (PDA) tests are available for predicting pile capacity, the use of a suitable pile driving formula to determine the allowable maximum final set values is much simpler, more convenient and cost effective for field application.

Numerous pile driving formulae are available in the literature (Chellis, 1944; Whitaker, 1976). The formula developed by Hiley (1922, 1925) over 80 years ago has been the most commonly used pile driving formula in Hong Kong although its application to long piles has been proven to be deficient time and again.

In this paper, a preliminary study on an alternative pile driving formula applicable to drop hammers and hydraulic hammers is presented. Pile loading tests carried out at a Hong Kong Housing Authority's (HKHA) site (hereafter referred to as Site A) on H-piles tested to failure or imminent failure indicate that the proposed pile driving formula gives good predictions of the ultimate capacity of driven piles.

BASICS OF PILE DRIVING FORMULA

In this paper, three pile driving formulae are discussed, including the Hiley formula, the formula proposed by the Hong Kong Construction Association (HKCA) in 1995 (hereafter called the HKCA formula) and the proposed alternative pile driving formula. All the three pile driving formulae are based on the energy approach which gives the following basic equation (Li *et al*, 2003).

[1] Director, Victor Li & Associates Ltd.
[2] Chief Structural Engineer, the Hong Kong Housing Authority
[3] Engineer, Victor Li & Associates Ltd.

$$R = E / (s + c / 2) \quad (1)$$

where E is the energy transferred to the pile-soil system after impact, s is the permanent pile settlement per blow (also called the set value) and c is the elastic compression of the pile-soil system.

There are two pile-soil systems depending on whether the pile anvil/cushion is included as part of the pile-soil system as discussed by Li *et al* (2003). If the anvil/pile cushion is included as part of the pile-soil system, energy will also be stored during elastic compression of the pile cushion. The elastic compression should therefore comprise three components, namely, $c = Cc + Cp + Cq$ where Cc, Cp and Cq are the temporary compression of pile cushion, pile and soil respectively.

If the anvil/pile cushion is NOT included as part of the pile-soil system, the energy transferred to the pile-soil system will be converted to energy stored in the pile and soil only. In this case, $c = Cp+Cq$ and E is simply the total energy transferred to the pile head, E_p, which can be measured directly using a PDA test. E_p can be expressed in terms of the energy transfer ratio X, defined as $E_p = X\ W\ h$, where W is the hammer weight and h is the drop height. The values of E_p and X are normally standard output in a PDA test report.

In some pile driving formulae, E is related to the kinetic energy of the hammer before impact E'. It is common to express E' is in terms of the hammer efficiency α defined as $E' = \alpha\ W\ h$. The hammer efficiency measures the energy loss during descend of the hammer. Some hydraulic hammer systems impart energy to the hammer during descend of the hammer and the input energy of the hammer for pile driving is actually higher than $W\ h$. This may give hammer efficiency higher than 1.0 even if there is energy loss before impact (see results in Figure 1 discussed later). As there is further energy loss after impact, E can be expressed in terms of the efficiency of hammer blow η. This gives $E = \eta\ E' = \alpha\ W\ h\ \eta$.

HILEY FORMULA

By considering the simple physics of impact of two rigid bodies, Hiley (1922) derived the following expression for the efficiency of hammer blow η :-

$$\eta = \frac{W + (W_p + W_r)\, e^2}{W + (W_p + W_r)} = e^2 + \frac{W(1 - e^2)}{W + (W_p + W_r)} \quad (2)$$

where W_p is the weight of pile, W_r is the weight of anvil and e is the coefficient of restitution. According to Eq.2, η decreases with pile weight. Therefore, the Hiley formula predicts higher energy loss after impact as the pile length increases. The Hiley formula considers the anvil as part of the pile-soil system. Combining Eq.1 and Eq.2 gives :-

$$R = \frac{\alpha W\ h}{s + \frac{1}{2}(C_c + C_p + C_q)} \times \frac{W + (W_p + W_r)\, e^2}{W + (W_p + W_r)} \quad (3)$$

HKCA FORMULA

Hydraulic hammers were introduced in Hong Kong in the late 80s and gained popularity in the early 90s. HKCA (1995) proposed the following pile driving formula for hydraulic hammers :-

$$R = \frac{K_h E'}{s + \frac{1}{2}(C_c + C_p + C_q)} \tag{4}$$

where K_h is the hydraulic hammer factor which in fact has the same meaning as efficiency of hammer blow η. The anvil/pile cushion is considered as part of the pile-soil system in the HKCA formula and therefore the C_c term appears in Eq.4.

The only difference between the HKCA formula and the Hiley formula is that a constant hydraulic hammer factor K_h and hence a constant η is used in the HKCA formula whereas η decreases with pile length in the Hiley formula. In the HKCA report, a K_h factor of 0.6 is recommended for a pile driven with cushion and 0.7 for a pile driving system without cushion. The recommended K_h factors that were derived a decade ago, based on the performance of the hydraulic hammers at the time, are too low and thus not applicable to modern hydraulic hammers with much higher efficiency. This often results in the inability to establish workable final set table using the HKCA formula for driven piles installed using modern hydraulic hammers. As explained by Li *et al* (2003), the contractors would usually switch to drop hammers and adopt the Hiley formula for final setting of piles while hydraulic hammers are used for pitching of piles.

ALTERNATIVE PILE DRIVING FORMULA

With the advent of foundation testing equipment, the energy transferred to the pile head during driving, E_p , can now be directly measured with high accuracy using the PDA test. This has led to the proposal of the following alternative pile driving formula by Broms & Lim (1988) and Paikowsky & Chernauskas (1992).

$$R = \frac{E_p}{s + \frac{1}{2}(C_p + C_q)} \tag{5}$$

In this formula, the pile anvil/pile cushion is not considered as part of the pile-soil system and therefore the term C_c does not appear in the denominator of Eq.5.

The above formula eliminates uncertainties in the assumption/measurement of parameters in pile driving formula such as hammer efficiency α, elastic compression of pile cushion C_c, efficiency of hammer blow η and coefficient of restitution e. Eq.5 can be presented in an equivalent form as follows :-

$$R = \frac{X\ W\ h}{s + \frac{1}{2}(C_p + C_q)} \tag{6}$$

Hussein *et al* (1992) observed that the energy transfer ratio X is not sensitive to the drop height. The same finding is made for data to be presented later in this paper. Therefore, a design value of X can be assigned for a particular pile driving system in determining the allowable final set values using Eq.6.

REVIEW OF EXISTING DATA

Energy Transfer Ratio

Figure 1 shows the data of energy transfer ratio *X* measured by PDA tests obtained by Li (2002) from a number of foundation sites in Hong Kong and additional data obtained from two other sites in Hong Kong. It can be observed that the value of *X* for a given pile driving system is generally independent of pile length and ground conditions within a site. The data in Figure 1(b) for Site A, covering a large range of drop heights from 1.5m to 2.7m, suggest that *X* is also not sensitive to drop height. If PDA tests are performed on selected piles for a given site during the initial phase of pile driving, a suitably conservative design value of *X* can be established for determining the allowable maximum final set values for the site.

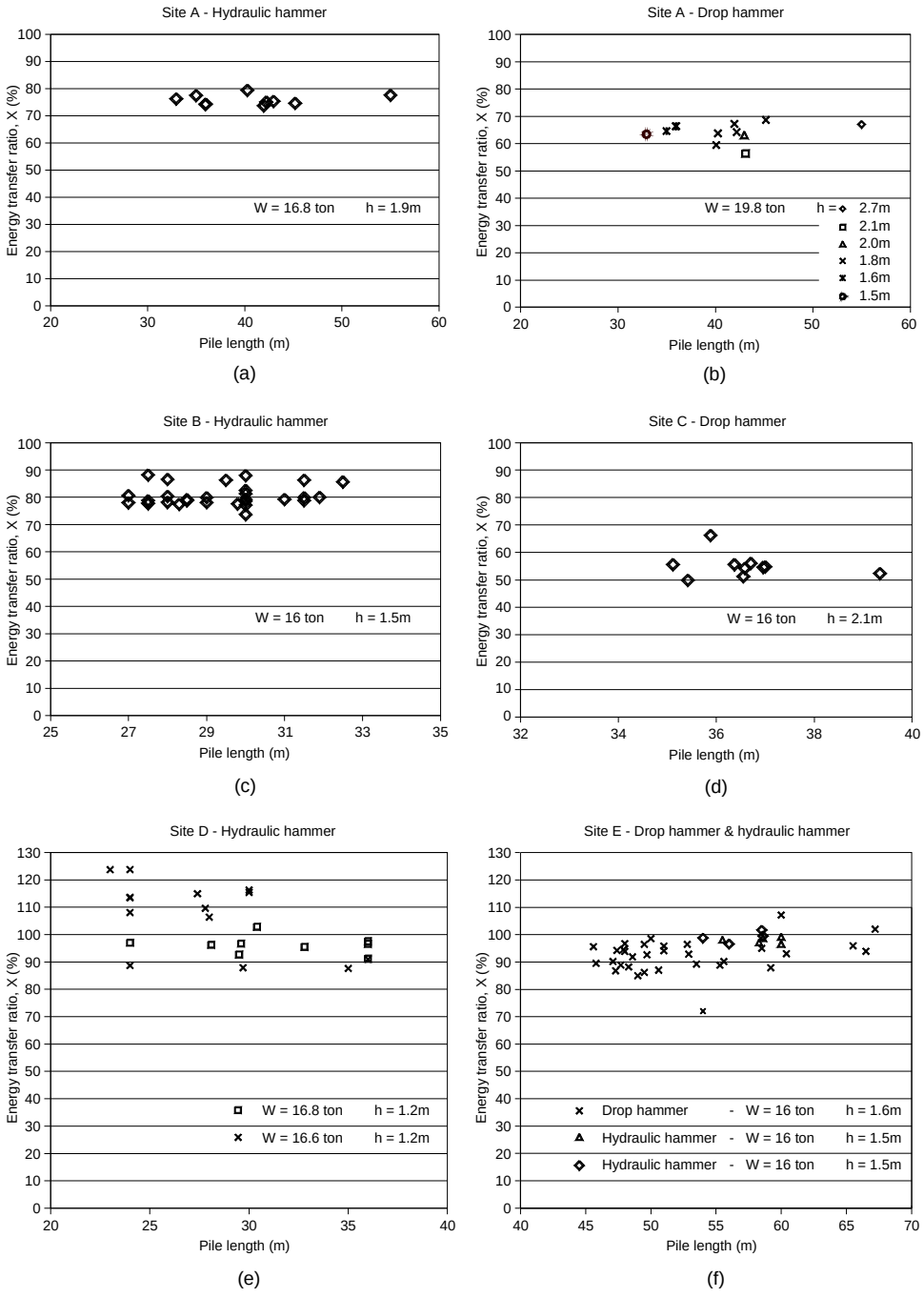

Figure 1 Energy transfer ratio at different sites

Efficiency of Hammer Blow

It has been recognized for a long time that the efficiency of hammer blow η tends to be constant for long piles (Cornfield, 1961; GEO, 1996; Triantafyllidis 2001). Li *et al* (2003) have derived the following relationship for η:-

$$\eta = \frac{X}{\alpha} \cdot \frac{\frac{1}{2}(C_c + C_p + C_q) + s}{\frac{1}{2}(C_p + C_q) + s} \tag{7}$$

Figure 2 shows the magnitude of η calculated for some piles for Site A based on the values of X, α, C_c, C_p+C_q and s measured by PDA tests and other field tests and measurements. Also shown in Figure 2 is the value of η calculated using the Hiley formula based on a coefficient of restitution of 0.32. The data in Figure 2 clearly demonstrate that the Hiley formula is not correct as the back-calculated values of η tend to be independent of pile length. If used, the Hiley formula will significantly underestimate the efficiency of hammer blow for long piles. The HKCA formula, which adopts a constant hydraulic hammer factor with implication of a constant value of η, is an improvement to the Hiley formula.

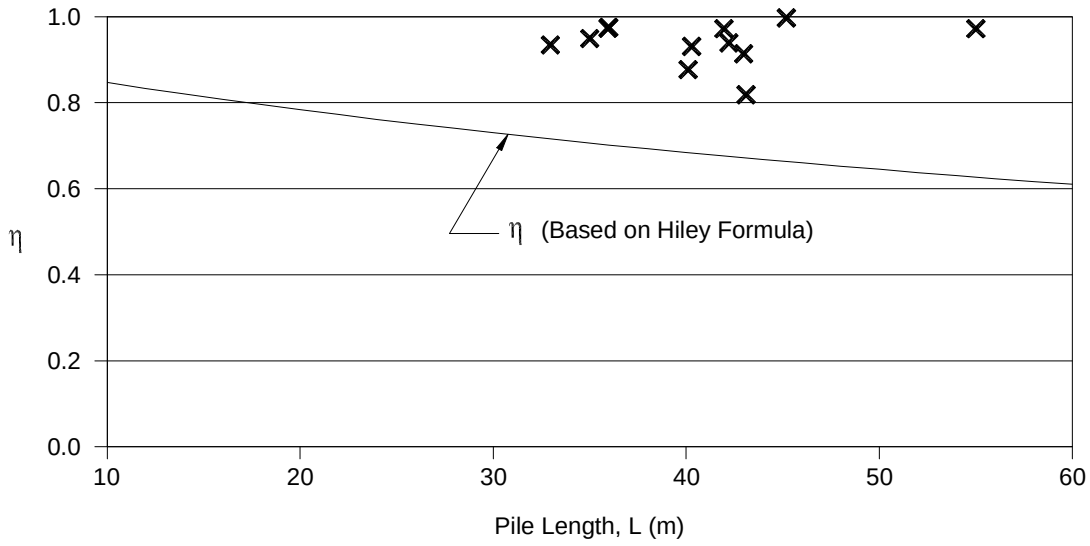

Figure 2 Efficiency of hammer blow for drop hammer

Accuracy of Alternative Pile Driving Formula

Figure 3 compares the ultimate capacity of piles predicted by the alternative pile driving formula of Eq.5 with that predicted by CAPWAP analysis or pile loading tests. The data in Figure 3(a & b) are obtained from Broms & Lim (1988), for which the failure loads of piles predicted by CAPWAP were used as a basis for checking the accuracy of the alternative pile driving formula. The data in Figure 3(c) are taken from Paikowsky & Chernauskas (1992), for which the failure loads were obtained from pile loading tests.

A total of 7 test piles of Grade 55C 305x305x224 kg/m H-piles were loaded to failure or 3.3 times the design pile capacity for Site A. Each test pile was initially driven to final set by hydraulic hammer, followed by a drop hammer. Therefore, two different final set values were obtained for each test pile.

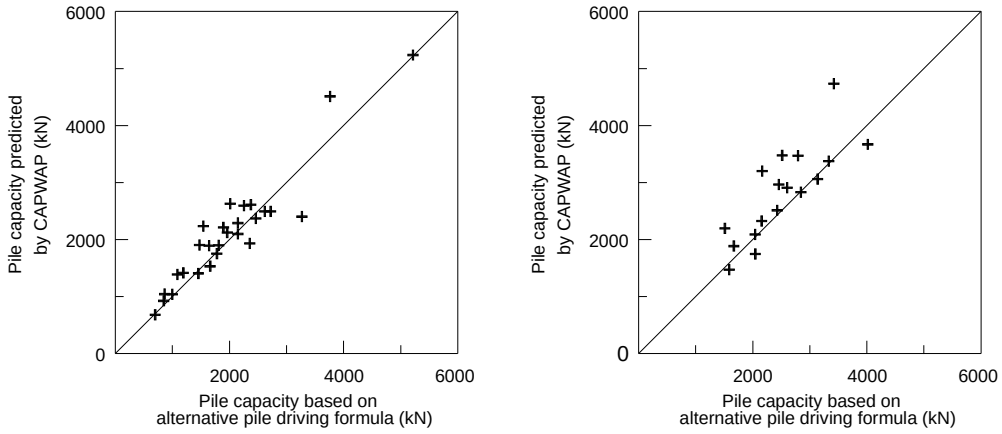

(a) Concrete Piles (b) Steel Piles

(a) Broms and Lim (1988)

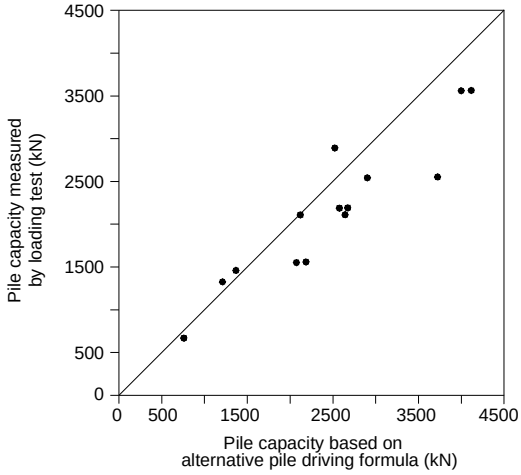

(b) Paikowsky & Chernauskas (1992)

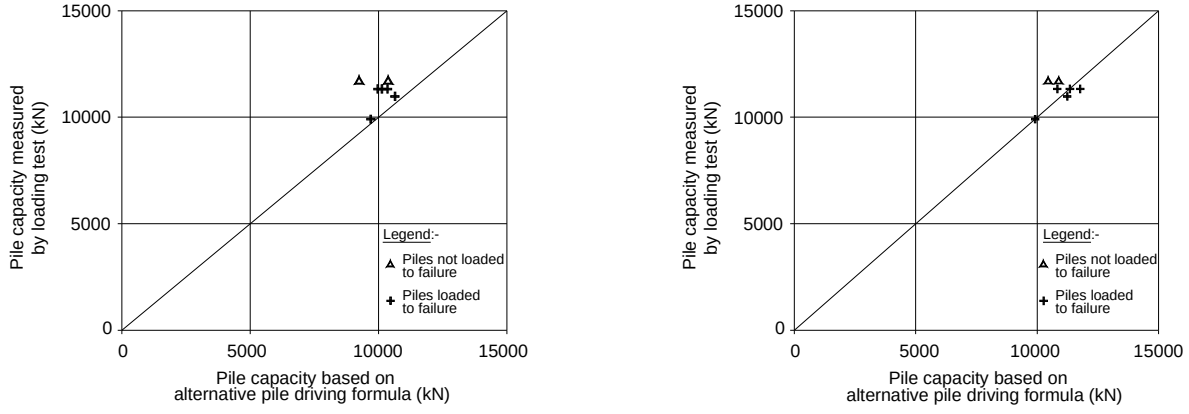

DROP HAMMER HYDRAULIC HAMMER

(c) Site A

Figure 3 Accuracy of alternative pile driving formula

To compare the maximum test loads or failure loads measured for the 7 test piles and the ultimate capacity predicted by the alternative pile driving formula of Eq. 6, the energy transfer ratio measured by PDA tests and the measured final set and $C_p + C_q$ values are used. Summaries of the pile length, hammer weight, drop height, the $C_p + C_q$ and final set values, the PDA test results and the loading test results of the test piles for driving by drop hammers and by hydraulic hammers are given in Table 1.

Table 1 Details of test piles

Pile no.	Pile length (m)	Hammer weight W (kN)	Drop height h (m)	Elastic compression $Cp + Cq$ (mm)	Final set s (mm/10 blows)	E_p measured by PDA (kN-m)	Emax = $W h$ (kN-m)	Measured energy transfer ratio X	Pile capacity from loading test (kN)	Predicted capacity (kN)
DROP HAMMER										
1	35.0	194.43	1.6	40	2	201.56	311.09	0.65	11328	9978
2	41.95	194.43	1.8	46	13	235.71	349.97	0.67	9912	9700
3	40.09	194.43	1.8	40	2	209.50	349.97	0.60	> 11682	10371
4	36.0	194.43	1.6	40	0	207.06	311.09	0.67	11328	10353
5	40.27	194.43	1.8	44	1	224.02	349.97	0.64	11328	10137
6	43.10	194.43	2.1	50	1	232.20	408.30	0.57	> 11682	9251
7	45.20	194.43	1.8	45	1	240.54	349.97	0.69	10974	10643
HYDRAULIC HAMMER										
1	35.0	164.81	1.9	38	20	238.38	313.14	0.76	11328	11351
2	41.95	164.81	1.9	41	28	231.20	313.14	0.74	9912	9923
3	40.09	164.81	1.9	39	12	225.20	313.14	0.72	> 11682	10879
4	36.0	164.81	1.9	39	4	234.23	313.14	0.75	11328	11770
5	40.27	164.81	1.9	42	4	231.82	313.14	0.74	11328	10833
6	43.10	164.81	1.9	44	3	233.10	313.14	0.74	> 11682	10453
7	45.20	164.81	1.9	41	14	246.15	313.14	0.79	10974	11240
Note: The measured energy transferred to pile E_p is based on average results of last 10 blows at final set.										

The soil profiles and load-settlement curves for the 7 test piles are presented in Figure 4. Figures 3(d) and 3(e) compare the predicted versus measured ultimate capacity of the test piles driven by hydraulic hammers and drop hammers.

The results in Figure 3 indicate that the alternative pile driving formula of Eq.5 or Eq.6 gives relatively good prediction of the ultimate pile capacity, both for drop and hydraulic hammers.

FINAL SET TABLE

In Hong Kong, it is common to restrict the applicable range of the final set values in a final set table to values between 25mm and 50mm per 10 blows. The former limit is based on a recommendation specified in an old foundation code, namely, the Code of Practice No. 4 – Foundation (ICE, 1954) that the weight of the hammer should be sufficient to ensure a final penetration of not less than 1/10 inch per blow. This code was superseded by the code CP2004 (BSI, 1972) and in turn by the British Standard BS8004 (BSI, 1986). The limit of 25mm per 10 blows was dropped, but a new recommendation that the final penetration should not be more than 5mm per blow was introduced in CP2004 and BS8004.

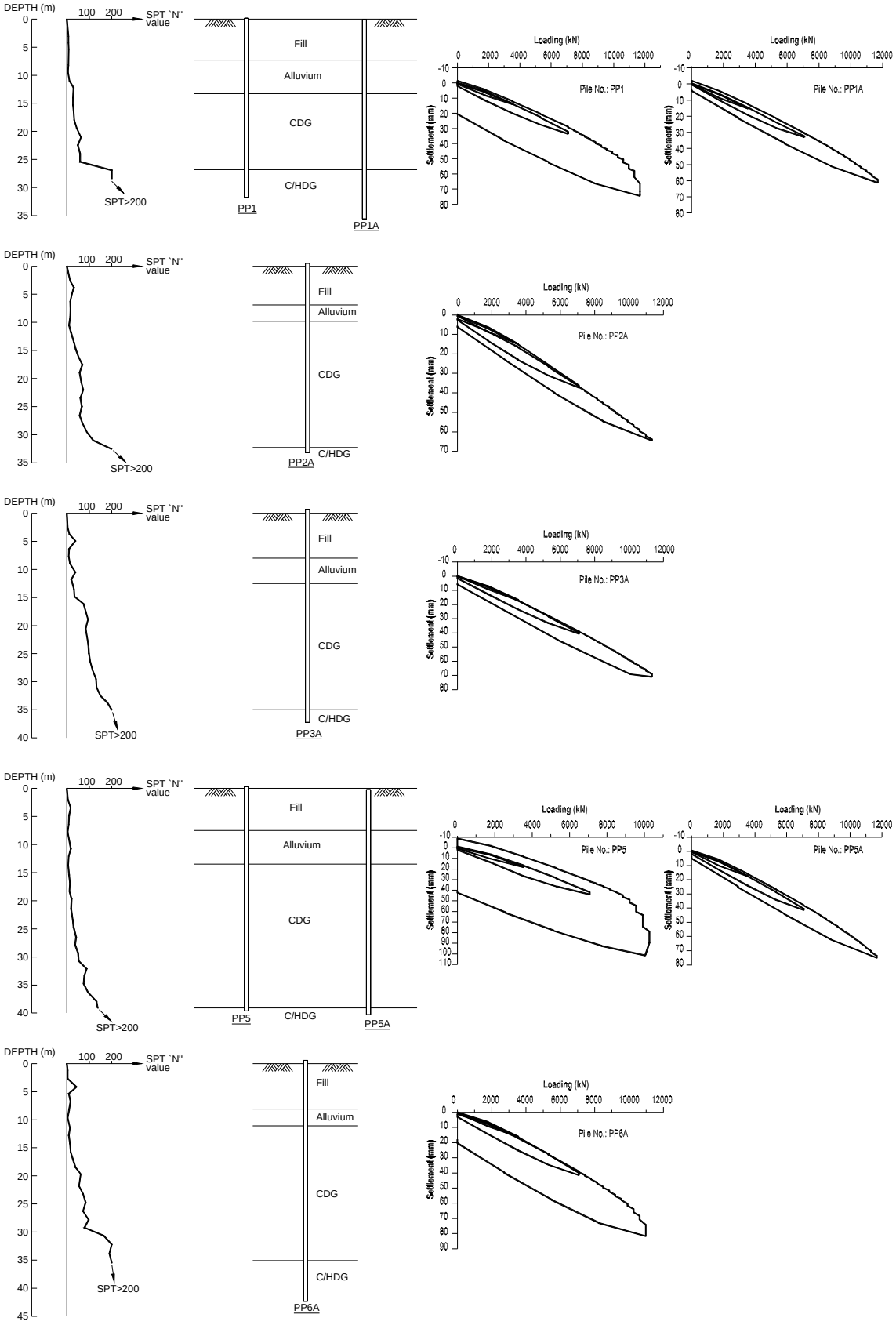

Figure 4 Details of test piles for Site A

One reason for setting a lower limit for the applicable range of final set value is to enforce piling contractor to use a heavy hammer for pile driving so as to reduce the driving stress that risks damaging the pile (Li *et al*, 2003). It is also commonly perceived by structural engineers that the limit of 25mm per 10 blows is set for the purpose of ensuring that the pile driving energy is sufficiently high. However, adequate pile hammer energy can be ensured through field measurements by PDA tests. Available data tend to suggest that the energy transfer ratio for a given site is independent of the final set or $C_p + C_q$ values. Very often, when a contractor drives a pile to a small final set value to reduce the residual settlement of the pile, the $C_p + C_q$ may progressively increase during pile driving. While the allowable maximum final set is within the applicable range and higher than 25mm per 10 blows initially for a smaller pile penetration, it may quickly drop to below the limit of 25mm per 10 blows with continued pile driving. The limit of 25mm per 10 blows may therefore deter a contractor from attaining a small set value although this will enhance the pile performance.

By imposing the limit of 50mm per 10 blows, it has the effect of limiting the weight of hammer for pile driving. Some may argue that the limit of 50mm per 10 blows is set to guard against piles from being damaged by heavy hammers. However, this seems contradicting with the recommendation in CP4, CP2004 and BS8004 that says "it is always preferable to employ the heaviest hammer practicable and to limit the stroke, so as not to damage the pile".

The above rule of setting the applicable range of allowable maximum final set values is too restrictive. Li *et al* (2003) recommended that that the limit of 25mm per 10 blows be dropped. Alternatively, a recommendation can be made to relax it to 10mm per 10 blows which is in line with the common practice in Hong Kong for piles subjected to hard driving. Li *et al* (2003) also suggested that if the calculated allowable final set value is larger than 50mm per 10 blows, it can be capped at 50mm per 10 blows. Based on experience from field PDA measurement, the chance of exceeding the allowable driving stress for steel H-pile is small. In this case, the contractor will be discouraged rather than banned from using a heavy hammer for pile driving.

CONCLUSION

An alternative pile driving formula which relates to the pile driving energy delivered to the pile after impact has been proposed. Available data indicate that the formula is applicable **to** both for hydraulic and drop hammers. As the energy transfer ratio X is relatively constant with pile length, drop height and ground conditions within a given site, the proposed formula can be implemented by adopting a single suitable design value of X for a particular pile driving system for various drop heights. The proposed formula obviates the need for measuring or making assumptions of parameters including the C_c value, hammer efficiency, coefficient of restitution. Recommendations for relaxing the applicable range of allowable maximum final set values are also made in determining the final set table for pile driving.

REFERENCES

British Standards Institution (BSI) (1972). *Code of Practice for Foundations – CP2004*: September 1972.

British Standards Institution (BSI) (1986). *Code of Practice for Foundations - BS8004*: 1986.

Broms, B.B. and Lim, P.C. (1988). "A simple pile driving formula based on stress wave measurements", *Proc. 3rd International Conference on Application of Stress-wave Theory to Piles*, 591-600.

Chellis, R.D. (1944). *Pile-driving handbook*: *Theory-Design-Practice of Pile Foundations*, Sir Isaac Pitman & Sons, Ltd.

Cornfield, G.M. (1961). Discussion on "Pile driving analysis by the wave equation", *Journal of Soil Mechanics and Foundations Division,* ASCE, Vol.87, no. SM1, 63-75.

Geotechnical Engineering Office (GEO), (1996). *Pile Design and Construction*, GEO Publication No. 1/96.

Hiley, A. (1922). "The efficiency of the hammer blow", *Engineering*, 673-674, 711-714, 745.

Hiley, A. (1925). "Rational pile-driving formula and its application in piling practice explained", *Engineering*, 657, 721.

Hussein, M., Rausche, F. and Likins, G. (1992). "Dynamics of pile driving as a function of ram drop height", *Proc. 4th International Conf. on Application of Stress-wave Theory to Piles*, (Editor: F.B.J. Barends), Balkema, 421-424.

The Institution of Civil Engineers (1954). *Civil Engineering Code of Practice No. 4 – Foundations.*

The Hong Kong Construction Association (HKCA) (1995). *Report on Hydraulic Hammer Performance.*

Li, K.S. (2002). Discussion on "On the application of the Hiley's formula in driving long piles", accepted for publication by *Geotechnique*.

Li, K.S., Lam, J. and Ho, Nick C.L. (2003). Chapter 3 : Driven Piles – in *Design and Construction of Driven and Jacked Piles*, Centre for Research & Professional Development, 51-72.

Paikowsky, S.G. & Chernauskas, L.R. (1992). "Energy approach for capacity evaluation of driven piles", *Proc. Conf. on Application of Stress-wave Theory to Piles*, (Editor: F.B.J. Barends), Balkema, 595-601.

Triantafyllidis, T. (2001). "On the application of the Hiley's formula in driving long piles", *Geotechnique*, Vol.51, No.10, 891-895.

Whitaker, T. (1976). *The Design of Piled Foundations*, 2nd Edition, Oxford: Pergamon.

ACKNOWLEDGMENTS

The authors would like to thank the Hong Kong Housing Authority for their permission to publish the field data of Un Chau Street Site.

靜壓樁在香港的應用實例

李啓信　　林早妮
李啓信工程顧問有限公司
何智凌
新利地基工程有限公司
李啓光
香港大學土木工程系

A CASE STUDY OF JACK PILING IN HONG KONG

K.S. Li and J. Lam
Victor Li & Associates Ltd.
Nick C. L. Ho
Sunley Engineering & Construction Co. Ltd.
P. K. K. Lee
Department of Civil Engineering, The University of Hong Kong

撮要

靜壓樁在香港是一種較新的樁基種類。靜力壓樁法在近年才引入香港， 但只是應用在少數的工程上，通常是作爲插樁用途。而最終完成樁基大多數還是依靠打樁法。 故此，現時仍然未有一套完善制定完成壓樁的方案，可以使靜壓樁能能夠合認受的標準。

本文載述了香港第一個純以靜壓樁法完成樁基的實例。採用方法是首先將所有靜壓樁加載到樁柱設計承載力的 **2.3** 倍， 並將此荷載維持一段短時間。最後荷載達至設計承載力的 **2.2** 倍，而這 **2.2** 倍的荷載會維持平穩直至樁柱沉降率是少於每 **15** 分鐘五毫米。本文會討論施工工序和預加荷載對靜壓樁的蠕動沉降及樁基深度的影響， 亦描述靜壓樁的荷載測試及其他現場測試數據。根據這些數據，本文建議了一套在香港適用的靜壓樁施工工序及完成壓樁方法。

A CASE STUDY OF JACK PILING IN HONG KONG

K. S. Li[1], J. Lam[2], Nick C. L. Ho[3] and P. K. K. Lee[4]

Abstract: Jacked pile is a relatively new type of pile in Hong Kong. It is not until recently that the technique of pile jacking has been used in a limited number of projects in Hong Kong, generally for pitching of piles. Final setting of pile is often achieved by percussive driving. There are no well-established set of termination criteria based on which jacked pile can be installed to meet the pile acceptance criteria.

This paper describes a case study of steel H-piles that were completely installed by jacking at a site in Hong Kong. All the jacked piles were loaded initially to 2.3 times the design pile capacity for a short period of time during installation and finally to 2.2 times the pile capacity, at which the load would be maintained constant until the settlement was less than 5mm in 15 minutes. In this paper, the influence of installation procedures and preloading on the creep movement and the pile penetration are described. Data of pile loading tests and other field tests will also be presented. Based on the test results and field observations, recommendations on pile installation and establishing the termination criteria for jack piling in Hong Kong are made.

INTRODUCTION

In Hong Kong, jacked piles have only been used in a limited number of foundation projects, all involving steel H-piles. Jacked piles are currently not an approved pile type endorsed by the Buildings Department (BD). Piling contractors have yet to build up sufficient experience in establishing suitable termination criteria for installing jacked piles that can meet the stringent pile acceptance criteria specified by the BD. There is thus a practical need to develop a general procedure for formulating the termination criteria of jacked piles in Hong Kong.

This paper presents details of a recent foundation project in which steel H-piles were completely installed by pile jacking. The performance of jacked piles at the site, hereafter referred to as Site A, is discussed and the experience gained from this site for establishing practical termination criteria for jacked piles will be presented.

FOUNDATION WORKS AT SITE A

Figure 1 shows the soil profile at the site, which mainly comprises thin layers of fill and/or alluvium overlying completely decomposed granite (CDG). Firm strata formed by completely/highly decomposed granite (C/HDG) with SPT "N" values exceeding 200 were found at a depth of about 25.5 to 27.5m below ground. No corestone was detected in the CDG layer in

[1]Director, Victor Li & Associates Ltd.
[2] Engineer, Victor Li & Associates Ltd.
[3] Senior Contracts Manager, Sunley Engineering & Construction Co., Ltd.
[4] Head, Department of Civil Engineering, The University of Hong Kong

all of the boreholes, making this site particularly suitable for jacked piles. Figure 2 shows the variation of SPT "N" values with depth for the site. The SPT "N" values increase with depth and attain a value of higher than 200 when the C/HDG layer is encountered.

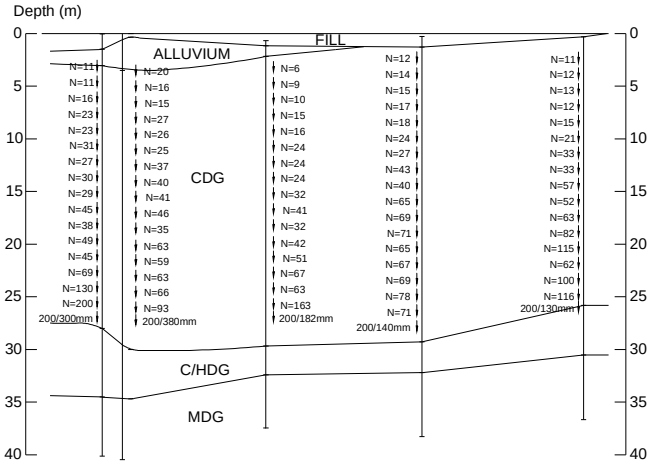

Figure 1 Soil profile at Site A

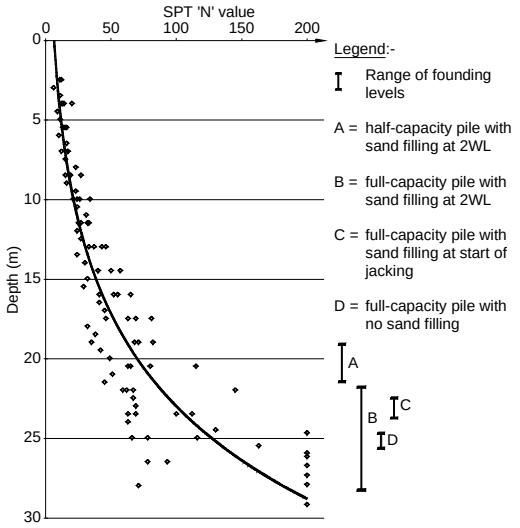

Figure 2 SPT 'N' versus depth

Grade 55C 305x305x180kg/m steel H-piles were used for the project. A pile jacking machine with a capacity of 9000 kN was used in installing the jacked piles. The construction procedures of jack piles have been described in detail by Yue & Ho (2002). Jacked piles can be placed at the centre or the end of the pile jacking machine during installation. Full capacity of the pile jacking machine can be mobilized if the jacked pile is placed at the centre location. If the jacked pile is placed at the end location, the capacity of the machine will be reduced by half.

A total of 65 jacked H-piles with a design capacity of 2950 kN (referred hereafter to as "full-capacity" piles) were installed by placing the piles at the centre location of the pile jacking machine. There were another 11 piles located near the site boundaries and they could only be installed by jacking at the end position of the machine. These piles have their design capacity reduced by about half to 1550 kN and will be referred to as "half-capacity" piles.

As discussed by Li *et al* (2003), pile buckling may occur if the voids on both sides of the web of an H-pile deepen to a certain critical depth during pile jacking. At Site A, three of the first five jacked piles had buckled during installation as no measure was taken at that time to control the development of void. To prevent pile buckling, the technique of filling up the voids with sand was employed for the remaining piles. Since then, no buckling of piles had occurred and sand filling had then become a standard working procedure for installing all the remaining piles.

The founding level of the full capacity jacked piles ranged from 22 to 28m below ground as shown in Figure 2. As the jacking machine had to remain at the pile location once the jacking process commenced, H-piles were spliced to give a total length of 30m before installation to eliminate the waiting time for splicing of piles, testing and/or cooling of welded joints during pile installation. At Site A, an average of 2 piles could be installed each day.

TERMINATION CRITERIA

Termination criteria refer to a set of working procedures such that jacked piles installed based on such procedures are expected to satisfy the pile acceptance criteria. For the foundation project at Site A, the pile acceptance criteria adopted were those used by the BD as described in the Practice Note PNAP66 published by the department. If we denote the design pile capacity as WL, the allowable maximum settlement at 2WL ranged from 35 to 43mm for the full capacity piles of the project and from 31 to 34mm for the half capacity piles according to the BD's pile acceptance criterion for total settlement, depending on the actual pile length. The allowable residual settlement was 6.7mm for both full-capacity and half-capacity piles.

Experiences show that if a jacked pile is subjected to a jacking force sufficiently higher than the design ultimate capacity and maintained for a sufficiently long period of time, it will pass the BD's pile acceptance criteria when subsequently tested at a load equal to the design ultimate capacity. Li *et al* (2003) used the term "pre-creeping" to describe this loading process. The idea of pre-creeping is similar to the well known concept of accelerating primary consolidation settlement and reducing residual settlement of a clay deposit by surcharging.

At the inception of the foundation project at Site A, there was little experience in the formulation of termination criteria or on how pre-creeping should be performed for jacked piles in Hong Kong. Chan *et al* (2002) reported a case study of an instrumented jacked pile for a public housing project. The pile was subjected to pre-creeping under a jacking force with magnitude varying between 2.0WL and 2.1WL for a period of about 2 hours. From a construction point of view, a pre-creeping duration of 2 hours is already too long to be practicable, yet the jacked pile failed to pass the BD's acceptance criterion for residual settlement. The unsuccessful case study reported by Chan *et al* (2002) does serve to indicate that if the duration of pre-creeping is to be reduced to a practical limit, say less than one hour, the jacking force has to be increased to above 2.1WL.

To develop the termination criteria for Site A, a series of tests were conducted for a working pile at the beginning of the project. The pile was subjected to 7 loading cycles with specified load levels. The settlement versus time curves for the 7 load cycles are shown in Figure 3(a). For each load cycle, the specified jacking force was maintained constant until the rate of settlement was less than 5mm per 15 minutes. The threshold settlement rate of 5mm per 15 minutes was adopted because it had been used earlier for another project described in Chan *et al* (2002).

Tests 1, 2, 4 and 6 involved virgin loading at increasing loads of 2.1WL, 2.2WL, 2.32WL and 2.43WL respectively. Tests 1 and 2 were each conducted in two stages to investigate the settlement behaviour of a jacked pile subjected to phased pre-creeping. In both tests, the pile settlement curve of the second stage of loading was largely a continuation of that of the first stage of loading. Therefore, dividing the pre-creeping process into several stages would not have any benefit in accelerating the creep settlement of the piles for Site A.

Tests 3, 5 and 7 were each carried out at a constant load of 2.1WL for a period of about 17 minutes. The aim was to investigate the settlement behaviour of the pile after it had been preloaded to different load levels. Figure 3(b) shows the settlement curves of Tests 3, 5 and 7 in a

larger scale. It can be observed that there was basically no pile settlement after 2 minutes. When the pile was unloaded, it rebounded essentially in an elastic manner giving very small residual settlements of 2mm, 1mm and 0.4mm respectively for Tests 3, 5 and 7. Based on these findings, it was judged that performing pre-creeping at 2.2WL until the settlement rate was less than 5mm per 15 minutes would be adequate for a pile to pass acceptance criteria at Site A. There was a concern that the pre-creeping process might take a long time to reach the threshold settlement rate of 5mm per 15 minutes. A decision was thus made to adopt the following two-stage pre-creeping:

a. An initial pre-creeping was carried out at 2.3WL until the settlement rate was less than about 3mm per minute.

b. The second stage of pre-creeping was carried out at 2.2WL until the settlement rate was less than 5mm per 15 minutes.

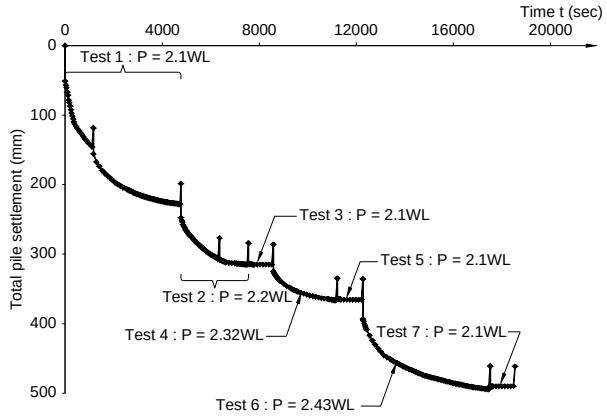

Figure 3 (a) Settlement curves for the 7 tests

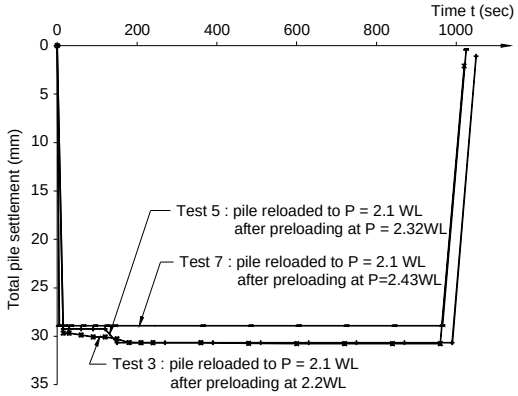

Figure 3 (b) Settlement curves for Tests 3, 5 and 7

The initial pre-creeping was intended to be carried out for a short period of time and hence a lower threshold settlement rate was adopted. It served two main purposes. First, if pre-creeping was carried out at a higher load level, it would be more confident that the jacked pile would pass the acceptance criteria. Second, the initial pre-creeping was intended to reduce the total time required for entire process of pre-creeping.

The procedures of the 2-stage pre-creeping process described above were adopted for installing all the jacked piles for Site A, providing practicable and workable termination criteria for the project. In addition, inelastic response of piles which gives significant pile settlement during reloading may occur for some sites, depending on the pile length and ground conditions (Li *et al*, 2003). Dividing the pre-creeping process into two stages would give a good indication of whether the pile would exhibit elastic behaviour during reloading. If inelastic behaviour is detected, the pile should be subjected to a few cycles of repeated loading to achieve elastic behaviour before commencement of pre-creeping. For Site A, the entire 2-stage pre-creeping process could normally be completed within 45 minutes.

REVIEW OF EXISTING DATA

P-d curve and δ-t curve

The force, *P*, required to jack a pile into the ground increases with pile penetration, *d*. Figure 4(a) shows a schematic load versus pile penetration curve of a jacked pile, called the P-d curve. Figure 4(b) shows a sample P-d curve of Site A and also the range of P-d curves of all jacked piles at the site. The P-d curves for Site A are very similar to each other, as evidenced by the relatively narrow range indicated in Figure 4(b). It could perhaps be attributed to the uniform soil profile of the site.

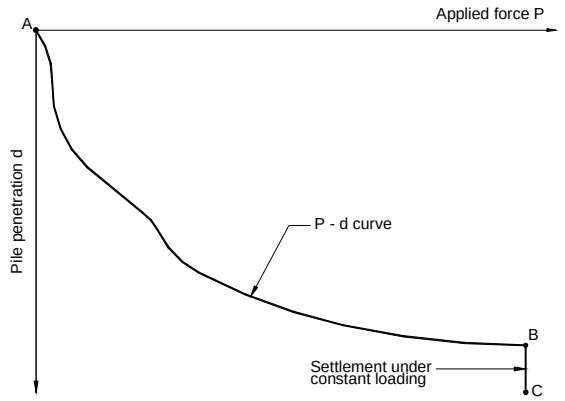

Figure 4 (a) P-d curve of a pile

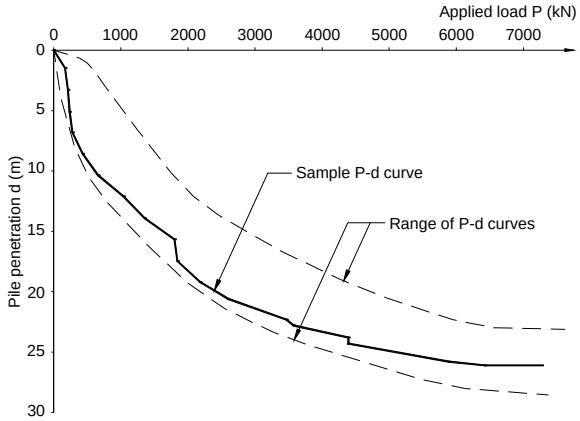

Figure 4 (b) Range of P-d curves for Site A

When the applied load reaches a specified level and maintained constant, say Point B in Figure 4(a), the pile will continue to settle slowly with time along the vertical path BC. The settlement versus time curve during constant loading is called a δ-t curve where δ means settlement under constant load and t denotes time. Li *et al* (2003) considered that the settlement δ is largely creep settlement. For this reason, a δ-t curve can be regarded as a creep settlement curve.

Figure 5(a) shows a typical δ-t curve for Site A when the jacked pile was subjected to a constant loading of 2.3WL. The creep settlement curve quickly approached an asymptotic value in about 30 minutes.

As discovered by Li *et al* (2003), the δ-t curve of a jacked pile can generally be fitted by a rectangular hyperbola of the form $\delta = t / (M\ t + C)$. By plotting δ/t versus t, the data will produce a straight line with gradient M and an intercept C as shown in Figure 5(b). The ultimate creep settlement of a jacked pile under constant loading, δ_{ult}, can be predicted using the relationship $\delta_{ult} = 1/ M$. Having obtained the parameters of the rectangular hyperbola, the rate of settlement at time t is given as:

$$\frac{\mathrm{d}\delta}{\mathrm{d}t} = \frac{C}{(M\,t + C)^2} \tag{1}$$

The residual creep settlement, δ_r at time t, i.e. the creep settlement which has yet to occur before reaching the ultimate creep settlement δ_{ult} after time t has elapsed, can be calculated using the following formula.

$$\delta_r = \frac{C}{M(M\,t + C)} \tag{2}$$

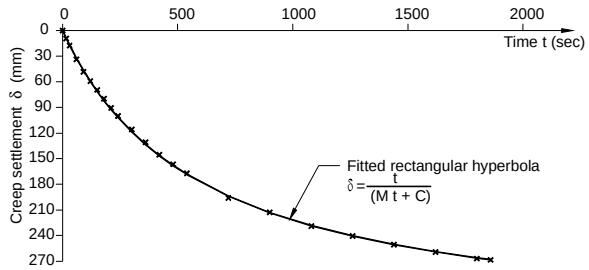

Figure 5 (a) δ-t curve

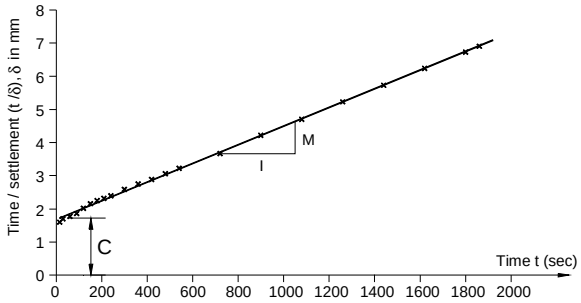

Figure 5 (b) δ/t vs t plot

Effect of preloading

All the jacked piles at Site A had been preloaded to a load level higher than the design ultimate capacity. The maximum preload of a pile with respect to any particular state of loading is defined as the highest load ever applied to the pile before reaching that stage of loading, i.e. P_B as defined in Figure 6(a). The preloading ratio is defined as the ratio of the maximum preload to the applied load at the current stage of loading, i.e. P_B / P_E in Figure 6(a).

Creep settlement of jacked piles can be reduced with preloading. If the pile is reloaded to a load level P_E lower than P_B and subjected to constant loading at Point E, the ultimate creep settlement δ_{ult} which will occur under a constant loading at Point E would be smaller than the residual creep settlement δ_r under a constant loading at Point C, i.e. $\delta_{ult} \leq \delta_r$. In addition, the ratio of residual settlement reduction, defined by δ_{ult} / δ_r, will decrease with an increase in preloading ratio. Based on this principle, pre-creeping at a higher load level could significantly reduce the total creep settlement that will occur when the pile is subsequently reloaded to a lower load level. However, the maximum load level at which pre-creeping can be carried out is controlled by the capacity of the jack piling machine and the likelihood of pile buckling at that load level.

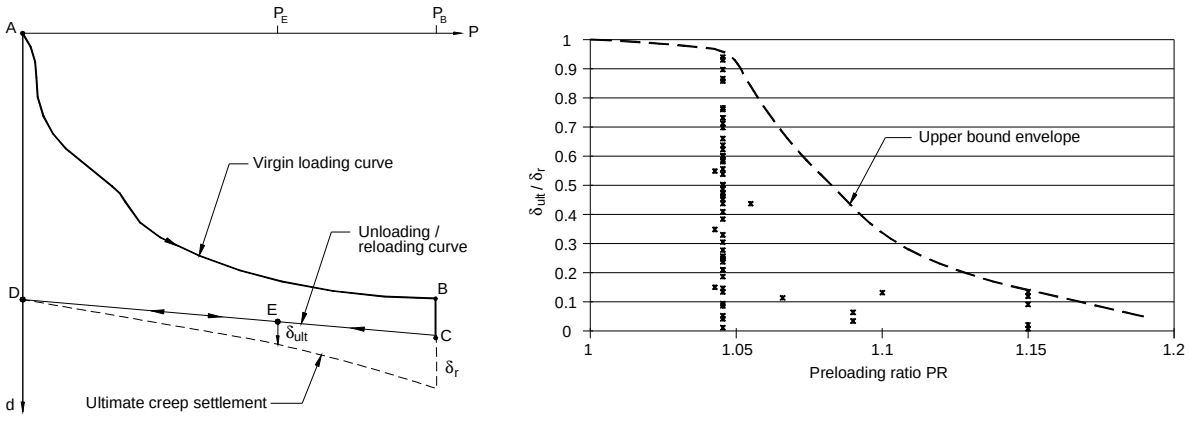

(a) P-d curve of a preloaded pile (b) Residual settlement reduction ratio

Figure 6 Preloading on creep settlement reduction

To study the creep settlement behaviour of a preloaded pile, the jacked piles at Site A were subjected to constant loading at different load levels (i.e. P_B in Figure 6(a)) of 2.1WL, 2.2WL or 2.3WL for a short period of time. The piles were then unloaded and reloaded to a lower load level (i.e. P_E in Figure 6(a)). The ultimate creep settlement δ_{ult} at P_E and the residual creep settlement δ_r at P_B were both predicted using the rectangular hyperbola method. Figure 6(b) shows the ratio of residual settlement reduction plotted against the preloading ratio PR = P_B / P_E, together with an upper bound envelope fitted to the data. It can be observed from Figure 6(b) that the ratio of residual settlement reduction decreases rapidly with an increase in preloading ratio. This suggests that preloading is very effective in reducing creep settlement of jacked piles for Site A.

Effect of sand filling

A jacked pile would exhibit different creep settlement behaviour if sand filling is carried out at different stages of pile installation. Figure 7 shows the settlement curves of 5 piles which were close to one another and all were subjected to the 2-stage pre-creeping process described earlier. Figure 7(a) shows the settlement curve of a full-capacity jacked pile (no.1), which was successfully installed without sand filling but remained unbuckled. Figure 7(b) shows the settlement curves for another two full-capacity jacked piles (nos. 2 & 3), which were installed with sand filling commenced at the start of jacking. Figure 7(c) shows the settlement curves of two typical full-capacity jacked piles (nos. 4 and 5), which were installed with sand filling carried out after the jacking force had reached 2WL.

Figure 7 indicates that sand filling has the effect of speeding up the process of pre-creeping. The settlement curves approached an asymptotic value in about 2 hours for the pile without sand filling (pile no.1 in Figure 7(a)), 40 minutes for piles with sand filling commenced at 2WL (pile nos. 4 and 5 in Figure 7(c)) and 15 minutes for piles with sand filling started at the beginning of pile jacking. The settlement curves in Figure 7 also indicate that sand filling has the effect of reducing the total creep settlement of the piles.

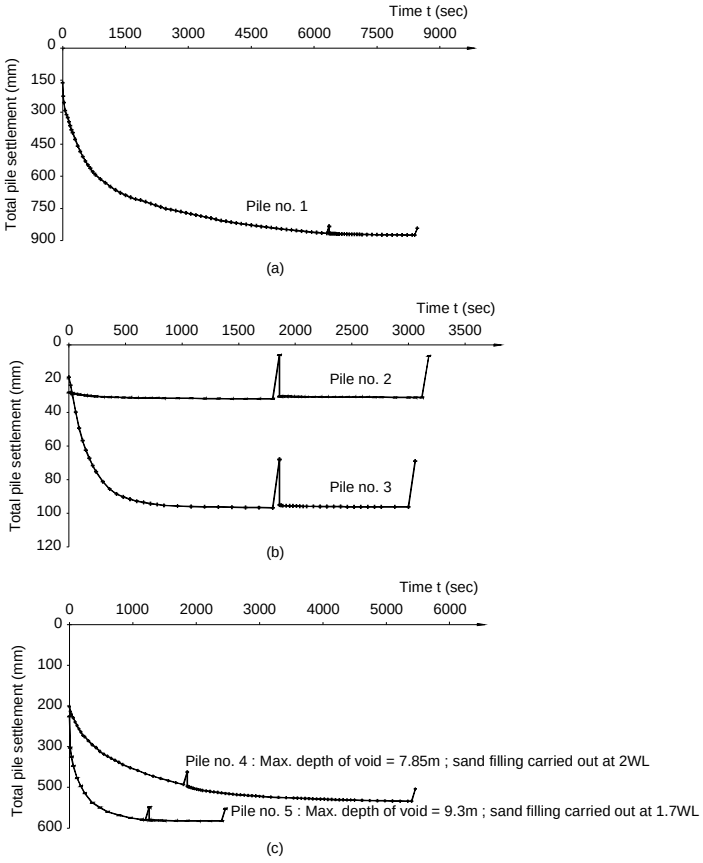

Figure 7 Effect of sand filling on pile settlement

The soil profile, the SPT "N" values with depth and the founding levels for the above 5 piles are shown in Figure 8. Sand filling increases the shaft friction of jacked piles to varying degree, depending on when sand filling is commenced during pile installation. Figure 8 indicates that the founding level was highest for pile nos. 2 and 3 with early sand filling. The SPT "N" values at the founding levels of pile nos. 2 and 3 were less than 70. The process of sand filling may have, to a certain extent, transformed the H-pile into a large displacement pile with significant shaft friction. The founding level of pile no. 1 was similar to that of pile nos. 4 and 5, indicating that delayed sand filling at 2WL will not significantly increase the shaft friction of jacked piles. However, the delayed sand filling is essential in preventing pile buckling.

As could be observed from Figure 2, the majority of the piles were founded at levels with SPT 'N' values of less than 150. This is in great contrast to driven piles which normally need to be driven to found on firm strata with SPT "N" values higher than 200 before they can pass the pile acceptance criteria.

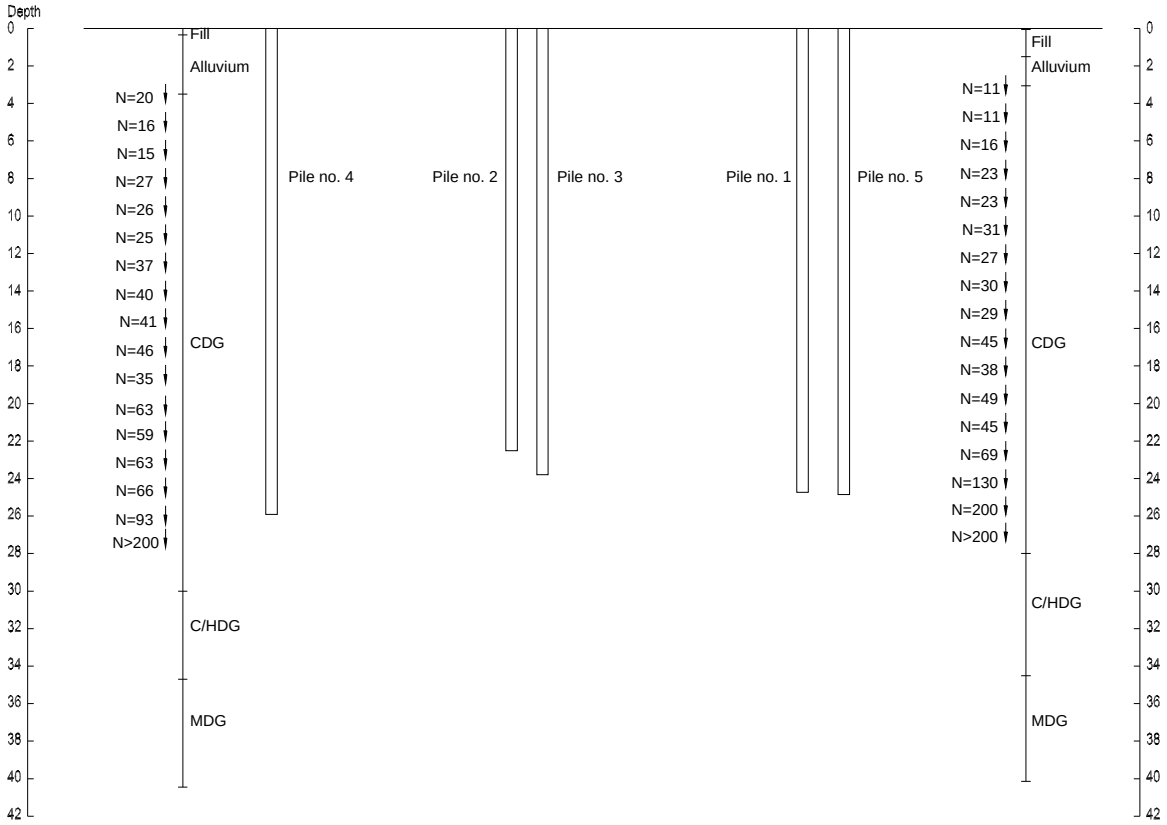

Figure 8 Founding levels of pile nos. 1 to 5

Pile loading tests

Four pile loading tests were conducted at Site A. Three of them were conducted on full capacity jacked piles and one on a half capacity jacked pile. The BD's procedures of pile loading test as described in PNAP66 were adopted. The piles were tested to a maximum applied load of 2WL for a period of 72 hours at the final stage of loading. Figure 9(a) shows the loading test results of the first successfully completed jacked pile at Site A, i.e. the same pile which gave the pile settlement curves in Figure 3.

Figure 9(b) shows the load test results of another full-capacity jacked pile of the site. During the loading test, the pile had been temporarily overloaded for a few hours up to a load of about 6600 kN, i.e. 2.24WL. During this period, the total pile settlement shot up to 30.228mm and later dropped back to about 29.2mm when the hydraulic jacks were readjusted to reproduce the target applied test load of 2WL. Even so, the total pile settlement had not exceeded the allowable value of 39.258mm. The residual settlement was still well within the allowable limit despite the overloading of pile during pile loading test.

Figures 9(c) and (d) show respectively the loading test results of the shortest full-capacity jacked pile and a relatively short half-capacity jacked pile at Site A. All the loading test results indicate that the jacked piles had passed the BD's acceptance criterion for both the total and residual

settlement with a good margin. They also confirmed that the termination criteria established for the jacked piles for Site A were practicable and viable.

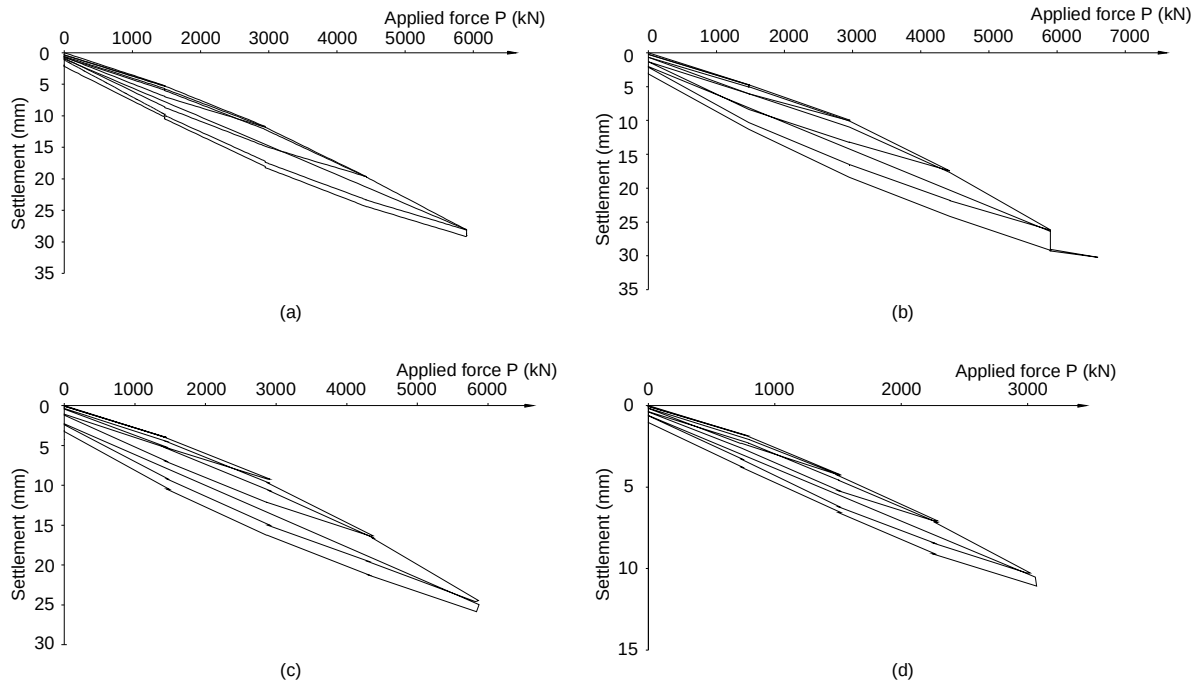

Figure 9 Pile loading test results

REVIEW OF TERMINATION CRITERIA

At the final stage of pile jacking at Site A, pre-creeping was carried out at a load of 2.2WL until the rate of creep settlement was less than 5mm per 15 minutes. It is useful to review whether this threshold settlement rate was indeed adequate for Site A.

When the pile is reloaded to 2WL during static loading test after completion of pre-creeping at 2.2WL, the pile would have experienced preloading at a preloading ratio of 2.2/2.0=1.1. According to 6(b), the ratio of reduction in creep settlement corresponding to this preloading ratio is about 30%. Therefore, to achieve an ultimate settlement not exceeding 6.7mm at 2WL, the residual settlement after pre-creeping at 2.2WL should be limited to less than 6.7/0.3 = 22.3mm.

Figure 10(a) shows the predicted ultimate creep settlement at 2.2WL, $(\delta_{ult})_{2.2WL}$, plotted against the predicted residual creep settlement at 2.3WL, $(\delta_r)_{2.3WL}$. Both quantities were predicted using the rectangular hyperbola method. It can be observed that the ultimate settlement at 2.2WL can be just a small fraction of the residual settlement at 2.3WL. This indicates that initial pre-creeping at 2.3WL was effective in reducing the creep settlement at 2.2WL for many of the piles at Site A, even if the preloading ratio of 1.1 was small for the initial pre-creeping.

The residual settlement at 2.2WL when the settlement rate reaches the threshold settlement rate of 5mm per 15 minutes, denoted by $\delta_{r\ (5mm/15mins)}$, can be calculated by means of

Eq.1 and Eq.2 and plotted against $(\delta_{ult})_{2.2WL}$ as shown in Figure 10(b). It can also be seen that the predicted values of $\delta_{r\ (5mm/15mins)}$ at 2.2WL are all smaller than the target value of 22.3mm, and mostly below 12mm. This indicates that the use of a threshold settlement rate of 5mm per 15 minutes as a criterion for terminating the pre-creeping process was adequate and, in fact, slightly conservative for Site A.

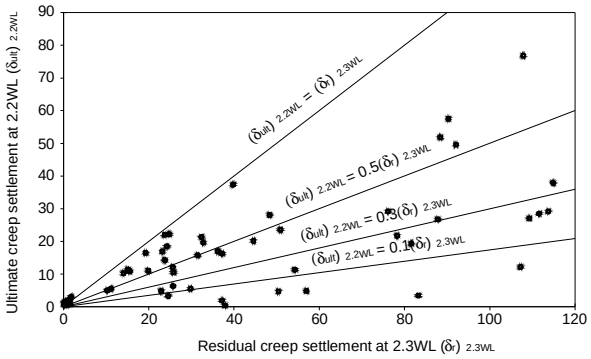

Figure 10 (a) Comparison of ultimate creep settlement at 2.2WL with residual settlement at 2.3WL

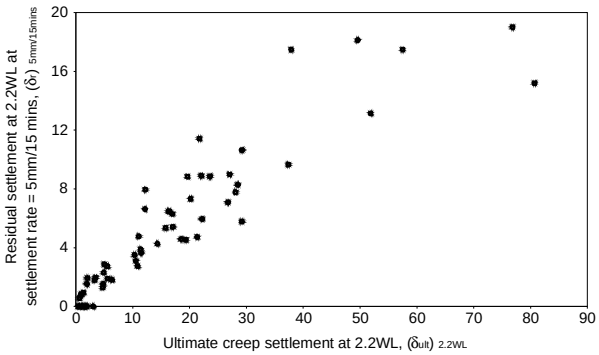

Figure 10 (b) Residual creep settlement at 2.2WL when the threshold settlement rate is reached

CONCLUSION

This paper presents a case study of jacked piles for Site A in Hong Kong. The influence of installation procedures and preloading on the creep settlement and pile penetration are discussed using the field test data obtained from the site. The paper discusses the thinking behind the formulation of termination criteria of jacked H-piles for Site A. The termination criteria established for the site are considered to be practicable, simple to implement and more importantly workable as confirmed by the good results of four loading tests. The experiences gained from Site A are useful for establishing the termination criteria for jacked piles for other sites in Hong Kong.

REFERENCES

Chan, S. T., Wong, F. C. C. and Tsoi, M. W. T. (2002). "Trial of jack piling in a Housing Authority foundation project". *Jack Piling in Hong Kong*, (Editor: K.S. Li), Centre for Research & Professional Development, 15-21.

Li, K.S., Ho, N.C.L., Lee, P.K.K., Tham, L.G. and Lam, J. (2003). Chapter 2 – Jacked Piles – in *Design and Construction of Driven and Jacked Piles*, (Editor: K.S. Li), Centre for Research & Professional Development, 23-50.

Yue, P. M. P. and Ho, N. C. L. (2002). "Construction aspect of pile jacking". *Jack Piling in Hong Kong*, (Editor: K.S. Li) ,Centre for Research & Professional Development, 23-30.

一九九九年八月石硤尾山泥傾瀉後的緊急斜坡鞏固工程

呂樂心　　潘偉強
香港特別行政區政府土木工程署土力土程處

URGENT SLOPE UPGRADING WORKS FOLLOWING THE AUGUST 1999 SHEK KIP MEI LANDSLIDE

L S Lui and W K Pun
Geotechnical Engineering Office, Civil Engineering Department
Government of the Hong Kong Special Administrative Region

撮要

一九九九年八月位於石硤尾村 **36** 及 **38** 座後的斜坡發生了一宗嚴重山泥傾瀉，導致三座位於斜坡前的住宅樓宇須永久封閉。而山泥傾瀉則引致斜坡表面嚴重鬆脫。事後，當局緊急鞏固斜坡，工程主要包括建造擋土牆及安裝泥釘。整項工程由探土、設計至施工在十六個月內完成。本文詳述了鞏固工程的設計及其主要考慮因素，並概述在工程上所遇到的困難及其解決方法。

URGENT SLOPE UPGRADING WORKS FOLLOWING THE AUGUST 1999 SHEK KIP MEI LANDSLIDE

L S Lui [1] **and W K Pun** [1]

Abstract

On 25 August 1999, a landslide occurred at a 50m-high cut slope behind the former housing Blocks 36 and 38 of Shek Kip Mei Estate, resulting in permanent evacuation of three housing blocks in front. The landslide primarily comprised distress with extensive slope surface cracking and localized detachments. The urgent upgrading works, mainly including retaining wall construction and soil nail installation, commenced shortly after the landslide. The works from the stage of investigation, design, to construction were completed within 16 months. This paper highlights aspects of the geotechnical design featuring the assessment of design options and the design considerations of the upgrading works. The project constraints and the solutions to overcome them are also presented. This project demonstrates the importance of proactive communication and partnership with other stakeholders.

INTRODUCTION

On 25 August 1999, a landslide occurred at a cut slope no. 11NW-B/C90 (slope C90) behind the former Blocks 36 and 38 of the Shek Kip Mei Estate (Figure 1). The landslide resulted in extensive surface cracks on the slope and localized detachment of soil mass from the slope. Three housing blocks, namely Blocks 35, 36 and 38 of Shek Kip Mei Estate, and the "Goddess of Mercy" temple located in front of the slope were evacuated after the landslide.

Slope C90 is about 100m long and has a maximum height of about 50m. The lower five batters of the slope stand at about 50° to the horizontal whereas the upper part is at 30°. The slope was covered with chunam before the landslide. Immediately after the landslide, the lower portion of the slope which exhibited significant signs of distress was covered with sprayed concrete as an emergency surface protection. In order to relieve the groundwater pressure, which might trigger further instability on the slope, twenty 12m-long prescriptive raking drains were installed along the toe of the slope. The slope movement was monitored closely by surveying at daily intervals in the first month after the landslide.

Following the landslide, the Government made a public pledge that the long-term upgrading works to slope C90 and three adjoining slopes no. 11NW-B/C68, C91 and C585 would be completed by the end of 2000. The Geotechnical Engineering Office (GEO) of the Civil Engineering Department (CED) undertook the design and construction of the urgent upgrading works under the Landslip Preventive Measures (LPM) Programme. The LPM Programme is a long-term strategy of the Government of the Hong Kong SAR to systematically upgrade substandard Government slopes to progressively reduce the landslide risk from slopes affecting the community.

[1] Geotechnical Engineering Office, Civil Engineering Department, Government of the Hong Kong Special Administrative Region.

THE LANDSLIDE

After the incident, the GEO initiated a comprehensive investigation on this landslide. The landslide investigation team discovered that the landslide had resulted in significant slope distress in the middle and lower parts of the slope, with cracks running along almost the entire slope length. The landslide debris was essentially intact and displaced downwards. It was estimated to have a volume of about 2,500m^3. The majority of the displaced material, despite local collapses of debris, had a limited mobility and remained on the slope.

Figure 1 – View of the Slopes (Dotted line shows extent of distressed zone)

After a series of investigation, a number of unfavourable factors leading to the landslide were identified. One of the factors was the existence of a persistent discontinuity with kaolin infill. This pre-existing discontinuity, which dips out at a shallow angle near the slope toe, was revealed by the landslide investigation team as the basal slip surface of the landslide. Another factor leading to the landslide was infiltration into the slope through pre-existing tension cracks, the defects on the chunam cover and an area with unauthorized cultivation above slope C90. The presence of old drainage lines on the slope would also have channelised subsurface water to the slope, leading to adverse groundwater condition. Details of the landslide investigation findings are documented in a report by the Fugro Maunsell Scott Wilson Joint Venture (2000). A good understanding of the mechanisms of failure and the unfavourable factors leading to the landslide was vital to the design of the slope upgrading works.

GROUND AND GROUNDWATER CONDITIONS

To gather information on the subsurface conditions of the slope and to obtain samples for laboratory tests, a comprehensive ground investigation (GI) was carried out shortly after the landslide. The GI works comprised 22 vertical and 5 horizontal drillholes, 14 trial pits, 10 trial trenches and 11 surface strippings. The vertical drillholes were sunk by rotary drilling with air foam flushing to various depths ranging from 12m to 60m. The horizontal drillholes were 20m to 50m long. Figure 2 shows the locations of these GI stations. Piezometers with Halcrow buckets were installed in the vertical drillholes for groundwater monitoring. Laboratory tests were conducted on soil samples retrieved from the GI fieldwork. These included classification tests for determining the broad characteristics of the material present in the slope, a series of consolidated undrained triaxial compression tests in mazier samples and direct shear box tests for measuring the shear strength of clay-infilled joints.

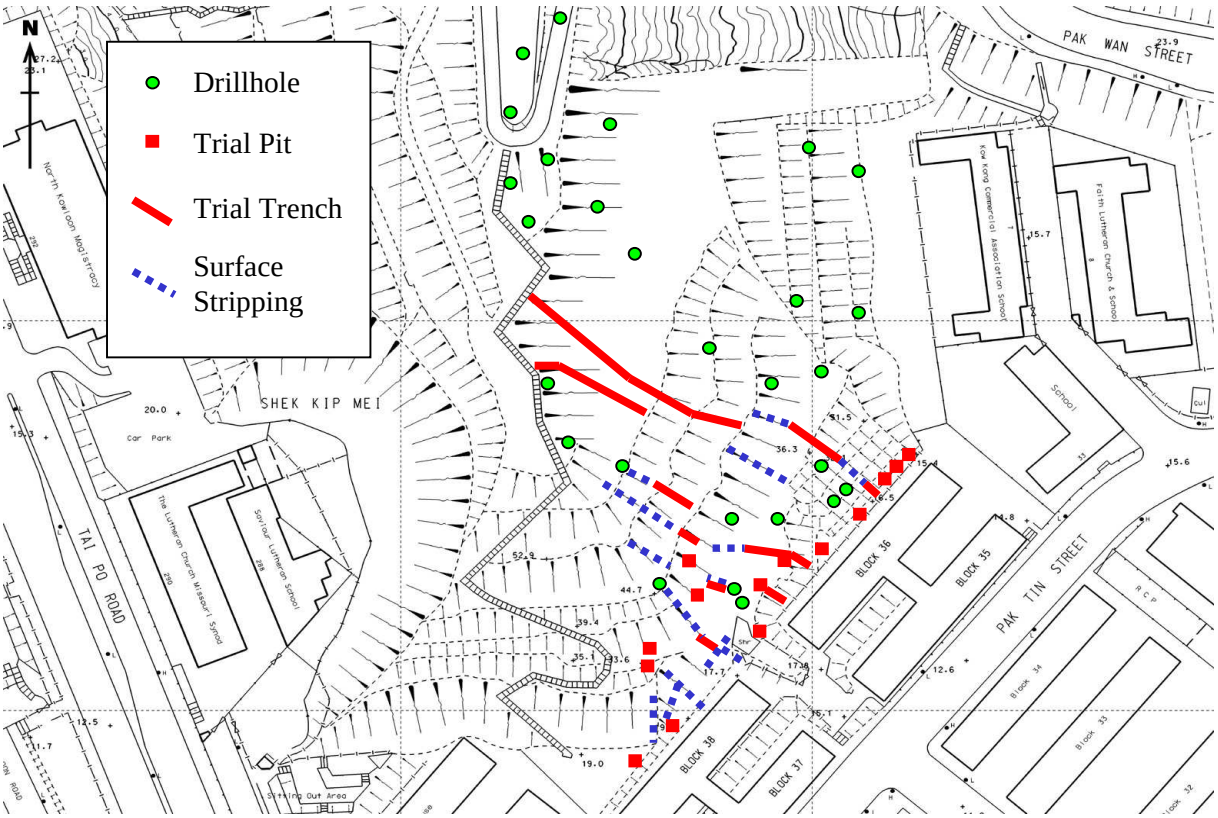

Figure 2 – Ground Investigation Plan

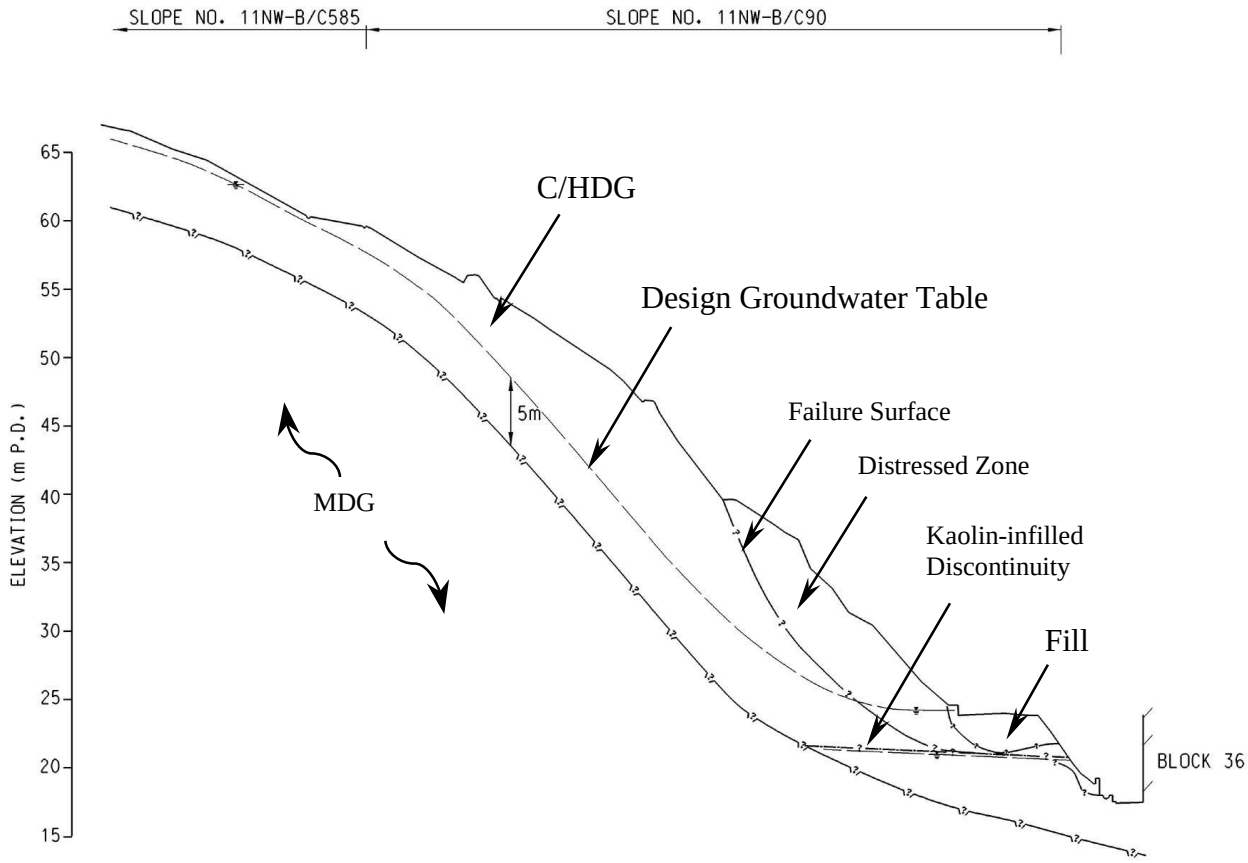

Figure 3 – Typical Geological Section of Slope C90

As illustrated by a typical geological section in Figure 3, the geology of the site comprises a soil mantle of completely to highly decomposed granite of thickness ranging from 4m to 16m, overlying moderately to slightly decomposed granite. Fill was present locally at the slope toe at the temple platform. The GI also revealed a persistent discontinuity infilled with slickensided kaolin and manganese oxide deposits with a maximum thickness of about 20mm and dipping at a shallow angle, at about 5° to 10°, out of the slope. This discontinuity had a lateral persistence of about 60m. Tension cracks, mostly infilled with soil, were found in the displaced soil mass with a maximum width and depth of about 300mm and 3m respectively.

Groundwater monitoring at the site was carried out right after piezometers were installed at a frequency of fortnightly in the dry season and weekly in the wet season. Halcrow buckets were provided in the piezometers for capturing the peak transient groundwater response. Return periods of the rainstorms related to the groundwater response were analyzed based on the statistical correlations of Lam & Leung (1994). By comparing the groundwater rise and the rainfall intensity of the corresponding rainstorms and that of a rainstorm with a 10-year return period, the design groundwater level was assessed to be at 5m above the inferred bedrock level as shown in Figure 3. In addition, the design allowed for a 3m-high perched water level above the persistent kaolin-infilled discontinuity to account for the possible perching of groundwater above this relatively less permeable feature.

The soil parameters used in the design were derived from the laboratory test results. The shear strength parameters of c'= 6 kPa and ϕ'= 39° were adopted for the CDG material. As the persistent kaolin-infilled discontinuity, which served as the basal slip surface of the 1999 landslide, could act as a weak plane for further instability, its shear strength was a critical parameter in the upgrading works design. The shear strength parameters of the discontinuity determined by the direct shear tests were c'= 0 kPa and ϕ' = 20°.

ASSESSMENT OF THE DESIGN OPTIONS

Three feasible design options were identified for the upgrading works for slope C90 (Figure 4). To

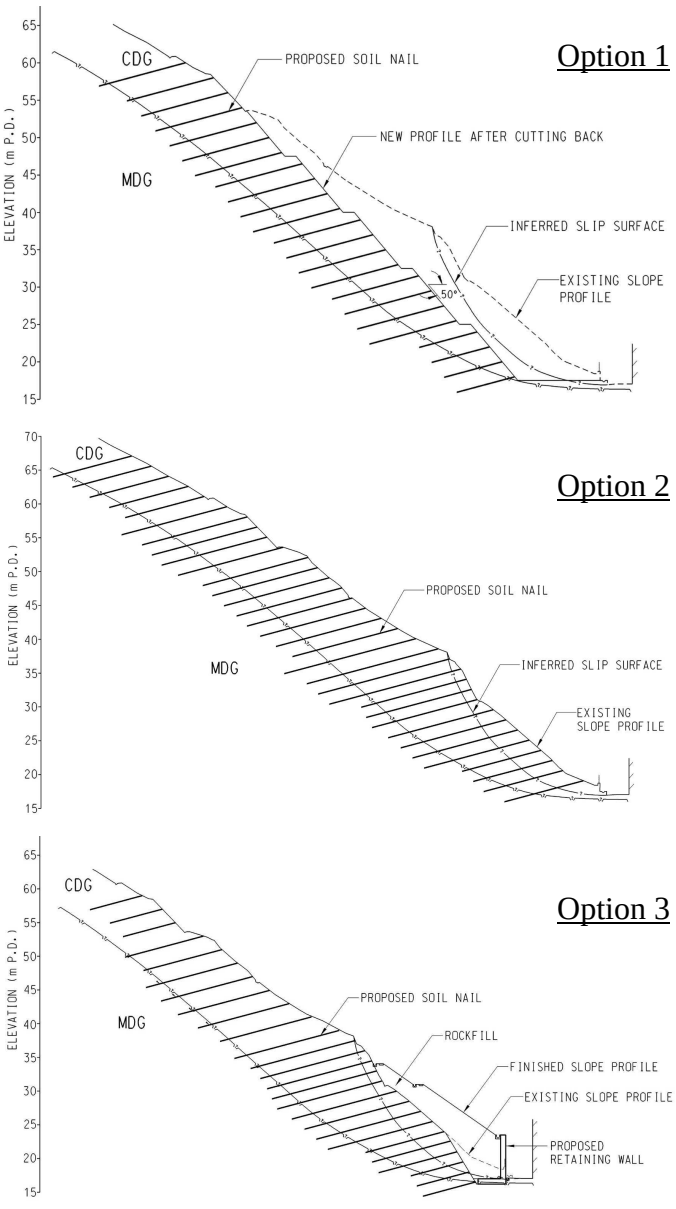

Figure 4 – Design Options of Upgrading Works for Slope C90

identify the most suitable scheme, an assessment of the options were carried out, considering the factors of reliability, ease of construction, site constraints, cost and environmental impact. The first option was to cut back the slope to trim away the slip mass. Soil nails would be installed on the new slope profile after cutting back. In the second option, soil nails would be installed without removing the distressed material. In the third option, a toe support would be provided by constructing a L-shaped reinforced concrete (R.C.) retaining wall at the slope toe and backfilling it with rockfill. A temporary cut slope at the slope toe was required to allow space to accommodate the wall. Soil nails would be provided on the temporary cut and on the upper part of the slope not supported by the rockfill. The pros and cons of the three options are summarized in Table 1:

Table 1 : Pros and Cons of the Design Options of Upgrading Works

Options	Pros	Cons
1	• The distressed material in the landslide would be removed. This scheme would be reliable.	• Extensive earthworks would be required to be carried out in the wet season of 2000. • Long construction period was anticipated. • Heavy machinery would be required to work at height on the slope with a steep profile.
2	• This option would have the shortest construction time. • No excavation works would be required and the works programme would therefore be less susceptible to delays caused by adverse weather.	• The distressed material involved in the landslide would be left in place, so this material might be subject to further movement well before the soil nail forces are mobilized. The robustness of this option would therefore be poor.
3	• Toe weight of the retaining wall and rockfill would be effective for stabilizing the slope with previous deep-seated move-ment. This would be a robust design. • The use of rockfill would be effective in providing drainage to the slope behind the wall. • Little earthworks would be required, so the construction would not be seriously affected by bad weather.	• This option would be the most expensive. • A small temporary cut into the distressed material of the slope would be required.

After evaluating the pros and cons of the various options, the third option was chosen as it could fulfill the requirements on stability, integrity, construction safety and time constraints, although it would be slightly more costly.

DESIGN RATIONALE

The detailed design of the upgrading works had to cater for all the unfavourable factors leading to the landslide. For instance, the persistent discontinuity with kaolin infill was taken

into consideration in the geological model for the design. Possible sliding failure along the discontinuity was analysed taking into account the low shear strength of the clay-infilled material and the potential for development of perched water on the discontinuity. The pre-existing tension cracks were sealed up during the works. Despite this, the potential adverse effects of the hydrostatic pressure brought by water induced in tension cracks were taken into account in the slope stability analysis. Also, all damaged surface protection covers were replaced by new ones. As slope C90 was located on old drainage lines, rockfill was used rather than soil fill as backfilling material to the toe retaining wall because it would be more effective in providing drainage for the slope. Also, the backfilling operation of rockfill would be less susceptible to delays due to adverse weather, so the tight construction programme would not be affected.

Though the project was quite urgent, stability and integrity of the slope during construction could not be compromised. The stability of the 8m-high 60° temporary cutting into the displaced soil mass for the retaining wall construction was of concern. The construction sequence was well-planned in the design stage in such a way that the majority of the soil nails at the lower and middle parts of slope C90 would have been installed before the onset of the first wet season after the landslide. A stage-by-stage excavation of the temporary cut slope followed by installation of soil nails was specified in detail in the contract drawings.

A total number of 826 soil nails was put on slope C90 and a 75m-long retaining wall with a maximum height of 8m was constructed. The cost of the works for slope C90 was $13.6M.

PROJECT CONSTRAINTS

Time Limit

A lot of constraints were faced by the project team. The tight time limit was a big concern. By the time the upgrading works were injected into the LPM Programme, only 16 months were available for the site investigation, detailed design and construction. All these activities were arranged to fit into a very tight programme. Right after the availability of preliminary GI results in mid-November 1999, the project team immediately commenced the design process of the upgrading works including formulation of ground model, design option assessment, project plan circulation, resolving land matters, detailed design and preparation of contract drawings. All these were fast-tracked and were completed in about two months, which usually would take about six months to complete. Within this short period of time, close liaison was maintained with the landslide investigation team to collect the most updated landslide investigation findings as input to the detailed design of the upgrading works. At around the same time, the Housing Department (HD) had decided to demolish the vacant housing blocks in front of slope C90. Close liaison was made with the HD staff to agree on the boundaries of the two sites for the demolition works and slope works respectively. The positions of the site boundaries would affect the alignment of the new retaining wall and more importantly the extent of the temporary cut slope.

The site works started in mid-February 2000, immediately after the Chinese New Year holidays. Usually it would take about 15 months to complete works of such a large scale, but only approximately 10 months were used and most of the works had to be carried out in the wet season of 2000. Close communication between the site staff and the design team was maintained throughout the course of the works. Site queries were resolved promptly to avoid

any delay. One major design amendment to facilitate construction was changing the retaining wall type from L-shaped R. C. wall to a mass concrete wall. This saved about one month.

Limited Working Space

The limited working space on site also posed a constraint to the project. The housing blocks, before they were demolished, were very close to the slope toe with a minimum clear distance of about 2m as shown in Figure 5. To have a robust design, it would have been better to build a higher retaining wall to retain more rockfill to cover all the distressed material. A higher retaining wall, however, would require a bigger wall base which in turn would require a higher temporary cut at the slope toe. A balance had to be achieved on this in view of the limited space. Access to the site was also limited. Only one vehicular access adjacent to a primary school was available, which had to be shared by the two contractors carrying out the demolition and slope upgrading works respectively and by the school students.

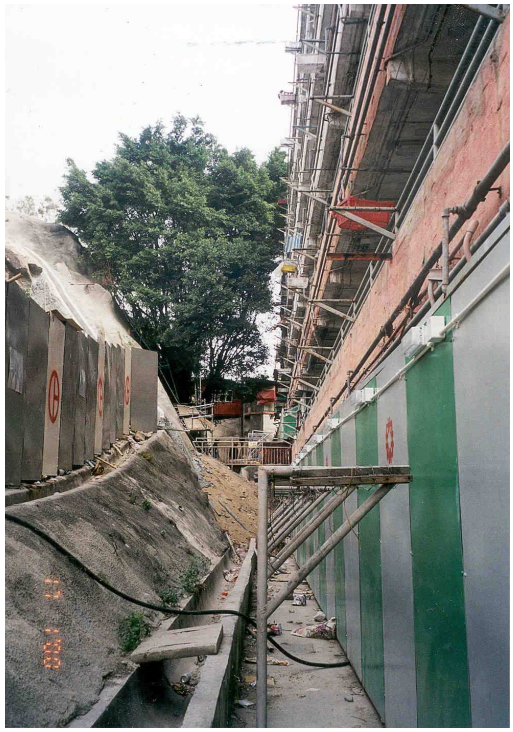

Figure 5 – Limited Working Space on Site

Clearance of the Temple

The goddess of mercy temple was located on a platform abutting the slope toe. It had to be cleared to make way for the retaining wall construction. One might imagine how much resistance there would be from the worshippers since this popular religious venue had been there for more than 35 years. Proactive discussion was held with the party in charge of the temple, District Councilors and worshippers to explain the reasons of clearance so as to minimize their discontent. With the assistance from a number of Government departments, the temple was finally cleared as scheduled for the construction of the slope upgrading works.

UPGRADING WORKS ON ADJACENT SLOPES

As mentioned before, after the landslide on slope C90, the three slopes adjacent to slope C90 were also

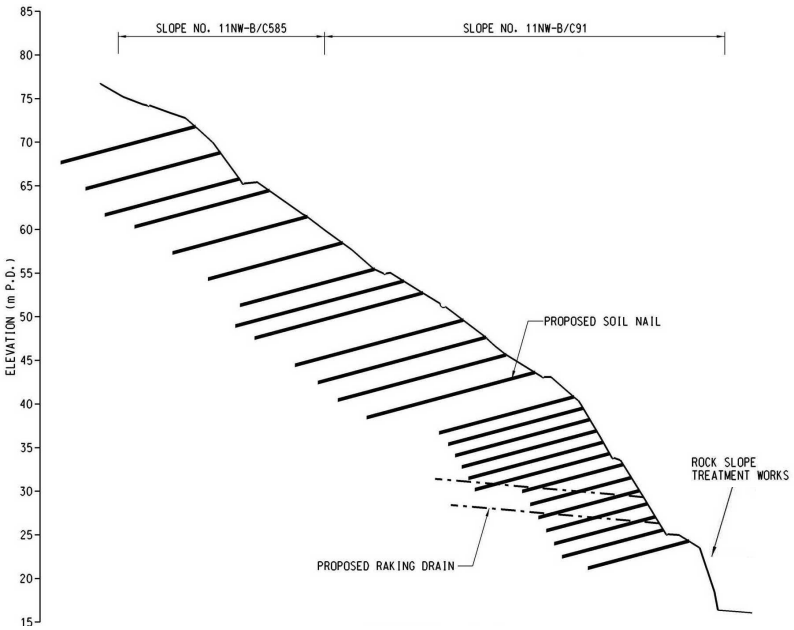

Figure 6 – Typical Section Showing Upgrading Works on Slopes C91 and C585

injected into the LPM Programme. The upgrading works on the slopes included installation of more than 1,900 number of soil nails of length ranging from 8m to 20m, installation of prescriptive raking drains, slope surface protection measures and rock slope treatment works as shown in the typical cross section in Figure 6. Construction works commenced in mid-September 1999 and was completed by April 2000. The total construction cost for these three slopes was $21.5M.

CONCLUSION

The project was completed safely, on time and within budget. As a concluding remark, proactive communication with all the concerned parties in the project was essential in such an urgent project. The teamwork of the various parties involved and the strong commitment of project team to meet the project objectives and target was the key to the success of the project.

REFERENCES

Fugro Maunsell Scott Wilson Joint Venture (2000). Report on the Shek Kip Mei Landslide on 25 August 1999. Fugro Maunsell Scott Wilson Joint Venture, 2 Volumes.

Lam & Leung (1994). Extreme Rainfall Statistics and Design Rainstorm Profiles at Selected Locations in Hong Kong. Technical Note No. 86, September 1994. Hong Kong Observatory.

ACKNOWLEDGEMENT

This paper is published with the permission of the Head of the Geotechnical Engineering Office and the Director of Civil Engineering, Government of the Hong Kong Special Administrative Region.

運用膨脹土泥漿於風化岩層中挖孔建造之磨擦樁樁身承載力計算及對端承樁之應用

庇高斯　李紹威　杜信

SHAFT CAPACITY OF FRICTION PILES CONSTRUCTED IN SAPROLITE UNDER BENTONITE AND IMPLICATIONS FOR END BEARING PILES

A R Pickles, S W Lee and R Tosen
Geotechnical Consulting Group (Asia) Ltd, Hong Kong

撮要

最近之九鐵東區鐵路延伸工程曾分別進行三次正規的磨擦樁承載力試驗。此等試樁皆於全風化花崗岩層中，利用膨脹土泥漿支撐之挖孔內建造，並由樁身與風化岩層所引發之磨擦反力承托樁頂附加之荷載。　每支試樁皆設有安裝於不同水平高度之應變儀及拉桿式伸縮儀等，用以測定樁身所受之壓力變化及樁底沉降情況。　本文論述此三個試驗之結果及提出樁身反力與標準貫入試驗抗力指數之相關處。

荷載試驗數據亦用於測度有限元差模型計算結果，並藉修正模型參數探討同樣利用泥漿挖孔建造之端承樁受力沉降之變化。　該等有限元差模型計算顯示絕大部份施加於長度較大之端承樁之垂直荷載皆由樁身(周邊面積)與其接觸之風化岩土引發之磨擦力互相抵銷，只有極少荷重真正直接由樁底地基岩土承接。　正如所料，該模型計算同時証明深長磨擦樁之荷載沉降抵抗力遠比深長端承樁一般假設並採用之抵抗力爲高。

SHAFT CAPACITY OF FRICTION PILES CONSTRUCTED IN SAPROLITE UNDER BENTONITE AND IMPLICATIONS FOR END BEARING PILES

A R Pickles[1], S W Lee[1] and R Tosen[1]

Abstract: Three full scale load tests have recently been carried out on friction piles constructed under bentonite slurry on the KCRC East Rail Extension project (Contract TCC300). The piles derived the majority of their load carrying capacity from shaft friction in completely decomposed granite. Each test pile incorporated multiple levels of strain gauges and rod extensometers to enable the load distribution down the pile and the pile shaft compression and toe settlement to be determined. The results of the three pile tests are presented and a correlation between the shaft resistance and SPT profile is given. The load test results have been used to calibrate finite difference models of the pile tests and the models have then been modified to investigate the load settlement behaviour for end bearing piles constructed under bentonite. The finite difference models demonstrate that the majority of the load applied to long end bearing piles is dissipated in shaft friction and little load is actually transferred to the toe of the pile. The models also demonstrate that, as expected, the load settlement behaviour of long friction piles is stiffer than generally assumed for long end bearing piles.

INTRODUCTION

KCRC East Rail Contract TCC300 includes the construction of approximately 220 friction piles with lengths typically in the range 50 to 70 m. The friction piles are large diameter bored cast-in-situ concrete piles and are designed to derive their ultimate load capacity from a combination of both shaft friction and end bearing in soil. The pile construction method envisaged in the construction contract comprised excavation of the pile bore within a temporary steel casing, which was to be advanced at least 2 m ahead of the excavation. Because of the presence of core stones within the weathered rock, the advancement of a steel casing ahead of the excavation is virtually impossible and this often requires a reduction in casing size as each obstruction is met. Penetration through the core stones and the requirement to "telescope" down the temporary casing sizes results in a very time consuming construction process.

The main contractor, Necso-China State-Hip Hing Joint Venture (NCHJV), proposed to construct the piles using bentonite slurry to support the pile bore. A short temporary casing was installed at the top of the pile to provide added stability near the ground surface. Bauer (Hong Kong) Ltd. was the piling sub-contractor for construction of all the friction piles. The proposed construction method was accepted by the Engineer and also accepted by Buildings Department subject to a number of conditions being met. In particular, the conditions relating to pile capacity and pile load testing included:

(a) At working load, the maximum allowable shaft friction should not exceed 0.45 x SPT 'N' value in the completely decomposed rock, with a limit of 55 kPa.

(b) At working load the maximum allowable end bearing pressure for piles founded in soil should not exceed 5 x SPT 'N' value with a limit of 1000 kPa.

[1] Geotechnical Consulting Group (Asia) Ltd, Hong Kong.

(c) A series of pile load tests would be required to demonstrate that the design ultimate capacity could be achieved (i.e. two times the maximum allowable working load).

(d) Settlement criteria for the loading tests would be in accordance with the requirements of PNAP 66, the de facto standard for pile test acceptance in Hong Kong for piles that require approval by Buildings Department.

Three friction pile load tests, referred to as P117, P131 and P125, were subsequently carried out. The test pile results demonstrated that the design capacity criteria would have a factor of safety significantly greater than 2 and the settlement of the test piles easily met the requirements of PNAP 66.

GROUND CONDITIONS

The thicknesses of the various soil layers at the three pile test locations are shown on Figure 1. At the location of test pile P117 the site is underlain by a succession of reclamation fill, marine clay, alluvium and completely to highly decomposed granite. The fill and marine clay at the location of pile test P117 would contribute to the negative skin friction loading on the working piles and as such this test pile was sleeved through the fill and marine clay. The alluvium layer at P117 is approximately 10 m thick and is predominantly a firm to stiff silty clay with a thin layer of sandy gravel at the base.

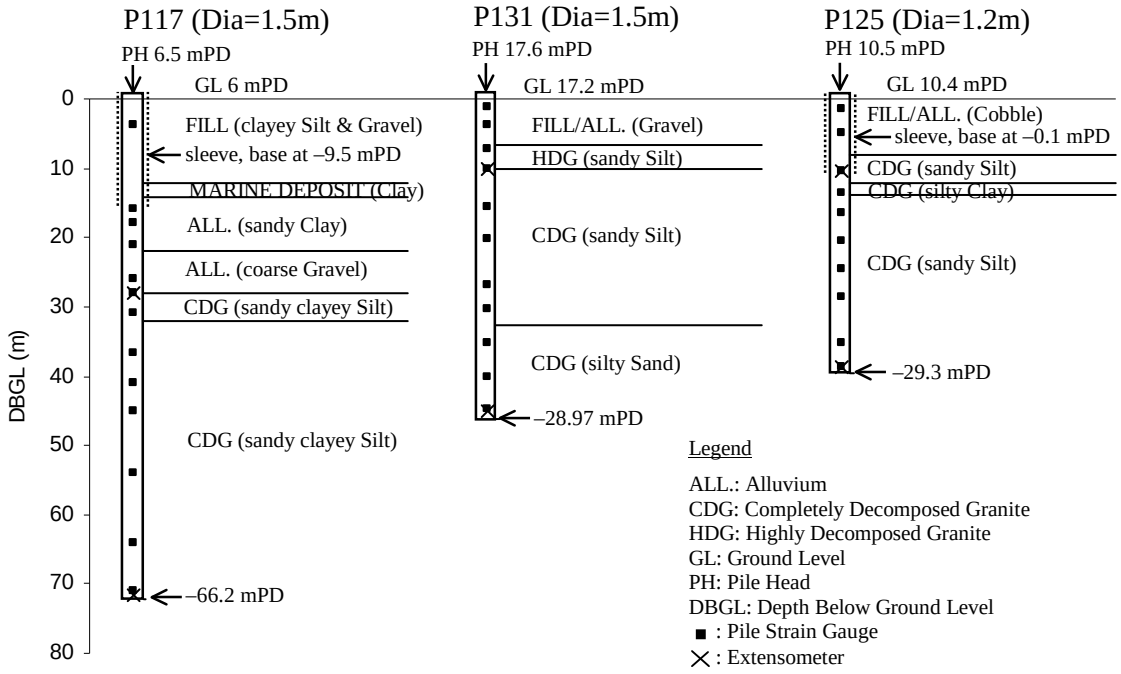

Figure 1: Ground conditions and details of the three test piles.

At the location of test piles P125 and P131 the site is underlain by relatively thin layers of granular fill and alluvium/colluvium. At both these locations the fill and alluvium/colluvium are directly underlain by completely decomposed granite. A sleeve was installed to the base of the colluvium at P125 and as such the pile test load at this location was carried entirely within the CDG. The upper six meters of P131 was constructed in a loose to medium dense sandy gravel.

A borehole was drilled at the location of each of the test piles with standard penetration tests (SPT) carried out at 2 m intervals. In addition, 5 further boreholes with SPT profiles were obtained in close proximity to each test pile. The SPT profiles at each test pile location

are shown in Figure 2 plotted as both the incremental and average cumulative SPT. The incremental SPT is equivalent to the actual SPT recorded at a particular level. The average cumulative SPT is a running average for the SPT from the top of the friction zone of the pile to the particular level at which the data is being analysed. It is noted that the SPT profile recorded at P125 above a level of –15 mPD is between 30% and 50% higher than that recorded at the 5 adjacent boreholes. The reason for this discrepancy is not known.

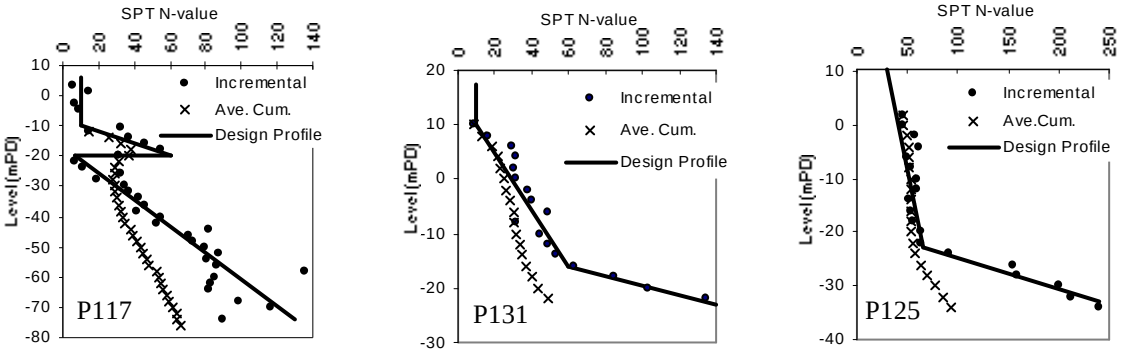

Figure 2: SPT N profiles at the locations of the three pile tests.

DETAILS OF TEST PILES CONSTRUCTION AND PILE LOAD TESTS

Details of the three test piles are shown in Figure 1. As noted above, two of the piles, P117 and P125, included a temporary outer and permanent inner steel liner to form a sleeve through the upper soil layers. The construction sequence for these two piles was as follows:

- Install the outer temporary steel casing and excavate to the base of the casing
- Fill the bottom 1 m depth of the casing with a weak bentonite cement grout
- Push the permanent steel casing approximately 1.5 m below the base of the temporary casing
- Excavate to the base of the pile under a bentonite slurry, maintaining the bentonite level at least 2 m above the ground water table
- Install steel reinforcement cage and pile instrumentation and then concrete the pile.

The construction sequence for pile P131 was as follows:

- Install an outer temporary steel casing to a depth of approximately 8 m below ground level
- Excavate to the base of the pile under a bentonite slurry
- Install steel reinforcement cage and pile instrumentation
- Place concrete in the pile, removing the temporary casing during concreting.

The construction timing for each of the three piles is summarised in Table 1. The excavation timing refers to excavation below the level of the permanent casing.

Table 1: Dates of construction and testing periods of the three test piles.

Pile	Commence Excavation Complete Excavation	Commence Concrete Complete Concrete	Commence Test Complete Test
P117	25/9/01 12h00 27/9/01 12h00	29/9/01 12h10 29/9/01 15h35	20/11/01 17h51 25/11/01 03h50
P131	13/12/01 14h30 14/12/01 10h00	14/12/01 16h30 14/12/01 19h00	11/3/02 16h26 16/3/02 08h50
P125	2/4/02 08h00 2/4/02 12h30	3/4/02 15h30 3/4/02 18h00	14/5/02 18h22 24/5/02 21h06

The pile test loading procedure for all three piles generally followed the requirements set out in PNAP 66. The pile was initially loaded in 4 increments to half the design pile capacity (nominally the working load, based on 0.45N on the shaft and 5N on the base). After unloading, the pile was reloaded in 4 increments to the design pile capacity (nominally two times the working load). The load was maintained at the design capacity for 72 hours. A third loading cycle was included at P125 with the pile load taken up to 1.25 times the design pile capacity (nominally 2.5 times the design working load).

RESULTS OF PILE LOAD TESTS

The pile head settlement and re-bound (residual settlement) at the working load and two times the working load are summarised in Table 2. The pile head settlement of P125 at 2.5 times the working load was 32 mm and the residual settlement on unloading was 23 mm.

Table 2: Summary of the test pile results.

Pile	Test Load (1xWL) kN	Head Settle. mm	Residual Settle. mm	Test Load (2xWL) kN	Head Settle. mm	Residual Settle. mm
P117	7500	4.7	0.6	15000	12.8	2.5
P131	5770	2.7	0.6	11540	6.1	2.5
P125	3800	2.5	0.3	7600	11.2	4.8

Each pile incorporated two rod extensometers, one fixed at the base of the pile to measure the pile toe movement and the other fixed at the level of the base of the temporary casing (or 10 m below the top of the pile in the case of P131). The pile compression can be determined from the rod extensometer data and, based on the known load applied to the pile, it is possible to back analyse the stiffness of the concrete. The average concrete stiffness determined for the three piles was 3.1×10^7 kN/m^2. The composite pile modulus for each of the piles is given in Table 3. The composite modulus makes allowance for the variation in reinforcement quantity in the pile and also the permanent steel liner.

Table 3: Variation of composite modulus of the test piles.

P117		P131		P125	
Pile Level From/to mPD	Modulus kN/m^2	Pile Level From/to mPD	Modulus kN/m^2	Pile Level From/to mPD	Modulus kN/m^2
6.0 to –7.3	4.2×10^7	17.6 to 8.7	3.9×10^7	10.5 to –0.1	4.2×10^7
-7.3 to –11.0	3.6×10^7	8.7 to –2.1	3.4×10^7	-0.1 to –29.3	3.1×10^7
-11.0 to –66.3	3.1×10^7	-2.1 to –29.0	3.3×10^7		

The load at various levels in the pile can be determined from the strain gauge output and the estimated composite modulus of the pile at any level. Figure 3 shows the variation in the load down each pile measured by each of the strain gauges for the loading stage to the design pile capacity (i.e. 2xWL). The data obtained from a small number of the strain gauges indicated load values which were not consistent with the pile test, for example load higher than the applied test load. For clarity the anomalous strain gauge data is not shown in Figure 3. A best-fit line representing the load distribution down each of the test piles is also shown in Figure 3. The predicted load shown in Figure 3 is based on finite difference modelling discussed later in this paper.

Review of Results of Pile Load Tests

It is common practice in Hong Kong to relate the shaft friction capacity of a pile (F_s) to the SPT 'N' value by a SPT load factor (C) (i.e. $F_s = C \times N$). For example, the purpose of the pile tests was to demonstrate that the ultimate SPT load factor was greater than 0.9 for the full depth of the pile. However, with the exception of pile P125 at 2.5 times the working load, it is clear from the test results that at the design pile capacity the ultimate skin friction had not been mobilised over the full depth of the piles (i.e. the ultimate shaft capacity is greater than 0.9N). The pile test data has therefore been analysed to determine the mobilised SPT load factor at various depths down the pile. This has been achieved by dividing the total load shed above a particular level in the pile by the average SPT N value for the pile above this level. For example, for P117 the load shed between the base of the temporary casing (-10 mPD) and a level of –30 mPD is 6400 kN (15,000 - 8,600 kN on Figure 3) and the average cumulative SPT value to this level is 29, see Figure 2. The mobilised SPT load factor to this level is therefore 2.3 (i.e. $6400/(1.5 \times \pi \times 20 \times 29)$).

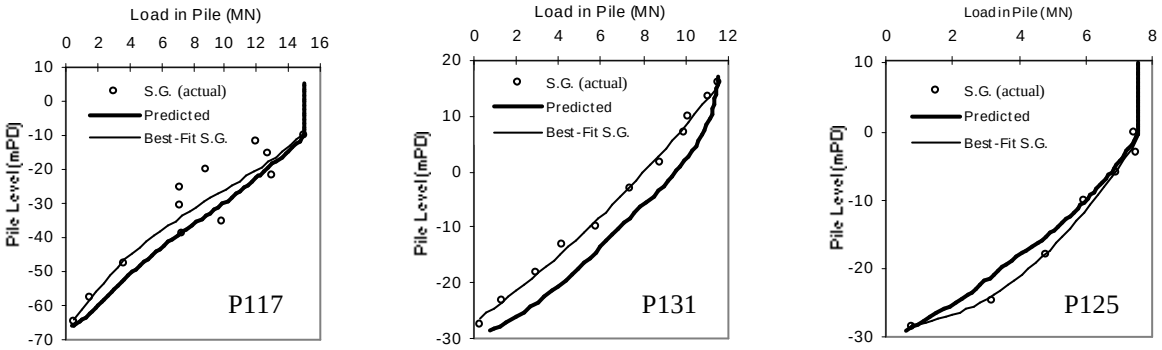

Figure 3: Measured and predicted load in pile for the three pile tests at 2xWL.

The variation of the mobilised SPT load factor with depth for each of the three pile tests at the design pile capacity (2xWL) is shown Figure 4. As a result of pile shaft compression the relative movement between the pile and the surrounding ground is greater at the top of the pile than at the toe. It can be seen from the results in Figure 4 that the mobilised SPT load factor varies down the length of the pile. It is likely that the ultimate skin friction has been mobilised over the upper portion of the test piles but that the ultimate shaft friction has not been mobilised towards the base of piles P117 and P131. As a result of the unexplained discrepancy in the SPT data at P125 it is considered likely that the mobilised SPT load factor at this pile has been underestimated, particularly above –15 mPD.

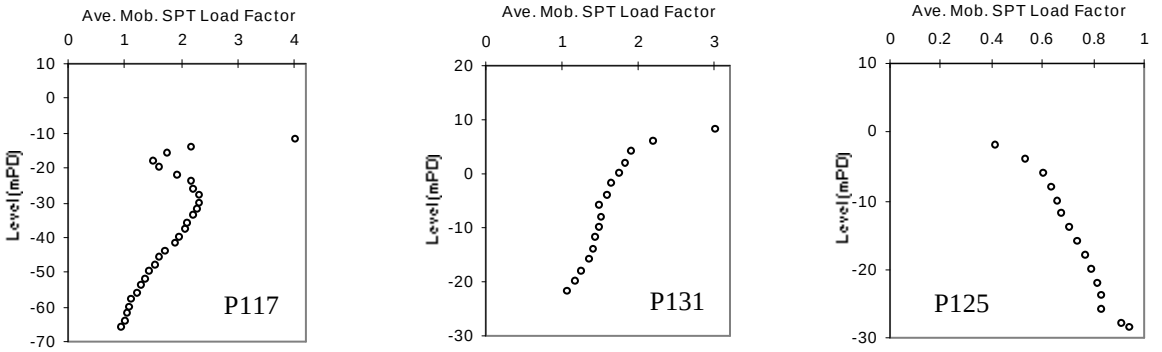

Figure 4: Average mobilised SPT load factor with depth for the three pile tests at 2xWL.

Figure 4 suggests that the relationship between SPT and shaft capacity is not a constant. This is not surprising as the SPT profile is taken in the undisturbed ground before pile bore

excavation and the excavation process will both loosen the soil around the pile and allow some stress relief in the ground around the pile. It may be more appropriate to determine the shaft capacity using an effective stress approach as follow:

$$F_s = K_s \times \sigma_v' \times \tan \delta$$

where F_s is the shaft friction at any depth down the pile, σ_v' the vertical effective stress, K_s the ratio between the horizontal and vertical effective stress around the pile after completion of construction and δ the interface friction angle between the pile and the soil. It is common practice to replace (K_s x tan δ) by a single factor β, such that

$$F_s = \beta \times \sigma_v'$$

At Test pile P125 a further load cycle was applied with the test load being taken up to 1.25 times the design pile capacity. The pile head settlement was 32 mm and the pile toe settlement was 26 mm. The pile settlement was therefore equivalent to approximately 2.5% of the pile diameter. Ultimate skin friction is generally considered to be mobilised at a displacement of between 1 and 1.5% of the pile diameter. The pile settlement at 1.25 times the design capacity was sufficient to mobilise the ultimate shaft friction over the full length of the pile. The test result was re-analysed using the 'β' method and the β value for the ultimate shaft friction was found to be in the range 0.2 to 0.3 with an average value of 0.28. Geo Publication 1/96 presents a relationship between β and the assumed soil friction strength. A β value of in the range 0.2 to 0.3 is equivalent to a soil friction angle of 35° to 36°, which is approximately the critical state friction angle of completely decomposed granite. The test result therefore shows good agreement with β values presented in Geo Publication 1/96.

BACK ANALYSIS OF PILE TESTS USING A FINITE DIFFERENCE MODEL

The three pile load tests have been back analysed using a finite difference model. The aim of this work was to investigate whether a relatively simple finite difference model could give a good approximation to both the load settlement characteristics and load distribution down the three test piles, using a consistent approach to the selection of ground stiffness and strength. The numerical modelling used the FLAC finite difference software. Axisymmetric analyses were carried out with an interface layer between the pile concrete and the surrounding soil. Figure 5 shows a part of a typical finite difference grid for the analyses. The test piles were modelled as an elastic material using the composite modulus values set out in Table 3 and a Poisson's ratio of 0.2. The soil was modelled as a Mohr Coulomb material with a cohesion of zero and a friction angle ϕ' for the various layers as set out in Table 4.

Table 4: ϕ'-values adopted in the FLAC analyses.

Soil Type	Typical Range of ϕ'	Adopted ϕ'
Fill	28 – 37	30
Marine Clay	26 – 28	27
Alluvial Sand	33 – 36	35
CDG	32 – 40	36

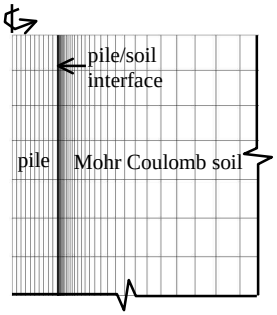

Figure 5: Close-up of FLAC mesh.

The interface friction strength was set to be the same as the adjacent soil. The in situ horizontal stress prior to pile loading was assumed to be (1–sin ϕ') times the vertical effective stress. The combination of interface friction and in situ horizontal stress results in a β value of 0.29 in the CDG, which is close to the average value determined from the final load stage of test P125.

It was considered appropriate to relate the soil stiffness to the SPT N profile. The results of pile load tests and also plate bearing tests generally show that the drained Young's modulus of soil (E' in MPa) falls in the range 1 to 3 times N value, Geo Publication 1/96. Analyses were carried out assuming both $E'=N$ and $E'=3N$ with a Poisson's ratio of 0.25. It was found that the use of $E'=N$ over-estimated the pile head settlement by approximately 50%, whereas $E'=3N$ gave a good correlation with the pile load test results. The finite difference models of the three load tests therefore adopted a stiffness profile using $E'=3N$. The SPT N profiles adopted for the ground stiffness are shown in Figure 2.

The results obtained from the finite difference modelling are shown in Figures 3 and 6. Figure 3 compares the calculated load distribution down the pile against the measured load distribution in the pile. Figure 6 shows the pile head settlement against applied load. It can be seen from both Figures 3 and 6 that the relatively simple finite difference model is able to give a good correlation with the observed behaviour of all three test piles.

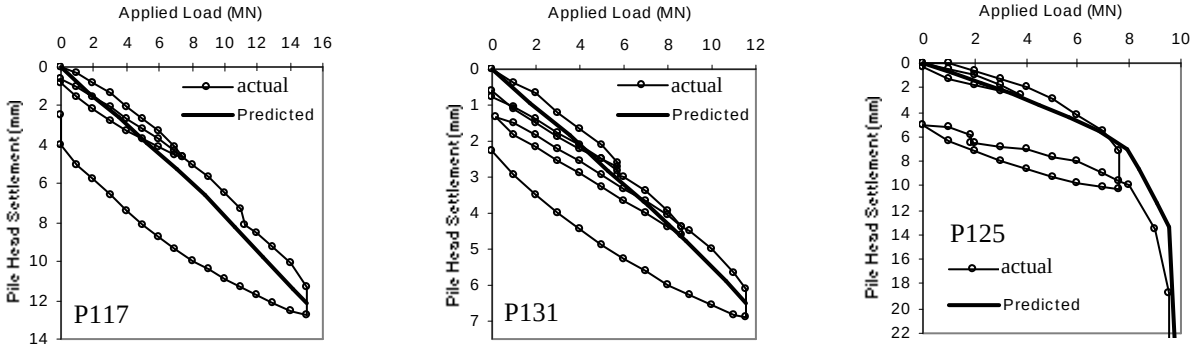

Figure 6: Measured and predicted load settlement curves for the three pile tests.

BEHAVIOUR OF LONG BORED PILES

It is common practice for piles in Hong Kong to be designed as end bearing on rock at depths in excess of 40 m and occasionally deeper than 100m. The design load on these piles typically results in an applied pile shaft stress in the range 5 to 10 MPa. Bell outs are constructed to limit the stress applied to the rock at the pile toe. Many designers assume that the full pile load will be transferred to the pile toe level and that pile head settlement will comprise elastic shortening of the pile and a small displacement of the pile toe.

It is a common misconception amongst many engineers that the load settlement response of end bearing piles on rock will be significantly stiffer than the response of friction piles founded in soil. In order to illustrate the difference in the response, the finite difference models of the three test piles were re-analysed with the inclusion of rock at the toe of the piles. Based on the results of end bearing pile load tests presented in Littlechild et al. (2000), the Young's modulus of the rock was assumed to be 2 GPa.

The results of the analyses are presented in Figure 7 for all three test piles. The figures compare the load settlement response of the friction test piles founded in soil (shown as "Friction" line) against the same piles acting as end bearing on rock (shown as "Fric+EB" line). Also shown on Figure 7 is the typical load settlement response often assumed by designers based on the assumption of all the pile load being transferred to the toe of the pile

(shown as “Pile Comp.+EB” line). The typical range of design loads applied to end bearing piles (i.e. shaft stress between 5 and 10 MPa) is also indicated in the figures.

The ground conditions at the locations of the three test piles are typical of many areas of Hong Kong with deep weathering profiles. It is clear from both the test pile results and the results of the finite difference modelling that, for piles longer than 40 m (P117 and P131), little load is actually transferred to the toe of the pile. Comparison of the “Fric+EB” and “Friction” lines in Figure 7 for applied load up to 2xWL indicates that the presence of rock at the toe of the pile does not have a significant influence on the load settlement characteristics of the pile. The comparison for pile P125 demonstrates that for a 40 m long 1.2 m diameter pile with a working load of 11300 kN (i.e. a shaft stress of 10 MPa) approximately 8000 kN is supported by shaft friction and only 3300 kN is transferred to the toe of the pile. It can also be seen that the settlement response often assumed by designers significantly over-estimates the settlement of end bearing piles founded on rock, refer to the “Pile Comp.+EB” lines.

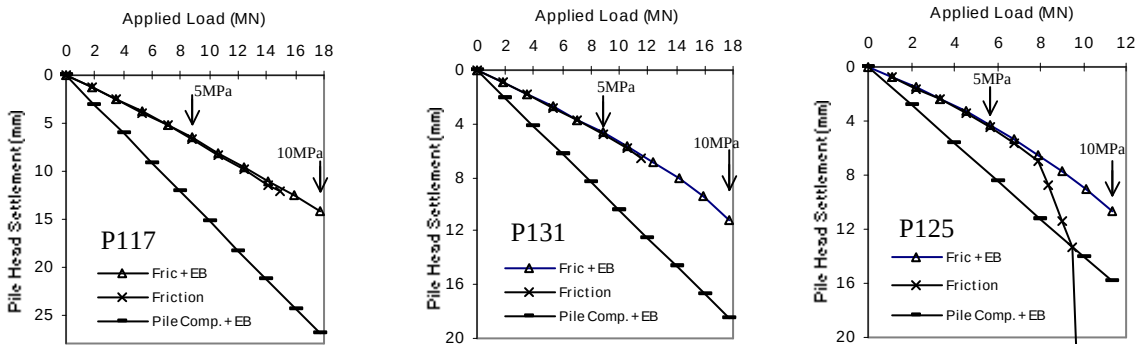

Figure 7: Load settlement curves of friction, friction plus end bearing and elastic shortening plus end bearing piles.

DISCUSSION AND CONCLUSIONS

The test pile results demonstrate that the adoption of a constant SPT load factor to design large diameter friction piles may not be appropriate. For piles constructed under bentonite slurry in soils with relatively low SPT ‘N’ values the ultimate SPT load factor is significantly greater than 0.9. However the SPT load factor is variable and reduces as SPT ‘N’ value increases. It is recommended that the pile design should always be checked using an effective stress approach. Large diameter end bearing piles with lengths in excess of 40 m and occasionally deeper than 100 m are common in Hong Kong whereas friction piles are infrequently used. This may be because a small number of load tests carried out on large diameter bored friction piles founded in saprolite have indicated very low friction capacity, see GEO Publication 1/96. However, it is known that speed of construction can have a significant influence on the capacity of friction piles founded in saprolite and this may be the cause of the previous poor test results. Traditional methods of pile construction can be relatively slow where obstructions are encountered and maintaining the casing ahead of the excavation can be extremely difficult. However, alternative methods of boring the pile based on the use of a drilling fluid (bentonite slurry, polymer etc.) instead of temporary casing can be significantly faster. This should result in both a higher pile capacity and a greater certainty of achieving the required load capacity.

Based on the test results presented in this paper it appears likely that the construction of bored piles to depths greater than 60 m is not cost-effective. At the typical working loads adopted in Hong Kong, negligible load will be transferred to the pile toe. This is because the

pile compression required to transfer significant load to the toe of a deep pile is sufficient to mobilise significant shaft friction in the pile shaft.

In conclusion, ignoring the contribution of pile shaft friction capacity in long piles is unnecessarily conservative. Further research into this subject is likely to result in major cost and program savings to the construction industry in Hong Kong. Perhaps more importantly the construction of unnecessarily deep end bearing piles is not in line with the commitment of the engineering profession to minimise the use of resources.

REFERENCES

Geotechnical Engineering Office (GEO) (1996). Pile Design and Construction – GEO Publication No. 1/96.

PNAP 66. Pile Foundations. Buildings Department, Practice Note for Authorised Persons and Registered Structural Engineers, Hong Kong, Latest Revision Jan 2002.

Littlechild B.D., Hill S.J., Statham I., Plumbridge G.D. and Lee S.C. (2000). "Stiffness of Hong Kong rocks for foundation design." Foundations, Proc., HKIE Geotechnical Division Annual Seminar, Hong Kong, 179-189.

告士打道頂管工程對鄰近建築的影響

溫立斯　　王建兵
百泰工程顧問有限公司
駱志聰　　馮炳權
香港特別行政區政府水務署

THE IMPACTS OF PIPE JACKING ACROSS GLOUCESTER ROAD

Leslie Swann and Jianbing Wang
Babtie Asia Ltd
C. C. Lok and P. K. Fung
Water Services Department
Government of the Hong Kong Special Administrative Region

撮要

2000 年末，告士打道近軍器廠街立交橋處頂管基坑開始了施工。立交橋橋墩採用淺埋獨立基礎，頂管基坑離其中一橋墩基礎僅 **1** 米。爲了減少沉降，頂管基坑支護採用了管樁。監測數據表明該橋墩對地面沉降非常敏感，在管樁安裝中已下沉了幾毫米。工程設計人員對此進行了詳細的勘查，制訂及執行了減少沉降的方案，但是橋墩繼續沉降。進一步調查表明該橋墩的沉降可能是由其他外部因素如 **50** 米外的降水工程及軟弱地層引起的。爲了控制沉降，進行了一系列的地基加固措施。盡管頂管中遇到了許多困難，如舊海堤等，工程順利完成。

本文著重闡述工程的施工，問題及解決方案。

THE IMPACTS OF PIPE-JACKING ACROSS GLOUCESTER ROAD

Leslie Swann[1], Jianbing Wang[2], C.C.Lok[3] and P.K. Fung[3]

Abstract: In late 2000 the construction of a jacking pit commenced on Gloucester Road near the Arsenal Street Flyover. The pit was 1 m away from one of the piers that was supported on a spread footing. In spite of the precautionary measures, movements of the bridge structure foundation and settlements in the surrounding areas occurred. Investigation showed the movement could be due to external factors such as dewatering of sites more than 50 m away, combined with very poor ground conditions. For the pipe-jacking extensive ground treatment was performed and the pipe-jacking was successful in spite of having to overcome obstructions such as old sea walls.

INTRODUCTION

In very congested urban areas, it is often impractical to install underground utilities by open trenching methods due to busy traffic, or the existence of numerous types of utilities / substructures. For such cases pipe-jacking techniques are frequently adopted. This paper presents a case study of the pipe-jacking project carried out under Gloucester Road, a busy road located on Hong Kong Island.

The pipe-jacking works were carried out for Water Supplies Department (WSD) Contract 17/WSD/97, Mainlaying at Wan Chai and Causeway Bay Area . The pipe-jacking work comprised installation of a DN1400 mild steel sleeve pipe (19 m in length) by an open shield pipe-jacking method with subsequent DN1000 M.S. pipes placed inside the sleeve pipe.

At an early stage of the construction works, prior to any excavation and pipe-jacking works, settlements of the ground and adjacent structures were recorded. Subsequently, an extensive programme of precautionary ground treatment works was implemented. In spite of having to overcome obstructions such as existing old sea walls, the pipe-jacking was completed successfully with little further ground settlements recorded. This paper presents the major difficulties and problems encountered during the works and the solutions adopted with a full discussion provided on the causes of ground settlements observed. Recommendations are made for pipe-jacking works in similar ground conditions in Hong Kong.

SITE AND GROUND CONDITIONS

The pipe-jacking work was carried out under Gloucester Road, with the Arsenal Street Flyover directly above. In particular, the Arsenal Street Flyover was supported on shallow spread footings (2 m below the existing ground), and one of the pier footings was 1 m away from the jacking shaft. Unsurprisingly utilities, including gas mains, water mains, telephone and power cables, were also present immediately adjacent to the excavation. Approximately 50 m away, there were two other construction sites where deep basement excavation and pipe-jacking works were being carried out.

[1&2] Director & Senior Engineer, Babtie Asia; [3] Engineer & Senior Engineer, Water Services Department, Government of the Hong Kong Special Administrative Region.

The ground investigation indicated that Marine and Alluvium deposits were present underlying the reclamation Fill. Layers of cobbles and boulders were identified in the Fill stratum. The observed ground water level was approximately 2.6 m below existing ground level, typically standing at around +1.3 mPD, though exhibiting tidal fluctuations.

BRIEF DESCRIPTION OF THE CONSTRUCTION WORK

Construction of Jacking and Receiving Shafts

The jacking pit site was handed over to the Contractor in late 2000 . The jacking pit was located within the central divider of Gloucester Road and was 1 m away from Pier No.4 of the Arsenal Street Flyover. The jacking pit had dimensions of 8m x 5.5m x 6.3m deep. The receiving pit was 6 m deep and 4m x 4m on plan (Fig 1). To overcome obstructions during installation of the supporting wall, steel pipe piles were installed and propped by three and two layers of walings and struts at the jacking and receiving shafts respectively.

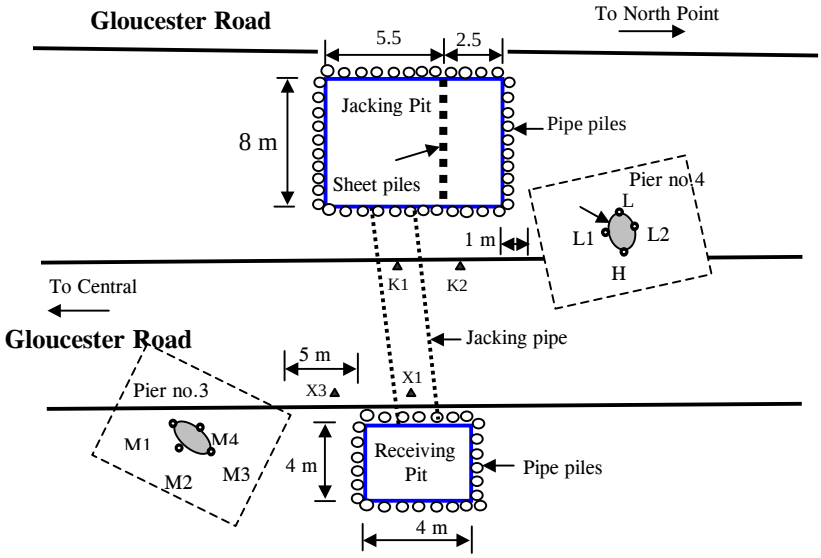

Fig.1 General Layout Plan

Installation of the pipe pile walls commenced in 2001. Steel pipe piles of 219 mm OD and 6.3 mm thick were installed to 12m depth at 250 mm centre to centre spacings using the ODEX drilling method. A layer of hard material (old sea wall, boulders) up to 3 m thick was encountered during pile installation at the jacking pit while at the receiving pit a boulder layer up to 4m thick had to be overcome.

To provide water cut-off for shaft excavation, a vertical grout curtain was installed into CDG or to the bedrock which required a two staged grouting operation - cement bentonite grouting followed by chemical grouting by Tube-A-Manchette method. The grout take was large (up to 600 litres of grout per metre was required in some locations) as the soil being grouted was generally loose with voids. Re-grouting was carried out after examination of the grouting pressures and grout takes. A large void was identified near Pier No.4 at a depth of 2 m below existing ground level, during trial trenching for a 132 kV power cable. The void was subsequently filled with cement bentonite grout.

Pumping tests carried out after the grouting works confirmed that the grout curtain had provided an effective water cut-off. The steady discharge rate of ground water from the

pumping well was measured at 0.19 m^3/hr and 0.40 m^3/hr at the jacking and receiving shafts respectively. Both shafts were excavated successfully with little groundwater inflow observed.

Precautionary Measures

Horizontal Grouting

To minimise groundwater ingress during jacking and to strengthen the subsoil, horizontal grouting work was carried out along the jacking alignment prior to pipe-jacking work. A total of seven. grout holes were drilled, covering the whole jacking length, and subsequently grouted.

To minimise water seepage during the drilling of the horizontal holes, as identified in a trial hole, four inclined grout holes were drilled from above the groundwater table to 1 m below the invert level of the jacking pipe and subsequently grouted. This technique proved to be successful in reducing water seepage during horizontal drilling and grouting.

Again large boulders were encountered during the drilling for most of the holes. Up to 500 litres of cement silicate chemical grout per meter was recorded at several locations, suggesting that the subsoil was in a very loose condition.

Voids Detection

Ground Probing Radar techniques were used to detect the presence of voids along the proposed pipe-jacking alignment across Gloucester Road prior to pipe-jacking work commencing. These showed minor near surface voids, but did not indicate a need for additional ground treatment.

Pipe-Jacking Across Gloucester Road

After a full technical review, it was decided to excavate the tunnel face manually with an open shield, given the existence of old sea walls and boulders along the jacking alignment.

Pipe-jacking work was carried out between 20th August 2002 and 28th September 2002. A DN1400 mild steel sleeve pipe was jacked from the jacking pit towards the receiving pit by two 250 ton hydraulic main jacks having a stroke of 1000 mm.

To minimise the disturbance to the ground due to the excavation, the maximum clearance between the shield and the excavated working face was limited to 300 mm. Ground and groundwater conditions ahead of excavation were assessed based on the probing holes drilled 3 m ahead of the working face and the drilling record of the horizontal grouting holes. The working face was sealed with steel channels and sand bags during non-working hours.

During pipe-jacking, inspection of the working face was carried out frequently. The working face was observed to be in a stable and dry condition throughout the whole period of pipe-jacking as a result of the good horizontal grouting, which was identified as layers and blocks of grout combined with grout veins. In addition to cobbles and boulders, concrete blocks (seawall), 2.5 m thick, were encountered between Chainage 8.5m and 11m.

The jacking force was relatively low, typically 10 bars to 20 bars, which was equivalent to 20 tones to 40 tonnes of jacking force or less than 5 kN/m^2 of pipe frictional resistance, which was much less than the empirical values obtained in Fill (Thomson, 1993). The lateral movements of the thrusting wall were monitored with dial gauges during the

jacking operation. The observed maximum movement was 2.2 mm with a typical value of 0.8 mm only. The alignment of the sleeve pipe was well controlled with a maximum deviation of only 16 mm recorded during the whole jacking process.

The pipe-jack broke through the receiving shaft on 26th September 2002. The total length of the jacked pipe was measured at 18.9 m.

MONITORING DATA

Given the existence of structures sensitive to settlements located immediately adjacent to the pipe-jacking work, an extensive monitoring scheme was developed, which included monitoring of ground / structure settlements and tilting, groundwater level and construction induced vibration. Void detection was also carried out prior to and after the pipe-jacking works.

Figure 1 shows the location of some critical settlement monitoring points within the site, including those installed on Piers No.4 and No.3, each having four points in four directions. Two tilting meters were also installed at Piers No.3 and No.4. In addition, standpipes / piezometers were installed around both shafts. All readings were taken daily except when there was no activity on site. As soon as the monitoring data indicated any undue movements, construction activities were ceased and a detailed review was undertaken to identify the cause of the movement and solutions proposed to further control the settlement.

Monitoring Data at Bridge Piers No.3 and No.4

Figures 2 and 3 summarise the results of the settlement monitoring against time and site activities for Piers No. 3 and No. 4 respectively. After completion of the pipe-jacking work, settlements of between 8 mm to 9 mm were recorded at four monitoring points M1 to M4 on Pier No. 3 while the measured settlements at Pier No.4 were between 9 mm to 11 mm. The observed tilting of the bridge piers was relatively small, being less than 1 in 1500.

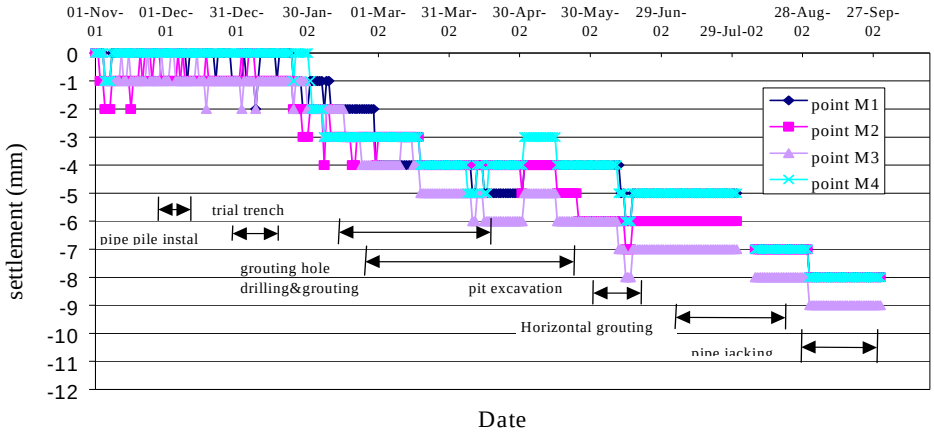

Fig. 2 Development of the observed settlements at Pier no.3 (up to 30/09/2002)

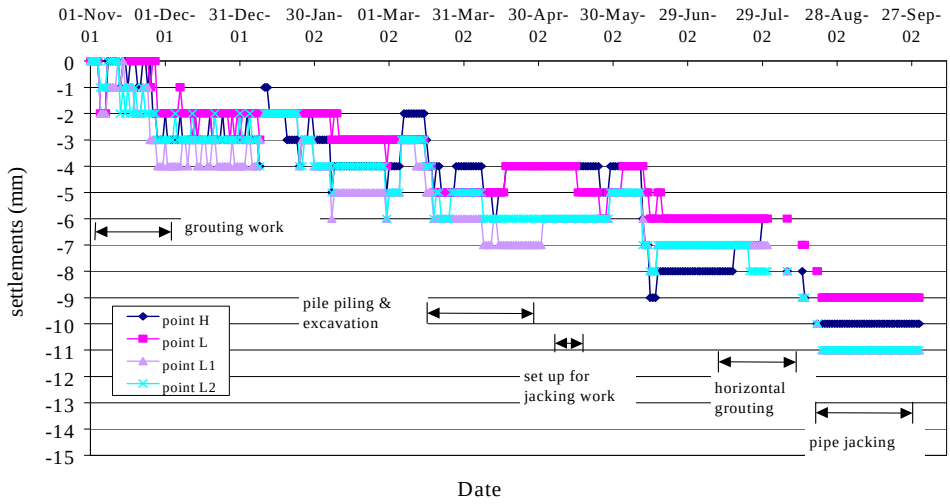

Fig. 3 Development of the observed settlements at Pier no.4 (up to 30/09/2002)

Based on the computer analysed deformation results and empirical methods (GEO, 1990 & 1993), the ground settlement at Piers No. 3 and No. 4 due to shaft excavation alone was predicted at around 4 mm. The settlement caused by pipe-jacking work alone was estimated at less than 2 mm based on normal probability distribution curve (Roe, 1995). Figures 2 and 3 show little additional settlement occurring during the excavation of the shafts and pipe-jacking work. As a result of precautionary ground treatment works carried out and good workmanship, the recorded additional settlement following the shaft excavation up to the completion of the pipe-jacking works was in the order of 2 mm to 6 mm only, being well within the estimated values.

Settlement Monitoring Around Site

Figure 4 summarises the results of the settlement monitoring against time and site activities at 10 critical monitoring points around the site. Of over 30 points, there were four settlement monitoring points, all located on road kerbs close to the site, at which the maximum settlement was observed to be over 10 mm. The maximum settlement observed occurred at point E, which was near to the installed pipe piles, reaching a cumulative settlement of 36 mm after completion of the pipe-jacking work. However during pipe-jacking work, only 4 mm further settlement was recorded at monitoring points K1 and K2 which were immediately above the pipe-jacking work, being less than the predicted 7 mm.

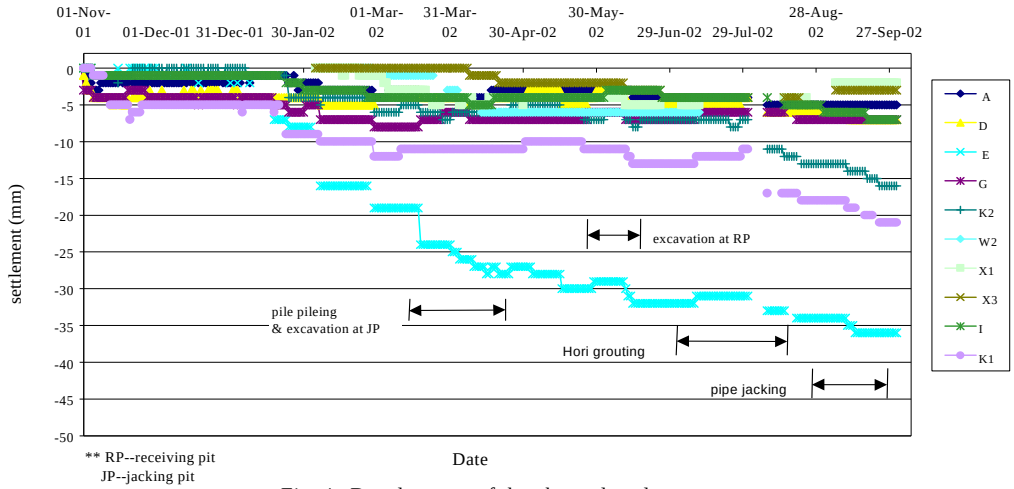

Fig. 4 Development of the oberved settlements (up to 30/09/2002)

Groundwater Monitoring

The ground levels recorded varied from +0.84 mPD to +1.96 mPD at the receiving shaft, and from +0.90 mPD to +1.50 mPD at the jacking shaft. The recorded variations in groundwater level were considered to be due to rainfall and tidal effects (Figure 5). No groundwater level drop was noticed during excavation for the shafts and pipe-jacking. However, a water level of as low as +0.16 mPD was recorded in September 2001 when only grouting work was carried out on site.

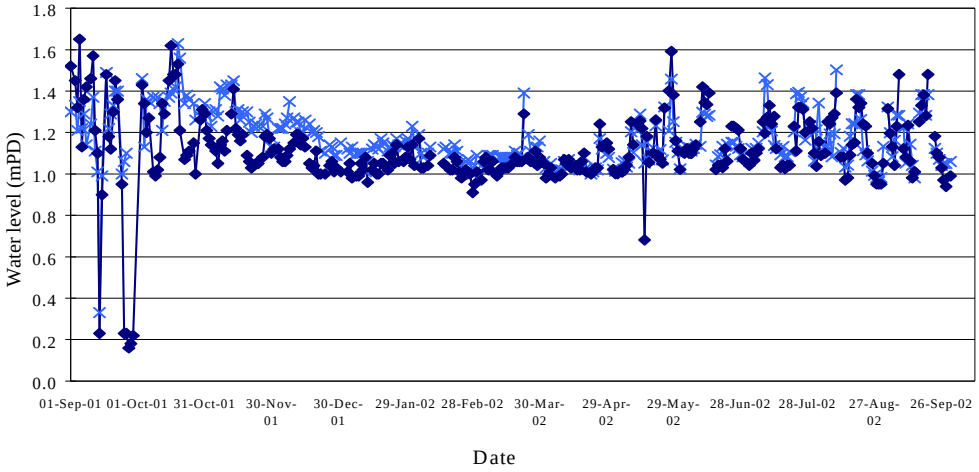

Fig.5 Groundwater Level Monitoring at Jacking Shaft

Vibration Monitoring and Void Detection

Vibration monitoring was carried out on the adjacent bridge piers with a Vibrograph during the installation of near side pipe piles. The peak particle velocities were measured at very small values, all being less than 8 mm/sec.

The report on the Ground Probing Radar suggests that there were a number of anomalies at shallow depths only. It was considered that while the loose fill may settle during the pipe-jacking it is generally above the level of the bridge foundations and, therefore, will not have any adverse effects on the bridge foundations. While it is possible that some settlement of the fill may occur which may affect the road surface slightly it should not have any impact on the flyover structure itself. Therefore it was decided to commence pipe-jacking.

PROBLEMS ENCOUNTERED AND SOLUTIONS ADOPTED DURING CONSTRUCTION

The pipe-jacking work was carried out under very difficult site condition, namely:

- Adjacent heavy structures - Arsenal Street Flyover founded on shallow footings.
- Numerous adjacent utilities sensitive to ground movements.
- Poor ground conditions, comprising loose ground with many cavities, old seawall, boulders/cobbles, for excavation and pipe-jacking, .
- Difficulty in controlling groundwater as the soil is highly permeable with a high groundwater table.
- Pipe-jacking under small overburden (3.5 m) with heavy traffic.

Up to end of October 2001, some ground settlements had been recorded although no dewatering or shaft excavation had commenced yet. Based on groundwater monitoring (Fig. 5), it was observed that the water level dropped by between 0.9 m to 1.2 m in September and early October 2001 while the drilling of grout holes and subsequent grouting were in progress. It was unlikely that that the above undue drop in water level was due to the work at this site. However, it was noted that deep dewatering work was being carried out in the basement construction site and remedial grouting work was underway for controlling ingress of ground water at another pipe-jacking site where a collapse had occurred in Gloucester Road. Both sites were approximately 50 m away.

Cracks were observed at several locations around the construction site adjacent to the Police Headquarters, which was immediately adjacent to a deep basement construction site. Pre-condition survey also identified old cracks on bridge Pier No.5, suggesting that the pier experienced settlement prior to the works. However, no signs of distress or new cracks developing on the piers were observed. Therefore, pipe-jacking work was allowed to continue with close monitoring.

In view of the undue ground settlements that occurred and the possible impacts from adjacent sites, various precautionary measures were taken to minimise the settlements of the bridge. In addition, an alternative arrangement to the original design was proposed to further reduce settlements, ie. relocate the jacking pit further away from Pier No.4 by 2.5 m and adopt double walls system at the side near the pier (Figure 1).

Careful precautionary engineering measures were adopted to minimise the disturbance to the ground and adjacent structures. During construction of the grout curtain, grout holes were drilled using bentonite slurry and casing, and sleeve grouting by tremie method was carried out immediately after drilling. Additional cement bentonite grouting was also carried out between the pier and the jacking shaft to improve the ground. Horizontal grouting was also carried out along the pipe-jacking alignment prior to the jacking.

The excavation of the shafts caused little ground settlements. The recorded settlement at Piers No. 3 and No. 4 were 1mm to 2 mm only. During pipe-jacking work, i.e., between 20th August 2002 to 26th September 2002, bridge Piers No.3 and No.4 settled 1 mm while a further 4 mm of settlement was recorded at monitoring points K1 and K2, which were located immediately above the pipe-jacking work (Fig. 2). This magnitude of further ground settlement is considered to be minimal given that the pipe was being jacked under a small ground cover with heavy traffic above. The contractor was instructed to minimise the excavation by carefully trimming the ground and limiting the distance between the shield and the excavation face to a maximum of 300 mm during jacking. The working face remained stable and dry throughout the pipe-jacking work as a result of good horizontal grouting and pipe-jacking workmanship.

In short, the advancing precautionary ground treatment work together with a well planned staged excavation, pipe-jacking and good workmanship, minimised the ground / structure movements. The pipe-jacking was completed successful.

CONCLUSION AND RECOMMENDATION

The pipe-jacking case presented above was carried out in a very difficult environment. Although great effort was made to minimise the effects to the ground and the adjacent structures, the measured ground and bridge piers settlements were more than expected. While little settlements occurred during shafts excavation and pipe-jacking work, settlements were recorded associated with minor site work, such as grouting and construction activities at nearby sites. Much of the settlements recorded were believed to be caused by activities from adjacent construction sites.

In general, the pipe-jacking work was considered to be successful with valuable experience gained and lessons learned through this difficult job. Particularly for pipe-jacking work, it cannot be over emphasised that a thorough understanding of the ground and groundwater conditions and adjacent development history is required. Except for long drives or small jacking pipes, manual tunnelling methods are preferred for pipe-jacking in old Fills, which often consists of many large obstructions, even old sea walls. Lessons learned from adopting TBM in such environments in Hong Kong have proven to be very expensive. Horizontal grouting along the jacking alignment is particularly useful for ground treatment and water cut-off. Sensible engineering judgement, practical and quick decisions must be made based on monitoring data, site conditions, and excavation and jacking technique adopted. Finally do not isolate your site from others – do your best to protect your site and others' sites too.

REFERENCES

Geoguide 1 (1993). *Guide to retaining wall design*, Geotecchnical Engineering Office, Civil Engineering Department, Hong Kong.

GCO Publication no. 1/90 (1990). *Review of design methods for excavations*, Geotecchnical Control Office, Civil Engineering Department, Hong Kong.

Roe, M.R. (1995). *Guide to best practice for the installation of pipe jacks and microtunnels.* Pipe-jacking Association.

Thomson, J.C. (1993). *Pipe-jacking and Microtunnelling.* Blackie Acadamic & Professional, London.

ACKNOWLEDGEMENTS

Acknowledgements are due to WSD of HKSAR, China and Yick Hing Construction Company Limited for permission to publish this paper. Comments from Advisory Division of GEO of HKSAR, China are also gratefully acknowledged.

中環現存地庫中深層地庫的設計與施工

施宏楚　　楊大明
奧雅納工程顧問公司

DESIGN AND CONSTRUCTION OF A DEEP BASEMENT THROUGH AN EXISTING BASEMENT AT CENTRAL

James W C Sze
Ove Arup & Partners Hong Kong Ltd.
Stephen T M Young
Ove Arup & Partners, USA

撮要

遮打大廈爲一座三十二層現代化商業大廈並擁有三層地庫，新廈於二零零二年六月竣工。爲了建造這座商廈，原建於六十年代之太古大廈在一九九八年十月被拆卸。

現存地庫及地基阻礙新地庫之施工，故需要用鋼管牆及帷幕灌漿進行部份拆卸，然後興建新地下連續牆來支承十五米深的基坑挖掘工程。 新地庫採用逆作法進行。新地下連續牆及大口徑鑽孔樁提供大樓豎向及橫向之支承。

本文介紹了地基及地庫之土力設計，討論了施工期遇到的困難和有關特殊處理。另外，比較了現場監測數據和數值方法預測之位移值。

DESIGN AND CONSTRUCTION OF A DEEP BASEMENT THROUGH AN EXISTING BASEMENT AT CENTRAL

James W C Sze[1] and Stephen T M Young[2]

Abstract: In June 2002, a 32-storey high quality commercial building with a 3-level deep basement, namely Chater House, was completed. To make way for this development, the demolition of the 1960's Swire House commenced in October 1998.

The existing basement structure and foundations obstructed the construction of the new basement. Temporary pipe pile walls with grout curtain were used to facilitate local trimming/demolition of the existing basement slab and pile caps. Diaphragm walls were constructed through the locally demolished basement to retain the soils for the 15m deep excavation and the new basement was constructed by top-down construction method. In addition to the diaphragm walls, large diameter bored piles were constructed to support the vertical loads and wind shear from the superstructure.

This paper describes the geotechnical design aspects of the new development. The difficulties and special issues during the substructure construction works are also discussed. Instrumentation monitoring results are also reviewed and compared with the predicted movements.

INTRODUCTION

Chater House is a new 32-storey 134m high commercial building located in the centre of the Central District of Hong Kong. The new development also includes a 3-level 15m deep basement for underground parking. The site is approximately 50m x 70m and is surrounded by sensitive structures and utilities, including

- a Mass Transit Railway station and tunnel with running tracks at a distance of 4m from the construction works.
- a tall building supported by shallow friction piles at a distance of 4.5m.
- a pedestrian footbridge and a pedestrian passageway at a distance of 7m.

In addition, the site was formerly occupied by Swire House, which had a one level basement and was supported on Franki piles. The existing basement and foundations imposed major obstructions to construction of the earth support wall, foundations and basement of the new development.

These site constraints were major challenges to both the design and the construction. This paper describes the geotechnical design aspects of the new development. The difficulties and special issues during the substructure construction works are also discussed. Instrumentation monitoring results are also reviewed and compared with the predicted movements.

---

[1] Senior Geotechnical Engineer, Ove Arup & Partners, Hong Kong

[2] Associate Principal, Ove Arup & Partners, USA (Formerly Associate Director, Ove Arup & Partners, Hong Kong)

GROUND CONDITIONS

Twenty-eight vertical boreholes were sunk using rotary drilling method to identify the ground condition at the site. Trial pits were also excavated to locate the existing utilities and underground structures. The typical geological profile under the site consists of 8-10m of Fill, overlying 6-8m of Alluvium/Marine Deposits. Below these strata is varying thicknesses of the Completely and Highly Decomposed Granite layers. The ground level of the site is at approximately +4mPD.

The rockhead, defined as Grade III or better rock, dips rapidly across the site, varying from a depth of 30m on the east to 70m on the west. Where the rockhead is deep, a thick layer of core stones and grade III/IV materials are apparent. The groundwater table is at approximately +2mPD.

MAJOR CONSTRAINTS AND CONSIDERATIONS

Existing Foundations and Basement Structures

The site was occupied by the former Swire House, which was a 22-storey concrete building with one level of basement supported by 1130 nos. Franki Piles. These piles extended into the decomposed granite and beared approximately at elevations –13mPD to –15mPD. As indicated in Figure 1, the building occupied the entire limit of the site and was originally constructed in two concurrent phases during the sixties. The structure had a one level basement which occupied 60% of the plan area. The Phase I structure was supported on isolated pile caps and the Phase II structure was supported by a piled raft foundation. The Phase I pile caps ranged from 1.5m to 3.6m in thickness and the elevation of the base of the caps ranged from +1.2mPD to –2.0mPD. The Phase II raft was 2.6m thick with a soffit level at approximately –2.3mPD. These existing pile caps and raft of Swire House obstructed the construction of the new earth support wall and foundations.

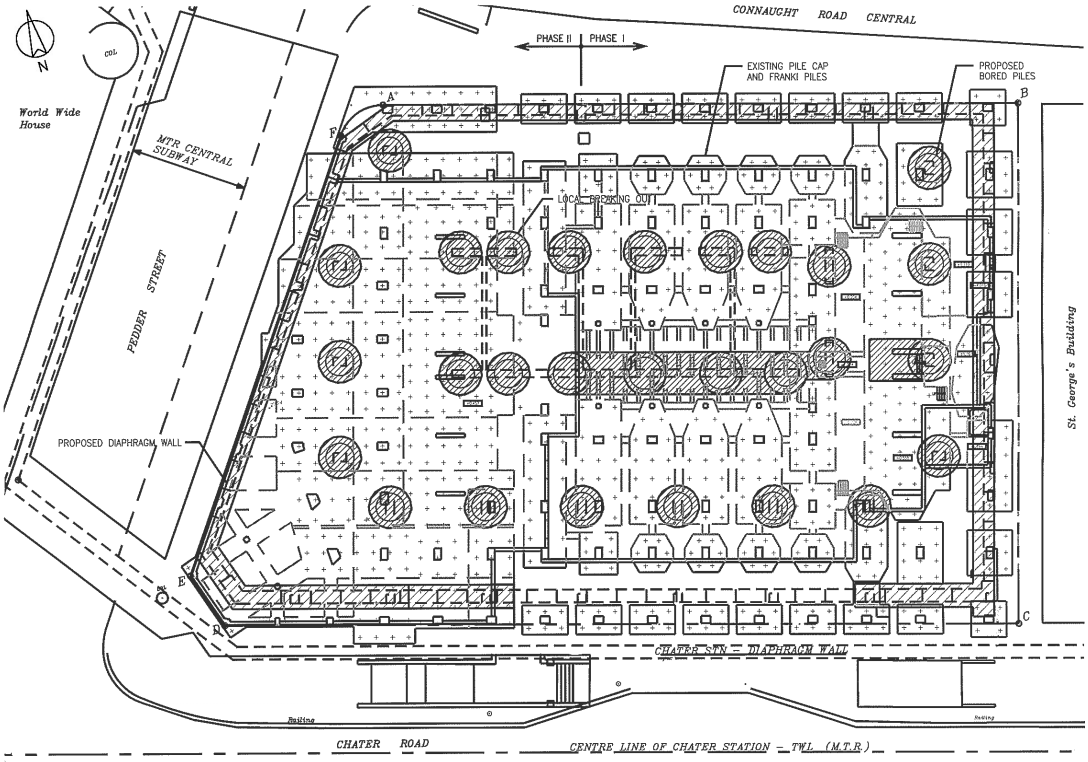

Figure 1 : Site Layout, Existing Foundation and Proposed Works

Adjacent Structures

The adjacent structures requiring particular attention include :

1. St. George's Building along St. George's Lane: A 26-storey high building supported by Franki piles, which extended into CDG. The building is located 2.2m from the site boundary and 4.5m from the new basement.
2. MTR Central Station along Chater Road. The station box is supported by 1.2m thick diaphragm walls bearing on rock. The depth of the Station is approximately 26m. The clearance between the station and the site boundary is 2m.
3. MTR Central Subway along Pedder Street. The subway is a floating structure located 7m from site boundary with a bottom level at -10mPD. The slabs are connected to Worldwide House by 125mm key-in with dowel bars at the intermediate slab level.
4. Footbridge on friction piles and Pedder Street Underpass at Connaught Road.

The new basement of Chater House is 15m deep and during construction of the basement, movement of adjacent ground is inevitable. Therefore it is important that the design of the retaining structures, the supporting system and the method of construction to consider the effects to these adjacent structures and not to cause distress to these structures.

Figure 2 shows a section of the Central Station and the Chater House basement, with the existing Swire House basement and Franki piles.

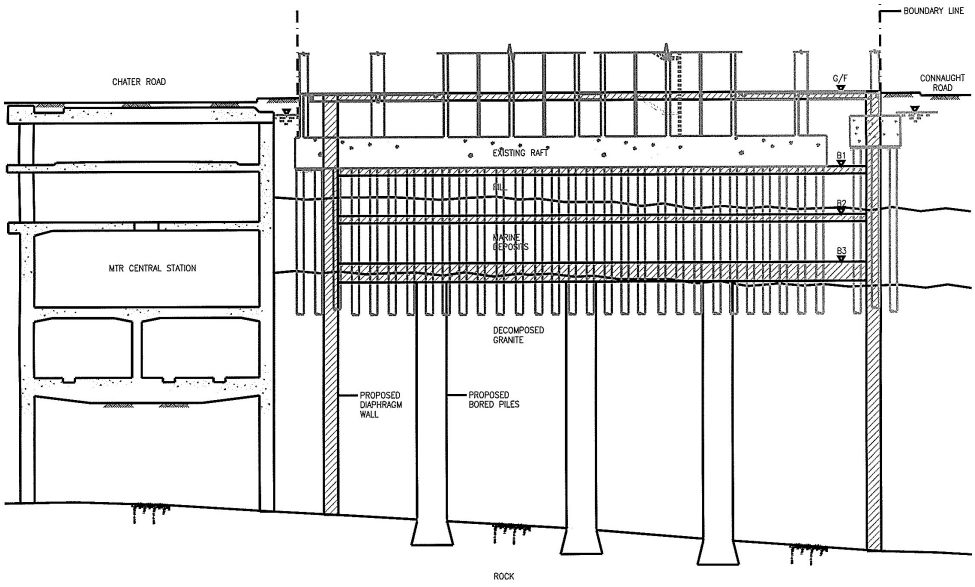

Figure 2 : North-south Cross-Section

Construction Program

The demolition of the existing Swire House commenced in October 1998 and the new Chater House structure, both basement and the superstructure, was completed in the end of 2001. The design and construction of the basement has to consider this fast track program.

DESIGN

Foundations of Chater House

Large diameter bored piles together with the diaphragm wall were adopted as the foundation system to support the gravity loads of the superstructure. The bored piles ranged from 2.5m to 3.0m shaft diameter with bell-out to a maximum of 4.4m and were founded on Grade III or better rock. To facilitate top down construction method, steel stanchions were installed to each of the bored piles. These stanchions were installed with very strict tolerance and were

encased into the concrete core walls and columns of the permanent basement structure. A 16m long temporary steel casing was installed to the top of each bored pile to facilitate the installation of the stanchions.

Peripheral Wall and Construction Sequence of Chater House Basement

In view of the movement constraints of the surrounding structures, the depth of the excavation and to allow for a fast track construction of the superstructure, top-down construction method for the 15m deep basement was adopted. The ground floor slab at +4.0mPD and the B1 slab at -1.7 to –3.0mPD were cast to act as supports to the earth support wall prior to excavation below the slabs. After the base slab was cast, local pits 1.5m deep were dug down below the base slab for lift pit structures. The B2 slab at –6.3mPD was constructed bottom-up after completion of the base slab.

Once the ground floor slab was cast, the design allowed the construction of the superstructure concurrently with the basement excavation up to 10-storey high which was governed by the limitation on the induced horizontal stress onto the adjacent MTR structure due to wind shear. After the B1 slab in the basement was cast, the core wall between the B1 slab and the ground floor slab was also constructed to transfer the wind shear down to B1 level that could resist the wind loading of the superstructure, and the superstructure could be constructed to its final height while the basement was excavating below the B1 slab.

Cast in-situ diaphragm wall was used as earth support wall to support the excavation as well as permanent retaining wall of the basement. A 1.0m thick wall was designed along Pedder Street, Connaught Road and St. George's Lane. Along Chater Road, a 1.2m thick wall was adopted in view of complying with the strict movement criterion of the Central Station. The wall was also offset from the site boundary to create a 4m clearance zone from the Station and to avoid clashing with most of the existing piles. The diaphragm wall was designed using the Oasys program "FREW" (Pappin et al 1986). In this program the wall is represented as elastic beam elements joined at the nodes and the soil is represented as an elastic-plastic continuum with the soil stiffness matrices being developed from pre-stored stiffness matrices calculated using the Oasys geotechnical FE program "SAFE". The program analyses the behavior for each stage of the construction sequence. For general ground settlement around the site, an empirical approach based on the observations made by Humpheson el al. (1986) relating the lateral wall movement and the ground settlement was applied.

In order to support the top down construction slabs and the podium load, the diaphragm wall was also designed as vertical load bearing elements. The panels were founded on various materials, from CDG to Grade III rock, depending on the loading conditions and utilized end bearing to support the vertical loads.

The behavior of the Completely Decomposed Granite during diaphragm wall panel installation has been described by Davies and Henkel (1980). The decomposed granite is both relatively compressible and relatively permeable and this allows rapid swelling to occur in response to the stress relief accompanying trench excavation. This leads to the formation of a compressible zone adjacent to the diaphragm wall panel which recompresses as arching develops during construction of adjacent panels. The resulting horizontal ground movements lead to settlement at the ground. From previous studies by Davies and Henkel (1980) and Humpheson et al (1986), the induced ground movements are strongly influenced by the excess slurry head (i.e. difference between bentonite level and groundwater level) during excavation of the trench. To limit the effects of the adjacent ground and structures due the diaphragm wall installation, the diaphragm wall panel lengths along Pedder Street, St. George's Lane and Chater Road were limited to approximately 3m to reduce the arching loads onto adjacent panels. A 1.7m slurry head above the existing groundwater table was to be maintained.

The effects of diaphragm wall trenching and basement construction on the adjacent sensitive structures like the St. George's Building, the MTR Central Station and the pedestrian subway connecting Hong Kong Station were analyzed using "SAFE". The soils have been modeled as elastic-plastic materials with Mohr-Coulomb strength limits. Two dimensional plane strain analyses were carried out to assess the induced movements and angular distortion onto these structures.

Seepage analysis was carried out using the OASYS finite element program "SEEP" to investigate the piezometric and groundwater drawdown outside the excavation. From the analyses, the amount of drawdown, required pump capacity and the associated ground settlement could be determined. In order to ensure an effective seepage cut-off and limit groundwater drawdown, toe grouting below the diaphragm wall, in the form of chemical grout in soils and fissure grout in rock, was required to a depth of 5m into Grade III or better rock.

CONSTRUCTION

Demolition of the Existing Basement Structures

Local trimming/demolition of the existing basement structures and foundations formed part of the advance work in the Swire House demolition contract to facilitate the construction of the new peripheral diaphragm wall and bored piles construction. Where the existing basement wall could not be used to support the local trimming/demolition, pipe pile wall was installed along the perimeter of the site to enable the trimming works, as shown in Figure 3. The pipe pile wall also acted as the outer guide wall for the subsequent diaphragm wall construction. In some areas, the existing pile caps and raft were located along the pipe pile wall alignment and diamond coring through the reinforced concrete caps was required to permit penetration of the pipe piles. A grout curtain was installed by performing chemical grouting through the slotted pipe piles. The pipe pile wall was supported by raking steel struts prior to trimming of the existing basement wall, piled raft and pile caps (Plate 1). Where pumping of water was required, local sump pumps were used.

Following the removal of the existing pile caps and raft within the limits of the proposed diaphragm wall and bored pile locations, the local openings were then backfilled with a cohesive concrete/bentonite mix. The existing basement was then backfilled to ground surface level to allow construction of the foundation works. The remaining existing pile caps and raft were removed during the top-down excavation of the new basement.

The installation of pipe pile wall commenced in October 1998 and was completed by March 1999. The local trimming and demolition works of the existing basement structures was carried out from June 1999 to August 1999.

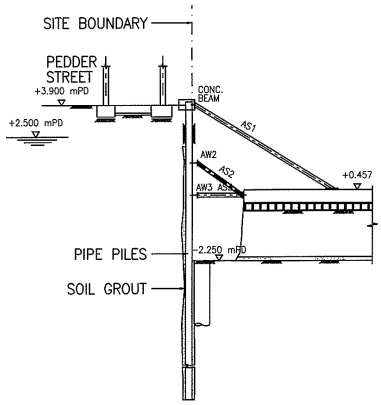

Figure 3 : Pipe Pile Wall for Trimming Works

Plate 1 : Existing Basement Trimming Works

Bored Piles and Diaphragm Walls

Due to the limited site area, the bored pile construction and the diaphragm wall construction were carried out sequentially. The bored pile works commenced in September 1999 and were completed by April 2000. The bored piles were constructed using traditional rotator and oscillator to advance the temporary steel casing in soils. Soils were removed using hammer grab. The shallow obstructions were overcome by chiselling while the deep obstructions and the rock socket for bell-out were penetrated using the Reverse Circulation Drilling (RCD) method.

Diaphragm wall and toe grouting works commenced in March 2000 and were completed in September 2000 (Plate 2). In general, diaphragm wall was constructed by the hammer grabbing method. Along Chater Road, a mill type reverse circulation trench cutter "hydromill" was used to excavate the diaphragm wall panels in order to reduce the induced vibration to the existing MTR Central Station.

The existing Franki piles caused various degrees of difficulty for the foundation works especially in controlling the overbreaking and verticality of the diaphragm wall panels. Removal of the Franki piles was carried out by light chiselling, breaking up the piles into smaller pieces and removed using the grabs. Timber piles, which were used to support an old building, known as Union House, before Swire House was built, were also encountered and which obstructed the foundation works as well as the basement excavation.

Plate 2 : Aerial View of Foundation Construction

Plate 3 : Basement Excavation

Pumping Test and Groundwater Drawdown

After the completion of the diaphragm wall, full size pumping tests were carried out to determine the performance of the cut-off system. The pumping tests were carried out in two stages in order to minimize the deflection of the diaphragm wall and the effects to the adjacent structures. The first stage was to dewater to –4mPD after the completion of the diaphragm wall. The second stage was to dewater to below the base slab at –12mPD after the completion of the ground floor slab.

The results of the Stage 2 pumping test revealed excessive drawdown along Chater Road while the targeted dewatering level within the basement construction had been reached. However, only slight ground and building movements were detected during the pumping test due to the excessive drawdown. It was considered that the excessive draw-down was due to confinement of the diaphragm walls surrounding the site and of the existing MTR Central station, which obstructed the natural recharging of the groundwater table.

As reported by Davies & Henkel (1980), the area had been subjected to substantial groundwater drawdown during the construction of the MTR Central Station and caissons of

Worldwide House. Since the soils had been preloaded, the measured magnitude of the settlement due to the ground water drawdown was small.

From both the pumping test results and back-analysis, a recharge well system was proven to be an effective way to minimize the groundwater drawdown. New recharge wells were installed along Chater Road and together with the recharge wells installed along St. George's Lane, an active recharge well system was proposed to maintain the water level outside the site. The wells were switched on automatically when the groundwater level measured in the monitoring standpipes dropped below +0.1mPD.

Basement Excavation

During the Chater House basement excavation, demolition of the existing basement structures was carried out using backhoe and hydraulic breaker (Plate 3). Since the majority of the existing Swire House basement structures and piles were to be removed, the Chater House basement excavation program was relatively long compared to normal excavation works. The new basement structure, together with the superstructure, was completed in December 2001. This was followed by the building services work and the occupation permit was obtained in June 2002.

INSTRUMENTATION AND MONITORING

A comprehensive instrumentation monitoring program outside the site was carried out to monitor the behaviour of the adjacent structures and to ascertain the predicted movements would not be exceeded. Ground, utility and building settlement points, inclinometers, piezometers, and tiltmeters were installed to monitor the ground/utility settlements, building movements, groundwater levels and tilting of adjacent structures. Inclinometers were also installed into the diaphragm wall panels to monitor the deflection of the wall. Observation wells were installed within the site to monitor the water level during the pumping tests and subsequent dewatering. In addition, vibration monitoring around the site was carried out to monitor the degree of vibration due to various construction activities.

The predicted and measured diaphragm wall movement at Pedder Street is shown in Figure 4. The predicted and measured movements at the adjacent ground and structures are compared and summarized in Table 1.

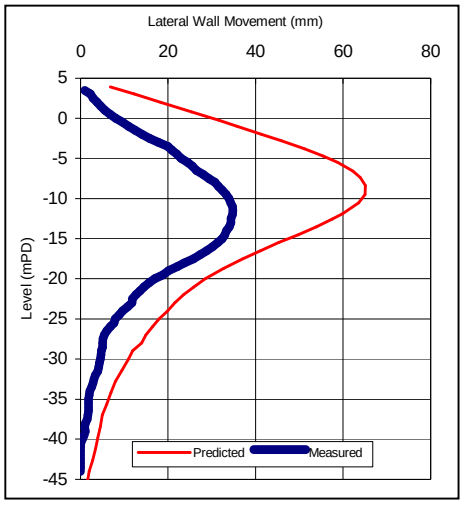

Figure 4 : Diaphragm Wall Movement

Table 1 : Summary of Movements

Area/Structure	Settlement (mm)	
	Predicted	Measured
Adjacent Ground	60	30
Connaught Road Footbridge	18	10
St. George's Building	21	8
MTR Central Subway	6	5
MTR Central Station Transfer Level	7 (lateral)	4 (lateral)

It can be seen that the measured movements are well within the predicted values. There are several reasons attribute to the differences :-

- Heaving of ground occurred during demolition of Swire House and offset part of the settlement;
- Only 2-D analyses were carried out and the 3-dimensional effect was ignored;
- Soil small strain stiffness has not been considered;
- Soils at the site and the surrounding areas are well pre-loaded due to substantial groundwater drawdown in the past, and due to loading of Swire House;
- No account has made for the influence of existing Franki piles within the site.

CONCLUSION

The foundations and the new basement structure of Chater House had been designed using various soil/structure interaction and finite element analyses. Although encountering some difficulties during construction, the works were carried out and completed without exceeding the acceptable movement of the adjacent ground and structures. The top down construction technique allowed a fast track construction program of the basement construction concurrently with the superstructure construction. The local trimming/demolition of the existing basement slab and pile caps at the diaphragm wall and bore pile locations allowed construction of the foundation works prior to removal of the entire existing basement and was a cost effective way to construct the new basement.

REFERENCES

Davies, R.V. and Henkel, D.J. (1980). "Geotechnical Problems Associated with Construction of Chater Station" *Proc. of the Conference on Mass Transportation in Asia, Hong Kong.*

Humpheson, C., Fitzpatrick, A.J.& Anderson J.M.D. (1986). "The basements and substructure for the new headquarters of the Hongkong and Shanghai Banking Corporation, Hong Kong" *Proc. Institution of Civil Engineers.*

Lui, J.Y.H. and Yau, P.K.F. (1995). "The Performance of the Deep Basement for Dragon Centre" *Proc. of the Seminar on Instrumentation in Geotechnical Engineering*.

Pappin, J.W., Simpson, B., Felton, P.J. and Raison, C. (1986). "Numerical analysis of flexible retaining walls" *Symposium on computer applications in geotechnical engineering, The Midland Geotechnical Society, April*.

ACKNOWLEDGEMENTS

The authors are grateful to the Hongkong Land Limited for permission to publish this paper.

香港天然山坡災害緩解措施

謝少雄，盧澳坤，徐向明 及 吳勝隆
香港特別行政區政府土木工程署土力工程處

SOME ASPECTS OF MITIGATION MEASURES AGAINST NATURAL TERRAIN LANDSLIDE HAZARDS IN HONG KONG

S H Tse, D O K Lo, H M Tsui & S L Ng
Geotechnical Engineering Office, Civil Engineering Department,
Government of the Hong Kong Special Administrative Region

撮要

在香港，天然山坡佔全港陸地約百分之六十，每年會發生約三百次的滑動。有些土地開發非常接近天然山坡，而天然滑坡的崩塌物有時會滾落到遠處，造成嚴重的後果。本文描述在香港用作防禦天然滑坡災害的一些緩解措施，包括現場鞏固隱定、防石欄、谷坊、欄砂壩和排水措施。此外，亦提及它們的實地操作和效用。

SOME ASPECTS OF MITIGATION MEASURES AGAINST NATURAL TERRAIN LANDSLIDE HAZARDS IN HONG KONG

S H Tse[1], D O K Lo[1], H M Tsui[1] & S L Ng[1]

Abstract: In Hong Kong, more than 60% of the total land is natural terrain and on average about 300 natural terrain landslides occur each year. Given the close proximity of some of the developments to natural hillsides, a failure may travel a long distance resulting in serious consequences. This paper describes some of the mitigation measures, which have been used in Hong Kong to protect developments against natural terrain landslide hazards. These measures include insitu stabilisation, boulder fences, check dams, landslide debris barriers, and drainage provisions. The effectiveness and practicality of these measures in mitigating natural terrain landslide hazards in Hong Kong are also discussed.

INTRODUCTION

The scarcity of flat land and the constant demand for land in Hong Kong means that there is an increasing pressure for developments to encroach onto the steep parts of its natural terrain. In Hong Kong, more than 60% of the total land is natural terrain. On average about 300 natural terrain landslides occur each year reflecting the inherent landslide hazards associated with the natural terrain. The vast majority of these landslides are shallow failures within the top few metres of the ground surface. Some failures have been observed to develop into channelised debris flows with a long runout. Given the close proximity of some of the developments to natural hillsides, a small channelised debris flow which can travel a long distance may result in serious consequences. This paper describes some of the mitigation measures, which have been used in Hong Kong to protect developments against natural terrain landslide hazards. These measures include insitu stabilisation, boulder fences, check dams, landslide debris barriers, and drainage provisions. The effectiveness and practicality of these measures in mitigating natural terrain landslide hazards in Hong Kong are also highlighted by some case histories.

MITIGATION MEASURES

Natural terrain landslide hazards have been broadly categorised into four groups, viz. open hillside failures (debris slides and debris flows), channelised debris flows, deep-seated failures and rock/boulder falls.

Landslide consequence can be reduced through landslide hazard mitigation measures, which can be divided into two categories: active and passive measures. Passive measures generally involve no direct engineering works and can include land-use regulations (e.g. no-build zones and land-use planning), education and safety precautionary messages. Active measures, on the other hand, involve engineering works and normally comprise preventive

[1] Geotechnical Engineering Office, Civil Engineering Department, Government of the Hong Kong Special Administrative Region

works on the slope to reduce the likelihood of failure, or protective works to mitigate failure consequences. Some of the active mitigation measures are summarised in Table 1.

Table 1 - Summary of Active Landslide Mitigation Measures

Source Area		Hazard Trail	
Action	Mitigation Measures	Action	Mitigation Measures
Inhibition of Occurrence	Scaling, splitting and removal of unstable rock Excavation of unstable material Modification of slope gradient, e.g. terracing, and construction of check dam	Flow Control	Promotion of deposition: e.g. unconfined deposition area, storage basin, debris flow breaker screen, and rock trap (ditch) Flow impediment and debris straining structure: e.g. sacrificial baffle, debris rack, steel cell dams, check dam (or cascaded dam), slit dam, and grid type Sabo dam Flow direction control: e.g. deflector wall, chute, lateral wall (or guideway), and lined channel
Stabilisation	Reinforcement: e.g. rock bolts, chains and cables, anchored mesh nets, anchors/dowels, soil nails, and piles Buttress Soil treatment: e.g. grouting, electro-osmosis, and thermal treatment Structural retention system Dentition Afforestation	Protective Structure	Terminal wall Debris barrier Boulder fence Debris shed and viaduct
Drainage and Infiltration Prevention	Surface drainage Subsurface drainage Surface protection		

Preventive measures, which are generally applied at the source area where the failure occurs, include strengthening of the slope by means of soil treatment, provision of reinforcement and drainage, removal of failure initiating factors (e.g. trimming of overhangs, removal of unstable material), regrading of slope, afforestation and construction of check dams.

Protective measures are generally constructed on the hazard trail along which the landslide debris is transported and deposited to protect the population and facilities at risk. These include, inter alia, rock/boulder fences, deflection berms, debris barriers and check dams. Debris racks, slit dams and steel cell dams have been used to help primarily to dissipate part of the energy of the debris and to screen out big boulders from the landslide debris. Unconfined deposition areas, debris containment basins and debris flow breaker screens have been provided to promote deposition by reducing the slope gradient and the confinement to the flow, or enhancing the separation of water from the debris. A number of techniques have also been deployed to encourage debris to continue to flow in a controlled manner through and beyond a developed area. These include lateral walls and debris viaducts to confine and divert the flow. Lined channels and guideways are sometimes constructed to minimise segregation of debris, increase flow velocity to prevent premature deposition, and to minimise degradation of the channel bed.

The applicability of particular mitigation measures or a combination of measures

depends on the type and scale of landslide hazards, the perceived elements at risk, and the consideration of costs, land-take and the associated reduction in risk that can be achieved.

The preferred approach for dealing with natural terrain landslide hazards is not to carry out extensive preventive/stabilisation works to large areas of natural terrain, which would be both very costly and environmentally damaging, but to mitigate the risk to a tolerable level through adjustment to development layouts taking due account of the site topography, provision of buffer zones and/or protective measures. In this connection, it is most effective to tackle the natural terrain hazards at the planning stage of the project so that the most feasible measures to mitigate the hazard can be incorporated in the design.

LOCAL PRACTICE AND CASE HISTORIES

The following sections give an overview of the types of mitigation measures commonly used in Hong Kong. The effectiveness of these measures is illustrated by some case histories.

Drainage Measures

Stability of natural hillside can be enhanced by reducing the groundwater pressure in the ground by means of subsurface drainage measures. Common drainage measures that have been employed in Hong Kong include vertical drainage wells (caisson drains), drainage tunnels, horizontal/raking drains or a combination of them.

Vertical drainage wells were installed by construction of a series of hand-dug caissons, which was a common form of construction in the 1980s. Horizontal drains were then installed through the caisson rings to draw water into the caisson. In some cases, the caisson rings were partly removed and the caisson was backfilled with suitable filter material to form a vertical drainage well. The water collected in the caisson was conveyed to the outlet via pipes or drainage tunnels connected to the bases of the caissons and the outlet (McNicholl et al 1985). Figure 1 shows an example of such a scheme adopted in a site in the Mid-levels area.

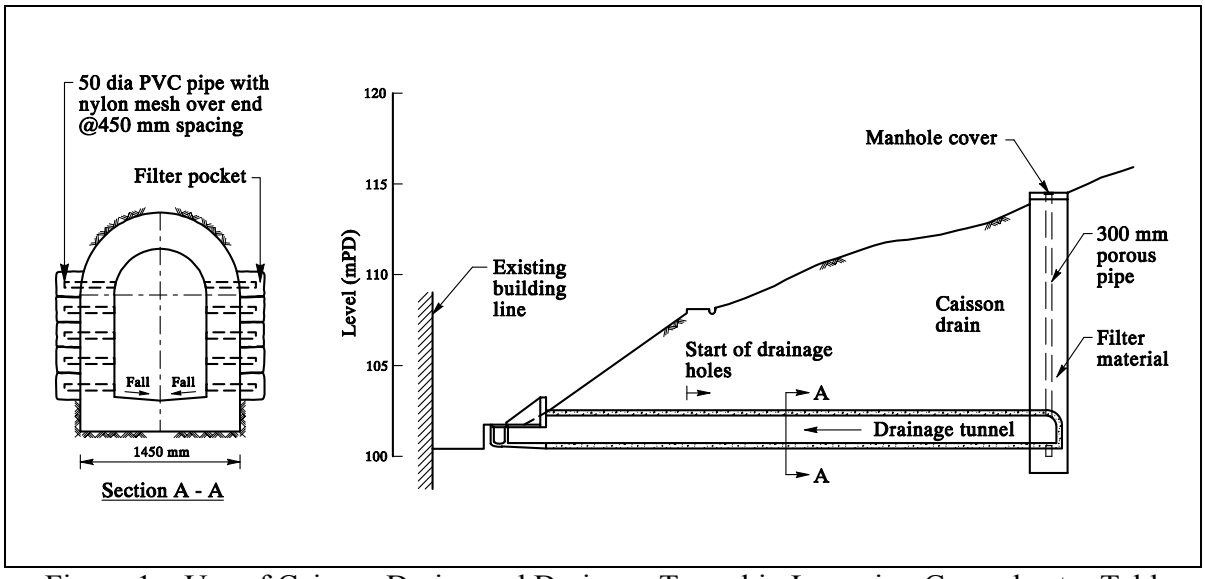

Figure 1 – Use of Caisson Drains and Drainage Tunnel in Lowering Groundwater Table

Drainage tunnels can be constructed to lower the groundwater behind a slope face.

When constructed in highly-weathered rock, the tunnels are lined using reinforced concrete with a drainage filter behind it. Drainage holes are provided through the lining to draw water into the tunnel. Owing to their high construction costs and possible disturbance to surrounding slopes during tunnel excavations, their use has been limited to control water levels in large slopes where no viable alternative scheme exists. The effectiveness of drainage tunnels can also be increased by provision of horizontal drains drilled from inside, similar to that of vertical drainage wells (see Figure 1).

Horizontal/raking drains typically comprise a 40 mm to 75 mm diameter perforated PVC pipe with an impermeable invert wrapped with a geotextile or a 35 to 40 mm diameter stainless steel pipe with slotted screen. The PVC pipe can be encased within another perforated PVC pipe to facilitate maintenance and the cleaning of the inner pipe. A comprehensive review of the design principles and consideration of horizontal drains is given by Martin & Siu (1996). In cases where satisfactory performance of the horizontal drains is vital to the stability of the hillside being drained, the drains are required to be regularly maintained and their effectiveness should be monitored and evaluated. Among the various subsurface drainage measures, horizontal drains are most commonly used in Hong Kong because of their ease of installation and relatively low cost.

Horizontal drains, up to 90 m in length, were installed in the natural hillside behind Po Shan Road. These drains constituted the longest horizontal drainage system so far constructed in Hong Kong. A total of 58 drains of length ranging from 40 m to 90 m with inclination between 5° and 10° with the horizon were installed at three different levels at the hillside. More than 50 piezometers were installed at the site to monitor the effectiveness of the drainage measures. As shown in Figure 2, the horizontal drains were able to bring about a ground water drawdown of about 5 m across most of the site and more than 15 m locally (Martin et al 1995).

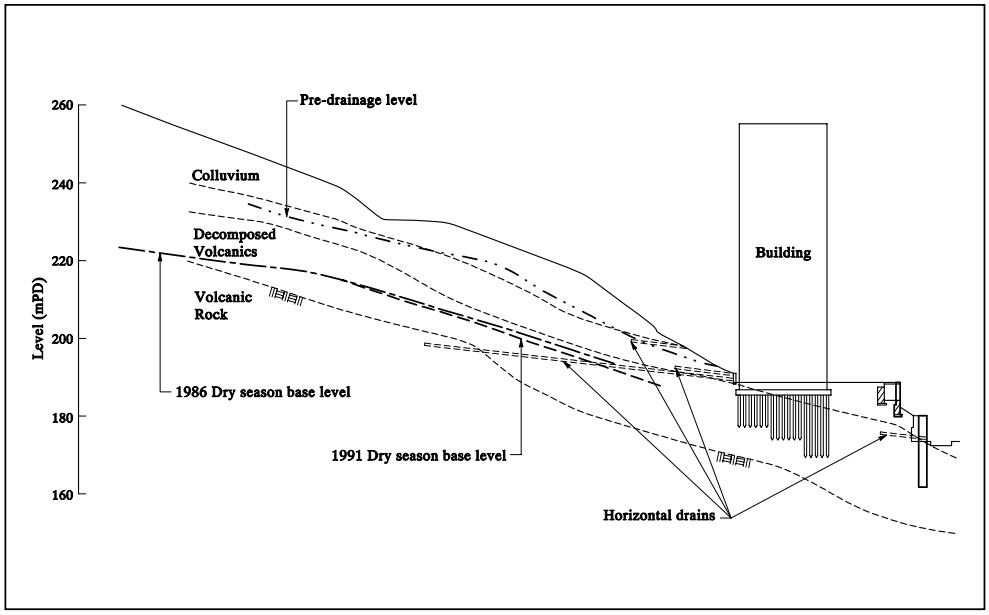

Figure 2 – Groundwater Drawdown Using Horizontal Drains at a Site in the Mid-levels (after Martin et al 1995)

Preventive and Protective Measures Against Boulder Falls

The strategy to mitigate boulder fall hazards is to immobilize the boulders by preventive measures, i.e. removal of the boulders or insitu stabilisation, or via provision of protective

measures, e.g. catch or arrest the moving boulder before it reaches the area of concern. Very often, a combination of both measures has to be adopted in order to achieve a cost-effective design to mitigate boulder fall hazards.

Boulder stabilization measures used in Hong Kong include splitting, surface protection, buttressing, strut/tie beams, anchorages, wire lashing/nets and proprietary rock fall fence. Au and Chan (1991) provide a detailed discussion on these measures and their applications. The suitability of these measures depends on actual site conditions and very often the best solution is a combination of the methods mentioned above. Engineering judgment based on common sense, experience, and sound engineering principles are crucial in designing insitu stabilization measures for boulders.

The most common protective method to mitigate boulder fall hazard in Hong Kong is by using catch/blockade structures. A number of protective structures have been built in Hong Kong. These include gabion boulder barriers below the eastern end of Lion Rock Ridge and in Shaukeiwan (Figure 3(a)), a reinforced concrete rock trap ditch below Beacon Hill and a collapsible fence on concrete foundation in the Mid-levels as reported respectively by Threadgold & McNicholl (1984), Grigg & Wong (1987), and Chan et al (1986). The design and construction of protective works are very often subject to physical constraints, such as access and ease of transportation of construction materials.

(a) Gabion-type Boulder Barrier at Yiu Hing Estate, Shaukeiwan

(b) Steel Boulder Fence below Seymour Cliff, Mid-levels

(c) Proprietary Steel Boulder Fence at a Site in Fanling

Figure 3 - Some Examples of Boulder Barriers in Hong Kong.

As mentioned earlier, it is sometimes economical to combine the protective method with preventive methods. One good example where a combination of these methods had been used to good effect is the Mid-levels boulder field preventive works reported by Chan and Au (1988). The mitigation strategy comprises preventive works for big boulders and protective works for smaller ones. The protection works consist of a catch fence of collapsible type which can absorb energy upon plastic deformation as shown in Figure 3(b). The fence consists of a 3 m high primary fence to catch boulders of design size plus a 1.5 m high secondary fence, which can be repaired at a lower cost, to catch smaller boulders. This post-wire rope fence could cater for falling boulders with an impact not exceeding 100 kJ. Boulders of large size were stabilized insitu by preventive methods. Nowadays proprietary boulder fences are also available to meet different energy-absorbing requirements of up to 2500 kJ, which have been constructed at a site in Fanling (Figure 3(c)).

Debris-resisting Barriers

Debris-resisting barriers have been employed in Hong Kong as protective measures against natural terrain landslide hazards. These include rock fences, gabions, reinforced concrete retaining walls, earthfill berms and check dams (Figure 4). They are generally less than 10 m high. These barriers have been designed to contain debris of up to about 2000 m^3

in volume. To enhance the impact capacity, some of these structures are founded on minipiles and some are integral with the building structure. The design of barriers generally involves the characterisation of landslide hazards, debris movement, the design event and the dynamic interaction upon debris impact at barrier. A comprehensive review of various approaches for debris runout assessment and suggestions for assessing debris mobility and debris impact loads in the design of landslide debris-resisting barriers is given by Lo (2000).

(a) Earthfill Berm in Tuen Mun

(b) Reinforced Concrete Retaining Wall in Fanling

(c) Check Dam in Sham Tseng

Figure 4 - Some Examples of Debris-resisting Barriers in Hong Kong.

Debris-resisting barriers could be in the form of counterfort walls, gabion walls, reinforced fill structures, and other types of gravity structures. The choice of a suitable barrier type should be made taking due cognizance of the construction and maintenance costs, land take and buildability.

For a barrier that straddles a streamcourse, special provisions such as straining structures that allow normal streamflow should be incorporated in the design as shown in Figure 4(c).

In the event where the debris impact loading is considerable, a second line of defence involving some form of sacrificial elements, e.g. rows of wooden piles, rubber tires, or rubble placed ahead of the barrier can 'soften' the impact on the primary barrier and minimise its damage.

MITIGATION STRATEGY

In practice, the mitigation strategy may comprise a combination of preventive and protective measures to effectively deal with different types of natural terrain hazards. This is best illustrated in the following case history. This site is located in the Mid-levels area below a natural hillside strewn with boulders (see Figure 5). The site is underlain with bouldery colluvium and decomposed granite. Ground water monitoring indicated that there was high and rapid rise (up to 7 m) in the groundwater table during heavy rainstorms.

To cater for the rapid rise in groundwater level and the possible damming effect of the caisson foundation of the building, a subsurface drainage system, as shown schematically in Figure 5 was built in the natural slope above the lot to lower the main and perched ground water tables to acceptable levels. The system consisted of large diameter caisson drains sunk into the top of the decomposed granite with horizontal drains installed to connect these caisson drains to the drainage outlets. The ground water table was monitored after completion of the drainage measures to verify the adequacy of the system and it was shown that the proposed drainage system had improved the stability of the hillside above the site to an acceptable level.

The site was located below a boulder field. In light of the existing boulder fence and insitu boulder stabilisation works previously carried out to mitigate the boulder fall hazards in the area, the designer decided, as a further precautionary measure, to locate the building further away from the hillside and to build a recreational area between the proposed building and the natural slope above the lot acting as a buffer zone and rock trap. This case highlights that a practical and cost-effective mitigation strategy can be achieved through engineering means and the importance of thoughtfully planning the development layout taking into account of the geotechnical constraints.

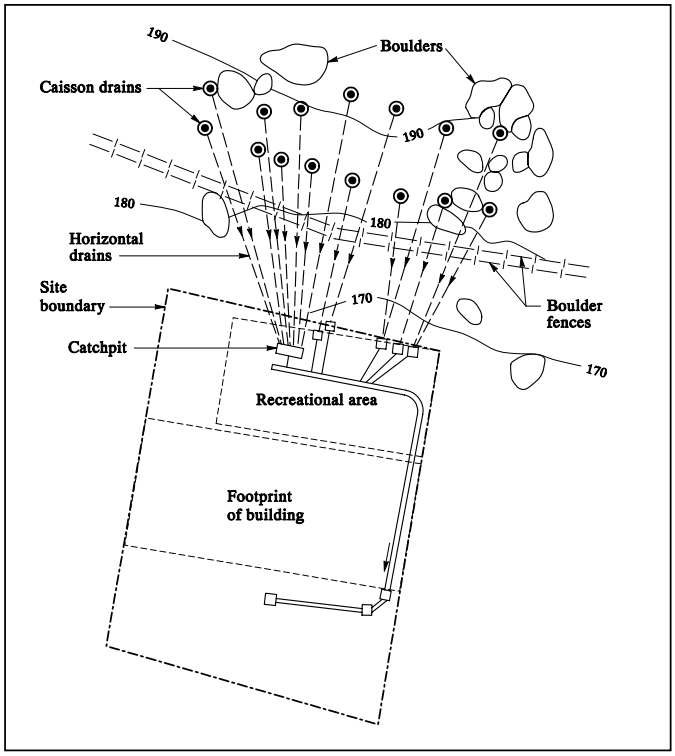

Figure 5 – Mitigation Measures Applied at a Site in the Mid-levels

Due consideration should be given to selecting an appropriate constituent material used in mitigation measures. For example, combustible material should be avoided where the risk of hill fire is high. There has been an incident in Hong Kong in 1989 in which the geosynthetic gabion material of four gabion barrier walls was badly damaged (Au & Chan, 1991).

It is worth noting that the mitigation measures should be maintained to ensure the physical integrity and continued satisfactory functioning of the measures during their service life. Recommended good practice for maintenance of natural terrain hazard mitigation

measures is given by GEO (2002).

CONCLUSIONS

A number of case histories have been reviewed which indicate that it is practical to mitigate natural terrain landslide and boulder fall hazards through engineering means or in conjunction with judicious choice of development layout. The applicability of a particular mitigation measure or a combination of measures need to be judged on a case-by-case basis taking due cognizance of the types and scale of landslide hazards, perceived elements at risk, effectiveness of individual mitigation measures, construction and maintenance costs, land-take and associated reduction in risk that can be achieved. It is important to maintain properly the mitigation measures during their service life to ensure the physical integrity and continued satisfactory function of the measures.

REFERENCES

Au, S.W.C. & Chan, C.F. (1991). "Boulder treatment in Hong Kong." *Selected Topics in Geotechnical Engineering – Lumb Volume*, edited by K.S. Li, pp 39-71.

Chan, T.C.F. & Au, S.W.C. (1988). *Mid-levels Boulder Field Preventive Works Pilot Scheme (Design Study Report No. DSR 1/88)*. Geotechnical Control Office, Hong Kong, 111 p.

Chan, Y.C., Chan, C.F. & Au, S.W.C. (1986). "Design of a boulder fence in Hong Kong." *Proceedings of the International Conference on Rock Engineering and Excavation in an Urban Environment*, Hong Kong, pp 87-96.

Geotechnical Engineering Office (2002). *Maintenance Requirements for Natural Terrain Hazard Mitigation Measures (GEO Technical Guidance Notes No. 8)*. Geotechnical Engineering Office, Hong Kong, 16 p.

Grigg, P.V. & Wong, K.M. (1987). "Stabilization of boulders at a hillslope site in Hong Kong." *Quarterly Journal of Engineering Geology*, vol. 20, pp 5-14.

Lo, D.O.K. (2000). *Review of Natural Terrain Landslide Debris-resisting Barrier Design (GEO Report No. 104)*. Geotechnical Engineering Office, Hong Kong, 93 p.

Martin, R.P. & Siu, K.L. (1996). "Use of horizontal drains for slope stabilization in Hong Kong." *Transactions of the Hong Kong Institution of Engineers*, vol. 3, no. 2, pp 25-36.

Martin, R.P., Siu, K.L. & Premchitt, J. (1995). *Performance of Horizontal Drains in Hong Kong (GEO Report No. 42)*. Geotechnical Engineering Office, Hong Kong, 109 p.

McNicholl, D.P., Pump, W.L. & Cho, G.W.F. (1985). "Groundwater control in large scale slope excavations - five case histories from Hong Kong." *Proceedings of the 21st Annual Conference of the Engineering Group of the Geological Society*, Sheffield, pp 513-523.

Threadgold, L. & McNicholls, D.P. (1984). "The design and construction of polymer grid boulder barriers to protect a large public housing site for the Hong Kong Housing Authority." *Proceedings of the Symposium on Polymer Grid Reinforcement in Civil Engineering*, London, pp 212-219.

ACKNOWLEDGEMENT

This paper is published with the permission of the Head of the Geotechnical Engineering Office and the Director of Civil Engineering, Government of the Hong Kong Special Administrative Region.

從山泥傾瀉汲取的經驗

汪學寧　　何建生
香港特別行政區政府土木工程署土力工程處

LESSONS LEARNT FROM LANDSLIDES

H N Wong and Ken Ho
Geotechnical Engineering Office, Civil Engineering Department
Government of the Hong Kong Special Administrative Region

撮要

研究山泥傾瀉，對我們更了解香港滑坡和改善斜坡工程，至爲重要。本文載述土木工程署土力工程處負責的系統性山泥傾瀉勘測工作，以及其在增強香港斜坡工程知識、作業及制度方面的功能。我們載列數宗山泥傾瀉個案，說明有關經驗如何令我們取得知識和技術的進展。這包括：**(A)1994** 年觀龍樓山泥傾瀉—對評估舊砌石擋土牆及維修地下帶水管道的專業方法帶來重大的改變；**(B)1995** 年翡翠道及 **1999** 年石硤尾山泥傾瀉—說明不良地質結構構成大規模滑坡的嚴重影響；及**(C)**全面分析在無支撐削土坡所發生的山泥傾瀉以顯示斜坡設計需要使用可靠的方案。

LESSONS LEARNT FROM LANDSLIDES

H N Wong[1] and Ken Ho[1]

Abstract: Studies of landslides have played an important role in improving the understanding of slope failures and enhancing slope engineering practice in Hong Kong. This paper describes the systematic landslide investigation programme operated by the Geotechnical Engineering Office of the Civil Engineering Department, and its functions in advancing Hong Kong's slope engineering knowledge, practice and system. Selected landslide cases are presented to illustrate how the lessons learnt have brought about technical insight and advances.

INTRODUCTION

Landslides can provide an invaluable source of information for advancing the understanding of the causes and mechanisms of slope failures. Experience has shown that it will pay dividends to study landslides in order to learn how best to prevent or mitigate similar failures in future. By studying landslides, one can learn how slopes really behave and perform in practice, what are the deficiencies in current practice and which areas are in need of improvement.

The findings of a detailed landslide study have resulted in technical advances and major impact on the professional practice whilst the overall diagnosis of a certain category of slope failures has given rise to important insights in respect of slope engineering practice. The systematic study of landslides in recent years has highlighted the need for improvement in slope engineering practice. This paper presents selected landslide case histories to illustrate how the lessons learnt have brought about technical insight and advances.

SYSTEMATIC LANDSLIDE INVESTIGATION PROGRAMME

A systematic landslide investigation (LI) initiative was introduced by the Geotechnical Engineering Office (GEO) in 1997. The main objectives of systematic landslide studies include the following:

(1) identification of slopes in need of early attention before the situation deteriorates to result in a serious problem,
(2) provision of evidence in forensic investigations of serious landslides that may involve coroner's inquest, legal action or financial dispute,
(3) provision of data for reviewing the performance of the slope safety system and identifying areas for improvement, and
(4) advancing the understanding of the causes and mechanisms of landslides to support technical development work and enhance the reliability of landslide preventive works.

Under the LI programme, all the landslides reported to the Government (which range from about 200 to 800 per year) are examined to identify cases that warrant follow-up studies. Typically, about 30 detailed or forensic investigations are carried out in a year. Between

[1] Chief Geotechnical Engineer, Geotechnical Engineering Office, Civil Engineering Department, Government of the Hong Kong Special Administrative Region

1997 and 2002, more than 1,800 genuine landslides have been examined under the systematic LI programme and some 180 cases selected for follow-up studies. A selection of case histories is presented below to illustrate how some of the key lessons learnt have brought about technical insight and advances.

The 23 JULY 1994 KWUN LUNG LAU LANDSLIDE

The 1994 Kwun Lung Lau landslide (Wong and Ho 1997) involved the sudden collapse of a 100-year old masonry wall that was in a good maintenance condition. The full height of the masonry wall together with the slope above failed and some 1,000 m^3 of debris was released. The masonry wall was of 700 to 800 mm in thickness, which was constructed against a steep cutting into natural ground (probably originally intended as a facing to the cut face). The 75^o steep masonry wall had a maximum height of 10.6 m and a base width of 0.8 m, i.e. a slenderness ratio was more than 13. This was exceptionally slender as compared with typical masonry walls of a similar construction in Hong Kong, which generally have a slenderness ratio of less than 4.

The forensic investigation established that the landslide involved buckling and brittle collapse of the thin masonry wall. The failure was triggered by subsurface infiltration from defective buried drainage systems, which saturated and weakened the soil mass. The state of knowledge at the time was that old masonry walls would fail in a ductile manner following deformation for some time. However, the Kwun Lung Lau masonry wall was in a good condition and yet it failed suddenly with little signs of deformation or distress. The failure mechanism was apparently different to the previous understanding and was investigated in detail.

Conventional stability analyses indicate that slope and retaining wall failure due to soil saturation is possible given the probable range of strength parameters of the soil and the masonry wall. The stability is especially sensitive to the assumed strength (viz. the cohesion component, c′) of the mortar joint between the masonry blocks. However, it is important to note that the actual failure mechanism of the slender masonry wall was very different to the assumptions made in conventional stability analyses.

Advanced numerical analyses using the distinct element computer program UDEC, were carried out to assist in the diagnosis of the mechanism and cause of the failure. The analyses investigated the response of the masonry wall upon wetting up of the retained ground due to water ingress. The wall was modelled as a discontinuum comprising an assembly of discrete blocks with cement mortar in between. The assumed constitutive model simulated the effect of damage to the mortar joints due to tensile or shear failure, with the c′ value of the failed portion of the joints being set to zero. It was not necessary to make any prior assumptions regarding the failure mode. Details of the analyses are given in GEO (1994).

The analyses predicted that the masonry structure would fail in a complex mode (see Figure 1). The masonry wall was found to bulge initially at about mid-height, accompanied by overturning of the portion of the masonry wall below this level. These deformation modes combined to lead to tensile failure and consequential sudden reduction of the shear strength of the affected mortar joints. The bulging and overturning action resulted in brittle fracture of the masonry wall at about mid-height, and the ground behind lost support and slid forward. The upper part of the masonry wall rotated backward as a result of the displacement of the detached mass and was predicted to come to rest on the surface of the debris with the front surface facing upward, which was consistent with the field observations. An important finding was that once tensile or shear failure of mortar joints was initiated, the wall would deform rapidly, with instability developing in an uncontrolled manner. The complex failure mechanism involved bulging and overturning modes followed by sudden

total collapse. The failure mode of the thin masonry wall was brittle which, once initiated, would develop rapidly. Such a complex failure mechanism is not considered in conventional retaining wall analyses, which could be unconservative in the case of thin masonry walls.

Following the Kwun Lung Lau landslide, the local professional practice in respect of assessment of stability of old masonry walls was rationalised. The assessment of the stability of old masonry walls is not straightforward because of their variable and non-monolithic construction. In general, the approach involved combined assessment of the calculated margin of wall stability and the state of wall deformation based on visual inspection and this continues to be applicable to well-proportioned masonry walls. However, thin masonry walls (defined as slenderness ratio of greater than 5) are liable to fail in a brittle manner without prior warning and these should be taken as being substandard, irrespective of the apparent wall condition.

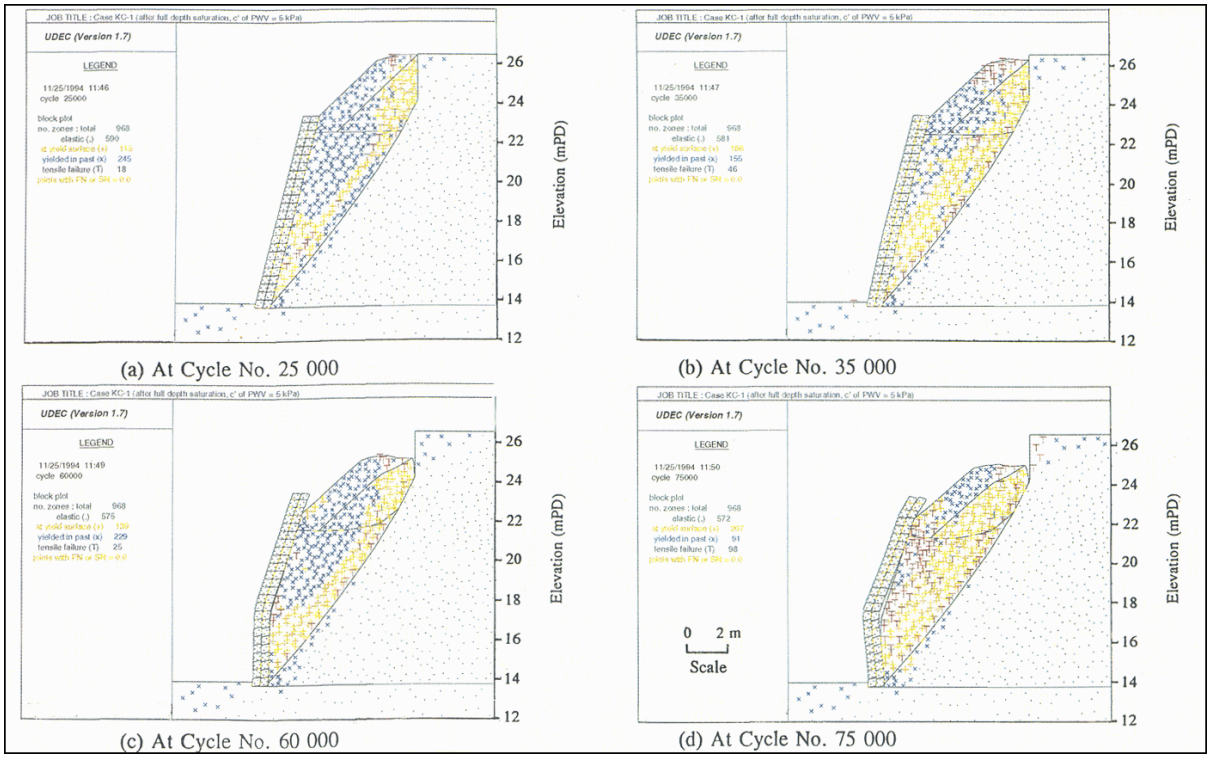

Figure 1 - Results of UDEC Analyses

The Kwun Lung Lau landslide also highlighted the critical importance of leakage from underground water-carrying services on slope stability. Rainfall analyses indicated that the 48-hour rainfall preceding the landslide was the most severe (return period about 28 years). The fatal landslide was a ‘delayed’ failure in that it occurred several hours after cessation of intense rain.

Finite element seepage analyses were carried out to assess the contribution of the different sources of water in saturating the ground behind the masonry wall. Transient seepage analyses were undertaken to examine the 50-hour period starting from the beginning of the rainstorm through to the time of the landslide, taking into account the actual rainfall profile by the nearest automatic raingauge and the suction measurements.

The pathway for subsurface seepage flow towards the landslide area established by the forensic investigation is shown in Figure 2. Subsurface seepage flow took place through the permeable fill layer at an elevation higher than the landslide. The source of water ingress was from defective sections of stormwater drains located beneath the yard area to the back of

the building block above the failed masonry wall. The seepage led to wetting up of the loose fill behind the masonry wall. The consequential settlement probably led to distress or rupture of a foulwater sewer running across the upper part of the landslide area, which had a rigid joint that was susceptible to ground deformation. This resulted in substantial saturation of the retained ground mass leading to the collapse.

The vital importance of environmental changes involving leakage from defective water-carrying services (due to deterioration and poor maintenance) in potentially destabilizing a slope is emphasized by the Kwun Lung Lau landslide. The fatal incident led to the issue of a Code of Practice on Inspection and Maintenance of Water Carrying Services by the Government to upgrade professional practice in the investigation and maintenance of underground water-carrying services (Works Branch 1996).

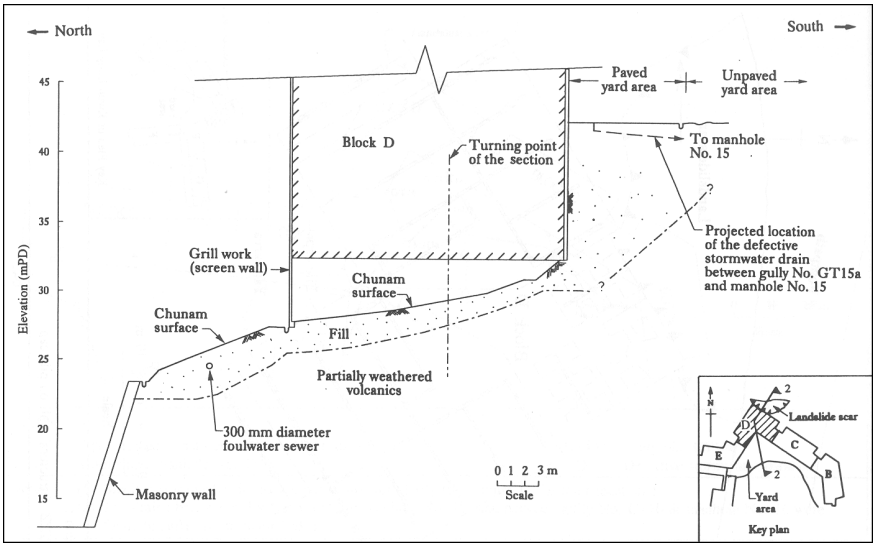

Figure 2 - Section through the Landslide Location, Block D and the Yard Area

EFFECTS OF ADVERSE GEOLOGICAL FEATURES

The 13 August 1995 landslide at Fei Tsui Road (GEO 1996) involved a large-scale failure (14,000 m^3) of a 27 m high engineered cut slope. The landslide consisted of a translational failure with the detached ground mass sliding outwards on a surface dipping gently out of the slope. Large failures of this type are unusual in Hong Kong, and this landslide is the largest reported rapid failure in a permanent cut slope in Hong Kong.

The post-failure investigation established that the basal slip surface of the landslide developed along a laterally extensive (>50 m) layer of kaolinite-rich altered tuff, which was about 15 m below the crest of the cut slope and dipping out of the slope at about 10^o to 25^o to the horizontal, whilst the backscarp of the landslide was defined by two sets of steep joints. Plate 1 shows that the layer (about 0.5 m thick) that controlled the basal failure plane is highly kaolinised and completely decomposed, with abundant kaolinite veins ranging from 2 mm to 20 mm in thickness.

It is noteworthy that the slope with the adversely orientated, persistent, clay-rich layer that controlled the failure was investigated on a number of occasions in the past. Signs of seepage were observed above the clay-rich layer. However, given the relatively shallow inclination of the layer (up to 25^o), all the various parties who previously studied the slope considered the chance of a large-scale translational failure along this layer to be remote.

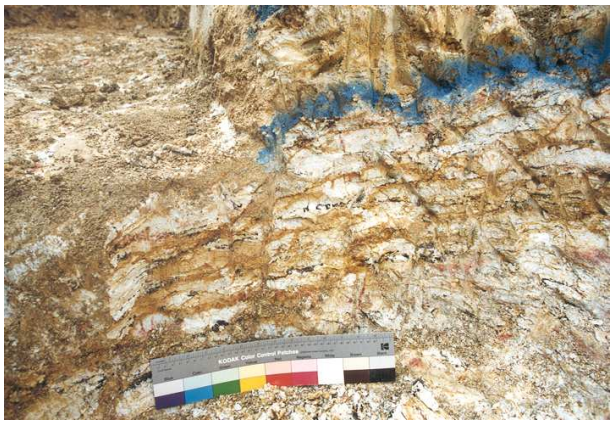

Plate 1 - Kaolinite-rich Altered Tuff at the base of the Fei Tsui Road Landslide

For the best estimate operational shear strength parameter ϕ' of 29^o for the clay-rich layer (based on direct shear box tests), theoretical stability analysis predicted that a perched water table of about 2 m above the layer would have been sufficient to cause a translational failure. The build-up of such a perched water table above the persistent clay-rich layer is credible following the prolonged rainfall that preceded the failure.

The adverse effect of significant adverse geological features on slopes previously subjected to engineering studies was also illustrated by the 25 August 1999 Shek Kip Mei landslide (GEO 2000). The slope displaced forward by about 1 m at the slope toe. The total volume of the displaced mass was about 6,000 m^3. A laterally-persistent (over 60 m long) discontinuity dipping at a shallow angle out of the slope formed the basal plane of the southern part of the landslide. This discontinuity was infilled with polished, slickensided kaolin and manganese oxide deposits up to 15 mm thick only (Plates 2 and 3), which was not mapped in the past geotechnical studies. The mean shear strength parameters of this clay-infilled discontinuity based on direct shear box tests are $c' = 0$ and $\phi' = 20^o$.

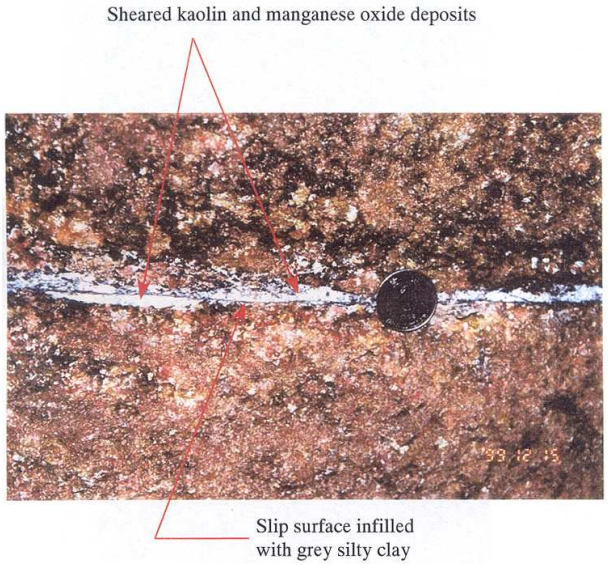

Plate 2 - Close-up View of the Slip Surface within the Sub-horizontal Discontinuity Infilled with Kaolin and Manganese Oxide in the Shek Kip Mei Landslide

Plate 3 - Laterally-persistent Discontinuity Infilled with Slickensided Kaolin and Manganese Oxide in the Shek Kip Mei Landslide

Adverse geological structures, such as persistent, clay-infilled discontinuities, can provide structural controls to potential large-scale instability and give rise to adverse hydrogeological conditions (e.g. conducive to build-up of perched water table), as highlighted by the 1995 Fei Tsui Road landslide and the 1999 Shek Kip Mei landslide. As the shear strength of weak infill to such adverse geological structures can be much lower than the matrix material of the soil/rock mass, the conventional safety margin will not be adequate to cover for such weak and impermeable seams if their presence is not taken into account in the ground model. Enhanced geotechnical input including in particular engineering geological input must be provided, especially for potentially problematic sites (Wong and Ho 2000), to look for such safety-critical geological features and assist in the formulation of representative ground model and hydrogeological model. The GEO has carried out a series of studies to improve the understanding of the effect of clay-infilled discontinuities on slope stability in Hong Kong. The key findings are summarised by Campbell and Parry (2001), and a GEO Technical Guidance Note No. 4 (GEO 2001) has been issued by the Geotechnical Engineering Office for reference by practitioners.

NEED FOR ROBUST SLOPE DESIGN

Between 1997 and 2002, 106 landslide incidents involved man-made slopes with past geotechnical engineering input and geotechnical design submissions checked and accepted under the slope safety system, 24 of which were major failures (i.e. $\geq$50 m^3 in volume). All of the 106 failures were studied to a sufficient detail to enable a meaningful diagnosis of the probable causes of failure. Of the 106 cases, 53 affected engineered soil cut slopes, 15 of which were major failures. All these 53 failures involved unsupported soil cuts, with no structural support, such as soil nails or earth retaining structures.

While insufficient control of surface water can sometimes be a contributory factor in major landslides, the most important causes of major failures on engineered soil cut slopes are:

(1) use of an over-simplified ground model which does not adequately cater for safety-critical weak geological structures in the ground mass, and

(2) use of an inadequate hydrogeological model which does not adequately account for adverse groundwater conditions (e.g. significant build-up of perched water pressure and/or rise in base groundwater table).

The comprehensive analysis of failures of engineered unsupported cut slopes highlights, inter alia, the need for robust slope design to enhance the reliability of engineered soil cut

slopes. Robustness reflects the vulnerability of a slope design to undetected (or unforeseen) conditions adverse to slope stability (e.g. high transient groundwater condition or presence of adversely orientated and weak clay seam) that are not accounted for in the stability analysis.

Measures that provide positive support to the slope, such as soil nails, reinforced concrete retaining wall, toe weighting, etc., are more robust than unsupported cuts because they are less sensitive to undetected or unforeseen conditions adverse to slope stability (e.g. high transient groundwater condition or adversely orientated, weak clay seam). Robust solutions are strongly recommended in view of the inherent uncertainties associated with the variability of the ground conditions and complex hydrogeological regimes in practice. In general, large unsupported cuts (particularly those with significant consequence-to-life or major economic consequence in the event of a slope failure) should be avoided as far as possible because these are especially vulnerable to undetected adverse ground conditions due to lack of system redundancy. Soil nails are robust because the nails can bridge over local ground weaknesses through stress redistribution and hence a soil-nailed slope behaves effectively as a reinforced ground mass. An added advantage of soil nails, from a risk perspective, is that the failure mode of a nailed slope is likely to be ductile, hence providing prior warning of impending failure (e.g. progressive development of slope distress) and with reduced debris mobility, see Figure 3.

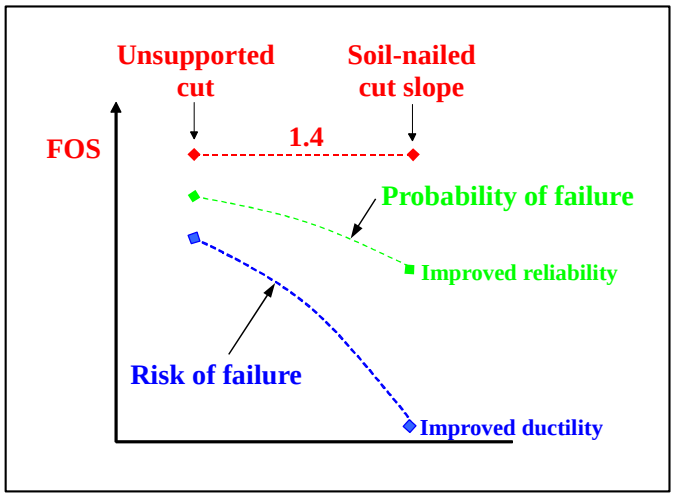

Figure 3 - Advantages of soil nailing over unsupported cut

Since the introduction of soil nails to Hong Kong in the late -1980's, there has been no reported failure of a permanent soil nailed cut slope. To ensure that the robust nature of the soil nail solution will be realized, it is important that the soil nails must be designed and constructed properly. Guidance on the use of soil nails in enhancing the stability of cut slopes, including cautions about its application in certain situations, is given in GEO Technical Guidance Note No. 11 (GEO 2003).

The vast majority of engineered unsupported soil cuts (i.e. with calculated Factors of Safety that meet the requirements stipulated in the Geotechnical Manual for Slopes (GCO 1984), geotechnical design submissions accepted by the checking authority, together with qualified supervision and design review carried out during construction) has hitherto not suffered any major failure. At the same time, significant and rapid failures of engineered unsupported soil cuts had occurred, resulting in dire consequences or 'near-misses'. Some of these significant failures occurred on unsupported cuts that had apparently survived many severe rainstorms in the past. Unsupported cuts can be susceptible to deterioration, environmental changes or more intense rainstorms of certain rainfall duration-intensity

characteristics. It is therefore important that designers must heed the lessons learnt from the past failures with a view to enhancing the reliability and robustness of engineered slopes.

CONCLUSIONS

Landslides are important case histories on the performance of slopes and our slope engineering practice. Landslide investigations are providing a useful feedback mechanism to improve the slope engineering practice and enhance the risk management system. With the insight gained from landslide studies, practitioners can better appreciate what to do as well as what not to do. There are considerable uncertainties in the assessment of stability of slopes in highly heterogeneous tropically weathered rocks and this must not be overlooked through the use of seemingly over-simplified ground models and computer analyses. Practitioners must pay special efforts to keep abreast of the lessons learnt from landslide case histories.

ACKNOWLEDGEMENTS

This paper is published with the permission of the Head of the Geotechnical Engineering Office and the Director of Civil Engineering, Government of the Hong Kong Special Administrative Region.

REFERENCES

Campbell, S. D. G. and Parry, S. (2001). "Report on the Investigation of Kaolin-Rich Zones in Weathered Rocks in Hong Kong." Special Project Report No. SPR 5/2001, Geotechnical Engineering Office, Hong Kong, 75 p. (GEO Report No. 132).

Geotechnical Control Office (1984) "Geotechnical Manual for Slopes. (Second edition)." Geotechnical Control Office, Hong Kong, 295p.

Geotechnical Engineering Office (1994). "Report on the Kwun Lung Lau landslide of 23 July 1994." Vol. 2 – Findings of the Landslide Investigation. Geotehnical Engineering Office, Civil Engineering Department, Hong Kong, 379 p.

Geotechnical Engineering Office (1996). "Report on the Fei Tsui Road landslide of 13 August 1995." Vol. 2 – Findings of the Landslide Investigation. Geotechnical Engineering Office, Hong Kong, 68 p.

Geotechnical Engineering Office (2000). "Report on the Shek Kip Mei landslide of 25 August 1999." Vol. 1 – Findings of the Landslide Investigation, Geotechnical Engineering Office, Hong Kong, 156 p.

Geotechnical Engineering Office (2001). "Guidelines on Recognition of Geological Features Hosting, and Associated with, Silt- and Clay-rich Layers Affecting the Stability of Cut Slopes in Volcanic and Granitic Rocks". GEO Technical Guidance Note No. 4, Geotechnical Engineering Office, Hong Kong, 8 p.

Geotechnical Engineering Office (2003). "Enhancing the Reliability and Robustness of Engineered Soil Cut Slopes". GEO Technical Guidance Note No. 11, Geotechnical Engineering Office, Hong Kong, 8 p.

Wong, H. N. and Ho, K. K. S. (1997). "The 23 July 1994 landslide at Kwun Lung Lau, Hong Kong." *Canadian Geotechnical Journal*, Vol. 34, 825-840.

Wong, H. N. and Ho, K. K. S. (2000). "Learning from slope failures in Hong Kong." Keynote Paper. Proc., 8th International Symposium on Landslides, Cardiff.

Works Branch (1996). "Code of Practice on Inspection & Maintenance of Water Carrying Services". Works Branch, Hong Kong Government.

香港大理石岩區建於泥土層內鑽孔樁之設計及施工

黃康祐
前香港特別行政區政府建築署

DESIGN AND CONSTRUCTION OF SOIL FRICTION BORED PILES IN HONG KONG, WITH PARTICULAR REFERECE TO MARBLE AREAS

Wong Hong-yau
Previously Architectural Services Department
Government of the Hong Kong Special Administrative Region

撮要

本文先敍述四項有詳盡紀錄並完善儀器裝置之樁柱測試。測試均在有大理石岩之地盤進行，一在元朗，另一在東涌，其 他兩地在馬鞍山。此等樁柱皆爲細口徑**(610MM)**鑽孔樁，基 本採用傳統之 **PIP(PAKT-IN-PLACE)**樁柱系統，但有一重大改 動，此爲在灌滿英坭沙漿之樁孔內加入一根最少長二十四米之工字鋼樁。經此改動，可將傳統之樁柱承托力增加最少一倍(由一百五十公噸增至三百公噸)。樁柱之測試結果將會隨地盤及土質之不同而改變，此會在本文詳細討論並與另外兩項較大及不同建造方法之鑽孔樁測試比較。最後本文將會提出影響樁柱沉降及承托力轉移之基本因素，並由此引申出一實際可行之樁柱設計方法。

DESIGN AND CONSTRUCTION OF SOIL FRICTION BORED PILES IN HONG KONG, WITH PARTICULAR REFERENCE TO MARBLE AREAS

Wong Hong-yau[1]

Abstract : This paper describes firstly four well documented and fully instrumented pile load testing cases in the various marble areas in Hong Kong : one in Yuen Long, one in Tung Chung and two others in Ma On Shan. All these are small diameter bored piles of 610mm nominal diameter, installed by advancing a continuous-flight hollow-shaft anger to the required depth and then backfilled with a specified sand cement mortar through the tip of the hollow anger during its withdrawal. This is basically the PIP (Pakt-In-Place) piling system, but with one very major modification, which is the lowering of a steel H-pile section (of length varying from 24m to 36m) into the fully grouted pile hole. With this modification the working load can be easily increased by at least 100% from about 1500KN (for conventional PIP piles) to about 3000KN or more. The variation of the above load test results with the various ground conditions will be discussed and these will be compared with two other load tests on considerably larger diameter soil friction bored piles installed by an entirely different method - bentonite supported bored piles. Finally the probable mechanisms contributing to the difference in load-settlement and load transfer behaviour of the various piling systems will be proposed and discussed, and a more practical design approach for such piles in Hong Kong will also be suggested.

INTRODUCTION

In Hong Kong, a very common piling system adopted is large diameter bored piles founding on rock. There are two major reasons for its frequent adoption. Firstly, rockhead in most of the areas in Hong Kong is not too deep, being on average at about 20m-30m below ground surface. Secondly, the high building load for buildings exceeding 20-30 storeys requires high bearing capacity.

Another very common piling system is driven steel H-piles. This has the advantages of being relatively cheap, quick to drive under favourable conditions and having relatively high capacity (normally over 3000kN).

However, the adoption of the above two piling systems will become very difficult as well as very expensive under the following ground/site conditions :

(1) Very deep rockhead in excess of 50m-60m or even exceeding 100m.
(2) Very stringent noise or vibration control or both.

In marble areas in Hong Kong, sound rock is normally at fairly great depth. Moreover, driven steel H-piles are practically ruled out as a result of GEO requirement to penetrate through all the rock cavities. In such areas, soil friction bored piles appear to be the most feasible solution unless the building load is extremely heavy or extremely light. In the

[1] Previously Architectural Services Department, Government of the Hong Kong Special Administrative Region

former case, bored piles founding on rock is practically the only solution whilst in the latter case, pad footing/raft foundation should be quite adequate.

DESCRIPTION OF SITE

There are the following common features for these four instrumented sites.

(1) All the four sites are in marble areas in Hong Kong. (See Figure 1)
Site 1 - Yuen Long, Site 2 - Tung Chung, Site 3 - Ma On Shan, Site 4 - Ma On Shan
(2) Sound rock is at fairly great depth, normally over 50m-60m to over 100m.
(3) The soil stratum is fairly thick, minimum over 30m to a maximum over 100m.
(4) The average SPT (Standard Penetration Test) value for the first 30m of soil is at least in the order of 20 or more, as summarized in the Table 1 (see also figures 3.1 to 3.4).

On the other hand, these four sites are different in the following aspects :

(1) Both Sites 2, 3 and 4 are in reclaimed land whilst site 1 is basically along the Yuen Long alluvial plain.
(2) As a result of (1) above, both Sites 2, 3 and 4 have a fill layer of more than 10m together with a thin layer of marine deposit.

FOUNDATION DESIGN CONSIDERATIONS

From the ground conditions as reviewed by ground investigations, one very striking fact is that rockhead (i.e. sound rock) is at very great depth, varying from at least 40-60m to over 100m. On the other hand, cavities are found at quite shallow depths in Site 1. In Site 2, cavities have not yet been found. Nevertheless, their existence cannot be ruled out as most of the drill holes terminate only at about 80m, at which rockhead has not yet been reached. Cavities are found at greater depths of 50m-60m for Sites 3 and 4.

In view of the above considerations, it appears that the more common piling systems such as large diameter bored piles founding on rock, steel H-piles socketing into rock and driven steel H-piles are practically ruled out. As for pad or raft foundations, these are also limited by the fairly low SPT values of 10-20 only in the surface layer.

Form the above considerations, it appears that any foundation design for the present sites must satisfy the following criteria :

(1) This must be a deep foundation (i.e. piling foundation) as the surface soil materials are not strong enough to support the building load.
(2) These piles cannot be founding on or socketing into rock as the rockhead is too deep, exceeding 100m in some areas.
(3) Driven steel H-piles are also ruled out. This criterion together with that in (2) above imply that these must be friction bored piles in soils.
(4) Any piles must be at least 10-20m above the shallowest cavities in order not to overstress the cavities.

For friction bored piles in soil, another important point to note is that too large a diameter is not cost effective. This is because double the pile diameter can only double the pile capacity, but the increase in piling cost is normally more than that. On the hand, too

small pile size (e.g. mini-piles of 300mm diameter or smaller) will reduce the pile capacity because of the high slenderness ratio.

With the above criteria in mind and considering also the piling systems currently available in Hong Kong, it appears that the most suitable piling system is the so-called PIP (Pakt-In-Place) piling system. This is a 610mm nominal diameter augered bored pile and from previous pile load test results, very high soil friction can be developed.

However, the working load of conventional PIP piles is only limited to about 1500kN, irrespective of the length of the pile, as the working load is limited by the working stress of the sand/cement mortar. With an allowable working stress (σ_{grout}) of 5 MPa and a nominal pile diameter (D) of 610mm, the working load (P_{grout}) based on σ_{grout} is limited to 1461kN. This is an intrinsic disadvantage of the PIP pile.

For the present 4 sites under consideration, only site I can accommodate such low bearing capacity piles. For the other 3 sites, the working load has to be increased to at least about 3000kN. In view of the above requirements, one very major modification has been made. This is carried out by simply inserting a steel H-pile into the pile after it has been completely grouted.

The design method of the conventional PIP piles is an empirical one based on SPT(N) values. For a pile bored to depth of H(m) below pile head, then the design working load (P_d) must be the lower of the following 2 values.

(1) $$P_f = 4.8\,\pi D\, N_{av} H/F + \pi \frac{D^2}{4}(5\, N_{base})$$

where P_f = Working load calculated from average SPT value over depth H (kN).

N_{av} = Average SPT (i.e. N) values over depth H, with local N value limited to 40

F = Factor of safety = 3, for conventional PIP design

N_{base} = SPT at pile base, limited to 200

(2) $$P_{grout} = \pi \frac{D^2}{4}\sigma_{grout} = \pi\frac{0.61^2}{4}(5000) = 1461\text{kN}$$

The following special features can be observed from the above empirical design :

(1) The contribution of the end bearing to the working design load is very small. Even with SPT as high as 200, the end bearing only contributes to about 20%. With PIP piles normally founding at SPT of 50-60, the contribution is only in the order of 5%.

(2) With average SPT over the pile depth in the order of 30, the maximum founding depth required is only in the order of 25m to 30m. Penetrating beyond this depth is meaningless as the working load is limited by the allowable working stress of the sand/cement grout of 5 MPa, thus limiting the maximum working load to the order of 1500kN only.

As boring to a greater depth of 40m to 50m does not impose any technical problems with the recent development of stronger augering machines, it follows that what is required is just to reinforce the sand/cement grout. Accordingly, the major modification in the present works is to insert a steel H-pile into the fully grouted pile. The initial objective is to increase

the working load of the conventional PIP piles by at least 100% from about 1500kN to 3000kN.

INSTALLATION OF TEST PILES

In general, the installation of all the test piles are essentially similar to that for the working piles, except that the steel H-pile is fully instrumented before final installation. The installation process is as summarized in Figure 2.

The physical and mechanical properties of the test piles and their constituent materials (grout and steel H-pile) in the various sites are as summarized in Table 2.

INSTRUMENTATION AND TESTING OF TEST PILES

The instrumentation and testing of all the test piles in these 4 sites were studied by HKU (University of Hong Kong) and the details were presented in HKU's reports (see Refs 1, 2, 3 & 4).

The instrumentation and testing works comprise majorly :

(1) Installation of strain gauges along both sides of the web of the steel H-pile at about 3m to 4m intervals (see Figure 2 for typical layout) and
(2) Taking readings of these strain gauges and the settlement at the pile top during the various load testing stages.

Ideally, with the elastic strain of the steel section at various depths available, the corresponding pile force at various depths can also be determined provided :

(1) The elastic modulus of the steel H-piles, elastic modulus of the sand/cement grout and the total cross-sectional area of the pile at various depths are known.
(2) There is no slip between the steel H-pile and the surrounding sand/cement grout.

In view of the above considerations, additional laboratory and field works are required. The following tests were carried out in the Structural Engineering Laboratory of The University of Hong Kong (see also Refs 1, 2, 3 & 4).

(1) Determination of elastic modulus of sand/cement grout, and steel H-piles.
(2) Determination of bond strength between steel H-pile and sand cement grout.

A summary of these properties is as given in Table 2.

In order to further confirm that there is no slip between the steel H-pile and the surrounding sand/cement mortar, the elastic strain in the sand/cement grout was directly measured in Site 1. This was carried out by installing strain gauge on opposite forces of a precast sand/cement grout cube, which was attached to the steel H-pile by a steel bracket.

DISCUSSIONS OF LOAD TEST RESULTS

In all these instrumented piles, there are two major sets of data to be measured :

(1) Settlement at pile top at various loading stages : A compliance test for a lot of piling works.
(2) Axial pile load at various depths for each loading stage : An investigative test for improvement of future design.

The load-settlement results are summarized in Table 3. The following points are to be noted :

(1) The load-settlement curve for all test piles is, in general, linear elastic up to the respective maximum load, i.e. failure of the piles has not yet occurred.
(2) The residual settlement in all the test piles is only in the order of 1-2mm and this further justify that failure of the piles has not yet occurred.
(3) Comparing the settlement at the same test load of about 3000kN, it is the highest in Sites 3 & 4 and the lowest in Site 2. This tends to agree with the average SPT value for the first 20m, as indicated in Tables 1 and 4.

With the axial pile load induced at any depth measured, the corresponding total pile shaft friction force developed at any depth $(P_f)_{measured}$, is given by :

$$(P_f)_{measured} = \text{Pile load applied at pile top} - \text{Axial pile load measured}$$

The total pile shaft friction load at any depth (H) for the four sites is as indicated respectively in Figures 3.1 to 3.4. The following features are to be noted from the $P_{measured}$ values in these figures :

(1) Fairly large pile shaft friction is developed in the first 10m. This is up to the range of 2000-3000kN, irrespective of the pile load applied at the pile top. The effect of the total pile length is also not very significant. This is not surprising if it is accepted that pile shaft friction is proportional to the SPT values of the surrounding soil.
(2) The axial pile load decreases quite rapidly with depth. At two-thirds of the pile length, about 80% of the total pile load applied has been dissipated. The remaining load at the tip of the pile is quite insignificant, normally less than a few percentages.
(3) The presence of a layer of soft marine clay in Sites 3 and 4 is accompanied by a much less rapid increase in the pile shaft friction at that level.

The relationship between pile shaft friction and SPT can be further assessed from Table 4. It should be noted that the ratio of average pile shaft friction load to average SPT is of the same order for each of the four sites.

COMPARISON WITH PREDICTION FROM EMPIRICAL EQUATION BASED ON SPT VALUES

The empirical equation for design of the working load (P_d) based on SPT values is as follows :

$$P_d = P_f = 4.8\pi DH(N_{av})/F$$

It should be noted that this is the original empirical equation as adopted in the conventional design (see Section 3), but with modifications that : (1) addition of steel H-pile, (2) ignoring

base resistance and (3) increasing local SPT to 50.

With nominal diameter (D) of 0.61m and F=3, the allowable design working load P_d for each of the 4 sites can be calculated (based on SPT values as in figures 3.1 to 3.4) and is summarized in Table 3.

The above table indicates that allowable design load (P_d) as calculated from the proposed empirical equation based on SPT values, in each site, exceeds the working load (which is equal to half of the maximum testing load) to be adopted in design. The development of P_d with depth for each site is also plotted in Figures 3.1 to 3.4, together with the measured results.

The following special features are to be observed in these figures :

(1) The rate of increase in pile shaft friction for P_d is increasing with increasing depth. This is to be expected as the SPT will in general increase with depth.

(2) On the contrary, the measured values increase initially very rapidly with depth, and the increase tends to be very slow at the lower third. This tends to imply that during load test, the full pile shaft friction has not been mobilized for more than half of the pile length.

The above difference in the variation in the development of pile shaft friction with depth does indicate the predicted trend can only be valid when the pile is loaded to failure. This is because the SPT value represent basically the shearing resistance at the limiting state of failure.

To have a better prediction of the actual variation of the pile shaft friction with depth, the empirical equation for prediction can be further modified by assigning different F values as follows :

(1)	F	=	1.0	for upper third	(i.e. at depth 0-H/3)
(2)	F	=	2.0	for middle third	(i.e. at depth H/3 – 2H/3)
(3)	F	=	3.0	for lower third	(i.e. at depth 2H/3 – H)

It can be seen from Figures 3.1 to 3.4 and Table 5 that with this modification, the predicted pile shaft friction profiles agree fairly well with the measured values.

COMPARISON WITH FRICTION BORED PILES IN SOIL INSTALLED BY OTHER METHODS

At this stage, it would be most useful to compare these results with friction bored piles in soil installed by other methods. The following two well documented cases have been chosen for comparison :

(1) Case (A) : A site in Kowloon Bay, with a barrette type pile of 2.8m x 0.8m x 40m deep (see Ref (5) for details).

(2) Case (B) : A site in Yuen Long area, with a 1.2m diameter and 50m deep pile (see Ref (6) for details).

In both cases, the wall of the piles are supported by bentonite during installation.

The general ground conditions of these two sites are as summarized below :

Case (A)	:	Kowloon Bay Site	Case (B)	:	Yuen Long Site
0-6m	:	Medium dense FILL	0-7.5m	:	Medium dense FILL
6-15.5m	:	Soft MARINE CLAY	7.5-25.5m	:	Soft clayey SILT
15.5-28.0m	:	Firm to stiff ALLUVIAL CLAY to medium dense ALLUVIAL SAND	25.5-33.5m	:	Stiff clayey SILT
			33.5-49.5m	:	Silty CLAY
28.0-40M	:	Completely to highly decomposed GRANITE			

The SPT values at various locations of these two sites for the first 40-50m are as summarized respectively in Figures 4.1 and 4.2.

The load-settlement results of the test pile in both Case (A) and Case (B) are as summarized in Table 3. The total pile shaft friction load developed at various depths has also been measured in both Case (A) and Case (B) and is as indicated in Figures 4.1 and 4.2 respectively. Based on the average SPT values, the predicted total pile shaft friction values at various depths have also been calculated as in Section 7 and plotted in Figures 10.1 and 10.2.

A comparison of the ground conditions in these two sites with the previous four sites (Sites 1, 2, 3 & 4), in particular the SPT values (Figures 3.1 to 3.4 and Figures 4.1 & 4.2) does indicate that :

(1) There is not any substantial difference between these sites.
(2) The Case (A) Kowloon Bay Site is, in fact, very similar to the two Ma On Shan Sites (Sites 3 & 4) as they are all in reclaimed land.
(3) The Case (B) Yuen Long Site is also quite similar to the Site 1 – Yuen Long Site, both being in the same area.

However, the measured pile shaft friction in these two sites is only about 50% of that predicted from SPT values, as can be seen from Figures 4.1 and 4.2. This is surprisingly low when comparing with the previous four sites (Site 1 to Site 4) as shown in Figures 3.1 to 3.4, which indicate that the measured pile shaft friction is in the order of 60%-70% higher than that predicted from SPT values. In other words, the average pile shaft friction mobilized in Site 1 to Site 4 is about 300% of that mobilized in the two sites in Case (A) and Case (B), and this is demonstrated more clearly in Table 4.

Bearing in mind that there is no substantial difference in ground conditions for all these sites, it follows that this major difference in pile shaft friction mobilized must be attributed to the very different pile installation methods.

PROBABLE MECHANISMS CONTRIBUTING TO DIFFERENCE IN PILE SHAFT FRICTION

From the comparison of the test results of the two groups of six sites, the following general conclusions appears to be valid :

(1) Prediction of the pile shaft friction from SPT values by the adoption of any one specific empirical equation is only valid for that particular type of pile installation method for which that empirical equation is initially designed for.
(2) The empirical equation for design of the working load (P_d) based on SPT values :

$$P_d = 4.8\pi DH(N_{av})/F, \quad \text{with } F = 3.0$$

is valid for the PIP (Pakt-In-Place) piling system. Nevertheless, this will lead to a very serious over-design up to 200% to 400% for piles installed by using bentonite as a temporary support during installation.

As there is no substantial difference in the original ground conditions between these two groups of sites, the drastic difference in the pile shaft friction mobilized can only be attributed to a change in the original ground conditions as a result of pile installation.

Firstly, it must be considered which set of ground parameters are affecting the pile shaft friction. Starting from a most basic consideration based on general physical laws as in Figure 5, which indicates the forces acting on an elementary pile surface area as well as the forces acting on a soil element immediately adjacent to this pile surface. From basic mechanics and basic soil mechanics principles :

$\tau_s = \sigma_h \tan\delta$ $\qquad$ $\sigma_h = K \sigma_{v'}$

in which

τ_s = Frictional shear stress acting on the pile surface by the surrounding soil

σ_h = Horizontal earth stress acting on pile surface

δ = Friction angle at pile/soil interface or friction angle of soil immediately adjacent to pile surface, whichever the smaller

$\sigma_{v'}$ = Effective vertical soil stress on soil element immediately adjacent to pile surface

K = Horizontal earth pressure coefficient (i.e. ratio of horizontal earth stress to vertical earth stress)

Combining the above two equations will yield :

$$\tau_s = K \sigma_{v'} \tan\delta$$

This means that the pile shaft frictional force developed is controlled by these three soil/site parameters : K, $\sigma_{v'}$ and δ. It is therefore essential to assess to what extent the pile installation process has altered the ground conditions and hence these three parameters.

For the first group of four sites (Sites 1, 2, 3 & 4) installed by a continuous flight hollow-shaft auger (see also Figure 2), the pile wall during installation will be fully supported all the time. Accordingly, inward yielding of the pile surface is quite unlikely and therefore a substantial reduction of the K parameter from its in-situ value is very unlikely. On the other hand, for the second group of two sites (Case (A) site and Case (B) site), the pile wall is only supported in most parts by a bentonite slurry during installation. As a result of this tremendous reduction in lateral support, the soil materials at the vicinity the pile wall will tend to yield inward, but the arching action prevents the collapsing of the pile wall. With the formation of such a loose zone around the pile wall, the subsequent replacement of the bentonite slurry by concrete is inadequate to re-compact the surrounding soil to its original state. It can be expected that the K value in this case will be reduced from K_o (at rest earth pressure coefficient) to a value below K_A (active pressure coefficient) and this already represents several times reduction in σ_h and hence in τ_s, even if there is no reduction in the other two parameter $\sigma_{v'}$ and δ.

The effective vertical overburden stress ($\sigma_{v'}$) is unlikely to be significantly reduced in both piling systems. This is because even in the bentonite supported case, the soil will yield inward along a horizontal direction and therefore any arching action will also be along a horizontal direction. Accordingly, the original in-situ vertical stress is unlikely to be affected. Nevertheless, in many text books and technical papers, it has been suggested that $\sigma_{v'}$ should remain constant instead of increasing with depth after reaching a certain depth. As for the other two parameters (K and δ), these are constants throughout the whole depth. As a matter of fact, this might just be a simple way of accounting for the decrease of δ with depth, as discussed below.

As for the δ value, it is again very common in most text books and technical paper that this is considered as a constant throughout the whole depth and is equal to the smaller of the following two values :

(1) The soil friction angle measured in triaxial compression test and calculated based on the Mohr-Coulomb criterion, or
(2) The friction angle between the soil material and the pile surface as measured in shear box test.

As a normal practice, the friction angle corresponding to the maximum shear stress developed will be adopted for design.

By referring to Figure 5, it is obvious that the above assumption is over-simplified and will result in over-design. From this figure, it can be seen that in the actual site, the δ value that can be mobilized will increase with strain (i.e. displacement at pile/soil interface) and this will reach a maximum value at a certain displacement, the amount of which will depend on the type of soil. For any working pile, the pile settlement is normally small and will also decrease with depth. Moreover, the soil materials immediately adjacent to the pile surface might be disturbed during installation. From the above considerations, it can be concluded that :

(1) The δ value that can be mobilized will decrease with depth.
(2) Depending on the type of soil and the method of installation, the maximum δ value might not be able to be mobilized at all in any part of the pile.
(3) Accordingly, the adoption of the maximum δ value as determined from triaxial testing on undisturbed soil samples will be basically meaningless in predicting the pile shaft frictional force that can be developed.

Summing up, the significant difference in the pile shaft friction mobilized in these two groups of site is due to the difference in the method of pile installation. To support the pile wall by bentonite slurry will result in local inward yield of the pile wall, thus creating a loose zone of soil immediately adjacent. The final result is a drastic reduction in K (horizontal earth pressure coefficient) and δ (friction angle), the amount of reduction being dependent on the degree of disturbance as well as the types of soil.

SUGGESTED FUTURE METHOD OF DESIGN FOR FRICTION BORED PILES IN SOILS IN HONG KONG

From the above two groups of well documented test sites on friction bored piles on soils in Hong Kong, it can be concluded that for piles that have been considerably disturbed at

and adjacent to the pile wall during installation, it will be extremely difficult to adopt any empirical equation for design. This is because it is extremely difficult, if not impossible, to quantify the extent and degree of soil disturbance in moving from one site to another. As discussed in Section 9, both the K and δ values will be reduced with soil disturbance, and the amount of reduction being increasing with the increase in the extent and degree of disturbance.

On the other hand, an empirical design method based on SPT values can be adopted, provided :

(1) The method of pile installation is consistent in moving from site to site.
(2) There is only minimal disturbance of the surrounding soil materials during pile installed.

For adopting into any empirical equation for design of these piles, the SPT value is a far superior parameter than that determined from triaxial compression test (or direct shear box test). This is because of the following reasons :

(1) The triaxial compression test (or direct shear box test) can only provide information on the δ parameter, out of the three parameters (K, $\sigma_{v'}$ and δ) required for calculating the pile shaft frictional. On the other hand, as the SPT is an in-situ test, therefore this will measure directly the shear frictional resistance and hence a combined effect of (K, $\sigma_{v'}$ and δ).

(2) As can be seen from Figure 5, the δ value thus provided is only the maximum value at a certain amount of soil displacement. For normal piles, the amount of soil displacement is relatively small and certainly lower than that required for the mobilization of the maximum δ. Moreover, even for two soils with similar δ value, the displacement required to mobilize the maximum δ value can vary quite considerably. On the other hand, the pile settlement in each case must be of the same order. This means that the pile shaft friction force that can be developed will also vary quite considerably.

(3) Another very serious limitation in adopting test results from triaxial compression test (or direct shear box test) is the difficulty in differentiating between the frictional and cohesive components in most of the weathered soils as well as the over-consolidated Alluvial Deposit in Hong Kong. Ideally, if the in-situ stress conditions can be measured, then the frictional force that can be developed in-situ can be accurately measured by the adoption of a true triaxial machine, in which the in-situ stresses along all three directions can be simulated. Unfortunately, such a device is not yet available for Hong Kong soils.

Nevertheless, it should be noted for empirical piling design equations adopting SPT values as the design parameter, there is still the limitation that this can only predict the maximum pile load (i.e. loading at which failure will occur). This basically cannot simulate the working condition of the pile. Under normal working condition, the pile settlement and hence the displacement at pile/soil interface decreases with depth. As a result of this, the unit pile shaft friction force developed will decrease with depth, as can be seen from the measured values in Figures 3.1 to 3.4 and Figures 4.1 to 4.2 On the other hand, the SPT values will

increase with depth. This is demonstrated by the fact that the calculated values from empirical equation based or SPT values have the unit pile shaft friction force developed increasing with depth (see also Figures 3.1 to 3.4).

In theory, if the pile load can be increased to such a state that pile failure starts to initiate, then the calculated unit pile shaft friction force developed might follow the same trend as that of the measured values. Nevertheless, it is, in practice, very difficult to load a full scale pile to failure.

To account for the above limitations so that a better simulation of the pile under working load condition can be made, a simple empirical approach as that in Section 7.6 has been carried out by assigning a lower factor of safety (F) near the pile top and a higher one near the bottom such that :

F	=	1	for top one-third	(i.e. at depth 0 – H/3)
F	=	2	for middle one-third	(i.e. at depth H/3 – 2H/3)
F	=	3	for bottom one-third	(i.e. at depth 2H/3 – H)

It can be seen from Figures 3.1 to 3.4 and Table 5 that the calculated values in this manner agree fairly well with the measured values, both the trend and the magnitude.

REFERENCES

LEE, P K K (1995). Field Monitoring of Load Distribution on Pakt-In-Place Piles in Yuen Long Civic Centre, Yuen Long, The University of Hong Kong, Department of Civil & Structural Engineering Report No. 95-68.

LEE, P K K and TSUI, Y (1998). Load Distribution Characteristics on Pakt-In-Place Grout Piles in Tung Chung, Lantau Island, The University of Hong Kong, Department of Civil & Structural Engineering Report No. 98-77.

TSUI, Y and LEE, P K K (1999). Load Distribution Characteristics on Pakt-In-Place Grout Piles at Area 90, Ma On Shan, The University of Hong Kong, Department of Civil & Structural Engineering Report No. 99-82.

TSUI, Y and LEE, P K K (1999). Load Distribution Characteristics on Pakt-In-Place Grout Piles at Area 100, Ma On Shan, The University of Hong Kong, Department of Civil & Structural Engineering Report No. 99-83.

NG, Charles, RIGBY, D, SHEN, C K, TANG, W, NG, S and LEI, G (1998). Some Preliminary Test Results from Kowloon Bay. Prediction Symposium on Large-Section Rectangular Friction Piles (Barrettes).

RIGBY, D B and NG, S (1998). Report on Loading Test of Instrumented Bentonite Slurry Supported Pile for the Village Flood Protection Works for Chau Tau Tsuen, Hong Kong University of Science and Technology, Civil Engineering Department Report.

Table 1 : Average SPT Values of Site 1 to Site 4

Site	Average SPT value (normally at 2m intervals)				
	2-10m	10-20m	20-30m	30-40m	40-50m
Site 1 – Yuen Long	15	23	18 (20-25m only)		
Site 2 – Tung Chung	18	43	38	39	64
Site 3 – Ma On Shan	23	12	30	43	39
Site 4 – Ma On Shan	11	17	28	62	56

Table 2 : Physical and Mechanical Properties of Test Piles and their Constituent Materials in Site 1 to Site 4

Site	No. of piles	Pile no.	Length (m)		$^{(3)}E_c$	$^{(4)}E_s$	$^{(5)}\sigma_{bu}$	$^{(6)}\sigma_c$	$^{(7)}\sigma_s$
			$^{(1)}$Overall	$^{(2)}$H-pile	(x 10^6 kPa)		(MPa)		
Site 1 Yuen Long	2	Pile 1 (No.208)	25	24	16-17	-	-	-	-
		Pile 2 (No. 836)	↓	↓	↓	-	-	-	-
Site 2 Tung Chung	2	Pile 1 (No.PP2)	38	36	21-27	200	-	46	380
		Pile 2 (No.PP2)	↓	24	↓	↓	-	↓	↓
Site 3 Ma On Shan	2	Pile 1 (No.P77)	45	36	17-21	↓	-	31	↓
		Pile 2 (No.P195)	↓	↓	↓	↓	-	↓	↓
Site 4 Ma On Shan	2	Pile 1 (No.P2)	↓	↓	20-20	↓	0.98	36	↓
		Pile 2 (No.P104)	↓	↓	↓	↓	↓	↓	↓

Notes : (1) Nominal pile diameter = 0.61m
(2) All H-piles being 305 x 305 x 149kg/m
(3) E_c = Elastic modulus sand/cement mortar
(4) E_s = Elastic modulus of steel H-piles
(5) σ_{bu} = Ultimate bond strength between steel H-pile and sand/cement grout
(6) σ_c = Compressive cube strength of sand/cement grout
(7) σ_s = Yield strength of steel H-pile

Table 3 : Relationship between SPT and Pile Shaft Friction in All Test Sites

Site	Pile no.	Pile length (m)	Maximum testing load, P_{max}(1) (kN)	Total/Residual Settlement (mm) at		Design working load, P_d (kN)
				$0.5P_{max}$	P_{max}	
Site 1 Yuen Long	Pile 1 (No.208)	25	2922	2.68/0.14	6.28/1.30	1770
	Pile 2 (No.836)	↓	↓	2.53/0.14	650/1.29	
Site 2 Tung Chung	Pile 1 (No.PP1)	38	5360	2.88/0.47	6.00/1.07	3300
	Pile 2 (No.PP2)	↓	5540	3.03/0.50	4.78/0.50	
Site 3 Ma On Shan	Pile 1 (No.P77)	45	4400	3.54/0.32	9.22/1.19	3600
	Pile 2 (No.P195)		4600	6.00/0.01	12.35/1.02	
Site 4 Ma On Shan	Pile 1 (No.P2)		5400	4.32/0.09	10.13/1.78	3600
	Pile 2 (No.P104)	↓	5200	6.00/0.01	12.69/1.02	
Case (A) Site Kowloon Bay	Pile 1	40	5430	2.60/-	9.35/1.94	10722
Case (B) Site Yuen Long	Pile 1	50	5400	7.27/2.34	21.9/9.00	9039

Notes : (1) The test load below which the load settlement curve still more or less linear elastic.

Table 4 : A Summary of Load-settlement and Predicted Design Working Load in Site 1 to Site 4

Site	Site 1	Site 2	Site 3	Site 4	Case (A) Site Kowloon Bay	Case (B) Site Yuen Long
Average SPT over first 20m	19	30	17	14	14	21
Average pile shaft friction load over full length per unit area at maximum load (kPa)	60.5	74.6	52.2	61.1	18.9	22.4
Ratio of average pile shaft friction to average SPT	3.18	2.48	3.07	4.36	1.35	1.07

Table 5 : A Comparison of Measured and Predicted Pile Shaft Friction Profile in Site 1 to Site 4

Site	Pile no.	Maximum load (kN)		Ratio of measured to calculated shaft friction developed at depth		
		Measured	Calculated	H/3	2H/3	H
Site 1 Yuen Long	Pile 1 (No.208)	2922	2780	1.108	1.034	1.051
	Pile 2 (No.836)	2922	2780	1.702	1.216	1.051
Site 2 Tung Chung	Pile 1 (No.PP1)	5360	5080	1.581	1.203	1.055
	Pile 2 (No.PP2)	5540	5080	1.865	1.312	1.091
Site 3 Ma On Shan	Pile 1 (No.P77)	4400	5790	1.020	1.039	0.760
	Pile 2 (No.P195)	4600	5790	1.025	1.003	0.795
Site 4 Ma On Shan	Pile 1 (No.P2)	5400	5384	2.170	1.580	1.003
	Pile 2 (No.P104)	5200	5384	2.058	1.454	0.966

多層大廈採用筏式基礎設計

黃偉儀　　吳力國　　陳杰東
輝固（香港）工程顧問有限公司

MULTI-STOREY BUILDING ON RAFT FOUNDATION IN HONG KONG

W Y Wong, Andy L K Ng, and Martin K T Chan
Fugro (Hong Kong) Limited

撮要

一座 **29** 層高及有 **3** 層地庫停車場的住宅大廈擬採用筏式基礎設計。該地基將坐於距離地面 **14.5** 米深的全/高度風化花崗岩，而石層則位於地面約 **30** 米之下。工程中，用了“**OSTERBERG LOAD CELL**”載荷試驗去驗證採用筏式基礎坐於全/高度風化花崗岩的可行性。試驗結果顯示位於基礎水平的全/高度風化花崗岩層的容許承載力是高於擬建大廈的設計荷載。本文旨在描述如何使用“**OSTERBERG LOAD CELL**”作爲是次載荷試驗，其試驗結果及在建築期間住宅大廈沉降監測的情況。

MULTI-STOREY BUILDING ON RAFT FOUNDATION IN HONG KONG

W Y WONG[1], Andy L K NG[2] and Martin K T CHAN[3]

Abstract: A 29-storey residential building with a 3-level basement carpark was proposed to be supported by a raft foundation founded on in-situ soil at 14.5 m below ground level. Bedrock is at approximately 30 m below the ground level. Plate load tests using Osterberg Load Cells were conducted to confirm the feasibility of adopting raft foundation on completely to highly decomposed granite (C/HDG) instead of deep foundation on bedrock. Tests results proved that the allowable bearing capacity of the C/HDG at the foundation level is greater than the bearing pressure to be imposed by the proposed building. This paper describes the method of plate load test using Osterberg Load Cell and presents results of the tests and the settlement monitoring during construction of the proposed building.

INTRODUCTION

The site is located at No. 1 Homantin Hill Road, three sides of the site boundary are surrounded by 30° to 40° downward slopes and the remaining side abuts an existing 6-storey building on the adjoining lot. The layout of the site and the surrounding features are shown in Figure 1.

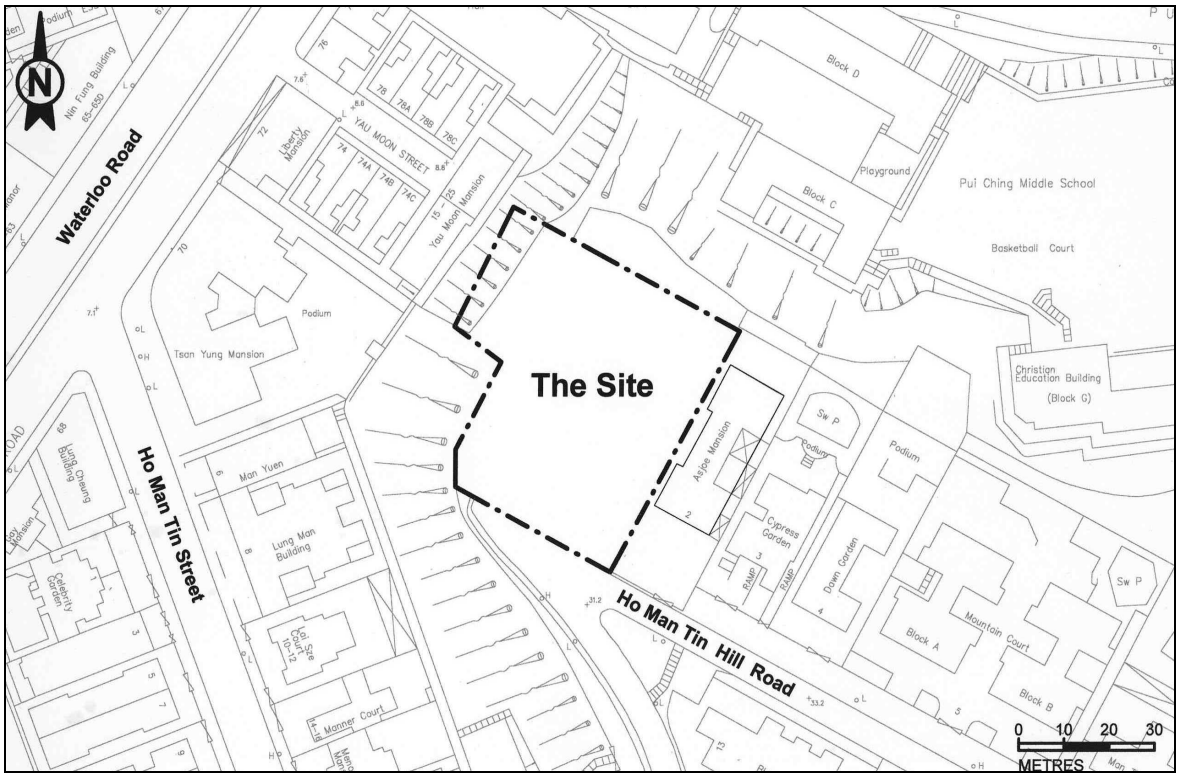

[1] Associate Director, Fugro (Hong Kong) Limited
[2] Principal Engineer, Fugro (Hong Kong) Limited
[3] Project Engineer, Fugro (Hong Kong) Limited

Figure 1 – Site Location Plan

The proposed development is a 29-storey residential building with a 3-level basement carpark. The proposed basement has a plan dimension of approximately 35 m x 50 m and a maximum depth of 14.5 m below existing ground level. The proposed residential building is located at the central portion of the basement and its footprint covers about one-third of the plan area of the basement (see Figure 2A).

The total design load of the residential building and the basement is approximately 550 MN and it was estimated that the maximum design bearing pressure over the footprint of the basement will be about 700 kPa based on a Young's Modulus (E) of the founding soil using a correlation of E=1.0N MPa.

FOUNDATION OPTIONS

A ground investigation comprising 15 drillholes and 6 trial pits was carried out to acquire sub-soil information for the design of foundation and basement excavation works. The ground investigation results revealed that the sub-soil geology was fairly uniform across the site with in-situ soil (completely decomposed granite) encountered at about 2 m below ground level and bedrock at approximately 30 m below ground level. The average blow count of the Standard Penetration Tests (SPT-N values) performed at the proposed level of the basement was 80 and the N value gradually increased with depth. The groundwater level was approximately 20 m below ground level. The drillhole locations and representative geological section of the site are shown in Figures 2A and 2B respectively.

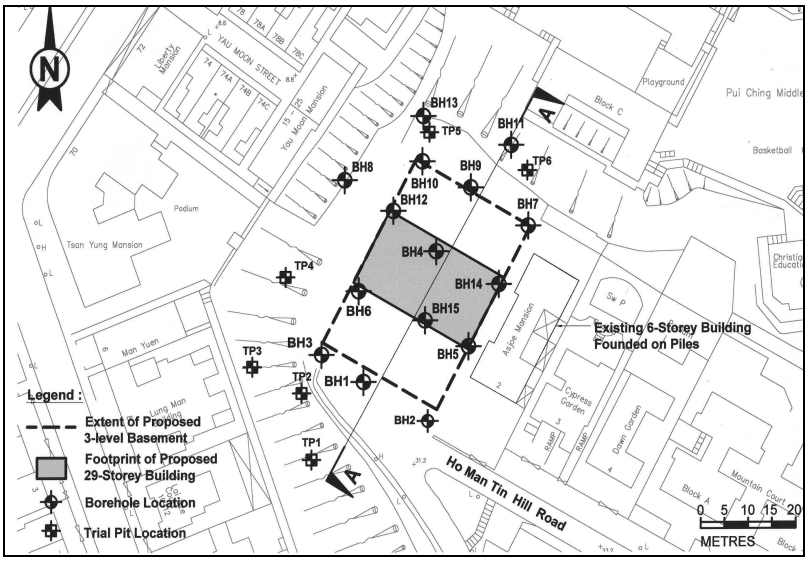

Figure 2A – Site Layout Plan

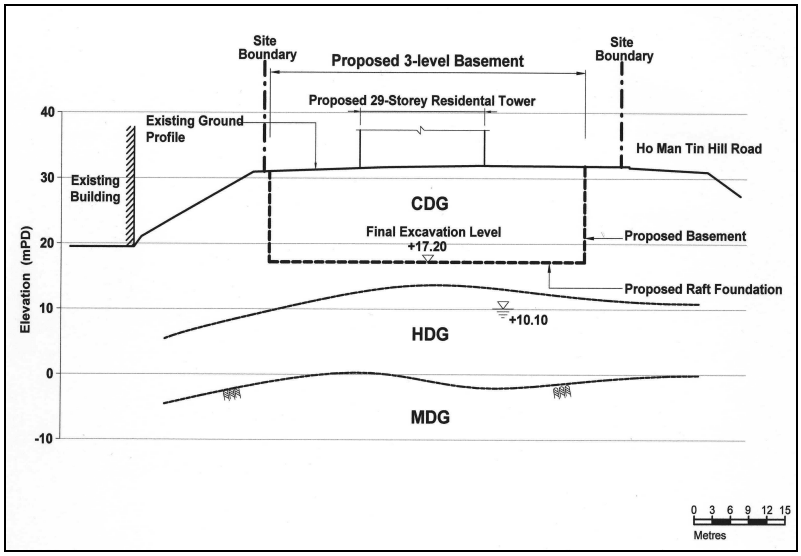

Figure 2B–Geological Section (Section A-A)

Based on the geological conditions and the building load, a piled foundation, such as bored piles founded on bedrock, would normally be adopted to support the residential building. However, in view of the configuration of the structure and the ground conditions, it was considered that it is feasible to use a raft to support the residential building but confirmation of the allowable bearing capacity of the founding stratum has to be carried out.

RAFT FOUNDATION

To verify the allowable bearing capacity of the raft, plate load test is normally conducted at the proposed founding level using the conventional method, in which the reaction load is provided by a kentledge that made up of concrete blocks or reaction piles as shown in Figure 3. However, the conventional method was unsuitable for this site because it could only be carried out after the excavation had reached the founding level. If the test results found that the bearing capacity at the tentative founding level was less than the required bearing pressure then it would be too late to change to another type of foundation. Therefore, the plate load test using Osterberg Load Cell (O-cell) was used for this site.

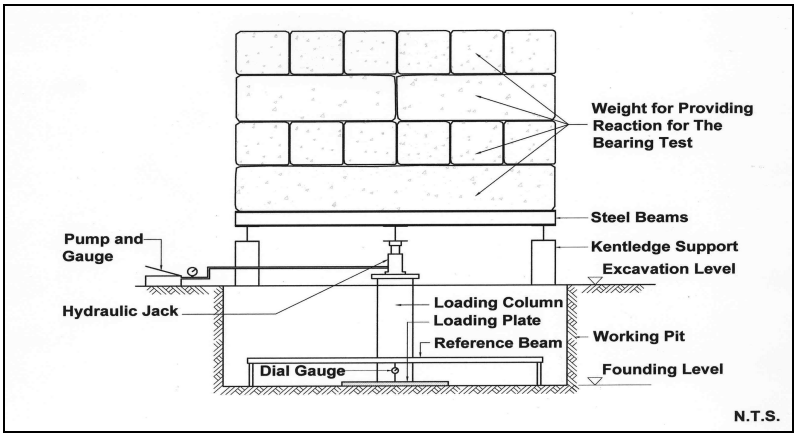

Figure 3 – Setup of Conventional Plate Load Test

OSTERBERG LOAD CELL

Osterberg Load Cell (O-cell) is a specially designed hydraulic jack developed by Professor Jorj O. Osterberg of the U.S.A. in 1980s for load testing in bored piles or deep

foundation. The O-cell is a high capacity, hydraulically driven, sacrificial jacking device installed within the testing pile with steel plates attached to the top and base of the cell. This assembled hydraulic jack-like device will then be attached to reinforcing steel cage and placed at the bottom or/and some distance above the bottom of a sacrificial bored pile. When hydraulic fluid is pumped into the cell, it exerts forces in two directions, upward against side shear and downward against end bearing of the test bored pile. End bearing provides reaction for the side shear portion of the load test and vice versa.

With this arrangement, the test will automatically separate the two resistance forces, namely the end bearing and the upward shear resistance. Rod extensometers can be connected to the top and bottom plates of the cell for recording the movement of the plates during the test. Instrumentation including vibrating wire strain gauges, linear vibrating wire displacement transducers can also be installed in the pile shaft or attached to reinforcing steel cage.

SEP UP OF THE PLATE LOAD TESTS

For this project, two sacrificial 1.2 m-diameter concrete bored piles were constructed at two selected locations of the site for performing the loading test. The selected locations (i.e. locations PLT1 and PLT2) of the tests are shown in Figure 4. These locations were selected based on that the SPT-N values adjacent to these two locations indicated that soil stratum may be relatively weaker when comparing with the SPT-N values at other drillholes locations.

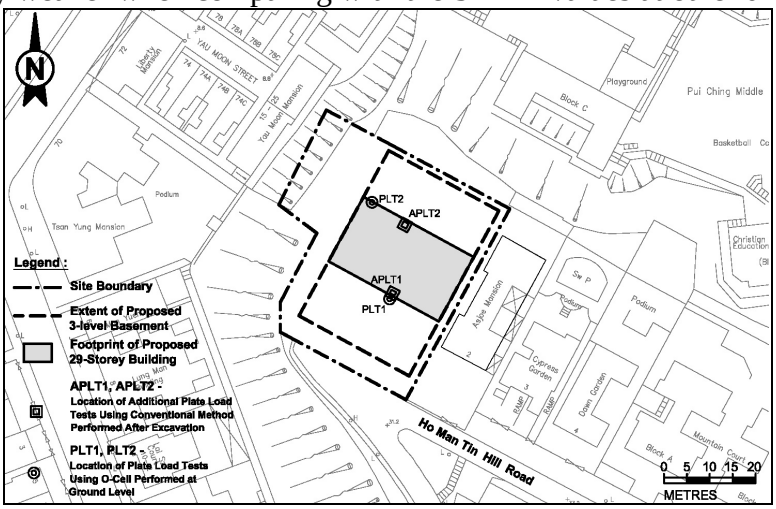

Figure 4 – Selected Location of Plate Load Test

The set up of the loading device was formed by assembling two 75 mm-thick and 900 mm-diameter circular steel plates to the top and bottom of a 230 mm-diameter O-cell. The O-cell and the assembled loading device are shown in Figures 5A and 5B respectively. Steel rod extensometers, strain gauges, transducer extensometer and displacement transducers were installed for monitoring the displacement and deformation of the test piles. Instrumentation set up of the test pile is shown in Figures 6A and 6B.

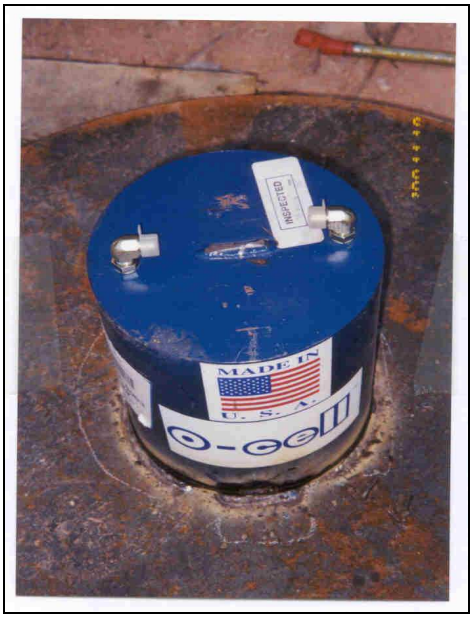

Figure 5A – 230 mm-dia. Osterberg Load Cell

Figure 5B – Assembled jacking device attached to the bottom of reinforcing steel cage

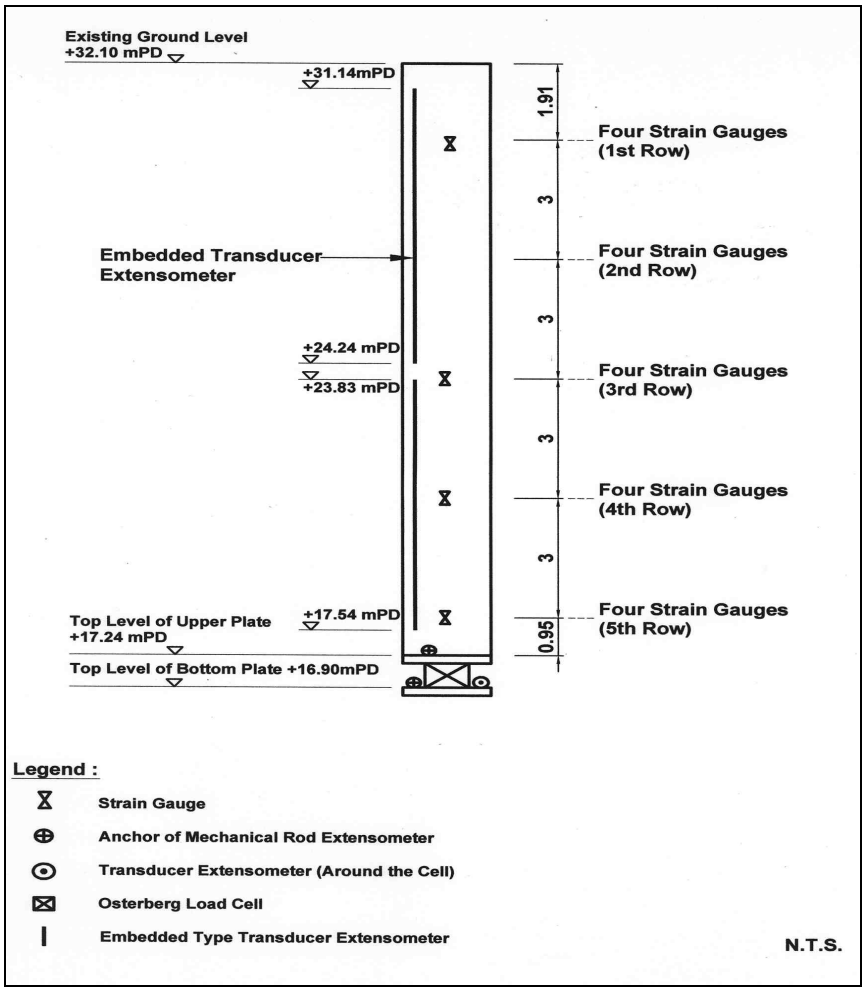

Figure 6A – Instrument Positions (Longitudinal Section)

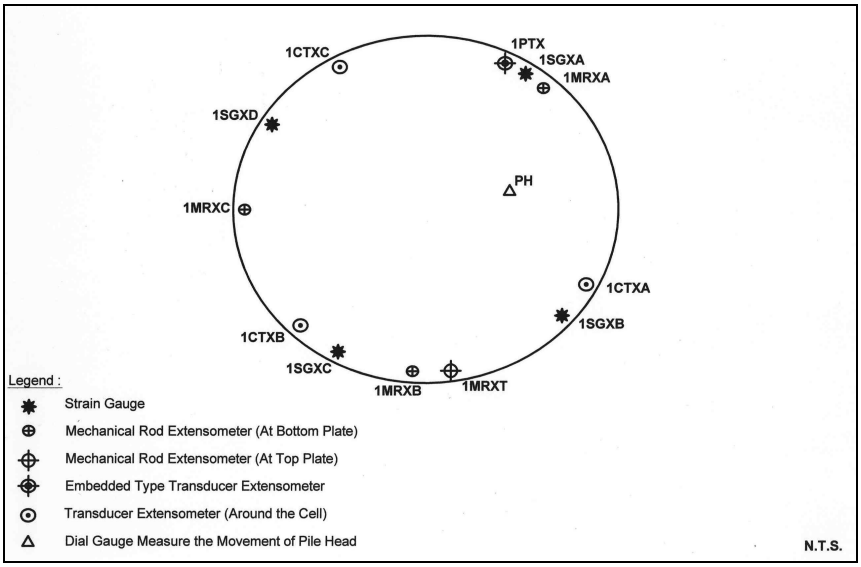

Figure 6B – Instrument Positions (Transverse Section)

After the pile shaft had been formed, the base of the hole was then cleaned carefully to avoid formation of loose layer above the bearing surface. Cement grout was then placed on the bottom of the hole before lowering the reinforcing steel cage into the hole to ensure uniform bearing over the bottom. The shaft of the bored pile was then filled with concrete.

The upper ends of rod extensometers and dial gauges for recording their movement during the test are shown in Figure 7. All dial gauges were mounted on a long reference beam staked to the ground a sufficient distance from the pile location to secure it in a fixed position (Figure 8). The deformation of the reference beam was also checked using a survey level. Signal cables for collecting data from strain gauges and transducers were connected to a central automatic data logging system as shown in Figure 9.


Figure 7 – Upper ends of extensometers


Figure 8 – Reference Beam


Figure 9 – Central Automatic Data Logging System

TESTING PROCEDURES

Testing commenced after the concrete of the pile shaft has gained sufficient strength. The testing pile was loaded by the O-cell and the reaction to the loading is provided by the friction on the pile shaft. This loading procedure has the advantage that the load was applied directly at the founding level instead of being applied at the top of the pile. If a top loading method was adopted, the applied load must overcome the shaft friction before the base resistance was mobilised. For a deep pile, the total shaft friction might be much higher than the base resistance and a very high applied load would be required. During the test, the applied load and the penetration of the base plate of the cell into the ground were measured by pressure gauge and extensometers respectively. At the same time the stress in the pile

shaft was measured by the strain gauges and the vertical movement of the pile head was also monitored by dial gauges.

A cyclic loading method including 4 cycles with a maximum testing load of 1800 kN, which is equivalent to an applied pressure of 2830 kPa (higher than 3 times of the design bearing pressure), was adopted for the tests. The loading was increased in 3 increments until the maximum test load of the first cycle was reached. Each increment was held until the rate of settlement was less than 0.05 mm in 10 minutes for a period of 30 minutes. Upon reaching the maximum test load, the load was maintained for 6 hours and the readings were taken at 1 hour interval. The test pile was then unloaded in 4 decrements and was allowed to recover for a period of 1 hour after unloading. The next loading cycle was then commenced until completion of the 4 loading cycles. The maximum test load of the 4th loading cycle was maintained for 3 days, during which time the settlement was monitored at fixed time interval, i.e. 8 hours.

RESULTS OF THE PLATE LOAD TESTS

The load-settlement curve of the tests at locations PLT1 and PLT2 are presented in Figure 10A and 10B respectively.

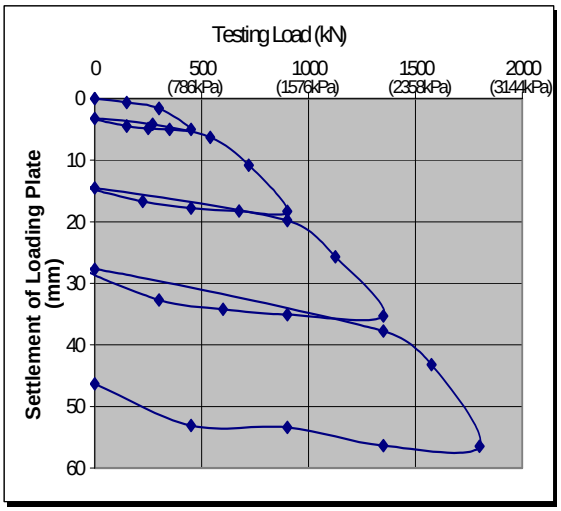

Figure 10A – Load-settlement Curve of Plate Load Test at PLT1

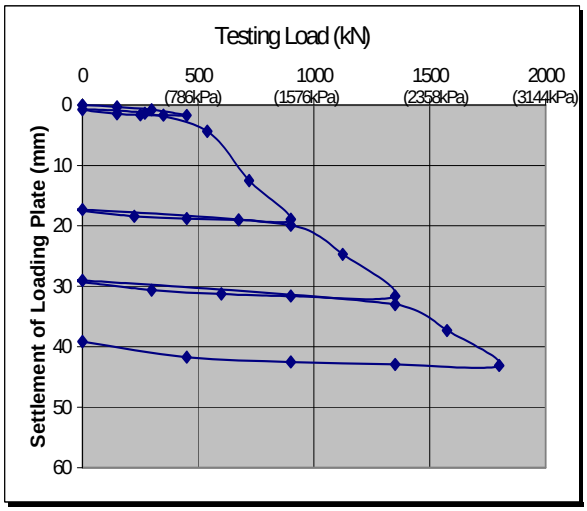

Figure 10B – Load-settlement Curve of Plate Load Test at PLT2

The test results indicate that the maximum applied pressure of the test, 2830 kPa (i.e. total load = 1800 kN) has not reached the ultimate bearing capacity of the soil stratum. As the test has not reached the ultimate bearing pressure, one third of the maximum applied pressure was therefore adopted as the allowable bearing pressure (i.e. 943 kPa). Under this applied pressure, maximum settlement at testing pile PLT1 and PLT2 was 8 mm and 7 mm respectively.

A finite element computer program – SAFE based on the method of Joseph E. Bowles (Ref. 6) was used to estimate the settlement of the raft foundation at the design loading. The predicted maximum settlement of the raft was 23 mm and the differential settlement was 1 in 1150. In the finite element computer program, an ‘equivalent modulus of elasticity’ – ‘E’ of

the bearing stratum was estimated based on the following expression for a rigid loaded area with a diameter – d on an elastic continuum:

$$\text{'E'} = \frac{q}{\rho}\frac{\pi}{4} d\,(1 - \nu^2)$$

where q is the average load intensity, ρ is the settlement and a poisson ratio (ν) = 0.3 was adopted. Based on results of SPT-N values at nearby drillholes and the plate load tests at PLT1 and PLT2, the relationship between 'E' and SPT-N value is given by 'E' = 0.7 N to 1.7 N (MPa). 'E'=1.0N MPa was adopted in assessing the settlement of the raft foundation under the design loading.

DESIGN VERIFICAITON

Upon completion of the plate load tests using the O-cell method, the results of which indicating that the bearing capacity of the soil stratum at the intended founding level is adequate, the basement excavation works were then proceeded. In order to compare the results of the plate load tests between using O-cell and the conventional method, two additional plate load tests using conventional kentledge method were carried out at the intended founding level upon completion of the excavation works. The general view and set up of the additional plate load tests are shown on Figures 11A and 11B respectively. The results of the additional plate load tests were in general agreement with that by the O-cell.

Figure 11A – General View of Plate Load Test Using Conventional Method

Figure 11B – Testing Set up of Plate Load Test

To monitor the settlement of the raft foundation during the construction stage, eight settlement check points were installed on the core structure of the high-rise building until completion of the construction works. No noticeable settlement and tilting were measured up to the completion of the building structure in late 2002.

CONCLUSIONS

A reliable prediction of the allowable bearing capacity of the sub-soil stratum at tentative founding level is a critical task for the production of a cost-effective foundation design. In this project, the use of O-Cell for verification of the bearing capacity of the sub-soil stratum for the design of raft foundation is an innovative and successful approach.

Significant savings on both construction cost and time have been achieved by eliminating the use of piled foundation for the high-rise building.

REFERENCES

Inter Pacific Ltd (1988). "Report on ground investigation work for No. 1 Homantin Hill Road".

Soil and Materials Engineering Co. Ltd (1998). "Laboratory Test Report", Report No. 98SR1461 and 98SR1562.

Chan, K.T. and Ng, L.K. (1999). "Report on Plate Load Test Proposal", Report No. S00301.09, Fugro (HK) Ltd.

Chan, K.T. and Ng, L. K. (1999) "Geotechnical Report on Foundation Design", Report No. S00301.07B, Fugro (HK) Ltd.

D.J. Sweeney and Ho C.S. (1982) "Deep Foundation Design Using Plate Load Tests", Fugro Guld Inc and Fugro (HK) Ltd. Respectively.

Bowles, J.E. (1988) "Foundation Analysis and Design", 4th Edition.

ACKNOWLEDGEMENT

The authors wish to thank Sun Hung Kai Engineering Ltd. for their permission to publish this paper and the review of the paper by Ir C S Ho and Ir Y C Koo is gratefully acknowledged.

穿越沉積岩地層 T7 幹道隧道的支護設計

楊文武　　梁文添　　盧耀宗
香港茂盛土力工程顧問有限公司

TEMPORARY SUPPORTS FOR TUNNELS OF TRUNK ROAD T7 IN METASEDIMENT GROUND

W.W. Yang, Man-Tim Leung and Joseph Lo
Maunsell Geotechnical Services Ltd., Hong Kong

撮要

位於馬鞍山區的 **T7** 幹道，總里程 **3.2** 公里，爲雙向雙車道主幹道。幹道西端連接馬鞍山公路，東端連接西沙公路，工程完工後將形成直接連接沙田和馬鞍山北的快速通道。本工程需穿過沉積岩和花崗岩岩體含斷裂 / 接觸帶的地層建造兩條總長約 **380** 米、跨度分別爲 **12** 米和 **16** 米的隧道，採用鑽爆法施工。在這種具複雜地質條件的地區建造最大開挖面積達 **148M2** 的大跨度隧道，其開挖支護設計具有挑戰性。本文討論有關隧道臨時支護設計和施工過程中實測的地層反應。

TEMPORARY SUPPORTS FOR TUNNELS OF TRUNK ROAD T7 IN METASEDIMENT GROUND

W.W. Yang [1] , Man-Tim Leung[2] and Joseph Lo[3]

Abstract: Trunk Road T7 is a dual 2-lane carriageway of 3.2 km long at the outskirt of Ma On Shan Town connecting Ma On Shan Road at the western end and Sai Sha Road at the eastern end. Upon completion, the road system would provide a direct link for the traffic between Sha Tin and to the north of Ma On Shan. Two tunnels, of approximate 380m total length and of 12m and 16 m span respectively, were bored in the rock mass of meta-sediments and granitic origin. A fault/contact intersecting both tunnels was identified. It posted a difficult and challenging job for the excavation and supports for the tunnels of large span with a maximum excavation section of 148m^2 in an area of complex geology. The design philosophy of temporary supports is discussed in this paper. Some monitoring results of ground response during tunnel construction are also presented.

INTRODUCTION

A new Trunk Road T7 in Hong Kong was proposed to connect the Ma On Shan Road in the south with the Sai Sha Road to the north as depicted in Figure 1(a). The Trunk Road T7 is designed as a dual carriageway of approximately 3.2 km in length, comprising 'at grade' and elevated sections. The alignment of Trunk Road T7 runs along the foot slopes of the Ma On Shan to Tate's Cairn Ridge which rises steeply to the south-east. At the Junction J22 near the northern end of T7 at the Sai Sha side, two relatively short sections of tunnels would pass through a Ma On Shan Mountain by drill and blast construction method to form the westbound off-slip Underpass C and on-slip Underpass D as shown in Figure 1(b). This project was tendered in December 2000. China Harbour Engineering Company (Group) won the construction contract in January 2001 of about HK$1.4 billion contract sum. Maunsell Consultants Asia Limited is the design engineer for the project.

The Underpass C and Underpass D tunnels are of 12m and 16m span respectively and with a total length of about 380m. The excavation cross-sectional areas are about 117m^2 and 148m^2 respectively for Tunnel C and D respectively. Two tunnels were driving approximately curved parallel on plan from the westbound at road level +20mPD towards the eastbound at road level +30mPD, with a minimum ground cover of about 5m. On the other hand, the minimum separation of Tunnels C and D is about 25m centre to centre which gives a minimum

[1] Senior Engineer, Maunsell Geotechnical Services Ltd.
[2] Project Engineer, Maunsell Geotechnical Services Ltd.
[3] Executive Director, Maunsell Geotechnical Services Ltd.

rock pillar width in-between the tunnel openings of only about 9m minimum. The major tunnel sections would be bored in rock mass of meta-sediments and granitic origin. A fault/contact zone intersecting both tunnels was identified during detail design stage (see Figure 1(b)). It posted a difficult and challenging job for the excavation and supports for the tunnels up to 16m span in an area of complex geology (see Figure 2).

This paper discusses the design philosophy of temporary supports. Some monitoring results of ground response during tunnel construction are also discussed.

DESCRIPTION OF GEOLOGICAL CONDITIONS

The underpasses are located in an area of complex geology, with a fault having been conjectured to closely follow the line of the eastern sections of the underpasses, through the portal locations. This fault divides the area into two significantly different elements, the northern comprising fine and medium grained granites, and the southern consisting of metasediments, fault breccia, and rhyolite. As a result of the ground movements the more brittle metasediments appear to contain a significant number of randomly orientated fissures, although frequently incipient. The general geological sections of the tunneling area as inferred from the results of the ground investigation are shown in Figures 3 and 4. The ground materials encountered during the tunnel excavation are:

Granites

The granites comprise both fine and medium grained and fine grained. The upper sections of the deposit are generally completely decomposed. At the level of the tunnel crown, the material is expected to be slightly weathered and moderately strong to strong. The joint surfaces frequently contain kaolin, chlorite and may be stained with iron or manganese.

Metasediments

The metasediments are generally grey and light fine grained or cryptocrystalline materials, with a complex interaction to the adjacent faulted and brecciated deposits. The strength of the material is frequently up to moderately strong but it appears that it is quite brittle. The structure of the material is relatively uniform but it is cross cut by many randomly oriented incipient fractures along which parting during coring has occurred. These fractures are frequently infilled with quartz, but penetrative weathering of the joint surfaces was evident when no quartz was present. The closely spaced joints are frequently coated with chlorite and calcite. This led to a general low recovery of core, and attendant low RQD values.

Faulted, Brecciated and Intruded Zone

These grey spotted white materials vary in strength from weak to moderately strong. The deposits vary according to the original rock type and it is suspected that the rhyolite may have intruded the fault zones also. The total core recovery varied markedly but RQD was frequently above 50%.

ROCK MASS CHARACTERIZATION

A rock mass is generally weaker than its constitute rock material as the mass contains structural weakness planes such as joints and faults. The stability of an excavation in a jointed rock mass is influenced by many factors including strength of intact rock, frequency of jointing, joint strength, confining stress, and pressure of water. The best practical way in which those factors could be taken into account is by applying rock mass classification methods. Quantitative classification of rock mass has become popular in the last decades, and justifiably so, since it provides a quick means of assessing rock mass quality, making comparison of previous experience and estimating support requirements. Two comprehensive classification systems have stood up, the Norwegian Geotechnical Institute (NGI) Q System developed by Barton, Lien and Lunde (1974) and Geomechanics Classification System by Bieniawski (1979). Both systems are substantially for civil engineering applications (Stacey and Page, 1986).

For the purpose of establishing appropriate level of temporary supports, the Norwegian Method of Tunneling (NMT) based on the Q system was used as the main guide in assessing systematic support requirements for the tunnels in rock mass. It should be noted that although application of the Q systems is straight forward, considerable insight, intuition, experience and engineering judgement are required. The Q System classification based on the three aspects of rock block size (RQD/J_n), joint shear strength (J_r/J_a), and confining stress (J_w/SRF). The rock mass quality number Q is defined as

$$Q = \frac{RQD}{J_n} \cdot \frac{J_r}{J_a} \cdot \frac{J_w}{SRF} \qquad (1)$$

Where, J_n is the joint set number; J_r is the joint roughness number; J_a is the joint alteration number; J_w is the joint water reduction factor, and SRF is the stress reduction factor.

The Q System classification was applied in this project. The results of rock mass quality assessments for expected metasediments based on available bore hole logs within this project area are given in Table 1 for a tunnel of 16m span. The likely ranges of Q to present the percentage of rock mass to exhibit a given rock quality for the depth ranges beneath rock head level of 0m to 10m; 10m to 20m; 20m to 30m; 30m to 40m; and greater than 40m are given. The Q ranges as shown in Table 1 are corresponding to NGI support classes 1 to 8 for a 16m span tunnel. In order to account for the increased degree of freedom of the blocks movement caused by the creation of extra free faces in the vicinity of portals, the Q values would be modified by multiplying the Jn value by 2 for tunnel portals. This would increase the support requirements and reduce shear strength and deformation characteristics of rock mass.

Table 1: Estimated Q range as percentage of total rock mass for a 16m span tunnel

	Support Class							
Depth	**8**	**7**	**6**	**5**	**4**	**3**	**2**	**1**
Range	**Q range**							
	< 0.003	**0.003 - 0.12**	**0.12 - 0.17**	**0.17 - 0.29**	**0.29 - 0.76**	**0.76 - 1.66**	**1.66 - 3.0**	**> 3.0**
0-10m	0	52	12	20	15	0	0	1
10-20m	0	41	8	24	17	7	3	0
20-30m	0	0	2	36	25	24	8	4
30-40m	0	0	5	30	59	5	0	0
>40m	0	0	0	0	36	25	40	0

DESIGN OF TEMPORARY SUPPORTS

Tunnels in Rock

The principal objective in the design of tunnel supports is to help the rock mass to support itself. Systematic temporary supports consisting of an integrated rock reinforcement of dowel and shotcrete would effectively act together with rock mass to limit rock deformation, and therefore help the surrounding rock mass in a self-supporting and stable state with an adequate safety during construction until the permanent tunnel lining could be installed. One of the most useful of Q-system is the support selection chart in which the tunnel support requirements are presented in a function of rock mass quality and ratio of the tunnel span to ESR (Excavation Support Ratio) that represents the safety of an excavation. Table 2 shows the temporary support guidelines corresponding to support classes for a 16m span tunnel based on the NGI Q-System (NCA, 1994). Analytical methods have been used to assess the stability of tunnel excavation and determine the requirement of support class 8 which was expected to be encountered the varying conditions of weak or mixed ground.

Table 2: Temporary Support Guidelines for a 16m span tunnel

NGI Support Class	**Minimum Systematic Support Requirements**	**Minimum Monitoring Requirements**
1 & 2	**Feature Dowels:** Installed in walls and crown as necessary. **Systematic Dowels:** none. **Shotcrete:** Min. 25mm applied as necessary to local fracture zones.	Convergence monitoring unlikely to be necessary
3	**Feature Dowels:** Installed in walls and crown as necessary. **Systematic Dowels:** 4m long on 2.4m grid in crown. None in walls. **Shotcrete:** Min. 25mm in crown. None in walls.	Convergence monitoring unlikely to be necessary
4	**Feature Dowels:** Installed in walls and crown as necessary. **Systematic Dowels:** 4 m long on 2.2 m grid in crown and walls with faceplates. **Shotcrete:** 70 mm in crown. None in walls.	Convergence monitoring at max. 34m intervals
5	**Feature Dowels:** Installed in walls and crown as necessary. **Systematic Dowels:** 4 m long on 1.8 m grid in crown and walls with faceplates. **Shotcrete:** 70 mm fibre reinforced in crown. 40 mm fibre reinforced in walls.	Convergence monitoring at max. 24m intervals
6 & 7	**Feature Dowels:** Installed in walls and crown as necessary. **Systematic Dowels:** 4 m long on 1.5 m grid in crown and walls with faceplates. **Shotcrete:** 120 mm fibre reinforced in crown and walls	Convergence monitoring at max. 1.2m intervals
8	**Steel Ribs:** Strengthened UC ribs of Grade 43A at 1.2 m centres with fibre reinforced shotcrete lagging and pipe-roof pre-supports. Subject to detailed analyses.	Convergence monitoring at max. 1.2m intervals

Tunnels in Weak or Mixed Ground

An assessment of the internal stability of the tunnel excavation in weak or mixed ground and including the portals has been made using Phase^2, a finite element program. A simplified model in two dimensions was established to simulate the complicated three dimensional behavior of staging excavation and ground relaxation. The Mohr-Coulomb constitutive model was used to present the plastic behavior of rock mass and roof canopy. Three elements of support have been included in the analyses, as follows:

- inclusion of pre-installed pipe roof canopy in the tunnel crown of about 120deg sectional zone, comprising one or two rows of 50mm diameter, 6m long pipes at 500mm center-to-center spacing through which grout would be pumped.
- steel arch ribs and an invert strut.
- fibre reinforced shotcrete to be sprayed immediately, covering the ribs by a minimum thickness of 40mm.

Due to the relatively large spans of the tunnels, the excavations were considered to be in stages, so that supports can be installed as soon as possible after exposure thereby not allowing significant deleterious convergence to occur. A two stage excavation strategy of Underpass D in a mixed ground condition is a top heading (maximum 7m height) with one row pile roof canopy , lower bench staging excavation and steel ribs of UC152mm x 152mm x 30kg/m with 200mm thick fibre reinforced shotcrete and without invert strut. The predicted ground responses are:

- vertical deflection at the tunnel crown in the order of 7mm and the invert heave of about 11mm at stage 1 top heading excavation as shown Figure 5(a), and
- responses of the composite temporary supports at both excavation stages are within the carrying capacity of the shotcrete-rib composite supports presenting in the interaction of normalized bending moments and thrusts as depicted in Figure 5(b).

TUNNEL EXCAVATION AND MONITORING

Most rock tunnel sections were excavated by conventional blasting method using cartridge explosives. In the poor and extremely poor rock masses, and where blasting might not be permitted, mechanical excavation by stages would be carried out, with supports installed close to the face for limiting ground deformations and convergence, and ensuring that ground movements would not exceed the limits. Prior to starting the excavation works from the weak or mixed ground section for construction of roof support canopy, probe holes of 64mm diameter were drilled in a manner to ensure that one probe hole is maintained to a distance of at least 20m ahead of the tunnel working face. A single probe hole was established in the tunnel crown and angled upwards at a gradient of about 1(V):3(H). Where a worse ground condition is encountered or expected, probe holes at the tunnel spring-line on either side of the face angling outwards at about 16° were also established at least 20m ahead of the face. A minimum lap of 1m was maintained between successive sets of probing.

Monitoring and the facility to upgrade support in the light of any adverse or unexpected results are also essential parts of the design and construction process. Monitoring and instrumentation along the alignment of the tunnel were established on the basis of the detailed design. Site monitoring during the whole construction process was controlled by relating the derived figures to alert, action and alarm levels. The instruments have been installed both within the tunnels to monitor the ground behavior, and above the tunnels, particularly near the portals, to monitor the effects of tunnel construction at the ground surface and existing utilities. Prior to the commencement of construction, instrumentation at some critical locations was installed to establish baseline readings. At the tunnel portals, inclinometers and survey reference points were installed to monitor the ground movements. Piezometers at selected

locations were installed to monitor the groundwater levels. Within the tunnels, convergence monitoring during excavation has been carried out using 3 or 5 point arrays, and the monitoring locations and frequency were determined according to the excavation stages, the support class.

The measured results of convergence arrays at a section of Tunnel D in a mixed ground are presented in Figure 6(a). It can be seen the convergence after top heading excavation was about 0.1% and increased up to about 0.3% after bench excavation (Array CLL1). The closure of walls at springline was up to 0.15% (Array CLU); and the closure of walls below springline after bench excavation was less than 0.05% (Array CLD). The crown settlement after top heading excavation was about 10mm and increased to about 15mm after bench excavation (see Figure 6(b). Comparison measured ground response with predictions showed a reasonable correlation.

DISCUSSIONS

Two large span tunnels of 380m total length were successfully excavated in meta-sediments, fault breccia/intruded zone and granitic origin. The NGI Q system was adopted to estimate systematic temporary supports of an integrated rock reinforcement of dowel and shotcrete for tunnels in rock. For tunnels in weak or mixed ground, staging excavation with temporary supports of steel ribs and shotcrete was designed with aid of numerical analysis methods. A tightly controlled excavation and comprehensive monitoring scheme were implemented during tunnel construction. Ground movements during the excavation showed reasonable correlation to the estimation.

REFERENCES

Barton, N., Lien, R. and Lunde, J. (1974), "Engineering classification of rock masses for the design of tunnel support", Rock Mechanics, 6(4), pp.189-236.

Bieniawski, Z.T. (1979), "The geomechanics classification in rock engineering applications", Proceedings, 4th International congress on rock mechanics, ISRM. Montreux, A.A. Ballkema, Rotterdam, 2, pp.41-48.

NCA (Norwegian Concrete Association) (1994), Spayed concrete for rock support – Technical specification and guidelines, Publication nr 7.

Phase^2: finite element analysis and support design for excavation, User's Guide, 1998-2001 Rocscience Inc.

Stacey, T.R. and Page, C.H. (1986), Practical handbook for underground rock mechanics, Tarans Tech Publications.

ACKNOWLEDGEMENTS

This paper is published with the kind permission of the Territory Development Department (TDD) of HKSAR who the authors would like to thank. The views expressed in this paper are those of the authors and not necessarily those of the TDD.

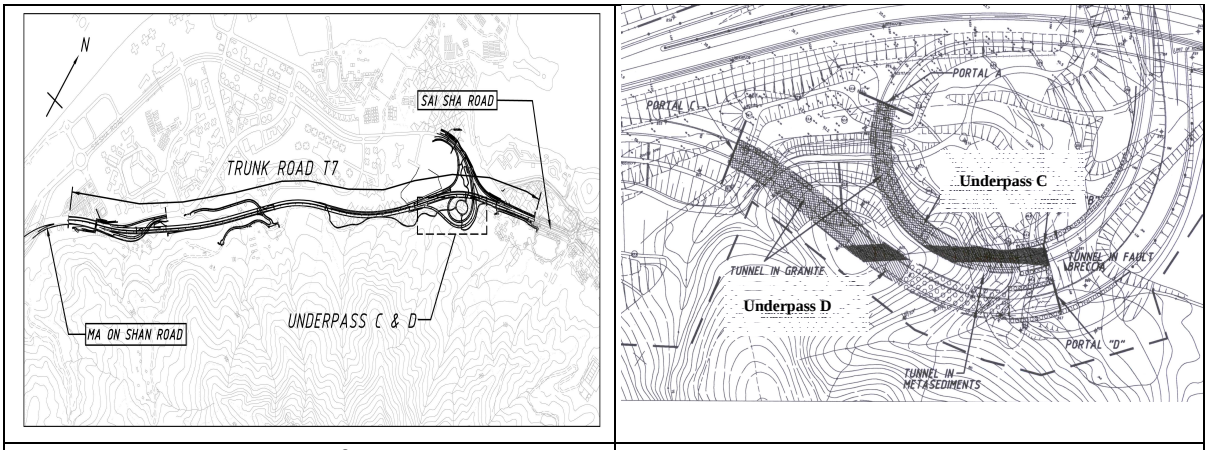

(a) General layout plan of Trunk Road T7 | (b) Tunnel alignment

Figure 1: Alignment of T7 and tunnels

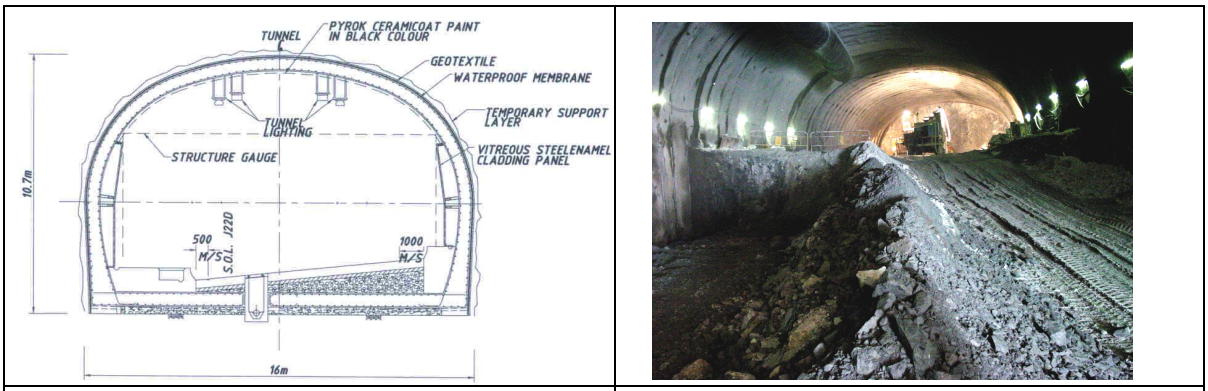

(a) Cross-section of Underpass D | (b) Tunnel excavation in stages

Figure 2: Typical tunnel section and an excavation photo

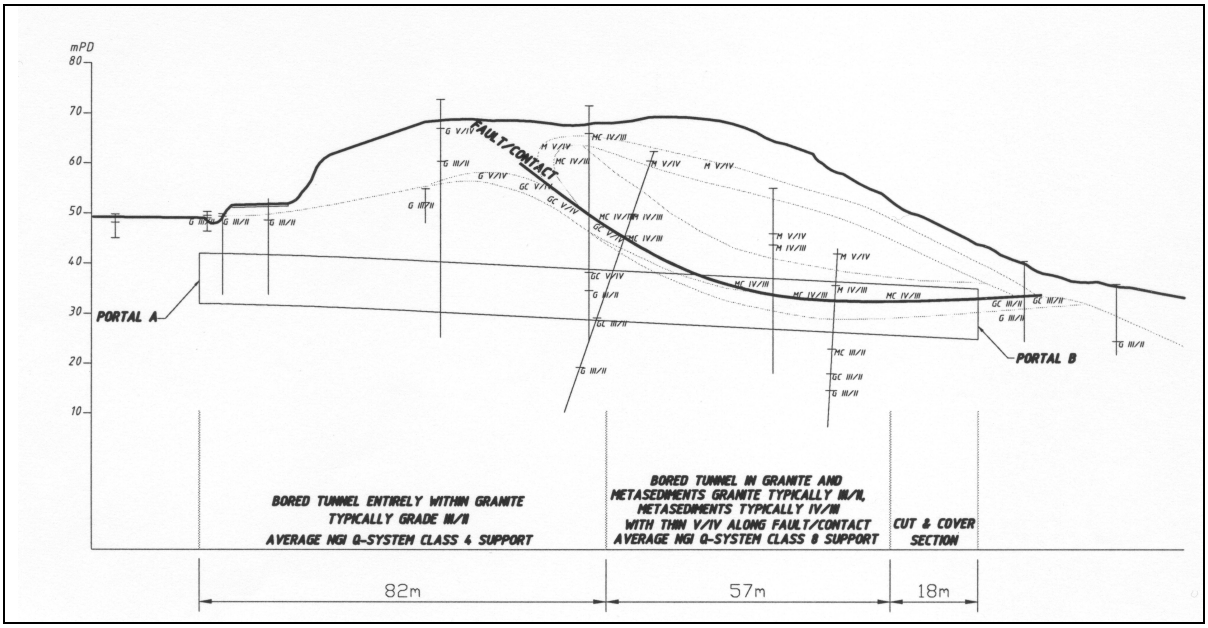

Figure 3: Longitudinal geological section of Underpass C

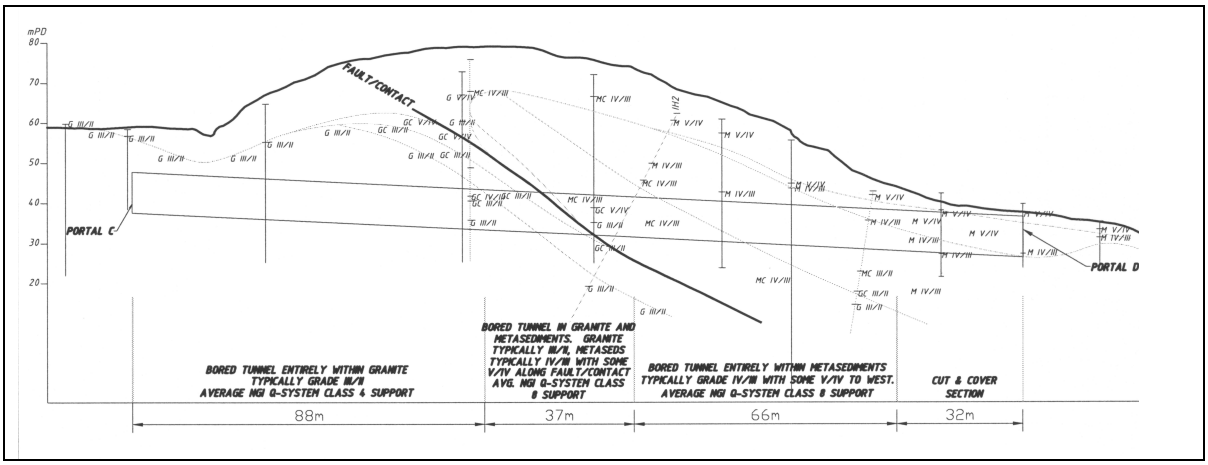

Figure 4: Longitudinal geological section of Underpass D

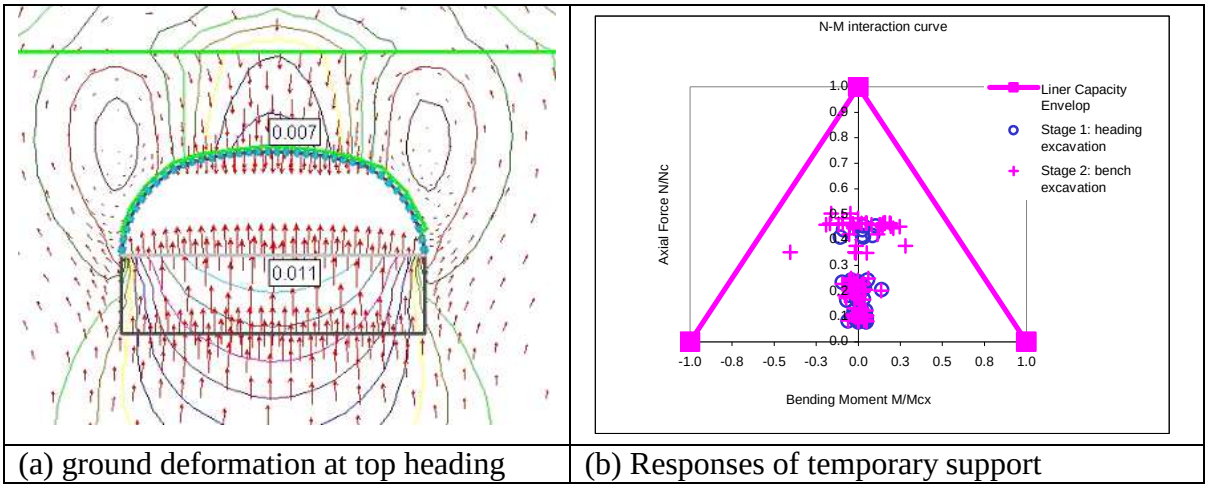

(a) ground deformation at top heading | (b) Responses of temporary support

Figure 5 – Numerical simulation of staging excavation and supports

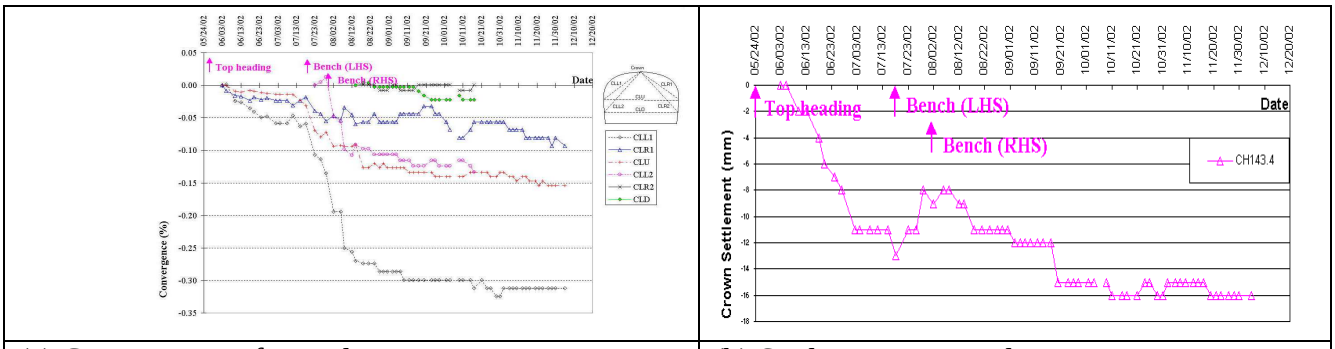

(a) Convergence of tunnel | (b) Settlement at tunnel crown

Figure 6: Measured deformation of tunnel opening at Ch. 143.4 of Underpass D

化複雜爲簡單的一個岩土工程個案

嚴建平
香港特別行政區政府建築署
陳宇華
香港特別行政區政府土木工程署

A CASE HISTORY OF SIMPLE SOLUTION TO A COMPLEX GEOTECHNICAL ENGINEERING PROBLEM

K P Yim
Architectural Services Department
Government of the Hong Kong Special Administrative Region
D Y W Chan
Civil Engineering Department
Government of the Hong Kong Special Administrative Region

撮要

在一個公路的改善項目中，需要興建一座行人天橋。根據項目的原有計劃，需要將一段山坡移去，以騰出空間建造通往天橋的梯級和斜路。工程需要將一段十二米高、五十米長的沉箱護土牆折去，以便興建另一幅十七米高雙排的大口徑樁護土牆。設計和建造一幅十七米高雙排的大口徑樁護土牆，是一項富挑戰性和技術複雜的工程。該項設計涉及多方面的資料搜集，並需要嘗試多個分析模型，進行複雜的電腦計算。

在接近完成詳細設計和準備招標的階段時，我們對這項目作出了全盤的檢討，在預計工程的六千多萬元費用中，四千多萬元屬於岩土工程，而施工時會相當困難和需時約三十六個月。在這一刻，我們嘗試將這項目的基本要求再次撿討，和試圖找出一個比較簡單的方案。在各方面的努力下，我們找到一個全新的方案，將現存的沉箱護土牆保留和加以利用，取替原先建議的雙排大口徑樁護土牆方案。新方案可將原有的工程費用大大減少四千萬元，又可減低對道路使用者所產生的危險。本文闡述這個案的內容，岩土工程的設計及討論轉變的過程。

A CASE HISTORY OF SIMPLE SOLUTION TO A COMPLEX GEOTECHNICAL ENGINEERING PROBLEM

K P Yim[1] and D Y W Chan[2]

Abstract : The original scheme of a highway footbridge improvement project required excavation into the uphill slope to make room for a standard pedestrian access ramp and staircase structure. The excavation might involve demolition of some 50m length of an existing 12m high caisson retaining wall, and replacement by a higher 17m double row bored pile wall, right next to an existing busy highway. Design of the 17m high double row bored pile wall was a challenging geotechnical assignment, involving complex technical issue of soil/structure interaction and construction technique. Detailed design had then proceeded, putting a lot of effort in both literature search for previous similar design cases, and sourcing for appropriate analytical models and computer programs to carry out the complicated design.

Towards the end of the detailed design stage and during the pre-tender stage, this original scheme was reviewed again. The works was estimated to cost some HKD 60M (of which over 40M was due to the geotechnical works), difficult to build, and requiring a long construction period of 36 months. At this point, the client's fundamental requirements were re-visited, with a view to developing a much simpler solution. With input from the project team, the client and major stakeholders, a revised scheme was finally drawn up which made full use of the existing caisson wall and dispensed with the double row bored pile replacement wall. There resulted in a consequent saving in construction time of 12 to 18 months and a huge cost reduction of HKD40M, not to mention the substantial reduction in risk to commuters close to a busy highway during the construction stage. This paper presents details of this case history, the geotechnical engineering designs, and discusses the change process.

INTRODUCTION

A project was initiated to improve the junctions at Ap Lei Chau Bridge Road, Ap Lei Chau Drive, Lei Tung Estate Road and Ap Lei Chau Praya Road to meet the increasing traffic demand. The project comprised re-aligning and widening of the road junctions and approach roads, and provision of a footbridge over Ap Lei Chau Bridge Road. In the original scheme, the standard pedestrian access ramp and staircase structure for the proposed footbridge would encroach into the existing caisson wall 15NW-B/CR100 and its upslope. Major geotechnical works of the original scheme might include demolition of part of the existing caisson wall, excavation into the upslope and the construction of a new gigantic replacement retaining structure to make room for the standard pedestrian access ramp and staircase structure. It was this

[1] Architectural Services Department, Government of the Hong Kong Special Administrative Region, China

[2] Civil Engineering Department, Government of the Hong Kong Special Administrative Region, China

unprecedented, unconventional new replacement wall, which gave rise to a very complex geotechnical problem involving both design and construction. This paper presents details of this case history, the geotechnical engineering designs, and discusses the change process.

THE SITE AND PROPOSED IMPROVEMENT WORKS

The site, on a sloping ground with a cantilevered caisson wall (feature no. 15NW-B/CR100), was built in 1994 as part of the Ap Lei Chau Bridge Road Improvement (Figure 1).

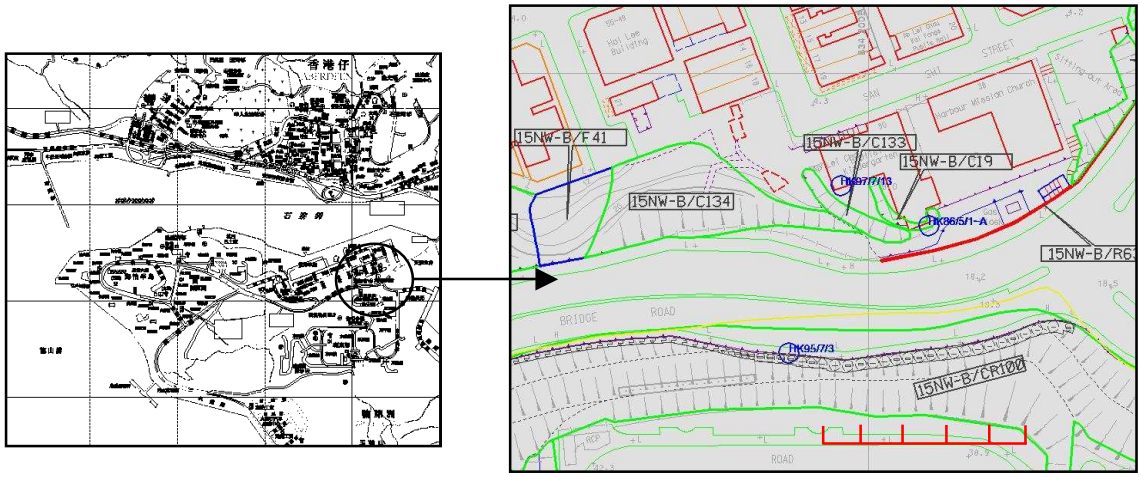

Figure 1 : Site Plan

The caisson wall 15NW-B/CR100 (Figure 2) comprises 2.6m diameter cantilevered caissons socketed into bedrock with a maximum retained height of about 12m above the road level. It supports a 40° slope, up to the platform of Yue On Court, which is at about 24 m above the Ap Lei Chau Bridge Road. Figure 3 shows the typical interpreted geological section based on the information collected from the ground investigation.

The preliminary layout of the proposed improvement works is shown in Figure 4.
The major geotechnical works would include demolition of some 50m length of the existing 12m high caisson wall 15NW-B/CR100, and excavation into the upslope by a maximum of 9m laterally to make room for the standard pedestrian access ramp and staircase structure, and to satisfy the requirement of leaving a gap separation between the staircase structure and the new retaining wall.

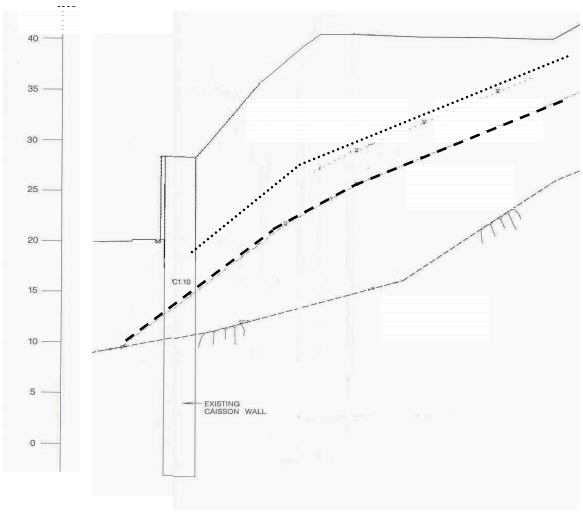

Figure 3 :Typical Geological Section

Figure 2 General Appearance of the Wall 15NW-B/CR100

OPTIONS ASSESSMENT OF THE ORIGINAL SCHEME

Three geotechnical options were considered in the early stage.

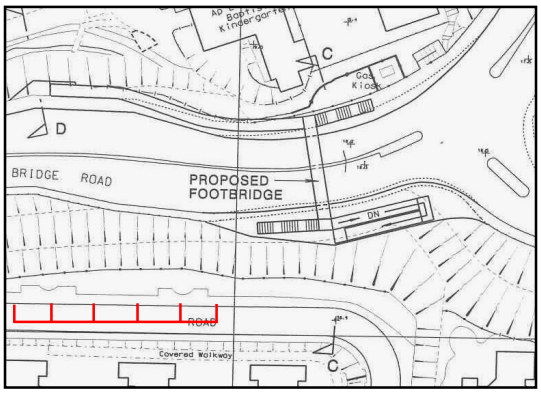

Figure 4 : Proposed Improvement Works of the Original Scheme

Option 1 : Caisson/Bored Pile Wall Option (Figure 5)

This Option required the construction of a line of concrete piles alongside the proposed ramp structure to replace the demolished section of caisson wall 15NW-B/CR100. Preliminary analysis showed that a replacement wall of 17m in height, comprising reinforced concrete piles of 2.5m diameter at 3m spacing, was required. To reduce the anticipated large deflection and the associated ground movement behind the wall, provision of intermediate supports was considered necessary to help reduce the bending stress, rock socket length and displacement of these concrete piles. Hand-dug caisson was initially considered as it was viewed as the simplest and cheapest method of construction for the concrete piles. However, because of health hazard associated with the caisson work, the authority would not approve the use of hand-dug caisson, unless it is proved to be the only practicable solution and when there is no other safe engineering alternative. Hand-dug caisson was therefore ruled out and, instead, large diameter bored pile was suggested.

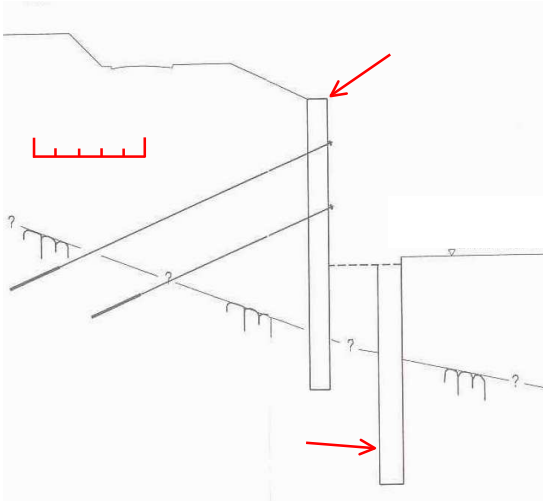

Figure 5 : Caisson/Bored Pile Wall Option

Option 2 : L-shaped Wall on Existing Caissons Option (Figure 6)

This was a proposal to construct a new retaining structure in the form of a new L-shaped wall tying to the existing caissons. Temporary lateral support would be necessary during the construction. Temporary ground anchors might also be required to prevent excessive lateral deflection of the lateral support. Similar to Option 1, permanent ground anchors were likely to be required to prevent excessive lateral deflection of the wall.

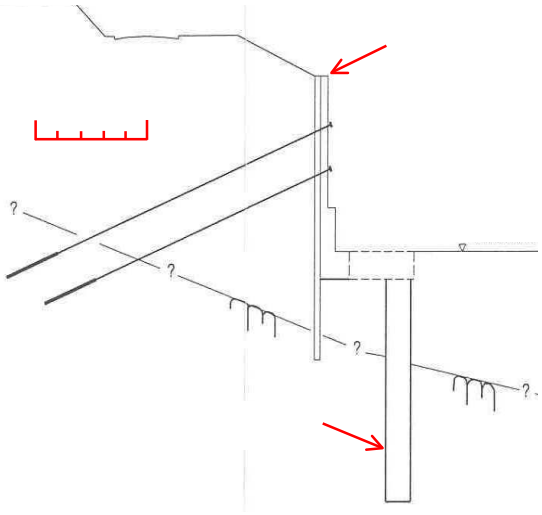

Figure 6 : L-shaped Wall on Existing Caissons Option

Option 3 : Subway Option (Figure 7)

The subway option was a viable solution to avoid the need of demolishing the caisson wall 15NW-B/CR100. However, the existing footpath would have to be widened to accommodate the pedestrian access ramp and staircase of the subway and hence reducing the width of the existing carriageway. On the grounds of cost and adverse impact on permanent traffic operation when compared to the footbridge options, the Client eventually rejected this option of a pedestrian subway.

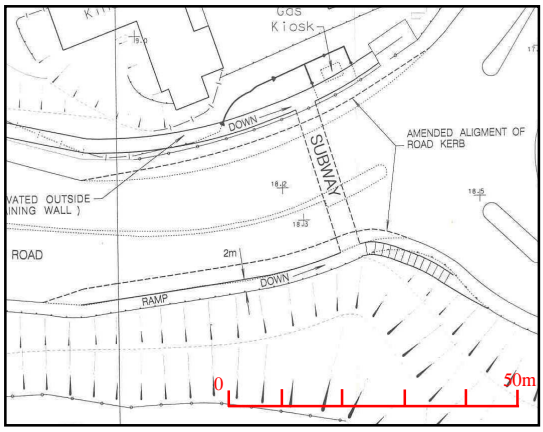

Figure 7 : Subway Option

DESIGN CONSIDERATIONS OF THE OPTIONS 1 AND 2 FOR THE ORIGINAL SCHEME

The two options of new retaining wall were considered geotechnically feasible. Option 1 was a new bored pile wall with intermediate supports by permanent prestressed ground anchors. Option 2 was a new L-shaped wall structure integrating into the existing caisson wall with intermediate supports by anchors.

One of the Client's requirements was that the proposed footbridge should be structurally separated from the retaining structure (Figure 8). Therefore, the wall stem of the L-shaped wall would need to be set back by about 9m out from the centre of the existing caisson wall to provide sufficient space for the ramp structure. With this restraint, the structural connection between the new L-shaped wall and the existing caisson wall in Option 2, thus, became not viable.

Furthermore, because of the complicated installation problem, the long term regular monitoring and maintenance burden in association with ground anchor, and hence the substantial recurrent expenditure, the ground anchor system was finally not accepted. Therefore, Options 1 and 2 (the anchor-supported cantilevered wall options) were not further pursued in the detailed design.

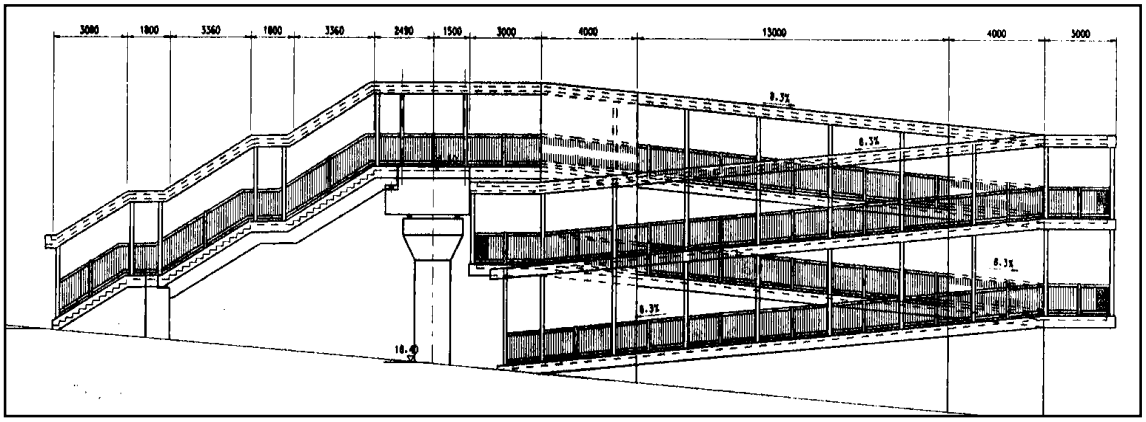

Figure 8: Typical footbridge with ramp structure

THE DOUBLE ROW BORED PILE WALL OPTION OF THE ORIGINAL SCHEME

The option of free cantilevered bored pile wall was further investigated and evaluated. Analysis showed that it would be extremely difficult, if not impossible, to design a stable 17m high one row free cantilevered bored pile wall. Eventually, a double row bored pile wall option was developed, with the highest retaining height of the wall to be supported by double rows of bored piles of 2.5m diameter. The front row piles were designed at 3m c/c, and the second row of piles at 6m c/c. Both rows would be connected by tie beams. Single row of bored piles was proposed to support those parts, where the retaining height was less than 10m. The layout plan and typical cross sections of this retaining structure is shown in Figures 9 and 10.

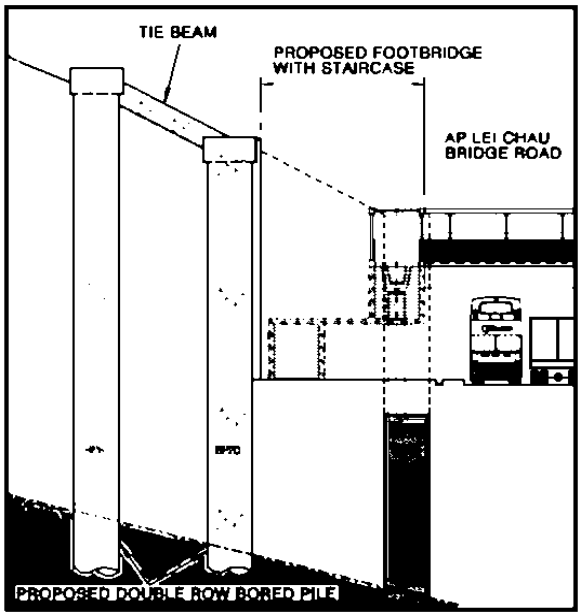

Figure 10 : Section of Double Row Bored Pile Wall Option

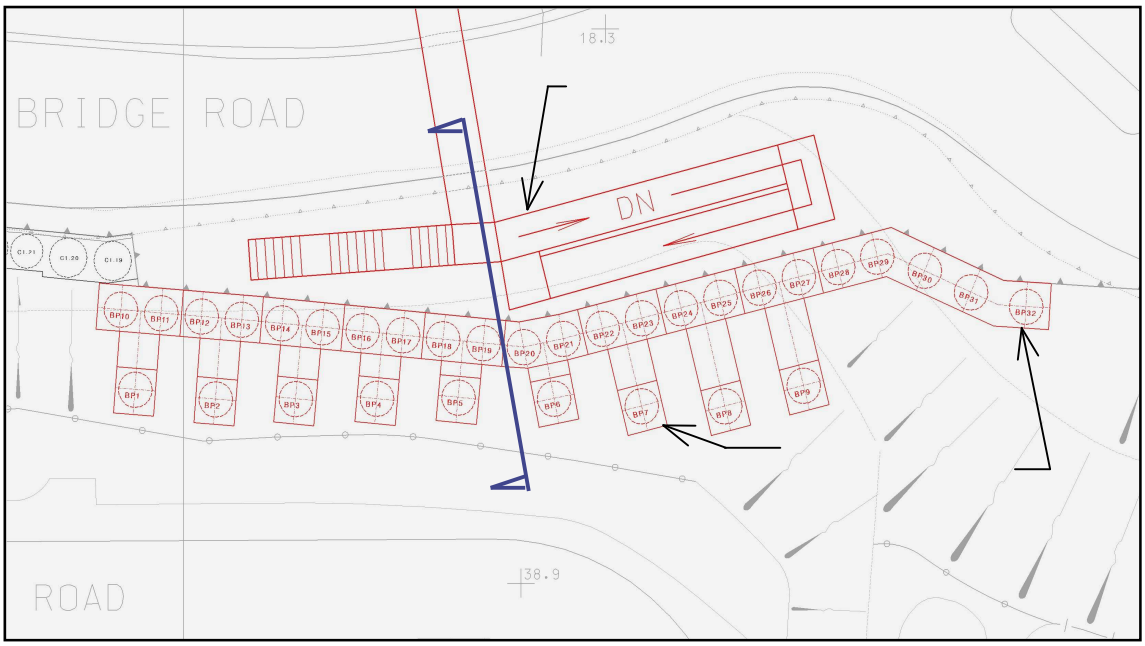

Figure 9 : Layout of Double Row Bored Pile Wall Option

DESIGN ASPECTS OF THE DOUBLE ROW BORED PILE WALL

The proposed bored pile wall will support the existing slope, access road and building platforms at some 20m above Ap Lei Chau Bridge Road. A very substantial and stiff structure will be required to serve the purpose in view of its considerable retained height.

Since there is little experience in the design and use of double row bored pile wall as an earth retaining structure, two different computer programme namely Fast Lagrangian Analysis of Continua (FLAC) and Linear Elastic Analysis Programme Ver.5 (LEAP5) have been adopted. In the structural design of bored piles, the bending moment, shear force and deflections are the key elements to be assessed. The results from the two approaches are compared and the larger values of bending moment and shear force are adopted. A typical example is discussed below.

Analysis Using A Two-Dimensional Finite Difference Computer Program FLAC

The analytical technique used in the program enables the effect of the site history to be modelled. The sequence of the construction events was considered in the analyses. The soil mass was modelled as a linear elasto-plastic material with a Mohr-Coulomb failure criterion. Both factored (for ultimate limit state) and unfactored (for serviceability limit state) soil parameters are adopted. A typical analysis starts with the site conditions prior to the construction of the existing caisson wall. Analysis is then carried out for different stages of construction to simulate what had happened on site, namely: initial stage; installation of the existing caisson wall; excavation in front of the existing caisson wall to the road level; installation of the proposed bored pile wall; and finally, excavation in front of the bored pile wall to the road level. The two rows of integrated bored pile comprise 23 nos. 2.5mØ RC bored piles at 3m c/c in the front row and 9 nos. 2.5mØ RC bored piles at 6m c/c in the rear row. The bored piles in the front row are linked up by means of a capping beam. In addition, the bored piles in the front row are tied back to the every single bored pile in the rear row by tie beams at 6m c/c. The grid for modelling is shown in Figure 11.

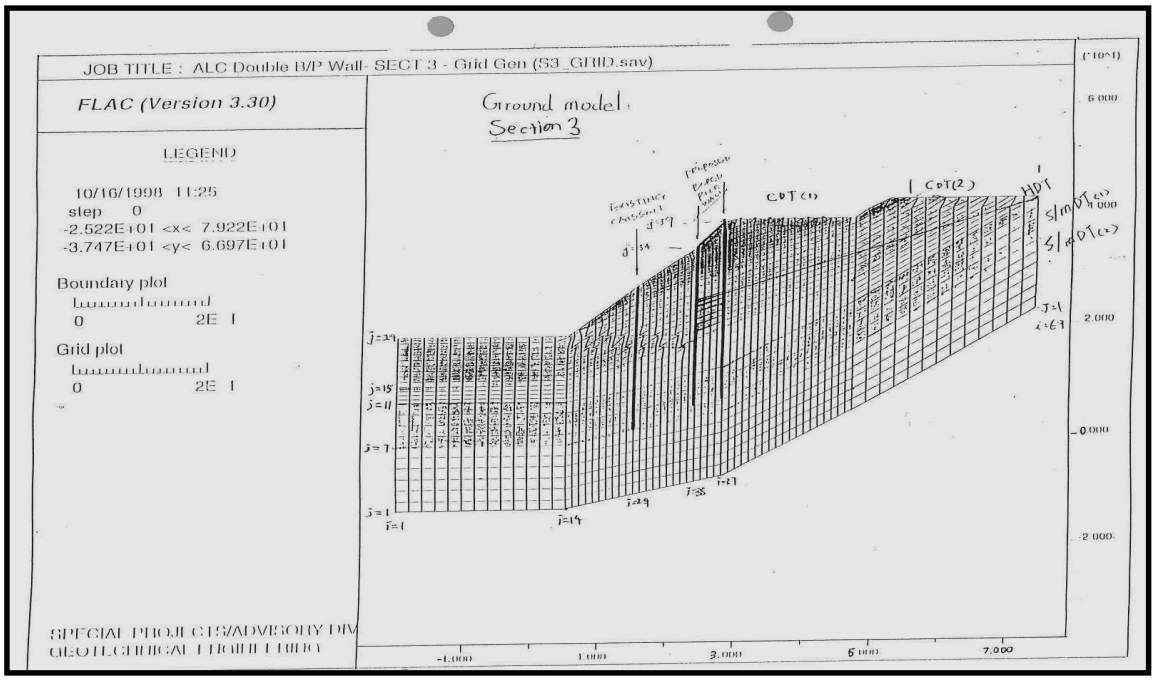

Figure 11 : Typical FLAC Model

Analysis Using A Two-Dimensional Structural Analysis Computer Program LEAP5

The computer program for general structural analysis, LEAP 5 has been used to calculate the stresses in the proposed structure under ultimate limit state (ULS). A

typical model of the analyses is shown in Figure 12. The structure was modelled as a plane frame with soil springs on the passive side below the excavation level. The soil mass enclosed between the two rows of bored piles was modelled as a series of internal beams that can carry compression but no tension nor bending moment.

Lateral earth loading was calculated using active earth pressure coefficients estimated with factored soil strength parameters for ULS in accordance with Geoguide 1. Horizon-tal geological layers are assumed in the estimation of the active earth pressure in order to simplify the calculations. All surcharge and water pressures are assumed to act on the rear bored piles.

Design Of Bored Pile Rock Socket Lengths

For the design of rock sockets of the bored pile wall under ULS condition, the following loaded cases were considered to determine the maximum stress envelope :

(a) The shear forces, bending moments and axial forces given by FLAC analyses based on **factored (**given in Geoguide 1) soil strength parameters and surcharges under ULS.

(b) The shear forces, bending moments and axial forces given by LEAP 5 analyses based on **factored (**given in Geoguide 1) soil strength parameters and surcharges under ULS.

(c) A factor of 1.4 (as recommended in BS8110 for earth and water pressure) applies on the shear forces, bending moments and axial forces derived from FLAC analyses based on **unfactored** soil strength parameters and surcharges.

Another exercise was carried out for (a), (b) and (c) above for the design of rock sockets for the rear bored pile. Difficulty was experienced when checking the lateral bearing capacity of the rock socket subjected to the lateral loads derived from the two rows of bored piles.

CONSTRUCTION ASPECTS OF THE DOUBLE ROW BORED PILE WALL

The major geotechnical works would involve construction of 32 nos. of 2.5m diameter bored piles over the existing slope, at a height of approximately 20m above the level of Ap Lei Chau Bridge Road. Since much of the bored pile excavation would be in rock of Grades II or III, massive reverse circulation rotary drilling machines would be required to avoid heavy chiselling and severe vibration, close to the existing occupied buildings. A gigantic temporary working platform (Figure 13), capable of supporting the bored pile machine and associated construction loads, would need to be erected over the slope at a high level up to the crest of the upslope. The foundation of the temporary working platform would need to be designed and carefully positioned to ensure that it would not impose any surcharge and adverse effect on the existing caisson wall and its upslope.

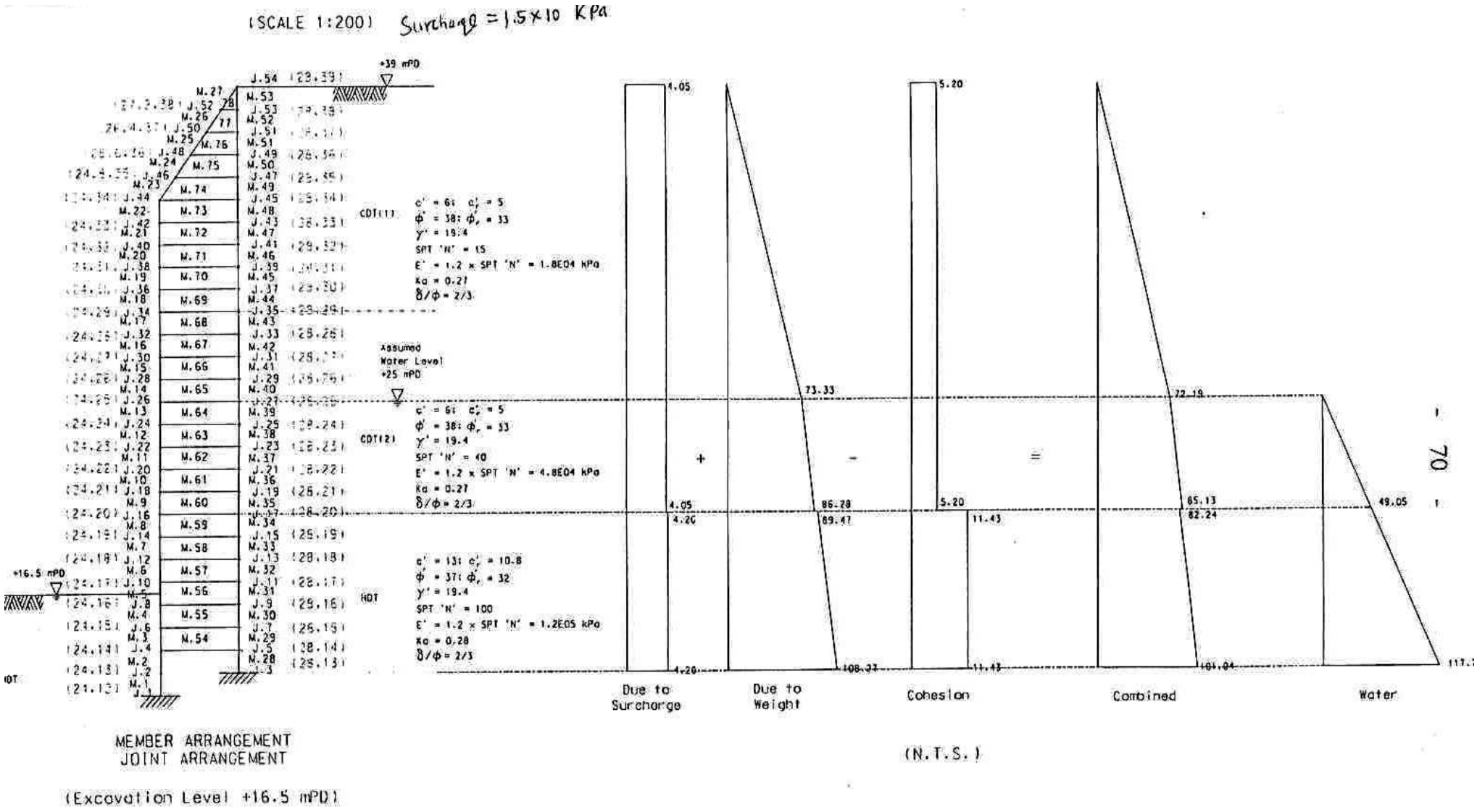

Figure 12 : Typical LEAP5 Model

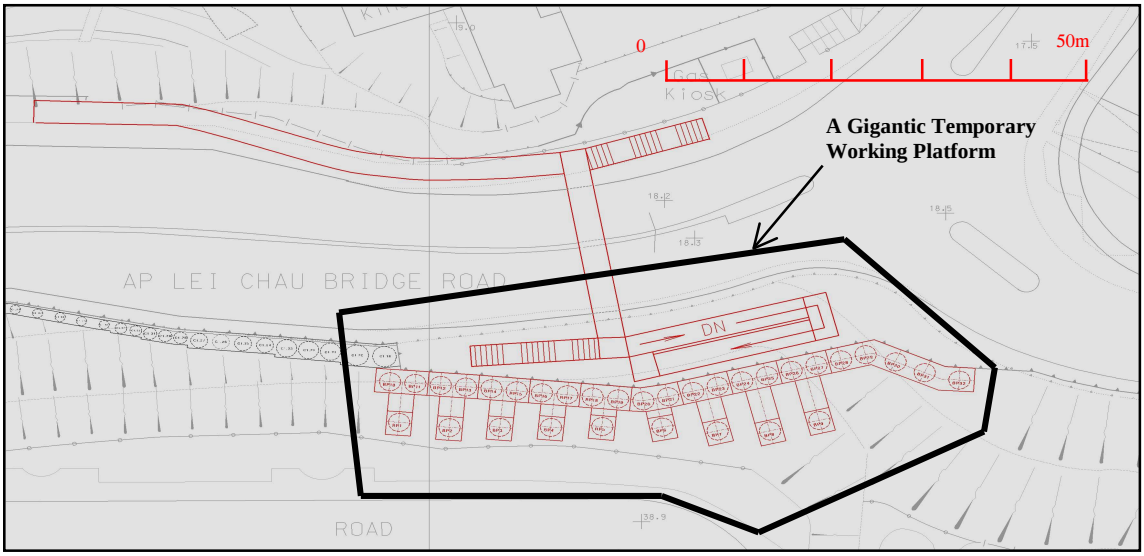

Figure 13 : Gigantic Temporary Working Platform

It was anticipated that there could also be a substantial risk and danger of accident to the public passing under the temporary working platform at some 20m below, as well as nuisance from noise, spoil, etc. Unless partial closure of Ap Lei Chau Bridge Road be implemented, the risk to the public during construction was considered unacceptable. A similar substantial temporary working platform is shown in Figure 14. It was envisaged that construction of the bored pile would involve excavation of 600m length of 2.5m diameter bored pile in soil, together with another 400m length of pile in rock. The works may take longer than 15 months to complete.

Figure 14 : Similar Gigantic Temporary Working Platform at Stubb's Road

Furthermore, suitable mitigation measures to protect the public and the residents of the housing estate at the upslope crest from nuisance caused by the construction activities should be duly allowed in the contract. In view of the significant impact, a public consultation and an environmental impact assessment would be required before finalising the scheme. Permission from the housing management should also be sought in advance for the proposed site access via the housing estate. If public response is negative, reduction of the works area and alternative construction method might need to be resorted. The project team was expecting a very difficult community lobbying work ahead.

EVOLUTION OF THE REVISED SCHEME

Towards the end of the detailed design stage and during the pre-tender stage, the difficulties and problems to be encountered with double row bored pile wall scheme were reviewed again. The works was estimated to cost some HK$ 60M (of which over HK$ 40M was due to the geotechnical works), difficult to build, and requiring a long construction period of 36 months. However, all design, drawings and contract documents,

public consultation, financing and pre-tender preparation work had been completed. Any drastic design change at this late stage would mean that most of the previous work would have become abortive and the accountability issue would be raised. At this stage, the project team was facing a dilemma, whether kept silent and delivered the design of the original scheme to the client, or questioned the overall layout in the light of the cost, construction difficulties, site safety and construction programme and looked for a better option.

In view of potential huge gain, a Value Engineering review was eventually applied to the original design, involving the project team, the client and the major stakeholders, trying to re-examine the basic functional requirements and reassess the design and construction options to pursue additional optimisation based on experience of the project team members. It was found and agreed that there was no strict requirement to separate the new footbridge from the existing retaining structure, and that the standard pedestrian access ramp and staircase structure was not a prerequisite requirement. These findings allowed greater flexibility in designing the layout and positioning the associated structures of the footbridge. Finally, it came up with a revised scheme basically fulfilling the redefined functional requirements of the client by providing a footbridge over Ap Lei Chau Bridge Road with a ramp and a staircase connecting to the footbridge as shown in Figures 15 and 16.

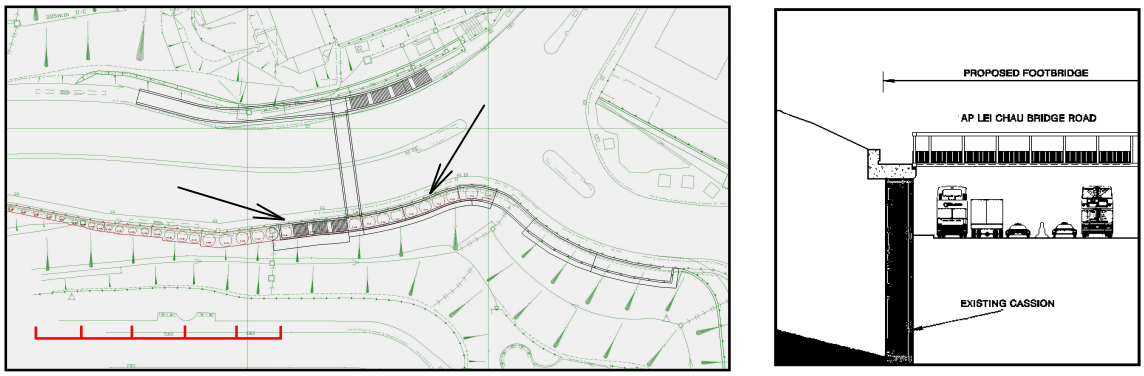

Figure 15 : Retaining wall layout and section under revised scheme

Figure 16 : Elevation of Retaining Wall Under the Revised Scheme

In the revised scheme, the layout of Ap Lei Chau Bridge Road westbound was maintained, with no change to the kerb line and footpath. Caisson wall 15NW-B/CR100 was to be preserved except some modification works to convert part of the wall into a staircase

and ramp. The proposed road improvement works of the revised scheme would mainly comprise the following works:

(a) Five existing caissons, namely C1.11 to C1.15 of the wall 15NW-B/CR100 would be trimmed down by 5m to 11m to accommodate the staircase connecting to the proposed footbridge. The wall section would be replaced with a new 2m thick cantilevered L-shaped retaining wall connected to the trimmed caissons by a 2m deep base slab at their cut-off level, with staircase to be formed on top of the base slab with handrail and roof;

(b) Existing caisson C1.10 would be trimmed down to support the proposed footbridge at +25.7mPD. The caisson head would be modified to provide a suitable support for the footbridge and a retaining wall connected to the caisson head would be built to support the upslope. The caisson C1.10 would be checked against the loadings derived from the footbridge;

(c) For the provision of pedestrian ramp connecting to the proposed footbridge, the capping beam to the east of the proposed footbridge would be filled up with concrete to the required level for the pedestrian ramp running towards Ap Lei Chau Drive (Figure 17). A new cantilevered wall section would be built with thickened base slab to replace the capping beam and suit the required gradient of ramp.

Figure 17 : Artist's Impression after completion of Works

ADVANTAGES OF THE REVISED SCHEME

(a) The revised scheme reduces the construction cost by deleting all those 32 no. bored piles in the original scheme, saving about HK$ 30M and shortening the construction time by about 15 months;

(b) No more bored piling machine will be on site and hence no more substantial temporary working platform is required. The works only involve cutting off of 5 caissons and building a replacement wall to cover the caissons. This will only involve a minor temporary lateral support works to build the replacement wall;

(c) Without the substantial temporary working platform, this will save about HK$ 10M and cut the construction programme by about 3 months;

(d) Geotechncial works have been kept to minimum and this will obviously shorten the whole construction programme very much;

(e) Minimum works mean minimum environmental impact to the public as works involve much less excavation in the revised Scheme;

(f) The access ramp is in the direction to the housing estate to give greater convenience to the majority of the pedestrians;

(g) Recurrent expenditure required for maintenance would be reduced as compared to the works of a higher bored pile wall if it is built; and

(h) Progress of works is now controlled by the footbridge construction, rather than any bored pile works or substantial temporary working platform. Construction programme could be better managed under less unforeseeable constraints.

DISCUSSION OF THE CHANGE PROCESS

In this case of the highway footbridge improvement project, the subway option was ruled out at feasibility stage, so detailed design had proceeded according to the client's request resulting in a very difficult preliminary design option. At the detailed design and pre-tender stage, and after the basic functional requirements were re-visited and redefined, the obvious question was raised:

> ***"Why could the layout not be revised to support the proposed footbridge on top of the existing caisson wall and straighten the pedestrian ramps to eliminate slope excavation?"***

These proposed scheme revisions were actually quite minor (re-aligning the pedestrian ramps; a lateral shift of the highway by less than one metre; a recess made at the existing caisson wall to accommodate a staircase and support the footbridge; and a new screen wall), but the determination to redefine the functional requirements and the necessary mind-shift by all members of the project team were enormous. There had also followed some grave concerns over whether the project content could be so radically changed at the detailed design stage, without causing severe delay and incurring substantial criticism from all walks. However, the revision finally proved to be totally feasible, with a consequent big saving in construction time and a huge cost reduction, not to mention the removal of a potentially

dangerous construction situation where works will be carried out close to a busy highway. After discussion amongst all affected parties and stakeholders, the project team proceeded with the new scheme, and received very good responses.

In the design of projects and in our concern to deal with the complex technical issues, we are used to taking for granted basic assumptions that, on critical examination, may turn out not only to be unnecessary but also cause false constraints on the project fulfilment. This can happen without realising and so it is useful to review basic assumptions and functional requirements during the inception, planning, design and even construction stages of a project. It can also occur as a result of agency multiple-handling, inadequate communication and different perception of function and purpose among project team members and the stakeholders. The real needs of the ultimate client may not be fully known by all project team members. In such cases, review of basic assumptions with the ultimate client is necessary.

CONCLUSIONS

The case history shows an application of the value engineering principles to seek for simple solution to a complex geotechnical engineering problem. It is vital to maintain good communication and clear understanding of the client's basic functional requirements among project team members, the clients and stakeholders at all phases of the project. Reviewing and questioning basic assumptions at all phases of the project should be encouraged, although it is not always easy. It also requires a certain detachment from the intricacies of the project and often not a little courage! Questioning basic assumptions can be achieved by asking very radical questions, questions that might appear too obvious and are therefore never asked. However, the possible improvements and savings can sometimes be very large and even mean the difference between a feasible project and no project at all, as is demonstrated by this case history.

ACKNOWLEDGEMENT

The authors would like to thank the Directors of Architectural Services Department, Civil Engineering Department and Highways Department for the permission to publish this paper.